2017

Deciphering the role of SerpinB2 in cancer invasion and metastasis

Nathanial L.E Harris
University of Wollongong

Deciphering the Role of SerpinB2 in Cancer Invasion and Metastasis

This thesis is presented as part of the requirement for the Award of the Degree of

DOCTOR OF PHILOSOPHY

The Illawarra Health and Medical Research Institute
School of Biological Sciences
Faculty of Science, Medicine and Health

UNIVERSITY OF WOLLONGONG

2017

Nathanial L.E. Harris **BMedSc BSc (Hons)**

DECLARATION

The work described in this thesis does not contain any material that has been submitted for the award of any higher degree in this or any other University and to the best of my knowledge contains no material previously published or written by any other person, except where due reference is made in the text of this thesis.

Nathanial L.E. Harris
2017

ACKNOWLEDGEMENTS

Firstly, the deepest gratitude and recognition is to my primary supervisor, Professor Marie Ranson. You have been akin to a Mother to me and I will not forget all the support and encouragement you have given ever since our first meeting. It has been an amazing journey and without you there I would not have completed this PhD. Secondly, Dr Kara Vine and Dr Darren Saunders - your continued support and encouragement has helped me on this journey in many ways, both on an academic and personal level and for this I am truly grateful. Kara, your guidance, even when you were exceptionally busy, will not be forgotten and I really appreciate that you had time for me during such demanding times, as well as many great extra-laboratory chats over coffee or drinks. Darren, I thank you for giving me many opportunities during my Ph.D experience, both with encouragement, time management and solid laboratory direction, not to mention the Cancer conferences! I would also like to thank Dr. Paul Timpson, for allowing me to be a part of your research group and without such laboratory experience, this thesis would not have been possible. Enormous appreciation to Dr Robert Shearer, your guidance at the beginning of the PhD was essential to the smooth running of this project! A big thanks to Dr Oliver Shilling and Dr Zon Weng Lai for your collaborative proteomic work. Thank you also to Dr Tony Romeo and Dr Mitchell Nancarrow for your training on the Electron Microscopy Centre (IPRI, UOW), as well as Anaiis Zaratzian and Alice Boulghourjian for all of your immunohistochemical assistance at the Kinghorn Cancer Centre, Sydney. Thank you to the University of Wollongong for financial support through an Australian Postgraduate Award (APA). Kudos to Dr Ben Buckley - many awesome memories inside and outside the lab were made – we got through it together brother! Thank you to the entire, amazing lab 210! For all the times and immense love we spread - Bless. To all my epic friends (you know who you are!) who kept me balanced and well loved through this odyssey, huge props. And last yet most of all, thank you to my amazing and inspirational family – Mum, Dad, Stef and Greer – you are all truly unique and miraculous! I would not be who I am or where I am today without each of you and I cannot thank you properly in words. One is truly blessed and honoured to be alive with you…

ABSTRACT

Pancreatic and breast cancer are both architecturally heterogeneous and insidious diseases of which 90% of patients succumb due to metastasis, the spread of tumour cells throughout the body. Tumour associated fibroblasts and other stromal cells have been implicated as major facilitators of tumour invasion and metastasis. Thus, there is a strong imperative to better elucidate tumour-stromal interactions in cancer as a means to develop more effective therapies. In that regard, this thesis focused on the urokinase plasminogen activation system (PAS) in stromal remodelling and invasion using two aggressive cancer types, pancreatic ductal adenocarcinoma (PDAC) and triple negative breast cancer (TNBC), as both are well known to utilise the PAS system during their invasion processes. The main activator of PAS is the serine protease, urokinase (uPA), and its overexpression is recognised as an important biomarker of metastatic disease and a therapeutic cancer target. Receptor bound uPA activates co-localised plasminogen into the broad-spectrum protease, plasmin. The combined proteolytic and signalling events initiated by this pathway drive extracellular matrix (ECM) degradation, cell proliferation, adhesion and migration. Negative regulation of this pathway is provided at several levels, including inhibition and clearance of protease activity by naturally occurring inhibitors, such as SerpinB2 (Plasminogen Activator Inhibitor Type-2). Elevated tumour SerpinB2 expression is associated with prolonged survival, decreased metastasis, or decreased tumour growth in a number of cancer types, with loss of stromal SerpinB2 expression associated with progression. However, specific mechanisms have not been addressed. To directly interrogate the role of SerpinB2 in pancreatic and breast cancer, *ex vivo* and *in vivo* models were developed using wild-type and SerpinB2$^{-/-}$ murine embryonic fibroblasts (MEFs). The potential role of SerpinB2 in tumour cell invasion *ex vivo* was also investigated in breast tumour epithelial cells with modulated SerpinB2 expression.

The effect of SerpinB2 deletion on the rate of collagen I matrix contraction and collagen density were measured utilising wild-type or SerpinB2$^{-/-}$ MEFs (Chapter 3). Significant decreases were observed using SerpinB2$^{-/-}$ MEFs in

matrix contraction rates, overall diameter, matrix integrity, collagen coverage and fibril network formation compared to wild-type MEFs ($P < 0.0001$). Second harmonic generation (SHG) and scanning electron microscopy (SEM) analyses of matrices formed by SerpinB2$^{-/-}$ MEFs revealed dysregulated, anisotropic dispersal of collagen I, compared with the ordered, isotropic distribution observed in matrices formed with wild-type MEFs ($P < 0.0001$). Further, stark differences in cellular adhesion, protrusion dynamics and migration between wild-type and SerpinB2$^{-/-}$ MEFs were observed, suggesting that SerpinB2 is important in regulating fibroblast migration, necessary for ECM remodelling.

Chapter 4 involved the implementation of 3D organotypic culture systems and *in vivo* models of PDAC to interrogate the role of PAS pathway in PDAC invasion. PDAC cell invasion through 3D organotypic matrices formed by SerpinB2$^{-/-}$ MEFs doubled compared to wild-type MEFs (27.2 % ± 1.9 versus 55.2 % ± 1.8; $P < 0.001$). Furthermore, a significant difference in invading PDAC cell morphology and migration mode was observed in matrices formed by SerpinB2$^{-/-}$ MEFs. PDAC cells invading through wild-type matrices also exhibited a predominantly mesenchymal migratory mode (>70% of cells), while PDAC cells in SerpinB2$^{-/-}$ matrices displayed a predominantly amoeboidal phenotype (>80% of cells). PDAC organotypic results were reproduced *in vivo*, as SerpinB2$^{-/-}$ MEFs in the PDAC mixed allograft model formed larger and more invasive tumours ($P = 0.0322$), with altered collagen deposition ($P = 0.0021$). Significant differences in uPA/uPAR expression on PDACs in allograft tumours formed with SerpinB2$^{-/-}$ MEFs was concomitantly reflected in an increased uPA activity by SerpinB2$^{-/-}$ tumours ($P < 0.05$), which lead to an increase in tumour cell local invasion through both muscle ($P = 0.0314$) and subcutaneous fat ($P = 0.0024$). These results thus indicate that SerpinB2 regulates stromal remodelling of collagen and in turn, influences tumour growth and local invasion.

The 3D organotypic culture system was also used to interrogate the role of SerpinB2 in TNBC cell invasion using the high uPA/uPAR expressing and invasive breast adenocarcinoma cell line, MDA-MB-231 (Chapter 5). In these models, SerpinB2 shRNA lentiviral vectors (Chapter 2) were also utilised to knock-down expression in these

cells. Down-regulation of SerpinB2 expression did not modify the invasion of MDA-MB-231 cells *in vitro* or *ex vivo* ($P > 0.05$), highlighting the important influence of stromal SerpinB2 on tumour cell invasion, similar to that reported in the PDAC cell invasion experiments. Further, a significant increase in breast tumour volume (1.88-fold) was observed in mice with allograft tumours formed with SerpinB2$^{-/-}$ MEFs versus with wild-type MEFs.

The *in vivo* models reported within this thesis show that co-injection of PDAC or TNBC cells and SerpinB2$^{-/-}$ MEFs resulted in increased tumour growth, aberrant remodeling of collagen ECM and increased local invasion from the primary tumour. Altogether, this confirms the significant role of SerpinB2 in the progression of cancer invasion and metastasis, providing valuable information on the role of PAS in tumour biology.

LIST OF ABBREVIATIONS

ACN	Acetonitrile
APS	Ammonium persulfate
ATCC	American Type Culture Collection
bFGF	Basic fibroblast factor
BSA	Bovine serum albumin
°C	Degrees Celsius
CAMs	Cellular adhesion molecules
CD loop	Interhelical loop between α-helices C and D in some serpins
DCC	Dicyclohexylcarbodiimide
dH2O	Distilled water
DMSO	Dimethyl Sulfoxide
ECs	Endothelial cell(s)
ECM	Extracellular matrix
FCS	Foetal calf serum
FDA	Food and Drug Administration
FPLC	Fast Protein Liquid Chromatography
EDTA	Ethylenediaminetetraacetic acid
EMT	Epithelial Mesenchymal Transition
ESI-MS	Electrospray Ionisation-Mass Spectrometry
FA	Formic Acid
FITC	Fluorescein isothiocyanate
x g	Gravitational force - 9.8 m/s
GPI	Glycophosphatidyl inositol
HGF	Hepatocyte growth factor (also known as scatter factor)
HIF	Hypoxia inducing factor
HMW	High Molecular Weight
IgG	Immunoglobulin G
IPTG	Isopropyl β-D-1-thiogalactopyranoside
kDa	Kilodalton
LB	Luria-Bertani broth
LDLR	Low density lipoprotein receptor
LRP	Low density lipoprotein receptor-related protein
LTT	Ligand targeted therapy
MALDI-MS	Matrix Assisted Laser Desorption Ionisation – Mass Spectroscopy
MDA-MB-231	Human breast adenocarcinoma cell line
MMPs	Matrix metalloproteinases
MOA	Mode of Action
***N*-AI**	5,7-dibromo-*N*-(*p*-hydroxymethylbenzyl)isatin
OD	Optical density
PA	Plasminogen activator
PAF	Platelet activating factor
PAGE	Polyacrylamide gel electrophoresis
PAI-1	Plasminogen activator inhibitor type 1 / SerpinE1
PAI-2	Plasminogen activator inhibitor type 2 / SerpinB2
PAS	Plasminogen Activation System
PBS	Phosphate-buffered saline
PDGF	Platelet derived growth factor

PEG	Polyethylene Glycol
pI	Isoelectric Point
Q-TOF-MS	Quadrupole-Time of Flight-Mass Spectrometry
RCL	Reactive Centre Loop
RME	Receptor-Mediated Endocytosis
rpm	Revolutions per minute
RPMI	Roswell Park Memorial Institute
RT	Room Temperature
SDS	Sodium dodecyl sulfate
SDS-PAGE	Sodium dodecyl sulfate polyacrylamide gel electrophoresis
SERPIN	Serine protease inhibitor
SERPINB2	Serine protease inhibitor type-II (also known as PAI-2)
SERPINE1	Serine protease inhibitor type-I (also known as PAI-1)
TB	Terrific broth
TEMED	*N,N,N',N'*-tetramethyl-ethane-1,2-diamine
TF	Tissue factor
TFPI	Tissue factor pathway inhibitor
TGF	Transforming Growth Factor
TGF-β	Transforming growth factor-β
TNF-α	Tissue necrosis factor-α
tPA	Tissue-type plasminogen activator
Tris	2-amino-2-hydroxymethyl-propane-1,3-diol
uPA	Urokinase-type plasminogen activator
uPAR	Urokinase-type plasminogen activator receptor
uPAS	Urokinase-type plasminogen activation system
UV	Ultra-violet
UV-Vis	UV-visible spectrum
v/v	Volume per volume
VEGF	Vascular endothelial growth factor
VLDLR	very low density lipoprotein receptor
w/v	Weight per volume

TABLE OF CONTENTS

DECLARATION ii

ACKNOWLEDGEMENTS iii

ABSTRACT iv

LIST OF ABBREVIATIONS vii

LIST OF PUBLICATIONS xix

CONTRIBUTIONS OF WORK xx

CONFERENCE PROCEEDINGS xxi

SCHOLARSHIPS AND AWARDS xxii

CHAPTER 1: INTRODUCTION TO SERPINB2 1

1.1 INTRODUCTION TO CANCER 2

1.2 Tumour invasion & metastasis 3

1.3 Tumour heterogeneity and stromal conscription 5

1.4 The plasminogen activation system (PAS) 8

1.4.1 The urokinase plasminogen activation system 9

1.4.2 uPA and the uPA receptor, uPAR 11

1.4.3 Plasminogen activator inhibitors 13

1.5 SerpinB2 15

1.5.1 Expression and structure 15

1.5.2 SerpinB2 function 19

1.5.2.1 uPA inhibition 19

1.5.2.2 Non-uPA inhibitory functions *21*

1.5.3 SerpinB2$^{-/-}$ mouse models 23

1.5.4 SerpinB2 in cancer 23

1.5.4.1 Tumour progression and inhibition *24*

1.6 The extracellular matrix (ECM) 27

1.6.1 The dynamic reciprocity of the ECM 28

1.6.2 Collagen I 29

1.6.3 Collagen crosslinking and fibrilogenesis 30

1.6.4 Lysyl oxidase (LOX) 32

1.6.5 Tissue transglutaminase-2 (TG2) 33

1.6.5.1 SerpinB2 and TG2 35

1.6.6 SerpinB2 and TG2 in the TME and development 36

1.6.7 TG2 in cancer 38

1.6.8 The Fibroblast & ECM remodeling 40

1.7 2D versus 3D *in vitro* models 43

1.8 The 3D organotypic model 45

1.9 Aims and Project Rationale 47

CHAPTER 2: PRODUCTION OF LENTIVIRAL VECTORS TO ASCERTAIN THE SPATIOTEMPORAL EXPRESSION OF SERPINB2 WITHIN THE TME 49

2.1 INTRODUCTION 50

2.1.1 Lentivirus 50

2.1.2 Lentiviral transfer vectors used for expression of cDNA and shRNA 51

2.1.3 Third generation lentiviral vectors 53

2.2 METHODS 57

2.2.1 Cell lines and culture conditions 57

2.2.2 Generation of SerpinB2 cDNA and shRNA 57

2.2.3 SerpinB2 expression clone generation 59

2.2.4 Creation of entry vectors 59

2.2.5 Creation of destination vectors 60

2.2.6 Transient transfections using SerpinB2 mutant cDNA 60

2.2.7 Lentivirus production 60

2.2.8 Viral titre optimisation for lentiviral transgene repression 61

2.2.9 Lentiviral infection 61

2.2.10 Characterisation 62

2.2.10.1 Western blotting 62

2.2.10.2 Immunofluorescence 63

2.2.10.3 Proliferation assays 63

2.3 RESULTS 63

2.3.1 Enzyme digestions and AGE 63

2.3.2 Entry clone analysis 64

2.3.3 Knock-in/overexpression constructs 65

2.3.4 Destination clone analysis 66

2.3.5 Transient transgene transfection of HEK-293T cells 74

2.3.6 LacZ infection for repression analysis 75

2.3.7 Stable transductions of MDA-MB-231 cell line 77

2.3.8 Western blotting - overexpression constructs 77

2.3.9 Western blotting - knockdown constructs 78

2.3.10 Long term stability of gene modification 80

2.3.11 Incucyte proliferation assay 81

2.3.12 Immunofluorescence 83

2.3.13 Stable GFP transduction of wild-type and SerpinB2-/- MEFs 86

2.4 DISCUSSION 88

CHAPTER 3: ELUCIDATING THE EFFECT OF SERPINB2 ON COLLAGEN CROSSLINKING AND STROMAL REMODELLING THROUGH APPLICATION OF THE 3D COLLAGEN CONTRACTION MODEL 93

3.1 INTRODUCTION 94

3.1.1 Imaging 3D systems 96

3.1.2 Second harmonic generation (SHG) 98

3.1.3 Multiphoton microscopy (MPM) imaging 99

3.1.4 Scanning electron microscopy (SEM) 100

3.1.5 SerpinB2 in the ECM 100

3.2 METHODS 101

3.2.1 Cell lines and culture conditions 101

3.2.2 Flow cytometry 102
3.2.3 Wound healing assays 102
3.2.4 3D organotypic contraction assay 103
3.2.5 Histological analysis 104
3.2.6 Ultrastructural SHG imaging 104
3.2.7 Tracking of fibroblast movements in matrices 104
3.2.8 SEM imaging 105
3.2.9 Pilot proteomic analysis of wild-type and SerpinB2$^{-/-}$ MEF matrices 105
3.2.10 Statistical analyses 106
3.3 RESULTS 106
3.3.1 Collagen I preparation 106
3.3.2 PAS expression in fibroblast lines 107
3.3.3 Differences in MEF migration/2D wound healing 108
3.3.4 Fibroblast contracted collagen I matrix formation and integrity 110
3.3.5 Stromal SerpinB2 effects on MEF migration and ECM remodelling 116
3.3.6 Pilot proteomic analysis of wild-type and SerpinB2$^{-/-}$ MEF matrices 118
3.3.7 Exogenous SerpinB2 effects on SerpinB2$^{-/-}$ MEF collagen contraction 119
3.4 DISCUSSION 124
3.4.1 Hypothetical effects of SerpinB2 in the ECM 129
CHAPTER 4: INVESTIGATION INTO THE EFFECTS OF SERPINB2 MODULATION ON PANCREATIC TUMOURIGENESIS AND LOCAL INVASION 141
4.1 INTRODUCTION 142
4.1.1 Genetic aberrations in the lead up to PDAC 142
4.1.2 Desmoplasia in PDAC 146
4.1.3 uPAS in PDAC 148
4.2 METHODS 150
4.2.1 Proteins and antibodies 150
4.2.2 Gene expression survival analysis 150

4.2.3 Cell lines and culture conditions 151
4.2.4 Flow cytometry 151
4.2.5 3D organotypic invasion assay 152
4.2.6 Mixed cell allograft model 152
4.2.7 Histological analysis 152
4.2.8 *In vivo* allograft local invasion scoring method 153
4.2.9 SHG and SEM imaging analysis 155
4.2.10 uPA activity assay 155
4.2.11 Statistical analyses 155
4.3 RESULTS 156
4.3.1 APGI PDAC gene expression survival analysis 156
4.3.2 PDAC cell invasion in the 3D organotypic culture model 158
4.3.3 Exogenous SerpinB2 inhibits PDAC cell invasion 162
4.3.4 Exogenous SerpinB2 does not inhibit PDAC invasion in contracted MEF matrices 163
4.3.4 PDAC tumour growth and local invasion *in vivo* 165
4.4 DISCUSSION 172
CHAPTER 5: TOWARDS AN UNDERSTANDING OF THE ROLE OF SERPINB2 IN BREAST TUMOURIGENESIS AND METASTASIS 181
5.1 INTRODUCTION 182
5.1.1 Breast cancer 184
5.1.2 TNBC 186
5.1.3 The role of uPAS in breast cancer 187
5.2 METHODS 192
5.2.1 Cell lines and culture conditions 192
5.2.2 Cell migration wound healing assays 193
5.2.3 Western blotting 194
5.2.4 3D organotypic culture 195
5.2.4.1 SerpinB2 knockdown in MDA-MB-231 effects on 3D invasion 195

5.2.4.2 MDA-MB-231HM invasion into 3D collagen matrices 195

5.2.4.3 Pilot 3D Organotypic breast tumour spheroid invasion assay 195

5.2.5 Mixed cell xenograft model 196

5.2.6 Statistical analyses 197

5.3 RESULTS 197

5.3.1 SerpinB2 expression in breast cancer cell lines 197

5.3.2 SerpinB2 and SerpinE1 characterisation in breast epithelial and stromal cells 198

5.3.3 Cell surface detection of uPA 199

5.3.4 SerpinB2 knockdown effects on migration in MDA-MB-231 cells 201

5.3.5 SerpinB2 knockdown effects on MDA-MB-231 3D organotypic invasion 203

5.3.6 Pilot 3D invasion assays with highly metastatic MDA-MB-231HM cells 204

5.3.7 High metastatic MDA-MB-231HM cells in wild-type and SerpinB2$^{-/-}$ MEF constructed collagen I organotypic matrices 206

5.3.8 Mammary tumour growth and local invasion in vivo 208

5.3.9 Pilot 3D Organotypic breast tumour spheroid invasion assay 209

5.4 DISCUSSION 210

CHAPTER 6: CONCLUSIONS AND FUTURE DIRECTIONS 219

REFERENCES 228

APPENDICES 277

APPENDIX A: SOLUTIONS AND MEDIA 278

APPENDIX B: IMMUNOFLUORESCENCE ANTIBODY CONTROL 282

APPENDIX C: LIST OF ANTIBODIES 283

APPENDIX D: SUPPLEMENTARY MOVIE LEGENDS 285

APPENDIX E: LENTIVIRAL CONSTRUCT SEQUENCES 286

LIST OF FIGURES

Fig. 1.1. Metastatic progression..... 5
Fig. 1.2. PAS and the role of the serpins – SerpinE1 and SerpinB2.....10
Fig. 1.3. Two-chain urokinase plasminogen activator.....12
Fig. 1.4. Serpin inhibitory mechanism.....14
Fig. 1.5. Structure of SerpinB2.....16
Fig. 1.6. SerpinB2 expression and activity.....19
Fig. 1.7. Structure of Collagen I.....31
Fig. 1.8. Invasion of human trophoblasts and PDAC cell invasion.....38
Fig. 1.9. Schematic representation of the biological activities undertaken by fibroblasts within the TME.....42
Fig. 1.10. Schematic of preparation and experimental progression of the 3D organotypic assay.....46
Fig. 2.1. Structure of wild-type lentivirus.....51
Fig. 2.2. Mechanism of RNA interference.....53
Fig. 2.3. Production of an inducible gene expression system.....55
Fig. 2.4. mRNA sequence of SerpinB2 and shRNA hairpin mRNA sequences.....58
Fig. 2.5. AGE analysis of PCR restriction digest reactions. 64
Fig. 2.6. pLenti6.3 SerpinB2 wt 1 sequence.....67
Fig. 2.7. pLenti6.3 SerpinB2 wt 2 sequence.....68
Fig. 2.8. pLenti6.3 SerpinB2 ΔCD 1 sequence.....69
Fig. 2.9. pLenti6.3 SerpinB2 ΔCD 2 sequence.....70
Fig. 2.10. pLenti6.3 ^{R380A}SerpinB2 full-length 1 sequence.....71
Fig. 2.11. pLenti6.3 ^{R380A}SerpinB2 full-length 2 sequence.....72
Fig. 2.12. pLenti6.3 ^{R380A}SerpinB2 ΔCD 1 sequence.....73
Fig. 2.13 Western blot of upregulated SerpinB2 expression in HEK-293T cells.....75
Fig. 2.14. Repression analyses for optimal transgene expression.....76
Fig. 2.15. Western blot of modified SerpinB2 expression in MDA-MB-231 cells using the pLenti system.....78
Fig. 2.16. Western blot of downregulated SerpinB2 expression in MDA-MB-231 cells using the pSLIK system.....79
Fig. 2.17. Long-term stability analysis of lentiviral constructs in MDA-MB-231 cells, using western blot analysis.....80
Fig. 2.18. Effect of SerpinB2 modification on the growth of MDA-MB-231 cells.....82
Fig. 2.19. Immunofluorescence imaging of overexpression constructs.....84

Fig. 2.20. Immunofluorescence imaging of knockdown constructs.....85

Fig. 2.21. FACS sorting of MEFs.....87

Fig. 3.1. 3D imaging systems.....97

Fig. 3.2. SDS-PAGE analysis of a representative sample of purified rat tail collagen I.....107

Fig. 3.3. Flow cytometry analysis of cell surface uPA and uPAR expression.....108

Fig. 3.4. Comparative time-course of migration of wild-type SerpinB2 versus SerpinB2$^{-/-}$ MEFs.....109

Fig 3.5. SEM ultrastructure analysis of TIFs matrices.....111

Fig 3.6. SHG imaging and quantification of wild-type and SerpinB2$^{-/-}$ MEF matrices.....113

Fig 3.7. SEM ultrastructure surface analysis of MEF matrices.....114

Fig 3.8. SEM ultrastructure sagittal section analysis of MEF matrices.....115

Fig. 3.9. Overnight 3D imaging of MEF migration and ECM remodelling.....117

Fig. 3.10. LC-MS/MS data analysis.....119

Fig. 3.11. 3D organotypic of SerpinB2 restoration effects on SerpinB2$^{-/-}$ MEF matrices.....121

Fig. 3.12. SEM ultrastructure surface analysis of SerpinB2$^{-/-}$ MEF matrices.....122

Fig. 3.13. SEM ultrastructure sagittal section analysis of SerpinB2$^{-/-}$ MEF matrices.....123

Fig. 3.14. Schematic of SerpinB2, LOX and TG2 in the ECM.....131

Fig. 3.15. Schematic of the roles of PAS and LOX in collagen cross-linking and ECM transformation from homeostatic tissue beds to pre-malignant, tumourigenic and metastatic tissue sites.....135

Fig. 4.1. Pancreatic epithelial neoplasia - PDAC initiation and progression.....144

Fig. 4.2. *In vivo* allograft local invasion scoring method.....154

Fig. 4.3. PAS expression in human PDAC after pancreatectomy.....157

Fig. 4.4. PDAC invasion through wild-type and SerpinB2$^{-/-}$ MEF/collagen I matrices.....159

Fig. 4.5. PDAC invasion through wild-type and SerpinB2$^{-/-}$ MEF/collagen I matrices.....160

Fig. 4.6 Fibroblast led PDAC invasion through 3D organotypic matrices.....161

Fig. 4.7. PDAC invasion in TIF/collagen 3D organotypic matrices.....163

Fig. 4.8. PDAC invasion in wild-type or SerpinB2$^{-/-}$ MEF/collagen I 3D organotypic matrices.....164

Fig. 4.9. *In vivo* mixed cell allograft model.....166

Fig. 4.10. Cleaved caspase-3 expression in mixed cell allograft model.....167

Fig. 4.11. Immunofluorescence - αSMA, uPA, uPAR and SerpinB2 expression in mixed cell allografts.....169

Fig. 4.12. Photomicrographs and quantification of PDAC tumour local invasion.....170

Fig. 5.1. Mammary gland development.....183

Fig. 5.2. Mammary gland tumourigenesis.....185

Fig. 5.3. SerpinB2 gene expression and recurrent free survival in breast cancer.....189

Fig. 5.4. SerpinB2 expression in malignant and non-malignant mammary cell lines.....198

Fig. 5.5. SerpinB2 and SerpinE1 expression in breast epithelial and fibroblast cell lines.....199

Fig. 5.6. Cell surface detection of uPA on the high metastatic TNBC cell line, MDA-MB-231HM.....200

Fig. 5.7. Effect of SerpinB2 knockdown on the migration of MDA-MB-231 cells.....202

Fig. 5.8. SerpinB2 KD MDA-MB-231 cell invasion through TIF/collagen I matrices.....204

Fig. 5.9. MDA-MB-231HM invasion through TIF and wild-type MEF constructed collagen I 3D organotypic matrices.....205

Fig. 5.10. MDA-MB-231HM cell invasion through wild-type and SerpinB2$^{-/-}$ MEF/collagen I matrices.....207

Fig. 5.11. *In vivo* mixed cell mammary xenograft model.....208

Fig. 5.12. MCF-7 breast tumour spheroid invasion through TIF/collagen I matrices.....209

Fig. 5.13. Triple cell breast tumour spheroid invasion through TIF/collagen I matrices.....210

Fig. 6.1. Schematic of the proposed effects of SerpinB2 within the TME.....221

Fig. A1. Immunofluorescence isotope controls.....282

Fig. A2. Entry clone analysis of pEN_TmiRc3-SerpinB2 shRNA1 vector sequence.....286

Fig. A3. Entry clone analysis of pEN_TmiRc3-SerpinB2 shRNA2 vector sequence.....287

Fig. A4. Destination clone analysis of pSLIK-SerpinB2 shRNA1 vector sequence. 288

Fig. A5. Destination clone analysis of pSLIK-SerpinB2 shRNA2 vector sequence.....288

Fig. A6. Entry clone sequence analysis of pDONR221 SerpinB2 ΔCD1 vector sequence.....289

Fig. A7. Entry clone sequence analysis of pDONR221 SerpinB2 ΔCD2 vector sequence. 290

Fig. A8. Entry clone sequence analysis of pDONR221 ^{R380A}SerpinB2 full-length 1 vector sequence.....291

Fig. A9. Entry clone sequence analysis of pDONR221 ^{R380A}SerpinB2 full-length 2 vector sequence.....292

Fig. A10. Entry clone sequence analysis of pDONR221 ^{R380A}SerpinB2 ΔCD1 vector sequence.....293

Fig. A11. Entry clone sequence analysis of pDONR221 ^{R380A}SerpinB2 ΔCD2 vector sequence.....294

LIST OF TABLES

Table 1.1. Individual PAS components involved in the prognosis of various human cancer types……..…..26

Table 2.1. Third-generation lentiviral transfer vectors used for expression of cDNA and shRNA knockdown…….. 56

Table 2.2. Overexpression entry clone concentration and DNA sequence analysis……..…65

Table 2.3. SerpinB2 knockdown entry clone concentration and DNA sequence analysis……..65

Table 2.4. Lentiviral destination constructs, expression type, concentrations and DNA sequence analyses……74

Table A1. List of antibodies used for IF, IHC and western blotting analyses……..…283

LIST OF PUBLICATIONS

1. Harris, N.L.E., Vennin, C, Conway, J.R.W., Vine, K.L., Pinese, M., Cowley, M.J., Shearer, R.F., Lucas, M.C., Herrmann, D., Allam, A., Morton, J.P., Australian Pancreatic Cancer Genome Initiative, Biankin, A.V., Ranson, M., Timpson, P., Saunders, D.N. (2017). "SerpinB2 regulates stromal remodelling and local invasion in pancreatic cancer". *Oncogene* - doi:10.1038/onc.2017.63

2. Vennin, C., Chin, V, Warren, S.C., Lucas, M.L., Herrmann, D., Melenec, P., Walters, S.N., Astrid Magenau, A., Allam, A.H., McCloy, R.A., Conway, J.R., Boulghourjian, A., Zaratzian, A., Heu, C., Nagrial, A.M., Chou, A., Steinmann, A., Drury, A., Froio, D., Giry-Laterriere, M., Harris, N.L.E., Mcghee, E.J., Whan, R., Grey, S., Johns, A., Samra4, J.S., Chantril, L., Gill, A.J., Biankin, A.V., Australian Pancreatic Cancer Genome Initiative, Wang, Y., Jeffry Evans, T.R., Anderson, K.I., Samuel, M.S., Burgess, A., Sansom, O.J., Morton, J.P., Pajic, M., and Timpson, P. (2017). "Transient tissue 'priming' via ROCK manipulation uncouples pancreatic cancer progression, chemo-resistance and the onset of the metastatic niche". *Science Translational Medicine* **9:**384.

3. Johnstone, C., Harris, N.L.E., Ranson, M., Rustgi, A.K. and Anderson, R. (2015). "Serglycin proteoglycan promotes progression and metastasis of triple-negative breast cancers". *Cancer Research* **75:**15.

4. Vine, K.L., Lobov, S., Indira Chandran, V., Harris, N.L.E. and Ranson, M. (2015). "Improved Pharmacokinetic and Biodistribution Properties of the Selective Urokinase Inhibitor PAI-2 (SerpinB2) by Site-Specific PEGylation: Implications for Drug Delivery". *Pharmaceutical Research* **32:**3; 1045-1054.

CONTRIBUTIONS OF WORK

Chapter 1: -

Chapter 2: Robert Shearer assisted with lentiviral design, cell line construction and PCR work.

Chapter 3: James Conway and David Herrmann assisted with 3D Organotypic culture technique and experimentation; Amr Allam, Claire Vennin and James Conway assisted with SP8 confocal technique and experimentation.

Chapter 4: Claire Vennin assisted with PDAC xenografts, Morgan Lucas carried out MEF migration polar plots with MatLab Software. Gene expression survival analysis was performed by Dr Mark Pinese.

Chapter 5: Dr Kara Vine assisted with TNBC allografts.

Chapter 6: -

CONFERENCE PROCEEDINGS

1. Ranson, M., Indira Chandran, V., Harris, N.L.E., Lobov, S. and Vine, K. (2013). "Site-specific PEGlation of human plasminogen activator inhibitor type 2: Fine tuning the pharmacokinetic and biodistribution properties for improved diagnostic and therapeutic potential". XIVth International Workshop on Molecular and Cellular Biology of Plasminogen Activation; University of Notre Dame. *Conference paper*
2. Harris, N.L.E., Indira Chandran, V., Locke, J.M., Skropeta, D., Vine, K.L. and Ranson, M. (2012). "Attachment of an Isatin Cytotoxin to an Inactive PAI-2 Mutant Confirms uPA Dependent Targeted Cytotoxicity". Plasminogen Activation System in Pathology Conference; University of Wollongong. *Poster presentation*
3. Harris, N.L.E., Vine, K.L. and Ranson, M. (2013). "The Urokinase System in Cancer Growth and Metastasis: Potential Prodrug Approaches". 2013 University of Wollongong Postgraduate Symposium. *Oral presentation*
4. Harris, N.L.E., Vine, K.L. and Ranson, M. (2014). "Deciphering the Role of PAI-2 in Cancer Invasion and Metastasis", Wollongong Hospital Grand Rounds - Drugs and Bugs. *Oral presentation*
5. Harris, N.L.E., Vine, K.L., Saunders, D.N. and Ranson, M. (2014). "Exploiting PAI-2 to Target Metastatic Disease". Medicinal Chemistry & Drug Discovery Symposium, Victor Chang Cardiac Research Institute. *Oral presentation*
6. Harris, N.L.E., Conway, J., Shearer, R., Vine, K.L., Pajic, M., Pinese M, Timpson, P., Saunders, D.N. and Ranson, M. (2014). "PAI-2 (SerpinB2) Inhibits Pancreatic Cancer Cell Invasion". Australian Metastasis Research Society Annual Scientific Meeting; Melbourne Convention & Exhibition Centre. *Oral presentation*
7. Harris, N.L.E., Conway, J., Shearer, R., Herrmann, D., Vine, K.L., Timpson, P., Saunders, D.N. and Ranson, M. (2014). "PAI-2 Inhibits Invasion of Breast and Pancreatic Cancer Via Inhibition of Urokinase (uPA)". 2014 Lorne Cancer Conference. *Poster presentation*
8. Harris, N.L.E. (2015). "PAI-2 as a Cancer Therapeutic". Sydney Catalyst International Translational Cancer Research Symposium (2015) *Oral presentation*
9. Harris, N.L.E., Vennin, C, Conway, J.R.W., Vine, K.L., Pinese, M., Shearer, R.F., Lucas, M.C., Herrmann, D., Allam, A., Morton, J.P., Biankin, A.V., Ranson, M., Timpson, P., Saunders, D.N. (2015). "PDAC Invasion and Stromal Remodelling is Dependent on uPA and Regulated by SerpinB2". 2015 Lorne Cancer Conference *Poster presentation*
10. Harris, N.L.E., Conway, J.R.W., Vine, K.L., Pinese, M., Pajic, M., Shearer, R.F., Lucas, M.C., Herrmann, D., Morton, J.P., Ranson, M., Timpson, P., Saunders, D.N. (2015). "SerpinB2 Inhibits Pancreatic cancer cell Invasion and facilitates stromal remodelling". Sydney Catalyst Translational Cancer Research - Early Career Researcher Symposium (2015) Kinghorn Cancer Centre; Garvan Institute of Medical Research *Oral presentation*
11. Harris, N.L.E., Conway, J.R.W., Vine, K.L., Pinese, M., Pajic, M., Shearer, R.F., Lucas, M.C., Herrmann, D., Morton, J.P., Ranson, M., Timpson, P., Saunders, D.N. (2015). "SerpinB2 Inhibits Pancreatic cancer cell Invasion and facilitates stromal remodelling". Australian Society for Medical Research Conference (2015) *Poster presentation*
12. Harris, N.L.E., Vennin, C, Conway, J.R.W., Vine, K.L., Pinese, M., Cowley, M.J., Shearer, R.F., Lucas, M.C., Herrmann, D., Allam, A., Morton, J.P., APCGI, Biankin, A.V., Ranson, M., Timpson, P., Saunders, D.N. (2015). "Pancreatic Cancer Invasion and Stromal Remodelling is Dependent on uPA and Regulated by SerpinB2". XVth International Workshop on Molecular and Cellular Biology of Plasminogen Activation; Rome, Italy. O*ral presentation*
13. Harris, N.L.E., Vennin, C, Conway, J.R.W., Vine, K.L., Pinese, M., Cowley, M.J., Shearer, R.F., Lucas, M.C., Herrmann, D., Allam, A., Morton, J.P., Ranson, M., Timpson, P., Saunders, D.N. (2016). "SerpinB2 regulates stromal remodelling and local invasion in pancreatic cancer". 2016 Lorne Cancer Conference. *Poster presentation*

SCHOLARSHIPS AND AWARDS

- Australian Postgraduate Award – 2013
- Lorne Cancer Conference Bursary – 2014, 2015, 2016
- British Council - Fame Lab; NSW Finalist – 2014
- ATA Scientific – Young Scientist Award – 2014
- 27th Lorne Cancer Conference – Novartis Oncology Poster Award – 2015
- Amplify Festival Bright Sparks Australian Finalist – 2015
- Thinkable Research Innovation Award – 2015
- XVth International Workshop on Molecular and Cellular Biology of Plasminogen Activation; Rome, Italy. Fellowship Award – 2015
- XVth International Workshop on Molecular and Cellular Biology of Plasminogen Activation; Rome, Italy. Best Oral Presentation Award – 2015
- Sydney Catalyst International Translational Cancer Research Symposium – Best Oral Presentation Award – 2015
- 28th Lorne Cancer Conference - Poster Award – 2016
- University of Melbourne Medical School Scholarship – 2016

CHAPTER 1

INTRODUCTION TO SERPINB2

CHAPTER 1

INTRODUCTION TO SERPINB2

1.1 INTRODUCTION TO CANCER

Cancer is known medically as a malignant neoplasm or tumour, comprising a broad group of diseases that involve unregulated cell proliferation, invasion and spread, known as metastasis, throughout the body. In 2014 in Australia, cancer was the fourth leading cause of all registered deaths (Australian Bureau of Statistics, 2014[1]). There are several hundred types of cancer reported (1), each initiated after one or more cells in a tissue undergoes progressive genetic mutations and chromosomal disruptions to produce a self perpetuating cell that possesses a malignant phenotype (2). The ability of a particular cancer cell type to invade and metastasise throughout the vasculature is the primary determinant of cancer prognosis (3), with metastasis responsible for 90% of all cancer deaths and the underlying cause of treatment failure (1,4,5). Tumours are architecturally heterogeneous (refer to section 1.3), which aids in remodeling the tumour microenvironment (TME) (1,6,7). These tumour systems differ in vasculature, host invasiveness, and connective tissue components (7-10), in which coagulation, cellular adhesion and angiogenesis, the growth of new capillary blood vessels from pre-existing vessels, each contribute critically to the metastatic capacity of a tumour (1,4). Furthermore, it is becoming increasingly clear that deregulated processes of stromal remodelling and collagen cross-linking within the TME perpetuates both an inflammatory and early-developmental phenotype, where the continuous cellular and molecular narrative aids malignant progression through local and distant tissues of the body (11-14).

1 Australian Bureau of Statistics
http://www.abs.gov.au/ausstats

Tumour-associated urokinase plasminogen activator (uPA) has long been recognised as a major cell surface marker of invasion and metastasis and proven for its prognostic relevance, and now as major player in ECM remodeling (15-23). The naturally occurring inhibitor of uPA, SerpinB2 (plasminogen activator inhibitor type-2), specifically and irreversibly binds to cell surface receptor bound uPA, forming a covalent inhibitor-protease complex, which is then internalised into the cell *via* receptor mediated endocytosis (RME) (24,25). Moreover, the establishment of an activated stroma within the TME enhances a tumours metastatic potential and it has been reported by many research groups that stromal fibroblasts and endothelial cells (ECs) overexpress uPA and uPAR while downregulating SerpinB2 in order to facilitate this process (26-31) (refer to section 1.9 and 1.10).

This Chapter will first briefly describe the process of invasion and metastasis and the nature of tumour heterogeneity before describing the different plasminogen activation system (PAS) members, with a particular focus on SerpinB2, and their modulated expression in cancer with reference to clinical relevance. Following this, an in depth assessment of the TME, with direct association to the biological functional importance of SerpinB2 in ECM remodeling and cancer progression will be described.

1.2 Tumour invasion & metastasis

Cancer metastasis involves a multifaceted process between the interaction of stroma and tumour cells (32,33). Initially a malignant cell must attain the ability to disengage from the biologically heterogeneous primary mass (32,33) and network of structural proteins that holds it in place to the basement membrane (BM) and traverse the protein rich, often dense extracellular matrix (ECM) (34,35). To accomplish this, the cell acquires an inappropriate constitutive expression of several enzyme systems, including the matrix metalloproteinases (MMPs) and the plasminogen activation system (PAS) (36). This affords the cell an ability to invade

surrounding host stroma, penetrate into the circulatory or lymphatic system, adhere to capillary beds of distant organs, invade the host tissue there and proliferate (Fig. 1.1) (5,18,35,37). Tumour invasion is also facilitated by the diminished expression of cellular adhesion molecules (CAMs) and epithelial–mesenchymal transition (EMT), by which tumour cells weaken E-cadherin-dependent cellular adhesion and enhance motility, making it possible for increased penetration into surrounding tissues (3,38). Through EMT, the tumour cell ultimately acquires a migratory phenotype, binding growth factor proteins and ECM molecules to its own membrane receptors, which generate a cascade of intracellular signals that promote invasion and metastases (3,38).

Furthermore, tumour invasion is greatly enhanced by the process of angiogenesis, as a tumour can only grow to 2 mm^3, before passive diffusion is inadequate to provide oxygenated blood, nutrients and removal of wastes (39). To overcome this, growth factor proteins are increasingly released by the tumour into the local environment, leading to the establishment of angiogenesis (5), and the conscription of host stromal cells into the TME (1,40) (41).

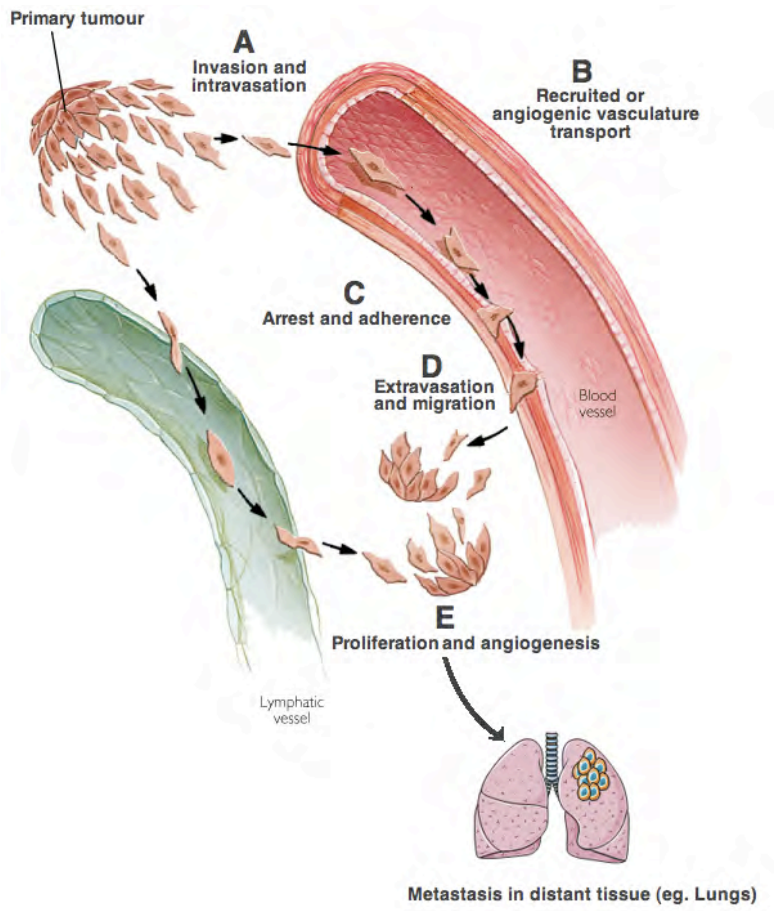

Fig. 1.1. Metastatic progression. Mutagenesis causes aberrant cell proliferation resulting in the formation of a primary tumour. **(A)** Invasive cells adapt a migratory phenotype, known as EMT, and produce proteases that degrade the ECM and BM, allowing them to break free of the primary tumour and enter the blood or lymphatic system through a process termed intravasation. **(B)-(D)** Tumour cells are transported to a distant site in the circulation where they adhere to and breakdown the ECM and BM to allow penetration to distant host tissue, known as extravasation. **(E)** Now at a secondary site in the body, the formation of a secondary tumour can occur. Adapted from (5).

1.3 Tumour heterogeneity and stromal conscription

Tumours can be considered disorganised organs that contain heterogeneous cell types. It is known that tumours contain evolving tumour cells, cancer stem cells (CSCs), conscripted 'stromal' cells such as fibroblasts and myofibroblasts (carcinoma-associated fibroblasts - CAFs), infiltrated leukocyte sub-types (immune and inflammatory cells), ECs, mesenchymal cells, such as pericytes and mural cells, as well as other vascular smooth muscle cells (40,42,43). In addition, the tumour infiltrate is composed of bone marrow–derived mesenchymal stem cells (MSCs), which along with CAFs, contribute both quantitative and qualitative changes

within the ECM (40). These tumour societies are highly adapted for survival against therapeutic intervention by producing new variants and utilising subpopulation interactions to counteract damaging stimulus. Thus, understanding tumour heterogeneity is one of the primary steps toward improving clinical efficacy and managing ongoing treatment in cancer therapy. In regards to specific tumour cell heterogeneity, one hypothesis proposed is the clonal evolution model. This model specifies that cancers evolve through random mutations, clonal expansion and clonal selection within 3D adaptive landscapes of tissue beds (44). There are highly variable and complex dynamics of gene expression that result in a multifarious clonal architecture. Through utilising sophisticated mutational analysis, Kandoth *et al.* (2013) has shown the presence of many sub-clones of tumour populations within solid breast tumours (45). It is proposed that these different sub-clone populations interact through paracrine signaling and even though therapeutic intervention can decimate certain cancer clones and destroy much of their habitat, there are inadvertent selective pressures for resistant sub-clone expansion (46-48). Many studies have demonstrated the presence of both genetically alike and genetically different sub-clones in primary tumours and metastatic lesions in the same patients, which is consistent with clonal evolution models (48,49). This Darwinian character of cancer is the crux of therapeutic failure, however this characteristic could eventually hold the key to more effectual control of cancer systems.

The second model proposed to account for tumour heterogeneity is the cancer stem cell (CSC) model. This ideal postulates that tumours are organised in a hierarchy, where cells with stem cell properties (CSCs) are at the zenith. There are two properties that are attributed to a CSC, the first is the ability for self-renewal, since differentiated cells cannot divide indefinitely (constrained by the Hayflick limit) (50). The second property of a CSC is the ability to generate differentiated tumour cells, which form the bulk of a tumour. These cells have been termed CSCs to reflect such stem cell-like properties and was first demonstrated by Dominique Bonnet and John Dick in human acute myeloid leukaemia in 1997 (51). Since that time CSCs have been demonstrated in many solid malignancies, including those of the brain (52), ovaries (53), lungs (54), breast (55), colon (56),

prostate (57), and pancreas (58), all of which exhibit a comparable hierarchical organisation. There is debate regarding the origin of CSCs, whether from dysregulation of normal stem cells or from a specialised population of tumour cells that acquired self-renewal ability (59). This cell plasticity is a significant feature of cancer due to lowering the activation barrier for increased cellular plasticity (60). This ability, coupled with the processes of EMT and mesenchymal-epithelial transition (MET), has profound implications for the plasticity between CSC types and their TME interactions. The Weinberg laboratory at the Massachusetts Institute of Technology have reported that EMT can result in increased numbers of CSCs (61), which causes significant challenges to therapy through several avenues including increased invasion and dissemination of cells, decreased proliferation of certain CSC populations avoiding chemo-cytotoxicity (62). Additionally, post-treatment, MET cells return to a highly proliferative state and can mediate tumour relapse at distant metastatic sites (63). Thus, compositional tumour heterogeneity and TME-induced selection pressures appear to guide a tumours evolution, which significantly underwrites both tumour development and clinical efficacy of treatment. This TME-imposed heterogeneity is produced by CSC self-renewal and differentiation (64). While normal stem cell niches are predominantly located in hypoxic tissue areas (mammary gland ducts, GI tract pits etc.), which promote this mesenchymal phenotype, poorly vascularised tumours also contain hypoxic regions that CSCs thrive within (65). Yeung *et al.* (2011) have demonstrated that hypoxia attenuates colon cancer cell differentiation maintaining a stem-like phenotype (66). In addition, it has also been recently shown that activated myofibroblasts within the TME can secrete factors (especially HGF) which impose the CSC phenotype (67). This interplay between stromal and CSCs is now beginning to emerge as a significant underlying factor causing intratumour heterogeneity (68), however the in-depth molecular mechanisms of this dynamic interplay are yet to be revealed. Advances in next-generation sequencing technology and the establishment of cBio Portal for Cancer Genomics (cBio) and The Cancer Genome Atlas (TCGA) have both significantly helped elucidate how heterogeneous cancer can be and the extent of the genetic mutational landscape of cancer. The molecular level interactions that these aberrations precede have profound mechanistic

and clinical implications. Thus, while the task remains unprecedentedly large, it is imperative to completely understand not only the pathophysiological context of disease but also the molecular and cellular events occurring within the entire TME. Deciphering the evolutionary code of tumour heterogeneity will both allow for better biomarkers and therapeutic strategies to restrain intratumoural heterogeneity and reduce selection pressures as well as making the dream of personalised medicine a reality (69).

1.4 The plasminogen activation system (PAS)

Dissemination of human cancers are characterised by the acquisition of novel functional competences in order to degrade the basement membrane, remodel the ECM, invoke angiogenesis and forming a TME, leading to tissue invasion and metastasis. Specifically, in the context of tissue remodelling, PAS is the human body's extracellular proteolytic enzyme system. The aberrant expression of PAS genes and/or upregulation of protease activity in tumourigenic tissue contributes to the attainment of important new cell capabilities that potentiate malignancy. PAS is comprised of extremely powerful serine proteases, protease inhibitors of the serpin family and various binding proteins (70). PAS is active under both physiological and pathophysiological conditions and responsible for a large range of biological processes from fibrinolysis (primarily), angiogenesis, tissue remodelling (17,71) and cell migration (17,72) to complement system activation (73), ovulation (74), and embryonic development (70,75-77).

There are two types of plasminogen activators, tissue-type plasminogen activator (tPA), and urokinase-type plasminogen activator (uPA). In contrast to tPA, which is fundamental in fibrinolysis (78), uPA plays an essential role in tissue degradation as part of physiological and pathological processes. As tPA is not inherently responsible for pericellular proteolysis or of emphasis in this research project, it will not be explored further in this thesis (refer to (79) for further information).

1.4.1 The urokinase plasminogen activation system

The urokinase plasminogen activation system (uPAS) directly consists of the serine protease uPA, its specific GPI (glycosylphosphatidylinositol)-anchored protein receptor uPAR, their two natural serpin inhibitors, PAI-1 (SerpinE1) and SerpinB2, as well as the plasmin inhibitor, α_2-antiplasmin (Fig. 1.3). uPA binds to uPAR, where it efficiently cleaves co-localised plasminogen at its Arg^{580}-Val^{581} bond, generating cell surface associated plasmin (16) (Fig. 1.3). The main physiological inhibitor of plasmin, α2-antiplasmin, is an important regulator of PAS, controlling the fibrinolysis process and facilitating degradation of many proteins within the ECM (80,81). Overexpression of the serine protease urokinase (uPA) is recognised as an important biomarker of metastatic disease and a therapeutic cancer target (19,82). uPA is responsible for plasminogen activation, the proteolytic conversion of the inactive zymogen, plasminogen, into the active serine protease, plasmin (72) (Fig. 1.2). Homeostatically, plasmin directly degrades fibrin and components of the ECM through conversion of procollagenases (pro-MMP) to active collagenase (MMP) enzymes. Plasmin also activates other pro-MMPs bound to the ECM, thus allowing basement membrane (BM) destruction, complete ECM deconstruction and latent/active growth factor stimuli, each contributing to tissue remodeling processes (20,71,78,83,84).

Reich *et al*. (1978) were the first to recognise the integral role of plasminogen activation and localised ECM proteolysis in cancer progression (75). Since then, numerous research groups have shown that malignant cells and/or associated stromal cells over-express various components of PAS constitutively, particularly uPA and its receptor uPAR, leading to unregulated proteolytic activity and a myriad of other non-proteolytic cell processes allowing tumour cell invasion and metastasis (15-17,19,21,71,76,77,84,85). For example, PAS is involved in multiple aspects of neoplastic evolution, including activation of pro-oncogenic cell signalling leading to enhanced tumour cell proliferation and altered cellular adhesion and migration, intravasation and extravasation of vasculature, growth at the metastatic sites and tumour neoangiogenesis (17,36,70,76,77,84,86-88).

Upon binding to its cellular receptor, uPAR, the pro-uPA zymogen is catalytically converted into its active form, which in turn activates co-localised plasminogen into the broad-spectrum protease, plasmin. The combined signalling and proteolytic outputs of this pathway activate a plethora of downstream events driving ECM degradation, cell proliferation, adhesion and migration (89). Negative regulation of this pathway is provided at several levels, including inhibition and clearance of protease activity by naturally occurring inhibitors, such as SerpinB2 (19,25).

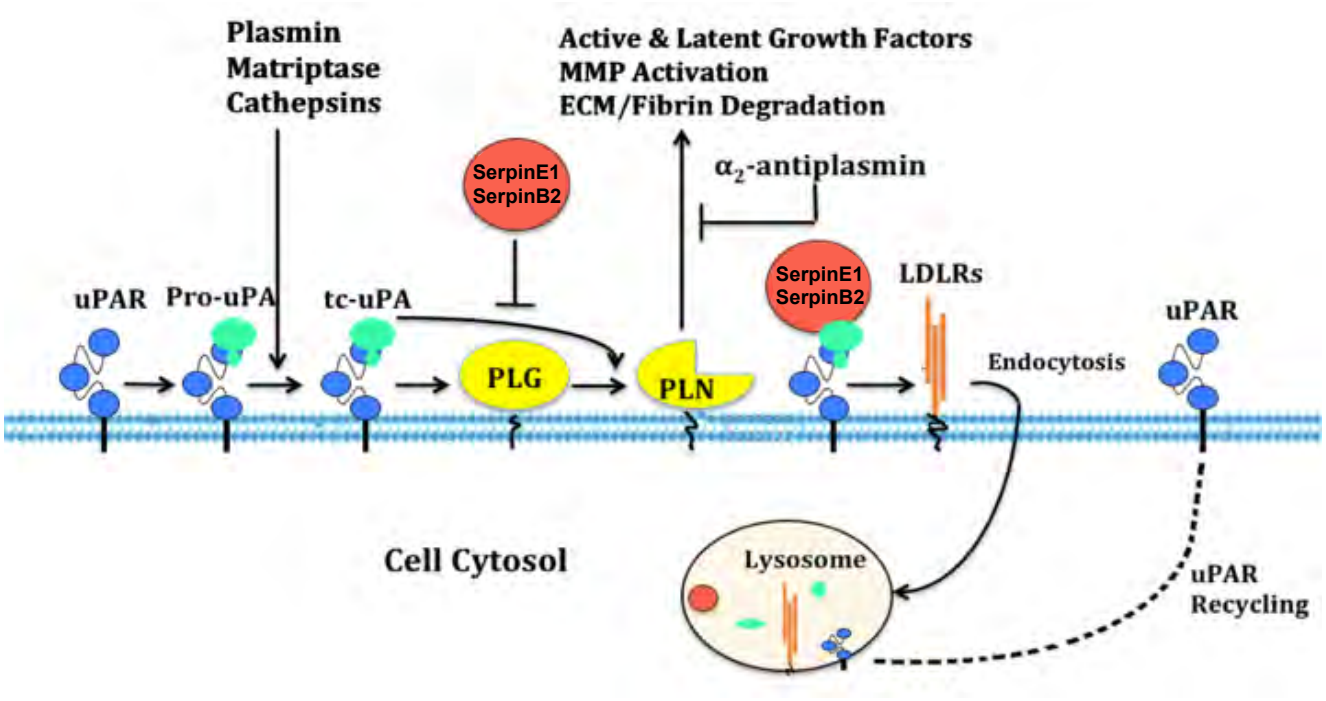

Fig. 1.2. PAS and the role of the serpins – SerpinE1 and SerpinB2. Plasminogen (PLG) binds to cell surface receptors *via* its lysine-binding sites. Plasmin (PLN), cathepsin B and matriptase reside in the pericellular space and cleave either sc-uPA (single-chain or pro-uPA) or plasminogen. The cleavage of sc-uPA initiates the plasminogen activation cascade by forming tc-uPA (two chain uPA), which cleaves nearby cell-bound plasminogen, forming cell surface-bound plasmin. This feed-forward loop facilitates matrix metalloprotease (MMP) activation, degradation of fibrin, fibronectin, laminin, and inhibition/activation of the complement system. α2-antiplasmin inhibits tc-uPA formation by inhibiting any soluble plasmin available. SerpinE1 and SerpinB2 prevent plasmin formation by inhibiting tc-uPA. Each serpin forms a complex with tc-uPA, which then binds to a member of the low density lipoprotein receptor (LDLR) family, promoting endocytosis and degradation of the Serpin:uPA inhibition complex, followed by recycling of the uPAR receptor. Modified from (19).

1.4.2 uPA and the uPA receptor, uPAR

uPA is synthesised as a single chain 53 kDa proenzyme - pro-uPA (17). Proteolytic activation of pro-uPA to the active two-chain serine protease uPA (tc-uPA) molecule occurs *via* plasmin-mediated (or cathepsin or matriptase) cleavage of the Lys^{158}– Ile^{159} bond of pro-uPA (20,90). The two chains are covalently linked by a disulfide bridge, Cys^{148}– Cys^{279} (Fig. 1.3) (17). Both pro-uPA and tc-uPA bind with high affinity (K_D, < 1 nM) to uPAR, however only tc-uPA is efficiently inhibited by SerpinE1 or SerpinB2 (37,84). Receptor uPAR binding potentiates the initiation of a pro-enzyme activation positive-feedback loop, resulting in increased plasmin production (refer to Fig. 1.2) (84,91). In addition to proteolytic functions, uPA binding to uPAR initiates a range of biological processes including initiation of intracellular signalling, leading to cell adhesion, proliferation and migration (84,92-95).

Duffy *et al.* (1988) were the first to demonstrate the prognostic value of uPA in cancer. Their research group later reported that patients with primary breast carcinomas and high levels of uPA activity had a significantly shorter disease-free interval and increased metastatic progression, in contrast to patients with low levels of activity (96). As plasmin is an efficient activator of pro-uPA, there is a strong positive feedback mechanism available, which can be exploited by a variety of malignancies, including breast (6), lung (97), endometrial (98), gastrointestinal (99), pancreatic (100) and colorectal cancers (101).

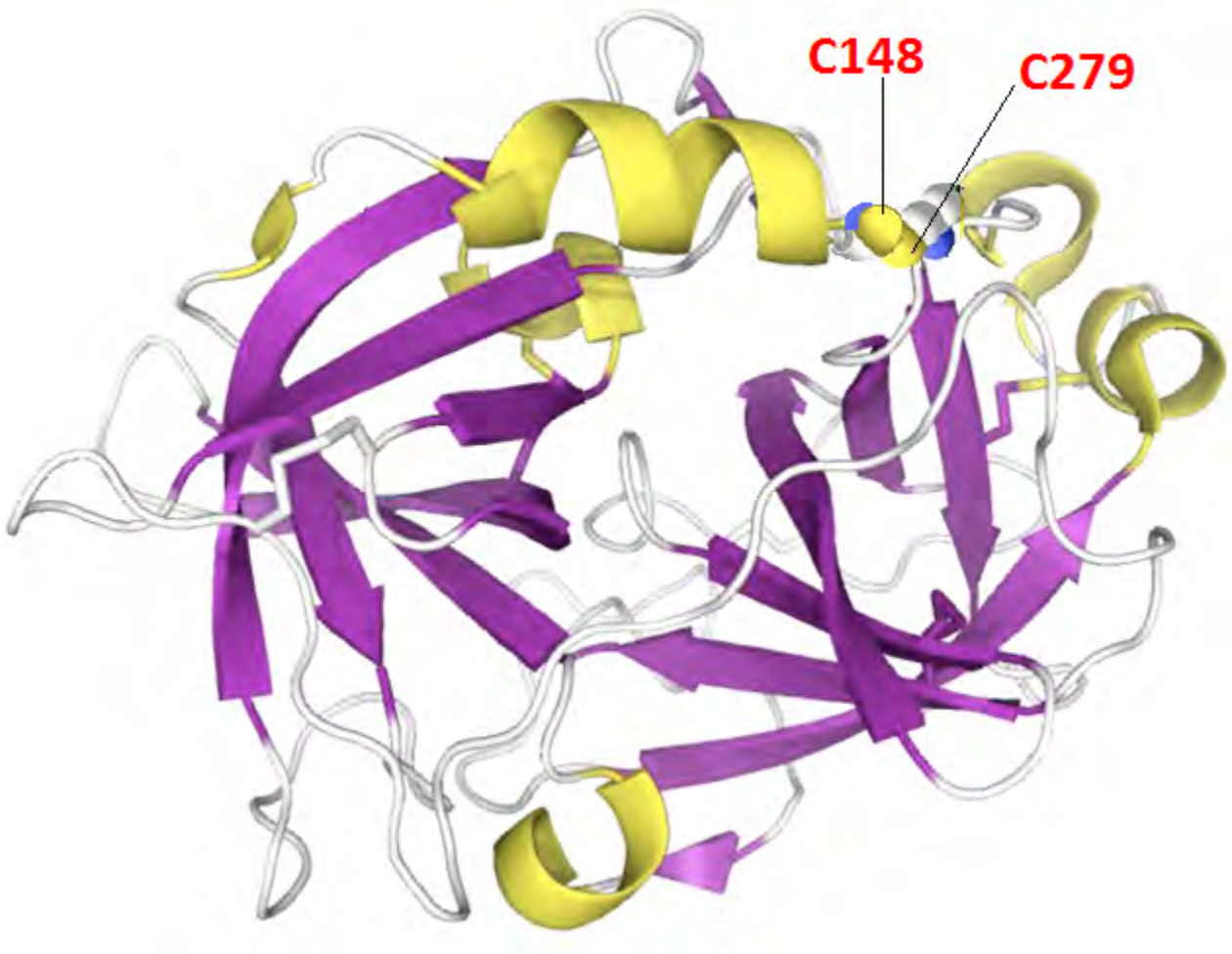

Fig. 1.3. Two-chain urokinase plasminogen activator. Synthesised as a 53 kDa serine protease, a single disulfide bond (Cys^{148}– Cys^{279}) holds the two chains together. Antiparallel, up-and-down β-sheet barrels shown in purple, and α-helices shown in yellow. Image constructed using PDB coordinates 1W0Z and the PyMOL molecular graphics system (102).

The uPA receptor, uPAR, is a 50-60 kDa (35 kDa deglycosylated) glycosylated phosphatidylinositol (GPI)-anchored single chain protein with three similar-sized domains (103). The binding of uPA to uPAR requires all three uPAR domains (103). As previously mentioned, uPAS also modulates cell responses such as migration, cellular adhesion, differentiation, proliferation and apoptosis (37,104). These are not necessarily related to proteolytic activity and require trans-membrane signalling, which is mediated by interactions between uPAR and a variety of extracellular proteins and membrane receptors, such as integrins, EGF, FGF-2 and HGF receptors, high molecular weight kininogen, caveolin, and the G-protein-coupled receptor (GPCR), FPRL1

(91,104). Further, stromal cells within the primary tumour's microenvironment may be activated to express proteins such as uPA and/or uPAR and are capable of modifying the behaviour of a cancer cell to promote angiogenesis, intravasation and metastasis (7,105). In a study by Hadler-Olden *et al.* (2011) the TME was found to have a greater impact on tumour invasiveness than individual cancer cells in their tumour xenograft mouse model (106). Moreover, increased levels of uPA and uPAR have been associated with a poor prognosis in patients with breast (6) ovarian (107), endometrial (108), kidney (109), prostate (110), head and neck (111), esophageal (112), colorectal (113), liver (114), lung (115,116), pancreatic (117,118) and leukaemic-associated cancers (119) (refer to Table 1.1 for further references).

It has been proposed that this transmembrane uPA/uPAR "signalosome" can activate intracellular signaling molecules such as tyrosine- and serine-protein kinases, Src, focal adhesion kinase (FAK), Rac, extracellular-signal-regulated kinase (ERK)/mitogen-activated protein kinase (MAPK) and the JAK/STAT pathways (104).

Overall, these activities confirm the inappropriate up-regulation of uPA and uPAR during pathophysiological states such as tumour invasion and metastasis (16). Conversely, within a homeostatic system, this unchecked activity is finely regulated by the protease inhibitors of uPAS, a superfamily of proteins known as the serpins.

1.4.3 Plasminogen activator inhibitors

Plasminogen activator inhibitors belong to the serpin (**ser**ine **p**rotease **in**hibitor) family. There are over 1000 known serpins, including 36 human proteins, making this the largest and most diverse family of protease inhibitors (120). The majority of serpins are involved in serine (as well as cysteine) protease regulation in a plethora of roles from coagulation, fibrinolysis, inflammation and complement activation to carcinogenesis, angiogenesis and apoptosis (121). All inhibitory serpins undergo structural changes in order to inhibit their target protease (122). Due to the far-reaching and potentially damaging effects of plasmin, regulation of uPAS activity is crucial for normal, non-invasive cell function. Both PAI-1 (SerpinE1) and SerpinB2 efficiently inhibit uPA in solution and at the cell surface (123), through the formation of covalent, irreversible enzyme:substrate

complexes (124). A diagrammatic representation of the inhibitory mechanism of serpins is shown in Fig. 1.4. SerpinE1 has been shown to be relatively unstable and rapidly convert to a latent form, which renders it incapable of interacting with uPA (125). Additionally, SerpinE1 may bind to either vitronectin, uPA or tPA, which causes exposure of integrins such as αvβ3, αvβ5 or αIIbβ3 binding sites on vitronectin, and activates the Jak/Stat pathway that facilitates angiogenesis, vital for metastatic spread (25,126-128). This paradox is observed in many tumour types where high levels of SerpinE1 are associated with a poor prognosis (refer to Table 1.1). In contrast, SerpinB2 does not display these properties and has been successfully exploited in many uPA-targeted therapies (129-131).

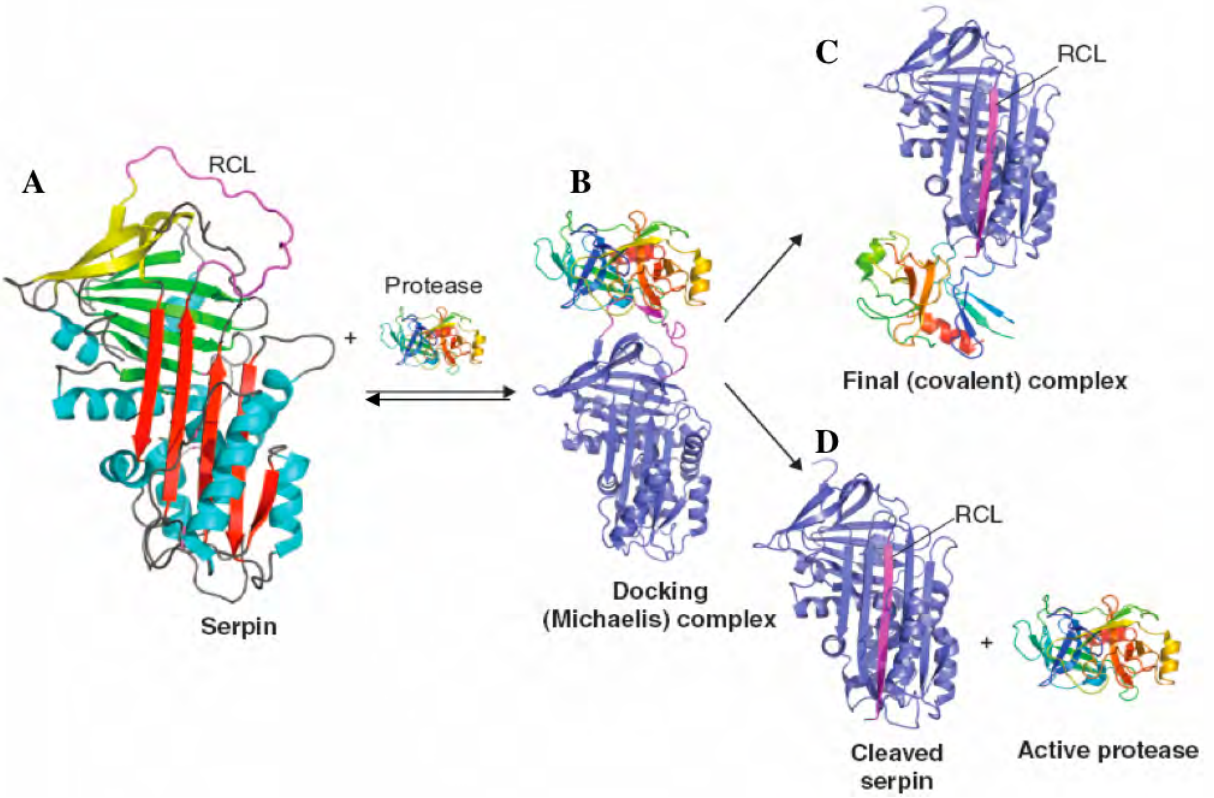

Fig. 1.4. Serpin inhibitory mechanism. Serpins exist in three main states. The secreted native ('stressed') serpin **(A)** is required for inhibitory activity. The first step in the inhibitory mechanism is the interaction of the serpin with an active protease to form the reversible, non-covalent Michaelis-like complex **(B)**. The serpin forms an oxy ester linkage and an acyl-enzyme intermediate by covalently bonding with the protease *via* the residues of the cleaved Reactive centre loop (RCL). The reaction can either proceed on an inhibitory or non-inhibitory pathway. The inhibitory pathway results in the formation of a covalent complex; the cleaved RCL of the serpin inserts into its own β-sheet and translocates the protease with it, distorting the active site resulting in an inactive protease and an inactive, relaxed serpin **(C)**. The non-inhibitory pathway results in the serpin not forming an acyl-intermediate, releasing the active protease and inactivating itself *via* insertion of the cleaved RCL into the β-sheet **(D)**. Adapted from (132,133).

1.5 SerpinB2

1.5.1 Expression and structure

SerpinB2 is a clade-B ov-serpin (ovalbumin family) comprised of 415 amino acid residues, encoded by a single gene – *SERPINB2* (120). Akin to all clade-B serpins, SerpinB2 is synthesised without a cleavable N-terminal signal peptide. However, unlike the traditional clade-B serpin, SerpinB2 is distributed bi-topologically, existing in two forms, as a 47 kDa non-glycosylated form mainly found intracellularly (134) and as a secreted, 60 kDa glycosylated form (135,136). The gene encoding SerpinB2 possesses an exon encoding a polypeptide loop between the α-helices, C and D (the CD-loop), which is the most extensive of all clade B serpins and the main site of protein binding (19). The CD loop has been reported to confer SerpinB2 the ability to interact with a plethora of largely intraceullar proteins (137-142), the exact functions of which are yet to be resolved (addressed in section 1.6). Uniquely to any other serpin, SerpinB2 can spontaneously polymerise under physiological conditions *in vitro*, dependent mainly on the CD loop and cellular redox status (143), without any known SerpinB2 serpinopathies unlike other serpins (19). In addition, it has been previously been shown that removal of the CD-loop does not affect the ability of SerpinB2 to fulfill it's protease inhibitory mechanism (19), explained in section 1.6.

The small percentage of glycosylated SerpinB2 is secreted *via* the golgi secretory pathway (144,145) making it one of only two clade B serpins (the other is Maspin) that are found both intra- and extracellularly. Of note, mouse SerpinB2 protein is 80% conserved to that of human SerpinB2 (146) meaning mouse studies have and continue to offer great insight into the pathophysiological modulated expression and function of human SerpinB2 (147). Recently, Udofa *et al.* (2013) reported five homologous regions between the human and murine promoters of SerpinB2, indicating that induction of SerpinB2 expression under certain physiological environments will be similar across both species (148).

The crystal structure of human SerpinB2 revealed the tertiary formation of SerpinB2 is that of a typical serpin,

with 9 α-helices (A-I) and 3 β-sheets (A-C) (Fig. 1.5) (149). SerpinB2 also possesses a reactive centre loop (RCL) for uPA inhibition (refer to section 1.5.3), which is yet to be resolved by X-ray crystallography (19).

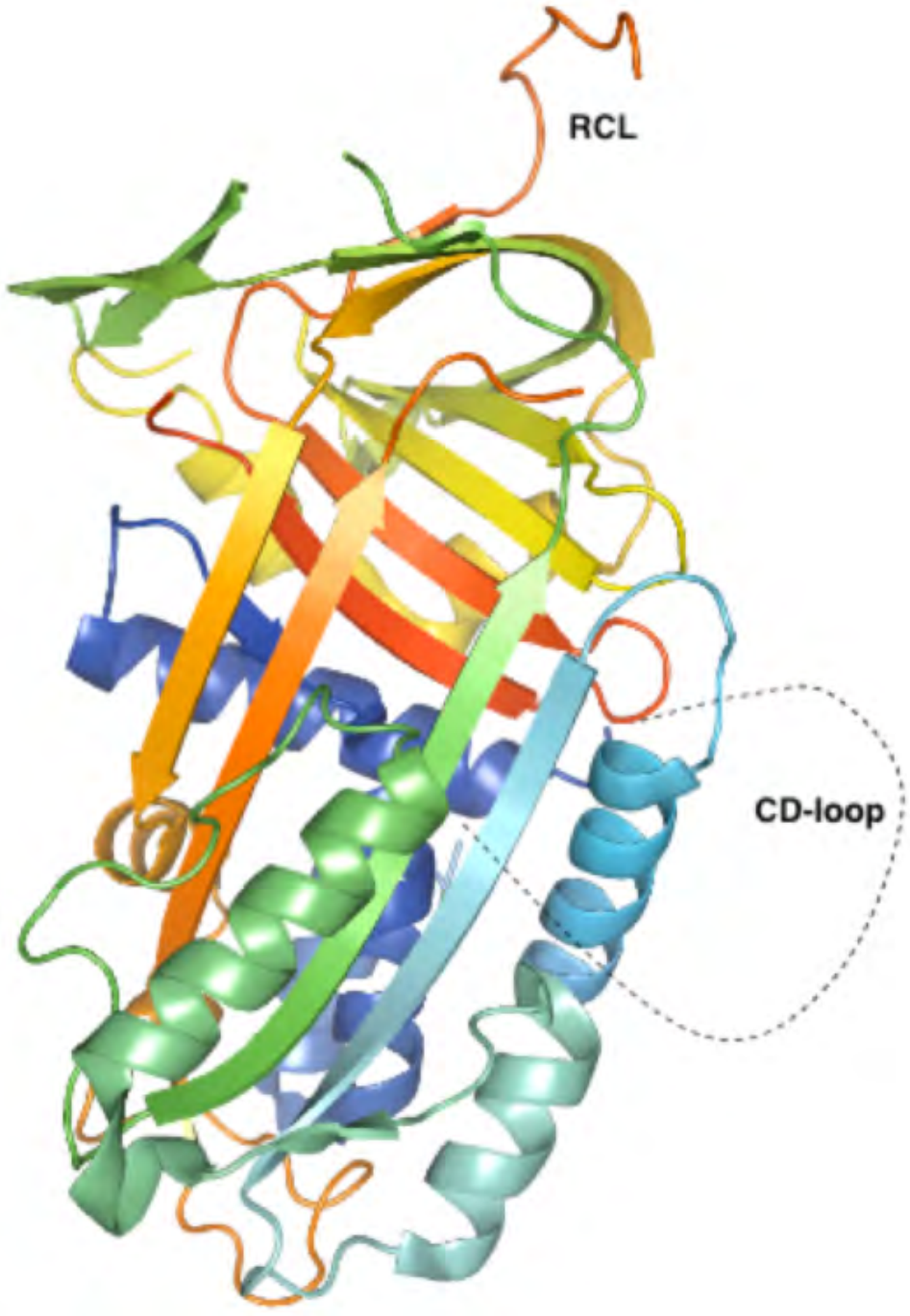

Fig. 1.5. Structure of SerpinB2. This serpin is comprised of 9 α-helices, 3 β-sheets and an RCL. SerpinB2 also possesses a CD-loop – a polypeptide chain between α-helices C and D (indicated by a dotted line). The conformation of the CD-loop has yet to be resolved and the structure shown is a CD-loop and RCL deleted mutant. Structure is coloured from *N*-terminus (blue) to *C*-terminus (red). Image was constructed using PDB coordinates 2ARQ (149) and the PyMOL molecular graphics system (102).

SerpinB2 is expressed by a number of cell types, including keratinocytes, trophoblasts, macrophages, monocytes, ECs, smooth muscle cells, dendritic cells, fibroblasts and cancer cells smooth mm cells (19,145,146,150,151). Expression of SerpinB2 is under strict regulation in homeostatic tissues (123), however during inflammatory conditions, cell differentiation, and wound healing it is heavily induced (145,146,151). Such inflammatory conditions can be invoked through viral (152-154), bacterial (142,155-157) and parasitic (158) conditions, as well as growth factors and cytokines in pathophysiological conditions such as asthma (159), lupus (160), adaptive immune system regulation (161)and cancer (24).

SerpinB2 expression is regulated through three genetic regions. Firstly, an inducible proximal promoter with two activator protein (AP-1)-like sites propagates both constitutive and PMA-activated transcription of SerpinB2 (162). This proximal promoter is conditionally dependent upon a CCAAT enhancer binding protein (C/EBP) element, which has been shown by Udofa *et al.* (2013) to bind the transcription factor C/EBP-P in order for both constitutive and LPS-inducible transcription of SerpinB2 (148). Secondly, SerpinB2 silencing is conducted by an upstream silencer [PAI-2 upstream silencer element 1 (PAUSE-1)], responsible for regulating both positive and negative control mechanisms of SerpinB2 (163). Thirdly, a distal AP-1 transactivator region reportedly controls transcriptional derepression of SerpinB2, important for fine-tuning SerpinB2 expression in both SerpinB2-expressing and -non-expressing cells (164). AP-1 has been described as a "nuclear decision-maker", critical for determining life or death cell fate decisions involved in apoptosis, cellular differentiation and proliferation (165,166). Through this ménage of transcriptional and post-transcriptional mechanisms, SerpinB2 is modulated homeostatically and pathophysiologically during stress, inflammation, cancer and when proteolytic and/or fibrinolytic operations have fulfilled their duties (Fig. 1.6). Recently, Schroder *et al.* (2014) reported that SerpinB2 expressed by B16 melanoma cells accesses the extracellular milieu upon the surface of 0.5–1 μm microparticles, through annexin-mediated binding to phosphatidylserine, where it still retained uPA inhibitory function (167). SerpinB2's binding modality is comparable to that reported for tissue transglutaminase-2 (TG2) (168). Interestingly, both SerpinB2 and TG2 lack the signal sequence for a classical

secretory mechanism (discussed further in Section 1.9.5). In addition, it was recently discovered that non-glycosylated (47kDa) SerpinB2 is secreted from ECs *via* trans-Golgi-network derived vesicles, upon stimulation with LPS (169). These two secretory mechanisms could have direct consequences for SerpinB2 release into the extracellular milieu during times of inflammation, ECM remodelling and stress (refer to Fig. 1.6). Further, it has been reported that the ecotropic virus integration site 1 (EVI1) transcription factor [associated with poor prognosis in human myeloid malignancy (170)] can bind and down-regulate SerpinB2 greater than 10-fold within leukemic cell lines, believed to inhibit myeloid differentiation (171). Glass *et al.* (2013) suggest that decreased SerpinB2 could play an important role in enhancing cellular proliferation by abrogating SerpinB2's protective function to Rb (171). Further, Glass *et al*. (2013) identified that the EVI1 binding site lies directly within the SerpinB2 silencer element, and propose that EVI1 potentially inhibits or alters normal binding and function of PAUSE-1. Bard *et al*. (2012) also showed that AP-1 physically interacts with EVI1 and that they both share promoter binding to an extensive range of target genes involved in malignant transformation, including SerpinB2 (170). Taken together, these two studies suggest that EVI/AP-1 could both collectively reduce expression of SerpinB2, increasing cellular proliferation in leukemic cells (171).

Additionally, SerpinB2 has been reported to be expressed over 105-fold by macrophages exposed to LPS (172), and has been shown to be up-regulated 2.9-fold by hepatic stellate cells under hypoxic versus normoxic conditions (173). Further, Copple *et al.* (2011) showed that HIF-1α activation not only up-regulated SerpinB2, but other important genes (including Ccr1, Ccr5, IL-13rα1, VEGF and PGF) involved in angiogenesis and collagen synthesis (173).

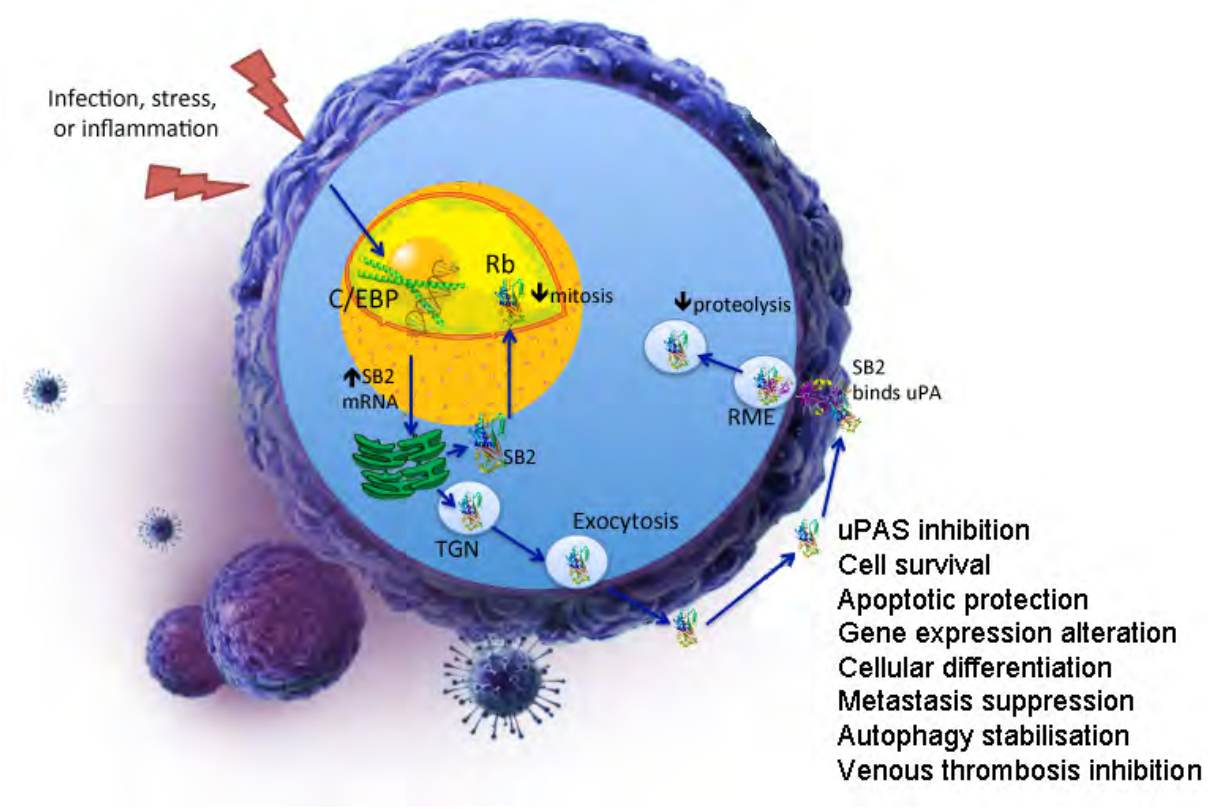

Fig. 1.6. SerpinB2 expression and activity. SerpinB2 (SB2) expression is induced by inflammatory and cell stress pathways and has a number of pleiotropic activities including uPA inhibition, cell survival, differentiation, immunity and extracellular matrix remodeling. The main extracellular role of SerpinB2 (after secretion on microparticles) is the inhibition of uPA, a powerful protease involved in proteolytic and fibrinolytic roles in vascular patency, ECM remodeling, cell migration and cancer. Rb – Retinoblastoma protein, TGN – Trans-golgi network, C/EPB - CCAAT enhancer binding protein element.

1.5.2 SerpinB2 function

SerpinB2 has been reported to bestow a plethora of biological functions of both an inhibitory and non-inhibitory nature (Fig. 1.6) [refer to (19) for an extensive review of SerpinB2 function].

1.5.2.1 uPA inhibition

SerpinB2 is an efficient inhibitor of tc-uPA (second order rate constant = 2.1×10^6 $M^{-1}s^{-1}$) and cannot stably inhibit pro-tPA or fibrin bound tPA (174), potentially allowing pro-uPA to initiate the plasmin generation cascade (refer to Fig. 1.3) (175). Unlike other serpins, SerpinB2 does not convert to a latent serpin conformation, remaining active until interaction with uPA or through renal clearance (176). It has been

previously been shown that removal of the CD-loop does not affect the ability of SerpinB2 to fulfill it's protease inhibitory mechanism of uPA or for the uPA:SerpinB2 complex to be internalised via RME (176). Furthermore, removal of the CD-loop allows for simpler and more efficient recombinant expression and purification of the protein (176).

SerpinB2 specifically inhibits uPA by the classical serpin inhibitory mechanism (refer to Fig. 1.4, B-C) forming a non-covalent Michaelis-like complex (when the interaction proceeds down the inhibitory pathway through interactions with the serpin's RCL residues (Arg^{380}–Thr^{381}), flanking the scissile bond (P1–P1) (120). Yu *et al.* (2002) have shown that a point mutation of the codon corresponding to the P1 (RCL) arginine residue at position 380 with an alanine residue abolishes the uPA inhibitory activity of SerpinB2 (172). Following attack of uPA at the active site on the scissile bond, a covalent ester linkage between Ser^{195} of the proteinase and the backbone carbonyl of the P1 residue is formed, which cleaves the peptide bond (120). Here, the RCL inserts into its own β-sheet (A) and transports the covalently bound uPA with it, distorting its active site. Upon inhibiting uPA, a covalent uPA:SerpinB2 complex is formed, which increases the binding affinity of uPA with endocytotic receptors of the LDLR family (*i.e.* VLDLR, LRP *etc.*), believed to be caused by conformational changes in uPA(177). The interaction of uPA:SerpinB2 and an LDLR receptor initiates rapid internalisation of the uPA:SerpinB2 complex from the cell surface into lysosomal compartments (124). This mediation results in the degradation of SerpinB2 and its attached protease along with the removal of any uPA-associated proteolytic activity from the cell surface (19,24).

Lastly, the strong inhibitory relationship between uPA and SerpinB2 within the TME appears to play a key role in tumour invasion and metastases (19,71,178-180). There are other contexts where SerpinB2 appears to take part in activities separate to uPA inhibition. In this perspective, a deeper elucidation of SerpinB2 roles within the TME could represent a vital component within the ongoing quest for metastatic cancer treatments.

1.5.2.2 Non-uPA inhibitory functions

Initially, extracellular SerpinB2 was identified as an inhibitor of uPA (refer to section 1.5.2.1), however it has been shown to bind tPA as well as tissue transglutaminase (TG2) of both trophoblasts during endometrial implantation, and keratinocytes of the cornified envelope (181) within both homeostatic and disease states (refer to Section 1.5.1). Intracellularly, there have been a multitude of functions assigned to SerpinB2, independent of uPA inhibition. These include cytoprotection [mainly in macrophages (152,182), dependent on the RCL in one study (183)], gene expression modification (184), immunomodulation of both innate and adaptive immunity (158), differentiation (135,185) inflammation and autophagy stabilisation (186), neuroprotection (187), protection from proteotoxic stress and cancer [reviewed in (19)]. Boncela *et al.* (2011) reported that SerpinB2 in ECs degraded the tumour suppressor gene, p53 (141). Moreover, it has also been reported in mouse models that SerpinB2 binds TG2 mediating an anti-apoptotic response through TANK-binding kinase 1 (TBK1), inactivating procaspase-3 (182). This is interesting as TG2 will be recurring within this project (refer to Sections 1.9.5, 3.4, 4.4) and has previously been shown to act on the Rb protein, playing an important role in the cell progression through apoptotic pathways (188). Several studies implicate SerpinB2 in cytoprotective activities and warrant further research into SerpinB2's interplay with TG2, defining exact mechanisms within these post-translational modification processes. SerpinB2 has also been shown to alter the secretory profile of cytokines in macrophages, specifically by blocking IL-1β secretion (189), indirectly inhibiting caspase-1 activation acting downstream of NF-κB (190), and regulating CCL2 production (involved in infiltration of monocytes, macrophages and T cells) in the development of Th2-mediated protective immunity following viral (161) and nematode infection (191,192), as well as in asthmatics (193,194). Additionally, SerpinB2 was recently shown to be up-regulated in middle cerebral arteries of hypertensive rabbits (195), while Palacios *et al.* (2015) have shown that rheumatoid arthritic (RA) macrophages subjected to ex-vivo isolated RA synovial fluid decrease expression of SerpinB2, reportedly in order to activate a pro-

inflammatory environment (196).

Interestingly, studies report SerpinB2 to be involved with neuroprotection. For a long time it has been known that neuronal cells express SerpinB2, especially proceeding kainite (an analogue of glutamate) dosing (187). It has previously been reported that SerpinB2 is an important "activity-regulated inhibitor of death (AID)" gene, produced in large concentrations by hippocampal neurons (197). Zhang *et al.* (2009) demonstrated that SerpinB2 promoted cell survival in both their cell culture and mouse models of neurodegeneration (197). Additionally, Lee *et al.* (2015) reported that SerpinB2$^{-/-}$ murine embryonic fibroblasts (MEFs) were much more sensitive to huntingtin protein aggregation versus wild-type MEFs, concluding that SerpinB2 is involved in the intracellular compartmentalization of aggregated proteins (198). Many studies report SerpinB2 to be involved with neuroprotection. Further, it has recently been shown that SerpinB2 assists in neuronal cell migration (199). Katie *et al.* (2014) demonstrated that SerpinB2 binds cell adhesion molecule close homologue of L1 (CHL1), which functions in neural cell proliferation, migration, differentiation, and survival. SerpinB2-CHL1 binding was shown to promote cerebellar granule cell migration and neurite outgrowth, involving interactions with integrins and vitronectin (199).

Further, SerpinB2 also appears to be involved in processes other than uPA inhibitory function, associated with cell adhesion and migration, through altering gene expression in many different cell types. These affects can occur either through direct or indirect cell-cell or cell-ECM association. It has been reported that SerpinB2-transfected HeLa cells expressed lower levels of intercellular adhesion molecule 1 (ICAM-1), which conferred protection from picornavirus-induced lysis (184). Ksiazek *et al.* (2010) showed that ICAM-l (a transmembrane glycoprotein) is expressed constitutively on many cell types and can promote tumour cell bindings to mesothelial tissue (200). Moreover, it was recently shown that SerpinB2 transcription is necessary for mammary cell migration induced through EGF, which activates a cascade linking the ERK-to-ERF axis migration-promoting pathway (201).

1.5.3 SerpinB2$^{-/-}$ mouse models

Apart from reduced adipose tissue development (202), SerpinB2$^{-/-}$ mice have been shown to progress normally through development, survival, maturity and fertility (203), until directly exposed to pathogenic stimuli, where they experience an impaired response to infection (19,151). It has been reported that SerpinB2$^{-/-}$ mice exhibit an increased susceptibility to Legionella pneumophila (157), HIV-1 (138) and schistosoma infection (158).

Recently, SerpinB2$^{-/-}$ mice were shown to have significantly increased venous thrombus resolution compared to wild-type mice, with a 12-fold elevation in active uPA levels within SerpinB2$^{-/-}$ thrombi reported (204). Siefert *et al*. (2014) found that SerpinE1 levels were concomitantly decreased (in SerpinB2$^{-/-}$ mice) potentially also responsible for the elevated uPA levels, however this did not affect both MMP-2 and MMP-9 activation, suggesting that enhanced thrombus resolution was *via* uPA-mediated mechanism (204). Moreover, SerpinE1$^{-/-}$ mice also exhibited increased thrombus resolution comparable to SerpinB2$^{-/-}$ mice, yet there was also reduced thrombus formation and altered MMP activity recorded (204). These data identify SerpinB2 as a novel regulator of venous thrombus resolution, modulating both inflammatory and uPA activity mechanisms, distinct from SerpinE1.

1.5.4 SerpinB2 in cancer

SERPINB2 is a multifaceted gene, constantly reappearing amongst experimental data across the wide realm of biomedical research. Given the multifarious nature of SerpinB2, it is not surprising that the roles ascribed to SerpinB2 within tumour systems are multifaceted and complex. There are many reports within the cancer field associating SerpinB2 expression with both tumour suppression and tumour advancement, dependent upon the specific tumour type, tissue context, ECM componency and TME regulation. This paradoxical nature of SerpinB2 effects on tumourigenesis, invasion and metastasis is quite complex, however many tumours express

SerpinB2 at tumourigenesis and at the initiation of metastasis, which could potentially be the body's homeostatic response, as a stress response modulator (198).

1.5.4.1 Tumour progression and inhbition

Recently, Kovacheva *et al.* (2014) have shown that sustained conditional knockdown of intracellular bone sialoprotein was essential for breast cancer skeletal metastasis, and that this was associated with up-regulated SerpinB2 expression (205), which otherwise is an indicator of good prognosis in breast cancer patients (19,82). Chambers *et al.* (1995) previously reported that increased intracellular SerpinB2 expression within metastatic ovarian tumour cells increased overall patient survival, while increased SerpinB2 levels detected in ascites correlated with a poor prognosis (206,207). Research by Ashton *et al.* (2012) demonstrated that SerpinB2$^{-/-}$ hematopoietic cells decrease leukemia stem cell (LSC) growth and survival leading to a significant reduction of leukemia cells in bone marrow versus wild-type hematopoietic cells (208). SerpinB2 shRNA LSCs revealed the same reduced phenotype of leukemia development demonstrating a new role for SerpinB2 specifically regulating leukemic populations *in vivo* (208). Additionally, Subimerb *et al.* (2014) reported that cholangiocarcinoma (a slow growing, highly metastatic bile duct tumour) patients with higher expression of both uPA and SerpinB2 in peripheral blood leukocytes had lower survival than patients with lower expression (209). Using a skin carcinogenesis model, Tonnetti *et al.* (2008) showed that SerpinB2$^{-/-}$ mice developed fewer tumours compared to wild-type mice (139). More recently, studies by Rushworth *et al.* (2014) showed that loss of dual-specificity phosphatase 5 (DUSP5) resulted in an increase in activated H-Ras/ERK-mediated by SerpinB2 gene transcription, leading to increased skin cancer progression (210). Both of these papers suggest that SerpinB2 expression is able to regulate the ERK pathway, necessary for cell migratory mechanisms. The association of SerpinB2 with poor patient prognosis has also been reported in endometrial, bladder, and colorectal cancers (211). SerpinB2 expression has also been reported to promote the development and progression of epidermal papillomas, induced by 12-O-tetradecanoylphorbol-13-acetate (TPA), in a manner

independent of uPA inhibition, proposed rather to be related to an apoptotic inhibition (212).

Furthermore, in regards to carcinomas of the brain, SerpinB2 has been shown to be prometastatic. In a recent study by Valiente *et al*. (2014), uPA and tPA produced by astrocytes from lung and breast cancer metastatic lesions were shown to be neuroprotective against metastatic advancement through activation of plasminogen to plasmin (213). Converted plasmin was reported to inhibit metastatic tumour cells through FasL activation, inactivating L1CAM, required for tumour cell spreading along capillaries, leading to cell apoptosis (213). The expression levels of both SerpinB2 and Neuroserpin (SerpinI1) in human metastatic tumours were associated with brain relapse, both individually and combined (213). SerpinB2 and SerpinI1 were suggested to be produced by these metastatic tumour cells to protect them from FasL action, allowing them to proliferate and migrate through the brain (213).

Contrary to the study by Valiente *et al.* (2014) and others described above, many *in vitro* and *in vivo* experimental models implicate SerpinB2 expression to have anti-invasive and anti-metastatic cancer consequences (24,167,214,215). There is also extensive clinical association between SerpinB2 expression and metastasis suppression clinically (216). High SerpinB2 expression in breast (6,85,96,217-219), lung (220), ovarian (221-223), prostate (224-227), head and neck (228-230), oesophageal (231,232) and pancreatic (118,233-238) cancers has been significantly associated with good prognosis, including increased relapse-free survival, disease-free survival, and mean overall survival time (Table 1.1). Further, in node negative breast cancer high tumour SerpinB2 is only statistically relevant if uPA levels are concurrently high (6,19).

Table 1.1. Individual PAS components involved in the prognosis of various human cancer types

(–) Poor Prognosis; (+) Good Prognosis; (NA) Not Associated; (ND) Not Determined.

Cancer type	uPA	uPAR	SerpinE1	SerpinB2	References
Breast	–	–	–	+	(6,85,96,217-219)
Ovarian	–	NA	–	+	(221-223)
Prostate	–	–	ND	+	(224-227)
Head & Neck	–	–	–	+	(228-230)
Oesophageal	–	–	–	+	(231,232)
Pancreatic	–	–	–	+	(118,233-238)

Recently, Huang *et al.* (2015) reported that low expression of SerpinB2 in head and neck squamous cell carcinoma (HSCC) tissue was associated with a higher chance of recurrence in HSCC patients (239). Further, Taoka *et al.* (2014) reported that SerpinB2 was up-regulated 1.5 fold in cisplatin resistant bladder cancer cells versus cisplatin naïve cells (240). Whether this relates to the anti-apoptotic ability conferred by SerpinB2 was not addressed. Importantly however, this is the first clinical finding where SerpinB2 has been shown to prevent chemo-acquired resistance in patients with HSCC (216). Most recently, a new player, ΔNp63α (a pleiotropic oncogene and member of the p53 transcription regulatory family), has been reported to negatively impact on the survival outcome of patients with squamous cell carcinomas (241). Moreover, King *et al.* (2014) showed that aberrant expression of ΔNp63α in keratinocytes, believed to precede squamous cancer development and progression, down-regulated SerpinB2 (241). This finding links p53 homologs and SerpinB2 together in the context of tissue homeostasis.

Furthermore, research by Li *et al.* (2014) demonstrated that down-regulation of SerpinB2 was essential to GPCR kinase-3 stimulated angiogenesis in a human prostate cancer *in vivo* model (242). This study and personal observations by our laboratory and collaborators indicate that SerpinB2 might suppress tumour angiogenesis. Several other animal models support these clinical findings. For example, Suwa *et al.* (2008) found that nude mice bearing a human colon cancer xenograft overexpressing SerpinB2 helped to inhibit primary tumour growth, decrease metastases and increase tumour apoptosis (243). Additionaly, treatment of uPA over-expressing tumour xenografts in animal models with SerpinB2 has been demonstrated to inhibit or complete prevent metastases (215,244). In a recent prostate cancer *in vivo* model, Zou *et al.* (2012) reported that SerpinB2 expression was suppressed by the tumour promoting molecules protein kinase D2 and D3, which increased the activity of uPA, uPAR and MMP9, suggesting that SerpinB2 loss contributes to prostate cancer progression (245).

Thus, these studies highlight the complex interplay of SerpinB2 activity between invading tumour cells and host tissue, revealing the enigmatic role this protein portrays. Interestingly, there are many studies that implicate SerpinB2 in cell migratory processes, within both developmental, homeostatic and pathophysiological systems and needs to be addressed. Studies over the last decade have shown that in cancer, tumour associated cells, such as fibroblasts and immune cells, are facilitating a strategic role in invasion and metastasis, helping attainment of cellular migratory pathways through engaging in cellular cross talk *via* exchange of proteases and cytokines with tumour cells (43,246-248). It is this diverse cellular presence within the TME that allows a tumour to facilitate a plethora of processes required through all stages of growth, migration, invasion and malignant progression throughout the ECM to access distant sites of the body.

1.6 The extracellular matrix (ECM)

The ECM is directly responsible for the homeostatic functioning of cellular and tissue functions within the human body. Strict control in regulating ECM turnover and remodelling is essential for proper embryonic

development, angiogenesis, wound healing, pregnancy and normative organ functioning. During pathological conditions, such as cancer, the dysregulated biochemical and biophysical functioning of the ECM perpetuates processes that aid in tumour invasion, metastatic niche formation and metastases (249). Exactly how ECM composition and remodelling is disrupted is of major concern to the field and is now widely accepted to be the crux for success or failure of many clinical therapies.

1.6.1 The dynamic reciprocity of the ECM

In 1982, Dr Mina Bissell proposed the model of 'dynamic reciprocity', where tissue-specific function is retained by information exchange between cells and their local ECM (250). This ongoing bidirectional interaction controls homeostatic functions performing pivotal roles in regulating tissue regenerative responses, from regulating cellular morphology, ECM contraction and remodelling, cellular differentiation, migration, proliferation, and survival during tissue development (251,252). These cell–ECM interactions are also impacted during pathologic processes including inflammation, haemostasis, cancer, diabetes, hypertension, and chronic wound healing (251). Each cell has access to the ECM through transmembrane cell surface receptors such as integrins, cadherins, selectins and syndecans (251). These receptor interactions occur with, and are not limited to, the ECM componenets laminin, fibronectin, collagen, vitronectin, proteoglycans and other cell surface anchored proteins eg. MT-MMPs, uPAR, and the Serpins, to name a few. Signal feedback moves from the cytoskeleton to the nuclear matrix and chromatin in a cyclical fashion and demonstrates that the ECM and cellular microenvironment are integral in determination of tissue specificity (250). This microenvironment additionally comprises cytokines, chemokines and growth factors, providing soluble paracrine signals from local cells, distant tissue beds, and CNS activity (253). Thus, this complex system of multifarious componency, in constant cell-ECM communications, determines both an organ's structure and function, and must act in cooperation to maintain homeostasis within tissues. These processes are best modeled using *ex vivo* 3D systems.

Prior to discussing these model systems an overview of collagen I, the major ECM component used in 3D models, is described.

1.6.2 Collagen I

In homeostatic tissues a precise balance is maintained between the processes of biosynthesis and degradation in order to preserve the physiological nativity of tissue collagens. Collagen makes up ~30% of all protein of the human body and 90% of collagen is type-1 collagen (254). Thus, collagen I is not only the most abundant protein the body, but also the most prevalent ECM component of breast and pancreatic tissue (the two cancer types under investigation in this project). Collagen I is a long, fibrous structural protein and the main constituent of skin, bones, tendons, cartilage, ligaments and fascia (255). It provides the framework and support for nearly all of the human body's tissues, though it can also be found intracellularly, particularly within fibroblasts and macrophages. All collagens have immense tensile strength, and when bundled, form large, eosinophilic fibers, known as collagen fibres (255). Collagens have more than fifty binding partners *in vivo,* believed to be due to the requirement of such diversity of fibril patterns, ranging from parallel bundles in tendon and ligament, to orthogonal lattices in cornea, and interlocking weaves in blood vessels, skin, and bone (256). In healthy tissue this is beneficial, however, having such a large number of binding partners can have detrimental impacts in diseased tissue states. Type-I collagen is first produced as the precursor molecule, Procollagen I, characterised by a triple-helical rod-like core domain with *N*- and *C*-terminal globular propeptides and linear telopeptides, respectively (255) (Fig 1.7 A). Procollagen chains are assembled into triple helices within the rough endoplasmic reticulum and contain a three-residue repeat of glycine-proline-X (where X can be any amino acid type) or glycine-X-hydroxyproline (257) and comprise three amino acids for every left-handed helix turn, stabilised by hydrogen bonds (257). Formation of collagen fibrils is first instigated by the enzymatic cleavage of Procollagen's N- and C-terminal pro-peptides performed by disintegrin and several metalloproteinases (BMP-1 and ADAMTS-2, -3, and -14), respectively (Fig 1.7 A) (255,258,259).

This causes the exposure of telopeptides, which engage in site-specific intermolecular interactions driving collagen self-assembly (Fig 1.7 B) (258). Procollagen I chains consist of two α1 (I)-chains and one α2 (I)-chain. These associate into (15 Å wide) trimers, with a molecular mass of ~270 kDa, nucleate and assemble into a triple-helix zipper formation and are translocated to the Golgi apparatus, where they are packaged into vesicles that eventually fuse with the cell membrane and extrude into the extracellular space (260). Collagen I packs together in thin ordered fibrils 10-300 nm in diameter, making them incredibly strong yet tensile, due to the intermolecular nature of their covalent cross-links (Fig 3.1 C-D) (255). Such covalence only occurs during the early stages of fibril development, when the N- and C- telopeptides are in a reactive site position, and not as a tissue bed reaches maturity (257). This is the native tertiary conformation of collagen I and it's fibres are the building blocks for collagen fibril bundles (Fig 1.7 D). These collagen superstructures are prevalent on a large scale in the body and exist in many types of tissues with diverse mechanical properties. While collagen I is a major determinant of the architecture of a specific tissue site, it has been observed to be both directly and indirectly involved in tissue specific functions including cell adhesion, proliferation, chemotaxis/migration, differentiation, as well as an antigen in immunopathological conditions
(255,261-264).

1.6.3 Collagen crosslinking and fibrilogenesis

As aforementioned, collagen has been shown *in vitro* to undergo a self-assembly/polymerisation process, spontaneously assembling into fibrils (256,265). However, the *in vivo* situation is vastly different. In mammals there are two major classes of ECM collagen cross-linking enzymes, the lysyl oxidase (LOX) family (containing 5 genes, LOX and LOXL1 to -4) and the transglutaminase family (eight have been characterised), of which LOX and the ubiquitous tissue Transglutaminase 2 (TG2) are the primary members of each family and essential for collagen I fibrillogenesis *in vivo* (Fig 1.7 C) (266-268). Both TG2 and LOX expression are induced by TGF-β (secreted by fibroblasts), which directly leads to increased cross-linking and reduced ECM degradation

indirectly stimulating enhanced ECM deposition, including collagens, elastin, proteoglycans, laminins and fibronectin, ultimately resulting in a greater tissue stiffness (269-271).

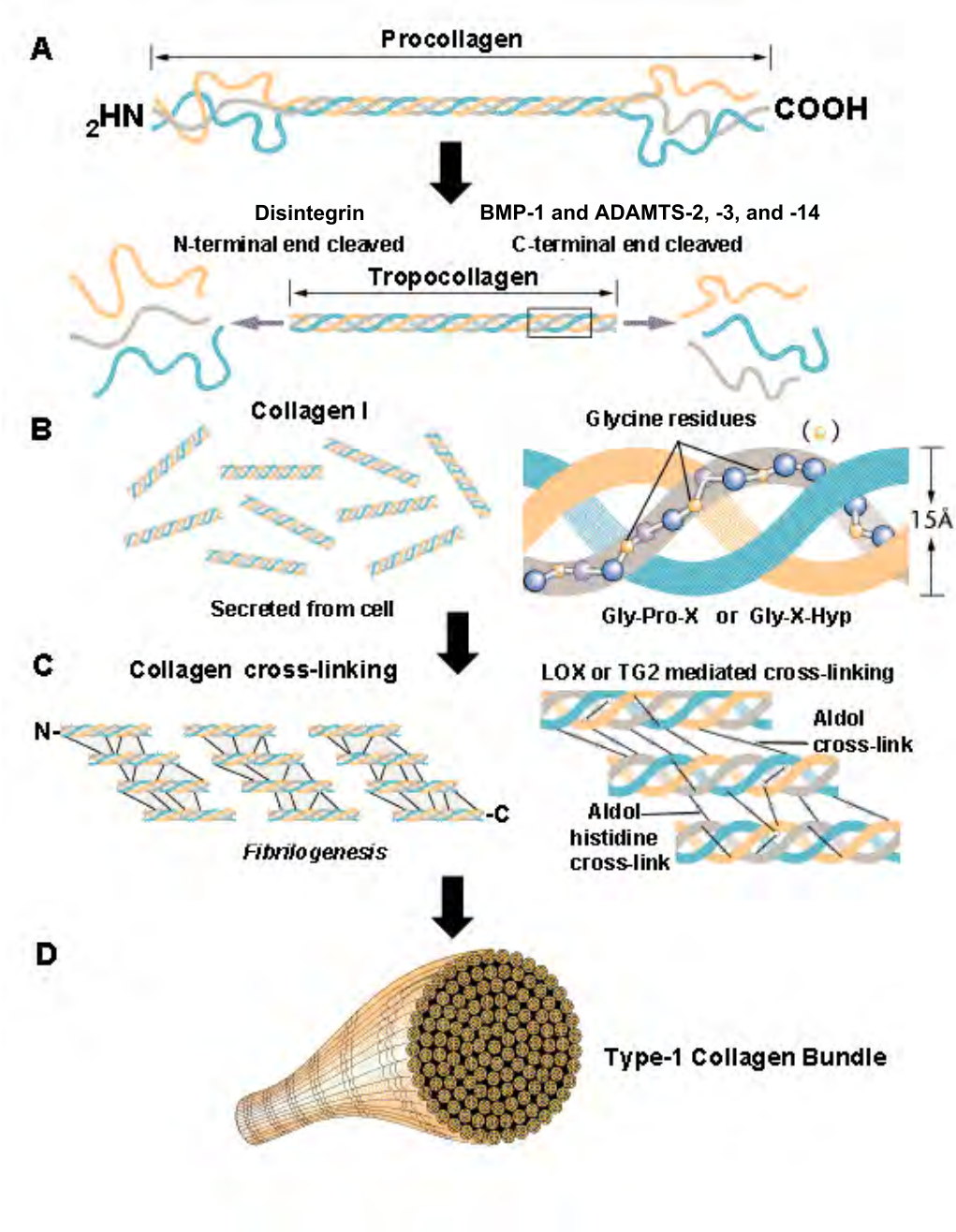

Fig 1.7 Structure of Collagen I. A. Procollagen I is the precursor to collagen I and contains two alpha-1 chains and one alpha-2 chains, assembled into a triple helix configuration. Procollagen peptidases cleave domains at the C- and N-terminals resulting in (**B**) formation of mature Tropocollagen I (~300nm long and ~1.5 nm in diameter), which is then secreted from the cell. **C.** Collagen I undergoes LOX and TG2 mediated cross-linking *via* aldol and aldol-histidine covalent reactions to form collagen I fibrils (up to 1 cm long and ~500 nm in diameter). **D.** The formation of a robust collagen I bundle or fibre is the major component of the body's ECM, supporting cell and tissue architecture as well as having many important biological functions in cellular adhesion, survival, migration and proliferation. Modified from (257).

Collagen molecules generally bind to fibronectin and then to the plasma membrane of cells through α11β1- and α2β1-integrins (256,272,273). This interaction has been shown to promote increased deposition of collagen I and III fibers, forming large extracellular collagen networks (266). During wound healing, increased biosynthesis is crucial for proper wound healing, where close cellular control over rapid collagen cross-linking is required. In certain disease states such as keloids, hypertrophic scars, scleroderma and many cancer tissue types, there is hyper-accretion of collagen bundling, forming desmoplastic, fibrotic tissue areas (274). Collagen I is also significantly up-regulated in end-stage liver cirrhosis, eventually preventing the entry of blood and oxygen to hepatic cells causing cell death. (275).

Furthermore, it is well established that many tumour types (including mammary, pancreatic and squamous cell carcinomas) contain high levels of collagen I in the TME (276-278). Tumour progression and metastatis is also positively correlated with collagen density and it has been demonstrated that stromal remodeling of collagen and ECM collagen cross-linking facilitates invasion (279), particularly through LOX facilitation (264). As this thesis involved effects on collagen crosslinking and ECM remodeling in the stroma of the TME, a summary of the two main ECM cross-linking enzymes, LOX and TG2, follows.

1.6.4 Lysyl oxidase (LOX)

The Lysyl oxidase family is a quintet of extracellular matrix modifying enzymes, with important roles in connective tissue formation, cellular adhesion, motility and migration, gene transcription regulation, and senescence, as well as cancer progression (280). LOX, the main enzyme of the family, is a copper dependent protein that covalently cross-links collagens (and elastin) within the ECM *via* converting lysine, histidine or hydroxylysine residues of *N*- and *C*-terminal telopeptides of collagen into peptidyl aldehydes (281) (refer to Fig. 1.7). These aldehydes then spontaneously condense with free lysine residues to form a variety of intra- and intermolecular covalent cross-links (281). This reaction gives collagen additional mechanical stability and helps

strengthen the surrounding ECM against degradation (255). As collagen fibril assembly is underway, LOX activity is increasingly expressed, believed to be due to its capacity to bind highly conserved sequences that are exposed on telopeptide regions of N- and C- terminals of fibrils (255). LOX expression is known to be up-regulated by hypoxia-inducible factors (HIFs), along with TGF-β (269), and thus is often over-expressed in hypoxic breast and pancreatic tumours, with poorer overall survival in patients with high LOX-expressing tumours (282,283). Other fibrotic disorders where LOX is implicated are connective tissues of the heart (260) and vasculature (284), lungs (264), skin (in particular keloid fibrosis and scleroderma) (274), kidneys (285), liver (cancer and liver fibrosis) (286), mouth (gingival atrophy) (287), and the colon (281). The consequence of correct LOX expression and resultant collagen cross-linking in homeostatic tissue is represented by the fact that $LOX^{-/-}$ mice are neo-lethal due to a fragile diaphragm and cardiovascular system collapse (288). Mutations in LOX, which can be recessive or as a result of nutritional copper deficiencies, are seen in Menkes disease and Occipital horn syndrome (289,290). Further, Osteolathyrism, a condition caused by ingestion of legumes from *Lathyrus sativus*, a plant rich in the LOX inhibitor β-aminopropionitrile (BAPN), reduces collagen cross-linking ability and can be fatal (23). LOX is directly able to modify the ECM, and its overexpression leads to the development of desmoplasia, with positive association reported between LOX, TIMP-1, SerpinB1 and MMP-9 in human colorectal cancer patients, enhancing tumour cell invasion (291) (280,292). In addition, it was recently demonstrated by Baker *et al.* (2013) that fibroblasts overexpressing LOX *in vivo* stimulate collagen cross-linking and matrix stiffness in colorectal cancer through FAK activation (293). Further, when LOX inhibitors have been used, reductions have been shown in the amount of activated fibroblasts, ECs, and a significant decrease in desmoplasia and TGF-β expression (294).

1.6.5 Tissue transglutaminase-2 (TG2)

The transglutaminases are a family of (8 known) enzymes that occur both intra- and extracellularly in all

mammals. Transglutaminases work by forming extensive cross-linked, mostly insoluble protein polymers, vital for native tissue barrier formation and structural networks. TG2 [(78 kDa), also known as tTG, or tissue TGase] is the most diverse and widespread of the transglutaminase family (295). This calcium dependent enzyme catalyses the reaction between the group of ε-amino lysine residues in collagen I and the γ-carboxamide group of glutamine residues in itself or other proteins (refer to Fig. 1.7), creating an inter- or intramolecular isopeptide bond, highly resistant to mechanical stress and proteolysis (296). In addition to collagen crosslinking ability of TG2, this ubiquitously expressed enzyme is a component of many cellular compartments, including exosomes, and is an intrinsic component of the plasma membrane. Furthermore, TG2 is able to catalyse many other biochemical reactions including GTP-binding/hydrolysing, deamidation and isopeptidase activity (296). TG2 is abundantly expressed in the cytosol of skin, heart, liver and small intestinal cells, while smaller amounts can also be found in the nucleus and mitochondria of cells (297).

Extracellularly, TG2 is known as nature's biological glue and its expression is elevated in multiple cancer cell types, implicated in drug resistance and metastasis due to its ability to promote EMT and stem cell-like properties of tumour cell populations (298). Like SerpinB2, TG2 is induced under inflammatory conditions and is deposited into the ECM after cell damage and stress to help in the remodelling and/or stabilisation of several ECM proteins, binding with great affinity to fibronectin (299). TG2 is now one of the earliest biomarkers of coeliac disease, stimulated mainly via TGF-β (300) and known to deamidate dietary gluten peptides and aggregations, acting as a target auto-antigen in the immune response, essential for coeliac disease pathogenesis (297,301). Interstingly, TG2 has been shown to have a positive feedback with TGF-β, increasing it's expression through NF-κB pathway activation (302). Extracellular TG2 increases cellular adhesion, proliferation, migration, differentiation, ECM stabilisation, wound healing and signal transduction (298). For a general review of the diverse roles TG2, refer to (303).

1.6.5.1 SerpinB2 and TG2

It has previously been shown that SerpinB2 cross-links to fibrin(ogen) *via* TG2 (in trophoblasts), through reaction with one of SerpinB2's three Glutamines in the CD Loop (Gln^{83}, Gln^{84} and Gln^{86}) (304). Jensen *et al.* (1993) stated that the TG2-catalysed/Ca^{2+}-dependent anchoring of SerpinB2 to ECM structures could be responsible for focally regulating fibrinolysis (181). In addition, they demonstrated that SerpinB2's uPA-inhibitory activity was not affected by cross-linking to fibrin(ogen), and activated peripheral blood monocytes still efficiently inhibited uPA-mediated fibrin clot lysis, through secretion of SerpinB2 into clots (181). Intracellular TG2 plays an important role in apoptosis and is known to use SerpinB2 as a substrate (182). Recent studies have linked SerpinB2 and TG2 as downstream mediators in the anti-apoptotic response triggered upon activation of TANK-binding kinase 1 (TBK1) (182). Studies by Delhase *et al.* (2012) show that TBK1 induces SerpinB2 expression, which stabilises TG2, cross-linking and inactivating procaspase-3, in a TNF-dependent manner (182). This study potentially provides explanation of the cytoprotective ability conferred to SerpinB2 (305). It has also been shown that $TG2^{-/-}$ mice are increasingly susceptible to cell death in acute liver trauma (182), and reported symptoms of mild onset of diabetes through ageing, thought to be related to insulin release disruption from pancreatic β-cells (295).

Interestingly, SerpinB2 has also been shown to be cross-linked to the cornified envelope of skin by plasma transglutaminase (TG1) (306). TG1 is anchored within the inner plasma membrane of keratinocytes, and activated with SerpinB2 in inflammatory conditions, such as congenital ichthyosis (306). Bechtel *et al.* (1996) reported that not only was SerpinB2 a major PAS inhibitor within normal epidermis, but within lupus erythematosus patients the increased epidermal SerpinB2 was not associated with an increase in epidermal uPA or tPA (307). Their data led them to hypothesise that epidermal SerpinB2 may have other functions than merely uPA inhibition (307). Further, Schroder *et al.* (2010) reported that $SerpinB2^{-/-}$ mice infected with *Schistosoma japonicum*, which can cause schistosomiasis in the liver and other tissues incurring fibrosis, had reduced collagen I fibrosis (as determined by collagen I picrosirius staining) versus wild-type (SerpinB2

expressing) mice (158). Interestingly, in the two most researched areas that SerpinB2 and TG2 bind, i.e. the skin (keratinocytes of the cornified envelope) and endometrium (endometrial cells, trophoblasts and the decidua), there is a reported increased SerpinB2 expression associated with tumour promotion (139,211). Whether there is a direct relationship within tumours of these tissues and SerpinB2 activity requires further elucidation. In regards to SerpinB2 activity within endometrial tissue, this could potentially be an area of great revelation for there are significant homologies between tumour biology and development.

1.6.6 SerpinB2 and TG2 in the TME and development

It has been shown that early embryonic cells share extremely similar phenotypes to tumour cells (308). Both undertake deprogramming to a proliferative stem cell state and develop immortal and invasive stages (308). These homologies were first speculated in 1892 by two French biologists, Lobstein and Recamier, but not since advances in genetics and developmental biology has this been further elucidated (309). Studies now show that embryonic development gene programmes are also being hijacked and used by invading tumour systems (308). It has been demonstrated that signaling pathways in patterning and morphogenesis within embryo development are co-ordinated by FGF, BMP, Wnt, Notch and Hedgehog signalling pathways (13). These pathways have been reported to be reactivated during tumourigenesis and contributing to tumour cell EMT, invasion and metastasis (14). Thus, through a functional and mechanistic understanding of trophoblast invasion many insights into metastatic cancer cell invasion are being revealed (310). Moreover, it has been reported that K-Ras mutation/over-activation coupled with developmental genetic elements (such as wnt-β-catenin, TGF- and Hedgehog) above crucial temporal thresholds drives differentiated pancreatic cells into a de-differentiated, ductal state (311,312). This has been shown to persist towards the formation of pancreatic epithelial neoplasia (PanIN) and can eventually result in pancreatic ductal adenocarcinoma (PDAC) (313) (Fig. 1.8). Further in-depth understanding could increase biomarker identification, new diagnostic techniques and future treatment

options to control the advancement and dissemination of metastatic cancer (309).

It is known that trophoblast differentiation throughout first trimester pregnancy involves cell proliferation, invasion and ECM remodeling (refer to Fig. 1.8). It is generally accepted that coordinated expression of MMPs/TIMPs and tPA/SerpinE1 play the key roles in fibrinolysis during early stages of placentation and separation of the placenta from maternal tissue at term (134,314). During pre-eclampsia, plasma tPA and SerpinE1 levels are distinctly increased and there is an association with increased concentration and pre-eclampsia severity (123,315). Interestingly, SerpinB2 levels are significantly reduced in pre-eclampsia and clinically the use of the ratio of high SerpinE1/SerpinB2 is associated with pre-eclamptic pregnancies [while the reverse ratio is associated with normal pregnancy (123,315)]. In patients of intrauterine growth retardation, uPA and SerpinB2 levels are prominently decreased, indicating that reduced uPA regulation and inhibition decreases placental function and potentiates intrauterine growth retardation (123). As uPA and SerpinB2 appear mainly to degrade trophoblast cell-associated ECM during early stages of placentation (314), it has also been proposed that cell membrane associated plasmin could impart directionality on migrating trophoblasts through basement membranes and interstitial tissues (316). Zini *et al.* (1992) also observed both SerpinB2 and SerpinE1 are secreted by trophoblasts in greater amounts than uPA (316), potentially to ensure critical uPA regulation, however it is proposed that there could be additional roles concomitant with uPA inhibiton (316). Further, trophoblast cell types (refer to Fig. 1.8) require the production of focal adhesions mediated by a cytoplasmic tyrosine kinase named focal adhesion kinase (FAK) (317). Within endometrial invasion by a blastocoele, FAKs are involved in trophoblastic cellular proliferation, migration/invasion, and ECM remodeling, specifically expressed within villous cytotrophoblast and extravillous trophoblast (EVT) cells, co-localised with integrin α5 and MMP2 (317). Additionally, it has been shown that cell–ECM adhesion is strengthened *via* TG2 cross-linking to integrin within cells causing receptor clustering, increasing integrins and

syndecan-4 causing increased signaling and activation of FAK, ERK1/2, Rho/ROCK, AKT and PKCα (318-320). This activity further stimulates TG2-mediated enhancement of cell adhesion and migratory processes (320). Robinson *et al.* (2006) reported significant TG2 protein and mRNA present in stromal and trophoblast cells from first trimester and at term, with higher levels appearing in third trimester (321). Further, it was demonstrated that primary cultures of embryonic trophoblast, fibroblast and decidual stromal cells all produce TG2 (321).

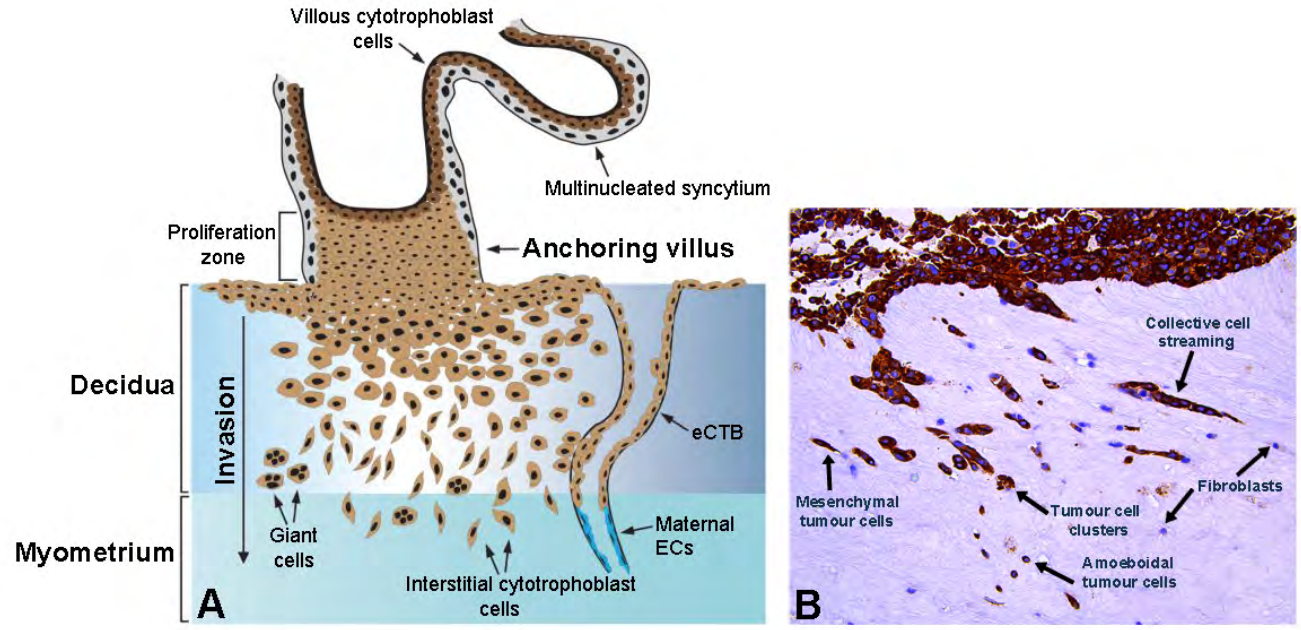

Fig. 1.8. Invasion of human trophoblasts and PDAC cell invasion. A. After blastocoele anchorage to maternal endometrial BM, villous cytotrophoblast precursor cells proliferate in cell columns. Extravillous trophoblasts (i.e. interstitial cytotrophoblasts) disconnect from cell columns and migrate into stromal areas of maternal decidua. Some interstitial cytotrophoblasts differentiate into giant cells in deeper placental tissue areas, while endovascular trophoblasts (eCTB) within maternal arteries replace maternal ECs and attain endothelial physiognomies. Adapted from (322). **B.** Within the pancreas, cells can acquire specific mutations that perpetuate metaplasia and dysplasia, leading to pancreatic ductal cell proliferation, progressing down a pathway to PanIN and towards a malignant phenotype. PDAC cells can reactivate developmental genes triggering BM degradation and EMT allowing invasion into the ECM. Different modes of invasion can occur including mesenchymal, amoeboidal and collective cell streaming. Invasion is also advanced with the assistance of stromal remodelling, paracrine signalling and growth factor secretion from carcinoma associated fibroblasts (CAFs); further addressed in Chapter 4.

1.6.7 TG2 in cancer

In a tumourigenic system, TG2 expression causes activation of FAK and the downstream PI3K/Akt1 pro-survival pathway (320). Furthermore, Chau *et al.* (2005) reported that treating collagen I with TG2

significantly increased cell attachment, migration and proliferation of both human osteoblasts and human foreskin dermal fibroblasts, in comparison to native collagen I (323). Interestingly, the TG2-treated collagen also had enhanced resistance to proteolysis over native collagen, due to increased cross-linking (323). Orban *et al.* (2004) showed that TG2 supplemented collagen I gels exhibit increased mechanical strengthen of fibrillar bundles, raising the denaturation temperature and burst pressure of gels, versus native Collagen gels (without TG2 mediated polymerization) (324). Moreover, Fortunati *et al.* (2014) demonstrated that cross-linking of collagen I by TG2 caused human osteoblasts to attach, spread, proliferate, differentiate and mineralise more rapidly compared to cells seeded onto native collagen (325).

Moreover, there is increasing evidence of TG2 as a substantial player in tumour progression. TGF-β, TNF-α, IL-1, IL-6 and NF-κB have all been shown to up-regulate TG2, driving inflammation and cancer progression (296,326,327). TG2 has been shown to be up-regulated in the stroma of invasive ductal breast cancers (328,329), and proposed as an independent risk factor for identifying patients at high risk of tumour recurrence (330). In one of the most aggressive cancer types, pancreatic ductal adenocarcinoma [(PDAC) – the focus of Chapter 4], Verma *et al.* (2006) showed that 42 of 75 (56%) tumour samples collected had higher basal protein expression levels of TG2 compared with normal pancreatic duct tissue (331). Increased TG2 expression in PDAC was strongly associated with nodal metastasis and lymphovascular invasion (331). Verma *et al.* (2006) also reported that TG2 induces activation of FAK and PI3K/AKT pathways, contributing to PDAC drug resistance and a more invasive PDAC phenotype (331). Subsequently, Verma *et al.* (2008) showed that siRNA down-regulation of endogenous TG2 abrogated the growth of PDAC tumours, through inhibition of PDAC cell proliferation, angiogenesis, and Akt phosphorylation (327). In addition they also reported a significant increase in gemcitabine efficacy with increased metastatic inhibition through TG2 knockdown (327). Consequently, both LOX and TG2 significantly impinge upon disease states of tissue fibrosis involving collagen I cross-linking malfunction. They are individually and dually expressed and secreted into the ECM by activated

fibroblasts, directly leading to enhanced collagen cross-linking, stromal remodelling, EMT migration and metastasis in cancer tissues (264,326,332). To this end, it is necessary to investigate their potential association with the PAS (in particular, SerpinB2), specifically one of the main cell types that secrete these enzymes - the fibroblast.

1.6.8 The Fibroblast & ECM remodeling

Fibroblasts are a heterogeneous population of cells of mesodermal origin and the most common cell type of the connective tissue cell family (333). Fibroblasts are able to transform into any of the other members of the family, including cartilage cells, bone cells, adipocytes, and smooth muscle cells (333). These transformations are dependent upon the structural and chemical composition of the surrounding ECM, as well as an individual cell's specific shape and growth cycle (333). The –blast suffix refers to a more active and plastic cell, while fibrocytes are considered less metabolically operational and unchangeable. Fibroblasts are generally distinguished from fibrocytes by their abundance of cytosolic RER and relatively larger cell size (334). Fibroblasts can synthesise and secrete collagens, collagenases, MMPs, TIMPs, uPA, uPAR, SerpinB2, glycosamino- and proteo-glycans, reticular and elastic fibres, fibronectin, many types of growth factors [FGF-2, TGF-β, PDGF, hepatocyte growth factor (HGF), insulin-like growth factors (IGFs), nerve growth factors (NGFs), Wnt1 and EGF], cytokines (IL-1 and others), chemokines [(monocyte chemotactic protein 1 (MCP1) and others], enzymes (LOX, TG2) and glycoproteins of the ECM (43,335-339). They provide the structural stromal network and are actively involved in remodelling this area during pregnancy, wound healing, fibrosis, cancer and other disease states (43). Originally considered a homogenous cell population (334), fibroblasts can exist morphologically in many shapes and sizes, from flat, plump, to spindle- or stellate shaped (activated) with multiple protrusions, processes and generally have a centrally placed oval or round nuclei, depending on the tissues specific properties and functions in which they exist (340). Fibroblasts can exist in dormant/quiescent

states as well as in an activated form (341). Their organ distribution and relative proportion of subpopulations is known to have a considerable impact on the regulation of that specific tissues function in both health and disease (341).

Moreover, fibroblasts have been shown to associate with tumour cells at all stages of cancer progression (43), and their structural and functional contributions to this process are only now beginning to emerge (Fig 1.9). Fibroblastic secretion of VEGF, TGF-β, GFs, chemokines and ECM facilitates the angiogenic recruitment of ECs and pericytes (43,247). Fibroblasts are instigated to transition into an activated 'myofibroblast' state by TGF-β, which ultimately leads to the pro-tumourigenic carcinoma-associated fibroblast (CAF) phenotype. However, not all CAFs originate this way and the CAF phenotype can have multiple cells-of-origin, including resident pericytes, ECs, adipocytes, epithelial cells and bone marrow-derived mesenchymal cells (BMDCs) (42,342,343). CAFs engage in continuous molecular cross talk with tumour cells and have even been reported to arrive at metastatic sites ahead of cancer cells (344).

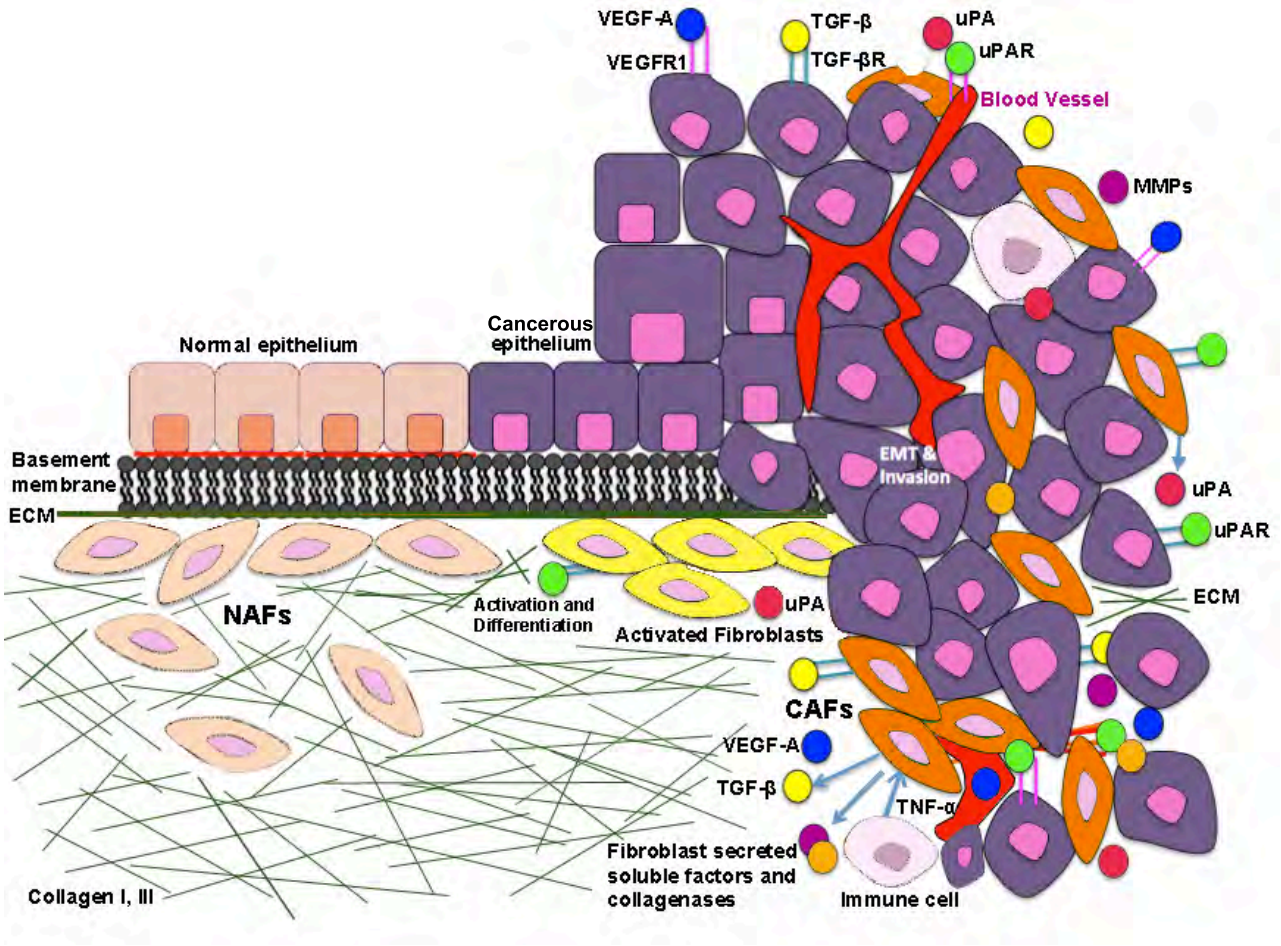

Fig. 1.9. Schematic representation of the biological activities undertaken by fibroblasts within the TME. Non-tumourigenic or normal associated fibroblasts (NAFs) transition to activated fibroblasts, which ultimately lead to pro-tumourigenic carcinoma-associated fibroblasts (CAFs). This figure also shows uPA/uPAR, VEGF-A and its receptor VEGFR-1, as contributing to the TME. Soluble-secreted factors, such as TNF-α, are capable of eliciting multiple effects within the TME [TNF-α induces TGF-β expression in lung fibroblasts (345)]; the figure depicts TGF-ß causing cells to undergo EMT/invasion and proliferation/differentiation of CAF. TGF-β is known to up-regulate expression of SerpinB1 and SerpinB2, MMP-2, TIMP-1 and plasmin (346). TGF-β up-regulates uPA in tumour associated macrophages (TAMs) (347) and stimulates uPA expression in cancer cells (348), while uPA (*via* plasminogen activation) activates secreted latent TGF-β, creating a pernicious positive feedback loop (349).

Traditionally, co-cultures of cancer cells with NAFs and CAFs have been used as *in vitro* models of EMT and tumour invasiveness. In order to test fibroblast cell types within models of collagen crosslinking, stromal remodeling and tumour invasion, more modern 3D systems are being employed.

1.7 2D versus 3D *in vitro* models

Historically, assessment of both genetic and molecular mechanisms has been conducted on tumour cells cultured on a flat monolayer (i.e. 2D *in vitro* system). However, pioneers in the cancer field demonstrated that tissue context profoundly affects tumourigenesis and progression. In 1984, David Dolberg and Mina Bissell demonstrated that the normal chicken embryonic microenvironment could override potent oncogenes [from Rous Sarcoma Virus (RSV)] to cause malignant transformation, and that wounding promoted tumour progression (11). Since that time it has been widely shown that tissue stroma can either promote or inhibit tumour progression (350-352), (353). Advances within biotechnology and increased understanding of biological tissue componency have made it both possible and ideal to develop 3D systems incorporating numerous cell types and ECM molecules and substrates. These models are biomimetic and correctly recapitulate the native *in vivo* scenario of tumour systems (354). It is now well known that cells behave extremely different in a 2D system to that of 3D systems, where spatial limitations do not allow true representation of cell-matrix interactions (354). 3D models show stark variances to 2D in regards to cellular behaviours such as differentiation, proliferation, and gene expression (355-357), allowing for greater assessment adequacy of complex *in vivo* whole organism approaches, where both cell–cell and cell-matrix interactions generate signaling pathways and cellular responses (358). It has been shown that specific genes are expressed in 3D, but not in 2D models. For example, Timpson *et al.* (2011) demonstrated that pancreatic cancer cellular protrusions at the leading edge are RhoA-dependent in a 3D organotypic culture model, but not in 2D cultures (359), and then further reported it's expression *in vivo* (359,360). Linder *et al.* (2003) showed that podosomes and invadopodia on migratory and invasive cells express high levels of actin, only observed in 3D and *in vivo* systems, yet not 2D models (361). It has also been shown that the classical focal adhesion proteins, paxillin and vinculin, were present within focal adhesions *in vivo* at a concentration comparable with cells within 3D matrices (362).

It is now known that 3D systems recapitulate a gamut of autocrine, direct and indirect paracrine signaling and cell type-specific behaviours as occurs *in vivo*, vital for cancer progression and not always observed 2D systems (358).

The increased reliability of 3D systems in pre-clinical application for the assessment of therapeutics in cytotoxicity, tumour progression, invasion and metastasis is unrivalled. Since the advent of 3D cancer models there have been increases seen in drug resistance versus 2D models (363). Such resistance can be attributed to many factors, one of which is limited diffusion through culture matrices facilitating hypoxia, shown to activate cell-survival genes and preclude drug sensitivity (364). Such chemoresistance is often demonstrated in 3D spheroid cultures first and then also observed *in vivo* (365). Another significant factor involved is the ECM and remodeling, undertaken by stromal cells. A recent study by Yip and Cheul (2013) showed using a multicellular 3D culture that hepatic tumour cells displayed increased chemoresistance due to the stromal cells present in their model (366). Talukdar *et al.* (2012) demonstrated in their 3D silk fibroin scaffold model that increased drug was required for cytotoxic effects and invasion inhibition of triple negative MDA-MB-231 breast cancer cells when compared with 2D cultures (367). In addition, 3D spheroids composed of either human or mouse pancreatic ductal adenocarcinoma (PDAC) cells showed an increased in drug resistance compared with 2D cell cultures, reflecting PDAC chemoresistance *in vivo*, believed to be due to integrin signaling effects (368). As such, in order to produce reliable laboratory models for drug design and testing, 3D models are becoming the gold standard.

One of the few downsides to some 3D culture systems is the decreased high-throughput nature in drug screening, time constraints and cost. In addition, much effort is still needed to assure reproducibility, matching of scorer analysis techniques, and automation in order to establish greater consistency. However, once a promising anti-cancer drug is in the pipeline, 3D cancer models are an ideal pre-animal tool to expose any flaws in drug efficacy or potential resistance mechanisms before commencing even more costly and time-consuming *in vivo* systems (358).

Additionally, it was recently proposed that cells can move rapidly through 3D fibrillar matrices *via* a 1D migratory mechanism, attaching to single fibres, not mirrored in 2D matrices (369). This work illustrates that cells interact and move within a wide range of dimensions *in vivo* from 1D, 2D and 3D, and as such it may be necessary to consider utilising both 2D and 3D systems for tumour invasion assessment (358,369). Nonetheless, the field is at a consensus that both the increased mimetic nature and utility of 3D systems in modeling cancer behaviour in live tissue is a significant advantage over 2D models.

Moreover, as aforementioned (refer to section 1.9.3 and 1.10) collagen remodeling and cross-linking is a major facilitator for tumour invasion, which means that pre-clinical cancer testing utilising collagen I is an important element. It has been shown that increasing the number of fibroblasts within collagen matrices can enhance tumour invasion. The addition of matrigel or cell-derived matrix (hyaluronic acid, laminins, FGF) factors to collagen matrices can produce a realistic tissue bed and stimulate the specific sets of surface receptors and activate signaling pathways as occurs within the TME (370). One such 3D investigatory apparatus is the organotypic model.

1.8 The 3D organotypic model

This model allows one to decipher the molecular and cellular mechanisms encompassing tumour and stromal microenvironment interaction. Once a matrix of fibroblasts and Collagen I is produced, it is considered appropriately similar to the tissue of the fibroblast cell origin (371). Formation of the substratum depends greatly upon the fibroblasts used and their ability to package and assemble collagen fibrils and bundles. Upon this stromal matrix is then seeded epithelial carcinoma cells, imitating the *in vivo* monolayer of the majority of early solid tumour tissue microenvironments. Once confluent, the carcinoma cells are then induced to invade into the underlying stroma by a chemotactic air-liquid interface over a predetermined period of time (7-21 days) (Fig 1.10). Quantitation of reductions in the extent of invasion can be used as a measure of anti-invasive

capacity of added compounds and assists in bridging the gap between traditional cell culture systems and animal studies. Additionally, advanced microscopy techniques are providing new insights on how cells behave in their native microenvironment thereby improving understanding of disease progression.

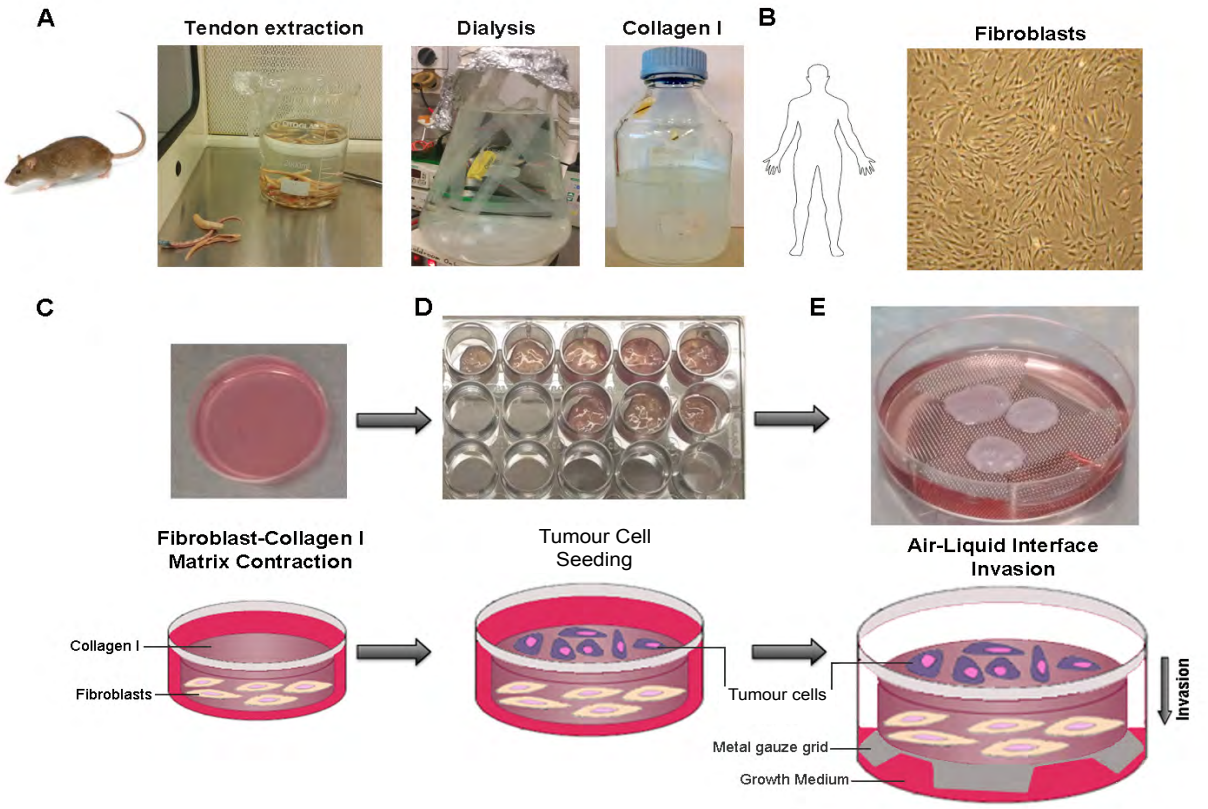

Fig. 1.10. Schematic of preparation and experimental progression of the 3D organotypic assay. A. Initial Collagen I extraction from rat tails is performed *via* tendon dissection, acetic acid extraction, NaCl precipitation and dialysis into 17.4 mM acetic acid, at physiological pH 7.4. **B-C.** Human or murine fibroblasts are co-cultured with harvested Collagen I and the matrices are contracted over a pre-determined time course (7-21 days). **D.** Contracted matrices are then seeded with carcinoma epithelial cells in 24-well plates and allowed to grow to confluency. **E.** After this time, matrices are partially submerged on top of a stainless steel, sterile grid to create an air/liquid interface. The carcinoma cells are then induced to invade into the underlying stroma by the chemo-attractive gradient and quantitation of reductions in the extent of invasion can be used as a measure of anti-invasive capacity of added compounds.

The organotypic model directly utilises this dynamic reciprocity ideal and, in a cancer research setting, offers researchers the foundations to explore the entire process of tumourigenicity, from ECM formation, stromal remodelling, fibroblast migration, autocrine/paracrine and cell-type specific signalling, tumour cell dissemination, migration and fibroblast-epithelial cell interaction. Invading tumour cells can be assessed for

paracrine, autocrine or specific signalling proteins, which can ultimately provide greater *in vitro* fidelity to support further *in vivo* models, reduce animal experimentation and increase drug discovery regimen (372). Previously, such deep insight has been particularly challenging, as these tissues are fairly inaccessible to experimental manipulation and optical observation. In the last decade there have been several novel innovations in 3D culture experimentation, such as the organotypic model. In combination with the capacity to isolate specific genes or proteins and manipulate individual microenvironmental factors, these systems have facilitated the real-time analysis of live biological tissue specimen. These techniques can now be used to visualise the cellular basis of fibroblastic migration, epithelial morphogenesis and migration modality, to test the roles of specific genes in regulating cell behaviour and the nature of cell-ECM interactions within equivalent carcinomatous tissues of the human condition. This is allowing for the elucidation of the contribution of microenvironmental factors to normal and disease processes. Collectively, this novel model can be used to answer fundamental biological questions and generate replacement human tumourigenic tissue, affording the increased fidelity and applicability of novel therapeutic approaches.

1.9 Aims and Project Rationale

From a review of the current literature it can be seen that there are significant roles of SerpinB2 within the TME of both primary and metastatic lesions. Overall, further understanding of the function of SerpinB2 in cell migration, collagen cross-linking, tumour invasion and metastasis is required in order to investigate it's mechanistic roles in tumour progression and/or inhibition. There is potential for the development and future utilisation of SerpinB2 based targeted therapies in the treatment of cancer and/or angiogenesis in patients with uPA over-expressing cancer, thus an additional outcome of this project is to provide further rationale for development of these novel therapeutics. The uPA binding properties of SerpinB2 has been exploited for utilisation in targeted anti-cancer therapeutic design (227,373). SerpinB2-cytotoxin conjugates with improved

pharmacokinetic properties hold promise for further development in this regard (129,130). However, a better understanding of the ideal context and applicatory schedule of benefit for SerpinB2's presence or absence within the TME, should lead to increased efficacy in treating metastatic tumours. As this thesis is focused on the role of the PAS in ECM remodeling, tumour invasion and metastasis, the cancers for experimentation were chosen with relation to their expression of PAS components as well as their stromal environment and ECM remodeling impingent on invasiveness. As Pancreatic ductal adenocarcinoma (PDAC) and triple negative breast cancer (TNBC) both utilise the PAS and form solid tumour malignancies characterised by a high stromal content, they were employed in this study. Thus, the overall aim of this thesis was to further investigate whether the primary role of SerpinB2 in both PDAC and TNBC cell invasion is through a uPA inhibitory role and/or additional mechanisms unrelated to protease inhibition. In order to investigate these potential activities, the specific aims of this study were:

1. To scrutinise the spatiotemporal effects of SerpinB2 expression, through development of lentiviral systems to modulate SerpinB2 gene expression and GFP reporter gene applications in epithelial and fibroblastic cell lines, respectively.
2. To elucidate the effects of SerpinB2 in collagen cross-linking and ECM remodeling using wt & SerpinB2$^{-/-}$ murine embryonic fibroblasts (MEFs) and functional imaging in a 3D organotypic contraction model.
3. To define the mechanism of SerpinB2 regulation in tumour invasion and metastasis in breast and pancreatic tumour organotypic invasion models, utilising advanced functional imaging assessment.
4. To investigate *in vivo* effects of modulated tumour cell SerpinB2 expression on tumourigenesis, collagen ECM remodeling and local invasion in an allograft mouse model of pancreatic cancer and a xenograft model of breast cancer.

CHAPTER 2

PRODUCTION OF LENTIVIRAL VECTORS TO ASCERTAIN THE SPATIOTEMPORAL EXPRESSION OF SERPINB2 WITHIN THE TME

CHAPTER 2

PRODUCTION OF LENTIVIRAL VECTORS TO ASCERTAIN THE SPATIOTEMPORAL EXPRESSION OF SERPINB2 WITHIN THE TME

2.1 INTRODUCTION

In order to elucidate underlying cell-specific effects of the spatiotemporal expression of SerpinB2 within the TME, the expression of SerpinB2 within epithelial cells was manipulated, through the use of third-generation lentiviral vectors. These lentiviral systems were utilised as they provide a fast and efficient means for modulating gene expression and GFP knock-in for reporter gene applications in live cell imaging of collagen remodeling and the TME (372).

2.1.1 Lentivirus

Lentiviruses belong to the large family, Retroviridae, spherical virions ~100 nm in diameter, with an outer envelope displaying glycoproteins. Two copies of linear viral RNA genome (approximately 10 kb) are enclosed, which contain three essential genes, *gag*, *pol* and *env* (374). The *pol* gene encodes three important viral enzymes: reverse transcriptase, protease and integrase. The *gag* gene encodes for the structural proteins: the capsid, nucleocapsid and matrix (375). Proteins are produced by a proteolytic separation of the *gag-pol* precursor (376) (Fig. 2.1). The *env* gene codes for the viral envelope glycoproteins, which bind and attach to target cell-surface receptors. Upon internalisation into a host cell, a pre-integration complex is formed (374), which is then transported into the nucleus, allowing transduction within both dividing and non-dividing cells (377,378). The viral enzyme integrase then initiates the proviral DNA integration within the host cell's genome. This process is made easier by long terminal repeats (LTRs), which can occur hundreds or thousands of times at both the 5' and 3' ends, acting as promoters to aid in viral DNA synthesis, integration and transcription regulation (379). Lentiviruses contain a complex genome, able to transduce a significant amount

of RNA into the DNA of a mammalian cell, irrespective of cell cycle phase (380-383). This is a valuable feature for utilising lentiviral vectors in modulating gene expression, with the ability to integrate and achieve long term expression in biomedical research, making them attractive tools for gene therapy (384).

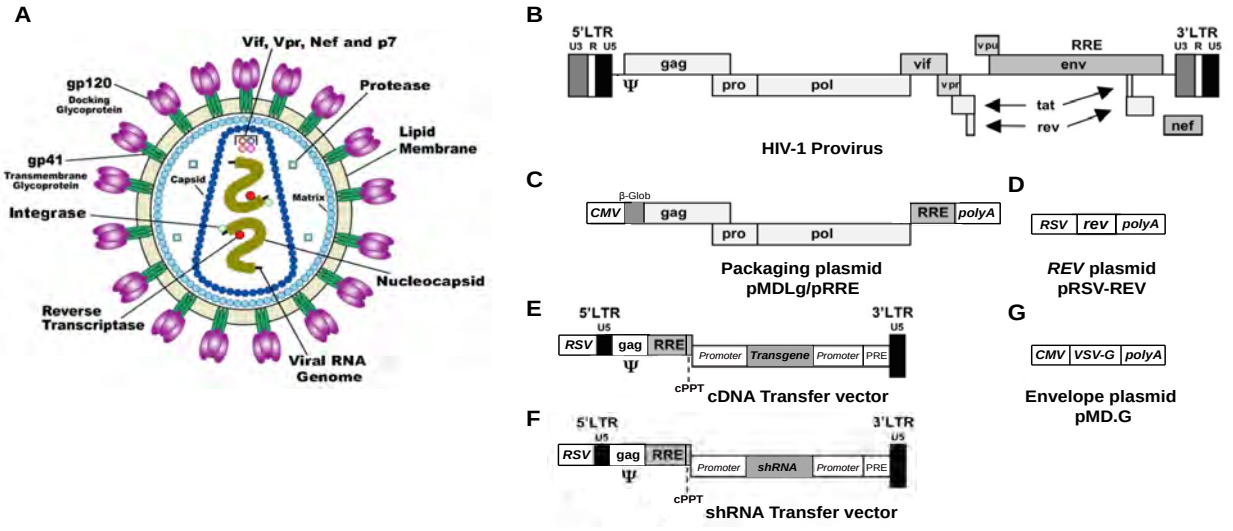

Fig. 2.1 A. Structure of wild-type lentivirus. Two ssRNAs are present within the nucleocapsid, covered by a capsid. The outer lipid membrane is formed from the host cell and is the surface is coated in glycoproteins. Lentiviruses contain the important viral enzymes: integrase, protease and reverse transcriptase (description is provided in the text). **B.** The wild-type HIV-1 genome – through differential RNA splicing, can obtain nine gene products. The viral LTRs, viral gene reading frames, Psi packaging signal (Ψ), and rev-responsive element (RRE) are shown. **C-F.** The third generation lentiviral vector system. **C.** The packaging plasmid (pMDLg/pRRE) contains both *Gag* and *Pol* genes under the stimulus of the CMV promoter and polyadenylation site (polyA) of the human β-globin gene. **D.** *Rev* cDNA-expressing plasmid, pRSV-Rev. **E-F.** These vector plasmids contain HIV-1 cis-acting sequences and an expression cassette for the transgene (cDNA or shRNA). Only the transgene is transported to target cells and no HIV-1 LTRs. **G.** The envelope plasmid, pMD.G – a vesicular stomatitis virus (VSV) pseudotype. Co-transfection of all vectors into dividing and non-dividing cells provides genomic integration of a specific transgene for gene expression modulation and concurrent experimentation. Only significant sections of each construct are shown. Adapted from (385).

2.1.2 Lentiviral transfer vectors used for expression of cDNA and shRNA

Lentiviral vectors are based on the first viral vectors made by Nobel laureate, Paul Berg. Berg and colleagues constructed hybrid viruses containing SV40 monkey virus and λ phage DNA segments, and were the first to propagate their replication inside cultured monkey cells (386). To this day SV40 viral polyadenylation sequences are used downstream of the 3' LTR of the latest generation lenti-vectors, as these greatly reduce the chances of transcriptional interference (387).

Lentiviruses can be stably integrated into dividing and non-dividing cells for long term transgene expression,

both *in vitro* and *in vivo* (379,382,388). Successful preclinical studies employed for treating Parkinsons, Alzheimers and Huntingtons diseases have been undertaken, as well as for the correction of genetic disorders such as immunodeficiencies and haemoglobin disorders (378,389,390). RNA interference has been readily used as a robust tool to down-regulate specific gene expression. Lentiviral vectors enclosing short hairpin RNA (shRNA) are extensively shown to induce efficient knockdown of specific individual and multiple cellular genes (391) (Fig. 2.2), as well as utilisation for the creation of transgenic animals (392).

A large effort has been made in the field to remove all non-essential HIV-1 sequences for viral replication, thus only viral proteins are transcribed within target host cells and the only genetic material that is incorporated into the transfer vector is the transgene cassette with non-coding viral elements [such as LTRs, Psi packaging signal, Rev responsible element (RRE)] (refer to Fig. 2.1). Another greate benefit of lentiviral vector systems are their low immunogenicity invoked within the host. However, there have been reports of immune responses directed against the VSV-G envelope (393). Due to the complexity of lentiviral vectors, and the adverse risks of HIV gene incorporation, the third generation lentiviral vectors were formulated with three or four plasmid lenti-vector production systems, with marginal sequence homology (394). At present, third generation lentiviral vectors are the most readily used vector systems for delivery of short-interfering RNA (siRNA) to cells (395) (refer to Fig. 2.1).

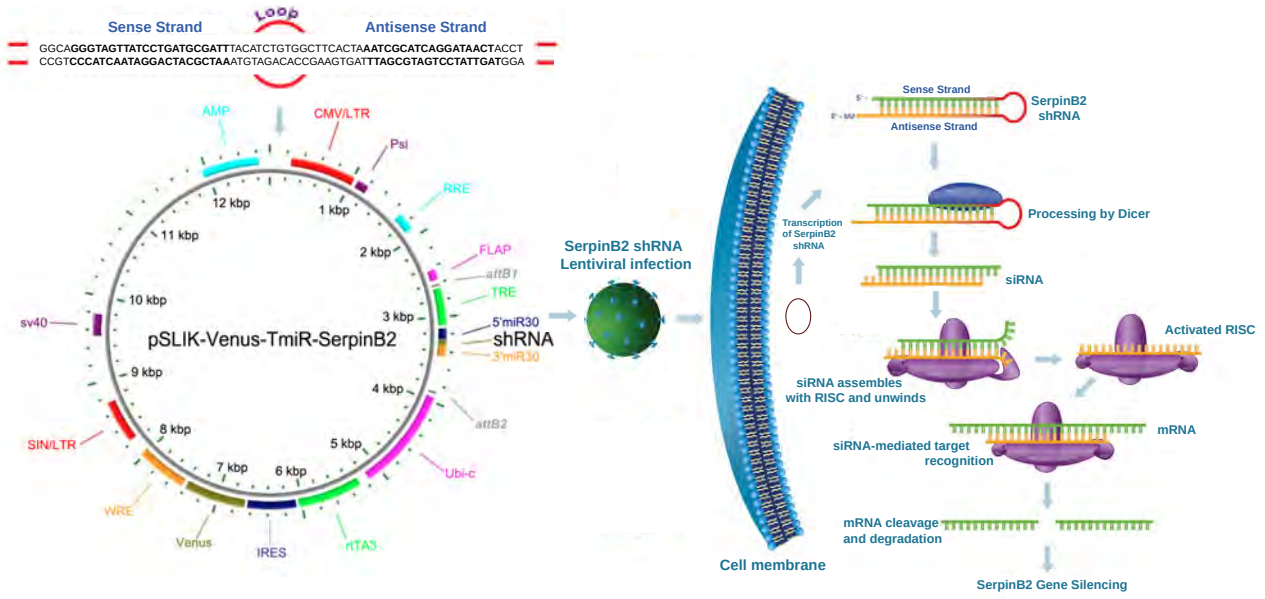

Fig. 2.2. Mechanism of RNA interference. To understand the effect of SerpinB2 knockdown, a lentiviral vector was created with a sequence of SerpinB2 that was cloned into a pEN_TmiRc3 plasmid for use with the pSLIK system (single lentivector for inducible knockdown). This lentivirus is then used to infect mammalian cells. In this process, SerpinB2 shRNA expressed from pSLIK lentivirus forms a double stranded stem-loop structure, which is cleaved at the loop by the cytosolic enzyme, DICER. This cleavage causes SerpinB2 shRNA to be integrated into the RNA-induced silencing complex (RISC). Herein, RISC guides the Serpin B2 shRNA strand to its complementary mRNA target, cleaves the specific SerpinB2 mRNA sequence and then targets it for degradation - coordinated by SLICER (396) .

2.1.3 Third generation lentiviral vectors

The overall difference between the second and third generation systems of lentiviral vectors is the increase in the safety of their organisation. This has been achieved through splitting up the *gag, rev* and *pol* packaging genes into two plasmids as well as splitting the *gag/gag-pol* gene into several parts (397). In addition, third generation lentiviral systems have no *tat* regulatory gene and the development of the self-inactivating (SIN) vector was accomplished by creating deletions in the 3´LTR (398,399). This abolished any LTR transcriptional activity, thus reducing the risk to form RCL and minimising the chance of endogenous gene interference (399-401).

Third generation lentiviral vector systems utilise four-plasmids, as shown in Fig. 1.1, that contain HIV-1's *gag, pol*, and *rev* genes inserted between LTRs with promoter activity at both ends. Through separation of the vector system into four plasmids [(three helper – one envelope (pMD.G) and two packaging vectors (pMDLg/pRRE and pRSV-Rev) - and one transgene vector) refer to Fig. 2.3], there is a large increase

required in the number of recombination events in order to form a complete replicative competent virus. In this respect, to date there have been no reported cases of replication competent lentiviruses (RCLs) occurring (385). With the addition of an extra plasmid, third generation lentiviral systems are potentially more difficult to use because they require transfection with four separate vectors to create fully operative lentiviral particles. Furthermore, third generation lentiviruses contain the incorporation of a central polypurine tract (cPPT) and a post-transcriptional regulatory element from woodchuck hepatitis virus (WPRE) into the 3′end of the transfer vector. This has been shown to improve transgene expression (402), increase transduction efficiency, nuclear localisation and the total amount of RNA integrated into the targeted host cell genome (403) (404). Newer generations of lentiviral systems have increased the application for viral vectors, including functional gene restoration and animal transgenesis, standard cellular biology and cancer research, and other types of clinical research (405). One of the latest lentiviral construction methods, based on a hybrid virus system, is the Gateway® lentivirus vector system, by Invitrogen™ (CA, USA). This system was used in this project as it offered a rapid and highly efficient site-specific recombination technology, through taking advantage of the properties of bacteriophage lambda. Lambda recombination happens within specific *att*achment (*att*) sites: *att*B on *E. coli's* chromosome with *att*P on the lambda's chromosome (406). These *att* sites have been well-characterised (407); upon lambda adherence and integration, recombination occurs between *att*B and *att*P sites, giving rise to *att*L and *att*R sites (406) (refer to Fig. 2.1).

Moreover, within *E. coli*, the Tet repressor protein (TetR) negatively controls the tetracycline-resistance operon (408). TetR blocks gene transcription through binding tet operator sequences (tetO) when Tetracycyline is absent (409). In the presence of Tetracycline, TetR cannot bind tetO and gene transcription can occur (410). Collectively, TetR and tetO are the foundation for the third generation Gateway® Tet vector systems, regulating gene expression (411). The Tetracycline responsive promoter element of the Gateway® TetR vector is inactive in the absence of tetracycline (or more frequently used, doxycycline). Once doxycycline is applied to the culture media (at a concentration that does not otherwise affect mammalian cell

behaviour), the tTA is allosterically modulated to bind to the CMV promoter and drive transgene expression (375). Thus, when co-transfected into mammalian packaging cells with Gateway® Lenti transgene vectors, the lentivirus produced to transduce target cells generates an effective apparatus to control the expression level of a specific gene of interest simply through adjusting the concentration of doxycycline, the system's inducer (Fig. 2.3).

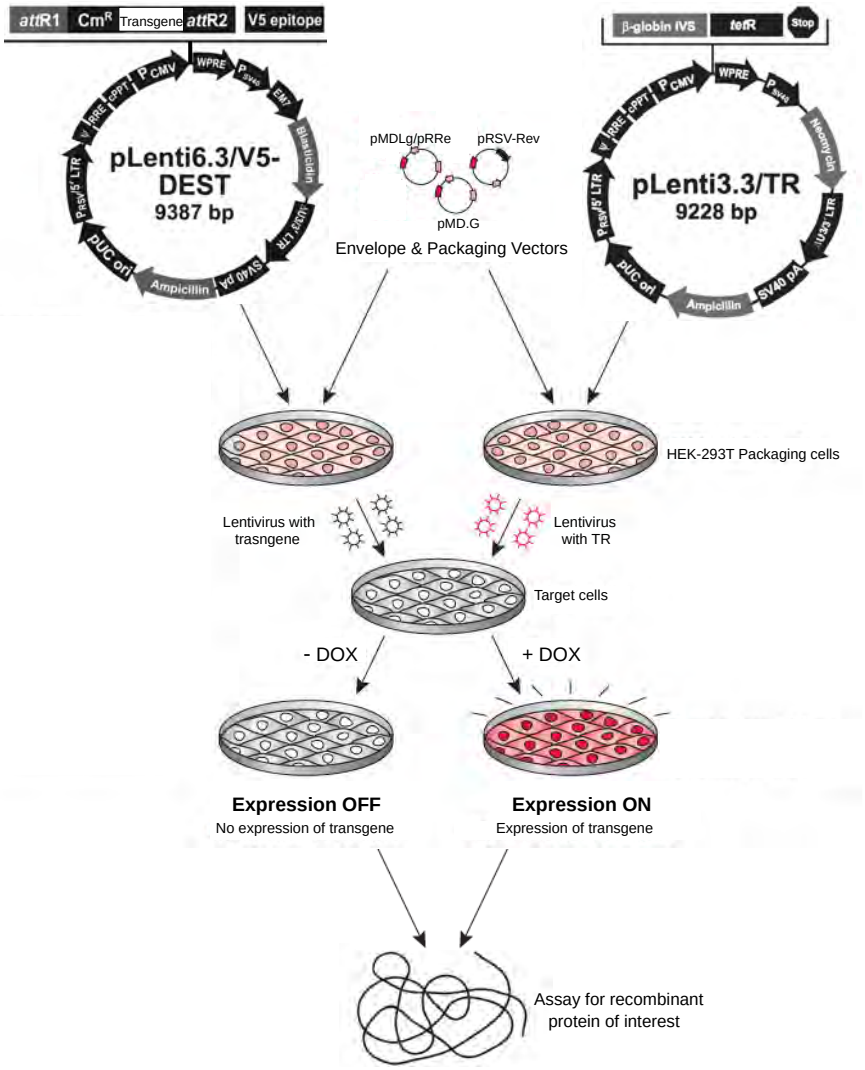

Fig. 2.3. Production of an inducible gene expression system. Co-transfection of envelope (pMD.G) and packaging vectors (pMDLg/pRRE and pRSV-Rev)(Gateway® Tet vector Systems) into 293T cells are used to generate high-titre lentiviral particles from both the pLenti3.3/TetR vector and pLenti6.3/V5-DEST vector, which contains the gene of interest. Target cells are then simultaneously co-transduced with the two lentiviruses. After antibiotic selection and culturing for an additional 48 h (+/– Doxycycline addition), the cells are harvested for recombinant gene analysis.

As this project involved both increased and decreased expression of SerpinB2, as well as GFP knock-in for reporter gene applications, different third generation lentiviral vectors were required to be constructed (shown in Table 1).

Table 2.1. Third-generation lentiviral transfer vectors used for expression of cDNA and shRNA knockdown.

cDNA Transfer Vector	Promoter	Cloning	Selection	Fusion tag	Citations
pLenti6.3/TO-DEST-V5	(TO)	Gateway	Blasticidin S	C-terminal V5	(398)
pLV-eGFP	CMV	MCS	GFP fusion	C-terminal EGFP	(398)
shRNA Transfer Vector	**Promoter**	**Cloning**	**Selection**		**Citations**
pSLIK	TRE	BfuAI/Gateway	UbC-Neo/Venus	--	(412)

The specific aims of this chapter were to:

1. Design and construct lentiviral vectors for the knockdown (shRNA) of SerpinB2; overexpression (cDNA) of SerpinB2, ^{R380A}SerpinB2 (inactive RCL mutant), and their ΔCD loop counterparts, SerpinB2 ΔCD loop and ^{R380A}SerpinB2 ΔCD loop.
2. Optimise and characterise these vectors within MDA-MB-231 mammary epithelial carcinoma cells.
3. Stably transduce GFP into both wild-type and SerpinB2$^{-/-}$ Murine Embryonic Fibroblasts (MEFs) for cell reporter functioning in proceeding experimental models, in Chapters 3,4 and 5.

2.2 METHODS

2.2.1 Cell lines and culture conditions

The invasive triple-negative (HER2-, PR- and ER-) human mammary epithelial carcinoma cell line MDA-MB-231 (luciferase expressing, referred to as MDA-MB-231) was originally purchased from American Type Culture Collection (ATCC, VA, USA) was maintained in Roswell Park Memorial Institute medium (RPMI-1640), supplemented with 10% fetal bovine serum (FBS), 10 mM HEPES buffer and 125 IU insulin, in a humidified 5.0% CO_2 atmosphere at 37 °C. Murine embryonic Fibroblasts (MEFs) originally isolated from wild-type and SerpinB2$^{-/-}$ mice (203) were a gift from Dr Wayne A Schroder (QIMR Berghofer Medical Research Institute, Australia). MEF primary cultures were then continually passaged in RPMI-1640 containing 10% FBS at 37°C with 5% CO_2 until spontaneous immortality was obtained. Identity of wild-type and SerpinB2$^{-/-}$ cells was confirmed by RT-qPCR (data not shown) and western blot. All experiments in this study were carried out using immortalised cells (unless specified otherwise) that were passaged ≤10 times before experimental use. Furthermore, passage-matched cells were used for the majority of experiments within this study. All cell cultures were routinely tested in-house for absence of mycoplasma contamination using the MycoAlert™ Mycoplasma Detection Kit (Lonza, Switzerland).

2.2.2 Generation of SerpinB2 cDNA and shRNA

Experimental design was carefully reviewed to minimise off target effects and to create the most efficient means of stable knockdown or overexpression of SerpinB2. In order to generate SerpinB2 lentiviral constructs, full length His-tagged SerpinB2, inactive ^{R380A}SerpinB2 and their ΔCD loop forms, SerpinB2 ΔCD loop and ^{R380A}SerpinB2 ΔCD loop, were created in our laboratory in pQE1 and pQE9 expression systems (Qiagen, Netherlands), respectively (176). Plasmids were prepared using the Wizard Plus SV Miniprep system (A1460, Promega) according to manufacturer's instructions. Transfections were performed using midiprep and maxiprep DNA only. Midiprep and Maxiprep DNA were prepared using the QIAGEN Plasmid Midi &

Maxi Kit (12163, QIAGEN), according to manufacturer's instructions. SerpinB2 plasmids were digested with BamHI and PstI enzymes and checked for correct size *via* agarose gel electrophoresis. Constructs encoding a hairpin targeting SerpinB2 were designed to knock down gene expression. SerpinB2 hairpins were created at two regions within SerpinB2 mRNA sequence, and oligonucleotides were purchased and supplied by the Garvan Institute's ACRF Facility for the Molecular Genetics of Cancer (Darlinghurst, Sydney) (Fig. 2.4). These DNA sequences were cloned into the pEN_TmiRc3 vector for use with the pSLIK system (412).

GTAACAACTCTCAGAGGAGCATTGCCCGTCAGACAGCAACTCAGAGAATAACCAGAGAACAACCAGCATTTCTTGCACT
ACAACTTGCTTAAGCTCTTACACTTCATAGTGAAGCTATGCACCACCGAGTGAAGCGATGTGGAACATTGGAAAGAGTG
GGCTTCCTTAGACAGACCTGGGCTTGAATCCCTGCTCCACTACCTACCAGCTGTGTGACCTTATACAAGTTACTTAATG
TTTCTGAGCATCAGGATATAATCTATAAAATAGGGAGAATCACCTCTACCTCATACAGATTCTGCAAAGATTAAACGAG
GAGAGGAGATTGAAACAATGGAGGATCTTTGTGTGGCAAACACACTCTTTGCCCTCAATTTATTCAAGCATCTGGCAAA
AGCAAGCCCCACCCAGAACCTCTTCCTCTCCCCATGGAGCATCTCGTCCACCATGGCCATGGTCTACATGGGCTCCAGG
GGCAGCACCGAAGACCAGATGGCCAAGGTGCTTCAGTTTAATGAAGTGGGAGCCAATGCAGTTACCCCCATGACTCCAG
AGAACTTTACCAGCTGTGGGTTCATGCAGCAGATCCAGAAGGGTAGTTATCCTGATGCGATTTTGCAGGCACAAGCTGC
AGATAAAATCCATTCATCCTTCCGCTCTCTCAGCTCTGCAATCAATGCATCCACAGGGAATTATTTACTGGAAAGTGTC
AATAAGCTGTTTGGTGAGAAGTCTGCGAGCTTCCGGGAAGAATATATTCGACTCTGTCAGAAATATTACTCCTCAGAAC
CCCAGGCAGTAGACTTCCTAGAATGTGCAGAAGAAGCTAGAAAAAAGATTAATTCCTGGGTCAAGACTCAAACCAAAGG
CAAAATCCCAAACTTGTTACCTGAAGGTTCTGTAGATGGGGATACCAGGATGGTCCTGGTGAATGCTGTCTACTTCAAA
GGAAAGTGGAAAACTCCATTTGAGAAGAAACTAAATGGGCTTTATCCTTTCCGTGTAAACTCGGCTCAGCGCACACCTG
TACAGATGATGTACTTGCGTGAAAAGCTAAACATTGGATACATAGAAGACCTAAAGGCTCAGATTCTAGAACTCCCATA
TGCTGGAGATGTTAGCATGTTCTTGTTGCTTCCAGATGAAATTGCCGATGTGTCCACTGGCTTGGAGCTGCTGGAAAGT
GAAATAACCTATGACAAACTCAACAAGTGGACCAGCAAAGACAAAATGGCTGAAGATGAAGTTGAGGTATACATACCCC
AGTTCAAATTAGAAGAGCATTATGAACTCAGATCCATTCTGAGAAGCATGGGCATGGAGGACGCCTTCAACAAGGGACG
GGCCAATTTCTCAGGGATGTCGGAGAGGAATGACCTGTTTCTTTCTGAAGTGTTCCACCAAGCCATGGTGGATGTGAAT
GAGGAGGGCACTGAAGCAGCCGCTGGCACAGGAGGTGTTATGACAGGGAGAACTGGACATGGAGGCCCACAGTTTGTGG
CAGATCATCCTTTTCTTTTTCTTATTATGCATAAGATAACCAACTGCATTTTATTTTTCGGCAGATTTTCCTCACCCTA
AAACTAAGCGTGCTGCTTCTGCAAAAGATTTTTGTAGATGAGCTGTGTGCCTCAGAATTGCTATTTCAAATTGCCAAAA
ATTTAGAGATGTTTTCTACATATTTCTGCTCTTCTGAACAACTTCTGCTACCCACTAAATAAAAACACAGAAATAATTA
GACAATTGTCTATTATAACATGACAACCCTATTAATCATTTGGTCTTCTAAAATGGGATCATGCCCATTTAGATTTTCC
TTACTATCAGTTTATTTTTATAACATTAACTTTTACTTTGTTATTTATTATTTTATATAATGGTGAGTTTTTAAATTAT
TGCTCACTGCCTATTTAATGTAGCTAATAAAGTTATAGAAGCAGATGATCTGTTAATTTCCTATCTAATAAATGCCTTT
AATTGTTCTCATAATGAAGAATAAGTAGGTATCCCTCCATGCCCTTCTGTAATAAATATCTGGAAAAAACATTAAACAA
TAGGCAAATATATGTTATGTGCATTTCTAGAAATACATAACACATATATATGTCTGTATCTTATATTCAATTGCAAGTA
TATAATAAATAAACCTGCTTCCAAACAACAATAAAAAAAAAAAAAAA

Fig. 2.4. mRNA sequence of SerpinB2 and shRNA hairpin mRNA sequences. Two hairpin loops (shRNA1 and shRNA2) were created for SerpinB2 gene editing, and these are displayed within the SerpinB2 mRNA sequence, highlighted in green (shRNA1) and blue (shRNA2), respectively.

2.2.3 SerpinB2 expression clone generation

Using the purified SerpinB2 plasmids as described in Section 2.2.2, homologous recombination attachment (*att)* sites, TGTTCAAACATGTTTTTTCGTCCGA (*att*B1) and TGGGTCGAAAGAACATG (*att*B2), were attached with a kozak sequence - (gcc)gccRccAUGG, *via* O/N PCR. Two separate PCR experiments were utilised in order to compare final purity of SerpinB2 expression clones using the pfu Turbo® (600250, Agilent, CA, USA) and Phusion® (E0553, New England Biolabs, MA, USA) PCR kits. Both were made up to final volumes of 50uL, using 50ng DNA for the pfu Turbo®, and 150ng DNA for the Phusion® PCR experiments. The amplification was performed using the following parameters: initial denaturation at 98°C for 30 sec and then 35 cycles of amplification consisting of 98°C for 10 s, 60°C for 10 s, and 72°C for 10 s. Primer sequences for PCR amplification of SERPINB2 mRNA were GCATGTTCTTGTTGCTTCCA (forward) and TTCAGCCATTTTGTCTTTGC (reverse).

2.2.4 Creation of entry vectors

Invitrogen Gateway® (California, USA) BP Clonase (11789-013) reactions were performed to create pDONR221-SerpinB2 entry vectors. *att*B-SerpinB2 PCR products (30ng/μL) and pDONR plasmid (150 ng/μL) were incubated with BP enzyme mix for 2 h. Each reaction was then transformed into heat-shock competent DH5α E. coli and grown O/N at 37°C. Cultures were grown and the plasmid DNA purified using Wizard® Plus SV Miniprep DNA purification system (Promega). Correct insertion by gel digest and sequencing using the following primers (3.2 pmol) M13 Fwd 5' –GTAAAACGACGGCCAGT – 3', M13 Reverse 5' – CAGGAAACAGCTATGAC – 3'. Sequencing was undertaken as previously specified using 20 ng per sample and genomic data was analysed using 4Peaks V1.8 software (Amsterdam, Netherlands). Sequences were again analysed using Finch TV analysis program (Geospiza Inc, USA). Translated sequences were BLASTed using blastx (NCBI; NIH, USA) in order to ensure correct sequences were maintained and in frame.

2.2.5 Creation of destination vectors

The pDONR221 entry plasmids (50 ng) were incubated with Gateway LR clonase enzyme mix (11791-019) and pLenti6.3/TO-DEST-V5 destination vector (150 ng) for 2.5 h at RT. Each reaction was then transformed into DH5α *E.coli* as before and grown O/N on Ampicillin agarose at 37°C. Cultures were grown and plasmid DNA was purified and sequenced as aforementioned in Section 2.2.4. Sequences were again analysed using Finch TV analysis program, translated and then BLASTed versus their appropriate SerpinB2 template, again using blastx. Once correct sequence homology was validated for each construct, lentiviral infections were undertaken. A summary of the experimental procedure for lentivector production is illustrated above in Fig. 2.3.

2.2.6 Transient transfections using SerpinB2 mutant cDNA

Prepared destination vector cDNA was transiently transfected into adherent HEK-293T cells, in order to ascertain if the produced SerpinB2 mutants could facilitate modified SerpinB2 expression. 5.0 x 10^5 HEK-293T cells/well were plated in a 6-well plate. After 2 days, when cells had reached 90-95% confluency, 2 µg of plasmid DNA was incubated with 10 µL Lipofectamine® 2000 (ThermoFisher) in 1.75 mL total volume Opti-MEM media (31985-070, Life Technologies) for 10 min. After this time, the HEK-293T cells were transfected with either 500 µL DNA/Lipofectamine mix, or 500 µL Opti-MEM for control wells. Media was changed in all wells after 4-6 h (as Lipofectamine can be toxic to cells) with 2mL DMEM/10% FBS and cells were assayed for transgene expression 48 h after this time.

2.2.7 Lentivirus production

In order to create lentiviral particles that could be used to infect mammalian cells of choice and produce stable overexpression or knockdown of target genes, the destination vectors produced above were transfected into the Human embryonic kidney cell line, HEK-293T. The destination vectors, pLenti6.3 LacZ (overexpression control) and pLV411 shGFP (knockdown control), were a kind gift from colleague Dr Robert Shearer at the

Kinghorn Cancer Centre, Sydney. All destination vectors, wt SerpinB2, full-length ^{R380A}SerpinB2, SerpinB2 ΔCD loop and ^{R380A}SerpinB2 ΔCD loop as well as control vectors, LacZ (overexpression) and shGFP (knockdown), were pre-incubated with Gateway packaging plasmids (pMDLg/pRRE, pRSV-Rev and pMD.G) for 30 min at RT in Opti-MEM (31985-070, Life Technologies) and Lipofectamine®, then applied to HEK-293Ts [CRL-3216, American Type Culture Collection (ATCC, VA, USA)] (2.0 x 10^6 seeded 24 h prior) in a 10 cm dish and incubated O/N at 37°C in 5% CO_2. After 24h, Optimem media was changed with 10 mL fresh DMEM/10% FBS (Gibco) and incubated for another 24 h. At this time, the lentivirus has been created and is collected in 1 mL aliquots and stored at -20°C, or used to infect any mammalian cell line.

2.2.8 Viral titre optimisation for lentiviral transgene repression

To ascertain the ideal repression concentrations for the tetracycline repression of the CMV promoter, MDA-MB-231 (Luciferase) cells were stably transduced using a two-vector expression system (A11144, Invitrogen). β-galactosidase (β-gal, blue) (pLenti6.3 LacZ) expression construct was co-transduced with increasing levels of the pLenti3.3TetR/CMV Vector. Three different dilutions of TR element construct were chosen for infection – 1/10 (high repression), 1/100 (mid repression) and 1/1000 (low repression). After 72 h, antibiotic selection was undertaken and 48 h post-induction of expression using 1 μg/mL doxycycline (Dox, 631311, Clontech), 231 cells were incubated with X-gal at 37 °C for 2 h. This LacZ gene was was chosen as a suitable control vector for the concurrent experiments as it is a extensively researched, reliable reporter gene and also because translated β-gal would put similar amounts of ribosomal and overall cellular mechanical strain to over-express.

2.2.9 Lentiviral infection

In order to infect adherent mammalian cell lines, each line was seeded (at 1.0 x 10^5 per well of a 6 well plate) to be sub-confluent on the day of infection (~60% confluency). Cells must grow for at least 72 h before adding antibiotic selection, thus cells were seeded at a density to ensure that they would not be over confluent too

quickly. Infections were performed in a 6-well plate, with virus diluted in normal media at 1/50, 1/100 and 1/100 dilutions. This allowed for different dilutions of virus to be tried as if the viral construct packages inefficiently (LTR bp length > 7kbp) then optimal concentration of the virus could be found. Viral dilutions were made up in 10 mL of media with 8 µg/ml Polybrene (107689, Sigma). Media was aspirated from the adherent cells and diluted virus added on top of the cells. After 24 h, viral media was replaced with fresh media to remove any excess virus not up taken by the cells. After 72 h from addition of lentivirus, antibiotic selection with Blasticidin S (R21001, Sigma) was added for overexpression pLenti constructs, at 6 µg/ml: initial selection, or 3 µg/ml: maintenance; or G418 (10131027, ThermoFisher) was added for knockdown pSLIK constructs (at 1 mg/mL: initial selection, or 0.5 mg/mL: maintenance) or sorting for fluorescent markers with a FACS Vantage instrument (Becton Dickinson, USA) was undertaken. To initiate SerpinB2 (and other gene construct) overexpression or knockdown, 1 µg/ml Dox was added to the media, to remove Tet repression upon the promoter, allowing for SerpinB2 transcription (refer to Fig. 2.3). Gene knockdown was confirmed by whole cell lysis, protein collection, western blot and immunofluorescence. Once selected, cells containing SerpinB2 shRNA (and wild-type cell controls) were transduced with a VSV-G pseudotyped lentivirus encoding pLV411 vector GFP. GFP-positive cells were then enriched by sorting with a FACS Vantage instrument (Becton Dickinson, USA).

2.2.10 Characterisation

2.2.10.1 Western blotting

Total cell lysates were prepared in standard radioimmunoprecipitation assay buffer (RIPA) extraction buffer supplemented with a protease inhibitor cocktail containing PMSF and EDTA (1183617001, Roche Diagnostics). 20-30µg of protein from these samples were separated under non-reducing conditions by 10% sodium dodecyl sulfate polyacrylamide gel electrophoresis (SDS-PAGE) and transferred to PVDF membranes (BioRad). The membranes were immunoprobed overnight at 4°C with antibodies against SerpinB2 (ab137588,

Abcam, Cambridge, UK) and Actin (ab3280, Abcam) or GAPDH (TA150046, OriGene, Maryland, USA) as per standard protocol (refer to Supplementary Antibodies Table of Appendix). The membranes were incubated with the appropriate HRP-conjugated secondary antibody and then developed according to enhanced chemilluminescence protocol (32106, ThermoScientific).

2.2.10.2 Immunofluorescence

For immunofluorescence analysis, MDA-MB-231 tumour cells (1.0 x 10^4 per well in a 6 well plate) were grown on cover slips, in the presence or absence of Dox (1 μg/mL). Cells were fixed using 4% paraformaldehyde for 10 min at RT and then blocked and processed with SerpinB2 antibody (Abcam), as described in Supplementary Antibodies Table of Appendix (Table A1). Cover slips were then placed onto glass slides mounted with Vectashield and cells imaged using a Leica DMI 6000 fluorescence microscope (Wetzlar, Germany).

2.2.10.3 Proliferation assays

All assays were performed at 37°C and 5% CO_2 using the IncuCyte ZOOM imaging system (Essen BioScience). Cellular proliferation was measured using a confluence mask algorithm optimised for MDA-MB-231 human mammary carcinoma cells. Wells were seeded with 1.0 x 10^4 MDA-MB-231 cells in a 24-well plate in triplicate and monitored at 2 h intervals until confluence was reached. Proliferation was expressed as percentage confluence over time.

2.3 RESULTS

2.3.1 Enzyme digestions and AGE

The PCR amplification of all SerpinB2, ^{R380A}SerpinB2, GFP and LacZ constructs yielded good product concentrations. Restriction digest reactions were performed with PstI enzyme on PCR products (with *att*B sites) of full length His-tagged SerpinB2, inactive ^{R380A}SerpinB2 and their ΔCD loop forms (as well as GFP and

LacZ, data not shown). These were checked for correct size *via* AGE (Fig. 2.5). Analysis of the DNA bands observed in the 1% agarose gel revealed dense bands migrating at ~1150 bp and ~1250 bp, consistent with the expected sizes of ^{R380A}SerpinB2 ΔCD loop mutant and full-length ^{R380A}SerpinB2, respectively (Fig. 2.5, Lane 1,2). Another band migrating at ~1150 bp was also observed (Fig. 2.5, Lane 3), which is consistent with the calculated size of SerpinB2 ΔCD loop.

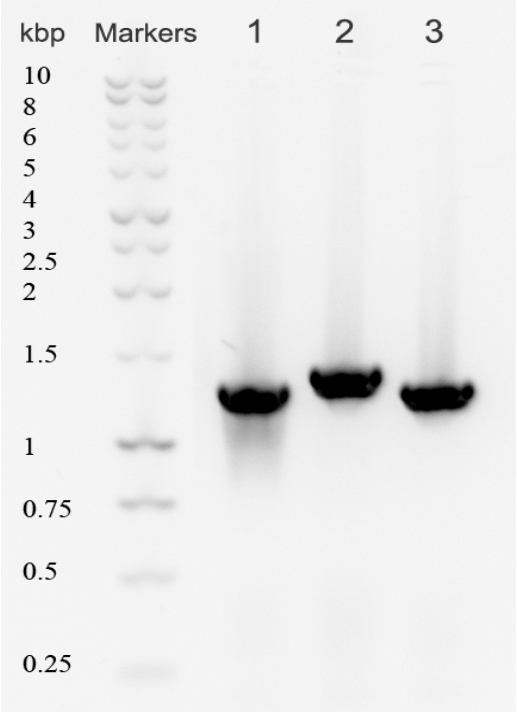

Fig. 2.5. AGE analysis of PCR restriction digest reactions. Restriction digestions were performed with PstI enzyme, fractioned on 1% agarose and stained with Ethidium bromide. Lane 1 – Inactive ^{R380A}SerpinB2 ΔCD loop cDNA, Lane 2 – Full length ^{R380A}SerpinB2 cDNA, and Lane 3 – SerpinB2 ΔCD loop cDNA.

2.3.2 Entry clone analysis

After incubation of PCR *att*B-constructs with pDONR entry vectors, subsequent transfection into DH5α *E. coli* and O/N growth, entry clone DNA extraction and purification was undertaken. Sequenced samples were then aligned and analysed as aforementioned in 2.2.4 (refer to Appendix E for raw sequence data). The sequences were in correct alignment (refer to Fig. A.2-A.11), thus further homologous recombination (LR) assays could be undertaken for transferal of SerpinB2 transgenes/shRNA into Gateway® destination vectors.

2.3.3 Knock-in/overexpression constructs

Entry clone reactions were undertaken in triplicate for each overexpression construct to ensure that correct sequences of each construct were maintained. Entry clone samples and their concentrations are shown in Table 2.2.

Table 2.2. Overexpression entry clone concentration and DNA sequence analysis.

Entry Clone Sample (pDONR221)	Concentration (ng/µL)	Size (bp)	Sequence Homology
Full length SerpinB2 - 1	**766.7**	**4,031**	**100**
^{R380A}SerpinB2 ΔCD - 1	573.2	3,932	100
^{R380A}SerpinB2 ΔCD - 2	**511.1**	3,932	100
Full length ^{R380A}SerpinB2 - 1	**552.1**	**4,031**	**100**
Full length ^{R380A}SerpinB2 - 2	517.4	4,031	100*
SerpinB2 ΔCD - 1	**573.2**	**3,932**	**100**
SerpinB2 ΔCD - 2	511.1	3,932	99.0

*Certain peaks were not as confident (<98%) as other constructs within cohort, samples in **bold** were chosen for further use. % Sequence homology refers to alignment of vector transgene to native gene of interest, using ncbi BLAST.

2.3.1 Knockdown constructs

Knockdown entry clone reactions were also undertaken in triplicate for each SerpinB2 hairpin as aforementioned in Section 2.3.2.1. Alignment and analysis revealed that peaks were quite confident and several clones could be chosen for further use (refer to Appendix E for raw sequence data). Table 2.3 displays the various clones with their concentrations and sequence homologies, matched to their respectively required SerpinB2 shRNA hairpin codes.

Table 2.3. SerpinB2 knockdown entry clone concentration and DNA sequence analysis.

Entry Clone Sample (pEN_TmiR_C3)	Concentration (ng/µL)	Size (bp)	% Sequence Homology
SerpinB2 sh1 - A	341.7	4,295	94
SerpinB2 sh1 - B	393.4	4,295	100 *
SerpinB2 sh1 - C	**371.0**	4,295	**100**
SerpinB2 sh2 - A	**392.4**	4,295	**100**
SerpinB2 sh2 - B	429.3	4,295	100 *
SerpinB2 sh2 - C	200.3	4,295	86

*Sequenced peaks were not as confident as other shRNA samples within cohort.

2.3.4 Destination clone analysis

Gateway® LR recombination reactions were undertaken in duplicate for each destination construct in order to limit errors in subsequent recombination reactions in an attempt to ensure that correct sequences of each construct were maintained. Sequence alignment and analysis was undertaken on both forward and reverse sequences of each construct. Robust peaks with good confidence (refer to Appendix E for raw sequence data) were observed and correct sequence alignment was then confirmed [as aforementioned in Section 2.2.5 (refer to Fig. 2.6-2.11)]. Thus, several clones were chosen for lentiviral packaging. Table 2.4 displays the various clones that were utilised in this project, revealing their concentrations and sequence homologies, matched to their respective SerpinB2 sequences. Forward and reverse sequences were performed and analysed to ensure correct alignment of the entire sequence of each construct [versus template SerpinB2 (and ΔCD and ^{R380A}SerpinB2 forms)]. pSLIK SerpinB2 shRNA vcctor sequences are shown in Appendix E (refer to Fig. A2-A8).

A

File: pLenti6.3_SerpinB2wt1

Sample Name: SerpinB2wt1_Forward
Mobility: KB_3130_POP7_BDTv3.mob
Spacing: 12.6587
Comment: NATHANIAL_HARRIS_14

Signal Strengths: A = 69, C = 52, G = 89, T = 71
Lane/Cap#: 1
Matrix: n/a
Direction: Native

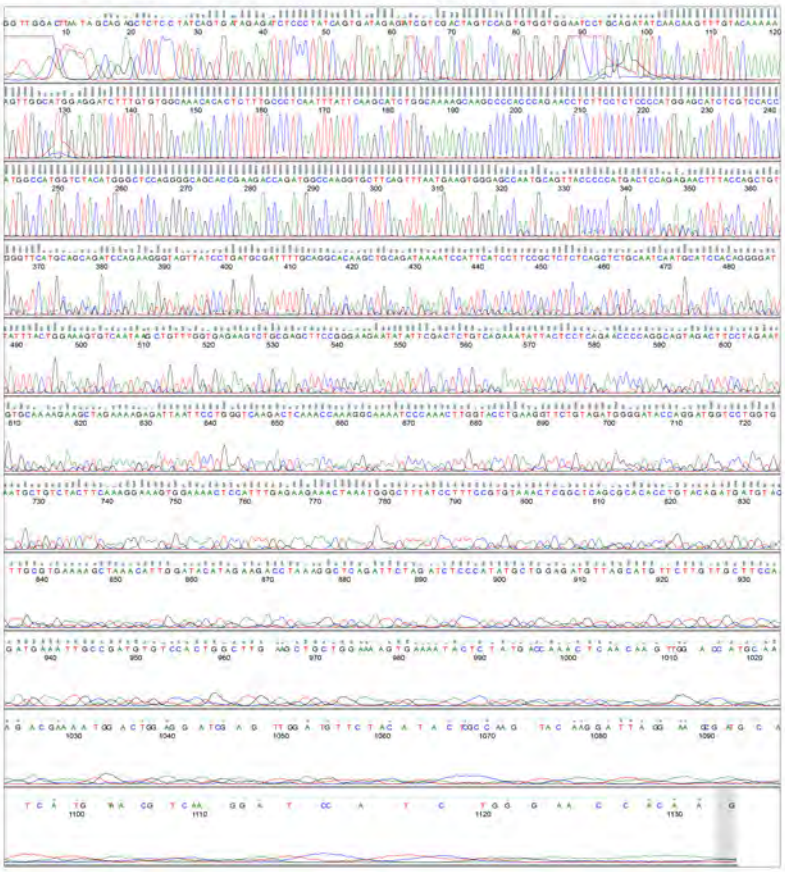

B

plasminogen activator inhibitor 2 [Homo sapiens]
Sequence ID: **gi|4505595|NP_002566.1** Length: 415 Number of Matches: 1

Range 1: 1 to 293

Score	Expect	Method	Identities	Positives	Gaps	Frame
583 bits(1504)	0.0	Compositional matrix adjust.	415/415(100%)	415/415(100%)	0/415(0%)	+2

Features:

```
Query  128   MEDLCVANTLFALNLFKHLAKASPTQNLFLSPWSISSTMAMVYMGSRGSTEDQMAKVLQF  307
wt SB2 1     MEDLCVANTLFALNLFKHLAKASPTQNLFLSPWSISSTMAMVYMGSRGSTEDQMAKVLQF  60
Query  308   NEVGANAVTPMTPENFTSCGFMQQIQKGSYPDAILQAQAADKIHSSFRSLSSAINASTGD  487
wt SB2 61    NEVGANAVTPMTPENFTSCGFMQQIQKGSYPDAILQAQAADKIHSSFRSLSSAINASTGN  120
Query  488   YLLESVNKLFGEKSASFREEYIRLCQKYYSSEPQAVDFLECAKEARKEINSWVKTQTKGK  667
wt SB2 121   YLLESVNKLFGEKSASFREEYIRLCQKYYSSEPQAVDFLECAEEARKKINSWVKTQTKGK  180
Query  668   IPNLVPEGSVDGDTRMVLVNAVYFKGKWKTPFEKKLNGLYPFRVNSAQRTPVQMMYLREK  847
wt SB2 181   IPNLLPEGSVDGDTRMVLVNAVYFKGKWKTPFEKKLNGLYPFRVNSAQRTPVQMMYLREK  240
Query  848   LNIGYIEDLKAQILELPYAGDVSMFLLLPDEIADVSTGLELLESEITYDKLNKWTSKDKM  1027
wt SB2 241   LNIGYIEDLKAQILELPYAGDVSMFLLLPDEIADVSTGLELLESEITYDKLNKWTSKDKM  300
Query  1028  AEDEVEVYIPQFKLEEHYELRSILRSMGMEDAFNKGRANFSGMSERNDLFLSEVFHQAMV  1207
wt SB2 301   AEDEVEVYIPQFKLEEHYELRSILRSMGMEDAFNKGRANFSGMSERNDLFLSEVFHQAMV  360
Query  1208  DVNEEGTEAAAGTGGVMTGRTGHGGPQFVADHPFLFLIMHKITKCILFFGRFSSP  1382
wt SB2 361   DVNEEGTEAAAGTGGVMTGRTGHGGPQFVADHPFLFLIMHKITKCILFFGRFCSP  415
```

Fig 2.6. pLenti6.3 SerpinB2 wt1 vector sequence. A. Nucelotide sequence analysis of destination vector, pLenti6.3 SerpinB2 wt1. **B.** Translated protein analysis of pLenti6.3 SerpinB2 wt1 construct versus translated wt SerpinB2 (Homo sapiens) sequence. Plasmid sample was extracted from transformed DH5α *E. coli* and sequenced as described in section 2.2.2. Sequence analysis performed using Finch TV and 4 Peaks analysis programs, compared to SerpinB2 template using blastx.

A

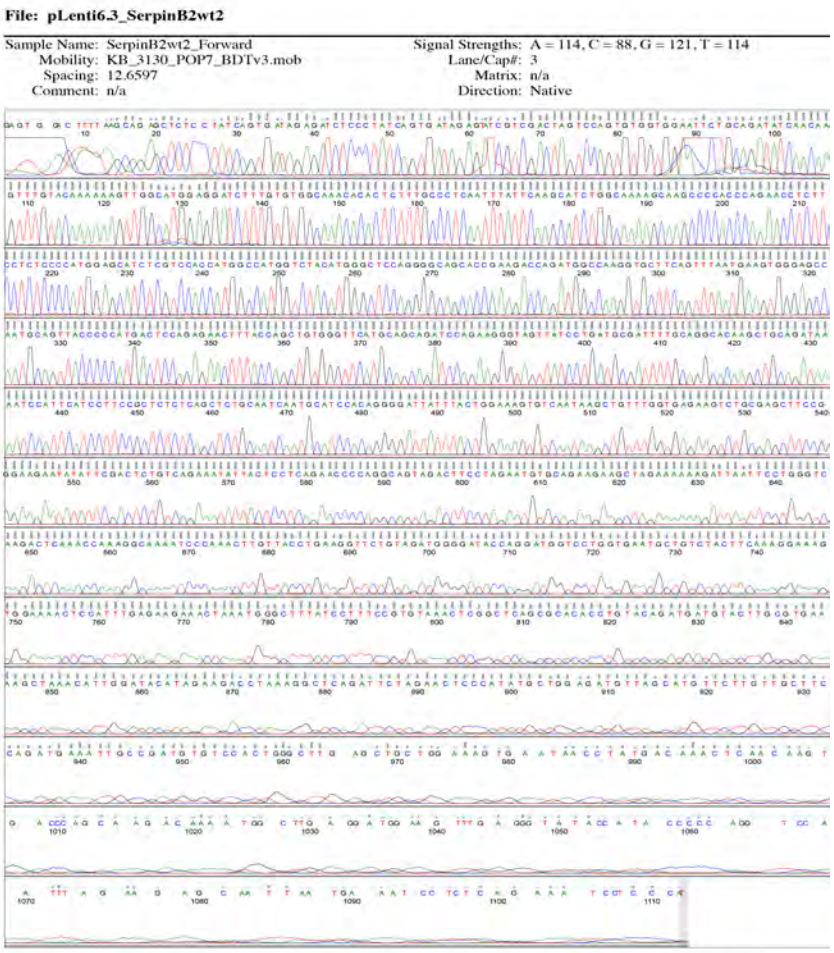

B

plasminogen activator inhibitor 2 [Homo sapiens]
Sequence ID: **gi|4505595|NP_002566.1** Length: 415 Number of Matches: 1

Range 1: 1 to 285

Score	Expect	Method	Identities	Positives	Gaps	Frame
592 bits(1527)	0.0	Compositional matrix adjust.	415/415(100%)	415/415(100%)	0/415(0%)	+2

Features:

```
Query  128  MEDLCVANTLFALNLFKHLAKASPTQNLFLSPWSISSTMAMVYMGSRGSTEDQMAKVLQF  307
wt SB2 1    MEDLCVANTLFALNLFKHLAKASPTQNLFLSPWSISSTMAMVYMGSRGSTEDQMAKVLQF  60
Query  308  NEVGANAVTPMTPENFTSCGFMQQIQKGSYPDAILQAQAADKIHSSFRSLSSAINASTGD  487
wt SB2 61   NEVGANAVTPMTPENFTSCGFMQQIQKGSYPDAILQAQAADKIHSSFRSLSSAINASTGD  120
Query  488  YLLESVNKLFGEKSASFREEYIRLCQKYYSSEPQAVDFLECAEEARKKINSWVKTQTKGK  667
wt SB2 121  YLLESVNKLFGEKSASFREEYIRLCQKYYSSEPQAVDFLECAEEARKKINSWVKTQTKGK  180
Query  668  IPNLLPEGSVDGDTRMVLVNAVYFKGKWKTPFEKKLNGLYPFRVNSAQRTPVQMMYLREK  847
wt SB2 181  IPNLLPEGSVDGDTRMVLVNAVYFKGKWKTPFEKKLNGLYPFRVNSAQRTPVQMMYLREK  240
Query  848  LNIGYIEDLKAQILELPYAGDVSMFLLLPDEIADVSTGLELLESEITYDKLNKWTSKDKM  1027
wt SB2 241  LNIGYIEDLKAQILELPYAGDVSMFLLLPDEIADVSTGLELLESEITYDKLNKWTSKDKM  300
Query  1028 AEDEVEVYIPQFKLEEHYELRSILRSMGMEDAFNKGRANFSGMSERNDLFLSEVFHQAMV  1207
wt SB2 301  AEDEVEVYIPQFKLEEHYELRSILRSMGMEDAFNKGRANFSGMSERNDLFLSEVFHQAMV  360
Query  1208 DVNEEGTEAAAGTGGVMTGRTGHGGPQFVADHPFLFLIMHKITKCILFFGRFCSP  1382
wt SB2 361  DVNEEGTEAAAGTGGVMTGRTGHGGPQFVADHPFLFLIMHKITKCILFFGRFCSP  415
```

Fig 2.7. pLenti6.3 SerpinB2 wt2 vector sequence. A. Nucelotide sequence analysis of destination vector, pLenti6.3 SerpinB2 wt2. **B.** Translated protein analysis of pLenti6.3 SerpinB2 wt2 construct versus translated wt SerpinB2 (Homo sapiens) sequence. Plasmid sample was extracted from transformed DH5α *E. coli* and sequenced as described in section 2.2.2. Sequence analysis performed using Finch TV and 4 Peaks analysis programs, compared to SerpinB2 template using blastx.

A **File: pLenti6.3_SerpinB2_CD1**

Sample Name: SerpinB2_CD1_Forward
Mobility: KB_3130_POP7_BDTv3.mob
Spacing: 12.6223
Comment: n/a

Signal Strengths: A = 85, C = 67, G = 119, T = 83
Lane/Cap#: 5
Matrix: n/a
Direction: Native

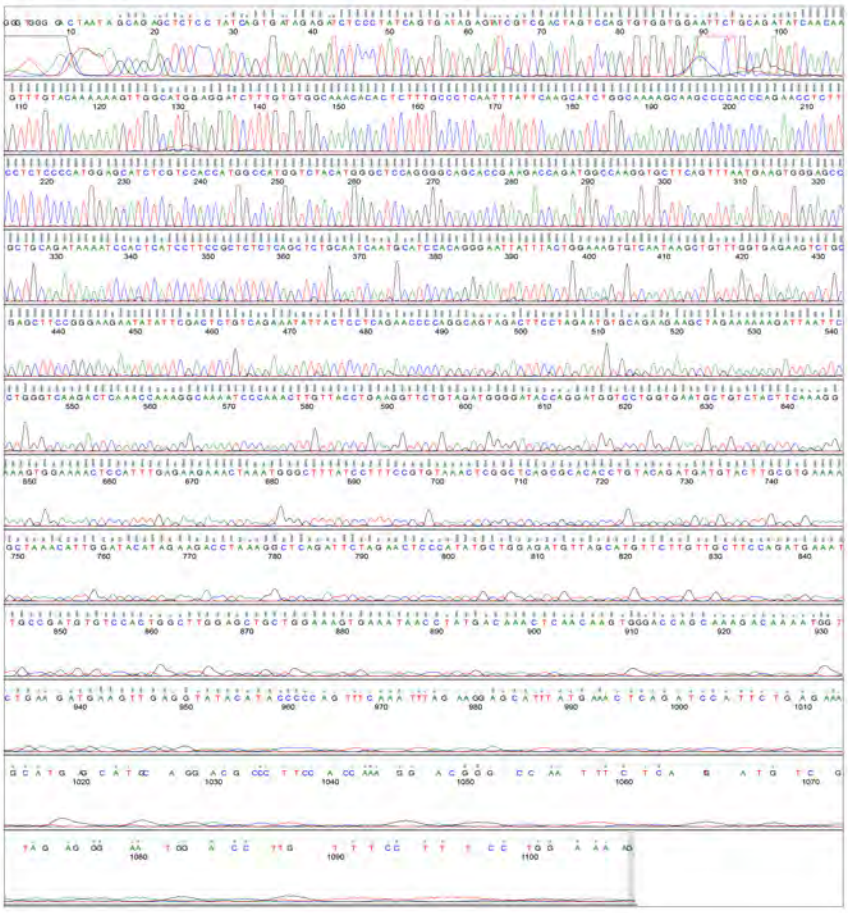

B

Chain A, Human Plasminogen Activator Inhibitor-2.[loop (66-98) Deletion Mutant]
Sequence ID: **gi|112489999|pdb|2ARQ|A** Length: 382 Number of Matches: 1

Score	Expect	Method	Identities	Positives	Gaps	Frame
545 bits(1403)	0.0()	Compositional matrix adjust.	382/382(100%)	382/382(100%)	0/382(0%)	+3

Features:

```
Query   129   MEDLCVANTLFALNLFKHLAKASPTQNLFLSPWSISSTMAMVYMGSRGSTEDQMAKVLQF  308
SB2 ΔCD 1     MEDLCVANTLFALNLFKHLAKASPTQNLFLSPWSISSTMAMVYMGSRGSTEDQMAKVLQF  60
Query   309   NEVGAAADKIHSSFRSLSSAINASTGNYLLESVNKLFGEKSASFREEYIRLCQKYYSSEP  488
SB2 ΔCD 61    NEVGAAADKIHSSFRSLSSAINASTGNYLLESVNKLFGEKSASFREEYIRLCQKYYSSEP  120
Query   489   QAVDFLECAEEARKKINSWVKTQTKGKIPNLLPEGSVDGDTRMVLVNAVYFKGKWKTPFE  668
SB2 ΔCD 121   QAVDFLECAEEARKKINSWVKTQTKGKIPNLLPEGSVDGDTRMVLVNAVYFKGKWKTPFE  180
Query   669   KKLNGLYPFRVNSAQRTPVQMMYLREKLNIGYIEDLKAQILELPYAGDVSMFLLLPDEIA  848
SB2 ΔCD 181   KKLNGLYPFRVNSAQRTPVQMMYLREKLNIGYIEDLKAQILELPYAGDVSMFLLLPDEIA  240
Query   849   DVSTGLELLESEITYDKLNKWTSKDKMAEDEVEVYIPQFQL*KEHY*ELRSILRSMGMED  1028
SB2 ΔCD 241   DVSTGLELLESEITYDKLNKWTSKDKMAEDEVEVYIPQFQL-KEHY-ELRSILRSMGMED  300
Query   1029  AFNKGRANFSGMSERNDLFLSEVFHQAMVDVNeegteaaagtggvmtgrtghggPQFVAD  1208
SB2 ΔCD 301   AFNKGRANFSGMSERNDLFLSEVFHQAMVDVNEEGTEAAAGTGGVMTGRTGHGGPQFVAD  360
Query   1209  HPFLFLIMHKITNCILFFGRFSSP  1230
SB2 ΔCD 361   HPFLFLIMHKITNCILFFGRFSSP  382
```

Fig 2.8. pLenti6.3 SerpinB2 ΔCD1 vector sequence. Nucelotide sequence analysis of destination vector, pLenti6.3 SerpinB2 ΔCD1. **B.** Translated protein analysis of pLenti6.3 SerpinB2 ΔCD1 construct versus translated SerpinB2 ΔCD (Homo sapiens) sequence. Plasmid sample was extracted from transformed DH5α *E. coli* and sequenced as described in section 2.2.2. Sequence analysis performed using Finch TV and 4 Peaks analysis programs, compared to SerpinB2 template using blastx.

A

File: pLenti6.3_SerpinB2_CD2

Sample Name: SerpinB2_CD2_Forward
Mobility: KB_3130_POP7_BDTv3.mob
Spacing: 12.5952
Comment: n/a

Signal Strengths: A = 71, C = 54, G = 90, T = 63
Lane/Cap#: 7
Matrix: n/a
Direction: Native

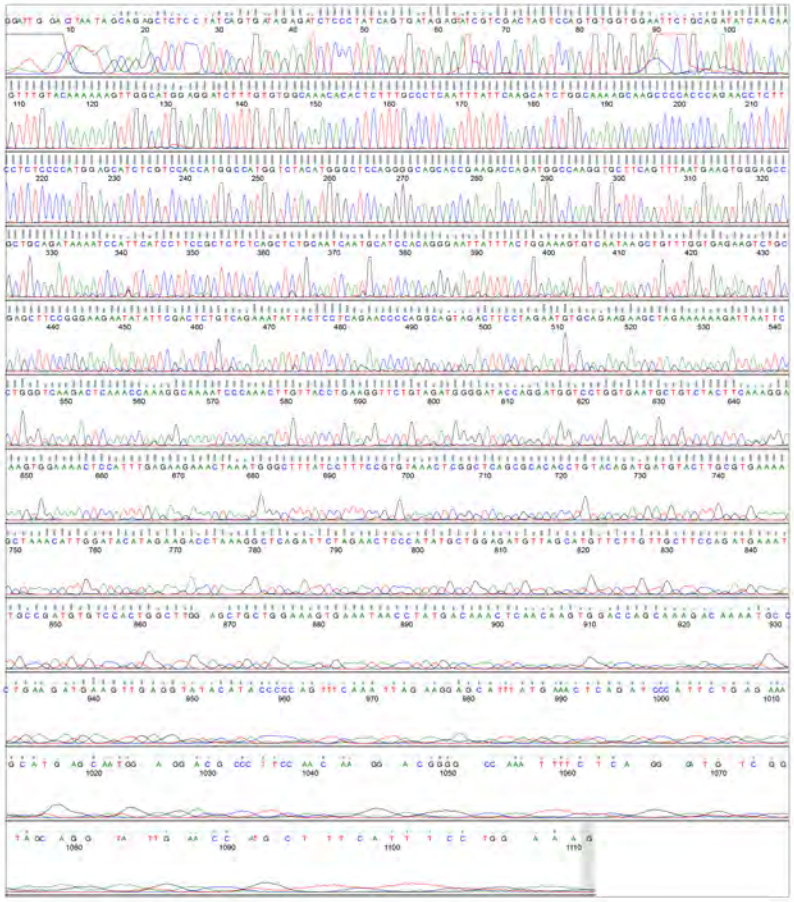

B

Chain A, Human Plasminogen Activator Inhibitor-2.[loop (66-98) Deletion Mutant]
Sequence ID: **gi|112489999|pdb|2ARQ|A** Length: 382 Number of Matches: 1

Score	Expect	Method	Identities	Positives	Gaps	Frame
545 bits(1403)	0.0()	Compositional matrix adjust.	382/382(100%)	382/382(100%)	0/382(0%)	+3

Features:

```
Query   129   MEDLCVANTLFALNLFKHLAKASPTQNLFLSPWSISSTMAMVYMGSRGSTEDQMAKVLQF  308
SB2 ΔCD 1     MEDLCVANTLFALNLFKHLAKASPTQNLFLSPWSISSTMAMVYMGSRGSTEDQMAKVLQF  60
Query   309   NEVGAAADKIHSSFRSLSSAINASTGNYLLESVNKLFGEKSASFREEYIRLCQKYYSSEP  488
SB2 ΔCD 61    NEVGAAADKIHSSFRSLSSAINASTGNYLLESVNKLFGEKSASFREEYIRLCQKYYSSEP  120
Query   489   QAVDFLECAEEARKKINSWVKTQTKGKIPNLLPEGSVDGDTRMVLVNAVYFKGKWKTPFE  668
SB2 ΔCD 121   QAVDFLECAEEARKKINSWVKTQTKGKIPNLLPEGSVDGDTRMVLVNAVYFKGKWKTPFE  180
Query   669   KKLNGLYPFRVNSAQRTPVQMMYLREKLNIGYIEDLKAQILELPYAGDVSMFLLLPDEIA  848
SB2 ΔCD 181   KKLNGLYPFRVNSAQRTPVQMMYLREKLNIGYIEDLKAQILELPYAGDVSMFLLLPDEIA  240
Query   849   DVSTGLELLESEITYDKLNKWTSKDKMAEDEVEVYIPQFQLKEHYELRSILRSMGMEDAF  1028
SB2 ΔCD 241   DVSTGLELLESEITYDKLNKWTSKDKMAEDEVEVYIPQFQLKEHYELRSILRSMGMEDAF  300
Query   1029  NKGRANFSGMSERNDLFLSEVFHQAMVDVNEEGTEAAAGTGGVMTGRTGHGGPQFVADHP  1208
SB2 ΔCD 301   NKGRANFSGMSERNDLFLSEVFHQAMVDVNEEGTEAAAGTGGVMTGRTGHGGPQFVADHP  360
Query   1209  FLFLIMHKITNCILFFGRFSSP  1230
SB2 ΔCD 361   FLFLIMHKITNCILFFGRFSSP  382
```

Fig 2.9. pLenti6.3 SerpinB2 ΔCD2 vector sequence. Nucelotide sequence analysis of destination vector, pLenti6.3 SerpinB2 ΔCD2. **B.** Translated protein analysis of pLenti6.3 SerpinB2 ΔCD2 construct versus translated SerpinB2 ΔCD (Homo sapiens) sequence. Plasmid sample was extracted from transformed DH5α *E. coli* and sequenced as described in section 2.2.2. Sequence analysis performed using Finch TV and 4 Peaks analysis programs, compared to SerpinB2 template using blastx.

A

File: pLenti6.3_R380ASerpinB2wt1

Sample Name: R380ASerpinB2wt1_Forward
Mobility: KB_3140_POP6_BDTv3.mob
Spacing: 12.1387
Comment: n/a

Signal Strengths: A = 70, C = 53, G = 90, T = 69
Lane/Cap#: 1
Matrix: n/a
Direction: Native

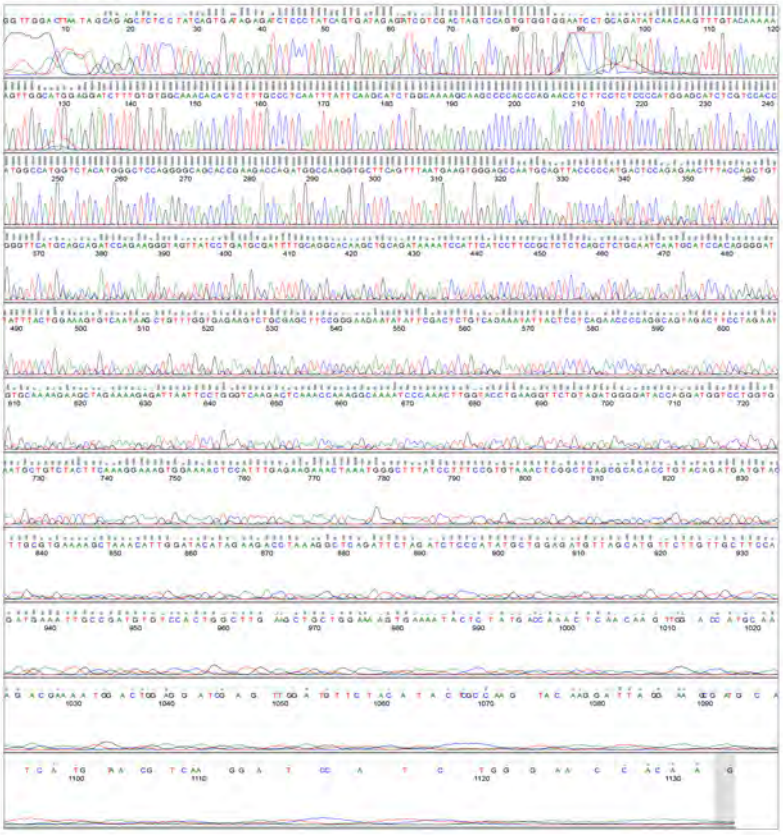

B

plasminogen activator inhibitor 2 [Homo sapiens]
Sequence ID: **gi|4505595|NP_002566.1** Length: 415 Number of Matches: 1

Range 1: 1 to 285

Score	Expect	Method	Identities	Positives	Gaps	Frame
592 bits(1527)	0.0	Compositional matrix adjust.	414/415(99%)	414/415(99%)	1/415(0%)	+2

Features:

```
Query  128   MEDLCVANTLFALNLFKHLAKASPTQNLFLSPWSISSTMAMVYMGSRGSTEDQMAKVLQF  307
wt SB2 1     MEDLCVANTLFALNLFKHLAKASPTQNLFLSPWSISSTMAMVYMGSRGSTEDQMAKVLQF  60
Query  308   NEVGANAVTPMTPENFTSCGFMQQIQKGSYPDAILQAQAADKIHSSFRSLSSAINASTGD  487
wt SB2 61    NEVGANAVTPMTPENFTSCGFMQQIQKGSYPDAILQAQAADKIHSSFRSLSSAINASTGD  120
Query  488   YLLESVNKLFGEKSASFREEYIRLCQKYYSSEPQAVDFLECAEEARKKINSWVKTQTKGK  667
wt SB2 121   YLLESVNKLFGEKSASFREEYIRLCQKYYSSEPQAVDFLECAEEARKKINSWVKTQTKGK  180
Query  668   IPNLLPEGSVDGDTRMVLVNAVYFKGKWKTPFEKKLNGLYPFRVNSAQRTPVQMMYLREK  847
wt SB2 181   IPNLLPEGSVDGDTRMVLVNAVYFKGKWKTPFEKKLNGLYPFRVNSAQRTPVQMMYLREK  240
Query  848   LNIGYIEDLKAQILELPYAGDVSMFLLLPDEIADVSTGLELLESEITYDKLNKWTSKDKM  1027
wt SB2 241   LNIGYIEDLKAQILELPYAGDVSMFLLLPDEIADVSTGLELLESEITYDKLNKWTSKDKM  300
Query  1028  AEDEVEVYIPQFKLEEHYELRSILRSMGMEDAFNKGRANFSGMSERNDLFLSEVFHQAMV  1207
wt SB2 301   AEDEVEVYIPQFKLEEHYELRSILRSMGMEDAFNKGRANFSGMSERNDLFLSEVFHQAMV  360
Query  1208  DVNEEGTEAAAGTGGVMTGATGHGGPQFVADHPFLFLIMHKITKCILFFGRFCSP  1382
wt SB2 361   DVNEEGTEAAAGTGGVMTGRTGHGGPQFVADHPFLFLIMHKITKCILFFGRFCSP  415
```

Fig 2.10. pLenti6.3 ^{R380A}SerpinB2 full-length 1 sequence. Nucelotide sequence analysis of destination vector, pLenti6.3 ^{R380A}SerpinB2 full-length 1. **B.** Translated protein analysis of pLenti6.3 ^{R380A}SerpinB2 full-length 1 construct versus translated wt SerpinB2 (Homo sapiens) sequence. Plasmid sample was extracted from transformed DH5α *E. coli* and sequenced as described in section 2.2.2. Sequence analysis performed using Finch TV and 4 Peaks analysis programs, compared to SerpinB2 template using blastx. The red line undermarks the R380A mutation – arginine residue at position 380 with an alanine residue.

A

File: pLenti6.3_R380ASerpinB2wt2

Sample Name: pLenti6.3_R380ASerpinB2wt2_Forward
Mobility: KB_3130_POP7_BDTv3.mob
Spacing: 12.6597
Comment: n/a

Signal Strengths: A = 114, C = 88, G = 121, T = 114
Lane/Cap#: 3
Matrix: n/a
Direction: Native

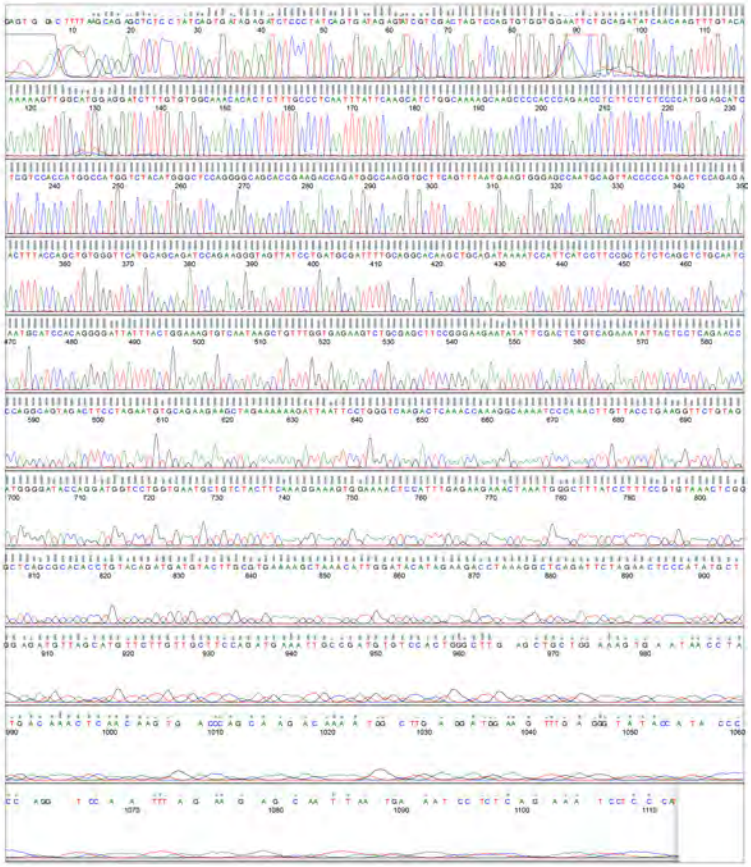

B

plasminogen activator inhibitor 2 [Homo sapiens]
Sequence ID: **gi|4505595|NP_002566.1** Length: 415 Number of Matches: 1

Range 1: 1 to 285

Score	Expect	Method	Identities	Positives	Gaps	Frame
592 bits(1527)	0.0	Compositional matrix adjust.	414/415(99%)	414/415(99%)	1/415(0%)	+2

Features:

```
Query  128   MEDLCVANTLFALNLFKHLAKASPTQNLFLSPWSISSTMAMVYMGSRGSTEDQMAKVLQF  307
wt SB2 1     MEDLCVANTLFALNLFKHLAKASPTQNLFLSPWSISSTMAMVYMGSRGSTEDQMAKVLQF  60
Query  308   NEVGANAVTPMTPENFTSCGFMQQIQKGSYPDAILQAQAADKIHSSFRSLSSAINASTGD  487
wt SB2 61    NEVGANAVTPMTPENFTSCGFMQQIQKGSYPDAILQAQAADKIHSSFRSLSSAINASTGD  120
Query  488   YLLESVNKLFGEKSASFREEYIRLCQKYYSSEPQAVDFLECAEEARKKINSWVKTQTKGK  667
wt SB2 121   YLLESVNKLFGEKSASFREEYIRLCQKYYSSEPQAVDFLECAEEARKKINSWVKTQTKGK  180
Query  668   IPNLLPEGSVDGDTRMVLVNAVYFKGKWKTPFEKKLNGLYPFRVNSAQRTPVQMMYLREK  847
wt SB2 181   IPNLLPEGSVDGDTRMVLVNAVYFKGKWKTPFEKKLNGLYPFRVNSAQRTPVQMMYLREK  240
Query  848   LNIGYIEDLKAQILELPYAGDVSMFLLLPDEIADVSTGLELLESEITYDKLNKWTSKDKM  1027
wt SB2 241   LNIGYIEDLKAQILELPYAGDVSMFLLLPDEIADVSTGLELLESEITYDKLNKWTSKDKM  300
Query  1028  AEDEVEVYIPQFKLEEHYELRSILRSMGMEDAFNKGRANFSGMSERNDLFLSEVFHQAMV  1207
wt SB2 301   AEDEVEVYIPQFKLEEHYELRSILRSMGMEDAFNKGRANFSGMSERNDLFLSEVFHQAMV  360
Query  1208  DVNEEGTEAAAGTGGVMTGATGHGGPQFVADHPFLFLIMHKITKCILFFGRFCSP  1382
wt SB2 361   DVNEEGTEAAAGTGGVMTGRTGHGGPQFVADHPFLFLIMHKITKCILFFGRFCSP  415
```

Fig 2.11. pLenti6.3 ^{R380A}SerpinB2 full-length 2 vector sequence. A. Nucelotide sequence analysis of destination vector, pLenti6.3 ^{R380A}SerpinB2 full-length 2. **B.** Translated protein analysis of pLenti6.3 ^{R380A}SerpinB2 full-length 2 construct versus translated wt SerpinB2 (Homo sapiens) sequence. Plasmid sample was extracted from transformed DH5α *E. coli* and sequenced as described in section 2.2.2. Sequence analysis performed using Finch TV and 4 Peaks analysis programs, compared to SerpinB2 template using blastx. The red line undermarks the R380A mutation – arginine residue at position 380 with an alanine residue.

A

File: pLenti6.3_SerpinB2R380A_CD1

Sample Name: SerpinB2R380A_CD1_Forward
Mobility: KB_3130_POP7_BDTv3.mob
Spacing: 12.4946
Comment: n/a

Signal Strengths: A = 25, C = 20, G = 36, T = 25
Lane/Cap#: 9
Matrix: n/a
Direction: Native

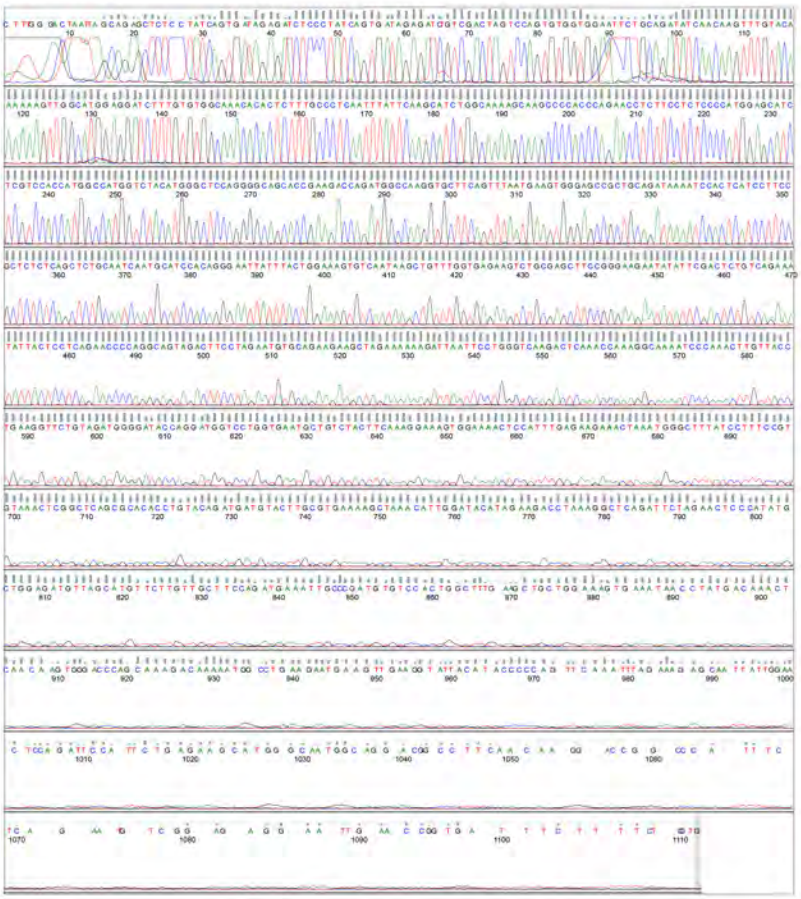

B

Chain A, Human Plasminogen Activator Inhibitor-2.[loop (66-98) Deletion Mutant]
Sequence ID: **gi|112489999|pdb|2ARQ|A** Length: 382 Number of Matches: 1

Score	Expect	Method	Identities	Positives	Gaps	Frame
545 bits(1403)	0.0()	Compositional matrix adjust.	381/382(99%)	381/382(99%)	1/382(0%)	+3

Features:

```
Query   129   MEDLCVANTLFALNLFKHLAKASPTQNLFLSPWSISSTMAMVYMGSRGSTEDQMAKVLQF  308
SB2 ΔCD 1     MEDLCVANTLFALNLFKHLAKASPTQNLFLSPWSISSTMAMVYMGSRGSTEDQMAKVLQF  60
Query   309   NEVGAAADKIHSSFRSLSSAINASTGNYLLESVNKLFGEKSASFREEYIRLCQKYYSSEP  488
SB2 ΔCD 61    NEVGAAADKIHSSFRSLSSAINASTGNYLLESVNKLFGEKSASFREEYIRLCQKYYSSEP  120
Query   489   QAVDFLECAEEARKKINSWVKTQTKGKIPNLLPEGSVDGDTRMVLVNAVYFKGKWKTPFE  668
SB2 ΔCD 121   QAVDFLECAEEARKKINSWVKTQTKGKIPNLLPEGSVDGDTRMVLVNAVYFKGKWKTPFE  180
Query   669   KKLNGLYPFRVNSAQRTPVQMMYLREKLNIGYIEDLKAQILELPYAGDVSMFLLLPDEIA  848
SB2 ΔCD 181   KKLNGLYPFRVNSAQRTPVQMMYLREKLNIGYIEDLKAQILELPYAGDVSMFLLLPDEIA  240
Query   849   DVSTGLELLESEITYDKLNKWTSKDKMAEDEVEVYIPQFQL*KEHY*ELRSILRSMGMED  1028
SB2 ΔCD 241   DVSTGLELLESEITYDKLNKWTSKDKMAEDEVEVYIPQFQL-KEHY-ELRSILRSMGMED  300
Query   1029  AFNKGRANFSGMSERNDLFLSEVFHQAMVDVNEEGTEAAAGTGGVMTGATGHGGPQFVAD  1208
SB2 ΔCD 301   AFNKGRANFSGMSERNDLFLSEVFHQAMVDVNEEGTEAAAGTGGVMTGRTGHGGPQFVAD  360
Query   1209  HPFLFLIMHKITNCILFFGRFSSP  1230
SB2 ΔCD 361   HPFLFLIMHKITNCILFFGRFSSP  382
```

Fig 2.12. pLenti6.3 ^{R380A}SerpinB2 ΔCD1 vector sequence. A. Nucelotide sequence analysis of destination vector, pLenti6.3 ^{R380A}SerpinB2 ΔCD1. **B.** Translated protein analysis of pLenti6.3 SerpinB2 ΔCD1 construct versus translated SerpinB2 ΔCD (Homo sapiens) sequence. Plasmid sample was extracted from transformed DH5α *E. coli* and sequenced as described in section 2.2.2. Sequence analysis performed using Finch TV and 4 Peaks analysis programs, compared to SerpinB2 template using blastx. The red line undermarks the R380A mutation – arginine residue at position 380 with an alanine residue.

Table 2.4. Lentiviral destination constructs, expression type, concentrations and DNA sequence analyses.

Transgene	Construct	Vector Size (bp)	Transgene Size (bp)	Concentration (ng/µL)	% Sequence Homology
SerpinB2 Wild-type 1	pLenti6.3/SerpinB2	9,668	2,180	833.7	100
SerpinB2 Wild-type 2	pLenti6.3/SerpinB2	9,668	2,180	147.5	100
SerpinB2 ΔCD loop 1	pLenti6.3/SerpinB2ΔCD1	9,569	2,081	827.5	100
SerpinB2 ΔCD loop 2	pLenti6.3/SerpinB2ΔCD2	9,569	2,081	41.4	100
Full length ^{R380A}SerpinB2	pLenti6.3/^{R380A}SerpinB2	9,668	2,180	72.8	100
^{R380A}SerpinB2 ΔCD loop	pLenti6.3/^{R380A}SerpinB2Δ CD	9,569	2,180	702	100
LacZ (Control)	pLenti6.3/LacZ	10,822	3,064	637.9	100
SerpinB2 shRNA (Hairpin 1)	pSLIK/SerpinB2 1C1	12,273	67	186.7	100
SerpinB2 shRNA (Hairpin2)	pSLIK/SerpinB2 2A2	12,273	67	283.2	100
GFP shRNA (Control hairpin)	pSLIK shGFP	12,254	48	141.6	100

2.3.5 Transient transgene transfection of HEK-293T cells

Transient transfections were initially undertaken in order to reduce reagent and consumable use (that is required for stable transduction experiments) while ensuring that the destination plasmids cDNA produced were target specific and transgene expression was effective. Expression of SerpinB2, SerpinB2 ΔCD loop and their ^{R380A}SerpinB2 mutant counterparts were assayed in the HEK-293T cell line after Lipofectamine transfection (Fig. 2.13). As the gene expression of each construct was increased in HEK-293T cells, versus the HEK-293T control cells (negligible levels of SerpinB2 expression), the destination vectors were deemed to be functional, consistent with the predicted outcome from sequencing analyses (refer to Table 2.4). Constructs chosen for further experimental use were full-length wild-type SerpinB2 construct 1 (refer to table 2.4), ΔCD loop construct 2, (Fig. 2.1.3, Lane 4), full-length ^{R380A}SerpinB2 construct 1 (Fig 2.1.3, Lane 5), and ^{R380A}SerpinB2 ΔCD loop construct 1 (Fig. 2.1.3, Lane 7).

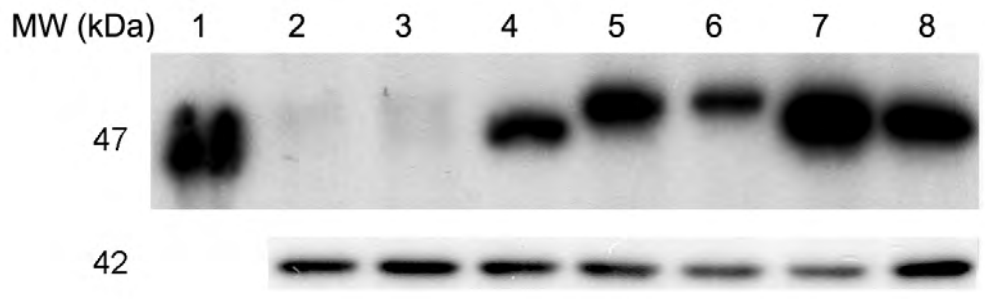

Fig. 2.13. Western blot of upregulated SerpinB2 expression in HEK-293T cells. Transiently transfected HEK-293T samples were fractioned by 10% SDS-PAGE, then transferred onto a PVDF membrane and probed with an anti-SerpinB2 antibody to detect the expression of serpinB2 mutant constructs. Lane 1 – Recombinant SerpinB2, Lane 2 – HEK-293T control, Lane 3 – SerpinB2 ΔCD loop construct 1, Lane 4 – SerpinB2 ΔCD loop construct 2, Lane 5 – Full length ^{R380A}SerpinB2 construct 1, Lane 6 – Full length ^{R380A}SerpinB2 construct 2, Lane 7 – ^{R380A}SerpinB2 ΔCD loop construct 1, Lane 8 – ^{R380A}SerpinB2 ΔCD loop construct 2. An anti-β-actin antibody was used as control (42 kDa).

2.3.6 LacZ infection for repression analysis

In order to reduce the chance of non-targeted gene disruption and to increase the likelihood of single transgene integrations per cell, optimisation of the Tet repression system was undertaken. MDA-MB-231 cells were stably transduced with a ß-galactosidase expression construct and increasing levels of the pLentiTetR Vector (at 1/10, 1/100 and 1/1000 dilutions) (Fig. 2.14). After 2 h staining with X-gal, 48 h after Dox induction (using 1 μg/mL), bright field microscopy images revealed stark differences in repression of the LacZ transgene (Fig. 2.14). The transduction of the pLentiTetR Vector demonstrated that effective repression of a transgene is possible with even a low dilution of virus (1/1000, Fig. 2.14A, far Right panels), however more concentrated TR lentiviral infection increased repression of the LacZ vector, as expected (1/10 and 1/100, Fig. 2.14A, Left and Middle panels, respectively). The control cells without lentiviral transduction had no ability to cleave X-gal, and thus produced no blue staining, ± Dox induction (Fig 2.14B, Left panels), while the MDA-MB-231s

transduced singly with the pLenti CMV/(TO)LacZ vector show intense blue staining, ± Dox induction (Fig 2.14B, Right panels).

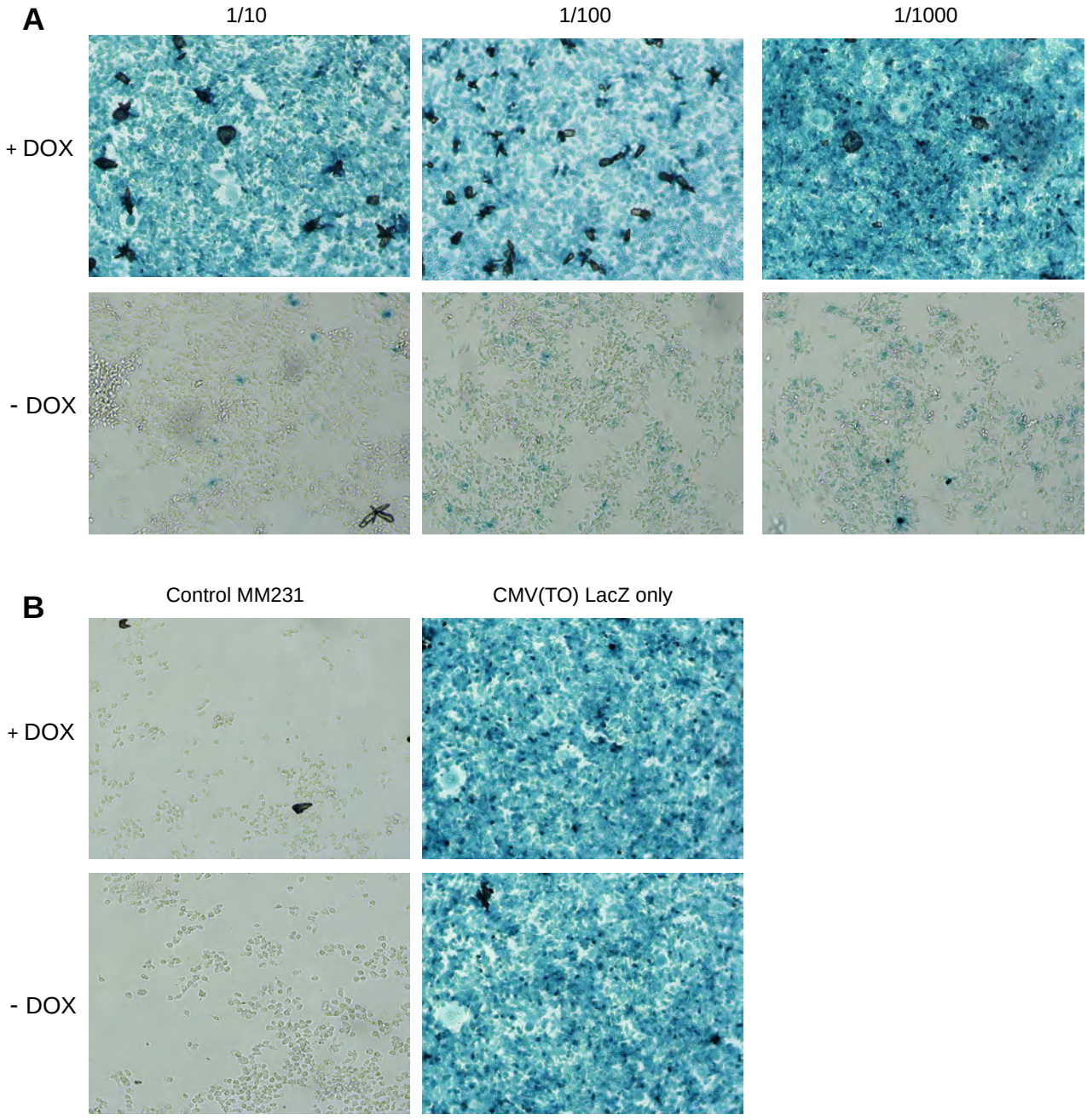

Fig. 2.14. Repression analyses for optimal transgene expression – MDA-MB-231 cells stably co-transduced with the pLenti CMV/(TO)LacZ vector and various levels of the pLentiTetR Vector were incubated for 2 h with X-gal stain, 48 h post-induction of expression using 1 µg/mL Dox, then imaged using bright field microscopy. **A.** Co-transduced 231 cells with decreasing dilutions (L-R) of pLentiTetR Vector (± Dox addition). **B.** Left panels show Control 231 cells without any lentiviral transductions (± Dox); Right panels show MDA-MB-231 cells singly transduced with pLenti CMV/(TO)LacZ vector (± Dox). Photomicrographs were imaged at 10x magnification.

2.3.7 Stable transductions of MDA-MB-231 cell line

Artificial destination constructs were prepared with SIN transgene vectors and the three Gateway® packaging vectors (pMDLg/pRRE, pRSV-Rev and pMD.G) and Lipofectamine 2K, incubated for 30 min at RT, then added into wells containing HEK-293T cells at 60% confluency. Following successful transient transfection experiments, concurrent lentiviral infections were also performed upon MDA-MB-231 cells. After antibiotic selection (72 h from infection), stably transduced MDA-MB-231s with knock-in SerpinB2, ^{R380A}SerpinB2 or LacZ (control); knockdown constructs SerpinB2 shRNA (both hairpins) or shGFP control, were collected and assayed using various modes for the evaluation of transgene modulation.

2.3.8 Western blotting - overexpression constructs

MDA-MB-231 (luc.) cells transduced with knock-in SerpinB2, ^{R380A}SerpinB2 or LacZ (control) lentiviral vectors were also transduced in combination with either 1/10 TetR or 1/1000 TetR, in order to individually evaluate the optimal repression for each gene expression lentiviral package. Three days after transfection and antibiotic selection, reporter gene expression was examined using western blotting (Fig. 2.15A-D). After confirmation of gene overexpression was achieved, cultures were kept under Dox conditions for at least ten days in order to confirm that overexpression could be maintained (Fig. 2.15 A-D). It should be noted that MDA-MB-231 cells do constitutively express SerpinB2, however this Dox inducible system revealed that all constructs with Dox addition dramatically increased the expression of SerpinB2 or ^{R380A}SerpinB2 within MDA-MB-231 cells, versus no Dox added control MDA-MB-231 cells. There was no significant difference observed in the expression of SerpinB2 or ^{R3880A}SerpinB2 in using either a 1/10 (Fig 2.15 A,B) or 1/1000 (Fig. 2.15 C,D) dilution of TetR Vector. Once confirmation of SerpinB2 and ^{R3880A}SerpinB2 knock-in was achieved, subsequent characterisation experiments could be performed.

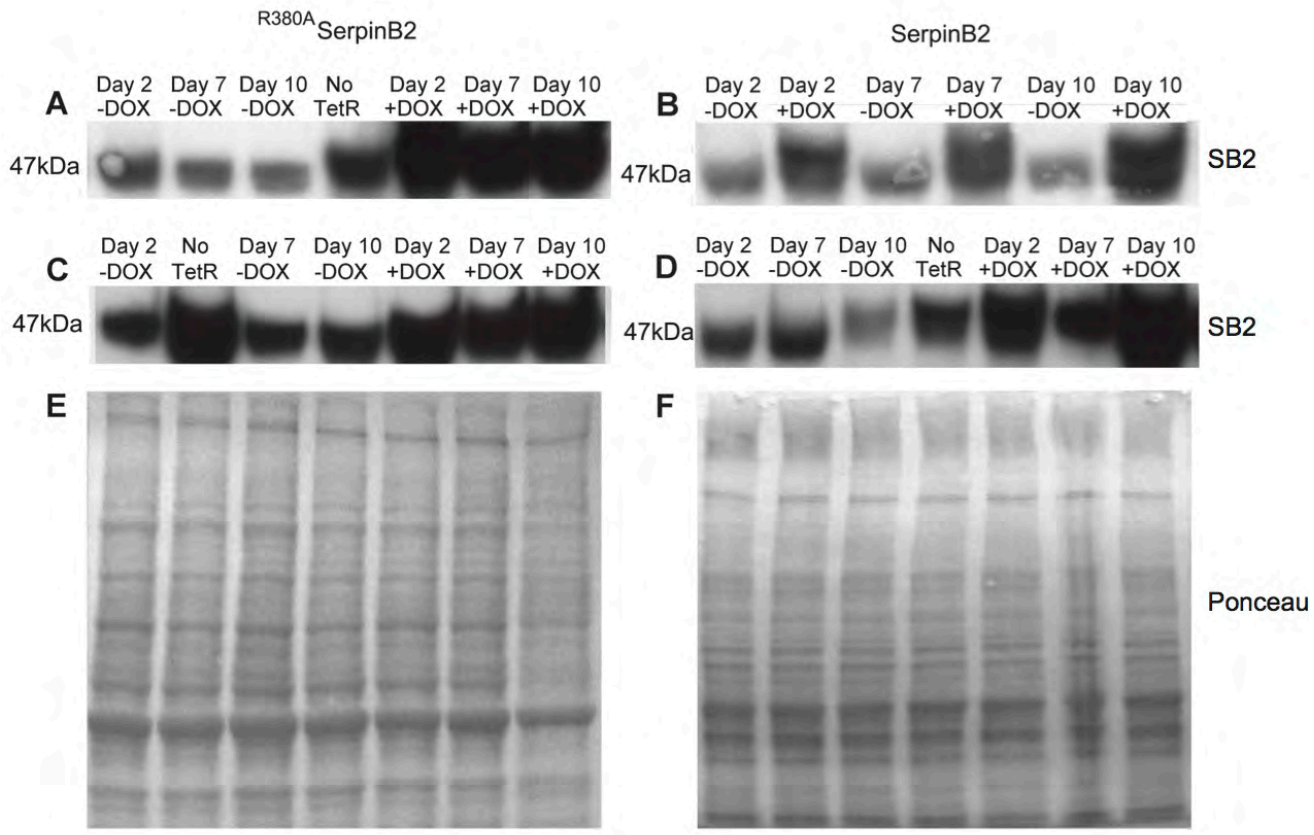

Fig. 2.15. Western blot of modified SerpinB2 expression in MDA-MB-231 cells using the pLenti system. Stably transduced MDA-MB-231 samples (± Dox induction) were fractioned by 10% SDS-PAGE, then transferred onto a PVDF membrane and probed with an anti-SerpinB2 antibody to detect the modified expression of SerpinB2. **A.** pLenti6.3/^{R380A}SerpinB2 (TO) and 1/10 TetR **(L-R)** Day 2 -10 (-Dox), No TetR, ^{R380A}SerpinB2 Day 2 -10 (+Dox); **B.** pLenti6.3/SerpinB2 (TO) and 1/10 TetR **(L-R)** Day 2 (-Dox), Day 2 (-Dox), Day 7 (-Dox), Day 7 (+Dox), Day 10 (-Dox), Day 10 (+Dox); **C.** pLenti6.3/^{R380A}SerpinB2 (TO) and 1/1000 TetR **(L-R)** Day 2 (-Dox), No TetR (-Dox), Day 7 (-Dox), Day 10 (-Dox), Day 2 (+Dox), Day 7 (+Dox), Day 10 (+Dox); **D.** pLenti6.3/SerpinB2 (TO) and 1/1000 TetR **(L-R)** Day 2 (-Dox), Day 7 (-Dox), Day 10 (-Dox), No TetR, Day 2 (+Dox), Day 7 (+Dox), Day 10 (+Dox). **E –F.** Ponceau S stained blot was used as a loading control.

2.3.9 Western blotting - knockdown constructs

MDA-MB-231 (luc.) cells were transfected with knockdown SerpinB2 shRNA (both hairpins) or shGFP (control) lentiviral vectors in serum-free medium for 24 hours. These constructs were diluted at various viral concentrations of either 1/50, 1/100 or 1/500, in order to evaluate the ideal amount for optimal SerpinB2 knockdown. Three days after transfection and subsequent Dox induction, reporter gene expression was examined using western blotting (Fig. 2.16 A). It was observed that knockdown was achieved with both hairpins using 1/50 and 1/100 dilutions (and Dox induction), yet there was no significant recorded

downregulation effect on SerpinB2 expression using a 1/500 dilution of shRNA, in either hairpin (Fig. 2.16 A). After confirmation of SerpinB2 knockdown was observed, cell cultures were kept under Dox conditions for up to 40 days (using only 1/50 and 1/100 lentiviral infected cells) in order to confirm that SerpinB2 knockdown could be maintained (Fig. 2.16 B). Western blot analysis revealed that knockdown was successful in all cohorts over a 40 day period, however, there was a greater knockdown of SerpinB2 observed in the 1/50 samples of both hairpins (Fig. 2.16 B,D). These data demonstrate that through using the pSLIK lentiviral vector, it was possible to introduce a tightly controlled miR-shRNA expression system for conditional knockdown of endogenous SerpinB2 mammalian gene from a single viral infection and opened up the attractive possibility of stable, robust, and reversible gene depletion in both primary and established cell lines for use in *ex vivo* and *in vivo* model systems.

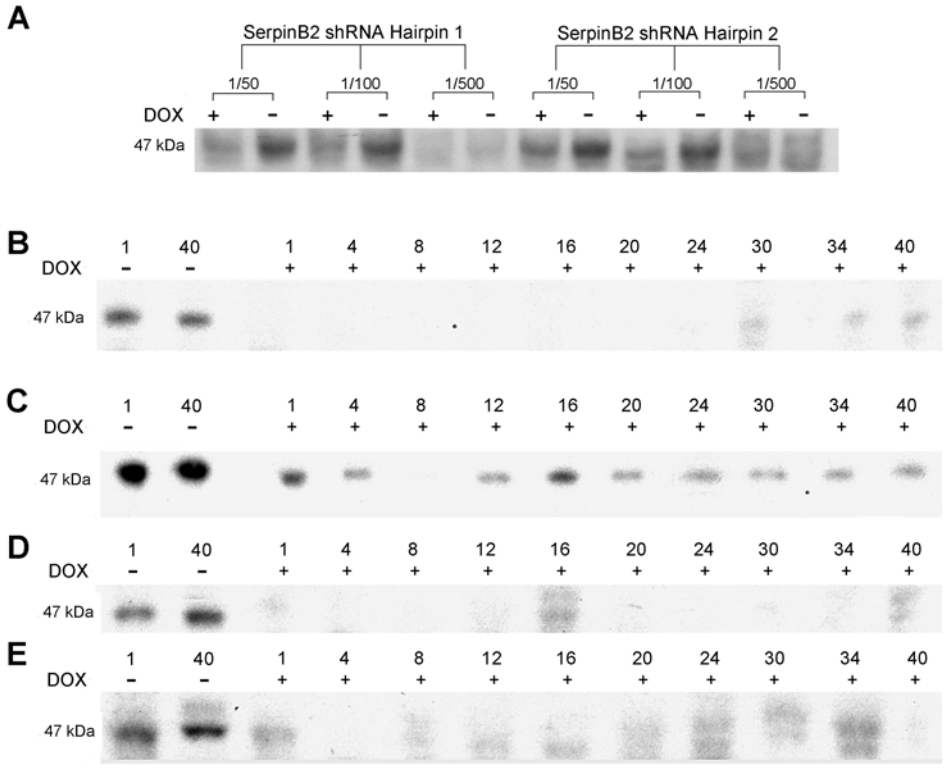

Fig. 2.16. Western blot of downregulated SerpinB2 expression in MDA-MB-231 cells using the pSLIK system. Stably transduced MDA-MB-231 samples were fractioned by 10% SDS-PAGE, then transferred onto a PVDF membrane and probed with an anti-SerpinB2 antibody to detect the modified expression of serpinB2. **A.** SerpinB2 shRNA1 Hairpins 1 and 2 (± Dox) at lentiviral dilutions of 1/50, 1/100 and 1/500; **B.** SerpinB2 shRNA Hairpin 1 at lentiviral dilution of 1/50 over a 40 d time course (± Dox); **C.** SerpinB2 shRNA Hairpin 1 at lentiviral dilution of 1/100 over a 40 d time course (± Dox); **D.** SerpinB2 shRNA Hairpin 2 at lentiviral dilution of 1/50 over a 40 d time course (± Dox); **E.** SerpinB2 shRNA Hairpin 2 at lentiviral dilution of 1/100 over a 40 d time course (± Dox).

2.3.10 Long term stability of gene modification

MDA-MB-231 cells were frozen and stored in liquid nitrogen. After more than a year, these cells were revived and grown in culture to ensure that transduced cells were still viable and maintained stable expression of transduced constructs. This was performed to ensure that future SerpinB2 knockdown or overexpression could still be achieved. Cells were collected and assayed for SerpinB2 expression using western blot analysis (Fig. 2.17). It was clear that the SerpinB2 knockdown and ^{R380A}SerpinB2 overexpression constructs were still viable, however this was not observed for the SerpinB2 overexpression construct (Fig. 2.17A).

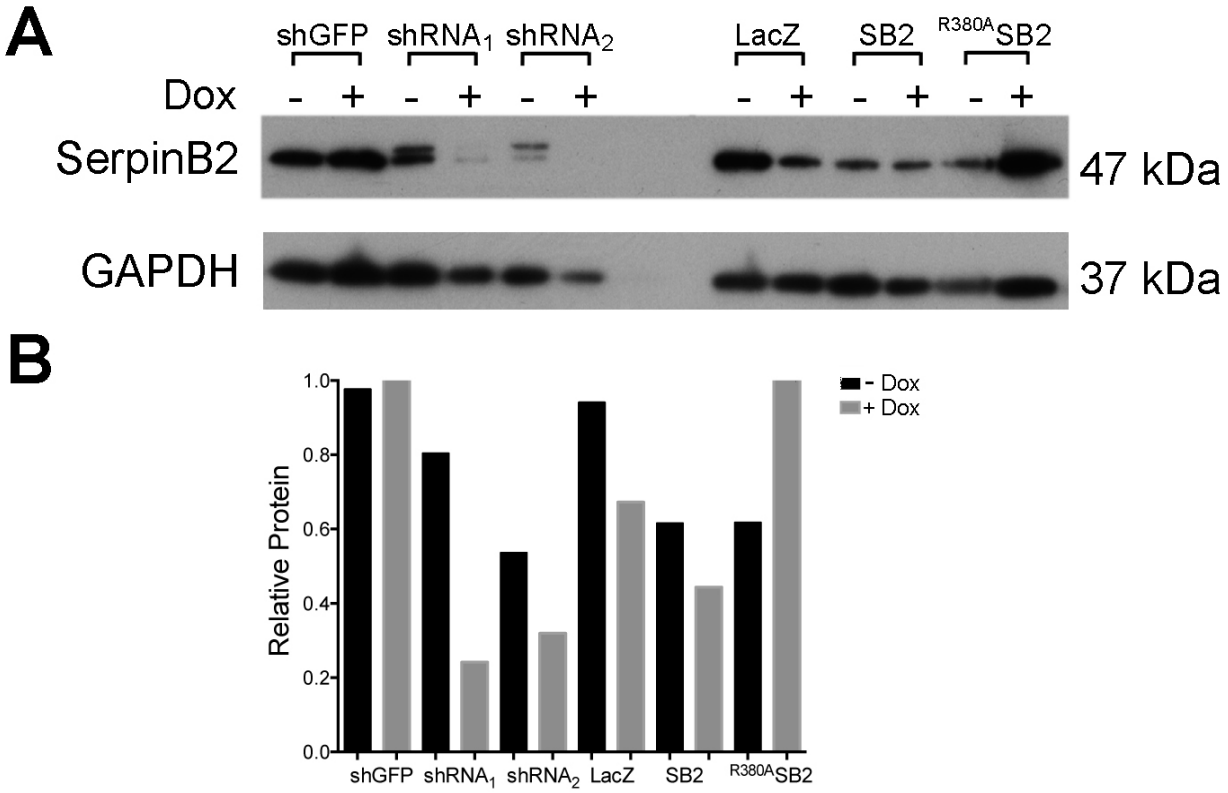

Fig. 2.17. Long-term stability analysis of lentiviral constructs in MDA-MB-231 cells, using western blot analysis. Stably transduced MDA-MB-231 samples were fractioned by 10% SDS-PAGE, then transferred onto a PVDF membrane and probed with an anti-SerpinB2 antibody to detect the modified expression of serpinB2. **A.** (**L-R)** shGFP KD control (± Dox), SerpinB2 shRNA Hairpin 1 (± Dox), SerpinB2 shRNA Hairpin 2 (± Dox), LacZ OE control (± Dox), SerpinB2 OE (± Dox), ^{R380A}SerpinB2 OE (± Dox). A GAPDH antibody was used as loading control; **B.** Relative SerpinB2 protein expression, each lane normalised to its respective GAPDH loading control lane.

The phenomena of the lower (~37 kDa) sized SerpinB2 band (observable in Lanes 3,4 and 5) is also observed by other SerpinB2 researchers and is believed to be a cleaved form of SerpinB2. Performing a gel digest, or

cutting out this band of interest to do an in-gel digestion with trypsin would be useful. Alternatively, to exactly interpret this band, this band could be cut out, purified by HPLC and sequenced using Edman degradation technology or HPLC/MS/MS sequence analysis. The loading controls revealed that this western blot should be repeated in order to ascertain more quantifiable SerpinB2 knockdown occurring withn each hairpin.

2.3.11 Incucyte proliferation assay

As there appeared to be problems with the longterm stability of SerpinB2 overexpression constructs, SerpinB2 knockdown constructs were selected for further experimentation. To ascertain if the modulation of SerpinB2 expression (i.e. knockdown) influenced cell growth, the confluency of MDA-MB-231 cells was measured over a period of four days using the IncuCyte Zoom live cell imaging system (Fig. 2.18). Results indicated that SerpinB2 knockdown constructs did not significantly affect the proliferative rate of MDA-MB-231 cells, both individually between Dox and No Dox addition, and versus shGFP control constructs (Fig. 2.18). It is possible that the inefficient knockdown of SerpinB2 with the shRNA Hairpin 1 (1/100 dilution) potentially influenced the proliferation rate (refer to Fig. 2.16 C, 1/100 dilution).

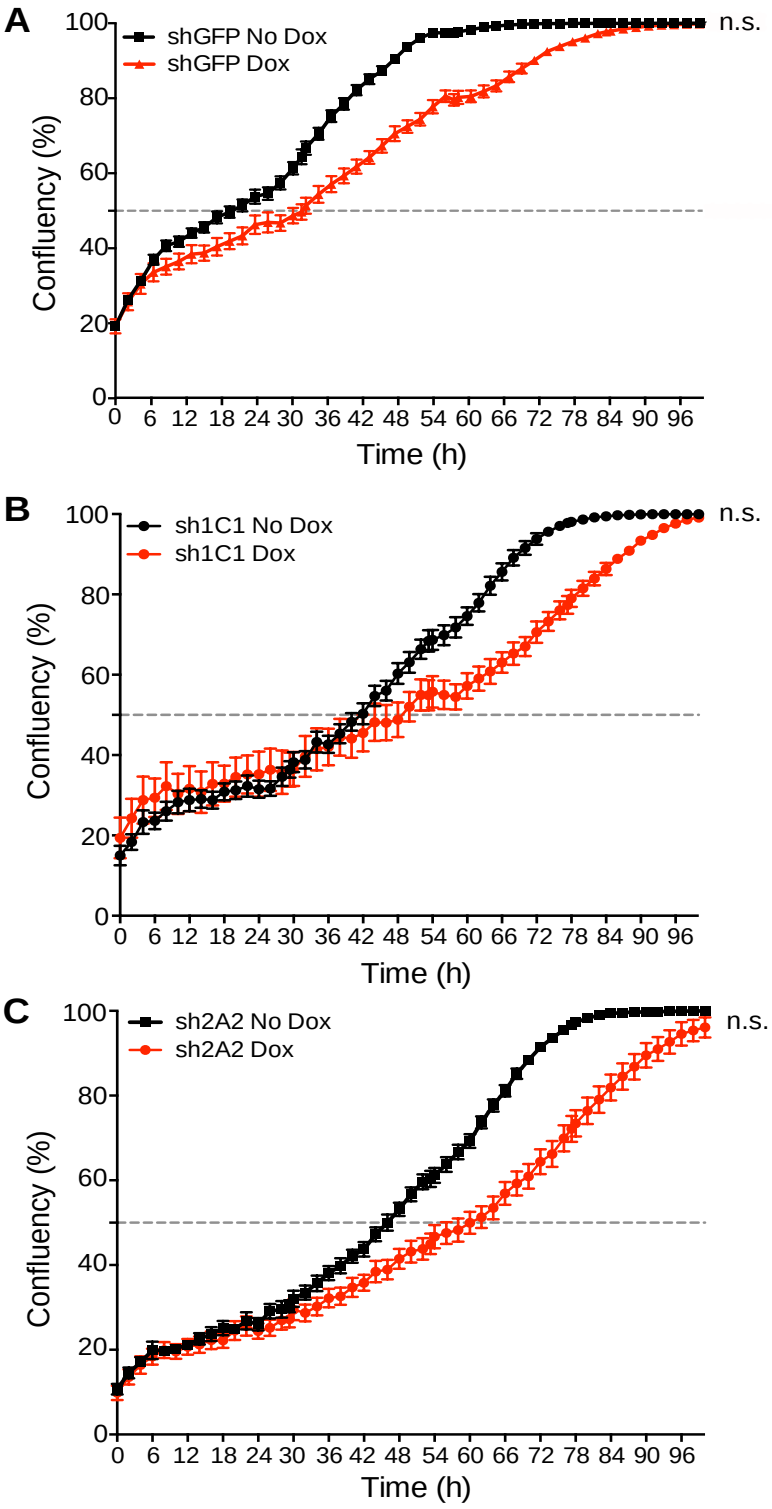

Fig. 2.18. Effect of SerpinB2 modification on the growth of MDA-MB-231 cells. Stably transduced MDA-MB-231 cells were seeded into individual wells of 96 well plates and then monitored over 4 days using the IncuCyte ZOOM imaging system. Stably transduced constructs were induced with (± 1 µg/mL) Dox. Constructs tested were **A.** GFP shRNA (shGFP), **B.** SerpinB2 shRNA1 (sh1C1), and **C.** SerpinB2 shRNA2 (sh2A2).

2.3.12 Immunofluorescence

In addition to western blotting, examination of MDA-MB-231 cells by immunofluorescence staining also confirmed that the lentiviral vector overexpression and knockdown constructs had worked successfully (Fig. 2.19 and Fig. 2.20, respectively). Both SerpinB2 and ^{R380A}SerpinB2 pLenti constructs (after Dox addition) effectively overexpressed SerpinB2 gene expression in MDA-MB-231 cells, when compared to the no Dox controls, detected by immunofluorescence (Fig 2.19). Concomitantly, both SerpinB2 1/50 and 1/100 dilutions of shRNA hairpins (with Dox induction) considerably reduced the expression of SerpinB2 versus no Dox controls, as observed by immunofluorescence (Fig 2.20). These studies validate the applicability of the pSLIK system to introduce conditional SerpinB2 RNAi into MDA-MB-231 cells from a single viral infection and allowed the modulation of SerpinB2 expression to study spatiotemporal expression of SerpinB2 in the 3D organotypic model, and more complex systems (Chapters 3, 4 and 5).

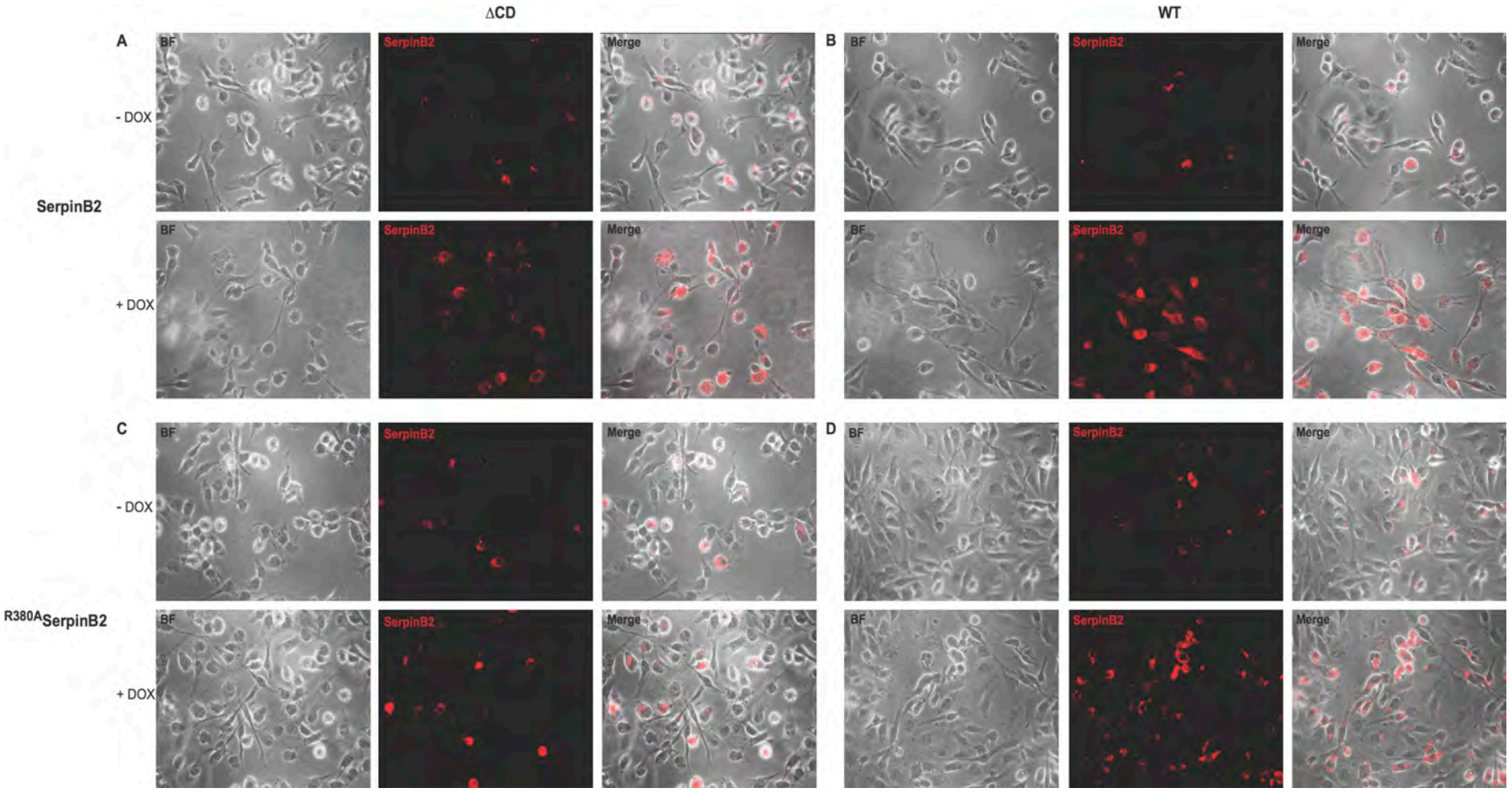

Fig. 2.19. Immunofluorescence imaging of overexpression constructs. Stably transduced MDA-MB-231 cells (± Dox) were fixed on glass slides and incubated with an anti-SerpinB2 antibody and secondary-HRP fluorescent antibody to detect the modified expression of serpinB2. **A.** SerpinB2 Δ CD loop transduced MDA-MB-231 cells, ± Dox; **B.** wild-type SerpinB2 transduced MDA-MB-231 cells, ± Dox; **C.** ^{R380A}SerpinB2 Δ CD loop transduced MDA-MB-231 cells, ± Dox; **D.** Full length ^{R380A}SerpinB2 transduced MDA-MB-231 cells, ± Dox. Photomicrographs were imaged at 20x magnification.

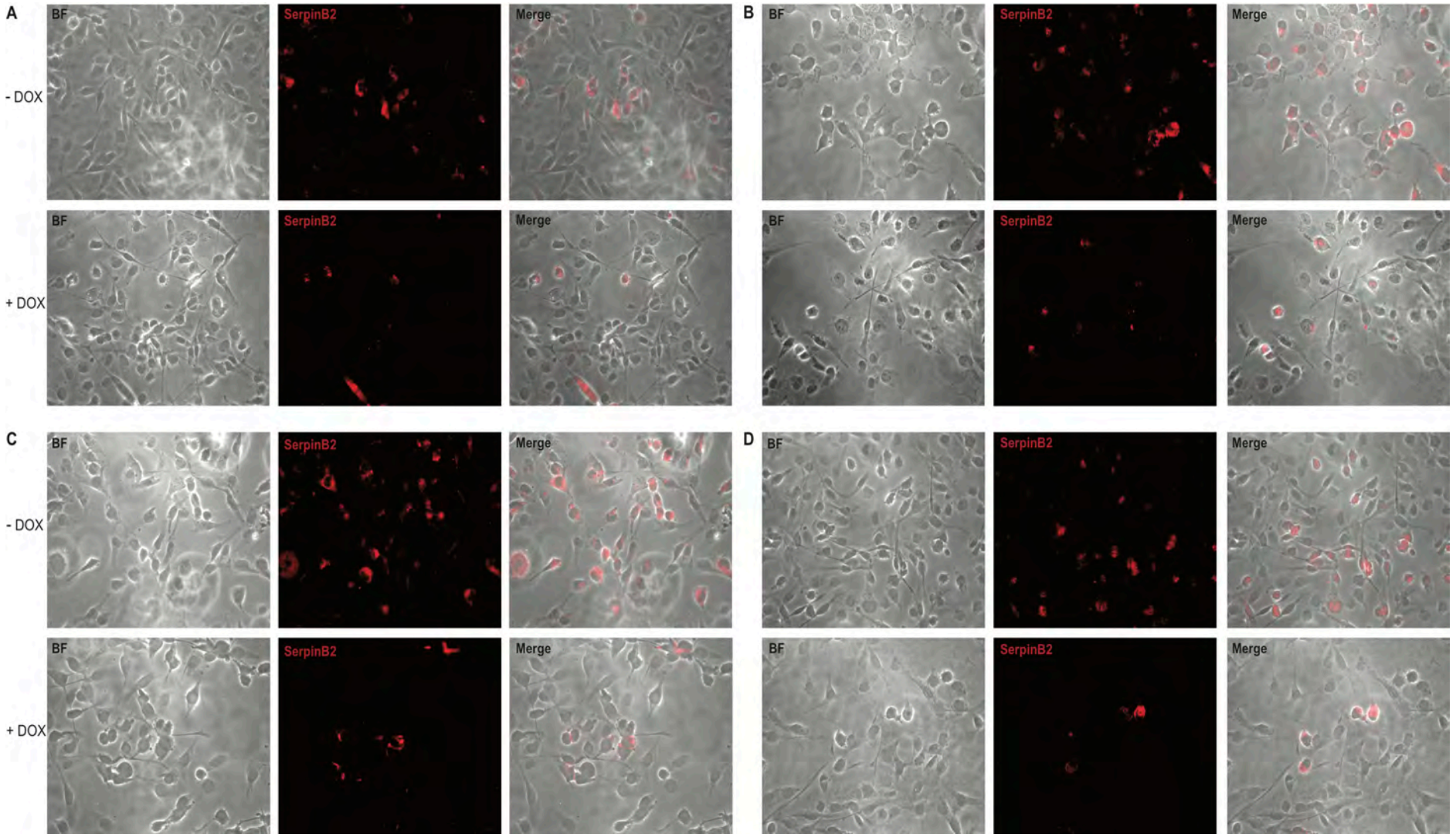

Fig. 2.20. Immunofluorescence imaging of knockdown constructs. Stably transduced MDA-MB-231 cells (± Dox) were fixed on glass slides and incubated with an anti-SerpinB2 antibody and secondary-HRP fluorescent antibody to detect the modified expression of serpinB2. **A.** MDA-MB-231 cells stably transduced with SerpinB2 shRNA1 at 1/50 dilution, ± Dox; **B.** MDA-MB-231 cells stably transduced with SerpinB2 shRNA1 at 1/100 dilution, ± Dox; C. MDA-MB-231 cells stably transduced with SerpinB2 shRNA2 at 1/50 dilution, ± Dox; **D.** MDA-MB-231 cells stably transduced with SerpinB2 shRNA2 at 1/100 dilution, ± Dox. Photomicrographs were imaged at 20x magnification.

2.3.13 Stable GFP transduction of wild-type and SerpinB2-/- MEFs

In order to have cell reporter function in future experiments of this research project, wild-type and SerpinB2$^{-/-}$ MEF cells expressing GFP were generated. This was achieved by lentiviral transduction using the VSV-G pseudotyped lentivirus encoding pLV411 vector. After infection, 20-30% of wild-type and SerpinB2$^{-/-}$ MEFs were GFP expressing (Fig. 2.21). GFP-positive MEFs were enriched by FACS sorting. Much cell gating was employed during FACS sorting, for isolating viable cells as well as doublet discrimination, in order to detect disproportions between cell size vs. cell signal. As Fibroblasts are morphologically heterogeneous, existing in ellipsoid, stellate and epithelial shaped appearance, this was taken into consideration when gating, as two distinct populations were observed [Fig. 2.21, A (i.)]. FACS MEF populations were collected, obtaining more than 83% of (KO MEF) cells stably expressing GFP (while 85.7% wt MEFs had stable GFP expression). These could then be used for imaging purposes in proceeding *ex vivo* and *in vivo* studies (Chapters 3,4, and 5). Further, cloning was not necessary and there were two populations of MEFs that were of round or elliptical appearance (identified through FACS sorting) and both were used for future experimentation (refer to Section 3.3.5).

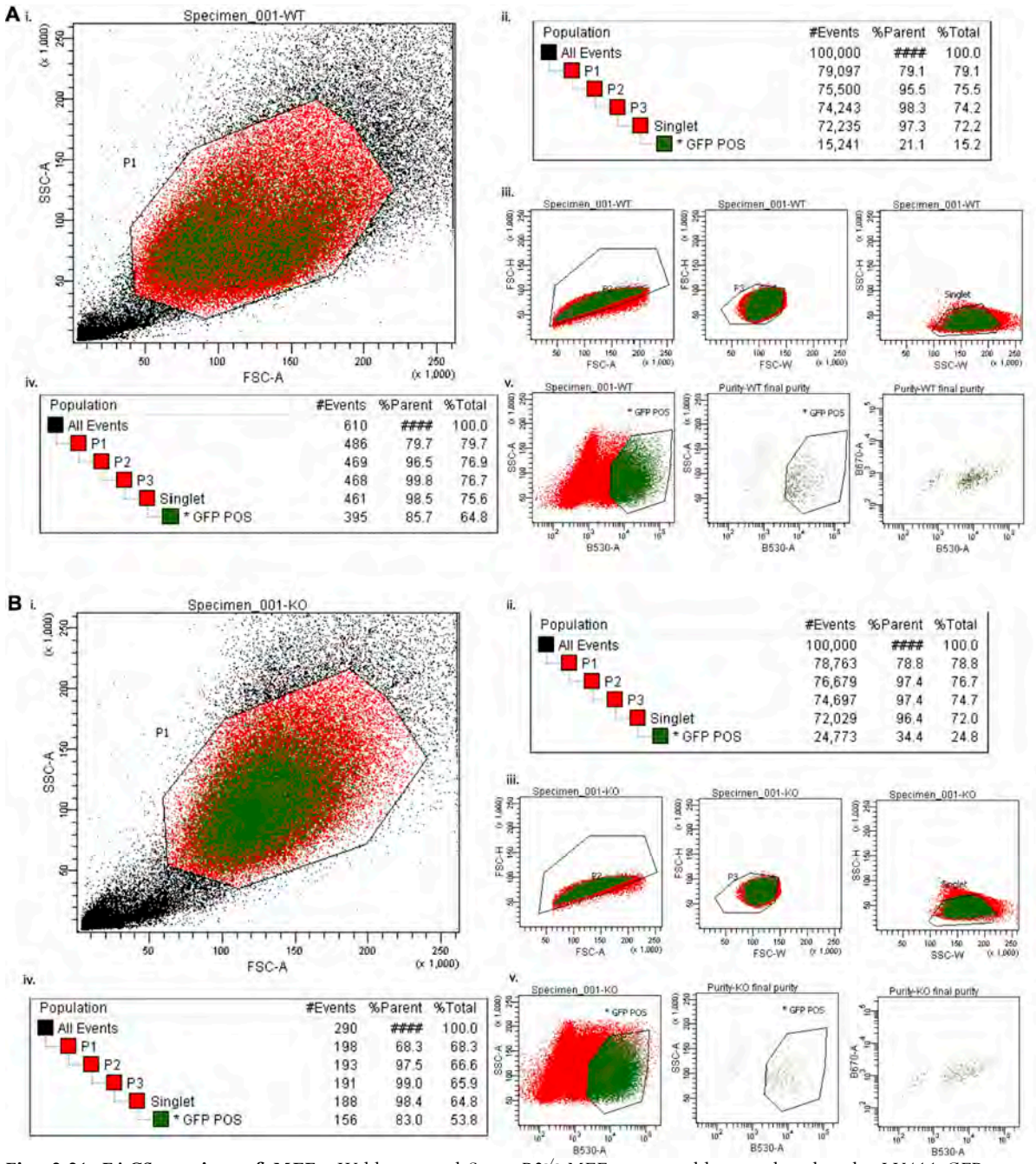

Fig. 2.21. FACS sorting of MEFs. Wild-type and SerpinB2$^{-/-}$ MEFs were stably transduced with pLV411 GFP vector and then sorted *via* FACS flow cytometry. **A. (i).** Light scatter plot of entire unsorted wild-type MEF population. To discriminate between healthy and damaged or dying cells, side scatter (SSC-A) and forward scatter (FSC-A) are plotted (P1); **(ii).** Panel displays the gating of initial wild-type MEF purity, during sorting; **(iii).** Gated populations are based on forward scatter height (FSC-H) v Area (P2), FSC –H v Width (P3) and Side scatter height (SSC-H) v width (singlet). To initially purify the population, gating for GFP-positive cells was done using 530-nm laser (B530-A) against SSC-A; **(iv).** Panel displays the gating of wild-type MEF purity after sorting; **(v).** Gated populations are based on SSC-A v B530-A (*GFP-POS) and final gating for GFP-positive cells was done using a 670-nm laser (B670A) against B530-A; **B. (i).** Light scatter plot of entire unsorted SerpinB2$^{-/-}$ MEF population. To discriminate between healthy and damaged or dying cells, SSC-A and FSC-A are plotted (P1); **(ii).** Panel displays the gating of initial SerpinB2$^{-/-}$MEF purity, during sorting; **(iii).** Gated populations are based on FSC-H v Area (P2), FSC –H v Width (P3) and SSC-H v width (singlet). To initially purify the population, gating for GFP-positive cells was done using B530-A against SSC-A; **(iv).** Panel displays the gating of SerpinB2$^{-/-}$MEF purity after sorting; **(v).** Gated populations are based on SSC-A v B530-A (*GFP-POS) and final gating for GFP-positive cells was done using B670A against B530-A.

2.4 DISCUSSION

This chapter outlines the development and validation of third generation lentiviral vectors for SerpinB2 modulation and GFP reporter gene applications. The production of these lentiviral vectors with a codon-optimised expression cassette under control of a TRE, CMV or (TO) promoter with high activity successfully modified the expression of SerpinB2 in MDA-MB-231 cells, and knock-in GFP within MEF cells. The Gateway® lentivirus vector system utilised in this project offered a robust and efficient tool for gene editing studies. Incorporation of a central polypurine tract (cPPT) and post-transcriptional regulatory element from woodchuck hepatitis virus (WPRE) in third generation lentviral vector systems has improved SerpinB2 transgene expression (402), versus earlier lentiviral systems used. This increase in transduction efficiency, nuclear localisation and the total amount of RNA integrated into cell genomes meant that phenotypic characterisations could be made much easier (403) (404), with increased reliability that effects were consequences of SerpinB2 modulation.

All necessary elements required for the production of the lentiviral vectors were cloned into the four donor plasmids and subsequently many high titre lentiviral stocks were produced. Homologous recombination reactions were always performed in triplicate to ensure that sequence homology was maintained. Sequencing consistently gave positive results, with evenly spaced peaks and a general lack of baseline 'noise' (refer to Fig. 2.6-2.11), proving that Invitrogen's Gateway® system offers rapid, highly efficient site-specific recombination methodology for gene editing. It is widely agreed that packaging of lentivirus inside HEK-293T cells proves to be an extremely efficient medium for production of viral particles (413), and in this body of work offered the best intermediate for reliable viral titres when comparing between constructs. For all SerpinB2, ^{R380A}SerpinB2, SerpinB2 ΔCD loop, ^{R380A}SerpinB2 ΔCD loop, GFP, LacZ and several scramble control (not shown) constructs, this system was effective in the production of lentiviral particles for subsequent infection of chosen mammalian cell lines and targeted gene modulation. Transient transfections were undertaken preliminarily (refer to Fig.

2.13), as these are straightforward to perform, versatile and avoid the time-consuming development and reagent use required when creating stable cells lines. It also allowed for easy and rapid testing of the various transgene constructs produced, and has been reported to be effective for testing viral pseudotypes (414). Since the transient transfection system allows virus production for a limited time only and co-transfection may increase the risk of recombination between the plasmids, stable packaging cell lines for SerpinB2 modulation were sought, in addition to moving towards *in vivo* models. Previously, much research has been undertaken to develop stable packaging cell lines for the production of lentiviral vectors (415-417). Lentiviral vectors are known to package with various concentrations (MOI 50-1000) of lentivirus, thus in order to minimise off target effects of gene insertion, such as non-targeted gene disruption, a single integration of virus per cell was optimal (375). The viral transfer vectors used in this study encoded tetracycline-based inducer/repressor elements, which are separate to the transfer vector, meaning that the inducible transgene could be independently titrated to achieve various levels of transgene activation. An advantage of this system was that it could be used to make cell lines with various base levels of repression for relatively comparable over-expression of multiple transgenes. Therefore, to determine the optimal level of repression for virus production and transduction, characterisation of the MOI of produced lentiviruses was determined by LacZ[-CMV(TO)] transduction of MDA-MB-231 cells and subsequent growth on X-gal plates of different viral dilutions (Fig. 2.14). This method was based on the amount of transgene copies per cell and allowed for evaluation of different dilutions to use in subsequent experiments, in order to ensure that the number of integrated proviral genomes was not affecting the tetracycline repression and thus not giving constitutive transgene expression without Dox treatment (418).

The pLenti6.3/TO-DEST-V5 vector was productively exploited to knock-in wt SerpinB2, full-length ^{R380A}SerpinB2 (and SerpinB2 ΔCD, ^{R380A}SerpinB2ΔCD loop constructs) and LacZ into MDA-MB-231 cells (refer to Fig. 2.15). Under tetracycline repression, this vector system was highly effective at overexpressing both SerpinB2 and ^{R380A}SerpinB2. Validation by Western blot and immunofluorescence confirmed the efficacy of all

lentiviral constructs produced (refer to Fig. 2.15-2.17 and Fig. 2.19-2.20, respectively). An essential characteristic difference between third generation lentivectors to older viral vectors is that they contain region-specific promoters. Many earlier lentiviruses used the constitutive CMV promoter to drive the ubiquitous expression of a downstream transgene, not confined to just one subtype of cells (418). Thus, it has previously been difficult to attribute whether phenotypic alterations caused by transgene transcription were due to intentional targeted manipulation in chosen cells or inadvertent effects on non-target cells (419). The generation of stable overexpression cell lines was time-consuming, however the ability to generate these within the same vector type greatly facilitated progression. Stable packaging cell lines not only lessen variation between vector stocks, but also reduce the likelihood of generating any forms of helper virus and allow reproducible propagation of RCLs (420). In order to counteract the toxicity of lentiviral protease (421), which abrogates constitutive vector production, inducible packaging cell lines were constructed, controlled with tetracycline-inducible systems (416,422). The pLenti6.3/TO-DEST-V5 vector highlights the value of restricting transgene expression within specific types of cells, with a selectable repressive element. Co-transducing these regulator and response viruses into target cells, creates a system that allows major control of the expression level of a gene of interest by adjusting the concentration of the system's inducer, Dox (418). In order to be sure that the pLenti system was successful in producing increased expression of SerpinB2, both western blot (Fig. 2.17) and immunofluorescence imaging (Fig. 2.19) were undertaken to confirm. These assays validated the knock-in of constructs used and provided enough evidence that the generated cell lines could be used for subsequent experimental models.

Concomitantly, the pSLIK system was efficaciously used to conditionally deplete the expression of SerpinB2 and GFP in MDA-MB-231 cells and MEF cells, respectively. Validation of both SerpinB2 shRNA knockdown constructs produced were observed over a 40 day period (with Dox treatment) in cell culture (refer to Fig. 2.16). This was performed in order to ensure as much as possible that knockdown cell lines produced could be

used in *in vivo* models with reliability that SerpinB2 knockdown would be maintained. The pSLIK system supported robust RNAi mediated knockdown of SerpinB2 and there was no recorded evidence of leaky expression from the TRE promoter. The Tet-inducible knockdown of SerpinB2 gene after transduction of cells with a single pSLIK lentivirus provides an important experimental platform for analysing the downstream effects on proliferation and the redundancy in signaling pathways associated with this gene. There is the potential for low basal expression of miR-shRNA, which has been reported to be a challenge with highly potent shRNA sequences (412). Shin *et al.* (2006) have reported that pSLIK's vector topology and optimised TRE-driven rtTA3 expression system counteract any problematic issues, driving fast integration and initiation into RISC (412). The presence of Dox creates a positive feedback loop, which drives higher rtTA3, and ostensibly, miR-shRNA expression (412).

In addition, subsequent cell confluency testing was recorded using the IncuCyte ZOOM digital imaging system, in order to see effects on cell proliferation (refer to Fig. 2.18). It was noted that the SerpinB2 shRNA hairpin 2 (+Dox) MDA-MB-231 cell line had reduced doubling time. This result requires to be followed up as time constraints unfortunately did not allow inquiry into further proliferation assays.

The pLV411 lentivirus expressed GFP as a transgene with minimal lentiviral cis-elements (LTR, packaging signal, RRE) (398). This allowed for the GFP mRNA sequence to be transposed with greater reliability of MOI as well as offering a good way to test the effectiveness of the promoter/enhancer elements in the pLV411 construct. After subsequent FACS sorting, a largely pure population of GFP-positive MEFs was produced (refer to Fig. 2.21), which were utilised in concurrent experimental models. The standard time frame for each pooled lentiviral infection in this study was approximately 2-3 weeks from the generation of the lentivirus to expansion of each genetically modified cell line. MOI can fluctuate naturally between groups of packaged lentivirus, due to differences in vector DNA quantity integrated during packaging, as well as the ability of chosen cells packaging efficiency, passage number and time of harvest post infection (420,423). In order to counteract this,

passage number was kept below five, harvesting was held time-period consistent and the same batch of packaged lentivirus was used for all generated constructs.

This study provides a rapid and effective modus operandi for the generation of lentiviral vectors, for both overexpression and attenuation of SerpinB2 gene expression. This work demonstrates specific transduction of transgene expression, which could be used for the potential development of serpinB2 gene therapies, within a cancer therapy approach. These data allow for further knowledge and insight to be gained when working with this powerful inhibitor gene of the Plasminogen activation pathway. Lentiviral vectors provide a powerful method to inducibly manipulate SerpinB2 (and GFP) gene expression in highly invasive breast cancer epithelial cells (and fibroblasts). With both the ability to over-express and knockdown genes of interest in a temporal, spatial, and cell-type specific fashion, this inducible genetic approach will allow for eventual understanding of the differential roles of SerpinB2 in the tumour microenvironment, which underlies the enormous complexity of tumour function and behaviour. GFP imaging in biomedical research is commonplace and extremely important not only as a diagnostic tool, but also in monitoring the progress of therapy. Molecular imaging provides a non-invasive opportunity to study diseases at the cellular or even the genetic level. In light of this, recent developments in gene editing technology are offering newer alternatives to lentiviral transduction, which minimise off-target effects, at the expense of time and cost. This study demonstrates the usefulness of lentiviral gene modulation for several targeted therapy applications offering a versatile tool for imaging of live cell culture and tumour microenvironment purposes. The progress of tumourigenesis and metastasis in carcinomatous mouse models is necessary for drug discovery and elucidating molecular aspects of how cells behave in their native microenvironment. This knowledge helps to improve our current understanding of disease progression. In conclusion, this chapter's work illustrates the versatile application of lentiviruses for SerpinB2 modulation, and the constructs produced herein can be useful for the modification of SerpinB2 in other cell types and research platforms, including those used to study tumour-stroma interactions within pancreatic and breast cancer (chapters 4 and 5, respectively).

CHAPTER 3

ELUCIDATING THE EFFECT OF SERPINB2 ON COLLAGEN CROSSLINKING AND STROMAL REMODELLING THROUGH APPLICATION OF THE 3D COLLAGEN CONTRACTION MODEL

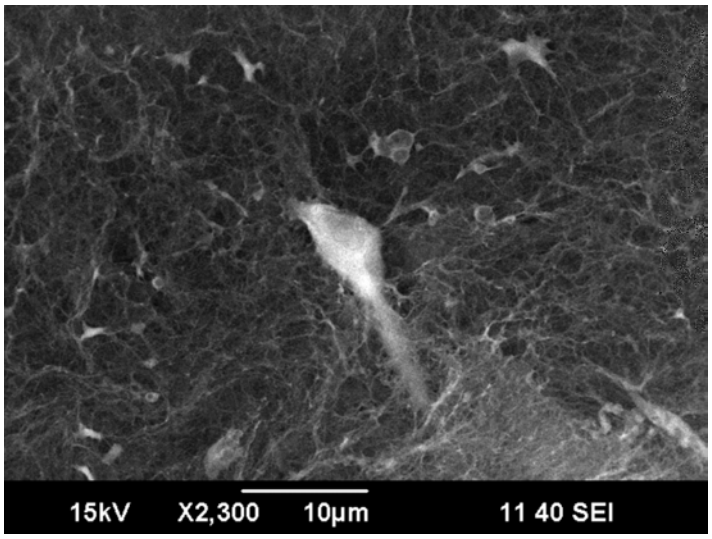

CHAPTER 3

ELUCIDATING THE EFFECT OF SERPINB2 ON COLLAGEN CROSSLINKING AND STROMAL REMODELLING THROUGH APPLICATION OF THE 3D COLLAGEN CONTRACTION MODEL

3.1 INTRODUCTION

In order to understand the processes of stromal remodelling and collagen cross-linking within the TME, extensive research into the structural and biological regulation of the ECM must be undertaken. As aforementioned, the ECM is directly responsible for the homeostatic functioning of cellular and tissue functions within the human body (refer to section 1.6). Strict control is essential for proper embryonic development, angiogenesis, wound healing, pregnancy and normative organ functioning. During pathological conditions, such as cancer, the dysregulated biochemical and biophysical functioning of the ECM perpetuates processes that aid in tumour invasion, metastatic niche formation and metastases (249). Exactly how ECM composition and remodelling is disrupted is still poorly understood, but is becoming increasingly accepted to be the crux for success or failure of many clinical therapies. Thus, this chapter aimed to elucidate the role of SerpinB2 on collagen matrix formation and stromal interactions within a TME context, through the use an advanced *ex vivo* 3D ECM model system. This novel model is based on the contraction of a type-1 collagen matrix, using human or murine fibroblasts (359), and was introduced to our laboratory by Dr Paul Timpson, Lab Head of Cancer Invasion and Metastasis at The Kinghorn Cancer Centre, Garvan Institute of Medical Research (Darlinghurst, Sydney). The primary function of this assay within a cancer research context is to mechanistically understand the process of ECM formation, tissue stiffness and collagen cross-linking, fibroblast/tumour association, tumour progression, migration and therapeutic efficacy of drug testing, as well as reducing the numbers of animal models by closing the gap between *in vitro* and *in vivo* research. Cell biology research has relied heavily on cell culture systems utilising cells grown on plastic in a 2-dimensional (2D) plane, which unfortunately do

not capture many effects of the tissue microenvironment as observed *in vivo*, including cell morphology, polarity and junctions, cellular interaction between the ECM and other tumour or stromal cells, and mechanotransduction, which affects intracellular signalling and cell fate (424). In the human situation, cancer invasion and metastasis occur in a complex 3D environment, with both autocrine and paracrine feedback loops in constant interplay from the surrounding host tissue and stroma. This governance of both cancer and stromal cell behaviour is both exceedingly complex and critical within the events that lead to dissemination and spread of a primary tumour thus, the use of 2D models are not comparable to the *in vivo* situation, creating conflicting results (358,425,426). The 3D organotypic model allows one to use the powerful fibroblast cell (discussed in more detail below) from nearly all tissue locations, which is the main cell type involved with the desmoplasia and fibrosis seen in invasive tumours (249,263,280). According to the type of tissue under investigation, a recapitulative ECM can be created utilising primary or immortalised fibroblasts, including those stably transduced with fluorescent markers. In this way, both stromal and tumour cells can be labeled in order to visualise cell-cell interactions during invasion. By mimicking the 3D TME, it is possible to couple *in vitro* and *in vivo* drug development with greater efficacy, utilising powerful advanced imaging techniques, with real-time, non-invasive imaging approaches for innovation of both biomarker target-based and phenotypic-based drug discovery experiments. In order to construct this TME, the 3D foundation substratum is produced by cultured fibroblasts, which actively contract collagen I into fibrils and bundles. Collagens have more than fifty binding partners *in vivo,* believed to be due to the requirement of such diversity of fibril patterns, ranging from parallel bundles in tendon and ligament, to orthogonal lattices in cornea, and interlocking weaves in blood vessels, skin, and bone (256). In healthy tissue this is beneficial, however, having such a large number of binding partners can have detrimental impacts in diseased tissue states. In the last decade there have been several novel innovations in 3D culture experimentation, such as the 3D organotypic model. In combination with the capacity to isolate specific genes or proteins and manipulate individual microenvironmental factors, these systems have facilitated the real-time analysis of live biological tissue specimen. These techniques can now be used to visualise the

cellular basis of fibroblastic migration, epithelial morphogenesis and migration modality, to test the roles of specific genes in regulating cell behaviour and the nature of cell-ECM interactions within equivalent carcinomatous tissues of the human condition. This is allowing for the elucidation of the contribution of microenvironmental factors to normal and disease processes. Collectively, this novel model can be used to answer fundamental biological questions and generate replacement human tumourigenic tissue, affording the increased fidelity and applicability of novel therapeutic approaches. Through combining advanced imaging with 3D systems, it is now possible to provide more informative and disease-relevant platforms for cancer behaviour and drug discovery.

3.1.1 Imaging 3D systems

In order to characterise and capture the continuous cellular and molecular narrative involved in tissue development and remodelling, advanced imaging in 3D cultures is being developed and helping to extend the frontiers of medical science (372). 3D Imaging of live (and fixed) tissue is typically undertaken overnight using an inverted microscope and requires constant control of temperature, humidity, 0_2 and CO_2 levels, and evaporation (427). As such, there are many new challenges involved to accurately visualise live cells in 3D cell cultures, techniques such as bright field and phase microscopy are usually not feasible as 3D culture tissue is often thick and light is not as easily transmitted through the specimen (428). In addition, to effectively visualise 3D cultures in a non-destructive manner, epi-illumination (light detected in a backward direction) imaging techniques are preferred for the observation of 3D tissue structure and dimensional characteristics (428). Different microscopic systems can be used in complementation for detection of fluorescent markers, cell/tissue autofluorescence, backscattered light, as well as label free proteins that are non-symmetrical (e.g. collagen I fibres) (428). Such imaging systems used in this study included second harmonic generation (SHG), two-photon (TPM) and multi-photon microscopy (MPM), and scanning electron microscopy (SEM) (Fig. 3.1).

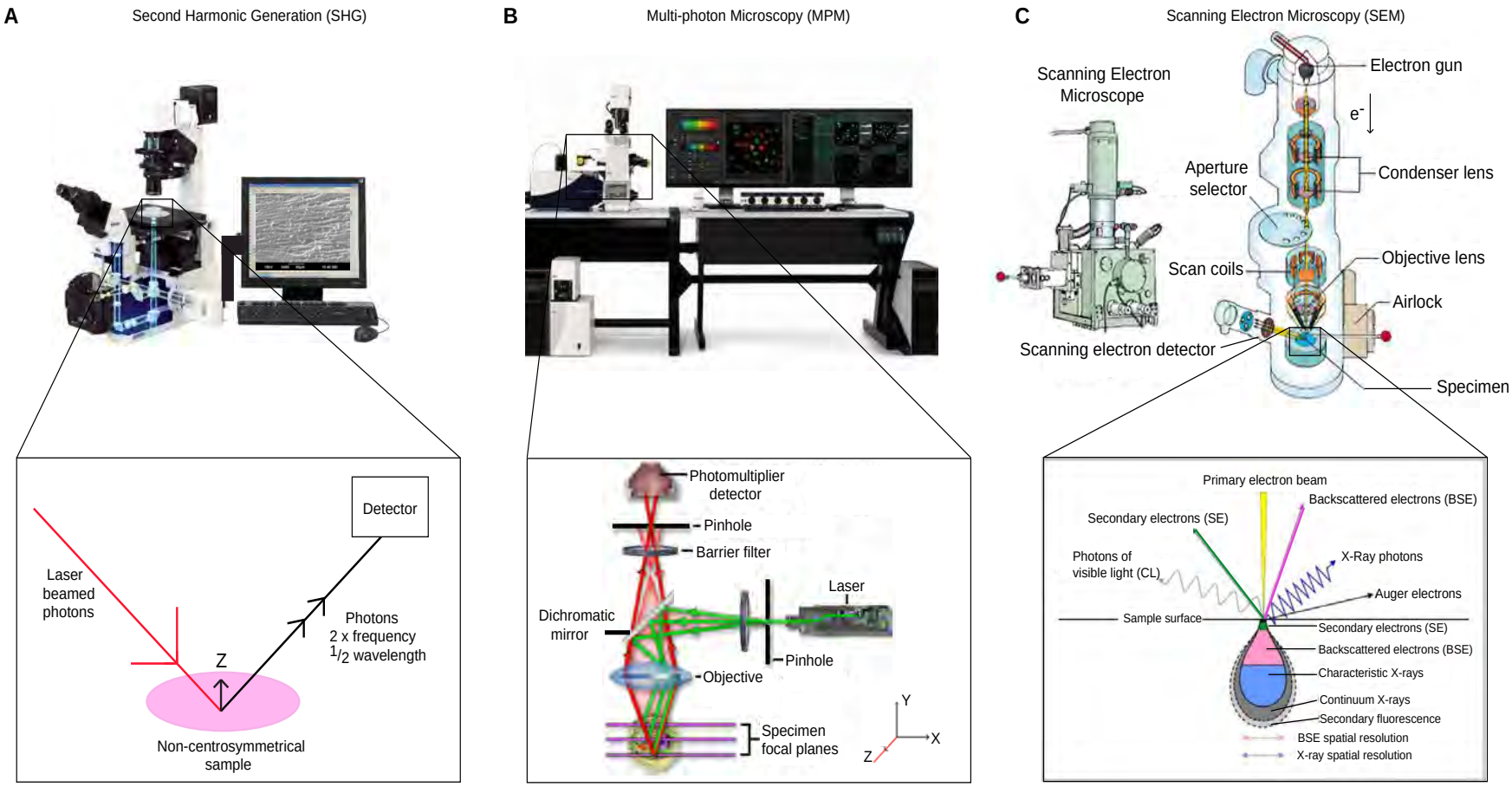

Fig. 3.1. 3D imaging systems. Diagrams of (**A**) second harmonic generation microscopy; (**B**) multi-photon microscope; (**C**) scanning electron microscope, and schematics of the signal paths of each system from the source, upon tissue sample and back to the detector for image generation. Images modified from http://www.leica-microsystems.com and http://binoculas.net.

3.1.2 Second harmonic generation (SHG)

In biomedical science, SHG microscopy is used for high-resolution, non-linear optical imaging that does not require fluorescent labeling for image detection (429). Instead, this technique involves two-photon fluorescence imaging, where a laser focuses two high-intensity photons upon a non-centrosymmetric tissue specimen to generate frequency-doubled light: the formation of one photon with twice the energy (and thus, frequency) yet half the wavelength of the initial photons (429) (Fig. 3.1A). In 1971, Fine and Hansen established SHG as a dynamic microscopic technique for visualisation of collagenous tissue samples (430). SHG differs from TPM in that it does not lose any photon energy after tissue absorption. The reason for this is because there is substantially less absorption into non-centrosymmetric tissue and thus, there is negligible thermal, photobleaching or phototoxic damage, valuable for live-imaging purposes (431). In addition, SHG imaging offers several advantages for live cell and tissue imaging as near infrared wavelengths of incident light can be used, meaning one can image deeper into thick tissues without any image loss or distortion. SHG laser photons are emitted coherently (432) and occur at non-centrosymmetric loci (433), such as collagen I fibres (434), myosin filaments (435), and in cellulose (436). Because SHG light is coherent, it is different to fluorescence microscopy in that it can capture dynamic information about the spatial organisation of molecules and tissue beds. Through the use of a high energy, short-pulse femtosecond laser and the correct filters, SHG excitation light can be easily isolated from the frequency-doubled emission signal (429). This means that pinholes are not required and very high axial and lateral resolution equivalent to confocal imaging can be obtained (429). In this regard, SHG microscopy has been extensively used to analyse tissues of the cornea and lamina cribrosa sclerae, both consisting primarily of collagen I (437). Within tissue specimen containing collagen I, SHG radiates from the shell of collagen fibrils, rather than from the core (434). The SHG signal may relate to the supporting element of each collagen fibril and thus, collagenous specimen can be resolved by directly imaging the backward-propagating SHG signal, which is an extremely useful tool for research within 3D live systems containing collagen I (434).

3.1.3 Multiphoton microscopy (MPM) imaging

MPM uses two pulsed long-wavelength photons to excite a fluorophore within a tissue sample. The two photons must simultaneously hit the fluorophore in order to excite an electron into a higher energy state, causing it to decay and emitting a fluorescent signal (438) (Fig. 3.1B). A MPM is different from a conventional fluorescence microscope, as the MP wavelengths of both excitation photons are longer than the wavelength of the resulting emission photon (438). MPM uses a raster pattern of focused laser light to generate an image, creating an optical section effect (439). Several advantages exist to multiphoton microscopy over confocal microscopy, including increased penetration depth with less damage to live tissue, higher contrast without bulk fluorescence, as well as all fluorescence light from the focus point being collected by the detector. The longer the emitted photon wavelength (typically infrared) the less damage there is to live tissue, meaning imaging can be undertaken for extended time periods without photobleaching or phototoxicity damage (439). In two-photon fluorescence microscopy (TPM), the synchronised absorption of two photons with half the frequency of the absorption spectrum of a fluorophore is necessary for fluorescence emission. The likelihood of simultaneous absorption of two photons within the natural light spectrum is small (calculated to be 1 event/106 years) (439). Thus, TPM fluorescence usually utilises a mode-locked laser, where photons are emitted at high intensity for extremely short (femtosecond) time periods (439). This technique allows for a multi-colour 3D image to be taken within tissue up to 70–100 μm deep, and also for time-lapse imaging. TPM was utilised within this study as it can both facilitate deeper imaging into specimen and visualise fibrillar ECM networks using SHG signals. Additionally, many novel techniques are being applied to MPM and TPM systems to help improve working length of biological samples without toxicity as well as attaining higher resolution images. Finally, 3D tissue samples can be prepared for ultrastructure imaging by scanning electron microscopy (SEM).

3.1.4 Scanning electron microscopy (SEM)

This technique has been used in cell biology since the early 1920's; however, as technology and methodology (cryogenic) has become increasingly better, sharp increases in resolution have been gained, specifically for biological matter. SEM produces a focused beam of electrons that interact with atoms in a sample, emitting a multitude of signals that contain information about the sample's surface topography, crystalline structure, chemical composition and electrical behaviour (440) (Fig. 3.1C). The types of signals produced by SEM include secondary electrons, back-scattered electrons, characteristic X-rays, light (cathodoluminescence) and specimen current and transmitted electrons (440). For biological matter, secondary electrons and back-scattered electrons are readily detected for image generation. The electron beam is scanned in a raster scan pattern predominantly (refer Fig. 3.1C), and the beam's position is combined with the detected signal to generate an image (440). SEM can achieve high resolution from >1 μm down to ~1 nm, and specimens can be observed in high or low vacuum, and at a wide range of cryogenic or elevated temperatures (441). The angle at which an electron beam contacts with the surface of a specimen is largely responsible for the resolution of the image as electron repulsion happens in a vast array, which must be optimised during each sample run. SEM was utilised in this project as it offered the ability to attain high-resolution ultrastructure information about the collagen networks formed in stromal matrices during fibroblast mediated ECM contractions.

3.1.5 SerpinB2 in the ECM

In order to facilitate proper ECM contraction, fibroblasts must appropriately regulate the PAS pathway. The combined signalling and proteolytic outputs of the PAS pathway activate a plethora of downstream events driving ECM degradation, cell proliferation, adhesion and migration (89). Negative regulation of this pathway occurs at several levels, including inhibition and clearance of protease activity by naturally occurring inhibitors, such as SerpinB2 (19,25). Elevated tumour SerpinB2 expression is linked with prolonged survival, decreased

metastasis, or decreased tumour growth in many cancer types (19,442,443). However, specific mechanisms have not been addressed. Therefore, to identify the role of SerpinB2 in collagen cross-linking and stromal remodelling it is necessary to interogate and dissect the role of the PAS pathway in collagen fibrillogenesis and ECM development. Through modulation of PAS activity in a context-dependent manner it should be possible to demonstrate the necessity of PAS activity in regulating cell-stromal interactions driving fibroblast adhesion and migration, collagen integrity and ECM remodelling.

Thus, the specific aims of this chapter were to:

1. Construct stromal equivalent collagen I matrices using fibroblasts with modified SerpinB2 expression.
2. Characterise the ultrastructural properties of these matrices using advanced microscopy techniques, including second harmonic generation (SHG), multiphoton microscopy (MPM) and scanning electron microscopy (SEM) analyses.
3. Identify and ascertain differences between the fibrillogenesis and stromal remodelling of matrices, in order to understand potential influences upon invasive capacity of epithelial breast and pancreatic carcinoma cells in proceeding experiments (Chapter 4 and 5).

3.2 METHODS

3.2.1 Cell lines and culture conditions

Human skin derived telomerase-immortalised fibroblasts (TIFs) (359) were maintained in Dulbecco's modified Eagle's medium (DMEM) supplemented with 10% FBS with 100 U/mL penicillin and 100 µg/mL streptomycin in a humidified 5.0% CO_2 atmosphere at 37°C. All cell cultures were routinely tested in-house for absence of mycoplasma contamination using the MycoAlert™ Mycoplasma Detection Kit (Lonza,

Switzerland). Spontaneously immortalised GFP-positive wild-type and SerpinB2$^{-/-}$ mouse embryonic fibroblasts (MEFs) were previously generated and cultured as described in Chapter 2 (section 2.2.1).

3.2.2 Flow cytometry

Expression of cell surface uPA and uPAR was analysed by indirect immunofluorescence using dual color flow cytometry (LSRFortessa^{TM}, Becton-Dickinson), propidium iodide (PI) was used to exclude non-viable cells as previously described (444). Data was analyzed using FlowJo software version 7.6.5 (FlowJO LLC, USA) comparing specific antibody binding to isotype controls to account for nonspecific binding (refer to Supplementary Antibodies Table of Appendix – Table A1).

3.2.3 Wound healing assays

Wild-type and SerpinB2$^{-/-}$ MEF migration differences were tested in 2D, prior to 3D model experimentation. All assays were performed in a humidified 5.0% CO_2 atmosphere at 37°C using the IncuCyte ZOOM imaging system (Essen BioScience, USA). Wells were seeded with either wild-type or SerpinB2$^{-/-}$ MEFs at even density (25,000/well) in triplicate in an uncoated ImageLock 96-well plate (Essen BioScience) and allowed to attach and spread over 16 h in RPMI containing 10% FBS. After a subsequent wash step with phosphate buffered saline (PBS), the wells were refreshed with RPMI in the presence or absence of 10% FBS. Scratch wounds were generated with the Woundmaker tool and images taken every 2 h. Images were processed using IncuCyte ZOOM system (10 x objective) and wound regions were measured using automated analysis. Relative Wound Density (%, value of 0 = no migration, value of 100 = completed migration, when the cell density inside the wound is the same as the cell density outside the initial wound) was analysed as a percentage (± SEM).

3.2.4 3D organotypic contraction assay

Contraction of collagen I matrices by either TIFs, wild-type or SerpinB2$^{-/-}$ MEFs were performed essentially as previously described (359). Briefly, rat-tail tendon collagen was extracted with 0.5 M acetic acid to a concentration of 2.0 mg/ml. The purity of the isolated collagen I was verified by SDS-PAGE. Contraction to a 3D matrix was stimulated by mixing fibroblasts ($5.0 \times 10^5 - 1.0 \times 10^6$ per 12 matrices) into neutralised (pH 7.4) collagen I solution and placing into 35 mm petri dishes (2.5 mL/dish). For use in this assay, TIFs were required to be quiescent, by leaving in culture for 4-14 days after confluency without change of media, while MEFs were used immediately upon reaching confluency. Detached polymerised matrices were then allowed to contract for 12-14 days (unless specified otherwise) in complete media (DMEM, supplemented with 10% FCS and pen/strep), refreshed every 2-3 days. It is of note that differences in overall matrix contraction time were observed due to different cell types used, or batch-to-batch variation in collagen I. This was controlled for by using the same collagen in triplicate experiments. Protein concentration was determined by performing SDS-PAGE alongside known concentrations of commercial collagen I (Sigma-Aldrich) and quantified *via* densitometry analysis.

Moreover, much literature has recently reported that doxycycline (Dox) is also an MMP inhibitor, decreasing MMP activity in wound healing (445), endometriotic lesions (446), reducing myocardial infarction size (447), as well as inhibiting MMPs and reducing brain damage after cerebral ischemia through attenuating hypertensive vascular remodelling in peripheral and cerebral vasculature (448). Therefore, supplement experiments were undertaken where either PBS (Control), 500 nM SerpinB2 ΔCD loop, ^{R380A}SerpinB2 (on ΔCD Loop backbone) or 20 μg/mL Dox were added to the media of contracting matrices, refreshed every two days. Dox is a broad spectrum inhibitor of MMPs, particularly MMP2, MMP9 (448), thus, Dox was used to elucidate the effect of MMP inhibition in collagen matrix contraction. Quantification of contraction rate was measured using photomicrographs and analysed by ImageJ (NIH, USA). After contraction, the matrices were fixed in 10%

neutral buffered formalin (NBF) for 2 days and either analysed or processed immediately, or kept in 70% ethanol at RT for 1-2 days before paraffin embedding or analyses. FFPE samples were then used for histological and microscopic analyses.

3.2.5 Histological analysis

Samples fixed in 10% NBF were processed using the Leica Peloris Dual Retort tissue processor (Germany). Histological staining was performed on 4 µm sections that had been deparaffinised in xylene and rehydrated using graded ethanol washes (70% - 100% EtOH). Haematoxylin and Eosin and picrosirius red (Polysciences, USA, #24901-250) staining were performed on a Leica Autostainer XL. Immunohistochemistry was performed used the Leica Bond RX system. Refer to Appendix Table 1 for antibody details. For scoring of invasive index, migration modality, cell cluster and immunohistochemistry staining, ten images per sample were acquired using a bright field microscope (Leica DM4000).

3.2.6 Ultrastructural SHG imaging

Live collagen I matrices or 20 µm sections of fixed contracted matrices, or tumours, were imaged using a 203 0.95 NA water immersion objective on an inverted Nikon TE-2000 microscope body. The excitation source was a Ti:Sapphire femto-second laser cavity (Coherent Chameleon Ultra II, USA), coupled to a LaVision Biotec Trim-scope scan-head. 840 ± 20 nm excitation wavelength/420 ± 10 nm emission wavelength was used to collect collagen 1 SHG signal. ImageJ was used to calculate percentage area detected by SHG signal per optical slice within a volume, after conversion to a binary image based upon a manually determined threshold value.

3.2.7 Tracking of fibroblast movements in matrices

Fibroblast motility through live collagen I matrices was computed by tracking cell position versus time with Imaris 8.0 (Bitplane, USA), using the cell-detection (built-in spots) and isosurface tracking routines (130 - 160 cells were tracked per experiment). Cells were selected for analysis if the cell centroid moved greater than one

cell diameter over the 14 h time course and blebbing cells were excluded. Visual confirmation was also used to exclude any cells displaying oscillations or shape changes to minimise artefacts associated with automated analysis. All cells were tracked in z-planes in the central part of the matrix (typically where the matrix was thickest for wild-type MEF matrices) to avoid any potential edge effects. GFP-tagged wild-type and SerpinB2$^{-/-}$ MEFs were detected using 488 nm excitation wavelength.

3.2.8 SEM imaging

Fixed matrices were sliced and clamped in a cooling chamber consisting of a 25mm x 10mm brass block with a sample chamber groove. The brass holder containing each sample was plunged into a bath of liquid nitrogen for 40 – 45 sec and then fractured with a liquid nitrogen cooled blade, to expose a cross-section surface which was flush with the surface of the brass block. The cooled holder with the fractured sample was then inserted into a JEOL 6490LV scanning electron microscope equipped with a secondary electron detector and a backscattered electron detector (scintillator type) using acceleration voltages between 10 and 20 kV. Images were recorded with an integrated JEOL digital image acquisition system, undertaken at the Australian Institute for Innovative Materials (AIIM), the UOW Electron Microscopy Centre (EMC), North Wollongong Australia.

3.2.9 Pilot proteomic analysis of wild-type and SerpinB2$^{-/-}$ MEF matrices

10 µm section of FFPE wild-type and SerpinB2$^{-/-}$ fibroblast mediated collagen I contracted matrices (n = 3) were sent to our collaborators, Dr Oliver Shilling and Dr Zon Weng Lai, at the University of Freiburg, Germany. Sections were deparaffinised with xylene and rehydrated in a decreasingly graded ethanol series, transferred into microreaction tubes and prepared for LC-MS/MS analysis by Dr Shilling and Dr Lai, as described in (449). LC-MS/MS analysis was performed on an Orbitrap XL (Thermo Scientific) mass spectrometer (MS) coupled to an Ultimate3000 micro pump (Thermo Scientific). The MS was operated in data dependent mode and each MS scan was proceeded by five MS/MS scans. LC-MS/MS data was obtained in raw format and converted to the mzXML format, using msconvert (86). For spectrum to sequence assignment X!

Tandem (version 2013.09.01) was used (449). The proteome database consisted of mouse and rat tissue reviewed canonical uniprot sequences (without isoforms) downloaded from UniProt (http://www.uniprot.org). Two different searches were conducted for light and heavy labelled peptides and mass tolerance for quantification was 0.02 Da. XPRESS data was $\log_2$-transformed yielding fold change (Fc)–values (449). Protein abundance was considered to be significantly altered if protein abundance increased or decreased with an average Fc-value > 0.70 or < -0.70.

3.2.10 Statistical analyses

Unless specified otherwise, data is presented as the mean (± SEM) of at least 3 independent experiments performed in either triplicate or sextuplet. Differences in the mean of two samples were analysed by an unpaired t-test. Comparisons of more than two groups were made by a one-way (or two-way) ANOVA with post hoc Holm-Sidak (or other post hoc) analysis for pairwise comparisons and comparisons versus control. *P* values < 0.05 were considered statistically significant. Unless stated otherwise, data and statistical analyses were performed using GraphPad Prism (version 6.0, USA).

3.3 RESULTS

3.3.1 Collagen I preparation

Collagen I is sequence conserved between rat and human, thus rat tails are the most convenient source for collagen I extraction within the laboratory, with a high content found in the tendon (four per tail). In order to ensure that the extracted collagen from rat-tails was in fact collagen I, a 7.5% SDS-PAGE was undertaken (Fig 3.2). Three bands can be observed in lanes 1 and 2, consistent with the sizes of collagen I monomers, alpha-1 chain [alpha-1(I) chain (139 kDa)] and alpha-2 chain [alpha-2(I) chain (129 kDa)]. As collagen I is a triple helix consisting of one alpha-2 chain and two alpha-1 chains, the third band present is the dimeric form

(~270 kDa) of alpha-1. Once confirmation of collagen I purity was achieved, proceeding contraction experiments using fibroblasts could be undertaken.

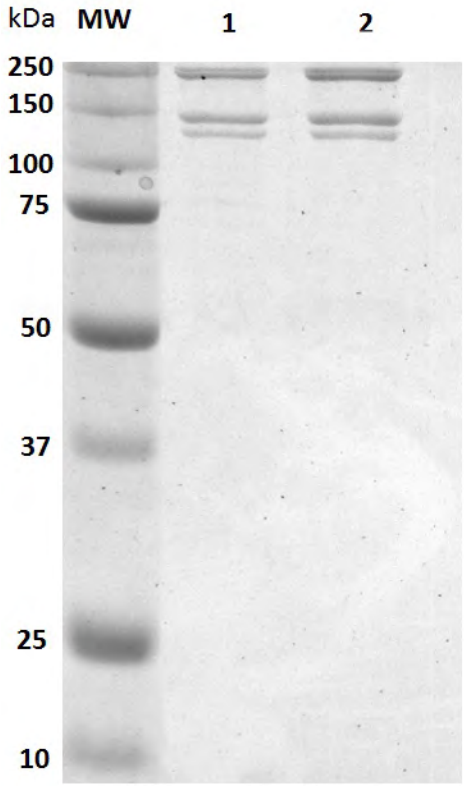

Fig. 3.2. SDS-PAGE analysis of a representative sample of purified rat tail collagen I. 7.5% non-reducing SDS-PAGE showing, Lane 1 – 0.5 µg collagen I; Lane 2 – 1 µg collagen I.

3.3.2 PAS expression in fibroblast lines

To determine PAS protein expression levels within the cell lines used for matrix formation, uPA and uPAR expression was undertaken using flow cytometry, and SerpinB2 expression by Western blot analysis (refer to section 2.2.10.1 for methodology) (Fig 3.3). Both wild-type and SerpinB2$^{-/-}$ MEFs expressed cell surface uPA (Fig 3.3B,C), however uPA fluorescence shift was 2.3-fold less in the SerpinB2$^{-/-}$ MEFs versus wild-type MEFs ($P < 0.0001$, Fig 3.3E). uPAR was significantly expressed on both SerpinB2$^{-/-}$ and wild-type MEFs, versus IgG isotype controls (Fig 3.3B,C), however there was no significant uPAR fluorescence shift recorded between SerpinB2$^{-/-}$ MEFs and wild-type MEFs ($P = 0.2927$, Fig 3.3F). TIF cells showed little to no expression of these

PAS activators, relative to IgG isotype controls (Fig 3.3C). Western blot analysis revealed that TIFs and wild-type MEFs both expressed moderate levels of PAI-2 (translated SerpinB2), while SerpinB2$^{-/-}$ MEFs were devoid of SerpinB2, as expected (Fig 3.3D).

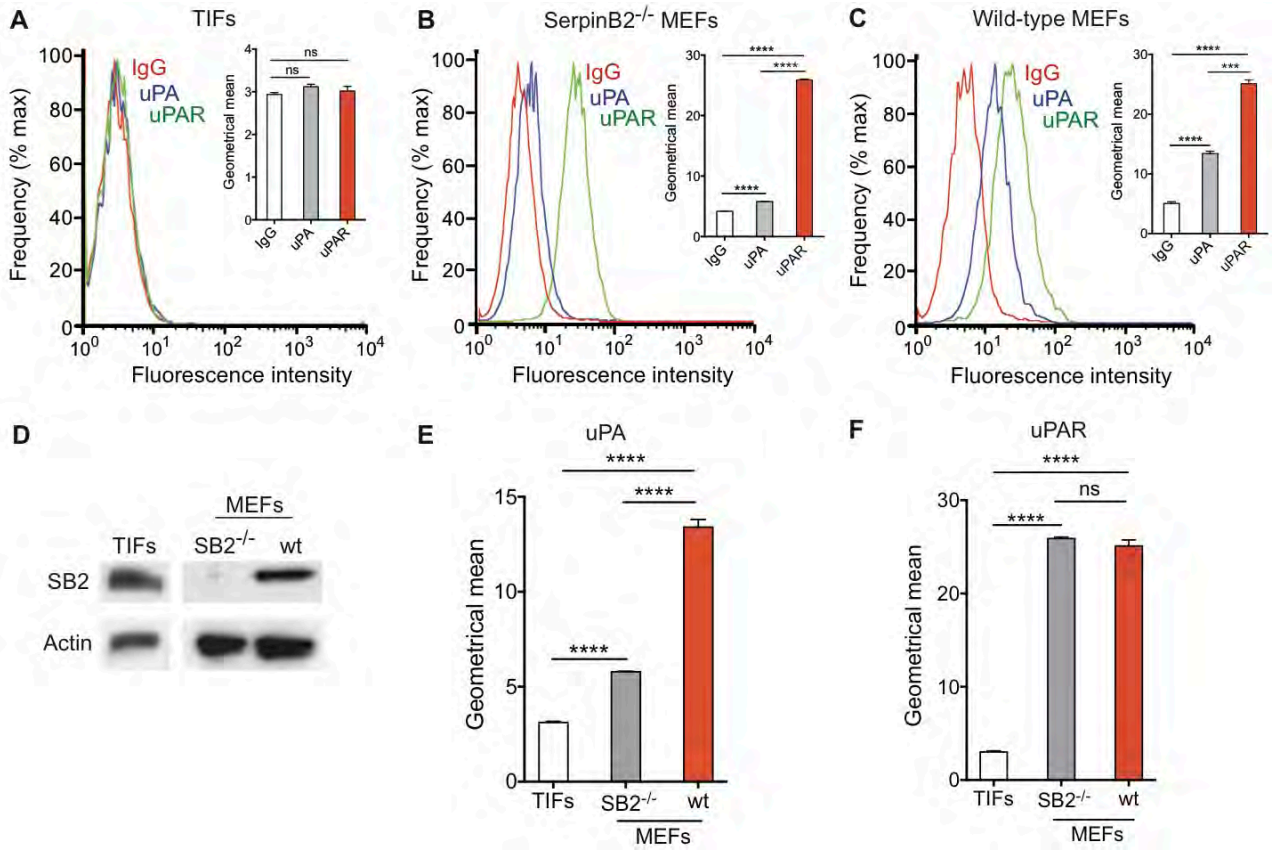

Fig. 3.3. Flow cytometry analysis of cell surface uPA and uPAR expression. A. Wild-type MEFs, **B.** SerpinB2$^{-/-}$ MEFs, and **C**. TIFs. Insets show the geographical mean of fluorescence intensity (± SEM, n = 3). **D.** Western blots showing expression of SerpinB2 in TIFs, SerpinB2$^{-/-}$ and wild-type MEFs. Blots were reprobed for actin as equiloading controls.

3.3.3 Differences in MEF migration/2D wound healing

The rate of proliferation of wild-type versus SerpinB2$^{-/-}$ MEFs was not significantly different in 2D systems [data not shown; reported by (167)]. Conversely, there was a significant difference observed in MEF cell migration as observed in 2D scratch wound assays, where the ability of SerpinB2$^{-/-}$ MEFS to polarise and migrate into the wound space over 24 h was significantly impaired under serum containing conditions, compared to wild-type

MEFs ($P < 0.0001$) (Fig. 3.4, A). This effect is not due to differences in MEF proliferation as aforementioned, and also observed in the serum free conditions of the assay ($P < 0.0001$) (Fig. 3.4, B).

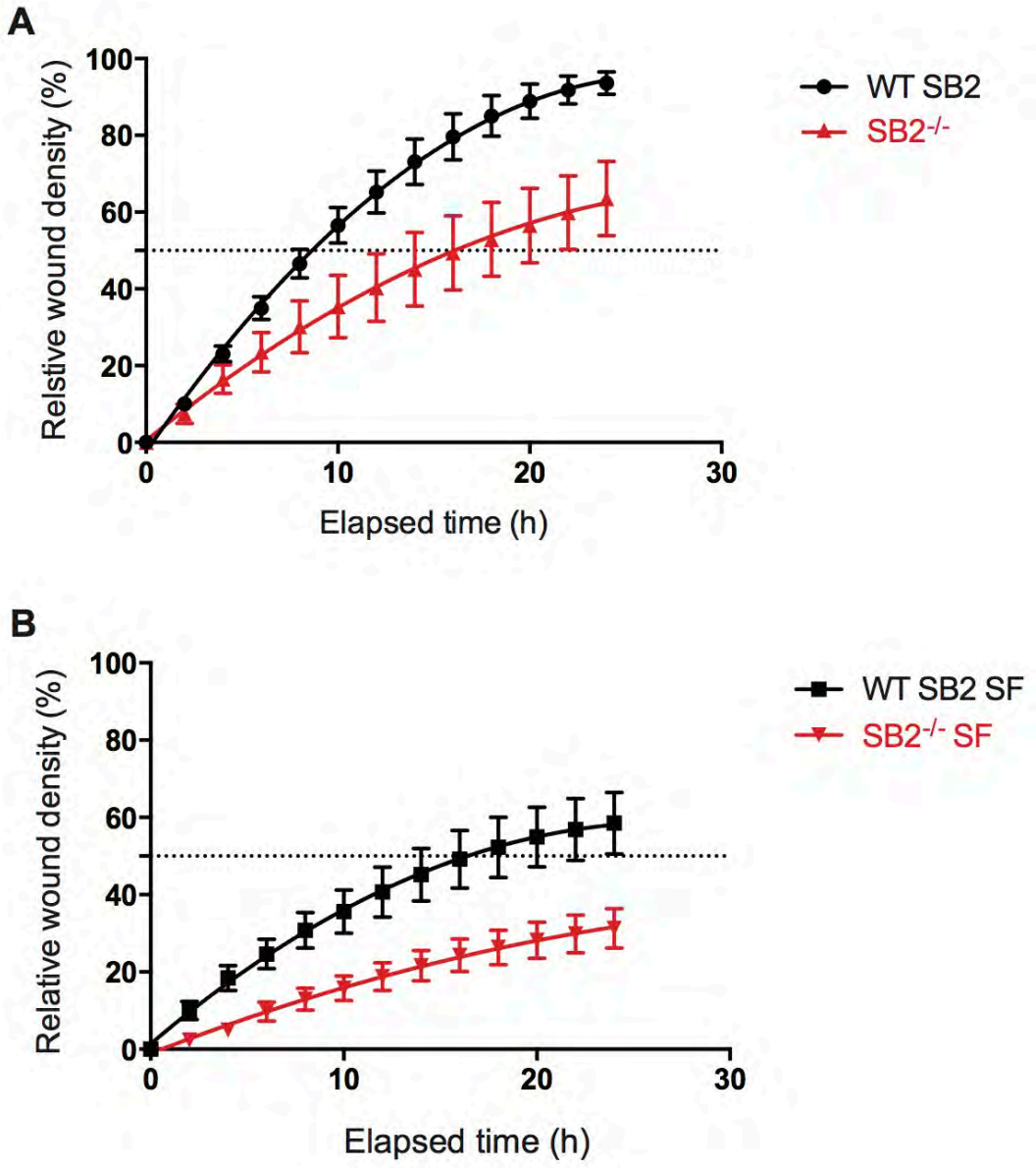

Fig. 3.4. Comparative time-course of migration of wild-type SerpinB2 versus SerpinB2$^{-/-}$ MEFs measured using IncuCyte ZOOM (Essen Biosciences). Cells (25,000/well) were added to an uncoated ImageLock 96-well Plate and allowed to attach and spread over 16 h in RPMI containing 10% FBS. After a subsequent wash step with PBS, the wells were refreshed with RPMI in the presence (**A**) or absence (**B**), of 10% FBS. Scratch wounds were generated with the Woundmaker tool and images taken every 2 h. Images were processed using IncuCyte ZOOM system and wound regions were measured using automated analysis. Relative Wound Density (%, value of 0 = no migration, value of 100 = completed migration, when the cell density inside the wound is the same as the cell density outside the initial wound). Each point represents the mean of 24 wells with the vertical bars showing the SEM. Generated by time-lapse imaging (Incucyte, 10 x objective) over time.

3.3.4 Fibroblast contracted collagen I matrix formation and integrity

Primarily, TIFs were used to verify that these cells could indeed contract collagen over a period of 12 days, forming robust dermal equivalent extracellular matrices (359). SEM imaging was then utilised to show the ultra-structure of these matrices (Fig. 3.5), revealing robust matrix integrity. Both surface (Fig 3.5A-E) and sagittal (Fig 3.5F-J) images were taken, revealing robust fibroblast-collagen contracted matrices, with homogenous collagen cross-linking, large fibril networks and dense matrix formation. This innovative technique was thus shown to be an ideal model for understanding collagen crosslinking and stromal remodeling, as well as for the elucidation of the effects of PAS on this process.

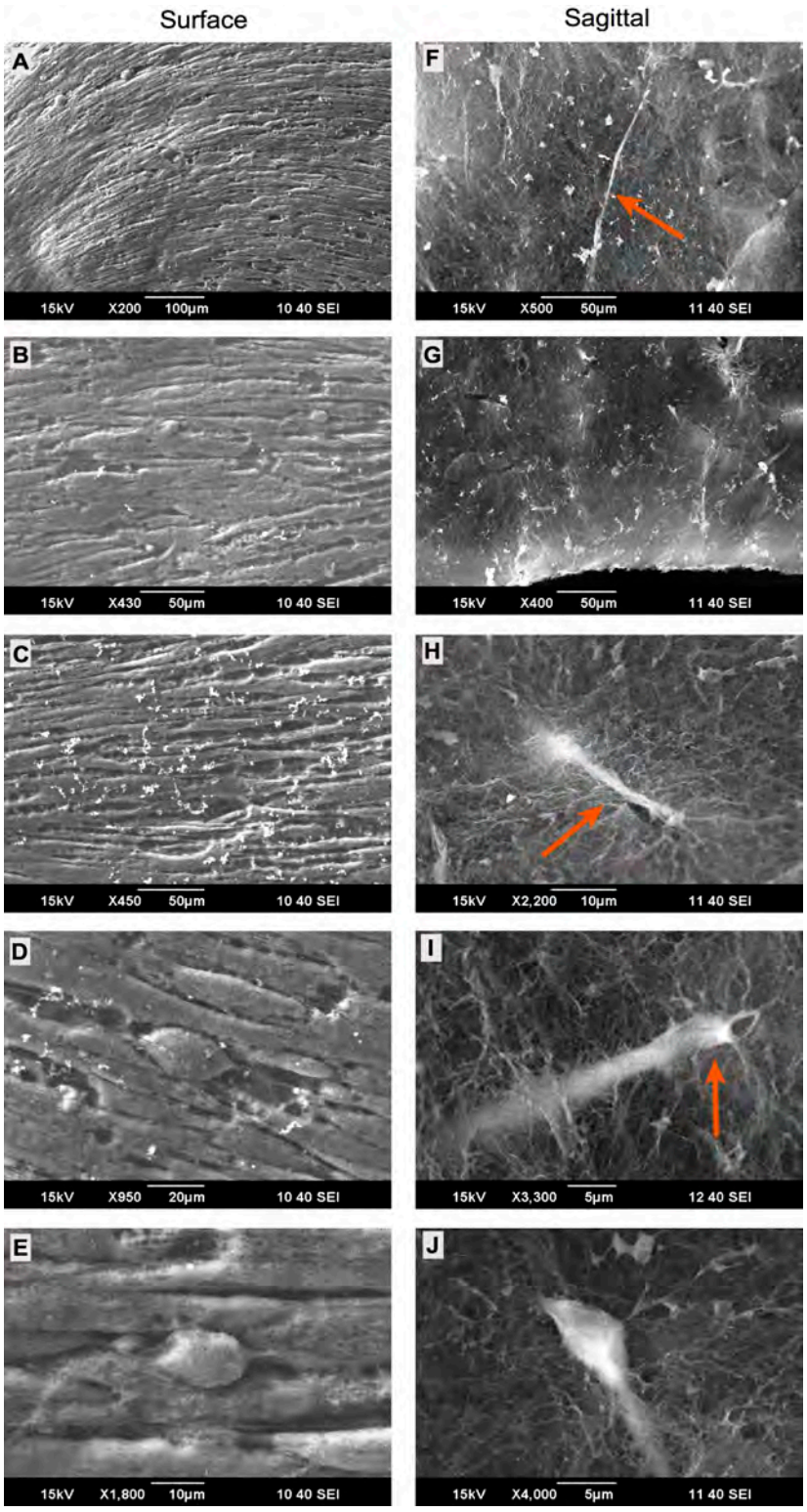

Fig 3.5. SEM ultrastructure analysis of TIFs matrices. SEM images show surface (**A-E**) or sagittal section (**F-J**) of TIF contracted collagen I matrices. Fixed sections were prepared (as described in section 3.2.7) at day 12 of contraction. Homogenous isotropic collagen cross-linking and large fibril networks in horizontal orientation can be seen in the surface section images (particularly images **A-C**). Solid matrix formation can be observed and TIFs (denoted by arrows) can be seen directly connected to the collagen networks.

Stromal expression of SerpinB2 is consistently linked to progression in a number of tumour types, as aforementioned. Therefore, to confirm the role of stromal SerpinB2 in regulation of the ECM and involvement with collagen fibrillogenesis, TIFs were substituted for wild-type or SerpinB2$^{-/-}$ MEFs to drive matrix contraction. Interestingly, matrices formed by SerpinB2$^{-/-}$ MEFs showed significant differences in the rate of collagen contraction to those generated by wild-type MEFs (Fig. 3.6). After a 12-day contraction period, wild-type MEF-contracted collagen I matrices were on average 2.3 x smaller than those contracted by SerpinB2$^{-/-}$ MEFs (Fig. 3.6D). This corresponded to a 58% reduction in the rate of matrix contraction in the absence of SerpinB2 (Fig. 3.96). This phenomenon was further characterised by a series of detailed structural analyses performed to interpret matrix integrity and organisation during matrix formation by either wild-type or SerpinB2$^{-/-}$ MEFs. SHG analysis of collagen coverage and density showed that wild-type fibroblasts formed a robust matrix composed of stable, covalent cross-linked collagen I, with homogenous density (Fig. 3.6A, Supplementary movies 1 and 2). Conversely, SerpinB2$^{-/-}$ fibroblasts formed disordered collagen networks with heterogeneous collagen I density and decreased diffusive hindrance (Fig. 3.6B; Supplementary movies 3 and 4). Quantification of SHG signal through z-stacks of each matrix showed a significant decrease in collagen coverage in the absence of SerpinB2. Maximum collagen coverage of 30% was observed in wild-type matrices at a depth of 20 μm, decreasing to 13% at a depth of 80 μm (Fig. 3.6C). In contrast, maximum collagen coverage only reached 10% in SerpinB2$^{-/-}$ matrices at the same 20 μm depth (Fig. 3.6C). 3D imaging of the SHG signal through matrices showed the stark differences between matrices constructed with SerpinB2 (Fig. 3.6F, Supplementary movie 5) or in the absence of SerpinB2 (Fig. 3.6G, Supplementary movie 5). The decreased diffusive hindrance recorded in the SerpinB2$^{-/-}$ MEF matrices shows the reduction in proper collagen I network formation, however more detailed ultra-structure characterisation was employed.

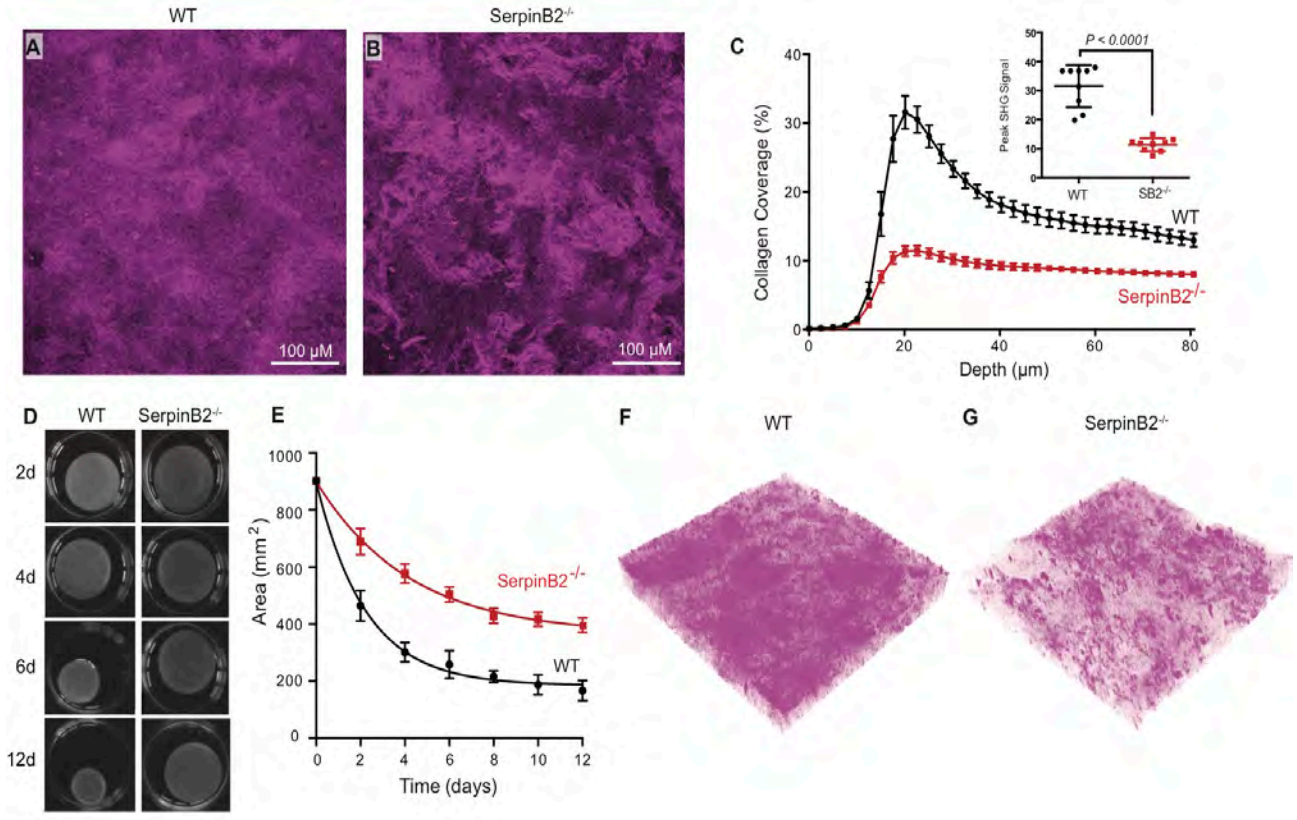

Fig 3.6. SHG imaging and quantification of wild-type and SerpinB2$^{-/-}$ MEF matrices. A-B: Maximum projection through 0 – 80 µm z-stack of SHG signal intensity of collagen I matrices formed with either (**A**) wild-type or (**B**) SerpinB2$^{-/-}$ MEFs; **C.** Total collagen coverage (quantified by intensity of SHG signal) within matrices formed by either wild-type or SerpinB2$^{-/-}$ MEFS, inset: Mean collagen coverage at SHG signal peak. Values shown are means ± SEM from 3 separate matrices (n = 9), statistical analysis performed using an unpaired t-test; **D.** Photographs showing collagen I matrix contraction over 12 days in the presence of either wild-type or SerpinB2$^{-/-}$ MEFS; **E.** Changes in area (mm^2) of collagen matrices shown in (**D**) over the 12 day contraction period. Values shown are means ± SEM from 3 separate matrices (n = 9); **F-G** 3D z-projections of multiphoton SHG imaging of matrices contracted by either (**F**) wild-type or (**G**) SerpinB2$^{-/-}$ MEFs, over a 12-day time course, demonstrating collagen crosslinking ability.

To this end, SEM imaging was undertaken and showed extensive fibril coverage, strong outer matrix structure and homogenous (isotropic) collagen distribution in the wild-type matrices (surface view Fig. 3.7A-E, sagittal view Fig 3.8A-E). Conversely, SerpinB2$^{-/-}$ MEFs formed disordered (anisotropic) collagen networks, with SEM revealing dense collagen bundles distributed in an unregulated fashion, resulting in poor collagen network integrity (surface view Fig. 3.7F-J, sagittal view Fig 3.8F-J). Hence, SerpinB2 expression by stromal fibroblasts is necessary for structural integrity in an *ex vivo* model of extracellular collagen matrix formation.

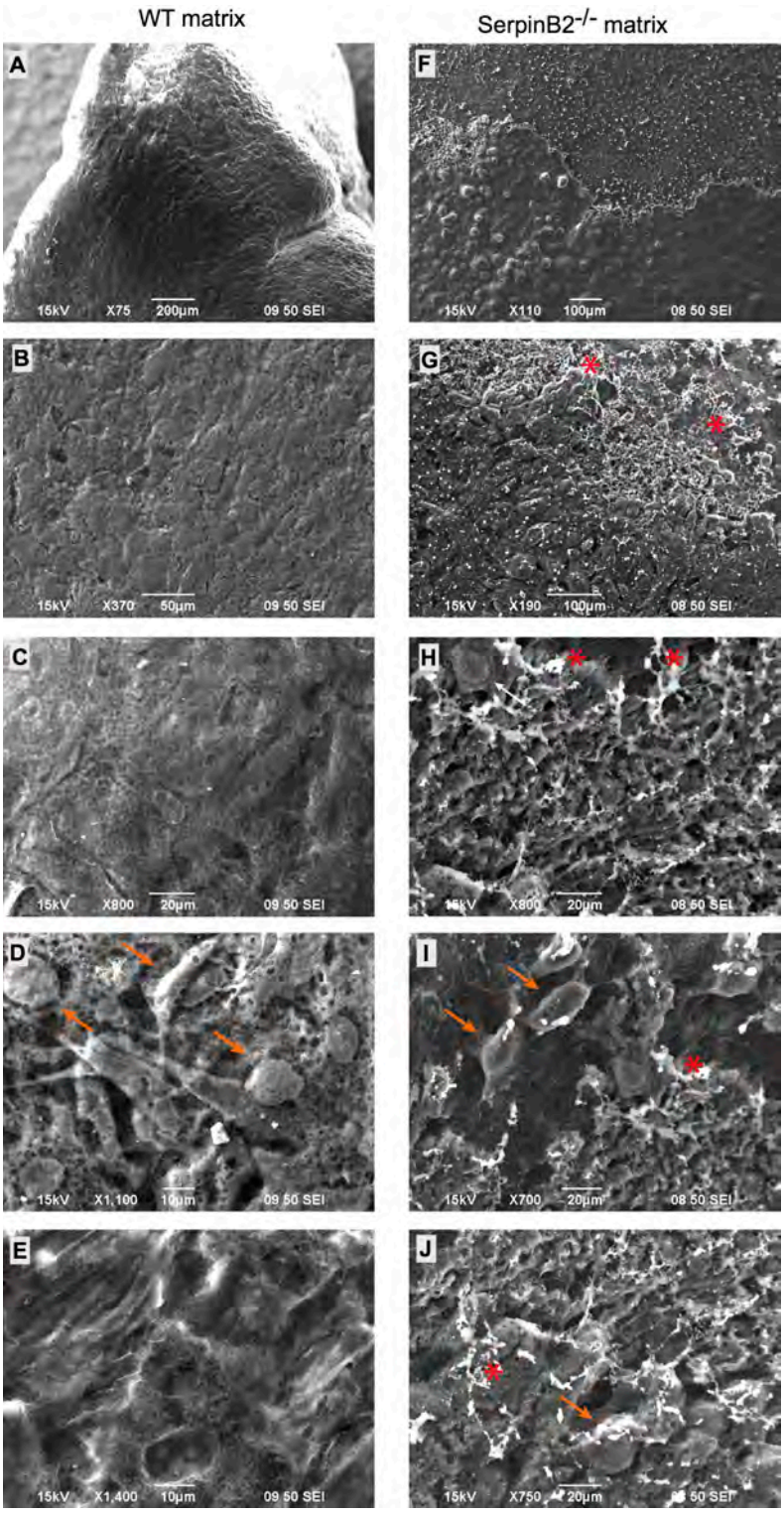

Fig 3.7. SEM ultrastructure surface analysis of MEF matrices. SEM ultrastructure analysis showing surface of either wild-type (**A-E**) or SerpinB2$^{-/-}$MEF (**F-J**) contracted collagen I matrices. Fixed sections were prepared (as described in section 3.2.7) at day 12 of contraction. Robust matrix formation can be observed in wild-type matrices (particularly images **B,C** and **E**), while SerpinB2$^{-/-}$ matrices show a malformed surface topography, with loose uncross-linked collagen (shown with a red *). MEFs (denoted by arrows) can be seen directly in the matrices, showing cell-cell contact and connected to the collagen networks in wild-type matrices, however this is considerably less in SerpinB2$^{-/-}$ MEF matrices.

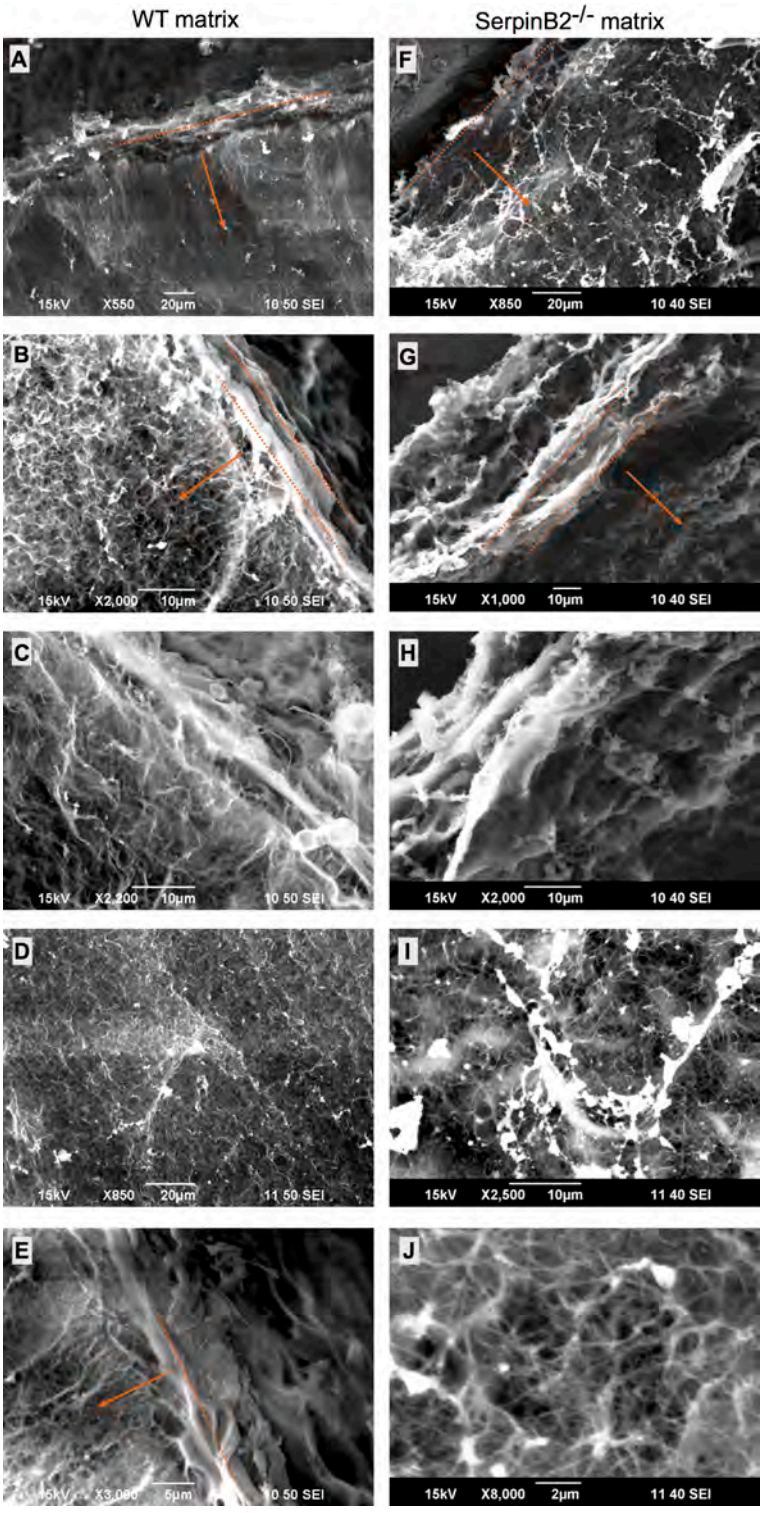

Fig 3.8. SEM ultrastructure sagittal section analysis of MEF matrices. SEM ultrastructure analysis showing sagittal sections of either wild-type (**A-E**) or SerpinB2$^{-/-}$MEF (**F-J**) contracted collagen I matrices. Fixed sections were prepared (as described in section 3.2.7) at day 12 of contraction. Collagen cross-linking of wild-type matrices can be observed with tighter networks and small pore size (**A-E**), while decreased collagen networks and decreased diffusive hindrance (large pore size) within SerpinB2-/- MEF fibril networks can be observed (**F-J**). Top of matrix is marked (**B** and **G**) with a dotted line and direction towards bottom of matrix marked with a red arrow.

3.3.5 Stromal SerpinB2 effects on MEF migration and ECM remodelling

The prominent differences shown above in ECM construction raised further questions into the individual cell specific effect within these matrices. Thus, in order to further understand the effect of SerpinB2 on matrix contraction, MEFs with stable GFP expression (refer to Chapter 2, section 2.3.7) were used to visualise their behaviour during collagen contraction. At day 6 - when matrix contraction was well underway (refer to Fig. 3.9), SHG and multiphoton imaging was undertaken over a 14 h period. Dramatic differences in the morphology and behaviour of wild-type versus SerpinB2$^{-/-}$ MEFs were observed (Fig. 3.9A). Morphologically, wild-type MEFs appeared larger than SerpinB2$^{-/-}$ MEFs, and were recorded consistently with higher motility, moving freely throughout the matrix, while SerpinB2$^{-/-}$ MEFs were virtually immobile (11.2 μm/s $\pm$ 0.4 versus 3.3 μm/s $\pm$ 0.1, respectively) (Fig. 3.9B and C; Supplementary movie 6). Notably, several wild-type MEFs were observed undergoing mitosis/cytokinesis, but this was not observed in SerpinB2$^{-/-}$ MEFs (Supplementary movie 7). Despite this, no difference in proliferation rate was observed between wild-type versus SerpinB2$^{-/-}$ MEFs in 2D systems [data not shown, reported by (167,198)]. Wild-type MEFs were predominantly multipolar, with dynamic cycling of numerous, short cellular protrusions. In contrast, SerpinB2$^{-/-}$ MEFs were predominately bipolar - with fewer but longer and more stable protrusions observed (Fig. 3.9D - H). Hence, the behaviour of MEFs within the contracting collagen matrix is significantly altered in the absence of SerpinB2, and this altered behaviour is likely responsible for the observed structural changes in matrices formed by SerpinB2$^{-/-}$ MEFs.

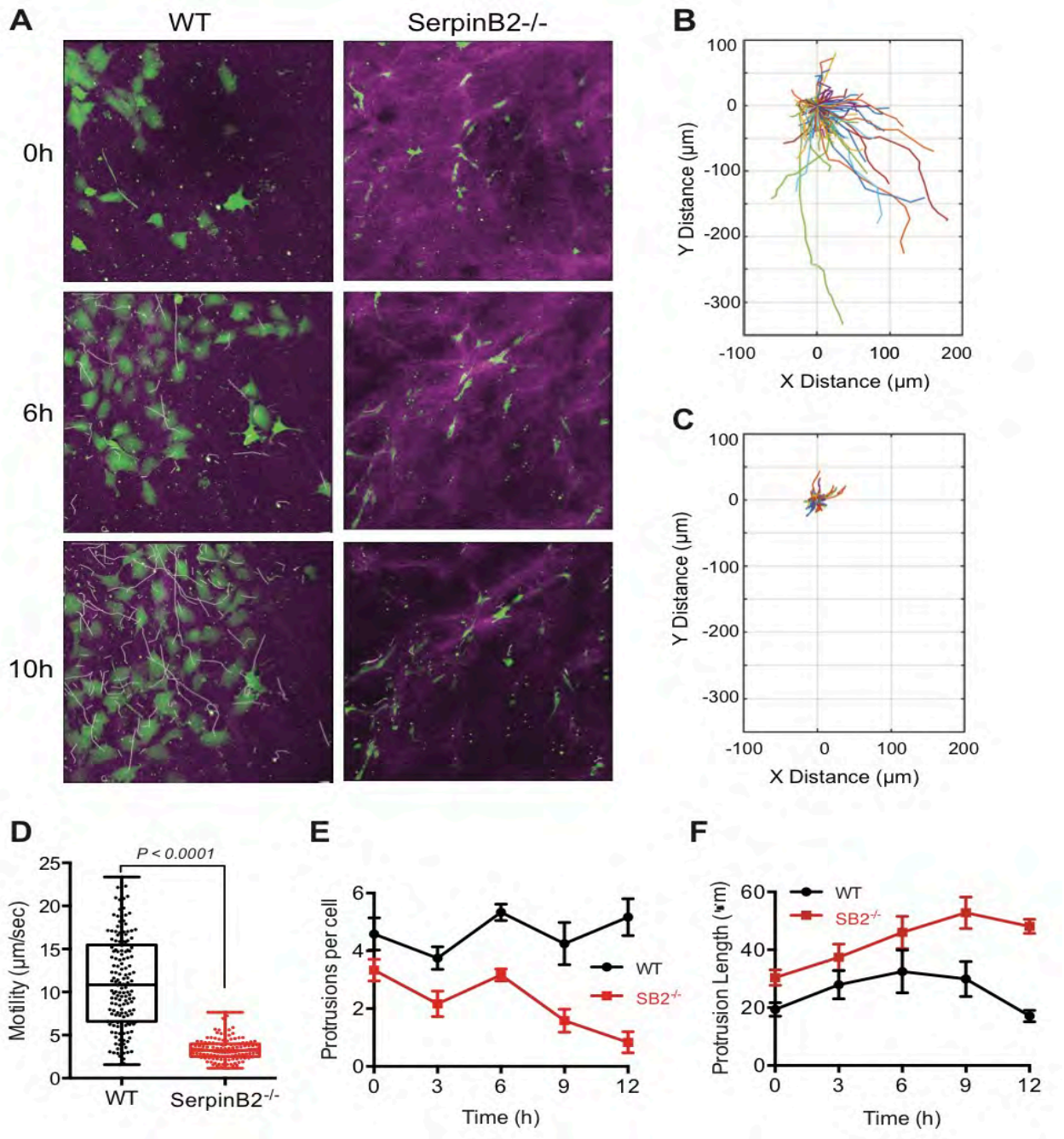

Fig. 3.9. Overnight 3D imaging of MEF migration and ECM remodelling. A. Migration of wild-type or SerpinB2$^{-/-}$ MEFs through collagen I matrices was tracked over 10 h at the midpoint of matrix contraction (day 6). collagen (magenta) was detected using SHG and wild-type or SerpinB2$^{-/-}$ MEFs were detected through stable GFP expression. Cell tracks are marked by a vector tail (white); **B-C.** Polar plots denoting cell directionality (x,y distance) and total displacement (µm) of either (**B**) wild-type or (**C**) SerpinB2$^{-/-}$ MEFs through collagen I matrices over the time course (14 h) of the experiment; **D.** Average motility of wild-type or SerpinB2$^{-/-}$ MEFs through collagen I matrices was computed by tracking cell position over time (n >130 for each, individual values are shown with bars representing mean ± SEM.); **E.** Average number of protrusions per cell across the course of the experiment; **F.** Average length of protrusions per cell across the course of the experiment. Statistical analyses were performed using unpaired t-tests.

3.3.6 Pilot proteomic analysis of wild-type and SerpinB2$^{-/-}$ MEF matrices

In order to begin to elucidate specifically the proteins present within this complex ECM remodelling process, a pilot LC-MS/MS analysis was performed on matrices derived using wild-type or SerpinB2$^{-/-}$ MEFs (Fig. 3.10). Interestingly, there were many proteins that were significantly decreased within SerpinB2$^{-/-}$ MEF matrices versus wild-type MEF matrices (Fig. 3.10), potentially responsible for the reduced contraction rate, increased overall diameter of matrices, lack of matrix integrity and decreased collagen cross-linking observed throughout (refer to Fig. 3.6-3.8). Those proteins found to be significantly less abundant were, and not limited to, LOX (2.6-fold less), collagen alpha-1(I) chain (0.8-fold less), collagen alpha-2(I) chain (1.2-fold less), EMILIN-1 (1-fold less), Biglycan (1-fold less), and SPARC (0.7-fold less) (Fig. 3.10). In addition, there were many proteins that were significantly increased within SerpinB2$^{-/-}$ MEF matrices, possibly in attempts at retaining functional roles for matrix integrity and collagen cross-linking, through SerpinB2 absence. Those proteins found to be significantly up-regulated were, and not limited to, Superoxide dismutase-1 [(SOD-1) 3.19-fold increase], Fibrinogen (2.28-fold increase), Zinc finger protein [(ZFAT) 2.2-fold increase], Actin-related protein 2/3 complex subunit 1B [(ARPC1B) 2.12-fold increase], and Actin (0.73-fold increase) (Fig. 3.10).

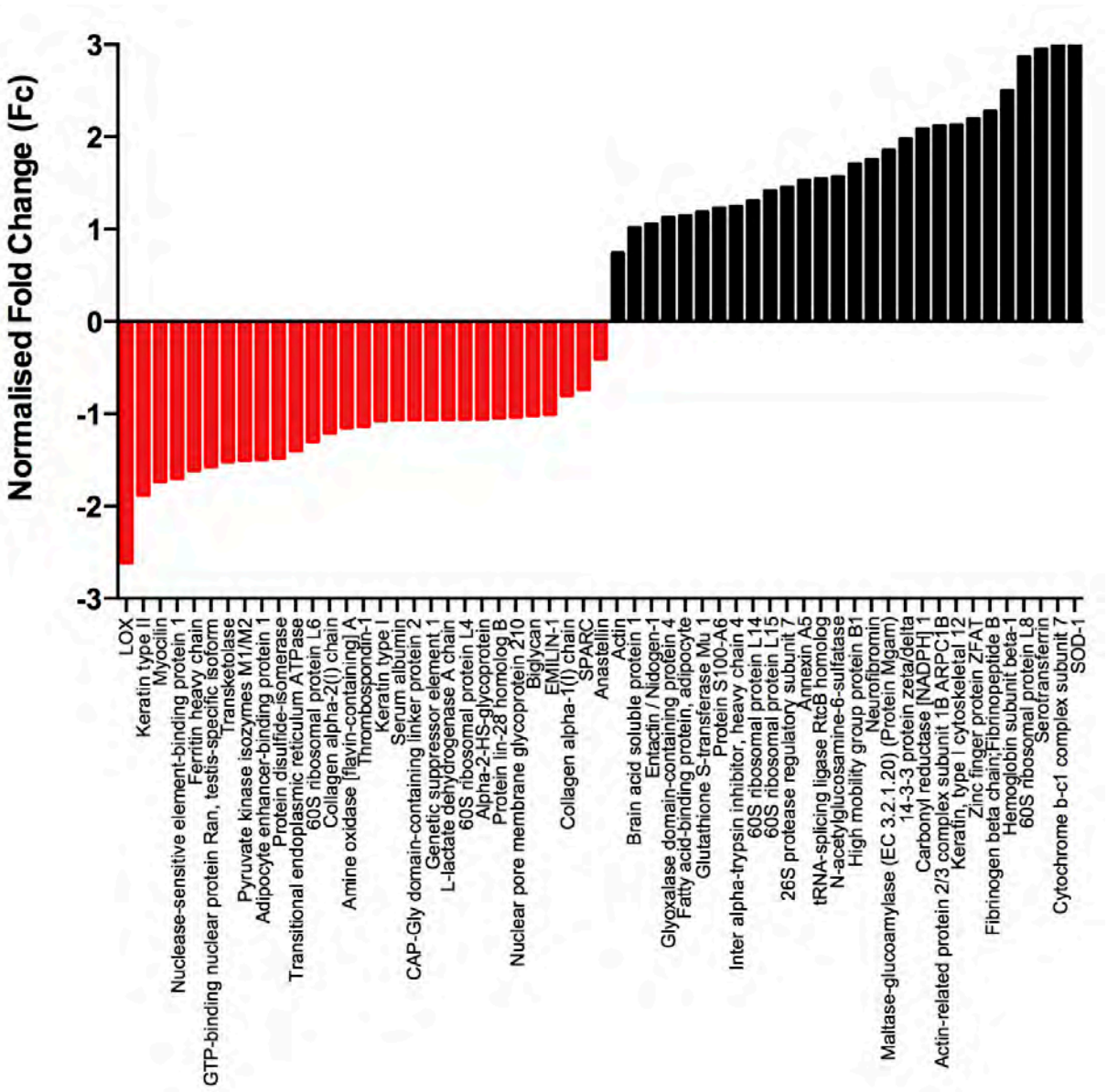

Fig. 3.10. LC-MS/MS data analysis. Normalised Fc values of proteins significantly altered within the SerpinB2$^{-/-}$ MEF matrices versus wild-type MEF matrices. Protein abundance was considered to be significantly altered if protein abundance increased or decreased with an average Fc-value > 0.70 or < -0.70.

3.3.7 Exogenous SerpinB2 effects on SerpinB2$^{-/-}$ MEF collagen contraction

SerpinB2 was lentivirally knocked back in to SerpinB2$^{-/-}$ MEFs as well as wild-type MEFs, using the pLenti6.3 vector system. However, after transduction and selection, the cells were phenotypically altered, displaying an epithelial-like phenotype with irregular lamellopodial protrusions (data not shown). The doubling time of both

transduced lines were also significantly decreased versus untransduced controls, and eventually the cells died. Thus, in order to determine whether the absence of SerpinB2 affected collagen cross-linking, *via* inability to inhibit potential uPA mediated effects on contraction, exogenous SerpinB2 was utilised in these SerpinB2$^{-/-}$ MEF mediated collagen I contraction experiments to ascertain whether the re-introduction of SerpinB2 could re-instate contraction rates, collagen cross-linking ability and proper fibrillogenesis, as observed within wild-type MEF matrices. Unfortunately, full length SerpinB2 was not available, thus SerpinB2 ΔCD loop, which maintains full uPA inhibitory activity (176), was used in its place, along with a PBS vehicle control and ^{R380A}SerpinB2 ΔCD loop as a uPA non-inhibitory control. As aforementioned, much literature has recently reported that Dox is also an MMP inhibitor (MMPs -2 and -9), while not causing cell death or effects on proliferation. Thus, contraction assays were setup using SerpinB2$^{-/-}$ MEFs in the presence of 500 nM SerpinB2 ΔCD loop, 500 nM ^{R380A}SerpinB2 ΔCD loop, PBS or 20 μg/mL Dox. There were no significant differences recorded upon the rate of matrix contraction using PBS, SerpinB2 ΔCD loop or ^{R380A}SerpinB2 ΔCD loop (Fig 3.11A,B), suggesting that SerpinB2 mediated uPA inhibition does not affect collagen cross-linking, but it is an intrinsic effect of SerpinB2 on cell behaviour. However, in the presence of 20 μg/mL Dox, matrices did not contract from the original size of the 35 mm petri dish (Fig 3.11A,B). This shows that through Dox induced MMP inhibition, SerpinB2$^{-/-}$ fibroblasts are not able to form viable collagen cross-linked networks and remodel the ECM. This suggests, not surprisingly, that impeded MMP -2 and -9 activity interferes with ECM remodelling within SerpinB2$^{-/-}$ MEF-collagen I matrices.

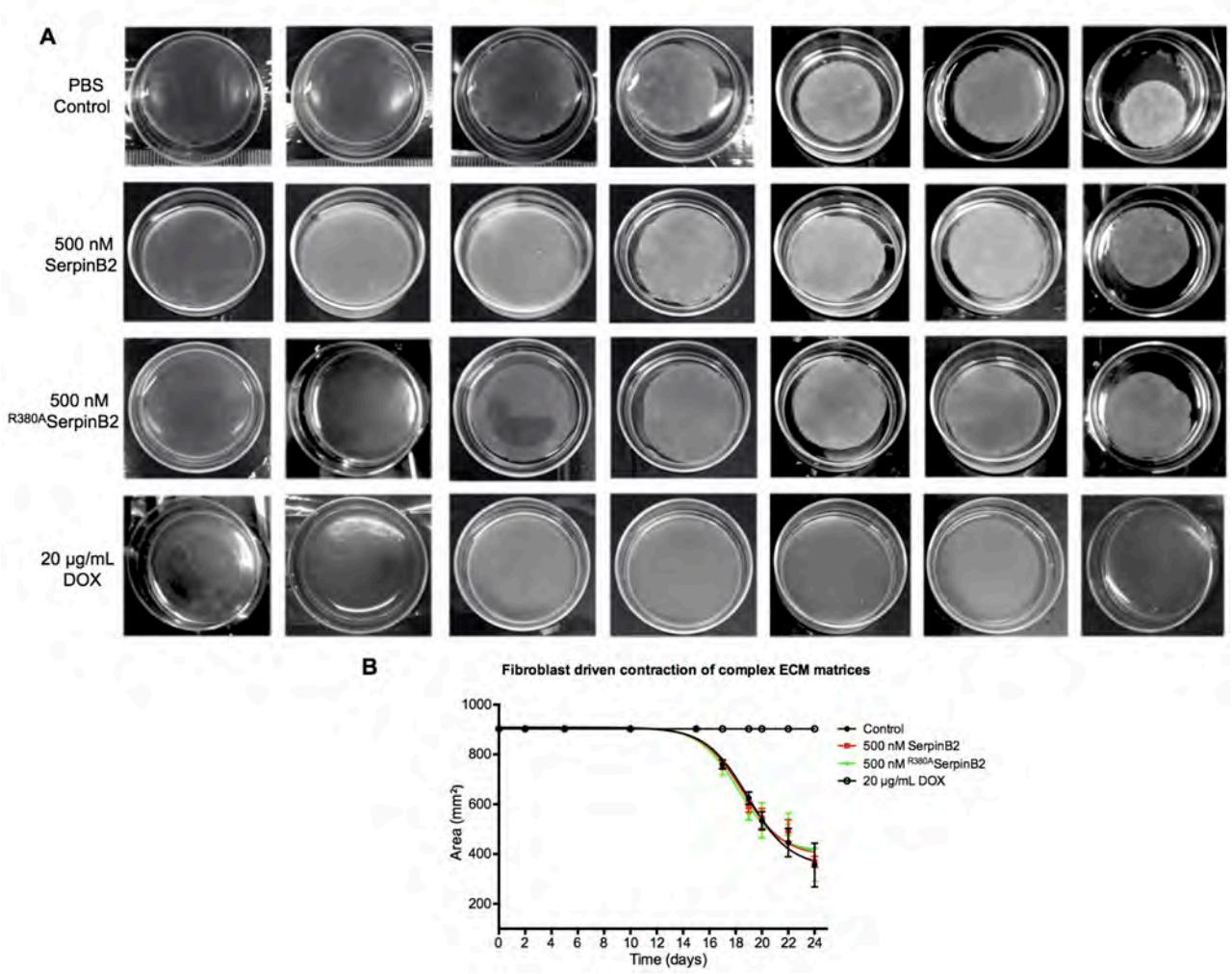

Fig 3.11. 3D organotypic of SerpinB2 restoration effects on SerpinB2$^{-/-}$ MEF matrices. A. Photographs showing SerpinB2$^{-/-}$ MEF collagen I matrix contraction over 21 days in the presence of either PBS Control, 500 nM SerpinB2, 500 nM ^{R380A}SerpinB2 and 30 µg/mL Dox; **B.** Changes in area (mm^2) of SerpinB2$^{-/-}$ MEF collagen matrices shown in (**A**) over the 21 day contraction period. Values shown are means ± SEM from 3 separate matrices.

This novel result is only preliminary in its findings, however, SEM imaging revealed that there were few, if any collagen fibrils in the Dox treated matrices (surface view Fig 3.12I-L, sagittal view Fig 3.13I-L), whereas extensive fibrillar collagen networks were observed within both SerpinB2 ΔCD loop (surface view Fig 3.12A-D, sagittal view Fig 3.13A-D) and ^{R380A}SerpinB2 ΔCD loop (surface view Fig 3.12E-H, sagittal view Fig 3.13E-H) treated SerpinB2$^{-/-}$ matrices. Additionally, there appeared to be thicker bundling of collagen in the SerpinB2 ΔCD loop matrices versus those formed in ^{R380A}SerpinB2 ΔCD loop matrices Fig 3.13D,H). This observation

could be due to higher uPA/uPAR expression effects on collagen cross-linking, as MMPs are required for remodelling and their presence is definitely required more than absence, as observed in Dox treated matrices (Fig 3.11A,B, Fig 3.12I-L, and Fig 3.13I-L).

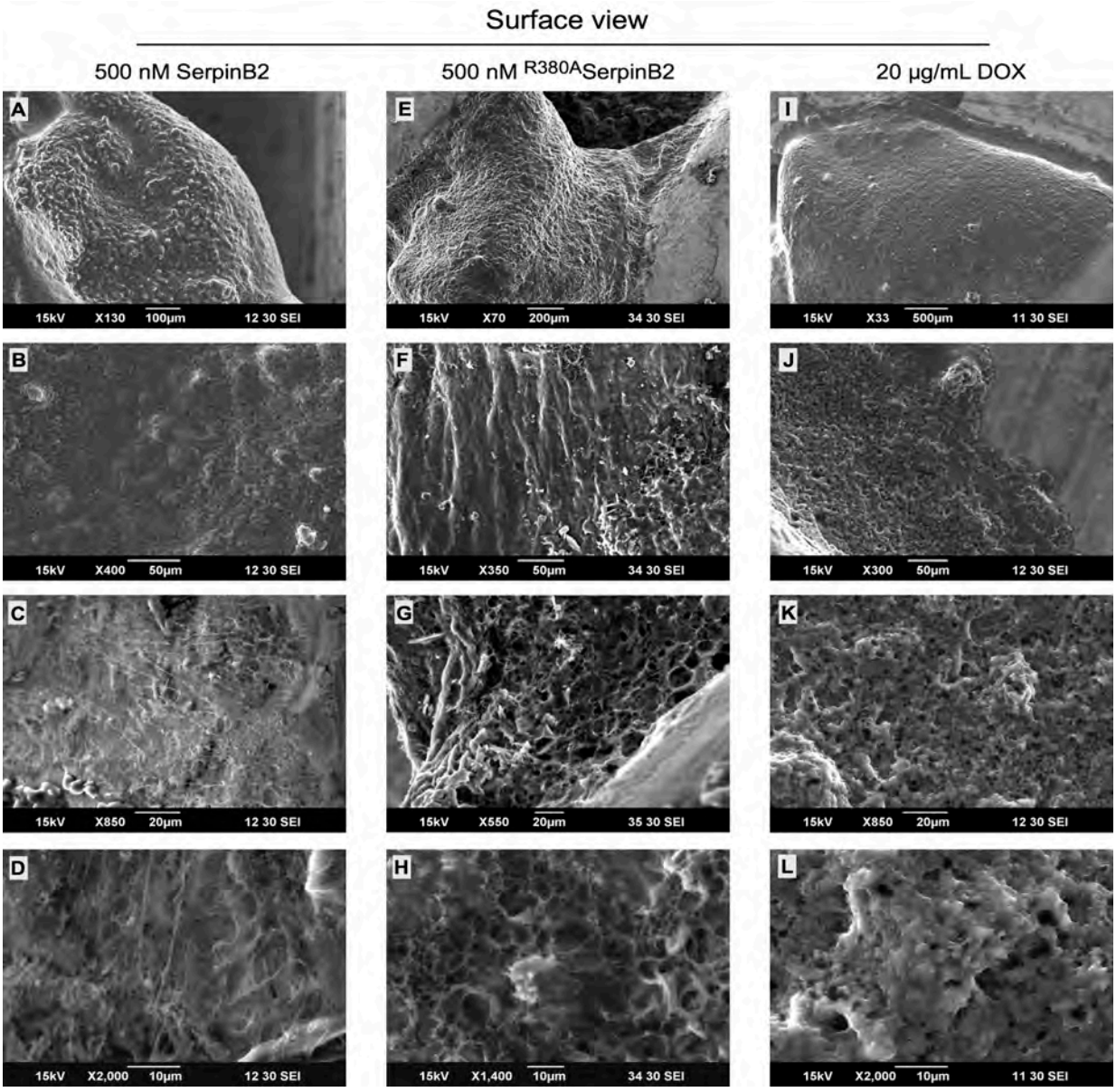

Fig 3.12. SEM ultrastructure surface analysis of SerpinB2$^{-/-}$ MEF matrices. SEM ultrastructure analysis showing surface of SerpinB2$^{-/-}$MEF contracted collagen I matrices in the presence of either 500 nM SerpinB2 ΔCD loop (**A**-**D**), 500 nM ^{R380A}SerpinB2 ΔCD loop (**E**-**H**), or 20 µg/mL Dox (**I**-**L**). Fixed sections were prepared (as described in section 3.2.7) at day 21 of contraction. Collagen cross-linking can be observed in SerpinB2$^{-/-}$MEF matrices formed in the presence of SerpinB2 ΔCD loop and ^{R380A}500 nM SerpinB2 ΔCD loop (images **A**-**H**), while SerpinB2$^{-/-}$ matrices in the presence of Dox do not show evidence of adequate collagen cross-linking.

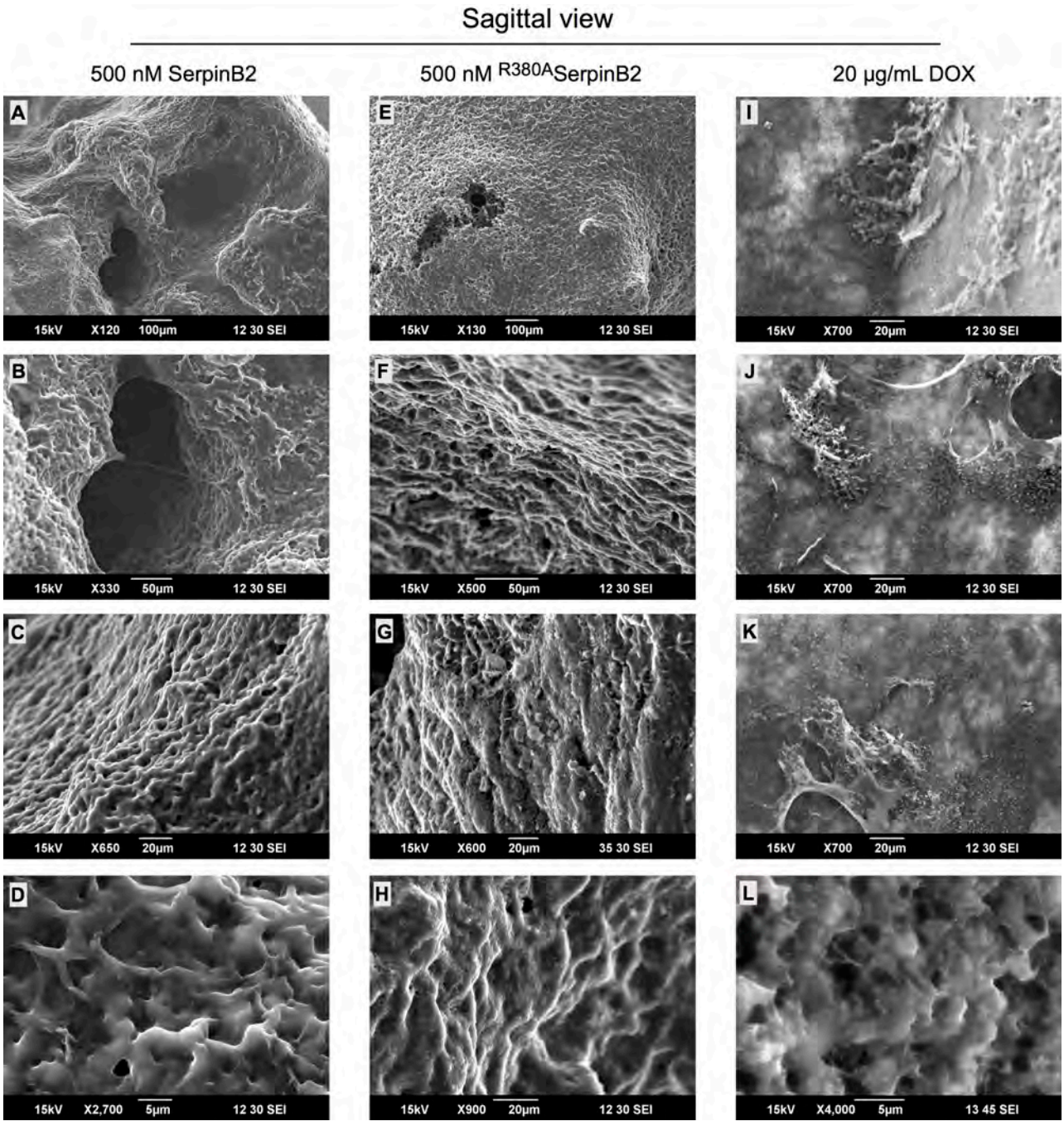

Fig 3.13. SEM ultrastructure sagittal section analysis of SerpinB2$^{-/-}$ MEF matrices. SEM ultrastructure analysis showing sagittal sections of SerpinB2$^{-/-}$MEF contracted collagen I matrices in the presence of either 500 nM SerpinB2 ΔCD loop (**A**-**D**), ^{R380A}500 nM SerpinB2 ΔCD loop (**E**-**H**), or 20 µg/mL Dox (**I**-**L**). Fixed sections were prepared (as described in section 3.2.7) at day 21 of contraction. Substantial collagen cross-linking in SerpinB2$^{-/-}$MEF matrices was observed in those contracted in the presence of SerpinB2 ΔCD loop and ^{R380A}500 nM SerpinB2 ΔCD loop with fibrillar organisation (**C** and **D**, **F** and **H**) evident, albeit with significant decreased diffusive hindrance (large pore size). SerpinB2$^{-/-}$ matrices contracted in the presence of Dox did not show any evidence of collagen I fibrilogenesis or collagen I bundle formation (**I**-**L**).

3.4 DISCUSSION

Indisputably, loss of ECM homeostasis is a key factor in tissue fibrosis and cancer progression (23). Interestingly, both of these pathologies are heavily shown to aid the other, shaping the way for malignant transformation, as cancer-associated fibrosis and desmoplasia are incriminated in primary tumour growth and metastases in many cancer types (23,249,263,353,450). Understanding ECM function within stromal formation and the TME is thus vital for the emergence of better treatment strategies and therapeutic options. As SerpinB2 has been linked to cancer inhibition as well as progression [(213) see Chapter 1, refer to section 1.5], we utilised SerpinB2 both genetically and pharmacologically for studies in 3D collagen I matrix contraction assays. The 3D matrix consists of collagen I, which is cross-linked into fibrils and contracted over a period of 7-21 days by both human and murine fibroblasts. The collagen was prepared by acetic acid extraction, which unlike enzymatic digestion, preserved the N- and C-terminal telopeptide reactivity aiding in collagen cross-linking (359,451). The acetic acid extraction method resulted in pure collagen I stocks that had robust polypeptide reactivity, as re-constituted collagen I successfully formed robust fibroblast-contracted matrices, confirmed by SEM (refer to Fig. 3.5). As collagen I has a homologous sequence between rat and human, rat-tails were sourced for collagen I extraction. Either from fresh or frozen starting material, adolescent rat tails were used, because collagen cross-linking is more labile in younger animals (N- and C- telopeptide residues available for aldol-lysine cross-linking) (359), thus essential for this technique. As stated by Timpson *et al.* (2011), collagen cross-linking is more labile in younger animals, thus collagen I was extracted from adolescent rat tedons and re-constitution occurred with higher fidelity (358,359,372). The collagen contraction assays utilising (both TIF or MEF) stromal fibroblasts were undertaken with success and proved that this is a highly useful model for assessing the impact of SerpinB2 on collagen cross-linking, matrix formation, stromal remodelling, as well as specific drugs which can be aimed at increasing or inhibiting these processes (358,359,372).

Initially, matrix formation with TIFs occurred over 12 days and indicated the ability of the collagen I extracted in-house to be used in this system and revealed that this assay would be not only a viable model (refer to Fig. 3.5), but also a robust tool for further interrogation of PAS activity in stromal formation. After successful pilot experiments with SerpinB2 expressing TIFs, the effects of genetically modified murine fibroblasts on collagen matrix contraction were conducted. The striking and somewhat unexpected effect of SerpinB2 absence on matrix integrity over a 12-day period suggested that SerpinB2 has a dramatic effect on collagen cross-linking (refer to Fig. 3.6-3.8). Significant decreases were observed in SerpinB2$^{-/-}$ MEF matrix contraction rates, overall diameter, matrix integrity, collagen coverage and fibril network formation (refer to Fig. 3.6-3.8). SHG and SEM analyses of matrices formed by SerpinB2$^{-/-}$ MEFs revealed dysregulated, anisotropic dispersal of collagen I, compared with the ordered, isotropic distribution observed in matrices formed with wild-type MEFs (refer to Fig. 3.6-3.8). Further, collagen matrices formed using wild-type MEFS formed robust matrices, with homeostatic fibrous layers, suggestive of good cell-cell cross talk, leading to proper fibril bundles formed due to stable covalent collagen I cross-linking, and apposite ECM construction. These large network coverings displaying an ordered ECM are normative of healthy tissue. Conversely, matrices prepared using SerpinB2$^{-/-}$ MEFs revealed that collagen I was not being crosslinked properly, with areas of large porosity in collagen networks. One of the major reasons for such profound differences in matrix construction is because there appeared to be poor cell-cell and cell-matrix communication, evidenced by many gap and overlapping regions of crosslinked collagen within the matrices, and a general lack of adequate bundle formation. This resulted in defunct construction of collagen I bundles, with unordered collagen matrices observed. Without proper fibrillogenesis and ordered collagen networks, the ECM contained larger pores (collagen cross-linked improperly) and where fibrils did form, there were denser bundles that were dispersed in an anisotropic fashion (refer to Fig. 3.7-3.8). This finding is supported in a different model of SerpinB2 deficiency. As aforementioned (refer to section 1.6.5), Schroder *et al.* (2010) reported that SerpinB2$^{-/-}$ mice infected with *Schistosoma japonicum* had reduced collagen I fibrosis versus wild-type (SerpinB2 expressing) mice (158),

suggesting that SerpinB2 is necessary for the fibroblast-dependent redistribution of collagen fibres around wound matrix contraction. The next challenge was to visualise the fibroblasts in collagen matrices to get a more in depth idea of the cellular behaviour. Improved MP microscopy techniques allow for continuous cell tracking exploring the subtle dynamics of biological processes in collagen cross-linking, fibroblast migration and stromal remodelling. To improve the imaging consistency and reliability, MEFs were modified to express GFP (refer to Chapter 2). This increased the ease of fibroblast detection by working in a spectrum with little collagen autofluorescence. Coupled with SHG detection, a solid framework was utilised where both collagen and fibroblast signals were captured separately (refer to Fig. 3.9), revealing stark differences between wild-type and SerpinB2$^{-/-}$ MEFs, suggesting that SerpinB2 is important in regulating fibroblast migration, necessary for matrix remodelling (Fig. 3.9). The significantly decreased motility of SerpinB2$^{-/-}$ MEFS together with the striking differences in cellular protrusion dynamics in these cells, suggest that the effect of SerpinB2 on matrix remodelling is primarily through regulation of MEF cellular adhesion and motility/migration. Fibroblast migration and cross-linking ability in this model somewhat mimics the proliferation/granulation and remodelling (but not re-epithelialisation) stages of wound healing. Proteases are important in these stages, particularly MMPs [stimulated by IL-1, TNF and TGF-β (452)], and uPA/plasmin are vital in a wound healing environment in order to break down the clot(s) as fibroblasts move into the area and start depositing collagen (452,453). Additionally, uPA/plasmin are important for keratinocyte migration to the area. MMPs are not constitutively expressed in cells in this environment, requiring regulation (452). SerpinB2 has a role in this context and moreover, in our models we propose that SerpinB2 potentially modulates MEF migration through stabilising TG2, binding *via* one or more of SerpinB2's three glutamine residues in the CD loop of its structure. SerpinB2 is known to be present on the focal adhesions of cells (454), thus interactions could be occurring with integrins and FAKs, potentially assisting fibroblasts during stromal remodelling and collagen crosslinking. Verma *et al.* (2006) reported that overexpression of catalytically active TG2 induced FAK and PI3K/Akt activation and siRNA mediated down-regulation of TG2 attenuated FAK phosphorylation in PDAC cells (331).

Further, they showed, *via* immunopreciptation and confocal microscopy, that activated FAK was colocalised with TG2 at focal adhesion points (331). This novel result proposes that elevated expression of TG2 induces constitutive activation of FAK. Given that TG2 is one of the major classes of collagen cross-linking enzymes, it is possible that SerpinB2 is utilised to assist in collagen fibrillogenesis, binding with fibronectin, fibrin(ogen) and other ECM molecules to achieve greater cell-matrix adhesion, communication and stability. Tissue stiffness in keloid fibrosis has been shown to increase expression of SerpinB2 (455). Suarez *et al.* (2013) showed that knockdown of SerpinB2 in keloid fibroblasts significantly reduced the intracellular expression of extracellular matrix components, α-SMA, fibronectin and collagen I (455). Further, SerpinB2 knockdown did not influence the viability or metabolic activity of keloid fibroblasts (455), as observed in MDA-MB-231 cells from Chapter 2 (see section 2.3.6.4). However, it has been reported that SerpinB2$^{-/-}$ MEFs are less able to withstand proteotoxic stress (198). In scleroderma and keloid fibrosis SerpinB2 is known to interact with FAKs, *via* integrin binding (455). FAK is a cytoplasmic tyrosine kinase encoded by the PTK2 gene (456), mediating integrin signalling during cellular adhesion and migration, as integrin binding enhances FAK phosphorylation (456). As its name would suggest, FAK is heavily localised to focal adhesions, coordinating the motility of a cell by inducing actin polymerisation and the throughput of cell-ECM contact and signalling (457). *In vitro* culturing of cells increases the levels of tyrosine phosphorylation in their focal adhesions, enabling proper adherence to culture flasks (457). FAKs have been implicated in the development of fibrosis, following mechanical force stimuli of inflammation, fibroblast activation and ECM (458). Myofibroblast differentiation has been shown to be initiated by TGF-ß and dependent on cell adhesion and integrin signalling *via* FAK (459). Mechanical tension induces α2β1-integrin expression, helping bind the cell cytoskeleton with the ECM, which in turn causes FAK formation between fibroblasts and collagen (460,461). FAK phosphorylation causes α-actinin stabilisation, inducing actin polymerisation and the throughput of cell-ECM contact and signalling (457). This increase in integrin binding consists of clustered, ECM-bound integrins, FAK and cytoskeletal adaptor proteins (such as

paxillin) within the cytoplasm (462), which not only mediates cell anchorage to the ECM, but also instigates 'outside-in' signalling cascades, which activate downstream pathways, regulating cell survival processes (462). In particular, increases in ECM stiffness in tumour and stromal tissue leads to increased integrin clustering (463), resulting in enhanced mechanotransduction that subsequently initiates cell migration (464). There is extensive crosstalk between integrins and TGF-beta signaling, where TGF-beta affects integrin-mediated cell adhesion and migration through regulating integrin expression (465). Conversely, integrins directly stimulate TGF-beta activation and reciprocal TGF-β-integrin signalling is implicated in normal physiology, as well as in a variety of fibrotic diseases, cancer and wound healing (465). In addition, TGF-β has been shown to up-regulate MMP-2, TIMP-1, SerpinB1, SerpinB2, and also plasmin (346). As aforementioned, TGF-β also increases expression of fibronectin, collagen, elastin, proteoglycans as well as LOX and TG2 by fibroblasts, leading to increased ECM synthesis, collagen cross-linking, decreased ECM degradation and overall ECM deposition and tissue stiffness (269). With respect to the observations seen in the real-time overnight imaging of wild-type MEF and SerpinB2$^{-/-}$ migration in collagen I matrices, it is tempting to hypothesise that such decreased tissue stiffness in SerpinB2$^{-/-}$ matrices potentially was caused through reduced integrin induction, reducing FAK activation and α-actinin stabilisation, meaning cell-ECM contact and signalling would be dramatically decreased, not allowing SerpinB2$^{-/-}$ MEFs to adhere or migrate as well as their wild-type counterparts (refer to Fig. 9; Supplementary movies 6 & 7). Furthermore, within SerpinB2$^{-/-}$ MEF matrices, excess activity by the uPA/uPAR system should lead to enhanced migration, cellular adhesion and proliferation mediated by uPAR binding to integrin receptors, EGF receptor, HMW kininogen, caveolin and the G-protein-coupled receptor FPRL1 (104). Although not tested within this thesis, overnight imaging revealed a reversed phenotype, which may mean that without adequate SerpinB2 regulation of uPA/uPAR complexes, signalosome interaction by uPAR and it's plethora of tyrosine- and serine-protein kinase partners (Src, FAK, Rac, ERK, JAK/STAT, MAPK) (103), could be impaired.

Proteomic analysis by Dr Zon Weng Lai revealed a (normalised) three-fold decrease of LOX within SerpinB2$^{-/-}$ MEF collagen matrices versus wild-type MEF matrices (refer to Fig. 3.10). This is a key finding and may be the major reason for such significant reductions in matrix contraction rates reported in collagen cross-linking and overall matrix integrity of SerpinB2$^{-/-}$ MEF matrices. To date there is no direct association between LOX and SerpinB2 published in the literature, revealing that this is a potentially novel result and one that certainly requires further investigation.

3.4.1 Hypothetical effects of SerpinB2 in the ECM

A potential link between LOX and SerpinB2 is *via* the FAK signalling pathway and this possible corollary link for collagen cross-linking and stromal remodelling would be mediated by integrin binding. A schematic of this proposed mechanism is shown in Fig. 3.14 It is well known that secreted LOX can interact with FAKs, increasing cell-to-matrix adhesion (282). Miller *et al.* (2005) previously reported that LOX facilitates MCF-7 breast cancer cell migration and cell-matrix adhesion formation through a hydrogen peroxide-mediated mechanism (HIF-1α), where LOX works upstream of the FAK/Src signalling pathway (282,466). As aforementioned, it was recently reported that fibroblasts overexpressing LOX stimulate FAK activation *in vivo,* causing increased collagen cross-linking and matrix stiffness in a colorectal cancer model (293). Many tumourigenic studies show decreased FAK activation with LOX inhibition (466,467) (282). Hypothetically, without SerpinB2, surplus uPA/uPAR activity may not allow adequate regulation of MMP activity, thus collagen exposure of telopeptides could be impaired, disabling LOX's post-translational activity in collagen cross-linking. Further, it has been reported that as collagen fibrils are being formed, LOX is involved in collagen linearisation, and fibril organisation (468). This requirement for LOX expression to facilitate collagen bundle formation could potentially be one of the reasons for the 3-fold decrease seen in the LC-MS/MS proteome analyses of SerpinB2$^{-/-}$ MEF derived versus wild-type MEF constructed collagen matrices (refer to Fig. 3.10). It is interesting to speculate that potentially there exist signaling mechanisms between

TG2/SerpinB2 and LOX to facilitate collagen oligomerisation, where SerpinB2$^{-/-}$ MEFs might have have decreased integrin ($\alpha 2\beta 1$) binding (without TG2-fibronectin/fibrin/integrin bond et), reducing FAK (Vinculin, Paxillin and FAK) activation/phosphorylation, attenuating actin re-organisation and eventually ECM remodelling, causing changes in cellular adhesion, proliferation, migration and cell survival. Conversely, as more collagen was being cross-linked in the wild-type matrices (where SerpinB2 stabilised TG2), LOX was activated moreso, thus helping to linearise the fibrils. Future experiments are essentially required to investigate further. Interestingly, actin-related protein 2/3 complex subunit 1B (ARPC1B) was present at twice the amount compared to that of wild-type matrices, as assessed by LC/MS. This increase was potentially to account for the decreased LOX pathway activity (refer to Fig. 3.10) as ARPC1B is a subunit of the Arp2/3 complex, involved in regulation of actin polymerisation and formation of branched actin networks. Welch *et al.* (1997) showed that Arp2/3 complex is localised to the lamellipodia of both stationary and motile fibroblasts and suggested that this complex promotes both actin assembly in lamellipodia and could facilitate lamellipodial protrusion (469). This 2-fold increase in SerpinB2$^{-/-}$ MEF ARPC1B level is potentially associated with the 0.73-fold up-regulation of actin within SerpinB2$^{-/-}$ MEF matrices (refer to Fig. 3.10) and may be a compensatory mechanism to stimulate proper fibroblast lamellipodial protrusion for adequate ECM remodelling. An explanation for this is not clear, but would most likely involve intracellular signaling cascades. EMILIN1 was also reportedly decreased (1-fold down-regulated) within SerpinB2$^{-/-}$ MEF matrices (refer to Fig. 3.10). This is interesting as EMILIN1 is a component of elastin fibres and reported to affect actin and paxillin distribution associated with cell polarity, ECM stress fibre formation and signalling (470). Numerous cell types migrate on EMILIN1 (471), however trophoblasts attach to EMILIN1 most efficiently (versus other cell types) and migrate using $\alpha 4\beta 1$ integrin without any stimulus, induction or activation (472). Further, Spessotto *et al.* (2006) showed ordered haptotaxis (directional motility) in trophoblasts was significantly more efficient toward EMILIN1 compared with fibronectin (472). In addition, Biglycan was also found decreased (1-fold down-

regulated) within SerpinB2$^{-/-}$ MEF matrices (refer to Fig. 3.10). Biglycan is a small, leucine rich ECM proteoglycan that binds with collagen I fibrils *in vivo* (473). Altogether, these data corroborate the extensive differences in cell-cell and cell-ECM communication observed in SHG, MPM and SEM experiments. To this end, SerpinB2 might be a key upstream regulator (with LOX and TG2) of extracellular matrix remodelling and collagen cross-linking (Fig 3.14).

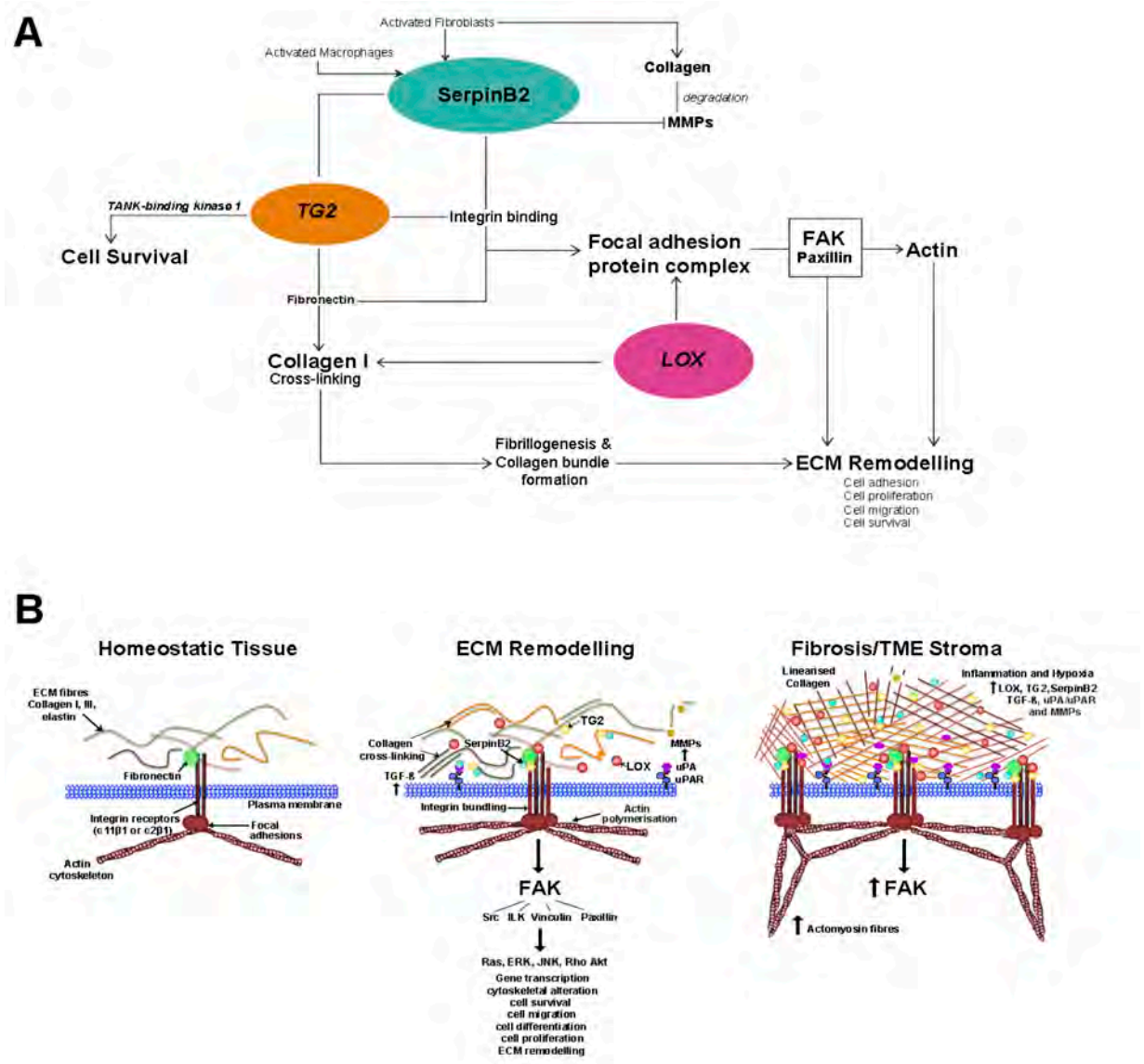

Fig 3.14. Schematic of SerpinB2, LOX and TG2 in the ECM. A. Potential molecular links between SerpinB2, LOX and TG2 in ECM remodelling and collagen cross-linking activities. Collagen and fibroblasts interact *via* focal adhesions, where SerpinB2 regulates MMP (through uPA/plasmin), promoting ECM accumulation. SerpinB2 also modulates cell migration mediated by integrins. LOX cross-links collagen within the ECM and promotes FAK and Paxillin activation, increasing cell motility and cell-ECM adhesions. TG2 binds to collagen *via* fibronectin, utilising secreted SerpinB2 (when present) as a stabiliser, mediating the binding, and affording enhanced cell-matrix communication and stability. **B.** In homeostatic tissue beds, collagen molecules interact with the cell *via*

fibronectin binding, which connects with the plasma membrane through α11β1- and α2β1-integrins. When ECM remodelling is initiated, biochemical and mechanical signalling from the ECM occurs through integrin receptors and leads to activation of a large number of pathways, particularly FAK [FAK, and integrin are both required for normal development: FAK, and integrin knockout mice are embryonic lethal (474,475)]. This and other kinase signalling cascades [Ras, Akt, ERK, Rho, Jun-N-terminal kinase (JNK)] can induce cytoskeletal alterations and lead to gene transcription changes in the nucleus. TGF-ß is relased into the ECM, activating collagen cross-linking enzymes, LOX and TG2, as well as SerpinB2 and B1, uPA/uPAR, MMPs. Lox is known to cause collagen linearisation. The modulation of both proteases and protease inhibitors is under disordered regulation in fibrotic/tumourigenic tissue beds, where inflammation and hypoxia activate increased expression of many matrix remodelling enzymes and proteins, leading to increased mechanical remodeling of the ECM. The contractile activity of the cells depends on activation of a number of pathways, including the Rho pathway, for assembly of stress fibres, integrin clustering, focal adhesion hyper-activation and increased tractional force at cell– matrix interface (463,476).

Concurrently, secreted protein acidic and rich in cysteine (SPARC), a matricellular glycoprotein that binds collagen and Ca^{2+}, was observed to be 0.73-fold less abundant in SerpinB2$^{-/-}$ matrices versus wild-type (refer to Fig. 3.10). SPARC is primarily involved in initiating nucleation during bone mineralisation (477) however, SPARC has also been reported to be secreted in non-ossifying tissues (478), during both ECM formation and tissue repair, arbitrating ECM remodelling, matrix turnover, and cell-ECM interactions (479,480). Interestingly, zinc finger protein (ZFAT) was also twice as abundant within SerpinB2$^{-/-}$ matrices (refer to Fig. 3.10), which could potentially be present in such concentration in order to facilitate zinc-dependent MMP processes (481).

Furthermore, proteomic analysis of the MEF-collagen I matrices revealed that SOD-1 was 3.2-fold more abundant in SerpinB2$^{-/-}$ matrices, potentially as a stress protein. SOD-1 is an important enzyme during apoptotic signaling and oxidative stress, most notably involved in the mitochondrial death pathway and cardiac myocyte apoptosis (482). Studies by Lee *et al.* (2015) reported that SerpinB2 loss lead to an inability to compartmentalise aggregating proteins and a reduced capacity of the ubiquitin-proteasome system, causing a proteotoxic phenotype (198). Thus, without SerpinB2, potentially a proteotoxic stressed environment may have activated SOD-1 in order to regulate apoptotic signaling and cell death. Fibrinogen was increased in SerpinB2$^{-/-}$ matrices (α-chain 0.84-fold more abundant, β-chain 2.28-fold more abundant), associating SerpinB2 expression with fibrinogen modulation (refer to Fig. 3.10). It has been reported that fibrinogen cleavage products can regulate cell adhesion and spreading, involved in chemotactic activities, and acting as mitogens for

several cell types (483). Further, Sahni *et al.* (2004) reported that fibrinogen binding to FGF-2 *via* αVβ3, induced expression of uPA, uPAR, and SerpinB1 in endothelial cells (484). SerpinB2 might crosslink to collagen *via* TG2 mediated fibronectin/fibrin binding, and this increase in fibrinogen observed in SerpinB2$^{-/-}$ matrices may be a direct attempt at SerpinB2$^{-/-}$ MEFs to facilitate collagen cross-linking using fibrinogen. In the absence of SerpinB2, TG2 potentially utilises fibronectin as a substrate for cross-linking to the α-chain of fibrin, which is why there is substantially less α-chain fibrinogen than β-chain fibrinogen. If true, this could also explain the decreased presence of anastellin (a peptide of fibronectin), as well as through plasmin degradation (36). Conversely, supra-expression of fibrinogen could be facilitating SerpinB1 expression, in order to regulate uPA/uPAR, and thus MMP activity. Alternatively, it may be that fibrinogen is two-fold more abundant within SerpinB2$^{-/-}$ MEFs due to the unnecessary formation of fibrin networks, which would only then be broken down by plasmin. This again demonstrates the similarity of this model with a wound-healing environment, except that fibrin network formation and breakdown is not required as the haemostasis stage is not present. It appears in our model that SerpinB2 helps to create ECM formation, separate to its uPA inhibitory functional acitivity.

Both collagen I and fibronectin confer mechanical strength to tissue beds (357) and fibronectin is found in tissue stroma as well as in the extracellular matrices of cultured cells (485). Fibronectin can be cross-linked *via* plasma transglutaminase to itself and the α-chain of fibrin. Mosher *et al.* (1979) previously have shown plasma transglutaminase-mediated crosslinking of fibronectin to alpha 1 type-1 collagen occurs at 37 °C and demonstrated that fibronectin-fibrin and fibronectin-collagen binding and cross-linking are highly related (486,487). Interestingly, there were no expression differences recorded by LC/MS in TG2 abundance. This could potentially be due to the fact that the matrices were analysed once fully contracted, thus TG2 may have fulfilled all specific purposes and was not present in detectable concentrations. This is potentially the case for certain proteases, such as MMPs, and may have been down regulated by the time the LC/MS analyses

occurred. Future experiments should analyse matrices at various stages of matrix contraction in order to determine whether this affects the detection of different proteins or levels of certain proteins (i.e. LOX).

Moreover, it has previously been shown that increased LOX expression results in increased collagen linearisation and tissue stiffness in pre-malignant tissue (485). Erler *et al.* (2009) demonstrated the crucial role LOX has in matrix remodelling in pre-metastatic niche formation, where tumour secreted LOX protein causes ECM remodelling and matrix stiffening in peri-tumour regions (485). This was actively aided by bone-marrow-derived cell (BMDC) recruitment and facilitated metastatic tumour cell colonisation and growth (485). Further, Erler *et al.* (2009) showed that matrix stiffening with LOX increased invasiveness of myeloid ($CD11b^+$) precursor BMDCs and also increased MMP activity (485). The importance of LOX cannot be overlooked, as this enzyme is vital for collagen cross-linking in ECM remodelling within pre-malignant tissue, stroma of early tumour invasion, pre-metastatic niche formation and at metastatic lesion sites. Recently, it was reported that prolonged exposure to hypoxia deactivates CAFs, leading to reduced collagen I organotypic contraction and decreased both ECM remodelling and stiffening of collagen I matrices (488). They showed that the ability of CAFs to remodel and invade matrices was impaired under hypoxic conditions, leading to HIF-1α stabilisation, reduced αSMA and periostin expression, decreased myosin II activity, abrogating CAF-mediated invasion of cancer cells (488). It would be interesting to see the expression of SerpinB2 in their models as they did not observe a difference in collagen cross-linking or oligomerisation in hypoxia (488). A potential path of tumourigenesis, invasion and metastasis utilising LOX and SerpinB2 is proposed herein (Fig. 3.15).

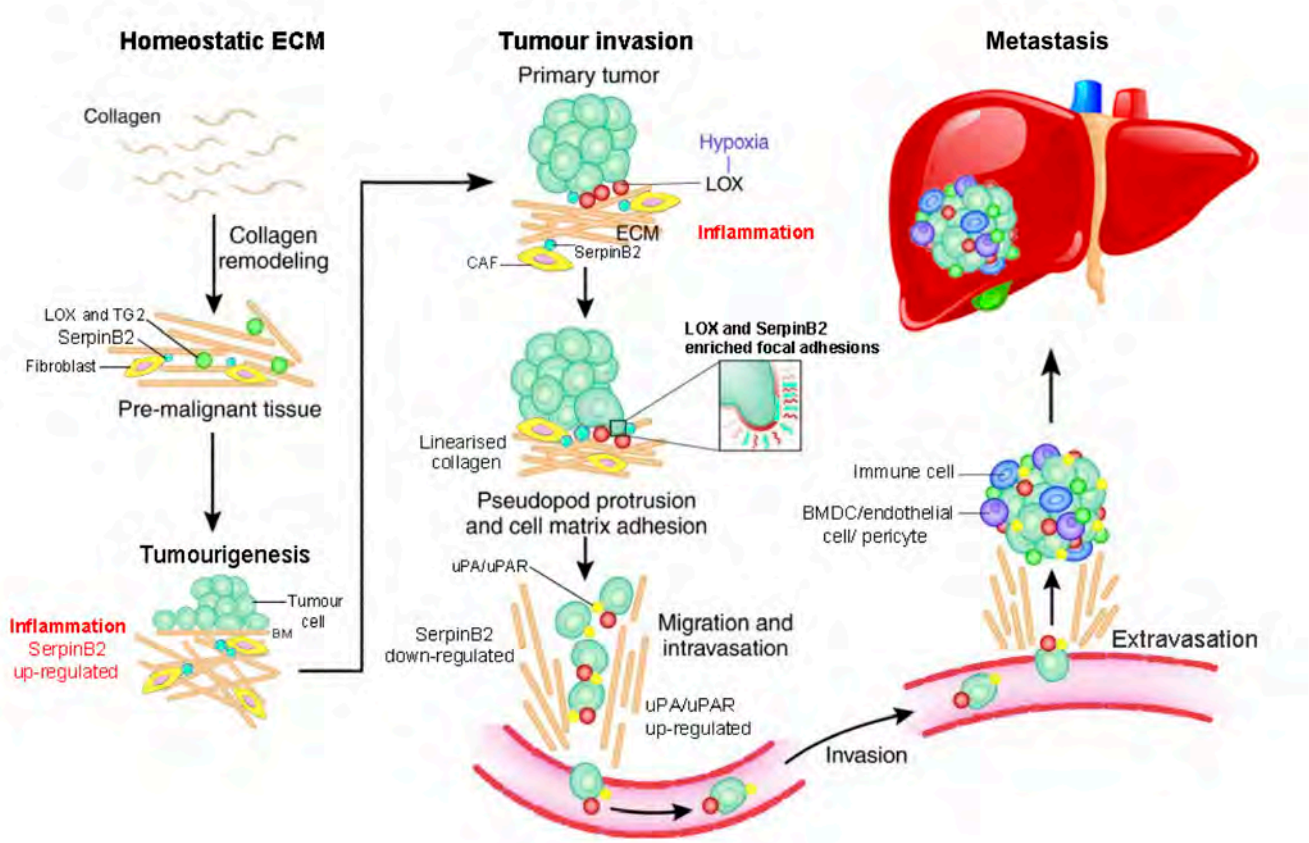

Fig. 3.15. Schematic of the roles of PAS and LOX in collagen cross-linking and ECM transformation from homeostatic tissue beds to pre-malignant, tumourigenic and metastatic tissue sites. SerpinB2 helps facilitate TG2-collagen I binding in the ECM. Premalignant and tumourigenic tissue increases secretion of soluble cytokines and chemokines, leading to inflammation, increasing local expression of SerpinB2. SerpinB2 aids the site with anti-plasmin/MMP activity in ECM remodelling, as well as anti-apoptopic roles. As tissue becomes more hypoxic, LOX is increasingly expressed, leafing to excess collagen crosslinking and bundle formation around the tumour. Both SerpinB2 and LOX are present on focal adhesions of tumour cells, facilitating increased ECM remodelling, and affording enhanced cell-matrix adhesion, communication and stability, allowing for tumour cell migration. Tumour secreted LOX causes peritumoural ECM stiffening and formation of a pre-metastatic niche for primary tumour cells to migrate easier. SerpinB2 is down-regulated as tumour cells undergo metastasis, increasing uPA/uPAR. BM: Basement membrane. Adapted from (249).

Much research has been conducted into MMPs, as they are heavily increased in the inflammatory response, normal tissue remodelling, wound healing, angiogenesis and cancer (481). The sustained presence of MMPs in stromal remodelling combined with increased ECM production and deposition, leads to the destruction of normal ECM and its replacement by invasive tumour-stromal ECM (23). Thus, MMPs are anti- and pro-tumourigenic, and ECM degradation and remodelling occurs *via* MMP regulation, which increases TME signals stimulating cellular proliferation and migratory mechanisms (23). These data align with the inadequate results of MMP inhibitors reported in cancer clinical trials where severe side effects and severe toxicity from both

short (e.g. marimastat) and long term (e.g. BMS-275291) dosing were reported (489). The reason for such disappointing trials is thought to be due to a functional redundancy between MMP family members (23), meaning that a combinatorial approach might be required for clinical efficacy. However, next generation MMPi antibodies are being created with higher binding for specific MMPs (particularly membrane anchored MMPs) offering renewed hope that this could be a renewed therapeutic pipeline(490,491). Conversely, within dermatology, there are two Dox drugs approved by the United States Food and Drug Administration, for adult periodontitis (Periostat), and rosacea (Oracea) (445). Both are administered as a 20 mg (twice daily) or 40 mg dose (slow-release) of Dox for MMPi and anti-inflammatory/anti-collagenolytic effects (445).

Moreover, MMPs have been shown to regulate FGF-2, VEGF and PDGF cell signalling, controlling cell growth, inflammation and angiogenesis (23). This is of particular importance because MMP expression and activity is highest in cells resident within the TME, and if there is not regulation of their expression, cytokine signalling can quickly move out of control. collagenase-1 (MMP1) degrades collagen IV (main constituent of the BM) and its expression is increased in highly metastatic cancer cells (492,493). Additionally, overexpression of MMP2 in transformed mammary epithelial cells and overexpression of MMP3, MMP11, MMP12 and MMP13 have been demonstrated in tumour stroma (494,495). As SerpinB2 is an upstream inhibitor of MMP1, MMP2, MMP3, MMP9, MMP12 and MMP13 (*via* uPA-plasmin inhibition) (496-499), its presence in the stroma biochemically modulates ECM remodelling. Thus, the ability to regulate MMP expression is of clinical significance and this study's finding highlights the important nature of MMPs in the ECM. In this chapters work, the effect of (20 μg/mL) Dox in the system, showed the importance of MMPs in ECM construction (refer to Fig.'s 3.11-3.13). There was zero contraction seen in the Dox cohorts. This result shows that MMPs are positive and negative regulators of stroma formation, vital for collagen breakdown, and necessary in the process of ECM remodelling. Interestingly, as of yet there are no reports or research evidence to show that Dox acts as a TIMP inhibitor (500). As the widely accepted primary extracellular biochemical function of SerpinB2 is

inhibition of uPA activity, the potential role of proteolytic activity in collagen matrix remodelling was considered. However, as the effect of SerpinB2 ΔCD loop addition to contracting SerpinB2$^{-/-}$ MEF collagen matrices had no effect on contraction versus PBS or ^{R380A}SerpinB2 ΔCD loop controls, this result potentially shows that contraction is independent of uPA activity (refer to Fig.'s 3.11-3.13). Interestingly, LOX is extracellular, and TG2 is both intra- and extracellular. Hence, there may be a response using full-length SerpinB2 exogenously versus SerpinB2 ΔCD loop, in SerpinB2$^{-/-}$ MEF collagen I contraction experiments. Thus, this experiment needs to be further elucidated, with incorporation of full-length wild-type SerpinB2. Furthermore, another reason for the lack of compensation observed in SerpinB2$^{-/-}$ MEF contracted collagen matrices by exogenous SerpinB2 addition could be related to the already irreversible effects of decreased LOX expression by the SerpinB2$^{-/-}$ MEFs. SerpinB2 may be a key upstream regulator for LOX and TG2 and other matrix proteins. Therefore, without its intracellular presence, the modulation of not only proteases and protease inhibitors is under disordered regulation, but potentially also LOX and TG2 expression. Thus, within the contraction experiments, the reintroduction of SerpinB2 exogenously is potentially too late, as a difference mechanism of action between intracellular and extracellular SerpinB2 maybe occurring.

However, the question whether uPA/PAS activity is necessary for matrix remodelling remains, as MMP inhibition by Dox clearly effected the contraction of collagen I by SerpinB2$^{-/-}$ MEFs (refer to Fig. 3.11). Though, undetectable levels of uPA/uPAR on TIFs suggest this in unlikely, and MMPs can be produced without uPAS activity. Notably, the immortalised fibroblasts (TIFs) normally used to drive efficient matrix contraction for organotypic experiments (i.e. similar to that observed with wild-type MEFs) express significant levels of endogenous SerpinB2 (Fig. 3.3), pointing moreso to intracellular signalling mechanisms affecting ECM remodelling.

As aforementioned in Chapter one (refer to section 1.7.1), Valiente *et al.* (2014) reported that increased SerpinB2 (and SerpinI1) expression is required for lung and breast metastatic cells to infiltrate the blood brain

barrier (BBB) (213). Cell adhesion to the surface of capillaries within the brain is attributed to increased SerpinB2 expression and shown to protect metastatic cells from astrocytic FasL apoptosis and L1CAM inactivation, facilitating further metastases (213). The pro-survival effects of SerpinB2 and cell adhesion and binding stability through integrins may allow enhanced cell-matrix attachment and help metastatic cells infiltrate the brain. This study allows one to ponder that perhaps the unique composition of the brains ECM (lecticans, proteoglycans, hyaluronic acid and tenascin family adhesive/anti-adhesive proteins) confers resistance to tumour invasion (501). Matrix proteins (especially type-1 collagen) common in other tissue beds are absent in the adult brain (501) and this unique composition of ECM may be responsible for the such cell motility activities, including tumour cells of non-neuronal origin. More cell migratory functions of SerpinB2 are addressed in section 1.9.5. In contrast, Yu *et al.* (2002) reported that SerpinB2 transfected THP-1 monocytes showed reduced adhesive properties and a decreased proliferation rate (172).

Interestingly, a study by Da Silva *et al.* (2015) reported there was no significant increase in LOX expression in astrogliomas (AGI, AGII and AGIII) compared to matched normal brain tissue samples (502). However, glioblastomas (GBMs), a more malignant astrocytoma, exhibited significantly enhanced LOX expression (502). The paradoxical difference in LOX expression between astrocytomas is of note, though da Silva *et al.* (2015) reported increased LOX expression, with increases from AGI-GBMII, which facilitated increase migration and angiogenesis within their models. It would be fascinating to see if SerpinB2 was expressed in these brain cancer cells, potentially working to facilitate both anti-plasmin activity and also cell-matrix adhesion.

Lastly, the results of this chapter demonstrate that ECM production and collagen deposition is influenced dramatically by SerpinB2 with regards to the development and remodelling of matrix architecture, from collagen cross-linking, tissue stiffness and porosity. The use of multiphoton-based SHG imaging in this study aided the investigation of ECM attributes and allowed for quantitative examination of collagen coverage and 3D modelling of organotypic matrices in real-time.

In the future, SerpinB2$^{-/-}$ 3D models could be imaged using imaging systems, such as FRAP and FLIM–FRET, to analyse SerpinB2-FAK co-localisation in fibroblast migration during matric contraction experiments. In addition, these imaging techniques could examine anti-uPA drugs that target the ECM, thereby offering early validation before more time-consuming, expensive and complex *in vivo* assessment. Additionally, there is a dire necessity for increased research and imaging of the stroma around primary, peri-tumoural, micrometastatic and metastatic sites, as this area remains poorly understood. This would be ideal for testing SerpinB2$^{-/-}$ tissues, as these are recapitulative of most advanced tumour systems and would be especially beneficial for the development of new combinatorial treatments targeting uPA/uPAR and/or the stroma of inoperable tumours.

Cancer therapies are increasingly targeting ECM remodelling enzymes in an effort to prevent changes in ECM homeostasis that promote tumour progression, and aiding in chemotherapy efficacy (23). However, the development of anti-fibrotic therapies for cancer treatment (such as imatinib, dasatinib and nilotinib) are not straightforward (503). Premature attempts to treat hypertrophic fibrosis and keloidal scars utilised the potent LOX inhibitor, BAPN, to reduce collagen cross-linking (23). Although these trials effectively reduced collagen cross-linking and associated scarring when applied upon the skin, clinical testing was stopped due to toxicity issues (23). Studies have reported that LOX inhibition reduced primary tumour growth and mechanotransduction in breast cancer (504). Although LOX is an encouraging therapeutic biomarker for fibrotic diseases and cancer, targeting specific ECM enzymes involved in stromal remodelling while avoiding unwanted side effects is extremely difficult and pursuing a single molecule within a large disease network can cause adverse side effects. Additionally, there can also be compensation by other ECM members, which can potentially lead to drug resistance. The TME has many overlapping molecules and pathways that help maintain a dysfunctional order. Thus, the field needs to elucidate all linkages within a specific network and every key individual and collective members response to dynamic modulation of the TME. This is a huge task and will only be achieved through worldwide, multi-disciplinary collaborations in order to attain a greater

understanding of how microenvironmental cues are driving fibrosis and stromal remodelling in tumourigenic systems. Through advancements in imaging technologies, utilised in this study, great insight is being gained to help elucidate these networks, and innovative imaging techniques are enabling accurate monitoring, imaging and quantification of the ECM when specific molecules are attenuated genetically or through drug dosage. Together, these technologies can help dissect both the spatial and temporal dynamics of the ECM in a TME setting, and promote understanding of the underlying mechanisms that influence cell-ECM interactions.

CHAPTER 4

INVESTIGATION INTO THE EFFECTS OF SERPINB2 MODULATION ON PANCREATIC TUMOURIGENESIS AND LOCAL INVASION

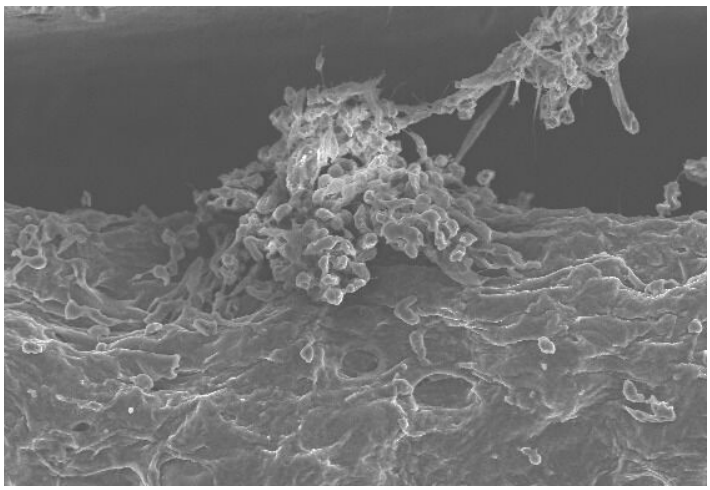

CHAPTER 4

INVESTIGATION INTO THE EFFECTS OF MODULATING SERPINB2 EXPRESSION ON PANCREATIC TUMOURIGENESIS AND LOCAL INVASION

4.1 INTRODUCTION

Pancreatic ductal adenocarcinoma (PDAC) represents ~92% of all pancreatic cancers and is the deadliest of all solid malignancies, with a 1-year survival rate of less than 20% and a 5-year survival rate of less than 5% (505,506). This is because approximately 85% of PDAC patients present with advanced stages of disease where local invasion or metastasis has occurred, or the primary tumour is surrounding arteries and is therefore inoperable (507). Further, prognosis remains poor even for those patients who do have surgery as tumour regrowth occurs ~85% of the time, meaning only 25-30% of patients are alive five years post-surgery (508). Thus, established approaches to PDAC therapy (i.e. resection and gemcitabine treatment) are largely ineffective and have severely limited impact on metastatic disease. Advances in adjuvant and metastatic chemotherapeutic regimens have resulted in modest improvements in outcome, but pancreatectomy remains the single most effective and the only potentially curative modality for the ~20% of patients suitable for such a procedure. Current treatment strategies for PDAC therefore remain ineffective and require urgent attention.

4.1.1 Genetic aberrations in the lead up to PDAC

Pancreatic duct epithelial cells undergo extensive atypical transformations in the lead up to PDAC morphology (509). Persistent epithelial de-differentiation and reactivation of embryonic/developmental signalling pathways, such as wnt-β-catenin, TGF-β and Hedgehog (Hh), contribute to a proliferative and anti-apoptotic phenotype of ductal epithelials, altering cell plasticity and increasing genetic variability (Fig. 4.1) (311,312). Considerable research has been conducted to determine the molecular foundations of PDAC. The almost universal K-Ras

mutation in over 90% of PDAC tumours, means that there is a constitutively active state of downstream signaling, through an inability to hydrolyse guanosine triphosphate (GTP), essential for signal transduction with G-proteins (494) (510). It is reported that K-Ras mutation/over-activation coupled with developmental genetic elements [wnt-β-catenin, Hedgehog (Hh)] above crucial temporal thresholds drives differentiated pancreatic cells into a de-differentiated, ductal state (313). This persists towards formation of pancreatic epithelial neoplasia (PanIN) and can eventually result in PDAC. The high degree of molecular heterogeneity associated with PDAC makes identification of suitable candidates for targeted therapy challenging (511). Approximately 2–10% of PDACs are associated with hereditary factors (312,512,513), however most are associated with somatic mutations of tumour suppressor genes p53 (75%) (514,515), p16/CDNK2A (~95% mutated and ~5% epigenetically silenced) (516), INK4A (~95%) (517), and SMAD4 (55%) (518). There are many large-scale genomic studies, such as the Australian Pancreatic Cancer Genome Initiative (APGI) [the Australian branch of the International Cancer Genome Consortium (ICGC)], which have been established in order to expand knowledge of the wider landscape of mutations associated with pancreatic cancer (511,519).

It is widely agreed that PDAC development arises from non-invasive, preneoplastic lesions (520). The materialisation of PanINs are the most common and extensively studied putative precursors to PDAC. PanINs are histologically classified into three stages of increasing cellular and nuclear abnomality (Fig. 4.1), and it has been found that each PanIN stage correlates with an increase in mutation frequency and gene association (521). PanIN1 lesions recurrently acquire a mutation in K-Ras (~20–40%), experience telomere shortening (~90%) (522), and have increased expression of HER2/neu (523), while PanIN2 more frequently harbour mutations in p53, SMAD4, and p16 (521,524). As these ductal lesions progress to a stage 3 PanIN, the ducts experience much higher mutations in K-Ras, p53, SMAD4 (and SMAD4 deletion) with additional mutations common in DPC4 and BRCA2 (523,525) (refer to Fig. 4.1). Further, Moriya *et al.* (2005) reported that K-Ras and SMAD4 regulate HER-2 expression in PanINs (523), which is known to dramatically increase signal transduction of kinase pathways MAPK, PI3K/Akt, and JAK-STAT, to name a few (526,527). This combination of genetic

elements creates a hyper cascade of downstream signaling, ultimately causing increases in genetic variability and cellular differentiation and activity.

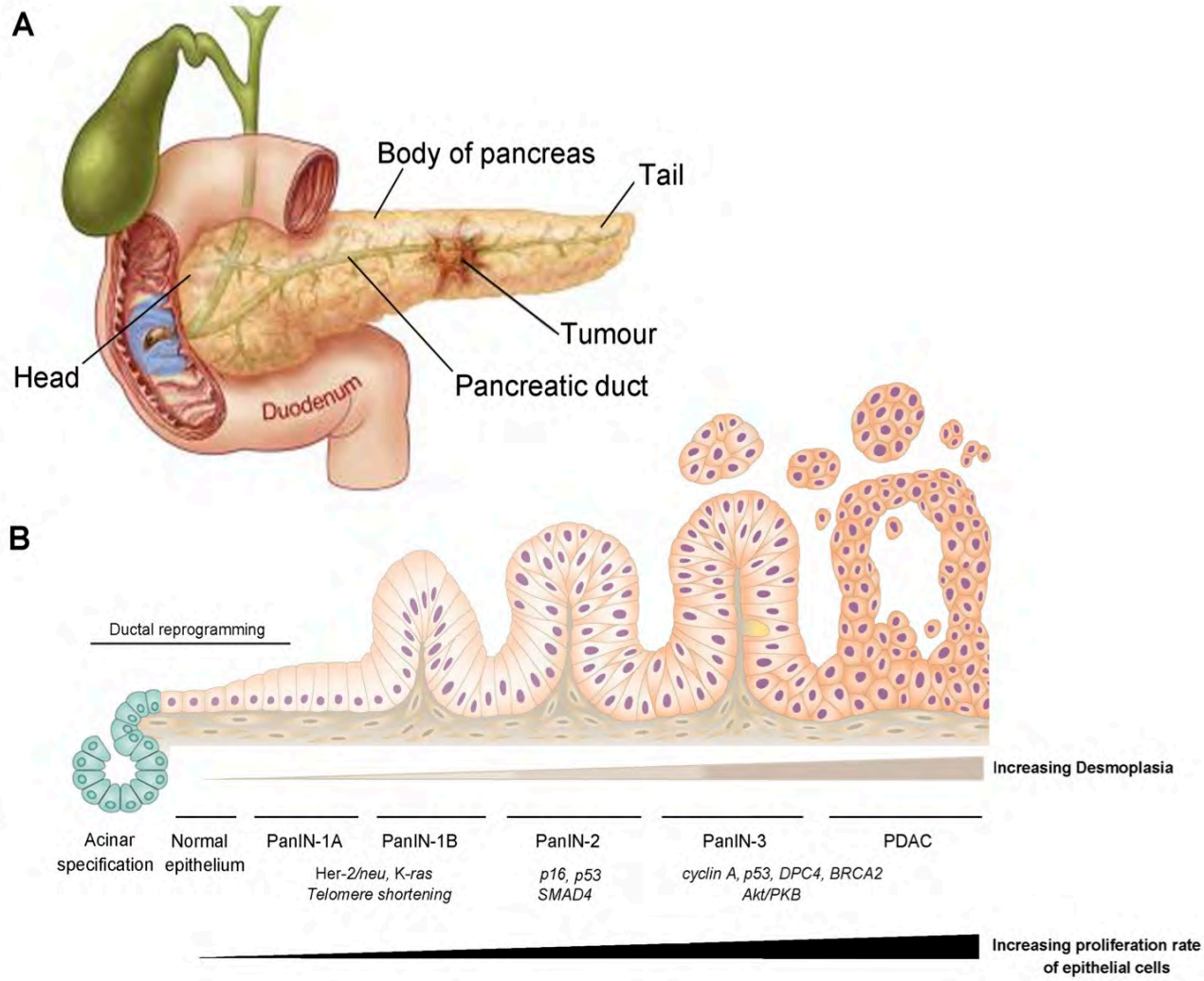

Fig 4.1. Pancreatic epithelial neoplasia — PDAC initiation and progression. A. Illustration of the gross anatomy of the pancreas (showing a PDAC in the pancreatic duct) indicating its close anatomical relationship with the duodenum and common bile duct. **B.** De-differentiated ductal cells can become PanINs, where β-catenin signalling is over-activated in parallel with increasing expression of Hh ligand and K-Ras, which temporally activates target genes in stromal cells of the developing desmoplastic response. Gene plasticity is altered and mutations can occur more frequently, causing ductal formation towards a PDAC state. Adapted from (313).

For these cell types, the reprogramming and dedifferentiation of their epithelial status into a 'ductal' cell type is required to undertake the PanIN–PDAC lineage. Initially, K-Ras was proposed as the instigating genetic lesion of PDAC, due to its widespread mutation frequency in patients. However, this was not successfully investigated until the development of transgenic models to assess such an hypothesis. Many pancreatic mouse

models have since been developed to understand which pancreatic cell types can develop into PDAC when mutant K-Ras is expressed (528,529).

Hingorani *et al.* (2003) were the first to produce the Pdx1-Cre;LSL-K-Ras$^{G12D/+}$ model (530). This Cre-inducible conditional allele [lox-stop-lox Kras^{G12D} (LSL-K-Ras^{G12D})] targeted to the endogenous K-Ras locus, allowed for expression of constitutively active K-Ras under both temporal and spatial control (530). This model unfortunately did not isolate a specific cell type, but instead targeted mutant K-Ras to most cells from all three epithelial lineages of the pancreas (ductal, acinar, islet). Nonetheless, the lesions slowly progressed through the entire human PanIN spectrum over increasing age of the mice into advanced PDAC disease, with a median survival of 15 months (530). This study suggested that K-Ras activation is a necessary tumour-initiating event in pancreatic carcinomatous states and that specific events are required for human PDAC progression. Based on this LSL-Kras^{G12D} model, three representative studies of invasive PDAC models have been reported (531-533). However, more recent models have been modified from the original Cre recombinase models, in order to begin to determine pancreatic cell type co-expression in the development of PDAC when mutant K-Ras is expressed. Hingorani *et al.* 2005 developed the *LSL-K-Ras$^{G12D/+}$;LSL-Trp53$^{R172H/+}$;Pdx- 1-Cre* model, where the concomitant expression of both *K-Ras^{G12D}* with *Trp53^{R172H}* manifested in the initiation of pancreatic tumourigenesis and widely metastatic PDAC (532). In addition, within this model, neither telomere shortening nor mutation of other major tumour suppressor gene pathways was required for the formation of ductal glandular histology, consistent with human PDAC patient histology (532). This model is both highly recapitulative of the human situation and also greatly hastens the development of locally invasive and largely metastatic PDAC, ideal for research purposes. Through using this strategy in 3D organotypic and xenograft models, observation into the effects of tumourigenesis, stromal remodeling and local invasion within the significant desmoplastic changes that occur in the PDAC TME could be made.

4.1.2 Desmoplasia in PDAC

PDAC generally arises in the head of the pancreas and within the developing TME, production of a dense stroma rich in collagen fibres, ECM proteins, fibroblasts and inflammatory cells, cytokines, chemokines, growth factors and ECM metabolising enzymes creates a fibrotic milieu, termed the desmoplastic reaction (450) (263) (refer to Fig. 4.1). It is only within the last five to ten years that the mechanisms contributing to this complex matrix process in PDAC have slowly started to be both elucidated and appreciated. This mechanical barrier surrounding the tumour is the defining reason why PDAC is one of the most drug-resistant forms of cancer. The main role in the formation and turnover of this near impenetrable stroma is assigned to the pancreatic stellate and fibroblast cells (discussed further below), leading to an increase in type I and V collagen and fibronectin, which could provide a valid reason for such poor drug penetration seen in PDAC treatments (534). This fibrous matrix surrounding PDAC also accumulates large amounts of hyaluronan, which increases interstitial fluid pressure and constricting tumour vasculature (535,536). Under these circumstances hypoxia and nutrient deficiency is in full effect, making it difficult for chemotherapy diffusion from the blood into the tumour, as well as leading to the selection of the most aggressive tumour cells through clonal expansion of resilient tumour populations (537).

Imamura *et al.* (1995) have reported that both lymph node and liver metastases have a similar increase in ECM proteins to that of PDAC desmoplastic tissue and that comparable amounts and type of collagens in PDAC desmoplasia are also features of alcoholic chronic pancreatitis and tumour-associated chronic pancreatitis tissue (276). Desmoplastic reaction in PDAC creates an inflammatory/immune cell front at the peripheral invasive edge of tumours (263). Morphological analyses of this sparse cell infiltrate in PDAC specimens has been shown to consist mainly of mast cells, macrophages, lymphocytes and plasma cells (538). Esposito *et al.* (2003) found that poorer survival was associated with PDAC patients who had higher numbers of mast cells in the stroma. These authors suggest the reason for this trend could be that mast cells secrete vascular endothelial growth factor [VEGF], largely responsible for facilitating angiogenesis (538). It is of note that there are contradictions

in the field about PDAC stroma and its influence on vasculature, invasion and metastasis [(353) also discussed below].

The presence of pancreate stellate cells (PaSCs) in the desmoplasia of PDAC are now recognized as playing an important role in the TME. PaSCs are a subset of pancreatic cancer-associated fibroblasts, which provide pro-survival signals to PDAC tumours (539). Homeostatically, PaSCs are a common cell feature of the exocrine pancreas and are usually located within the periacinar space, existing in a quiescent state (540). They have long cytoplasmic processes, which are used to encircle the base of the pancreatic acinus (263). When in a quiescent state, PaSCs exhibit a low rate of proliferation and small amount of ECM production. However, within pancreatic disease progression, these cells help facilitate and renovate tissue sites, after transforming from their normal quiescent state into an activated 'myofibroblastic' state (540). Once activated, PaSCs become significantly more proliferative, migrate towards areas of inflammation and produce ECM proteins, cytokines, chemokines, and growth factors (450,541). Apte *et al.* (1998) were the first to isolate PaSCs (542), and showed that these produced the ECM proteins that comprise the stroma of PDAC, as well as demonstrating the presence of activated PaSCs in the tumour stroma (450). They found that activated PaSCs were indeed the specific cellular source of ECM proteins and that these cells expressed α-SMA and co-localised with mRNA encoding procollagen, within PDAC stroma (450).

Thus, much evidence has come to light that PaSCs have a mutually beneficial relationship in PDAC etiology, resulting in an overall increase in growth rate of pancreatic tumours and potentially helping to facilitate their metastases. In this regard, studies have shown that culture supernatants from human pancreatic tumour lines can stimulate PaSC proliferation and their production of ECM proteins (543). This is believed to be due to the ability of pancreatic tumour cells to produce and secrete PDGF, TGF-β and FGF-2, which promote the activated state and proliferation of PaSCs as well as increasing ECM production (450). Furthermore, Bachem *et al.* (2005) showed that the growth rate of PDAC cells injected subcutaneously into nude mice markedly

increased when co-injected with PaSCs and that PDAC tumours grown with both cell types exhibited a desmoplastic reaction also observed in the human situation (543).

Of major interest to this project is the knowledge that PaSCs and PDAC cells both have the ability to produce matrix metalloproteinases and tissue serine proteases, specifically those generated by PAS (544). Moreover, the stroma of the PDAC TME is now widely believed to be the major facilitator of tumour invasion and metastasis (43). The field's relatively limited understanding of tumour-stromal interactions in PDAC is likely hindering the development of effective therapies and there is a strong imperative to better elucidate these processes. In that regard, this chapter focused on the role of uPAS in stromal remodelling, tumour growth and local invasion in PDAC.

4.1.3 uPAS in PDAC

PDAC has been reported to express significantly high levels of uPA and uPAR, which also potentially play a major role in PDAC invasion and metastasis. One of the first studies on the role of uPAS in PDAC was conducted by Takeuchi *et al.* (234). In 1993, their group analysed 97 PDAC specimen and found uPA expression predominated in 76 of these (a total of 78.4%), which correlated with shorter survival (234). SerpinB2 was present in 79 carcinoma specimens (81.4%) and was found to be significantly lower in PDAC specimen from patients with peritoneal metastasis ($P < 0.02$) (234). Further, higher SerpinB2 expression was associated with significantly higher survival than negative or weak PDAC SerpinB2 expression ($P < 0.05$) (234). Harvey *et al.* (2003) reported high uPA expression in PDAC cells in 93% of patients and also in surrounding stromal cells in 87.5% of patients, however, they recorded no uPA expression in normal pancreatic tissue distant from the PDAC site (233). A study by Xue *et al.* (2009) reported that the overexpression of uPAR predicted short survival in PDAC patients and that uPAR siRNA inhibited PDAC cell proliferation, migration and promoted apoptosis (545). Asuthkar *et al.* (2013) examined the role of uPA in the generation of PDAC cancer stem cells (CSCs), concluding that uPA interacts directly with transcription factors (Lhx2, HOXA5 and

Hey) to promote PDAC CSCs (546). In addition, Asuthkar *et al.* (2013) showed decreased tumourigenicity and increased gemcitabine sensitivity after suppressing uPA in PANC-1 and Mia-PaCa-2 cells (546). Winter *et al.* (2015) directly analysed uPA blood serum concentration in 90 PDAC patients and found a threefold increase of uPA serum concentration in patients with PDAC (3,23 ng/ml), compared to the control group (1.01 ng/mL; $P < 0.01$) (117). Further, they reported that higher uPA serum concentration was observed in patients with shorter survival time as well as significant differences between uPA levels of lower and greater concentration (than 2 ng/ml) and overall survival time (117).

Thus, the presence of uPA, uPAR and SerpinB2 in both fibroblasts and PDAC cells raises the question of how functionally relevant the PAS is within PDAC tumourigenesis, stromal remodelling, and tumour invasion and metastasis. Stromal expression of SerpinB2 has been linked to reduced disease progression and improved patient outcome in PDAC (19,238). In addtition, SerpinB2 expression in esophageal squamous cell carcinoma associated fibroblasts (CAF) correlated with prolonged patient survival (232). Elevated tumour SerpinB2 expression is commonly linked with prolonged survival, decreased metastasis, or decreased tumour growth in a number of other cancer types (19), including three small-scale studies in human PDAC (238,442,443). However, specific mechanisms have not been addressed and there is much to gain through looking at the cell specific effects of SerpinB2 modulation of the PDAC TME. Through the development of 3D organotypic culture systems (refer to section 3.2.3) (358), mouse models of pancreatic cancer that closely recapitulate the human disease (547), and mouse models of SerpinB2 deficiency (198), this may provide a unique and powerful opportunity to dissect the role of the PAS in the PDAC TME. By combining these models to modulate PAS activity in a context-specific manner, this chapter aimed to demonstrate that uPA activity is necessary for PDAC invasion *ex vivo* and *in vivo* and that SerpinB2 regulates tumour-stroma interactions driving stromal remodelling, collagen integrity, PDAC tumour growth and local invasion.

Thus, the overall aim of chapter four was to investigate the effects of stromal SerpinB2 modulation on PDAC growth, local invasion and progression in our *in vitro* and *in vivo* models. The **specific aims of chapter four were to:**

1. Interrogate the ICGC data for uPA expression analyses with PDAC patients
2. Utilise the 3D organotypic invasion model to functionally assess the effects of SerpinB2 upon tumour cell invasion, migration and clustering.
3. Characterise the influence of SerpinB2 upon local invasion and tumour growth in a mixed cell allograft mouse model of PDAC.
4. Characterise the collagen properties of wild-type and SerpinB2 modified tissue from both *in vivo* and *ex vivo* models using advanced microscopy techniques (including IVIS, SHG, multiphoton imaging and SEM analyses), immunofluorescence and uPA enzymatic assays.

4.2 METHODS

4.2.1 Proteins and antibodies

Recombinant human SerpinB2 and SerpinB2^{R380A} inactive mutant were purified and characterised as aforementioned. High molecular weight (HMW) human and murine uPA was purchased from Molecular Innovations (USA). Refer to Table 1 of Appendix for all antibody details.

4.2.2 Gene expression survival analysis

Collaborations with Dr Mark Pinese and Dr Marina Pajic at the Kinghorn Cancer Centre (Darlinghurst, NSW) afforded our laboratory access to outcome data and gene expression measurements from the APGI PDAC cohort (511). These data are available from the ICGC DCC (https://dcc.icgc.org/). Gene expression measurements were undertaken by our collaborators at at the Kinghorn Cancer Centre from bulk tumour,

performed on the Illumina Human HT-12 V4 platform, and were processed using the Bioconductor lumi package (v 2.18.0), using "bgAdjust.affy" background subtraction, "vst" transformation, and "quantile" normalization. Outcome data were current as of March 2016. The influence of log-expression on disease-specific survival was examined separately for each probe. Martingale residual plots were used to assess functional form, and no departures from linearity were observed. The prognostic significance of each probe was then evaluated by likelihood-ratio tests, comparing a Cox model with probe log-expression as a linear predictor, against a marginal model. Multiple testing correction was performed by Holm's method. All data processing was performed in the R environment (version 3.1.1, survival package version 2.37-7). Analysis of gene alteration frequencies in PAS components across various tumour types in the TCGA database was performed using the cBioPortal for Cancer Genomics (442,443).

4.2.3 Cell lines and culture conditions

The invasive murine pancreatic ductal adenocarcinoma cell line, $PDAC^{p53R172H/+}$ (and referred to as PDAC hereafter), harvested from *Pdx1-Cre, LSL-KRas*$^{G12D/+}$*, LSL-Trp53*$^{R172H/+}$ mice (547), were maintained in Dulbecco's modified Eagle's medium (DMEM) supplemented with 10% FBS with 100 U/mL penicillin and 100 µg/mL streptomycin in a humidified 5.0% CO_2 atmosphere at 37°C. Human TIFs and wild-type and $SerpinB2^{-/-}$ MEFs were generated and cultured as described in section 3.2.1.

4.2.4 Flow cytometry

Expression of cell surface uPA and uPAR was analysed by indirect immunofluorescence using dual color flow cytometry (LSRFortessa™, Becton-Dickinson) and PI used to exclude non-viable cells (444). Data was analysed using FlowJo software version 7.6.5 (FlowJO LLC, USA) comparing specific antibody binding to isotype controls to account for nonspecific binding. Antibody details and dilutions are described in Table 1 of Appendix.

4.2.5 3D organotypic invasion assay

Invasion of PDAC cells through collagen I matrices contracted by either TIFs, wild-type or SerpinB2$^{-/-}$ MEFs were performed as described in detail in section 3.2.2. After contraction, 2.0 x 10^5 PDAC cells were seeded on top of the matrix in 24-well plates and grown for 2-3 days or until confluent. The matrices were then transferred to a liquid-air grid interface for invasion, as previously described (359). Matrices were refreshed every 2-3 days with DMEM supplemented with 10% FBS with 100 U/mL penicillin and 100 µg/mL streptomycin ± compounds (500 nM SerpinB2, 500 nM ^{R380A}SerpinB2 or PBS control). After 14 days, the matrices were fixed in 10% NBF for 2 days and kept in 70% ethanol at room temperature prior to embedding and sectioning as described in section 3.2.2. Sections were then processed for histological and microscopic analyses.

4.2.6 Mixed cell allograft model

Subconfluent PDAC cells and MEFs were harvested and resuspended in cold PBS, pH 7.4. 7.5 x 10^5 MEFS (wild-type or SerpinB2$^{-/-}$) were mixed with 2.5 x 10^5 PDAC cells (totalling 1 x 10^6 cells in 100 µL at a 3:1 MEF:PDAC ratio) and injected subcutaneously into the rear flank of four week old female BALB/c-Fox1nuAusb mice (5 per group). Tumour volume was quantified using a digital vernier caliper while mice were conscious and calculated using the equation, $xy^2/2$ (548). Mice were monitored daily in compliance with the Garvan/St Vincent's Hospital Animal Experimentation and Ethics Committee guidelines (approval #13/17). Mice were anesthetised seven days post injection and analysed using an IVIS fluorescence/luminescence imaging platform. After euthanasia, tumours were dissected into 3 parts and either formalin fixed or frozen for further processing and analyses.

4.2.7 Histological analysis

Dissected tumour sections from mixed allografts above were fixed in 10% cold NBF and processed and embedded in paraffin using the Leica Peloris Dual Retort tissue processor (Germany). Histological staining was

performed on 4 μm sections deparaffinised in xylene and rehydrated using graded ethanol washes. Haematoxylin and Eosin (H&E) and picrosirius red (Polysciences, USA, #24901-250) staining were performed on a Leica Autostainer XL. Immunohistochemistry was performed using the Leica Bond RX system. Refer to Table 1 of Appendix for antibody details. For scoring of invasive index, migration modality, cell cluster and immunohistochemistry staining, 10 images per sample were acquired using a bright field microscope (Leica DM4000).

For immunofluorescence analysis, pancreatic tumour allograft cryosections (4 μm) were cut and air-dried on glass slides. Sections were then fixed in 100 % acetone for 10 min at -20 °C and air-dried. Rehydrated sections were blocked and processed with antibodies as described in figure legends and Table 1 of Appendix. Slides were then mounted with Vectashield containing DAPI (Vector) and cells imaged using a Leica DMI 6000 SP8 laser scanning confocal fluorescence microscope (Germany). Staining specificity was shown with isotype controls.

4.2.8 *In vivo* allograft local invasion scoring method

Single and collective cell invasion into local tissue (subcutaneous fat, muscle and skin) was analysed by histoscore on 4 μm H&E stained sections. Local invasion was quantified as shown in Fig. 4.2, and scored by three separate researchers.

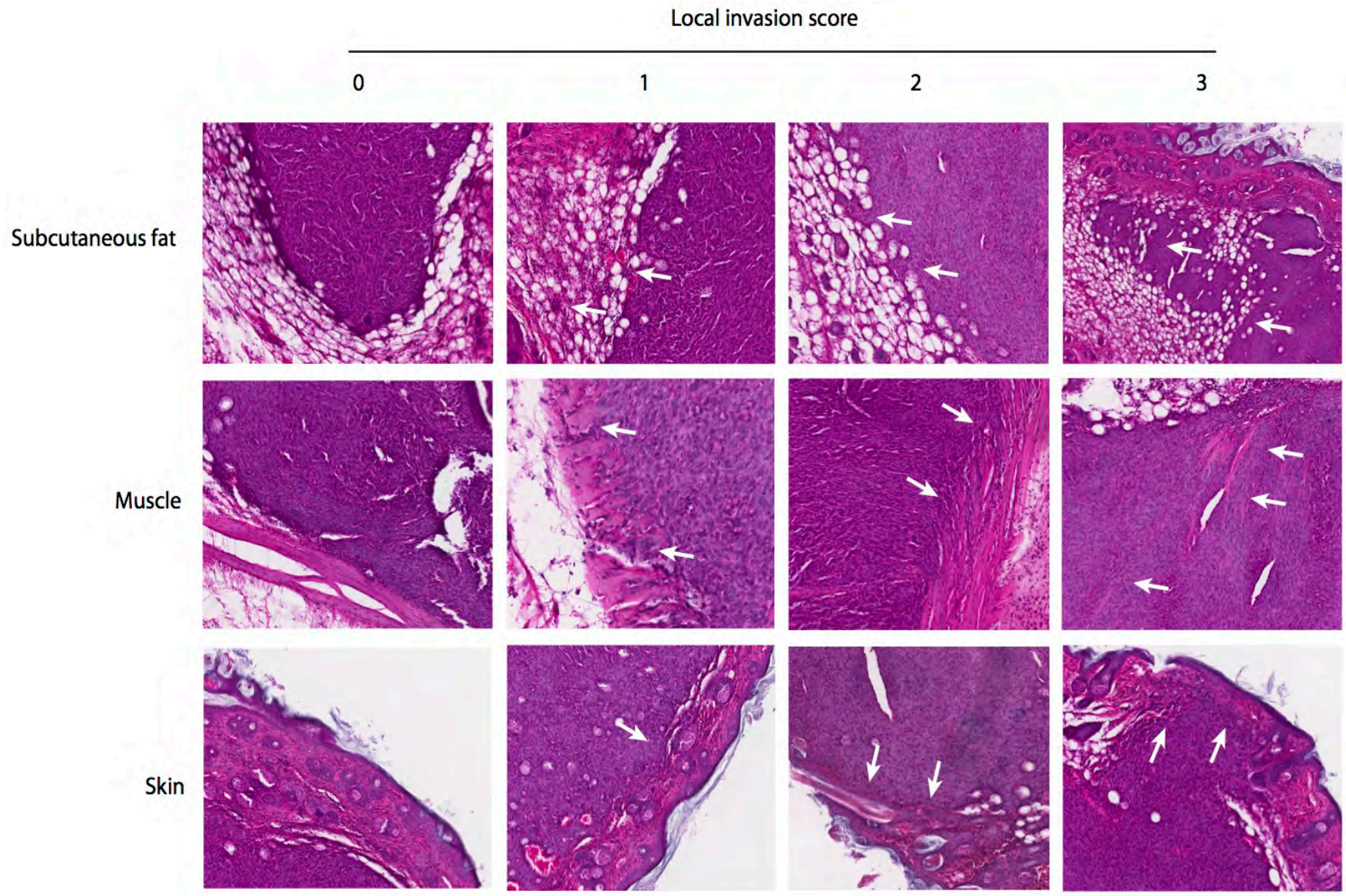

Fig. 4.2. *In vivo* allograft local invasion scoring method. Representative photomicrograph images defining quantification system of local invasion by either wild-type or SerpinB2$^{-/-}$ MEF:PDAC tumours. Single and collective cell invasion into local tissue (subcutaneous fat, muscle and skin) was analysed by histoscore on 4 µm H&E stained sections. No invasion was quantified as 0; single cell invasion into local tissue was scored as 1, collective cell invasion as 2, and in the event where the tissue was completely penetrated by tumour, a score of 3 was given. Arrows show invasion of tumour cells into specific tissue area. Quantification of local invasion was scored blind by three separate researchers.

4.2.9 SHG and SEM imaging analysis

20 µm FFPE sections of 3D matrices or tumours were analysed using SHG and SEM imaging systems as described in section 3.2.6 and 3.2.8, respectively.

4.2.10 uPA activity assay

Activity assays were performed as previously described (176). Briefly, frozen tumour samples were defrosted on ice and homogenised in 10 mM Tris (pH 8.0), 0.15 M NaCl, & 0.1% Triton X-100. Total protein levels were determined and lysates diluted to 3 mg/mL in 100 µL reaction buffer (20 mM HEPES, pH 7.6, 100 mM NaCl, 0.5 mM EDTA, 0.01% (v/v) Tween 20) containing 0.25 mM uPA fluorogenic substrate (Z-Gly-Gly-Arg-AMC – Chemicon, USA). Fluorescence was measured over time at 37 °C using a POLAstar plate reader (OMEGA) and activity determined against a murine uPA standard.

4.2.11 Statistical analyses

Unless specified otherwise, data is the mean (± SEM) of at least three independent experiments performed in either triplicate or sextuplet. Differences in the mean of two groups were analysed by an unpaired t-test. Comparisons of more than two groups were made by a one-way (or two-way) ANOVA with post hoc Holm-Sidak (or other post hoc) analysis for pairwise comparisons and comparisons versus control. P values < 0.05 were considered statistically significant. Unless stated otherwise, data and statistical analyses were performed using GraphPad Prism (version 6.0, USA).

4.3 RESULTS

4.3.1 APGI PDAC gene expression survival analysis

The PAS has previously been shown to drive invasion and metastasis in numerous cancer types (19). In the specific context of pancreatic cancer, expression of various individual components of this system have been associated with differential survival/outcome in a small cohort of PDAC patients (238,549). Therefore, the association of mRNA expression of PAS components (PLAU, PLAT, PLAUR, SERPINB2, SERPINE1) and disease-specific survival in a large cohort of resected PDAC (APGI) were analysed (Fig. 4.3) (511). Increasing PLAU expression was significantly associated with poorer survival (1.6 years reduced) following pancreatectomy (Cox model coefficient 0.387; likelihood ratio $P = 0.00019$, n = 141, Fig. 4.3A and B).

Further, at the genomic level, PAS component genes (PLAU, PLAUR, SERPINB2) were found to be frequently altered in PDAC (22% of cases, Fig. 4.3C). Interestingly, genomic alterations of the enzyme (PLAU), receptor (PLAUR), or inhibitor (SERPINB2) of the PAS pathway appeared to be mutually exclusive in PDAC (Fig. 4.3D). Mutual exclusivity of genomic alterations within a particular pathway are strongly predictive of a role for that pathway in driving tumourigenesis (550). Together, these data suggest a functional role for the uPA/SerpinB2 axis in PDAC progression. These genomic data imply that PDAC invasion could be facilitated by PAS, and thus needed to be interrogated through various experimental models.

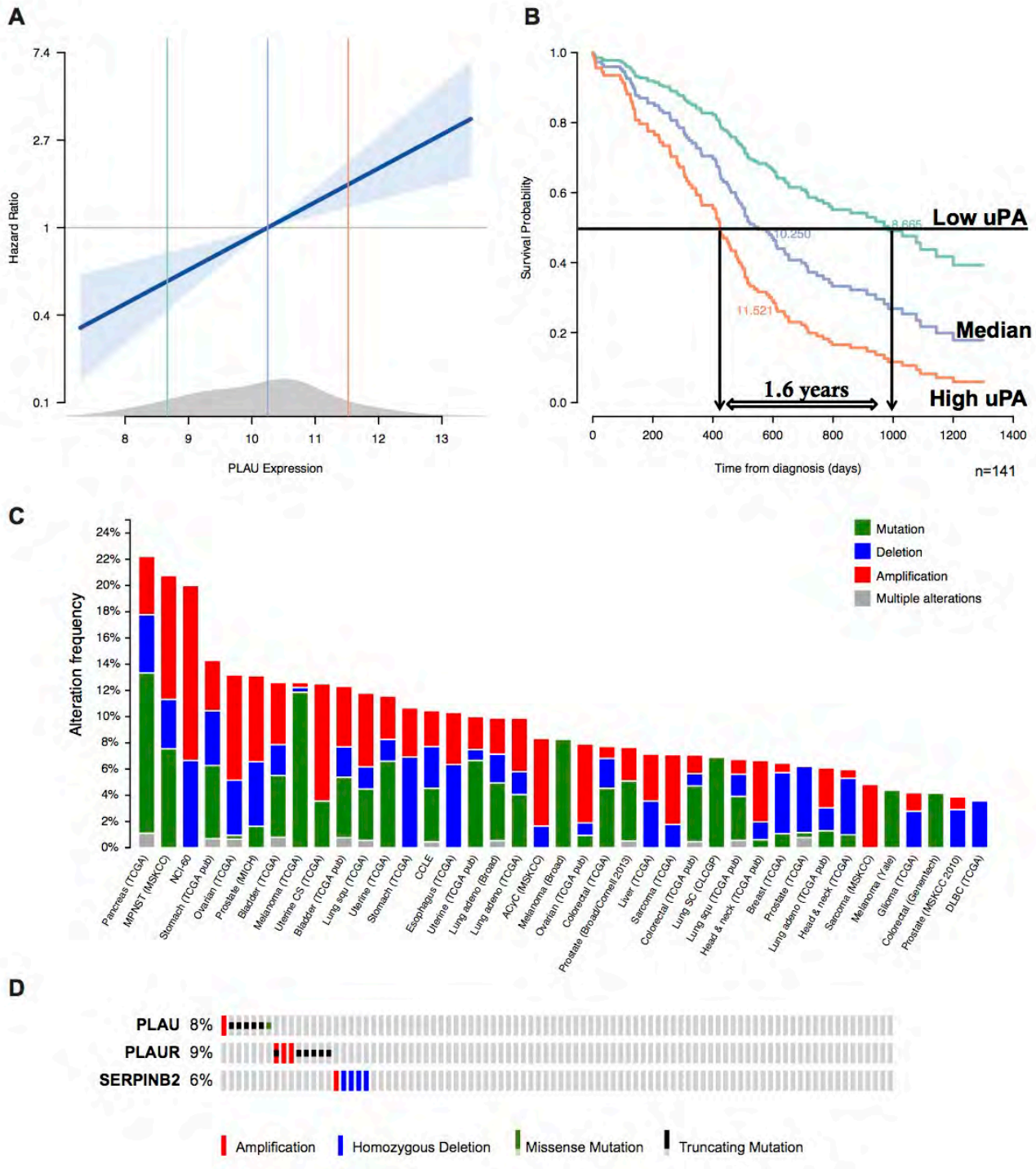

Fig. 4.3. PAS expression in human PDAC after pancreatectomy. Hazard ratio (**A**) and overall survival (**B**) in relation to uPA expression for a cohort of patients with resected PDAC (n=141). Standard error of the fit is shown as a light blue band, and the distribution of PLAU expression in the cohort as a grey density distribution. 10th, 50th, and 90th percentiles of the PLAU expression distribution are indicated by vertical green, blue, and orange lines, respectively. The Cox model predicted survival paths for these three percentiles of PLAU expression are further illustrated in (**B**). Inset lines denote the extended survival time of 1.6 years for patients in the 10th percentile for PLAU expression versus patients in the 90th percentile of PLAU expression distribution. **C.** Alteration frequencies of the PAS component genes PLAU, PLAUR and SERPINB2 across various cancer types in TCGA database; **D**. Mutual exclusivity of PLAU, PLAUR and SERPINB2 genomic alterations in pancreatic tumours in TCGA database (n=90).

4.3.2 PDAC cell invasion in the 3D organotypic culture model

To further assess the role of uPA and SerpinB2 in PDAC invasion, the 3D organotypic culture system described in Chapter 1 (refer to Fig. 1.11) was employed. In this model, invasion of PDAC cells into the fibroblast-contracted collagen I matrix was induced by a chemotactic air-liquid interface (359). PDAC cells are an appropriate functional model for understanding the role of PAS in pancreatic cancer as they express cell surface uPA/uPAR (refer to Fig. 4.7E). This model closely recapitulates the interaction between cancer cells, stromal cells and the ECM (547). In order to determine the effects of altered matrix integrity in the absence of stromal SerpinB2 (matrices outlined in Chapter 3) on migration and invasive capacity of pancreatic tumour cells, a 14-day invasion using the air-liquid interface method was undertaken. PDAC cell invasion through matrices formed by SerpinB2$^{-/-}$ MEFs doubled compared to wild-type (27.2 % $\pm$ 1.9 versus 55.2 % $\pm$ 1.8; $P < 0.001$) (Fig. 4.4A-C). Furthermore, a significant difference in invading PDAC cell morphology and migration mode was observed in matrices formed by SerpinB2$^{-/-}$ MEFs. PDAC cells invading through wild-type matrix exhibited a predominantly mesenchymal migratory mode (>70% of cells) (Fig. 4.4A, D) while PDAC cells in SerpinB2$^{-/-}$ matrices displayed a predominantly amoeboidal phenotype (>80% of cells) (Fig. 4.4B, D).

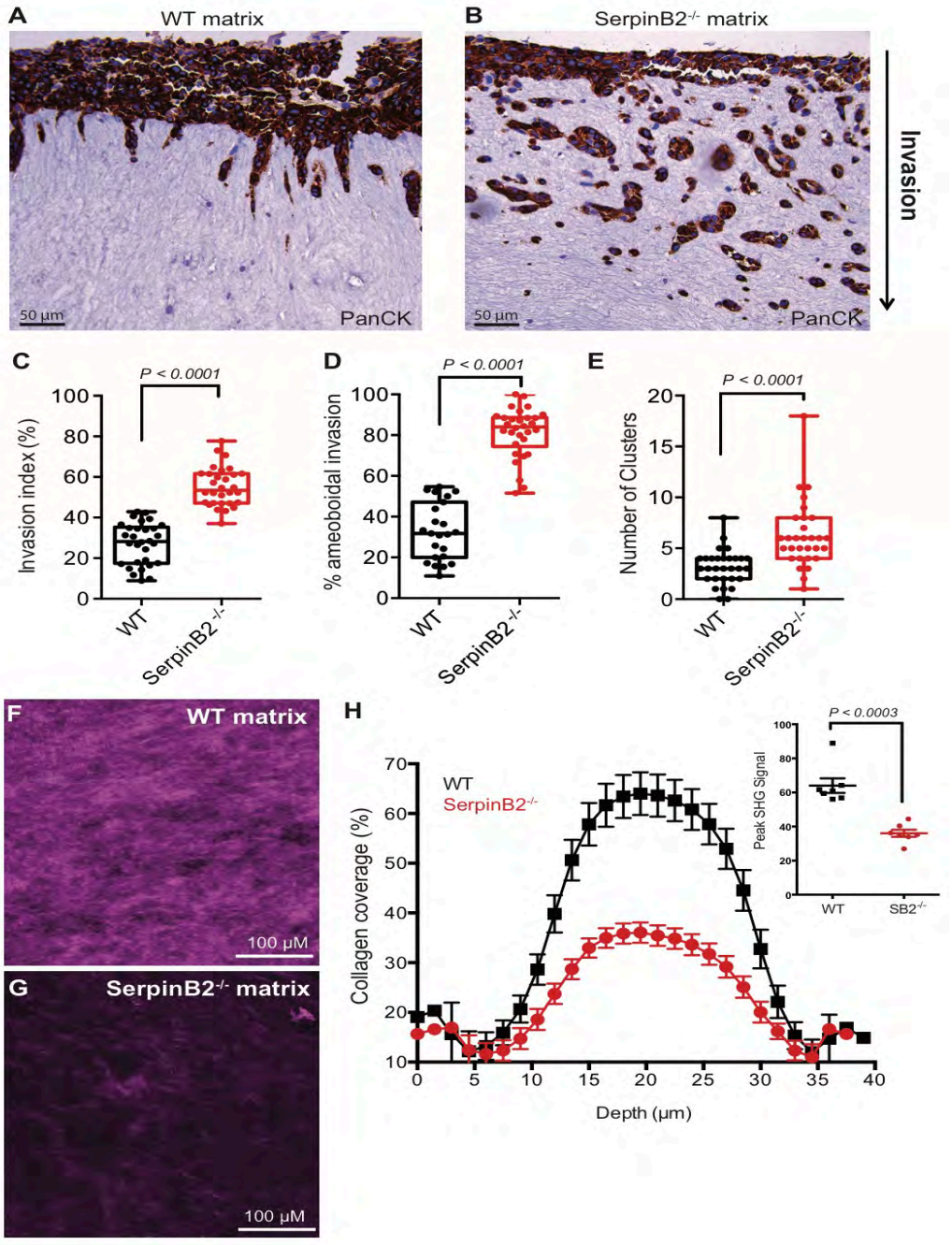

Fig. 4.4. PDAC invasion through wild-type and SerpinB2$^{-/-}$ MEF/collagen I matrices. A-B: Photomicrographs of pan-cytokeratin stained sections of organotypic cultures showing invasion of PDACs through collagen I matrices formed in the presence of either (**A**) wild-type or (**B**) SerpinB2$^{-/-}$ MEFs; **C.** Invasion index - calculated as the percentage of PDACs invading the matrix relative to PDACs present in the layer overlaying the matrix; **D.** Migration mode analysis - PDAC cells were scored as displaying either amoeboidal, mesenchymal or collective migration modes; **E.** Cluster analysis – Clusters per field of view (FOV) were scored when ≥3 PDAC cells were together in a complex. **C-E** analysis was performed on images taken at sites of maximal invasion after 14 days, using 10 fields of view. Individual values are shown with bars representing mean ± SEM from 3 separate matrices. Statistical analyses were performed using unpaired t-tests; **F-G**: Maximum projection of SHG signal intensity of collagen matrices formed with either (**F**) wild-type or (**G**) SerpinB2$^{-/-}$ MEFs (bars = 100 µm); **H.** Total collagen coverage (quantified by SHG) within PDAC invaded matrices formed with either wild-type or SerpinB2$^{-/-}$ MEFS, inset: Mean collagen coverage at SHG signal peak. Values shown are means ± SEM from 3 separate matrices (n = 9), statistical analysis performed using an unpaired t-test.

These observations were supported by increased expression of E-cadherin in PDAC cells within SerpinB2$^{-/-}$ matrix, but not in wild-type matrices (Fig. 4.5). Expression of E-cadherin is required for epithelial cell adhesion mechanisms, forming adherens junctions to bind epithelial cells tight together and to the tissue bed (551). E-cadherin down-regulation reduces cellular adhesion strength within a tissue bed, resulting in increased in cellular motility and migration. As PDAC cells in the wild-type matrices exhibited a decreased expression of E-cadherin, this potentially allowed them to break adherens junctions and separate from the monolayer, acquiring the classic epithelial-mesenchymal transition (EMT) to invade down into the collagen matrix. Further, there was a significant increase in PDAC cell clustering observed within matrices prepared with SerpinB2$^{-/-}$ MEFs compared with wild-type MEFs (6.2 $\pm$ 0.6 clusters versus 3.1 $\pm$ 0.7; ($P < 0.0001$) (Fig. 4.4E). This cluster phenotype coupled with significant E-cadherin expression, suggested that collective invasion did not require EMT within SerpinB2$^{-/-}$ collagen matrices, and revealed PDAC cellular control of CDH1 (E-cadherin encoding gene).

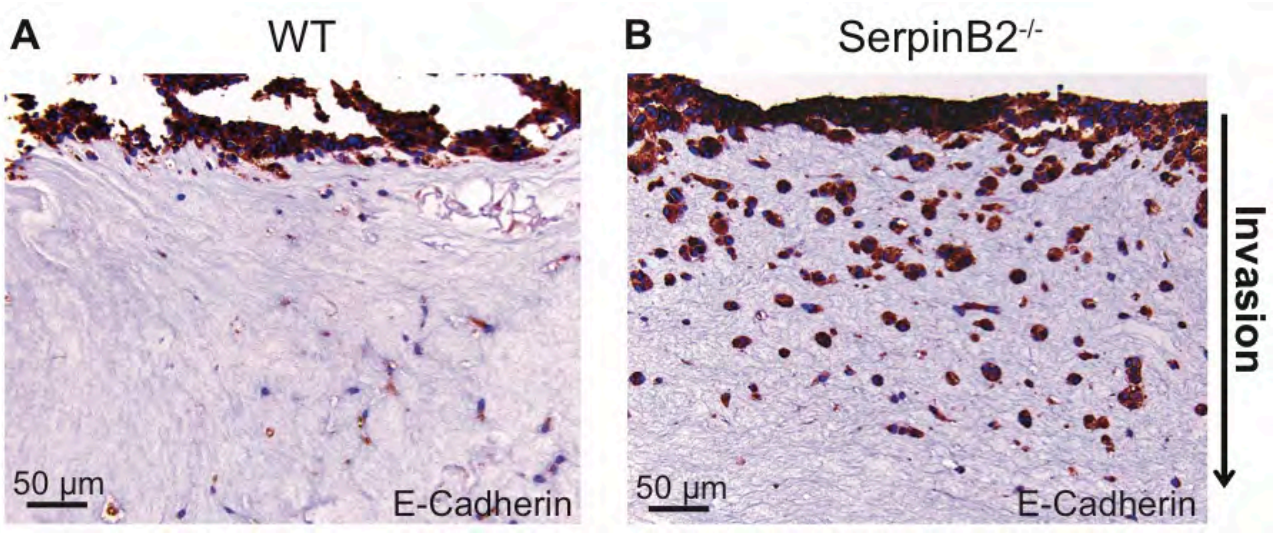

Fig. 4.5. PDAC invasion through wild-type and SerpinB2$^{-/-}$ MEF/collagen I matrices. A-B: Photomicrographs of E-Cadherin stained sections of organotypic cultures showing invasion of PDACs through collagen I matrices formed in the presence of either (**A**) wild-type or (**B**) SerpinB2$^{-/-}$ MEFs.

Moreover, fibroblast led PDAC invasion was observed in both wild-type and SerpinB2$^{-/-}$ MEF/collagen I matrices (Fig. 4.6), which is a novel result for SerpinB2$^{-/-}$ MEF constructed matrices, however well-known to

occur in the TME and reported by others (344,552). Additionally, ultrastructural SEM analyses observed fibroblast constructed tunnels in both wild-type and SerpinB2$^{-/-}$ MEF/collagen I matrices, which potentially provides insight into one of the pathways that both epithelial and mesenchymal PDAC cells may traverse and invade down into the collagen matrices (Fig. 4.6).

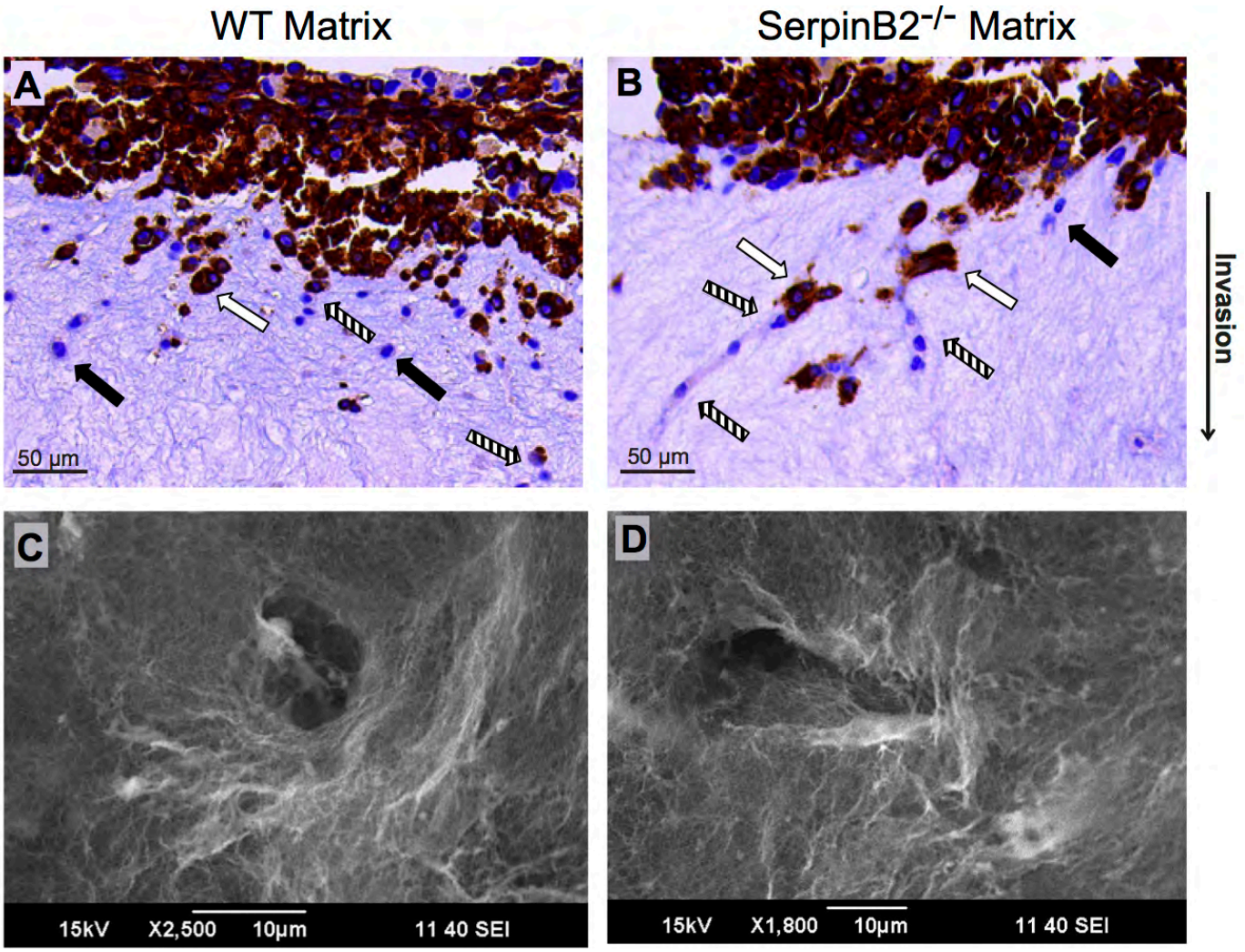

Fig. 4.6 Fibroblast led PDAC invasion though 3D organotypic matrices. PDAC cells being guided into both (**A**) wild-type and (**B**) SerpinB2$^{-/-}$ MEF collagen I matrices. Inset: Black arrows denote fibroblasts; white arrows denote PDAC cells; black and white striped arrows denote fibroblasts leading PDAC cells into the matrix. **C.** SEM analysis of a fibroblast constructed tunnel within (**C**) wild-type and (**D**) SerpinB2$^{-/-}$MEF collagen I matrices.

SHG analyses of the matrices at the end of the 14-day invasion assay confirmed the reduced structural integrity of SerpinB2$^{-/-}$ MEF (36 ± 2.1 % collagen coverage) versus wild-type MEF matrices (64 ± 4.3% collagen coverage), respectively, corresponding to a 56% decrease in the mean collagen coverage between matrices

(Fig. 4.4F-H). Hence, the compromised structural integrity of matrix formed in the absence of stromal cell SerpinB2 markedly influenced PDAC cell migration and invasion.

4.3.3 Exogenous SerpinB2 inhibits PDAC cell invasion

After it was elucidated that SerpinB2 deletion with the stroma significantly increases PDAC invasion, the next question posed was what effect SerpinB2 directly has upon epithelial PDAC cells. Importantly, the telomerase-immortalised fibroblasts (TIFs) used for matrix contraction express low if not negligible levels of uPA/uPAR (Fig 4.7F). This was necessary in order to ascertain individual uPA/uPAR effects of PDAC cells in this model. Under control conditions (PBS), PDAC cells were highly invasive (invasion index = 71.1 % ± 4.1) with extensive penetration into the underlying dermal-equivalent matrix (Fig. 4.7A, D) as previously reported (359,553). In contrast, there was a significant inhibition of PDAC cell invasion observed in the presence of exogenous SerpinB2 over the 14-day invasion period (invasion index = 42.9 % ± 6.2, $P < 0.0001$) (Fig. 4.7B, D). Importantly, invasion of PDAC cells was not affected by SerpinB2^{R380A}, an active-site mutant that is unable to inhibit uPA (invasion index = 71.1 % ± 4.1, $P = 0.2087$) (Fig. 4.7C, D). Hence, invasion of PDAC cells into the underlying stroma in an organotypic culture model was uPA-dependent and regulated by SerpinB2, one of the key endogenous inhibitors of uPA activity.

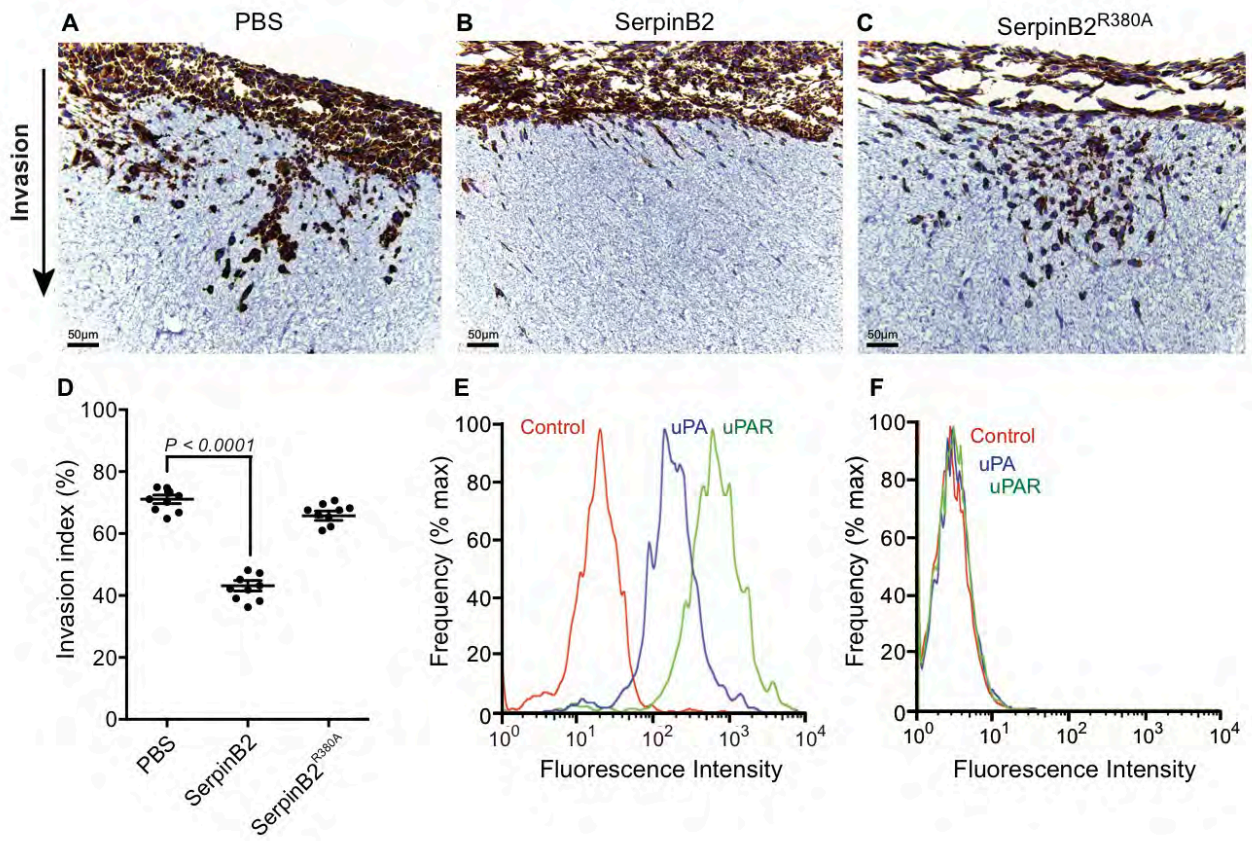

Fig. 4.7. PDAC invasion in TIF/collagen 3D organotypic matrices. A-C: Photomicrographs of pan-cytokeratin stained sections of 3D organotypic cultures showing invasion of PDACs through the TIF/Collagen I matrix, (**A**) PBS control, (**B**) 500 nM wild-type SerpinB2, **C.** 500 nM SerpinB2^{R380A} (uPA non-inhibitory mutant); **D.** Invasion index - calculated as the percentage of PDACs invading the matrix relative to PDACs present in the layer overlaying the matrix (pan-cytokeratin stain) from 10 fields of view at areas of highest invasion. Individual values are shown with bars representing mean ± SEM from 3 separate matrices. Statistical analysis performed using an unpaired t-test. **E-F**: Flow Cytometry analysis of cell surface uPA and uPAR expression on (**E**) PDAC and (**F**) TIFs. Figures are representative of triplicate determinations.

4.3.4 Exogenous SerpinB2 does not inhibit PDAC invasion in contracted MEF matrices

As SerpinB2 showed successful PDAC cell inhibition of invasion through TIF contracted matrices (with moderate to high SerpinB2 expression level in these fibroblasts), it was necessary to observe if this would occur in the context of stromal SerpinB2 absence. Thus, organotypic invasions were undertaken using PDAC cells in both wild-type and SerpinB2$^{-/-}$ MEF contracted matrices, with exogenous addition of either wild-type SerpinB2, ^{R380A}SerpinB2 or PBS control (Fig. 4.8). Significant differences were observed in PDAC cell invasion between wild-type or SerpinB2$^{-/-}$ matrices (Fig 4.8, $P < 0.0001$), as previously shown in section 4. (refer to Fig 4.4C). PDAC cell invasion through wild-type MEF matrices was also significantly abrogated with the addition

of wild-type SerpinB2 versus ^{R380A}SerpinB2 ($P < 0.0001$), and PBS ($P < 0.0001$), Fig. 4.8A-C, G). However, no significant PDAC invasion differences were observed between exogenous addition of wild-type SerpinB2, ^{R380A}SerpinB2 or PBS through SerpinB2$^{-/-}$ MEF contracted matrices ($P > 0.05$, Fig. 4.8D-F).

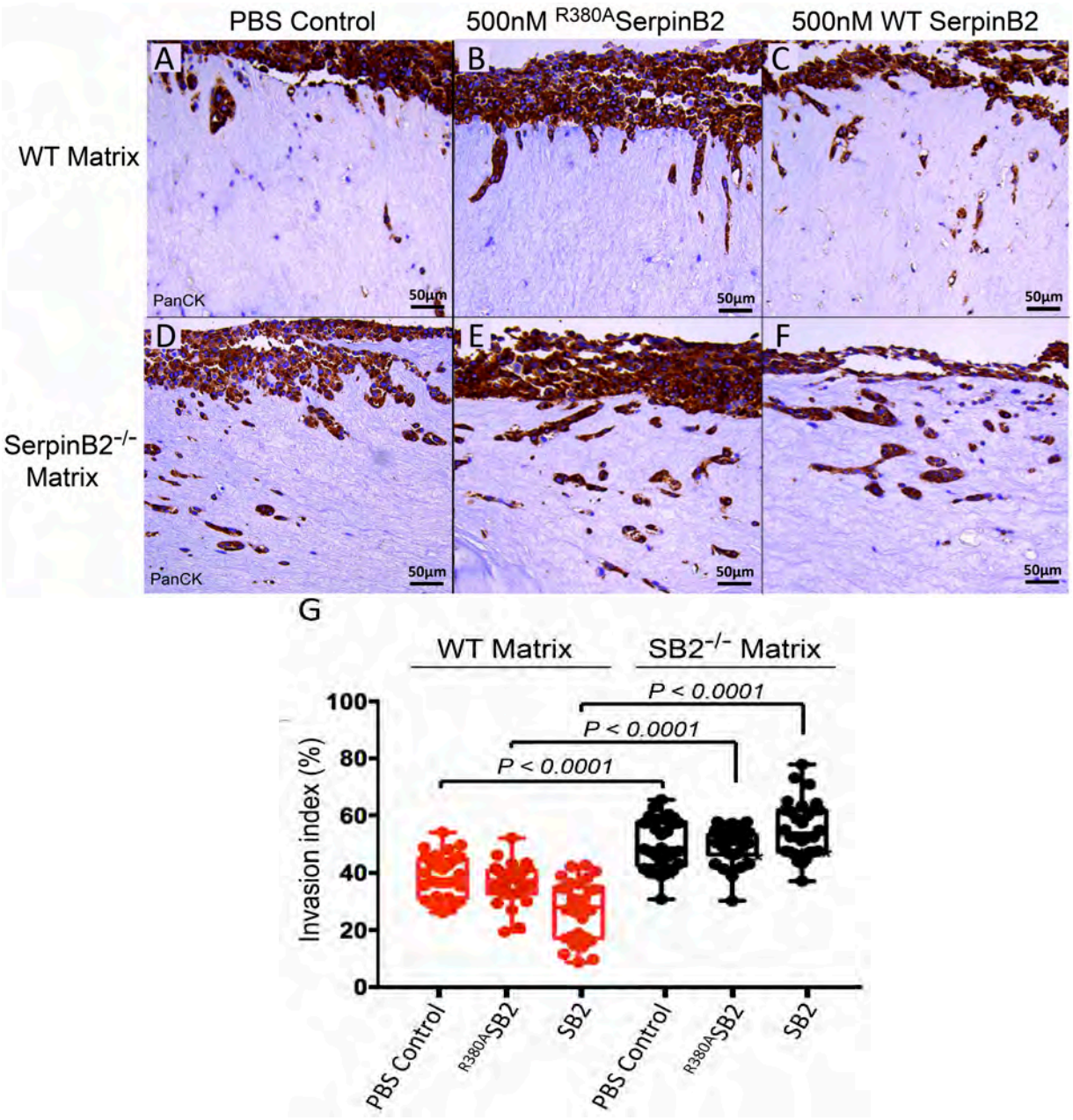

Fig. 4.8. PDAC invasion in wild-type or SerpinB2$^{-/-}$ MEF/collagen I 3D organotypic matrices. A-C: Photomicrographs of pan-cytokeratin stained sections of 3D organotypic cultures showing invasion of PDACs through the wild-type MEF/Collagen I matrix, (**A**) PBS control, (**B**) 500 nM ^{R380A}SerpinB2 (uPA non-inhibitory mutant), (**C**)**.** 500 nM wild-type SerpinB2; **D-F:** Photomicrographs of pan-cytokeratin stained sections of 3D organotypic cultures showing invasion of PDACs through the SerpinB2$^{-/-}$ MEF/Collagen I matrix, (**D**) PBS control, (**E**) 500 nM ^{R380A}SerpinB2 (uPA non-inhibitory mutant), (**F**)**.** 500 nM wild-type SerpinB2; **G.** Invasion index - calculated as the percentage of PDACs invading the matrix relative to PDACs present in the layer overlaying the matrix (pan-cytokeratin stain) from10 fields of view (of triplicate experiments) at areas of highest invasion. Individual values are shown with bars representing mean ± SEM from 3 separate matrices per experiment. Statistical analysis performed using an unpaired t-test. Figures are representative of triplicate deeterminations.

4.3.4 PDAC tumour growth and local invasion *in vivo*

To determine the effects of modulating the expression of SerpinB2 in the stroma *in vivo*, an allograft experiment was performed, where PDAC cells and MEFs (wild-type or SerpinB2$^{-/-}$) were co-injected into Balb/c nude mice. A MEF:PDAC ratio of 3:1 was used in order to reflect the high fibroblast content and low tumour cellularity of PDAC tumours (554-556). Seven days post subcutaneous inoculation into the hind flank of the animal, PDAC tumours formed. Tumours containing SerpinB2$^{-/-}$ MEFs were significantly larger and more elongated than those formed with wild-type MEFs (mean volume 205 mm^3 ± 29, versus 143 mm^3 ± 29 respectively, $P = 0.0322$, Fig. 4.9B). Consistent with the increased size of tumours formed with SerpinB2$^{-/-}$ MEFs, IHC showed significantly elevated cell proliferation as evidenced by increased Ki-67 staining in these tumours compared to those formed with wild-type MEFs (tumour border = 819 ± ± 53.3 vs 506 ± 48.1 positive cells per field of view (FOV), $P = 0.0024$; tumour centre = 576 ± 65.7 versus 208 ± 48.2 positive cells per FOV, $P = 0.0020$; Fig. 4.9C).

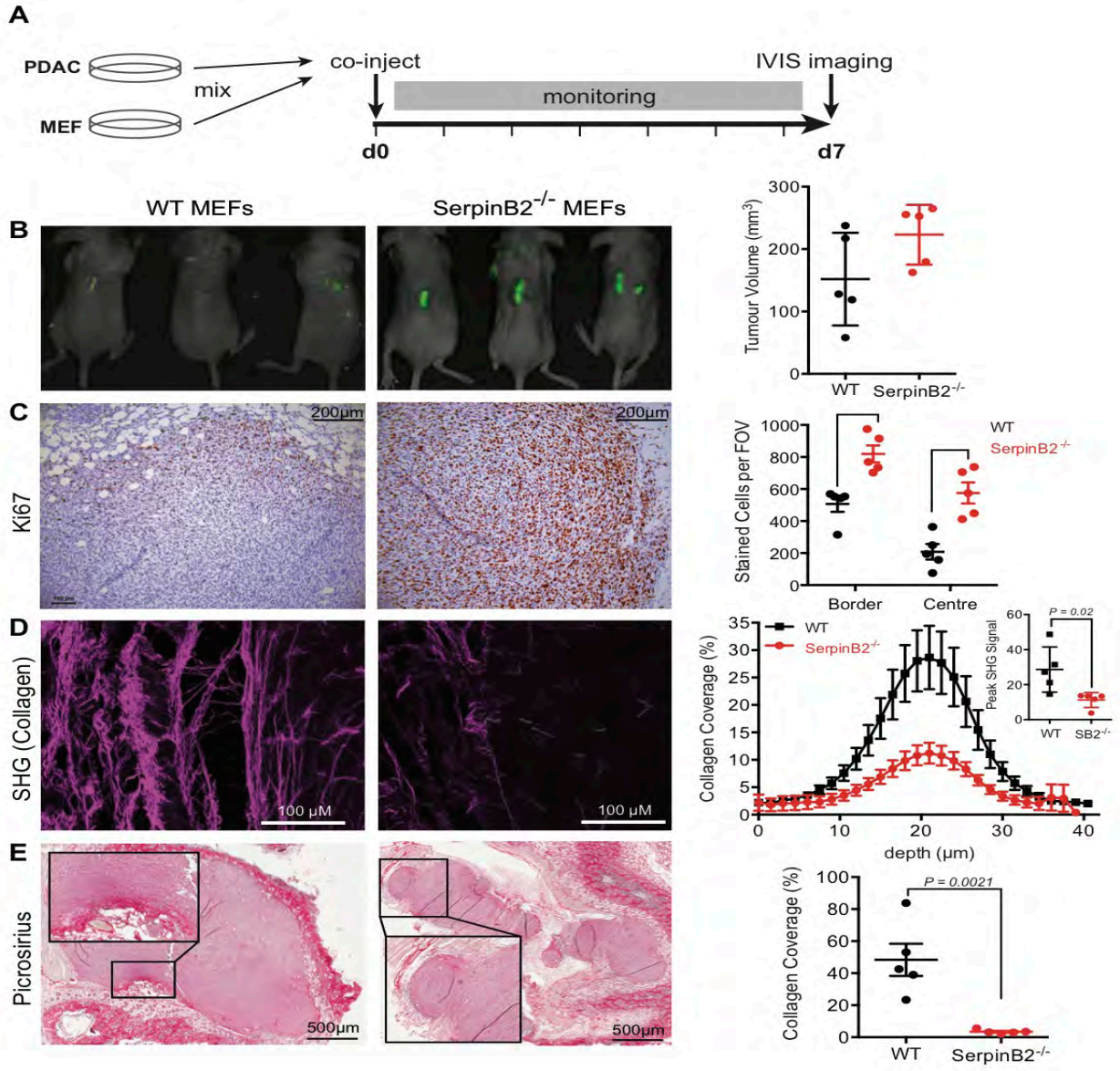

Fig. 4.9. ***In vivo*** **mixed cell allograft model. A.** A mixture of MEFs (wild-type or SerpinB2$^{-/-}$) and PDACs (at a 3:1 MEF:PDAC ratio) were inoculated into nude mice and allowed to grow for 7 days prior to the following analyses; **B.** IVIS imaging of MEF-GFP fluorescence; tumour volume quantification (mean ± SEM, n = 5); **C**. Ki-67 staining and quantification at both the border and centre of tumours; **D.** Maximum projection of SHG signal intensity of collagen coverage formed within MEF:PDAC tumours (inset: mean collagen coverage at SHG signal peak); **E.** Picrosirius staining (with insets showing high magnification view) and quantification of collagen I/III coverage of tumours. Individual values shown are means from 3 representative images per tumour from 5 animals per group with mean ± SEM denoted. Statistical analyses were performed using unpaired t-tests.

Consistent with the results from 3D organotypic experiments, significant changes in collagen matrix integrity of allograft tumours in the absence of SerpinB2 were observed. SHG analysis (Fig. 4.9D) showed a significant decrease in collagen content at tumour margins in the absence of MEF SerpinB2 (mean collagen coverage 28.7 ± 5.8 % versus 11.2 ± 1.9 % in wild-type versus SerpinB2$^{-/-}$ MEF respectively. $P = 0.0209$). Quantification of Collagen I and III content in allografts by picrosirius staining (Fig. 4.9E) also revealed significantly decreased

collagen coverage in tumours formed with SerpinB2$^{-/-}$ MEFs compared to wild-type (48.4 ± 10.1 % versus 3.5 ± 0.6 % respectively, $P = 0.0021$). No significant difference in apoptosis (detected by IHC analysis of cleaved caspase-3) was detected in the PDAC cell allograft tumours formed with either wild-type or SerpinB2$^{-/-}$ MEFS (Fig 4.10).

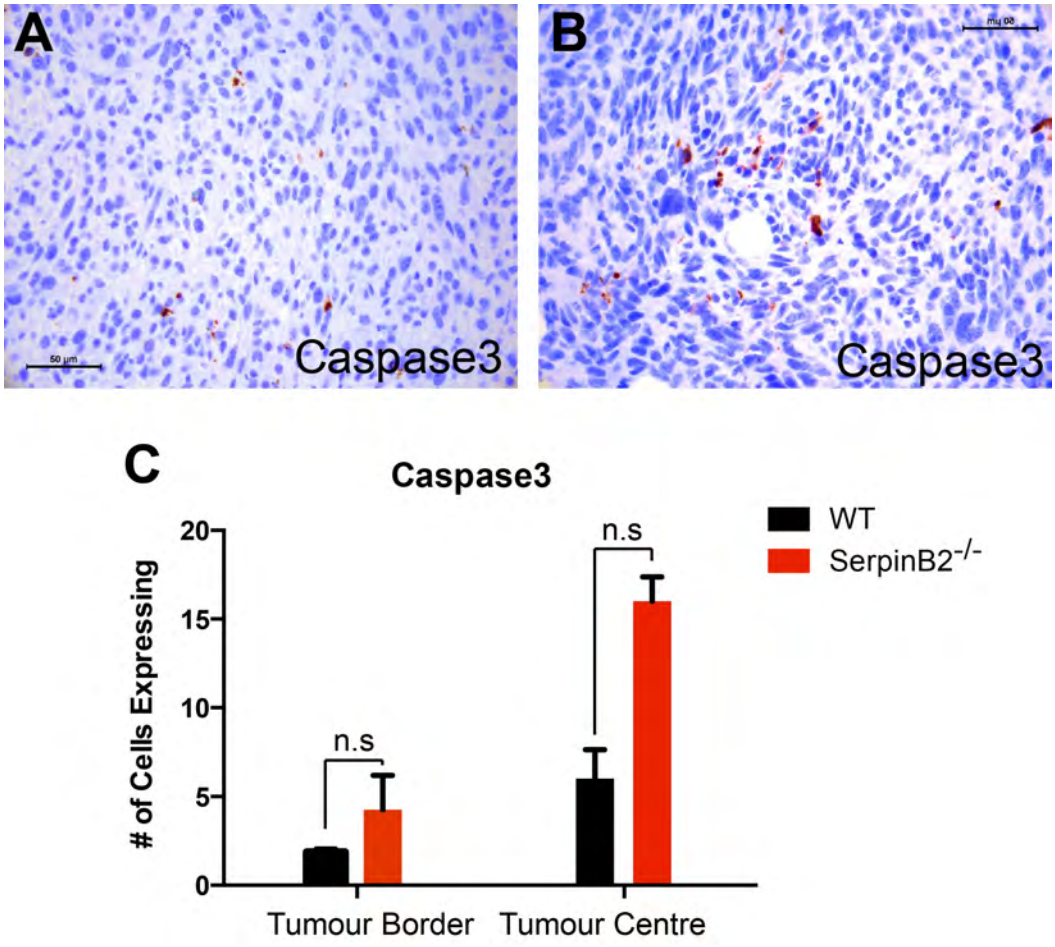

Fig 4.10. Cleaved caspase-3 in mixed cell allograft model. A-B: CC3 staining at centre of **(A)** wild-type and **(B)** SerpinB2$^{-/-}$ MEF tumours; **C:** Quantification of CC3 staining at both tumour border and centre of wild-type and SerpinB2$^{-/-}$ MEF:PDAC tumours (n = 5; Error bars = SD).

This result is quite novel, as most findings in the field report an increase in collagen bundling at the border of tumours (263,280,557). This result could explain the difference in local invasion, suggesting that PDAC collective migration is increased when there is less desmoplasia/collagen coverage surrounding the primary tumour mass (addressed further in the discussion). Loss of E-cadherin (or gain of N-cadherin) was not required in such a SerpinB2 null ECM (Fig. 4.5), thus traditional EMT migration appeared less advantageous for the

spread of the tumour. It appears from these results, that for loco-regional progression of PDAC in a SerpinB2 down regulated system, advantages appear to reside in collective tumour migration over disseminating individual PDAC cells. It is known that large tumour masses produce higher autocrine and paracrine concentrations of promigratory factors and matrix proteases while also protecting inner cells from immunological targeting (558,559). Examination of allograft tumour margins by immunofluorescence (Fig. 4.11) revealed that many cells were positive for alpha-smooth muscle actin (α-SMA), marking activated fibroblasts which are known to lead tumour invasion (344) (see Appendix B for isotype control immunofluorescence, refer to Fig. A.1). No obvious co-localisation between SerpinB2 and α-SMA was observed, suggesting that host derived myofibroblasts may have been recruited to the TME over the seven day experimental time period. This analysis also revealed significantly higher expression of uPA in tumours formed with SerpinB2$^{-/-}$ MEFs compared to those formed with wild-type MEFs (Fig. 4.11). Expression of uPAR, the cellular receptor for uPA, was also higher in these tumours (Fig. 4.11). Further, uPA distribution appears to be localised to discrete regions within tumours formed with wild-type MEFs, with a more homogenous distribution was observed in tumours formed with SerpinB2$^{-/-}$ MEFs (Fig. 4.11). While many cells showed clear expression of SerpinB2 in tumours formed with wild-type MEFs, there was only some SerpinB2 detected in tumours derived using SerpinB2$^{-/-}$ MEF/PDACs, suggesting host derived fibroblast or other stromal cells may contribute SerpinB2 (Fig. 4.11). In addition, there was only a small amount of observable co-localisation of uPAR and SerpinB2 within SerpinB2$^{-/-}$ MEF/PDAC tumours versus a moderate amount within wild-type MEF/PDAC tumours. This result was expected in the SerpinB2$^{-/-}$ MEF/PDAC tumours and suggests that SerpinB2 expression observed in the wild-type MEF/PDAC tumours may be contributed by intracellular pools of SerpinB2 that is independent of its extracellular uPA inhibitory role (Fig. 4.11, B).

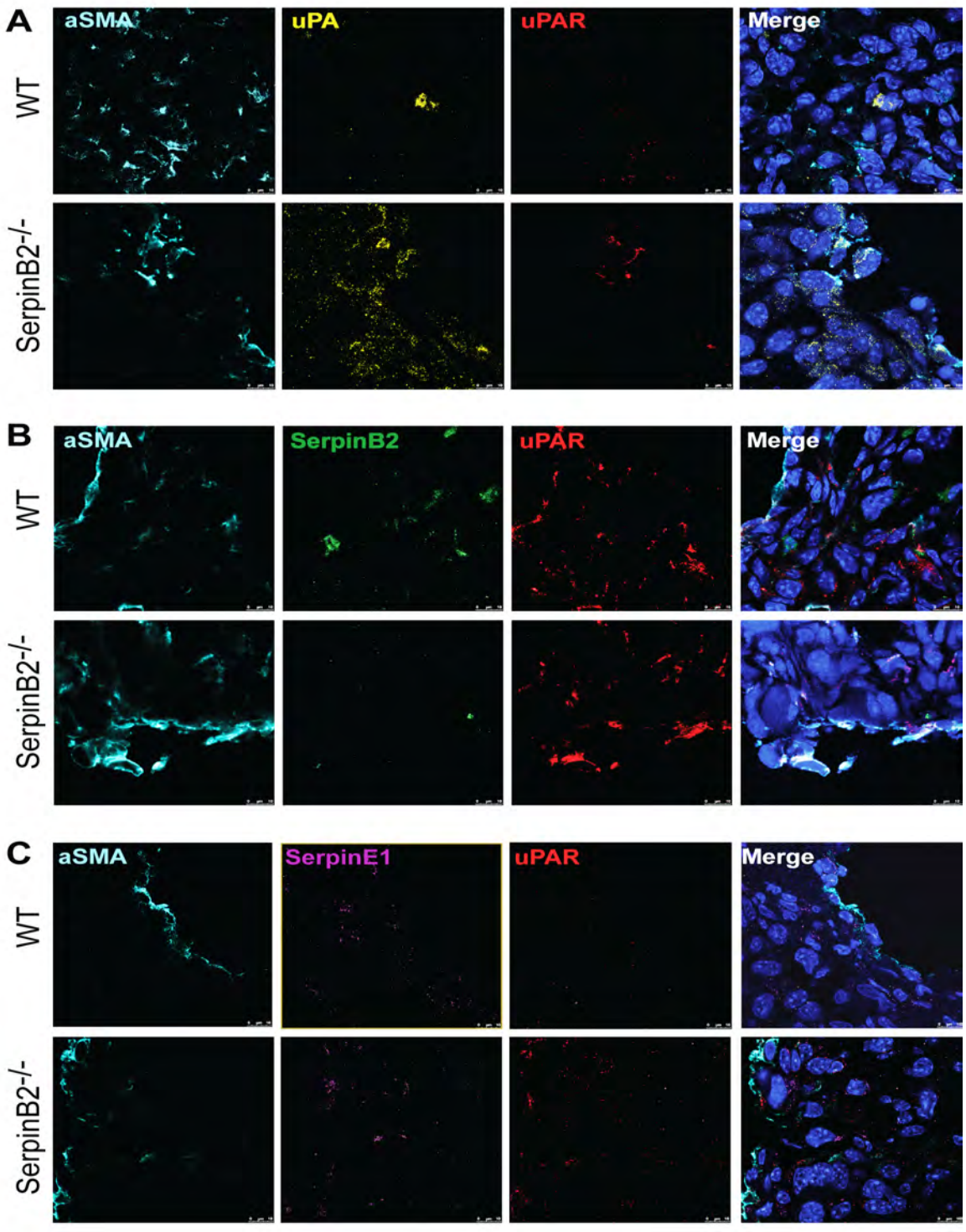

Fig 4.11. Immunofluorescence - αSMA, uPA, uPAR, SerpinB2 and SerpinE1 expression in mixed cell allografts. Immunofluorescence imaging of cryosections from wild-type or SerpinB2$^{-/-}$ MEF:PDAC tumour allografts showing expression of **(A)** α-SMA, uPA, uPAR, **(B)** α-SMA, SerpinB2, uPAR or, **(C)** (B). α-SMA, SerpinE1, uPAR. Merged images include DAPI nuclear staining;

Histological analysis of excised tumours showed that those formed with wild-type MEFs were largely encapsulated (Fig. 4.11A), while tumours formed with SerpinB2$^{-/-}$ MEFS showed significantly enhanced local

invasion into both muscle (Fig 4.12A,B) and subcutaneous fat (Fig 4.12C,D). Notably, this result reveals the differential invasive capacity of tumours with or without stromal SerpinB2 expression.

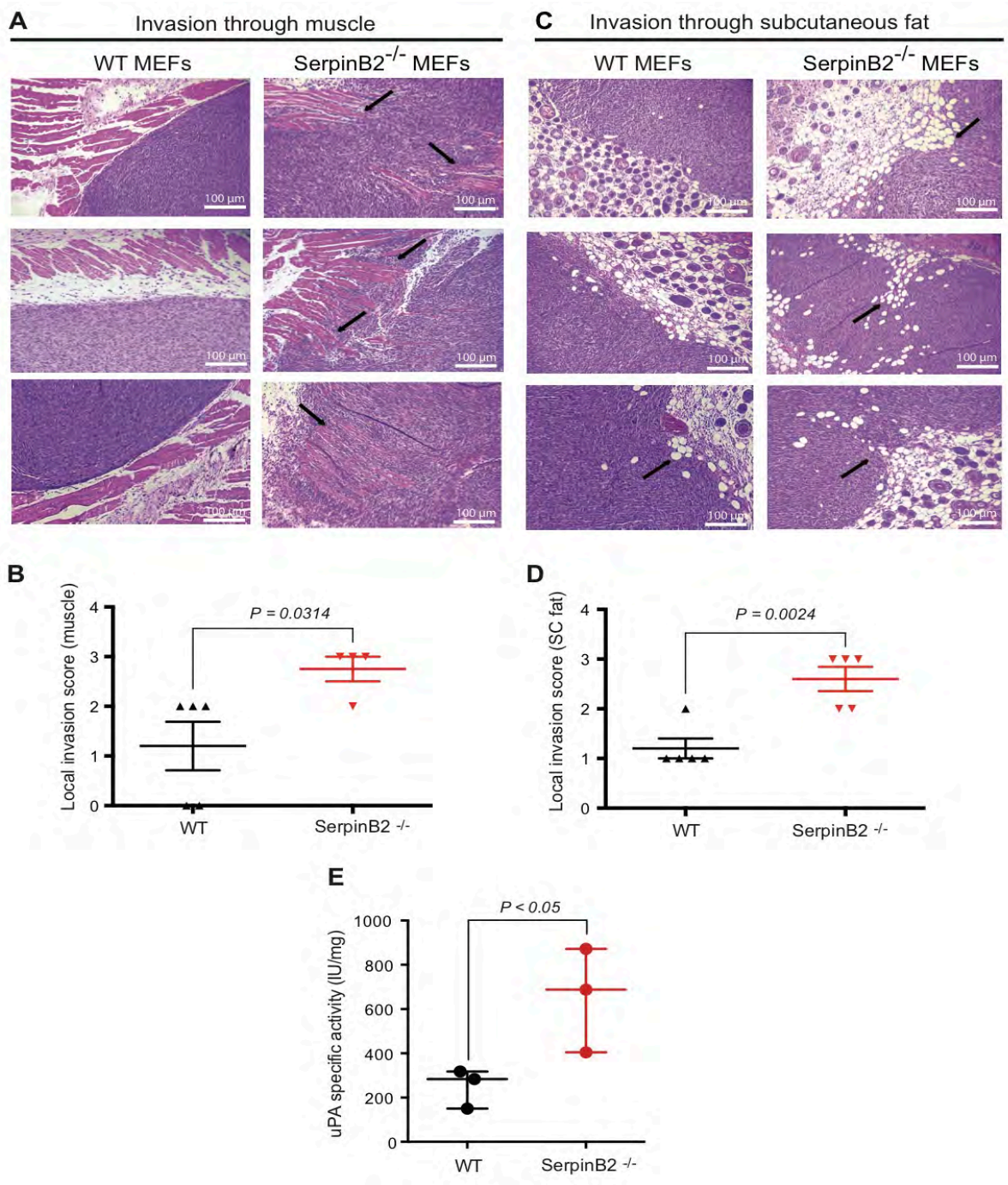

Fig 4.12. Photomicrographs and quantification of PDAC tumour local invasion. Cell invasion into local muscle tissue (**A**) or subcutaneous fat (**C**), by either wild-type or SerpinB2$^{-/-}$ MEF:PDAC tumours. Black arrows denote single and collective PDAC local invasion into either muscle or subcutaneous fat tissue; quantification of invasion into local muscle tissue (**B**) or subcutaneous fat (**D**) are shown. **E.** uPA enzymatic activity (IU/mg) from either wild-type or SerpinB2$^{-/-}$ MEF:PDAC tumour lysates (bars represent mean ± SEM, n = 3).

Consistent with increased immunofluorescent detection of uPA protein in allografts formed with SerpinB2$^{-/-}$ MEFs (refer to Fig. 4.12), we also observed increased uPA proteolytic activity in these tumours (250.4 $\pm$ 51.1 IU/mg versus 654.10 $\pm$ 136.0 IU/mg in wild-type and SerpinB2$^{-/-}$ respectively. $P = < 0.05$, Fig 4.12E).

In summary, the increased proliferation and local invasion observed in mixed cell allograft tumours formed with SerpinB2$^{-/-}$ MEFs is accompanied by changes in the expression and distribution of uPA and uPAR, and increased uPA proteolytic activity. These robust changes most likely reflect altered dynamics of uPA/uPAR turnover on PDAC cells. It seems that SerpinB2 expression within the stroma impinges greatly upon the migration modality and ability of PDAC cells to locally invade, collectively or singly. Altogether, these novel findings from two organotypic invasion assays and a mouse model of PDAC provide evidence that the spatiotemporal expression of SerpinB2 impacts greatly upon stromal remodelling of the ECM as well as the invasiveness of PDAC cells.

4.4 DISCUSSION

PDAC represents a worldwide causation of human morbidity and mortality, ranking among the top five causes of cancer death after gastric, breast, lung and prostate cancer (560). About 55 per cent of pancreatic cancer cases occur in developed countries (561), where the delayed prognosis for the majority of patients diagnosed with PDAC means that advanced stages of disease are already in effect. Beyond surgery, current PDAC treatment options are extremely limited and have not substantially improved the survival of patients with resectable disease over the past 25 years. Thus, there is an urgent need for new therapeutic strategies to treat advanced disease, as only 10-20% of patients are eligible for pancreatectomy (562). Tumour-stroma studies are vital in the understanding PDAC biology and will provide the key to wholly understanding the tumourigenic process and for the generation of new therapeutic strategies against this insidious disease.

A strong association between increased PLAU mRNA expression and decreased survival in a large cohort of resectable pancreatic cancer patients (refer to Fig. 4.3) confirmed the power of uPA overexpression as a marker of disease outcome/survival in PDAC. At the genomic level, there are observed mutually exclusive alterations of various PAS components in a significant proportion of PDAC cases. PLAU expression is associated with poor prognosis following pancreatectomy and PAS component genes are frequently altered in PDAC. The predicted effects of these mutually exclusive alterations are functionally equivalent. That is, deletion of SERPINB2 is functionally equivalent to amplification of its enzyme target PLAU or enzyme receptor PLAUR. Mutual exclusivity of genomic alterations within a particular pathway is strongly predictive of a role for that pathway in driving tumourigenesis (550). In this respect, the pattern of genomic alterations in PAS components is consistent with a role in driving PDAC tumourigenesis and highlights its potential as a therapeutic target.

An important consideration in interpreting genome and transcriptome data on whole tumour extracts is the relatively low tumour cellularity, high stromal content, and related desmoplasia that it characteristic of PDAC (511). Therefore, to understand the role of uPA in PDAC biology it is critical to consider functional effects in a

cell-specific context. Only a few clinical studies have looked closely at cell-specific expression in human PDAC (234,238,549), with varying results that may be confounded by limited sample sizes. Given these limitations, a functional approach was applied to understand the role of the PAS in PDAC biology. 3D organotypic culture systems and *in vivo* models of PDAC were utilised to interrogate the role of the PAS pathway in PDAC development. These models were successfully used to modulate SerpinB2, and in turn, PAS activity in a context-dependent manner and demonstrated that uPA activity is necessary for PDAC invasion *in vitro* and *in vivo*. Further, these models proved that SerpinB2 regulates stromal remodeling of collagen and in turn influences tumour growth and invasion. Organotypic culture models provide an excellent platform for understanding functional effects of cell-specific interactions in a complex 3D environment. More than 80% of cancers in the human body originate from the epithelium (23). This means that TME components during tumourigenesis, invasion and metastatic processes are potentially common between ostensibly distinct tumour types. The 3D oranotypic model has shown the fidelity and advanced insight into stromal mechanics, made possible through the creation of a histologically similar tissue bed equivalent to the stroma of tumour systems, using fibroblasts and collagen I for matrix construction. Such a powerful model is quite time consuming to prepare, but once the technique has been learnt, can be undertaken with astonishing ease. In order to study cell migration and remodeling within a 3D context, limiting animal work, yet acquiring a much more realistic model of the human situation, organotypic models are revolutionising cancer biology research (354,358,425,563). This approach has provided our laboratory with valuable information in the form of stromal SerpinB2 effects versus epithelial effects, and is continuing to be found effective in a wide range of different uses. Future studies will build on these basic principles by increasing the complexity of cell types included in the cultures, for instance, using lymphocytes, keratinocytes in dermal matrices, and endothelial cells. The inclusion of endothelial cells, together with fibroblasts in the matrix or separately beneath the matrix, could allow modelling of angiogenesis concomitantly with the study of tumour-stroma interaction. The addition of immune cells to this model is another area for development within our laboratory, since it is widely

reported that tumour-associated macrophages (TAMs) have a large impact on tumourigenesis and metastasis *in vivo* (564). Previous studies by Chioni *et al.* (2008) have reported that co-cultured macrophages with cancer cells on collagen gels increases autocrine and paracrine signalling loops enhancing cell movement, and similar experiments are definitely possible with this organotypic culture (565).

Inhibition of PDAC invasion within TIF matrices by recombinant SerpinB2 (but not an inactive mutant) demonstrated that uPA activity is necessary for PDAC invasion in organotypic culture (refer to Fig. 4.7,B-C). The underlying mechanisms for this effect likely involve altered dynamics of ECM degradation and remodelling *via* attenuated protease activation (including Plg, MMPs etc). Further, SerpinB2 mediates the specific, rapid inhibition and clearance of cell surface-bound uPA (19,176) and altered dynamics of uPAR recycling and associated signalling pathways are also likely involved in the dramatic inhibition of PDAC cell invasion by SerpinB2. The lack of significant inhibition to PDAC cell invasion through SerpinB2$^{-/-}$ matrices with the addition of wild-type SerpinB2, ^{R380A}SerpinB2, or PBS (Fig. 4.9G) suggests that once the collagen I matrix has been formed without proper collagen fibrils and bundles, uPA may not have as great importance on tumour cell migration. Once the tissue structure is comprised with such poor integrity and porous structure, once the tissues structure is already composed and is porous and compromised, lacking a robust matrix system, that the tumour cells can mobilise more effectively and addition of exogenous SerpinB2 has negligible effect, as uPA/uPAR axis is not needs to navigate such large routes (utilising Rho/Rock pathways instead).

The major histopathological hallmark of PDAC is the severe fibrosis and desmoplastic reaction that generates a high stromal-to-epithelial ratio (566). This aberrant inflamed microenvironment surrounding the tumour site is implicated in the reduced chemoresponse of PDAC patients (536,567,568). PDAC fibrosis is composed of abundant ECM proteins, of which, several paracrine and autocrine factors between stromal and tumour cells induce their deposition (566). Fibroblasts/myofibroblasts secrete the precursors of many components of the extracellular matrix, including collagens, fibronectin, hyaluronic acid, collagenases and many growth factors (IGF, EGF, TGF-β *etc.*). Within the TME, tumour (and stromal) cells use the surrounding interstitial matrix as

a passive substrate while actively promoting increased type-I collagen deposition within the peritumoural space, in order to enhance invasive activity, local growth, and cancer stem cell formation (569). Myofibroblast depletion led to extensive remodeling of tumour ECM with a significant decrease in tumour stiffness and total collagen content, resulting in worse prognoses (570). Myofibroblasts contribute to the production of collagen I. Other groups have reported this *in vivo*, where cancer cells migrating away from the primary tumour site move into a nascent ECM deposited by infiltrating stromal cells, which potentially contain defects in collagen cross-linking (261,571-573). Sabeh *et al.* (2009) reported that protease-independent mechanisms of cell migration are only possible when the collagen network is bereft of adequate covalent cross-linking that characterise homeostatic tissues (451), as likely occurred in this study, and also *in vivo* in desmoplastic pancreatic carcinoma tissue. In this study, the *ex vivo* platform concurred such findings and demonstrated that protease-independent invasion programs, such as amoeboidal and collective cell clustering, can thus be accommodated by an immature, wound-like environment at sites surrounding the primary neoplasm (refer to fig. 4.4 and 4.5). In general PDAC tumourigenicity, advancement of malignancy has classically been reported to proceed through collagen-rich areas where penetration occurs through EMT style progression, in a slower advancement through the ECM by proteolytically active neoplastic PDAC populations (536,574-576). The increased synthesis of collagen by the stroma appears to serve as a pathway for such tumour invasion.

Even though both wild-type and SerpinB2$^{-/-}$ MEF ECM matrices allowed efficient PDAC invasion, the disordered networks of the SerpinB2$^{-/-}$ MEF matrices increased PDAC permissiveness (Fig. 4.4). Excess collagen I bundling, enhances PDAC cell proliferation and capacity for escaping the epithelial cell compartment. Thus, in the context of an *in vivo* tumour, the ability of CAFs to deregulate the ECM structurally may be made easier in the absence of SerpinB2. On the basis of differences observed in the morphology and activity between wild-type and SerpinB2 MEF migration movies in the Collagen I matrices (refer to Fig. 3.6), the increase in local invasion observed in SerpinB2$^{-/-}$ tumours (Fig. 4.12) and the increased positive staining of α-SMA on SerpinB2$^{-/-}$ tumours (Fig. 4.11), we can say that fibroblasts displayed an active, cancer associated

phenotype. There are many previous reports of activated fibroblasts having pro-cancerous effects (263,450,540,544,577), as found in this study.

Mode and efficiency of PDAC cell migration likely affected by interplay of proteolysis/remodelling and physical hindrance of the tissue/surrounding stroma. It has been shown that ECM stiffness effects morphogenesis of tumour cells (558). Altered structural integrity has significant effects on PDAC migration and invasion. The increase in PDAC invasion in the SerpinB2$^{-/-}$ matrices could explain the differences observed *in vivo* in local invasion, suggesting that PDAC migration (and thus, metastasis) is increased when there is less desmoplasia/collagen coverage surrounding the primary tumour mass. The invading cells from tumours with SerpinB2$^{-/-}$ MEFS appear to have increased paracrine, autocrine or cell type-specific signalling, as their migration into muscle and fat was significantly higher than local invasion by cells from tumours formed with wild-type MEFs. This phenomena has also been reported by other researchers in the PDAC field (352,570). Ozdemir *et al.* (2014) found that α-SMA myofibroblast depletion in their PDAC mouse models significantly reduced ECM stiffness, without increasing gemcitabine efficacy, leading to more undifferentiated tumours, increased EMT, tumour cell proliferation and EMT invasion, altered immune cell infiltrate profiles and faster death (570). In addition they showed that tumour angiogenesis was diminished in α-SMA myofibroblast$^{-/-}$ mice, without altering glycolysis or hypoxia. Rhim *et al.* (2014) deleted Sonic Hh from mice and reported earlier onset of undifferentiated PDAC, stroma formation attenuation, increased angiogenesis, more aggressive PDAC tumours that metastasised and led to faster succumbing of death versus control mice (352). Both Rhim (2014) and Ozdemir *et al.* (2014) concluded that desmoplasia protects the host from metastasis and when stroma is reduced in PDAC, there is an increase in EMT, proliferation, invasion and reduction in overall survival (352) (570). Both authors also suggest that stroma depletion leads to greater dependence on VEGF, which intriguingly, should mean enhanced uPA/uPAR activity in such tumour systems, as uPAS activators are are required on the surface of activated, migrating endothelial cells through VEGF stimulation (29). Ozdemir *et al.* (2014) also reported that LOX levels were unchanged in α-SMA myofibroblast$^{-/-}$ mice, despite dramatic

reductions in ECM stiffness (570). This result further supports the potential role of SerpinB2-TG2 in mediation of type-I collagen crosslinking, as explained in Chapter 3 (refer to section 3.4).

A major result in this chapter was the loss of E-cadherin by PDACs through the wild-type matrices recapitulated classical EMT migration (Fig 4.5). This result suggested that PDAC cells might recognise differentiated features in new tissue sites and up or down-regulate E-cadherin expression. This result has been observed by others, who report that those cancer cells can transition between EMT and MET, forming cell-cell adhesions again and returning to an epithelial state (578). E-cadherin is crucial for cell-cell adhesion, holding epithelial cells tight together upon the basement membrane. When epithelial cells lose E-cadherin expression, they release β-catenin into their cytoplasm (578). These β-catenin molecules have been shown to migrate into the nucleus and trigger EMT-inducing transcription factors, which can activate RTK and cause tumour cells to undergo transformation to a mesenchymal state, initiating metastasis (578). While EMT is a fairly rigid process completed through widespread alterations in gene transcription, mesenchymal–amoeboid transition (MAT) or amoeboid–mesenchymal transition (AMT), involve rapid modifications in migratory mode, arising from the specifics of the tissue microenvironment (579). These transitions are known to play a significant role in several stages of the metastatic process, when a certain microenvironment requires phenotypical adaptation of the tumour cells. Metastatic cells are able to undergo significant epigenetic alterations in order to regulate molecular mechanisms to induce MAT/AMT. Cells using amoeboid-like or cell clustering invasive strategies are afforded enhanced contractility, promoted by the Rho/ROCK signaling pathway (580), allowing them to pass through apertures in the passive collagen networks and adapt their cell bodies to the pre-existing spaces, or by exerting a sufficient actomyosin force, which can be generated to deform their surrounding ECM (536,571,581). This study observed such a phenomenon, where amoeboidally migrating PDAC cells moved at significantly higher rates through the SerpinB2$^{-/-}$ versus wild-type matrices, without adhesion attachment to collagen I substrate. The sustained expression of E-cadherin suggests that the pore sizes of the SerpinB2$^{-/-}$

matrices were of sufficient size and that collective cell migration was available. This type of migration is also seen *in vivo* within tumourigenic systems. Cancer cell migration through lymph nodes can occur through stromal cell–lined conduits that support rapid movement through matrix-free zones, orchestrated by fibroblasts (582). Further, tissues without interstitial collagen networks, e.g., the brain (583), are infiltrated by tumour cells without necessitating proteolytic remodeling, merely requiring ROCK-regulated pathways to squeeze a migrating cell through matrix openings smaller than the short axis of its nucleus (584). As aformentioned in chapter 1 and 3, Valiente *et al.* (2015) reported that increased SerpinB2 (and SerpinI1) expression was required for lung and breast metastatic invasion through brain tissue (213). It has been shown that type-I collagen organisation into fibrils has a significant role in limiting the diffusion of large molecules into the tumour area (262,583). Pluen *et al*. (2001) reported that molecules with diameters similar to the interfibrillar space had much slower diffusion, associated with a higher density of host stromal cells that synthesise and organize type-I collagen (583). Obviously, type-1 collagen influences PDAC tissue resistance to macromolecule transport, believed to be caused by proteoglycan/glycosaminoglycan binding and stabilizing of the ECM (262). This, coupled with hypovascularity, has major implications in chemo-resistance to macromolecule-based therapy. It therefore necessary to develop site-specific drug carriers to improve the delivery of molecular medicine to solid tumours, like PDAC (583). The findings presented of PDAC invasion and migratory modality through SerpinB2$^{-/-}$ matrices, as well as those through dermal fibroblast matrices, support a model wherein the type-I collagen architecture of the normal interstitium presents itself as a structural barrier to cancer cell traffic (585). However, when rigid structural barriers occur and pore size is not permissive for collective cell movement, such as occurs in PDAC desmoplasia, cancer cells appear to be reliant on the PA system and MT1-MMP activity, and conceivably the associated membrane-anchored collagenase (585,586).

3D Organotypic results were reproduced *in vivo,* as SerpinB2$^{-/-}$ MEFs in the mixed allograft model formed larger and more invasive tumours, with altered collagen deposition (refer to Fig.4.9). Also significant

differences in uPA/uPAR expression on PDACs in SerpinB2$^{-/-}$ allograft tumours, was concomitantly reflected in increased uPA activity in SerpinB2$^{-/-}$ tumours (refer to Fig. 4.11C).

Future therapeutic treatments for pancreatic cancer should consider targeting critical pathways in the growth, advancement, and prolongation of the tumour stroma. In the pursuit of more effective therapeutic intervention, researchers must attain deeper understanding of the tumour stroma in the specific context of PDAC. The unfortunate failure of systemically administered chemotherapy in PDAC can attest to this perspective; clearly extensive tumour–stromal interactions affect PDAC malignancy, such as SerpinB2 alteration. Through acquiring a better understanding of the signaling mechanisms most vital in the development and perpetuation of PDAC stroma, drug design and development can be enhanced with clearer rationale, leading to an increased stromal-targeting efficacy, offering better outcomes for PDAC patients.

Given that PaSCs regulate ECM turnover, one such approach could include co-administration of an anti-fibrotic reagent such as pirfenidone, to target the desmoplastic regions around PDAC tumours, initiating fibrolysis and potentially reducing chemoresistance in PDAC patients. This chapter clearly establishes a definitive role for uPA in pancreatic cancer and reveals novel evidence for both tumour and stromal cell specific effects of SerpinB2 on PDAC invasion. The availability of this well characterised mutant K-Ras/p53 PDAC model histologically recapitulates PDAC in human pathology and has revolutionised the field of PDAC research. This model mimics both the central epithelial component of human PDAC but also the incredibly complex TME, a feature for which much of treatment failure is accredited. Due to the failure of therapies targeting the TME, work in our lab is aimed at stromal targets, which are being evaluated in mouse models of PDAC.

The advent of this model with uPAS enquiry has generated much knowledge about how PDAC migration can be initiated around the TME and potentially how the disease progresses. Both uPA and SerpinB2 clearly affect PDAC TME development and stromal maintenance. SerpinB2 deletion within stroma impinges on ECM formation/structural integrity and influences invasive capacity and migratory mode of stromal and tumour

cells. The results presented in this chapter suggest that a better understanding of stromal biology and desmoplasia in the mechanism of PDAC will likely provide significant opportunities for better treatments for this devastating cancer. Fibroblasts clearly play a major role in PDAC, and it is well reported that interactions between PaSCs and cancer cells of PDAC are disease limiting. Hwang *et al.* (2008) reported that PaSC conditioned media increased PDAC cell proliferation, migration, invasion, while also decreasing the effectiveness of radiation and chemotherapy (gemcitabine) (577). These data strongly point out important roles for the desmoplasia of PDAC in the mechanism of stromal remodeling and local invasion, implicating SerpinB2 heavily within these processes. The next challenge for our laboratory is to understand when is an ideal timeframe to exploit the PAS pathway for therapeutic success. Crucial to this effort will be determining the molecular basis of how SerpinB2 is activated and exactly which other pathways it is sigThus, it is vital to understand how these interactions in the tumour epithelium and the microenvironment impact upon other pathways, such as Rho/Rock. As these important milestones are achieved, new paths of opportunity will be uncovered to offer new routes of therapeutics for PDAC malignancy.

Finally, the findings in this chapter identified the uPA/SerpinB2 axis as a driver of PDAC invasion and a marker of disease outcome/survival, strongly supporting the further development of uPA-targeted therapeutics for the treatment of PDAC. Development of new anticancer therapies represents a crucial challenge for the biomedical community and these data present significant insight into mechanisms of PDAC invasion and impact upon the potential use of SerpinB2 in a drug delivery system to target PDAC stroma. Heavily expressed on PDAC tumours, uPA inhibition by SerpinB2 warrants further preclinical investigation as a potential therapeutic target. Increased uPA activity in SerpinB2$^{-/-}$ allograft tumours, could represent a paracrine-like inhibition of PDAC uPA by SerpinB2 from the wild-type MEFs tumours.

CHAPTER 5

TOWARDS AN UNDERSTANDING OF THE ROLE OF SERPINB2 IN BREAST TUMOURIGENESIS AND METASTASIS

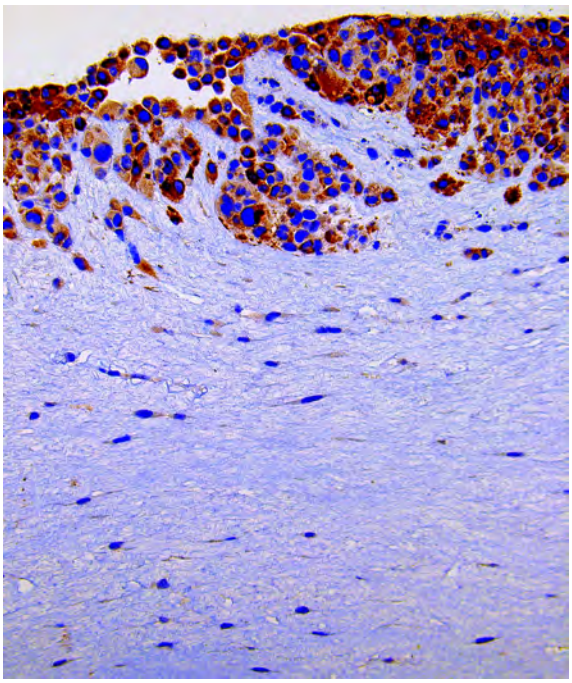

CHAPTER 5

TOWARDS AN UNDERSTANDING OF THE ROLE OF SERPINB2 IN BREAST TUMOURIGENESIS AND METASTASIS

5.1 INTRODUCTION

The mammary gland is a complex secretory organ composed of epithelial cells, endothelial cells, adipocytes, fibroblasts and immune cells. It is one of the human body's most physiologically and structurally dynamic organs, continually developing through several distinct stages (587). From prenatal life, early development and puberty, to reproduction and menopause, there are extensive processes, which are critical for normal gland development and breast tissue homeostasis (587). Processes such as proliferation, angiogenesis, migration, invasion, and resistance to apoptosis are vital for normative mammary function, yet these aforementioned processes also facilitate the origination and advancement of breast cancer (587). Endocrine hormones and many different growth factors must act synergistically in order to develop a healthy mammary gland and normative breast tissue bed. Initially, prenatal mammary gland development occurs *via* epithelial cell proliferation and invasion into the mammary fat pad (Fig. 5.1). These cells then differentiate into small networks of branched ducts. Mammary gland development pauses here until puberty, when oestrogen release from the ovaries (combined with IGF-1 and growth hormone) causes these epithelial duct cells to proliferate, swelling the ducts and forming bulbous structures, known as terminal end buds (TEBs) (refer to Fig 5.1) (587). TEBs are the most proliferative cell type of the developing mammary gland and they will continue to proliferate, migrate and branch out into the mammary fat pad (Fig. 5.1). The next phase of mammary gland development occurs during pregnancy and is the most active phase of growth for the organ. High concentrations of oestrogen and progesterone (in preparation for lactation) cause rapid proliferation of the mammary gland epithelium (587). The epithelial cells of TEBs are highly proliferative and homeostatically invasive (during puberty and pregnancy) during this time, while anti-apoptotic signalling pathways (PI3K/AKT, and RAS/MEK/ERK) prevent

premature involution of mammary gland tissue (588). These functions are essential for post-natal care, however extremely detrimental when redeployed within a tumourigenic environment. Once lactation has concluded, apoptotic signalling is vastly up-regulated (PTEN protein turns off PI3K/AKT pathway) (588), causing gland involution.

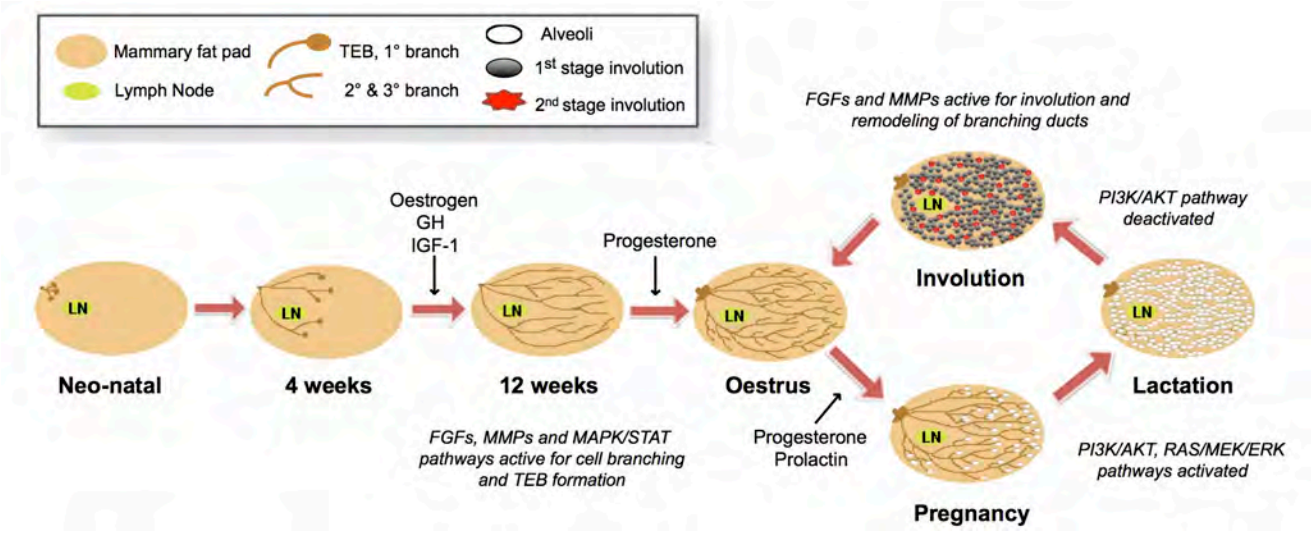

Fig 5.1. Mammary gland development. The mammary gland epithelial cells proliferate and invade into the mammary fat pad. Cell differentiation results in the formation of epithelial ducts, which swell to form terminal end bud (TEBs). During pregnancy, TEBs proliferate and undergo branching into the fat pads. Gland involution occurs following lactation whereby the mammary gland epithelial cells die by apoptosis. There are two branching mechanisms within the mammary gland: Side branching and bifurcation of TEBs. Neonatally, the mammary epithelium consists of only a few small ducts that grow allometrically until puberty. After 4 weeks post birth, short tertiary branches form under the influence of progesterone. At the onset of puberty, expansive ductal morphogenesis and growth is initiated, and the epithelial tissue branches out to fill the fat pad with ducts (stimulated by GH, oestrogen and IGF-1), achieved by cooperation between plasminogen/plasmin and MMPs. Upon pregnancy, prolactin and progesterone induce alveologenesis - the growth of alveolar cells. Prolactin stimulates milk production that continues until cessation of weaning, when signals induce involution – the mammary gland is remodeled back to its original adult state. Modified from (351).

The mammary epithelium consists of two main cell types, basal and luminal. The basal epithelium contains myoepithelial cells (and a small population of stem cells), which are attached to the basement membrane and generate the outer layer of the mammary gland (589). The luminal epithelium directly forms the ducts and milk secreting alveoli, while the myoepithelial cells squeeze milk from the alveolar luminal cells. These two cell types are most active during puberty and reproduction, when significant hormone presence activates signaling networks, influencing epithelial-mesenchymal cell interactions (590). These networks involve MAPK and STAT proteins for cell branching, lactation and gland involution, as well as FGFs and MMPs in mesenchymal

remodeling of branching ducts and involution (591). Plasminogen has previously been shown essential for normal mammary development, as plasminogen$^{-/-}$ mice show delays in early ductal expansion and maybe unable to lactate due to secretory epithelial deficits (592). Conversely, uPA$^{-/-}$ mice display normal mammary development and gland involution (592). Because of this, evidence by Selvarajan *et al.* (2001) suggests that plasma kallikrein is the protein responsible for activating plasminogen within the mammary gland (593). Previously, Simian *et al.* (2001) reported that MMPs work in collaboration with PAS during mammary epithelial morphogenesis and branching in 3D collagen I matrices (594). These studies imply that even if uPA is not directly responsible for the induction of mammary duct branching, plasmin is still activated and plays a major role, in an MMP-dependent manner (591). Other studies suggest that MMP-2 promotes ductal elongation, while MMP-3 stimulates lateral side branching (595).

Normal signaling between developing mammary cell populations is tightly controlled by TGF-β, Wnt, FGF, hedgehog (also present in PDAC biology, refer to 4.1), EGF, neuregulin3 (an EGF receptor), oestrogen and notch signaling pathways (1). Furthermore, in the last decade it has come to light that normal mammary gland functioning is dependent on stem cell processes, involving these key signaling pathways (589). Stem cells in the mammary gland are thus of key importance for physiological tissue renewal and regeneration following post-natal care. It has previously been shown that deregulation of these specific pathways in the mammary gland can facilitate breast cancer progression and are hijacked in cancer cells fueling unregulated tumour growth, invasion and instigating metastatic processes (589).

5.1.1 Breast cancer

Breast cancer is the most common cancer in the world for women, and in 2015 there was an estimated 15,740 new cases of the breast cancer diagnosed in Australia (145 males and 15,600 females) (596). Breast cancer is a multifaceted and heterogeneous disease (of which there are ten molecular subtypes) involving distinct histological and genetic aberrations (597). These cancers most commonly originate from basal cells lining the

inner milk ducts (i.e. basal cells -80% of cases) or the luminal cells of lobules that supply milk to the ducts (15 % of aetiology) (Fig. 5.2). In the majority of cases, breast cancer takes many years to arise and become diagnosable. Breast tissue is particularly sensitive to tumourigenesis, for several reasons. Oestrogen, the primary female sex hormone, stimulates breast cell division and is activated strongly and at many occasions during a woman's life. Not only does enhanced cell division increase the risk of DNA damage, but breast cells do not fully mature in women until their first full-term pregnancy (598). Immature breast cells bind carcinogens much stronger than mature breast cells and are also less efficient at the DNA damage response (599). When coupled with oestrogen-stimulated mitosis, it unfortunately dramatically increases the risk of developing breast cancer for many women, especially nulliparous women.

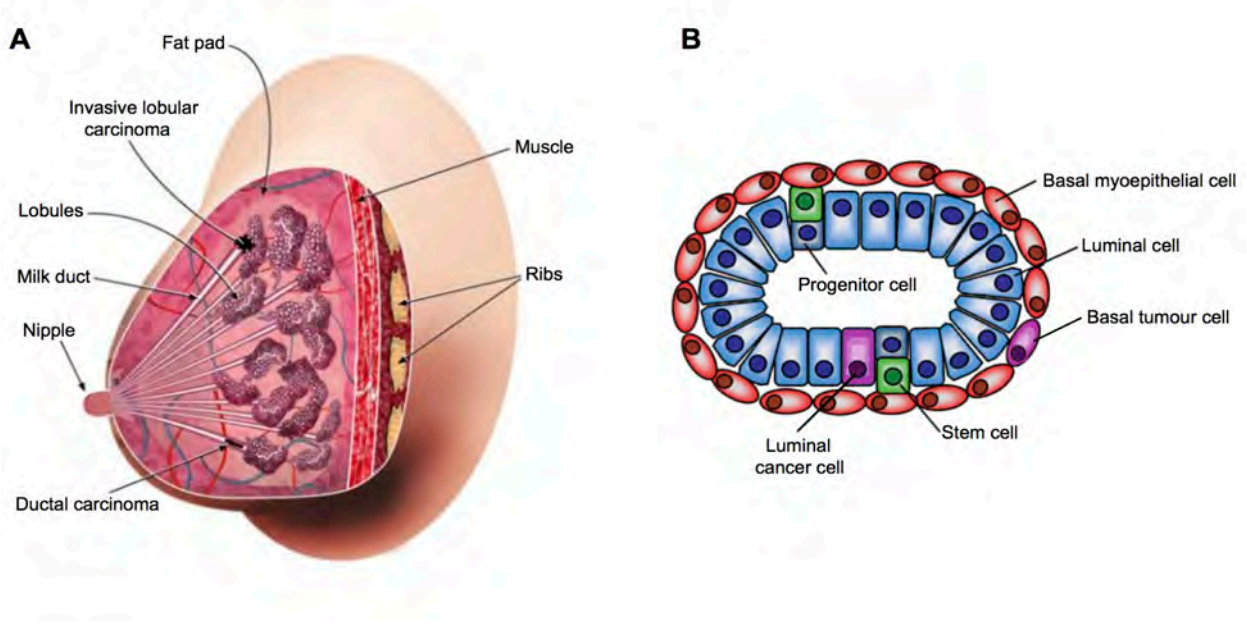

Fig 5.2. Mammary gland tumourigenesis. A. Illustration of the gross anatomy of the mammary gland (showing both an invasive lobular carcinoma and a ductal carcinoma *in situ* - DCIS). **B.** The two layers of a mammary duct composed of luminal and basal myoepithelial cells (and their tumourgenic counterparts) as well as stem and progenitor cells. Adapted from (600).

Breast cancers are divided into 5 intrinsic sub-divisions known as luminal A, luminal B, human epidermal growth factor receptor 2 (HER-2)-enriched, basal-like and normal-like, and are further placed into 3 specific sub-groups by their receptor expression type (601). These sub-groups are hormone receptor [oestrogen (ER+) or progesterone (PR+) receptor] positive, HER-2+, and triple negative (lacking ER, PR and not over-

expressing HER-2) breast cancer (TNBC). ~ 75% of all breast cancers are ER+, where patients tumours grow in response to oestrogen stimulation (602). ~65% of ER+ tumours are also PR+ (603). HER-2+ breast cancers account for ~20-25% of all breast tumours, and tend to be rapid growing and aggressive in their phenotype (604). Lastly, TNBCs account for between 10-17% of all breast cancers, tend to be highly aggressive (605), and are commonly associated with the breast cancer gene, BRCA1 (606).

5.1.2 TNBC

TNBC is commonly taken for a basal-like sub-type of breast cancer as approximately 75% of TNBCs express basal cell markers (601,607,608). TNBC tumours carry a poorer prognosis than luminal tumours (609,610), with African-American, African and menopausal women having a threefold higher risk of developing TNBC versus all other women (611). TNBC also has been associated with deprivation status, younger age at diagnosis, with more advanced stage tumours, hereditary and BRCA1 mutations (611). As TNBCs lack the traditional targetable receptors, common treatments like hormone therapy and cyto-toxic or –static drugs targeting estrogen, progesterone, and HER-2 are ineffective, often requiring combinatorial therapeutic regimen (606). In addition, women with TNBC are more likely to experience a peak risk of recurrence within 3 years from diagnosis, and mortality rates are increased for 5 years after diagnosis (611). Standard treatment for TNBC is chemotherapy, allowing for a higher rate of breast-conserving surgeries, followed by adjuvant chemotherapy and radiotherapy (if required). Evaluation of the response to chemotherapy gives important individual clues to particular chemo-sensitivity or –resistance. TNBCs are usually sensitive to chemotherapy however, some cases do not elicit any or a complete response, and the response does not correlate with overall survival (612). This makes TNBC particularly complicated to curatively treat. However, chemotherapy is still an effective option, as many women do respond well initially. Five years post-diagnosis, TNBC patients have the same rate of relapse as women with ER+, PR+ or HER-2+ breast cancers (613). Further, after 10 years from diagnosis, recurrence is even less likely in TNBC patients versus recurrence in patients with other breast cancer types (613). Pooled data of all TNBC subtypes versus other breast cancer types indicate that with adequate treatment

plans, 20-year survival rates are not significantly different between TNBC patients and patients with hormone positive breast cancers (614). Paradoxically, some types of TNBCs are extremely aggressive, exhibiting poor prognosis and an unpredictable relapse pattern (615). These TNBC subtype cases are often fatal within the first 1-2 years from diagnosis and have a much higher risk of relapse in the first 3–5 years and also absolute relapse and survival rate differences across subtypes (614,615). One explanation for this is that TNBCs comprise a vastly heterogeneous cancer group (616). Within these tumour systems the TME is a major constituent in determining the behaviour of each tumour, thus depending on the composition of stromal cells and ECM factors present, these can influence a tumours aggressiveness and potentiate an invasive system that is extremely difficult to treat. By taking into account the role of the neoplastic epithelium and the local microenvironment, medical science is elucidating the powerful interplay that tumour systems participate in. Upregulation of MMPs which digest fibrillar and membranous collagens can result in a tissue microenvironment of altered fibrillar composition, where degraded basement membrane is a key feature in the instigation of cancer cell migration and intravasation into the vasculature (18). Furthermore, altered ECM impairs molecular diffusion in tissue beds, which impacts upon drug delivery to breast tumours (364). At present, ECM alteration is recognised as a hallmark in the progression of breast cancer, with many observable changes in tissue signaling during tumour invasion and metastasis (617). In order to begin to understand the complex tumour-stromal interactions in breast cancer that are hindering the effectiveness of current therapies, there is an essential need to enhance the field's knowledge of these processes. In that regard, this chapter focused on the role of uPAS in tumour growth, migration and local invasion in breast cancer.

5.1.3 The role of uPAS in breast cancer

The proteolytic activity of uPA is negatively regulated by SerpinB2, and in many human malignancies, levels of uPA are significantly higher than in the corresponding normal tissues, directly related to patient prognosis (refer to Table 1, section 1.5). Current literature strongly supports that individual uPAS factors are involved in the process of rendering malignant breast tumours invasive, and high levels of tumoural uPA are associated with

metastasis and shorter survival than those with lower uPA tumour expression, therefore signifying uPAS as an attractive target for cancer therapy (16,18,71,84,98,101,124,618,619). Genetic expression of PAS inhibitor, SerpinB2, in recurrent free survival in breast cancer subtypes Luminal (A and B), Basal, HER-2+, or all sub-types combined can be observed in Fig. 5.3. High SerpinB2 expression levels are advantageous for patient survival without relapse in both Luminal A and B sub-types (but not basal and HER-2+ individually) or when all BC sub-types are combined (Fig. 5.3, E). This interesting finding indicates that SerpinB2's control over the feed-forward plasmin and uPA/uPAR loop is advantageous and may, in part, inhibit disease progression in these tumour types.

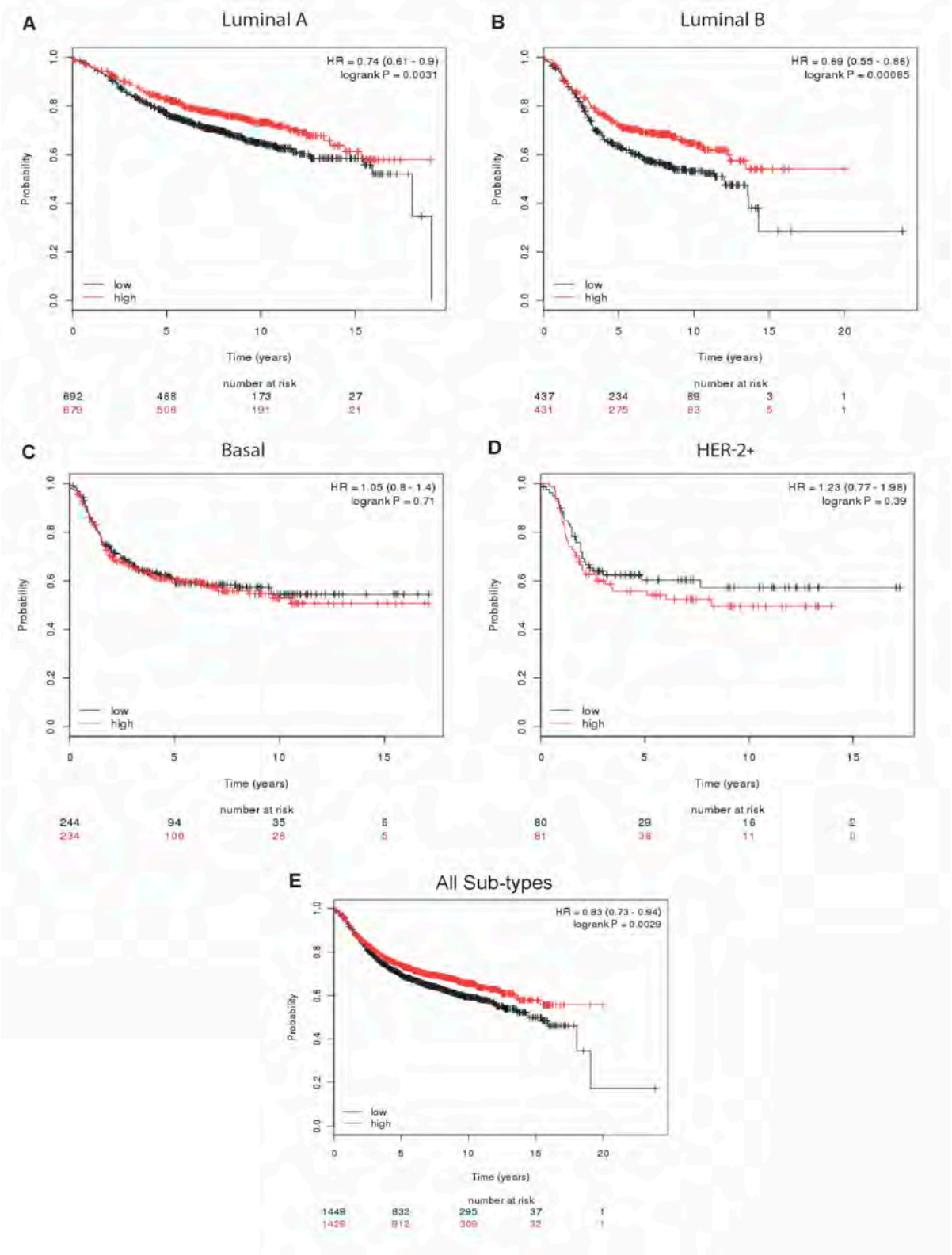

Fig. 5.3. SerpinB2 gene expression and recurrent free survival in breast cancer. Kaplan-meyer plots showing overall survival in relation to SerpinB2 expression for cohorts of patients with (**A**) Luminal A, (**B**) Luminal B, (**C**) Basal, (**D**) HER-2+, and (**E**) All sub-types (grouped together) of breast cancer. Red lines indicate high SerpinB2 expression and black lines indicate low SerpinB2 expression. Data from KM Plotter. Accessed June 2015.

Like all solid tumour systems, in order for invasion and metastasis to occur, the ECM must be remodeled. ECM-directed mammary morphogenesis is currently not well understood, however, involves epithelial 'invasion' into adipose tissue, a process that also occurs by normative epithelial cells within ductal branching, during puberty and pregnancy, as discussed above (Section 5.1). Exactly how this mammary morphogenesis is dysregulated and subverted in the progression of BC in the specific context of PAS is of paramount importance. Thus, this chapter sought to address various aspects of ECM alteration in the context of breast tumour invasion and metastatic progression in the metastatic derived (pleural effusion) invasive triple-negative human mammary epithelial carcinoma cell line, MDA-MB-231, and it's even higher metastatic daughter cell line, MDA-MB-231HM. These cells are aneuploid female (range = 52 to 68), with chromosome counts in the near-triploid range (620). They both express epidermal growth factor (EGF), transforming growth factor alpha (TGF-α), as well as the WNT7B oncogene (621). In addition, our laboratory has previously shown that MDA-MB-231 cells over express uPA and uPAR (622).

In a study by Finak *et al.* (2008), stromal SerpinB2 gene expression was reported to be significantly reduced (>16-fold) in isolated invasive tumour stroma compared with matched normal stroma in breast cancer patients (623). This dramatic reduction in SerpinB2 expression is also a robust predictor of clinical outcome in breast cancer, with greater recurrence free survival in patients with higher levels of SerpinB2, see (19). As previously mentioned (see Chapter 1, refer to section 1.5.3), SerpinB2 efficiently, specifically and irreversibly binds and clears uPA from uPA over-expressed cell surfaces, without activating pro-invasive pathways in tumour cells (19,25). Furthermore, SerpinB2 lacks individual binding sites for LRP, VLDLR and vitronectin and thus does not stimulate the pro-invasive phenotype that is associated with SerpinE1 (24,25,177,624). SerpinB2 is also non-toxic and even at highest known *in vivo* concentration during third trimester pregnancy, where it can consistently reach levels above 250 ng/mL in plasma (134,625), there are no reported associated health risks (626). Additionally, SerpinB2 cannot inhibit pro-tPA or fibrin bound tPA (627), meaning there are no overactive fibrinolysis side effects when administering high doses of SerpinB2. High tumour SerpinB2 levels are

associated with improved patient outcome in breast cancer (see Fig. 5.3), and in node negative breast cancer high tumour SerpinB2 is only statistically relevant if uPA levels are concurrently high (6,19). Moreover, high levels of SerpinB2 expression in breast carcinomas has been correlated with increased, relapse-free survival (fig. 5.3) (17,18,221,628-631), while low expression has exhibited the opposite effect. Furthermore, treatment of uPA over-expressing tumour xenografts in animal models with SerpinB2 demonstrated inhibition or complete prevention of metastasis (215,244).

The aforementioned studies indicate that SerpinB2 is a valid therapeutic option in breast and other cancer states, and can be directly delivered to cell surface uPA and internalised into tumour cells *via* receptor-mediated endocytosis (RME). This system avoids any damage to normal, healthy cells, and this approach could potentially be used combinatorially with chemotherapy treatments to enhance efficacy or provide cytostatic effects for uPA expressing cancers.

Previous studies have reported conjugation of SerpinB2 to ^{213}bismuth (an α-emitting radioisotope) preferentially targeted breast, prostate and melanoma cancer xenografts in animal models and micrometastases *in vivo* (227,373,632,633). In addition, our laboratory has shown that 2'-deoxy-5-fluorouridine (a pro-drug form of the common chemotherapeutic 5-fluorouracil) or an anti-mitotic dibrominated-*N*-alkylisatin (a potent cytotoxin), conjugated to SerpinB2 was able to preferentially kill uPA/uPAR over-expressing cell lines (130,619).

Overall, further understanding of the spatiotemporal expression of SerpinB2 in breast tumourigenesis and metastasis is required in order to investigate this powerful PAS inhibitors potential as a novel chemotherapeutic and provide further rationale for the development of SerpinB2 based targeted therapies in the treatment of breast and various cancer types.

The specific aims of this chapter were to:

1. Characterise the effects of SerpinB2 knockdown upon MDA-MB-231 cell invasiveness in the 3D organotypic model.
2. Investigate the invasiveness of highly metastatic MDA-MD-231HM cells through SerpinB2 null organotypic matrices.
3. Elucidate the effects of SerpinB2 upon tumour growth in a mixed cell xenograft mouse model of TNBC.

5.2 METHODS

5.2.1 Cell lines and culture conditions

The invasive triple-negative human mammary epithelial carcinoma cell line MDA-MB-231 originally purchased from American Type Culture Collection (ATCC, VA, USA) was maintained in Roswell Park Memorial Institute medium (RPMI-1640) (Invitrogen, USA), supplemented with 10% fetal bovine serum (FBS), 10 mM HEPES buffer and 125 IU insulin, at 37 °C in a HERAcell incubator (Kendro Laboratory Products, Germany) in 95% humidified atmosphere, containing 5% CO_2. The highly metastatic breast adenocarcinoma (MDA-MB-231HM) cell line [passaged six times through lung metastases (634)], was a gift from Professor Zhi Ming Shao and Professor Zhou Luo Ou (Breast Cancer Research Institute, Fudan University Shanghai Cancer Center, China). Three of these MDA-MB-231HM cell lines were stably transfected with fluorescent markers by Dr Cameron Jonstone (Peter MacCallum Cancer Centre, Victoria, Australia) and donated as a gift to our laboratory. The three cell lines initially tested were MDA-MB-231HM luciferase expressing (MDA-MB-231HM Luc), MDA-MB-231HM tomato expressing (MDA-MB-231HM Tom) and MDA-MB-231HM luciferase and tomato expressing (MDA-MB-231HM Luc and Tom). All MDA-MB-231 parent and daughter cell lines were routinely cultured as mentioned above. Fibroblast cell lines, normal Fre-85 (NAFs) (635), and

Breast CAF (CAFs) line, were a gift from Dr Lily Huschtscha (Children's Medical Research Institute, New South Wales, Australia). Both NAFs and CAFs were routinely cultured in DMEM:F12 medium containing 100IU insulin, 1 ng/mL FGF-2 and 10% (v/v) heat-inactivated FBS. For subculturing, cells were detached at subconfluency (80-90% confluency) using sterile 1 × PBS containing 5 mM EDTA (pH 7.4) followed by 0.05% (w/v) trypsin-EDTA (1×), centrifugation at 1,200 rpm for 5 min at RT using a Heraeus Megafuge 1.0R (ThermoFisher Scientific, USA) and resuspension in fresh culture medium, prior to each experiment. All cell experiments were conducted using cells in exponential growth, passaged 48 h prior. Cell viability and cell number were assessed prior to experimentation using the Trypan blue (Sigma-Aldrich) exclusion method, with viable cells counted using a haemocytometer. Cell lines were also routinely tested for Mycoplasma contamination (in-house testing conducted by IHMRI technical staff) and found to be negative.

5.2.2 Cell migration wound healing assays

Individual wells of an Imagelock 96-well plate (Essen Bioscience, USA) were coated with 50 µL of collagen I (300 µg/mL) in 17.4 mM acetic acid, on ice. All assays were performed in a humidified 5.0% CO_2 atmosphere at 37 °C using the IncuCyte ZOOM imaging system (Essen BioScience). Individual wells were seeded with either MDA-MB-231 (shGFP ±Dox, sh1C1 ±Dox, or sh2A2 ±Dox) cells at even density (25,000/well) in octet of the pre-coated ImageLock 96-well plates and allowed to attach and spread over 8 h with aforementioned media, in the presence or absence of 2 µg/ml Dox. After two subsequent wash steps with PBS, the wells were refreshed with media in the presence or absence of 2 µg/ml Dox. Scratch wounds were generated with the Woundmaker tool and images taken every 2 h. Images were processed using IncuCyte ZOOM system (10 × objective) and wound regions were measured using automated analysis. Relative Wound Density (%, value of 0 = no migration, value of 100 = completed migration, when the cell density inside the wound is the same as the cell density outside the initial wound) was analysed as a percentage (± SEM).

5.2.3 Western blotting

To ascertain the relative expression of translated SerpinB2 within different breast cancer cell lines, western blot analysis was undertaken, as previously explained (refer to 2.2.10.1). 30 µg protein from whole cell lysates of either non-malignant human mammary epithelial cell lines (184B5, MCF10A, MCF12A), human mammary luminal carcinoma cell lines (T-47D, MCF7, MDA-MB-134, MDA-MB-175, MDA-MB-330, MDA-MB-361, BT483, BT474) or human mammary basal carcinoma cell lines (HCC1569, HCC1954, HCC38, HCC70, HCC1187, HCC1500, HCC1532, BT20, BT549, MDA-MB-157, MDA-MB-231, MDA-MB-436, MDA-MB-468) were used for separation under non-reducing conditions by 10% SDS-PAGE and transferred to PVDF membranes. The membranes were immunoprobed overnight at 4°C with antibodies against SerpinB2, or Actin as per standard protocol (refer to Supplementary Antibodies Table of Appendix – Table A1). The membranes were incubated with the appropriate HRP-conjugated secondary antibody and then developed according to enhanced chemilluminescence protocol (32106, ThermoScientific).

In order to elucidate the relative expression of translated SerpinE1 and SerpinB2 within both the epithelium and stroma of the breast TME, western blot analysis was undertaken (refer to 2.2.10.1). 20-30 µg protein from whole cell lysates of either human mammary basal carcinoma cell lines (MDA-MB-231, MDA-MB-231HM), primary human mammary normal- and carcinoma-associated fibroblasts (NAFs, CAFs), or telomerase immortalised human fibroblasts (TIFs) were used for separation under non-reducing conditions by 10% SDS-PAGE and transferred to PVDF membranes. The membranes were immunoprobed overnight at 4°C with antibodies against SerpinB1, SerpinB2 or GAPDH as per standard protocol (refer to Supplementary Antibodies Table of Appendix – Table A1). The membranes were incubated with the appropriate HRP-conjugated secondary antibody and then developed according to enhanced chemilluminescence protocol.

5.2.4 3D organotypic culture

5.2.4.1 SerpinB2 knockdown in MDA-MB-231 effects on 3D invasion

Invasion of MDA-MB-231 cells with SerpinB2 knockdown through TIF contracted collagen I matrices was performed using 3D organotypic assays as aforementioned (refer to 3.2.2). After fibroblast-mediated collagen I matrix contraction, 2.0×10^5 MDA-MB-231 (either shGFP ±Dox, sh1C1 ±Dox, or sh2A2 ±Dox) cells were seeded on top of each matrix in 24-well plates and grown for three days – after this time a wholly confluent monolayer was formed. The matrices were then transferred to a liquid-air grid interface for invasion (359), in which the liquid phase was supplemented with or without 2 µg/mL Dox. After 14 days, the matrices were fixed in 10% NBF for 2 days and kept in 70% ethanol at room temperature. Samples were embedded in paraffin wax and sections were then acquired for histological and microscopic analyses.

5.2.4.2 MDA-MB-231HM invasion into 3D collagen matrices

Invasion of the highly metastatic MDA-MB-231HM cell line through collagen I matrices contracted by either TIFs, wild-type or SerpinB2$^{-/-}$ MEFs was performed as aforementioned (refer to 3.2.2). After fibroblast-mediated Collagen I matrix contraction, 2.0×10^5 MDA-MB-231HM cells were seeded on top of each matrix in 24-well plates and grown for three days – after this time a wholly confluent monolayer was formed. The matrices were then transferred to a liquid-air grid interface for invasion (359). Initially, pilot assays were conducted through both TIF and MEF contracted collagen I matrices in order to determine the optimal length of invasion for this cell line. After 7 or 14 days, the matrices were fixed in 10% NBF for 2 days and kept in 70% ethanol at room temperature. Samples were embedded in paraffin wax and sections were then acquired for histological and microscopic analyses.

5.2.4.3 Pilot 3D Organotypic breast tumour spheroid invasion assay

A pilot experimient was undertaken to investigate the effects of tumour spheorids in this 3D organotypic model. This system would recapitulate the *in vivo* situation with greater biomimicry and potentially allow for increased therapeutic insight when testing novel drugs. The 3D spheroid culture differed from the models above in that

contraction of collagen I matrices was undertaken by TIFs and MCF-7s, or TIFS and MCF-7s, MDA-MB-231s and SK-BR-3s. Initially, breast cancer cells were seeded (5.0×10^3 of MCF-7 or 1.66×10^3 each of MCF-7, MDA-MB-231 and SK-BR-3, per well) in 60 wells of a round bottom 96-well ultra-low adherent cell plate (Corning, USA - distributed by Sigma). After 3 days, fully formed spheroids were collected and 60 spheroids (either MCF-7 or MCF-7/MDA-MB-231/SK-BR-3) were co-cultured with quiescent TIFs (8.0×10^4 per matrix) in Collagen I solution per matrix (V_2: 2.5 mL) in a 35 mm petri dish. Matrices were then allowed to contract for two days in complete media (DMEM, supplemented with 10% FBS and penicillin-streptomycin). After this time, MCF-7/TIF/Collagen I or MCF-7/MDA-MB-231/SK-BR-3/TIF/Collagen I matrices were moved to a 24 well plate and incubated for a further 2 days in the presence of either 500 nM SerpinB2 or PBS control. After this time, the matrices were fixed in 10% neutral buffered formalin for 2 days and kept in 70% ethanol at RT. Samples were embedded in paraffin and sections were then acquired for histological analyses [H&E, PanCK, Picrosirius red and Ki-67; refer to Supplementary Antibodies Table of Appendix (Table A1. for further details)].

5.2.5 Mixed cell xenograft model

In order to better understand the intrplay between stromal and tumour cells *in vivo*, MDA-MB-231HM cells and MEFs were trypsinised and resuspended in cold PBS. 7.5 x 10^5 MEFS (wild-type or SerpinB2$^{-/-}$) were mixed with 2.5×10^5 MDA-MB-231HM cells (1×10^6 cells in total at a 3:1 MEF:MDA-MB-231HM ratio) and injected into the intramammary fat pad (IMFP) of the 1st mammary gland of of 4 week old female BALB/c-Fox1nuAusb mice (5 per group). Tumour volume was quantified using a digital vernier caliper while mice were conscious and calculated using the equation, $xy^2/2$ (548). Mice were weighed and monitored daily in compliance with the University of Wollongong's Animal Experimentation and Ethics Committee guidelines (approval #AE13/18). Mice were anaesthetised 15 days post injection and tumour weight and volume compared between treatments.

5.2.6 Statistical analyses

Unless stated otherwise, data is presented as the mean (± SEM) of at least three independent experiments performed in either triplicate or sextuplet. Differences in the mean of two groups were analysed by an unpaired t-test. Comparisons of more than two groups were made by a one-way (or two-way) ANOVA with post hoc Holm-Sidak (or other post hoc) analysis for pairwise comparisons and comparisons versus control. *P* values < 0.05 were considered statistically significant. Unless stated otherwise, data and statistical analyses were performed using GraphPad Prism (version 6.0, USA).

5.3 RESULTS

5.3.1 SerpinB2 expression in breast cancer cell lines

Western blot analysis was undertaken to compare SerpinB2 protein levels in normal (transformed) breast cell lines as well as luminal, basal and HER-2+ BC epithelial cell lines (Fig. 5.4). Compared to the control (1 µg) recombinant SerpinB2 used in the western blot, the normal (transformed) breast epithelial cell lines, 184B5 and MCF10A, expressed moderate to high levels of SerpinB2, while the MCF12A line expressed low to negligible levels of full-length SerpinB2 (Fig. 5.4). The lower (~37 kDa) sized SerpinB2 observed on western blots [of which MCF12A cells expressed moderate and similar levels to that of 184B5 (labeled as 184 in Fig. 5.4) and MCF10A cells] is potentially a cleaved form of SerpinB2. All of the human mammary luminal carcinoma cell lines (T-47D, MCF7, MDA-MB-134, MDA-MB-175, MDA-MB-330, MDA-MB-361, BT483, BT474) expressed low to negligible levels of both full-length and cleaved SerpinB2 (Fig. 5.4). Lastly, the human mammary basal carcinoma cell lines, HCC1954, HCC1500, HCC1532 and MDA-MB-436, all expressed moderate to high levels of full-length SerpinB2, while HCC1500, HCC1532, BT549, MDA-MB-157, MDA-MB-231, MDA-MB-436 and MDA-MB-468 cells expressed moderate to high levels of cleaved SerpinB2 (Fig. 5.4).

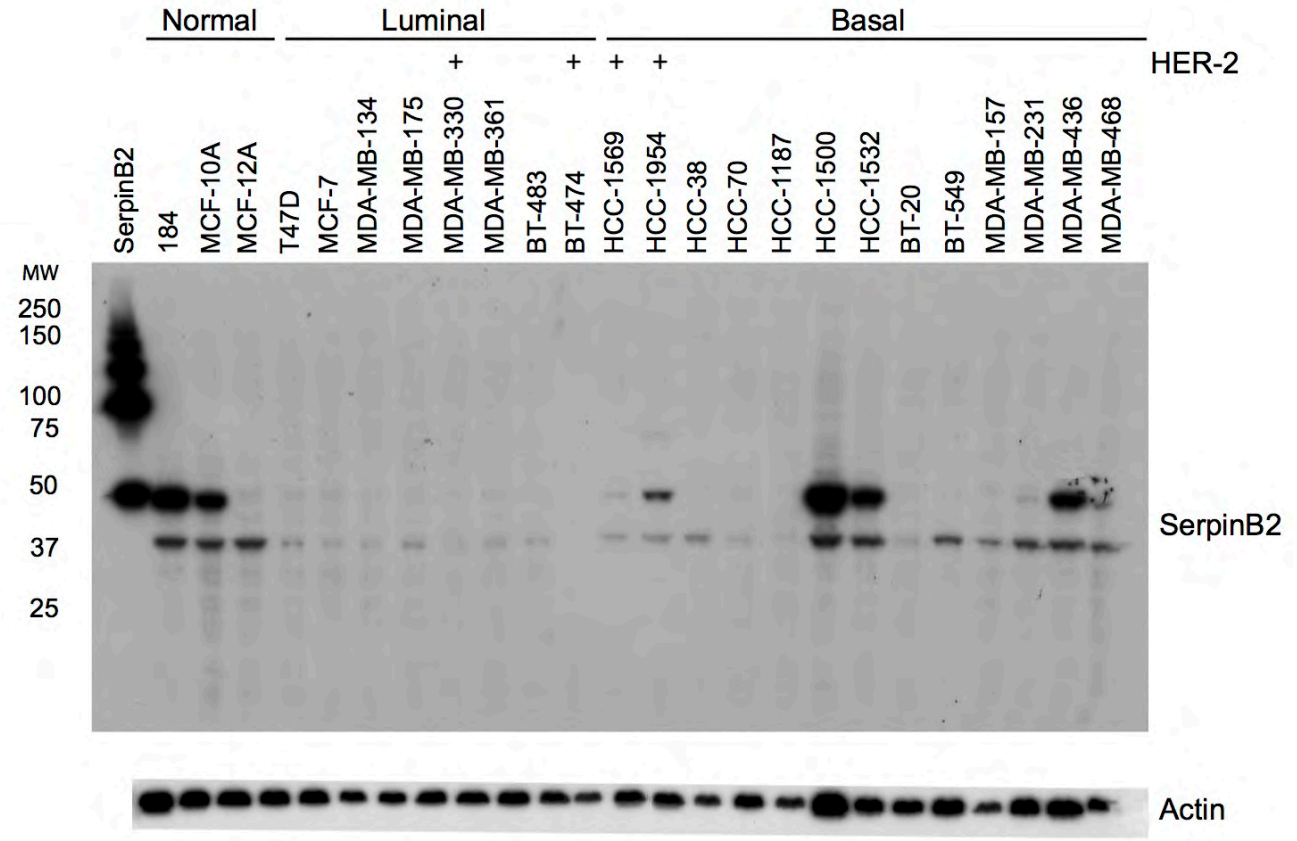

Fig 5.4. SerpinB2 expression in malignant and non-malignant mammary cell lines. Western blots showing expression of SerpinB2 in non-malignant human mammary epithelial cell lines (184B5, MCF10A, MCF12A), human mammary luminal carcinoma cell lines (T-47D, MCF7, MDA-MB-134, MDA-MB-175, MDA-MB-330, MDA-MB-361, BT483, BT474) or human mammary basal carcinoma cell lines (HCC1569, HCC1954, HCC38, HCC70, HCC1187, HCC1500, HCC1532, BT20, BT549, MDA-MB-157, MDA-MB-231, MDA-MB-436, MDA-MB-468). Blots were reprobed for Actin as equiloading controls.

5.3.2 SerpinB2 and SerpinE1 characterisation in breast epithelial and stromal cells

Further, it was necessary to understand the expression levels of both PAS inhibitors, SerpinE1 and SerpinB2, within both epithelial and stromal cells for use in proceeding *in vitro* and *in vivo* experiments. Analysis of stromal cell expression of both PAS serpins revealed that NAFs express little to negligible levels of SerpinB2, while CAFs and TIFs express moderate to high levels of SerpinB2 (Fig. 5.5). SerpinE1 levels were comparable to SerpinB2 within CAFs, however not so for NAFs and TIFs. NAFs expressed moderate to high levels of SerpinE1, while TIFs expressed lower levels to that of SerpinB2. Within epithelial BC lines tested, the parent MDA-MB-231 cell line expressed relatively high levels of SerpinB2, while it's daughter metastatic cell line, MDA-MB-231HM, expressed no SerpinB2 (Fig. 5.5). SerpinE1 levels were comparable to SerpinB2 within

MDA-MB-231HM cells, while MDA-MB-231 cells expressed lower SerpinE1 levels to that of SerpinB2 (Fig. 5.5).

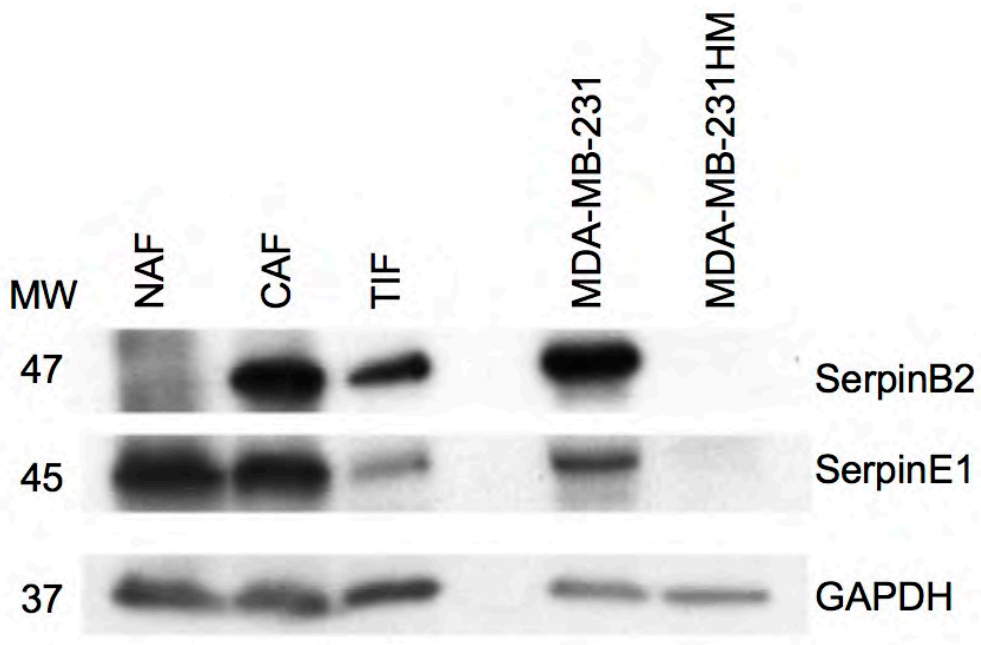

Fig 5.5. SerpinB2 and SerpinE1 expression in breast epithelial and fibroblast cell lines. Western blots showing expression of SerpinB2 and SerpinE1 in NAFs, CAFs, TIFs, MDA-MB-231 and MDA-MB-231HM (Tom and Luc) cells. Blots were reprobed for GAPDH as equiloading controls.

5.3.3 Cell surface detection of uPA

An immunofluorescence assay was performed to determine MDA-MB-231HM cell surface uPA expression. Three MDA-MB-231HM cell lines, differing only in fluorescent reporters, were used in order to determine which was the best line to utilise for continuing experiments. All lines appeared to express high levels of cell surface uPA when analysed by flow cytometry in comparison to the fluorescence peak obtained using a non-induced rabbit IgG_{2A} antibody control (Fig. 5.6). MDA-MB-231HM Tom cells expressed high levels of uPA (geometric mean = 40 ± 3.08 fluorescence units, versus IgG_{2A} control geometric mean = 9.67 ± 2.23 fluorescence units) (Fig. 5.6, A,D; $P > 0.001$). Similarly, MDA-MB-231HM Luc cells also expressed high levels of uPA (geometric mean = 43.4 ± 2.14 fluorescence units, versus IgG_{2A} control geometric mean = 11.7 ± 1.16 fluorescence units) (Fig. 5.6, B,E; $P > 0.001$). Lastly, MDA-MB-231HM Luc and Tom cells expressed

the highest levels of uPA (geometrical mean = 57 ± 2.49 fluorescence units, versus IgG_{2A} control geometrical mean = 11.7 ± 3.36 fluorescence units) (Fig. 5.6, C,F; $P > 0.001$), of all the MDA-MB-231HM cell lines. These data suggest, that as a transformed TNBC model for understanding PAS expression spatiotemporally, these cell lines were ideal given the high uPA expression levels. As MDA-MB-231HM Luc and Tom cells expressed the highest cell surface levels of uPA, this cell line was used for 3D organotypic and *in vivo* experiments.

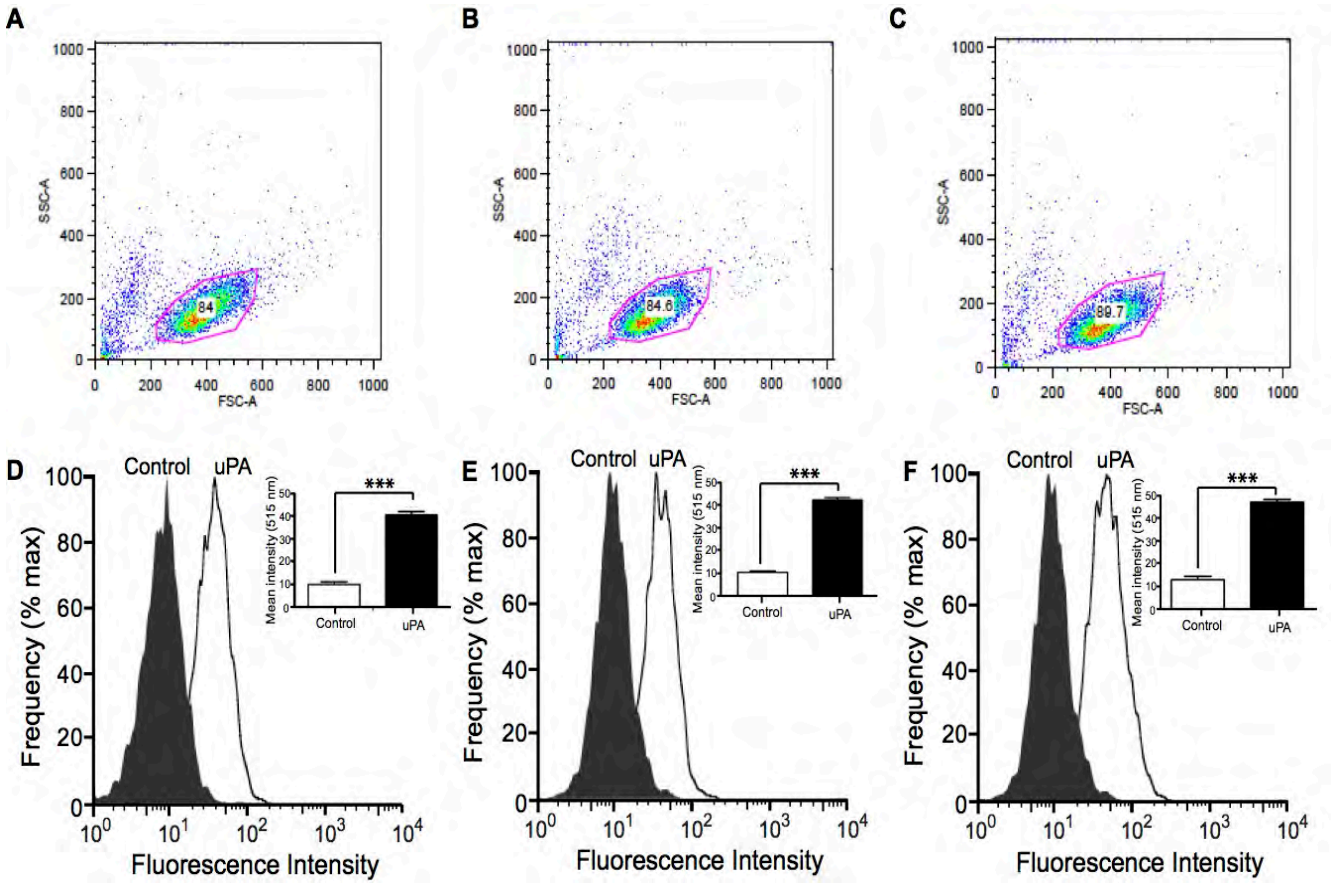

Fig. 5.6. Cell surface detection of uPA MDA-MB-231HM cell lines. A,D. MDA-MB-231HM Tom, 84% of cell population (gated) analysed; **B,E.** MDA-MB-231HM Luc, 84.6% of cell population (gated) analysed; **C,F.** MDA-MB-231HM Tom and Luc, 89.7% of cell population (gated) analysed. Charcoal shaded histograms represent cells probed with negative control (non-induced rabbit IgG antibody). White histograms represent cells probed with rabbit anti-mouse uPA polyclonal antibody. Bound primary antibody was detected with goat anti-rabbit, FITC-conjugated antibody. Inset boxes of **D**, **E and F** display mean intensity of fluorescence at 515 nm.

5.3.4 SerpinB2 knockdown effects on migration in MDA-MB-231 cells

Before 3D experimentation was undertaken, investigations into the effects of SerpinB2 knockdown on MDA-MB-231 cell migration on collagen I was employed. MDA-MB-231 cells were used as these express SerpinB2 (see Fig. 5.2). Wound healing assays showed that through separate Dox induced GFP- (Fig 5.7, A) and SerpinB2-hairpin (sh1C1 Fig 5.7, B; sh2A2 Fig 5.7, C) production in MDA-MB-231 cells, there were no significant differences recorded on cell migration between either ±Dox induction of individual hairpins or between cohorts (Fig. 5.7). Trends towards decreased wound healing rates in Dox induced MDA-MB-231 cells across all cohorts were observed, however this slower migration rate was not dramatic or significant. Thus, SerpinB2 knockdown in MDA-MB-231 cells had no effect on cell migration in a 2D collagen I wound healing system. This is unlike the effects observed in fibroblast 2D migration experiments (see Chapter 3, refer to secion 3.3.3)

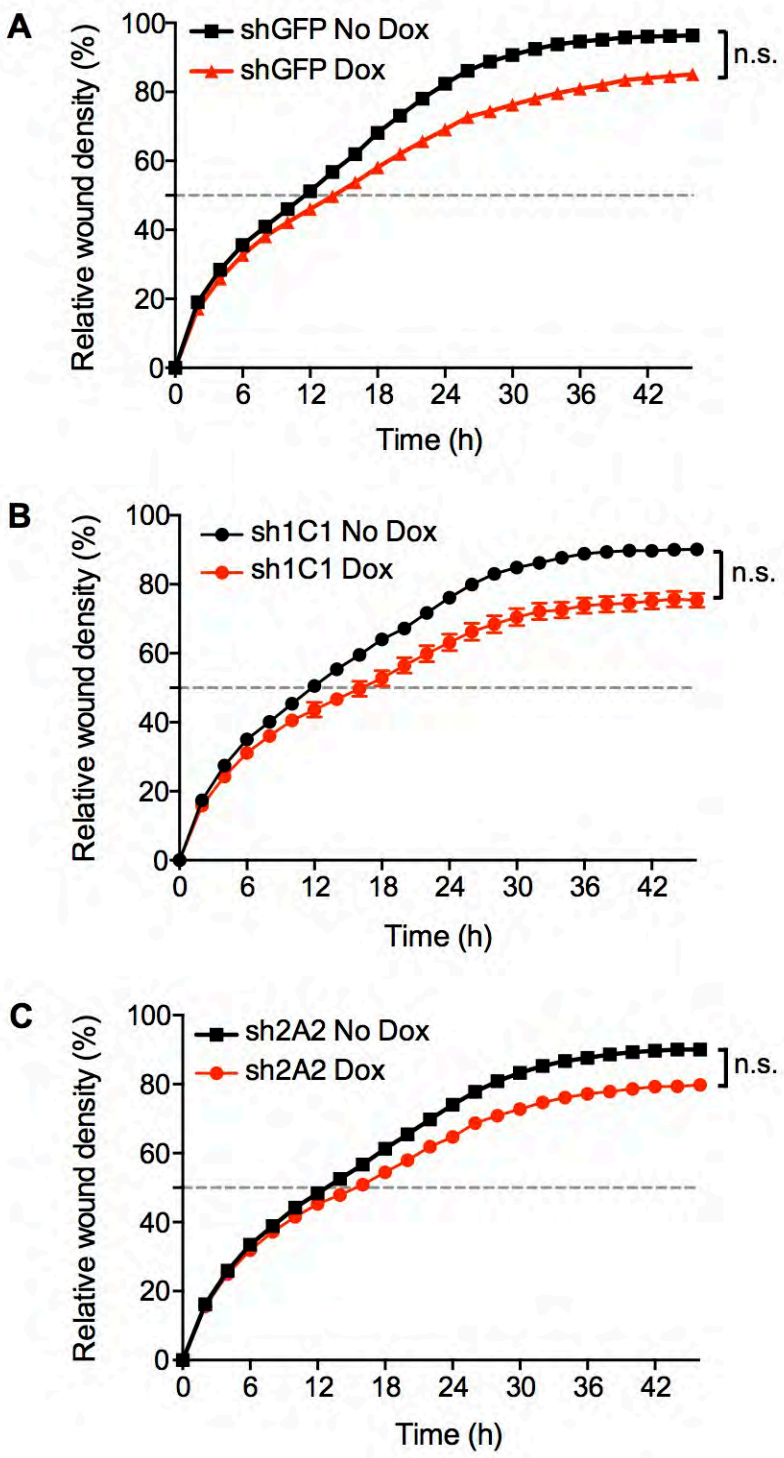

Fig 5.7. Effect of SerpinB2 knockdown on the migration of MDA-MB-231 cells. Comparative time-course of migration of stably transduced MDA-MB-231 cells measured using IncuCyte ZOOM (Essen Biosciences). Constructs tested were **A.** MDA-MB-231 shGFP ±Dox, **B.** MDA-MB-231 SerpinB2 sh1C1, and **C.** MDA-MB-231 SerpinB2 sh2A2. Images were processed using IncuCyte ZOOM system and wound regions were measured using automated analysis. Relative Wound Density (%, value of 0 = no migration, value of 100 = completed migration, when the cell density inside the wound is the same as the cell density outside the initial wound). Each point represents the mean of 8 or 16 wells with the vertical bars showing the ±SD.

5.3.5 SerpinB2 knockdown effects on MDA-MB-231 3D organotypic invasion

Next the effects of SerpinB2 knockdown in MDA-MB-231 cells was tested in the 3D organotypic invasion assay. Over a 14-day invasion period MDA-MB-231 cell invasion into matrices formed by TIFs was not significantly different between +Dox or no Dox induction of individual hairpins, and not significantly different between any of the cohorts (Fig. 5.8). shGFP MDA-MB-231 cells [(+ Dox = 320.6 μm ± 20.64 invasion distance, versus no Dox = 314.3 μm ± 16.49 invasion distance) (Fig. 5.8 A,D; $P = 0.8123$)] were not significant to either SerpinB2 sh1C1 MDA-MB-231 cells [(+ Dox = 329.8 μm ± 12.31 invasion distance, versus no Dox = 302.3 μm ± 13.78 invasion distance) (Fig. 5.8 B,D; $P = 0.1473$), or SerpinB2 sh2A2 MDA-MB-231 cells [(+ Dox = 337.1 ± 12.32 invasion distance, versus no Dox = 330.3 ± 10.84 invasion distance) (Fig. 5.8 C,D; $P = 0.6788$)] within TIF constructed collagen I matrices (Fig. 5.8). The similar invasion distance detected between cohorts potentially indicates that intracellular SerpinB2 does not affect epithelial invasion into TIF contracted collagen I matrices. Further, no significant difference was observed in invading MDA-MB-231 cell morphology and migration mode between any of the SerpinB2 or GFP control hairpins (data not shown).

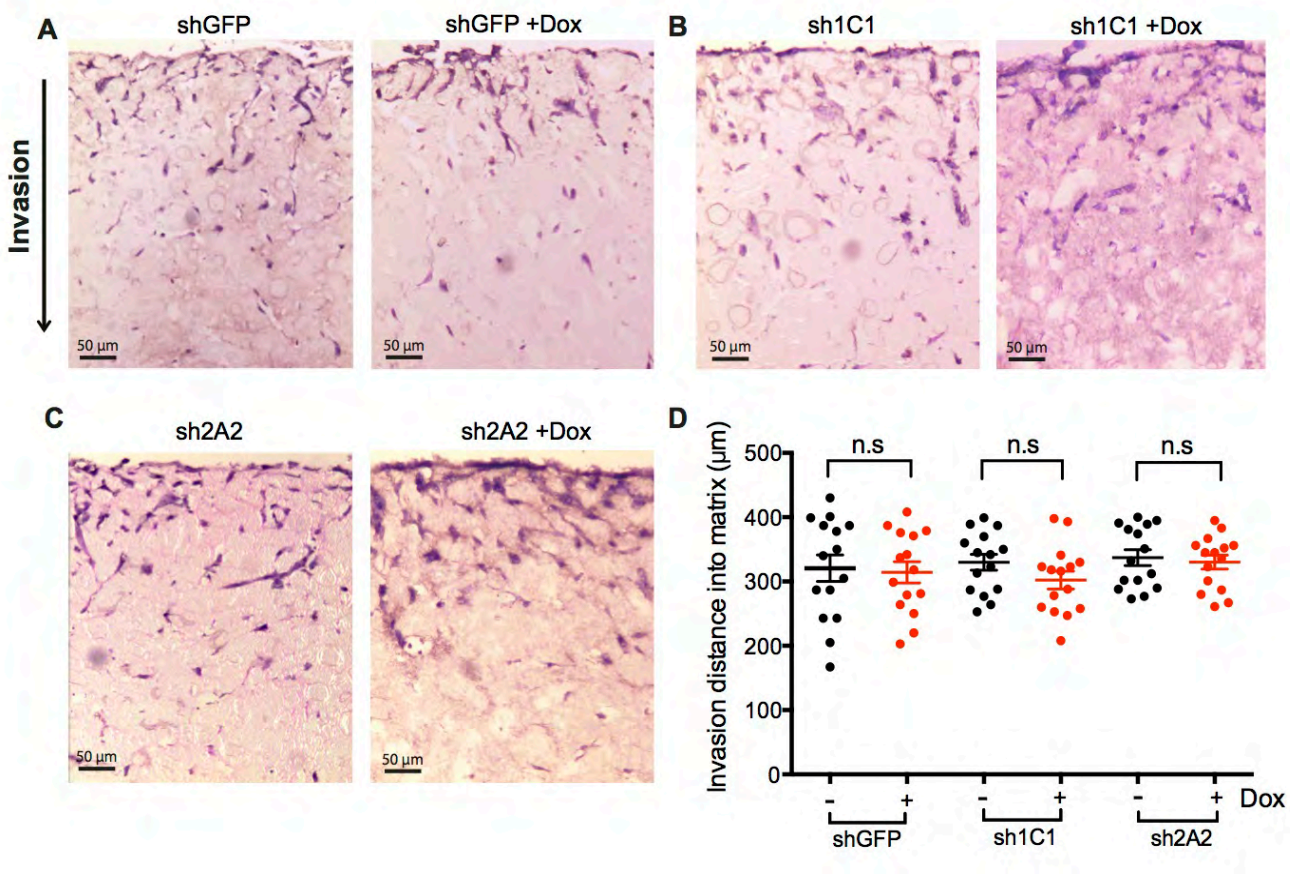

Fig 5.8. SerpinB2 KD MDA-MB-231 cell invasion through TIF/collagen I matrices. Photomicrographs of H&E stained sections of organotypic cultures showing invasion of **A.** shGFP MDA-MB-231 cells (± Dox), **B.** sh1C1 MDA-MB-231 cells (± Dox), and **C.** sh2A2 MDA-MB-231 cells (± Dox) through collagen I matrices formed in the presence of TIFs. **D.** Invasion distance analysis was performed on images taken at sites of maximal invasion after 14 days, using 15 fields of view. Individual values are shown with bars representing mean ± SEM from 4 separate matrices. Statistical analyses were performed using unpaired t-tests.

5.3.6 Pilot 3D invasion assays with highly metastatic MDA-MB-231HM cells

To determine the invasive potential of MDA-MB-231HM cells through TIF or wild-type MEF constructed collagen I matrices, the 3D organtoypic method was employed. Both 7- and 14-day invasions were undertaken in order to identify the optimal time length for invasion experiments. After both 7- and 14-days, MDA-MB-231HM cells invaded into matrices (Fig. 5.9), however 14-day invasion periods resulted in obvious and maximal differences for this cell type. Interestingly, MDA-MB-231HM cells invaded further into TIF matrices than wild-type MEF matrices over a 14-day invasion period, potentially due to species specificity. Also of note,

the parent MDA-MB-231 cell line did not invade into TIF or wild-type MEF matrices after 7 day invasion period (data not shown).

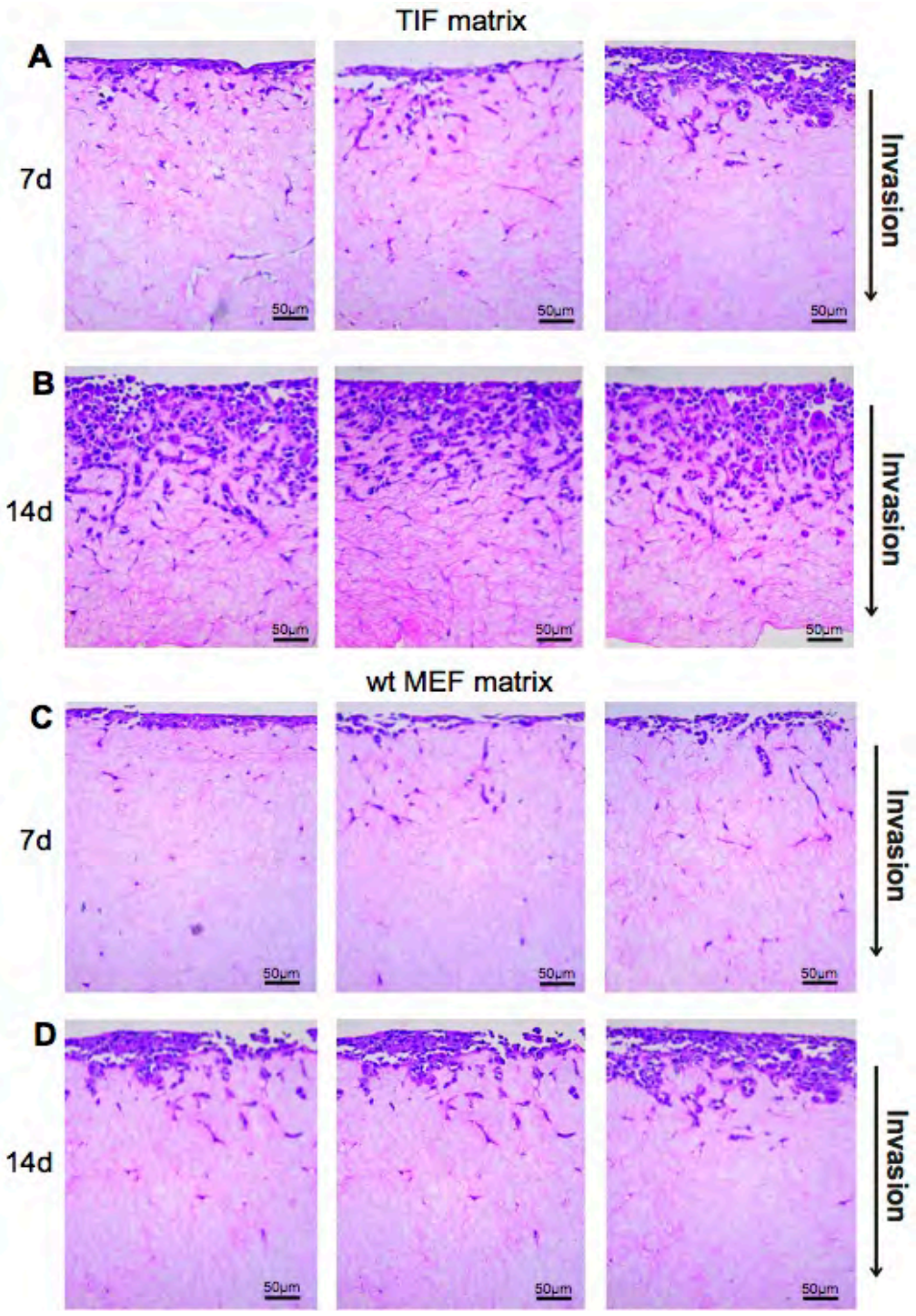

Fig. 5.9. MDA-MB-231HM invasion through TIF and wild-type MEF constructed collagen I 3D organotypic matrices. Photomicrographs of H&E stained sections of 3D organotypic cultures showing invasion of MDA-MB-231HM cells through either (**A**-**B**) TIF or (**C**-**D**) wild-type MEF constructed collagen I matrices over a 7 or 14-day time period. Each image represents a separate matrix.

5.3.7 High metastatic MDA-MB-231HM cells in wild-type and SerpinB2$^{-/-}$ MEF constructed collagen I organotypic matrices

As it was earlier confirmed that MDA-MB-231HM cells express negligible levels of SerpinB2, the stromal contribution of SerpinB2 to the invasion process of these cells within the TNBC microenvironment could be determined without potential confounding effects of epithelial cell SerpinB2 expression. Invasions using the 3D organotypic system were undertaken over both 7- and 14-day time periods. After 7-days invasion, MDA-MB-231HM cell invasion through matrices formed by SerpinB2$^{-/-}$ MEF matrices was 4.37-fold greater than invasion of wild-type MEF matrices (36.02 % ± 1.67 versus 8.24 % ± 3.37; $P < 0.0001$) (Fig. 5.10, A-C). After a 14-day invasion period, MDA-MB-231HM cell invasion through matrices formed by SerpinB2$^{-/-}$ MEF matrices was 2.87-fold greater than epithelial invasion through wild-type MEF matrices (45.39 % ± 3.51 versus 15.79 % ± 1.6; $P < 0.0001$) (Fig. 5.10, D-F).

There was no significant difference observed in invading MDA-MB-231HM cell morphology or migration modality in matrices formed by SerpinB2$^{-/-}$ MEFs versus wild-type MEFs. MDA-MB-231HM cells invading through either matrix exhibited a predominantly amoeboidal phenotype (refer to photomicrographs in Fig. 5.10).

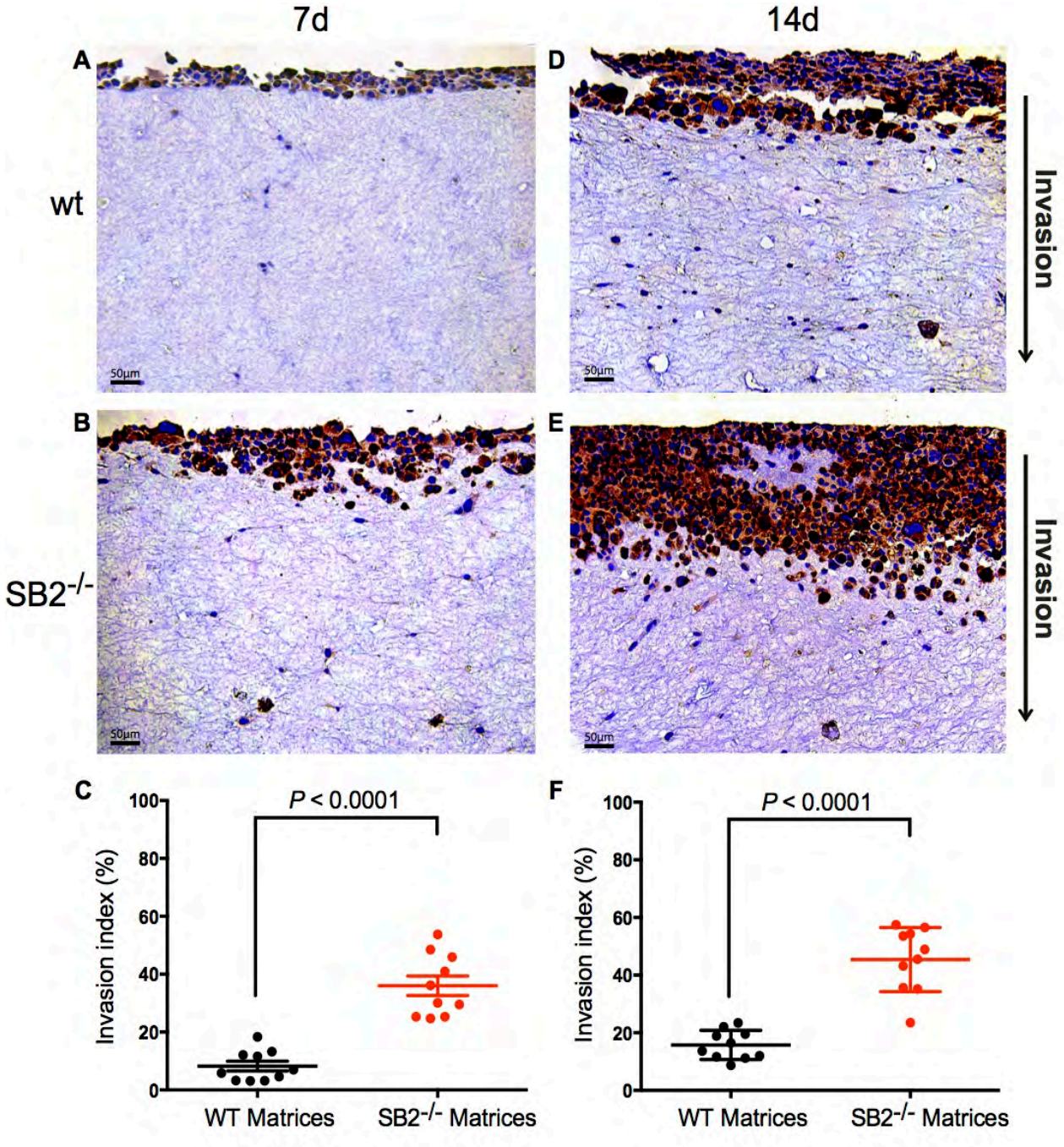

Fig. 5.10. MDA-MB-231HM cell invasion through wild-type and SerpinB2$^{-/-}$ MEF/collagen I matrices. A-B: Photomicrographs of pan-cytokeratin stained sections of organotypic cultures showing invasion of MDA-MB-231HM cells over a (**A-B**) 7-day or (**D-E**) 14-day time period through collagen I matrices formed in the presence of either (**A**,**D**) wild-type or (**B**,**E**) SerpinB2$^{-/-}$ MEFs; **C,F.** Invasion index - calculated as the percentage of MDA-MB-231HM cells invading the matrix relative to MDA-MB-231HM cells present in the layer overlaying the matrix. Analysis was performed on images taken at sites of maximal invasion after 7- or 14-days, using 10 fields of view. Individual values are shown with bars representing mean ± SEM from 3 separate matrices. Statistical analyses were performed using unpaired t-tests.

5.3.8 Mammary tumour growth and local invasion *in vivo*

After recording such significant invasion differences in our 3D model, these cells were then utilised in an animal model. To determine whether SerpinB2 absence in MEFs would affect TNBC tumour growth and local invasion *in vivo*, a xenograft mixed cell experiment was performed, where MDA-MB-231HM cells and MEFs (wild-type or SerpinB2$^{-/-}$) were co-injected into the 1st mammary gland (IMFP) of four week old old female Balb/c nude mice. A 3:1 MEF:MDA-MB-231HM ratio was utilised as this is clinically representative and allows for the formation of a pathophysiologically relevant TNBC TME (636,637). Fifteen days post inoculation, TNBC tumours formed with SerpinB2$^{-/-}$ MEFs were significantly larger (and increasingly oblate spheroid) than those formed with wild-type MEFs (mean volume 114.5 mm^3 ± 7.812, versus 60.98 mm^3 ± 5.230 respectively, P = 0.0005; Fig. 5.13).

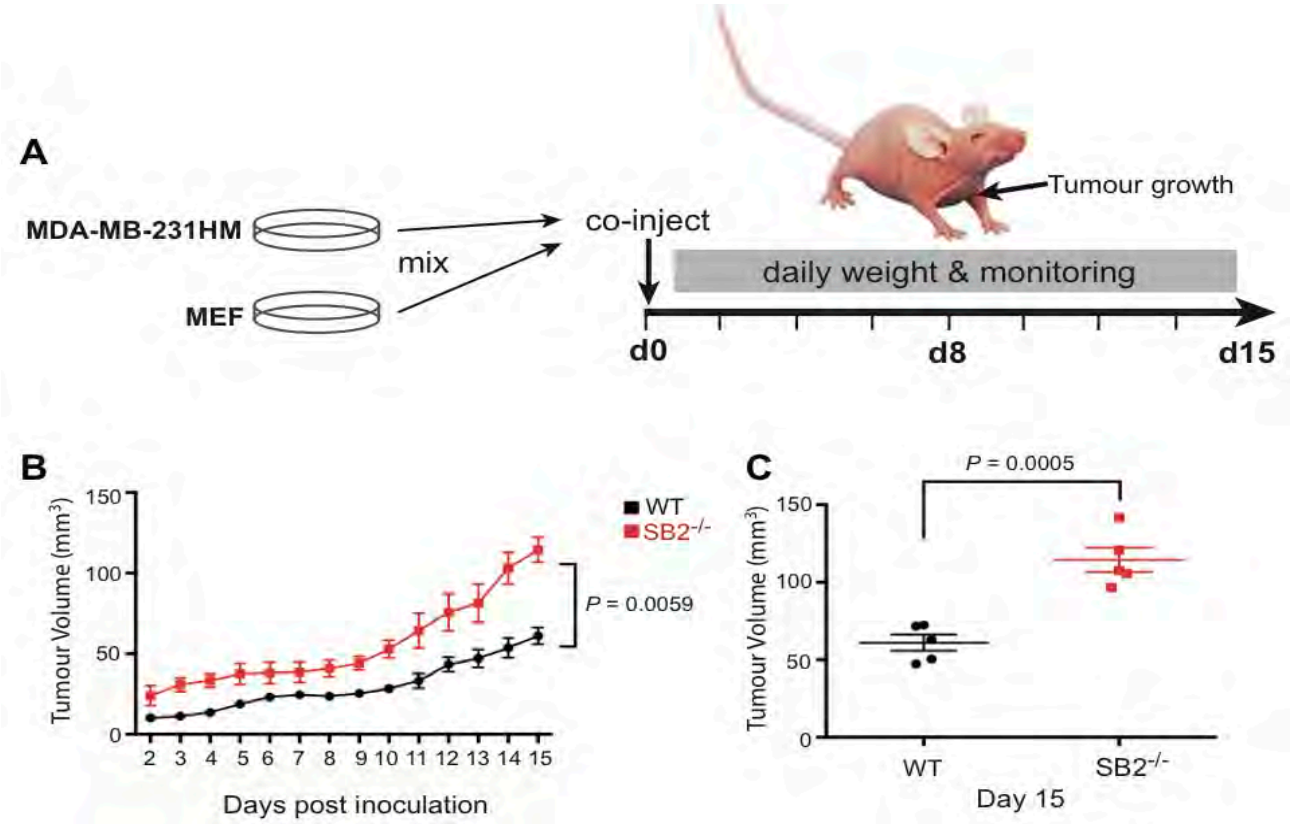

Fig. 5.11. *In vivo* mixed cell mammary xenograft model. A. A mixture of MEFs (wild-type or SerpinB2$^{-/-}$) and MDA-MB-231HMs (at a 3:1 MEF:MDA-MB-231HM ratio) were inoculated into the IMFP of the 1st mammary gland of nude mice and allowed to grow for 15 days. **B.** Analysis of tumour volume (mean ± SEM, n = 5) was undertaken daily starting from day 2, when tumours were palpable. **C.** Quantification of tumour volume after 15 days. Individual values shown are tumour volume measurements taken from 5 animals per group with mean ± SEM denoted. Statistical analyses were performed using unpaired t-tests.

These data suggest that SerpinB2 deletion in stromal cells is more influential upon breast tumour invasion. The decreased tumour-associated SerpinB2 levels in this system reflected a decreased host response to a rapidly growing and potentially invasive TNBC tumour (Fig. 5.11). Ethical endpoint at day 15 was only an issue for the SerpinB2$^{-/-}$ MEF cohorts, concurring the protective effect of SerpinB2 overexpression in cancer seen by many in the field (6,19,98).

5.3.9 Pilot 3D Organotypic breast tumour spheroid invasion assay

In order to make the 3D organotypic model more recapitulative of the human situation, a pilot experiment was undertaken. The initial aim was to understand primarily if it was feasible for tumour spheroids to both survive and invade within collagen I beds. Initially, after talks with PhD colleague, James Conway (The Kinghorn Cancer Centre, Sydney, NSW), MCF-7 breast cancer cells were employed to determine whether they would survive, and potentially migrate through the collagen matrices. After matrix contraction and a subsequent liquid-air interface invasion period, the matrices were sectioned and it was observed that the spheroids were both viable and migratory (Fig. 5.12).

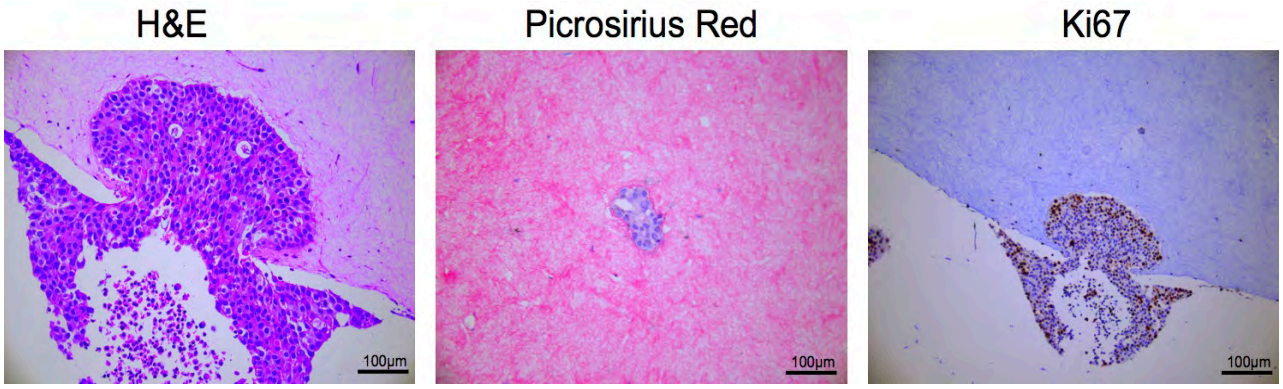

Fig. 5.12. MCF-7 breast tumour spheroid invasion through TIF/collagen I matrices. A-B: Photomicrographs of H&E, Picrosirius red and Ki-67 stained sections of organotypic cultures showing MCF-7 breast tumour spheroids within collagen I matrices formed in the presence of TIFs. Photomicrographs were obtained at 20 x magnification.

This experimental idea was then applied using MDA-MB-231HM, MCF-7 and SK-BR-3 breast tumour spheroids in TIF/collagen I matrices, with the addition of ± 500 nM SerpinB2 (Fig. 5.13). Examination of

H&E, pan-cytokeratin, Picrosirius red and Ki-67 stained sections did not show any significant differences between invasions with or without 500 nM SerpinB2. This experiment revealed that the breast cancer cells invaded out from the spheroid and that this experimental model is viable and requires further testing.

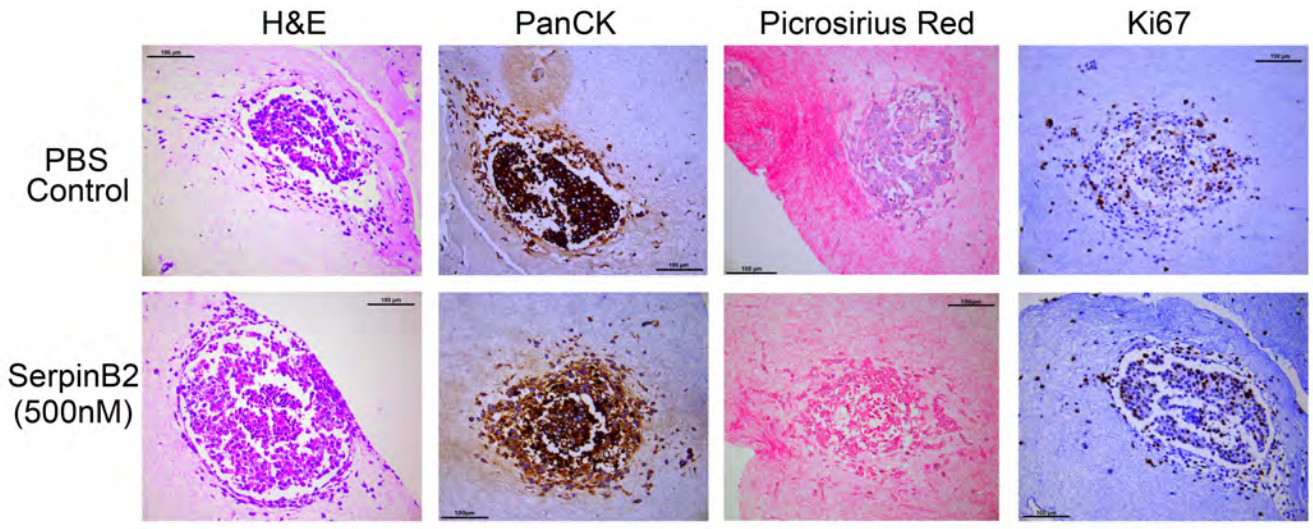

Fig. 5.13. MDA-MB-231HM, MCF-7 and SK-BR-3 breast tumour spheroid invasion through TIF/collagen I matrices. A-B: Photomicrographs of H&E, pan-cytokeratin, Picrosirius red and Ki-67 stained sections of organotypic cultures showing invasion of MDA-MB-231HM MDA-MB-231HM, MCF-7 and SK-BR-3 breast tumour spheroid cells over a 2-day time period through collagen I matrices formed in the presence of TIFs. Photomicrographs were obtained at 20 x magnification.

5.4 DISCUSSION

Breast Cancer (BC) is the most common type of cancer in women world-wide and the incidence is only increasing (611). Approximately 10-12% of BCs are TNBCs, which are usually more invasive and have a poorer prognosis than the majority of other BC sub-types (601), thus it is essential to understand the aetiology of these tumours. The advancement of TNBC marks a critical phase in breast cancer evolution, wherein dynamic tumour-stroma interactions are in constant interplay and affecting host response and treatment efficacy. Direct genetic mutations, deletions, amplifications have all been demonstrated to play an important role in the progression and metastasis of TNBC (616). Thus, tumour-stroma studies are essential for understanding TNBC biology in order to attain a deeper knowledge off all the key players and further develop therapeutic strategies

for TNBC patients. This chapter outlines the development of a TNBC model to investigate the effects of SerpinB2 modification on TNBC (MDA-MB-231 and MDA-MB-231HM cell) invasion. Initially, analysis of SerpinB2 expression within both mammary epithelial and fibroblast cells was undertaken. It was shown that all normal (yet transformed) human mammary epithelial cell lines expressed SerpinB2 and human mammary basal carcinoma cell epithelial lines expressed moderate to high levels of cleaved SerpinB2 (refer to Fig. 5.4). Conversely, the entire collection of human mammary luminal carcinoma cell lines tested (T-47D, MCF7, MDA-MB-134, MDA-MB-175, MDA-MB-330, MDA-MB-361, BT483, BT474) expressed low to negligible levels of SerpinB2 (refer to Fig. 5.4). This is interesting because high SerpinB2 expression levels are associated with recurrent free patient survival in both Luminal A and B sub-types (Fig. 5.3, E), which infers that luminal BCs benefit without intratumoural SerpinB2 expression. Potentially, luminal BCs require control over PAS activation in order for tumour progression (to activate endothelial cells and/or migrate further etc.), as they have the basal myoepithelial layer as an additional barrier before the basement membrane and mammary ECM. Alternatively, it has been reported that luminal epithelial cells display reduced polarity due to the loss of myoepithelial cells within luminal tumour systems, which leads to progression and invasion *via* collective cell migration (638). These results also suggest that perhaps it is not so much a function of the epithelial cellular expression of SerpinB2 that drives invasiveness, but a stromal component. Indeed, this remodeled TME would definitely benefit the tumour without uPA inhibition. Thus, the 3D organotypic culture system was used to interrogate the role of SerpinB2 in BC development and invasion. These models were efficaciously used to elucidate SerpinB2 effects in a context-dependent manner and demonstrated that endogenous SerpinB2 activity is not required for MDA-MB-231 invasion *in vitro* or *ex vivo* (refer to Fig. 5.7). Potentially, the endogenous SerpinE1 that is still expressed within SerpinB2 shRNA MDA-MB-231's may be compensatory. However, these unexpected results infer that epithelial cell invasion does not require SerpinB2 for invasion through collagen I matrices in both an *ex vivo* or *in vitro* system. This result was made even more interesting when using the higher metastatic daughter line, MDA-MB-231HM, for proceeding experimentation. The rationale being that this cell

line expresses no apparent SerpinB2 or SerpinE1 (refer to Fig. 5.5). After initial pilot experiments (14 days was optimal; refer to Fig. 5.9) through TIF and wild-type MEF matrices, MDA-MB-231HM cells were found to be 1.6-fold more invasive than the parent MDA-MB-231 line, and thus ideal for this 3D invasion model. These cells were employed in order to understand the role of SerpinB2 in TNBC biology. As it is critical to consider functional effects in each cellular compartment of tumour tissue, MDA-MB-231HM cells were used in experiments with wild-type and SerpinB2$^{-/-}$ MEF matrices. This was ideal as there was little to no SerpinB2 in the system for these assays (MDA-MB-231HM/SerpinB2$^{-/-}$ MEF matrices) and this approach yielded valuable information, highlighting the stromal SerpinB2 effects influencing upon tumour cell invasion. Even though both wild-type and SerpinB2$^{-/-}$ MEF ECMs allowed efficient MDA-MB-231HM invasion, the disordered collagen networks of matrices generated by SerpinB2$^{-/-}$ MEFs (refer to Chapter 3, section 3.3.4) increased MDA-MB-231HM penetration by nearly 3-fold (after 14 days; refer to Fig. 5.10). Thus, without fibroblastic SerpinB2 expression, it appears that MDA-MB-231HM cells can invade collectively (ameboidal-based migration) and further within collagen I matrices, which was similarly reported in the PDAC cell invasion experiments (refer to Chapter 4, section 4.3.2).

On the basis of the insignificant invasion distances between the parent line MDA-MB-231 SerpinB2 knockdown cohorts (refer to Fig. 5.8), coupled with an increase of invasion using the MDA-MB-231HM cells (lacking SerpinB2 expression; refer to Fig. 5.10), *in vivo* testing was undertaken. A significant increase in tumour volume (1.88-fold) was recorded in mice with SerpinB2$^{-/-}$ MEF tumours versus mice with wild-type MEF tumours (Fig. 5.11), potentially demonstrating an active CAF phenotype related to SerpinB2 absence within the TME. Unfortunately time constraints did not allow for further post-hoc analyses of tumours, and only tumour volume was quantified in this experiment. Nonetheless, the tumour volume differences recorded were extremely significant and may be due, at least in part, to the serpin function of wild-type MEFs. This is supported by data showing that epithelial SerpinB2 knockdown in MDA-MB-231 cells does not alter invasion

into collagen I matrices (Fig. 5.8), while MDA-MB-231HM invasion into MEF constructed collagen I matrices is higher without fibroblastic SerpinB2 expression (Fig. 5.10). Thus, these data infer that stromal cell SerpinB2 activity potentially reduces the invasive and metastatic capacity of breast tumours. The efficiency of tumour growth in this *in vivo* model was potentially affected by interplay of both proteolysis and local ECM remodelling, reducing physical hindrance of the surrounding stroma by MEFs lacking SerpinB2 (Fig. 5.11). Similarly, as was observed in Chapter 4 (refer to section 4.3.4), within the *in vivo* PDAC allograft model, the increase in MDA-MB-231HM tumour growth in the SerpinB2$^{-/-}$ MEF cohorts suggest that MDA-MB-231HM progression and local invasion is increased when there is less desmoplasia/collagen coverage surrounding the primary tumour mass. Although not tested here, the invading cells from tumours with SerpinB2$^{-/-}$ MEFs seem to increase cell type-specific signalling within the TME, affording increased tumour growth rates. Future tumour studies utilising both MDA-MB-231 and/or MDA-MB-231HM cells with SerpinB2$^{-/-}$ MEF in to look at metastases in this model would be ideal to ascertain whether SerpinB2$^{-/-}$ MEF tumours have increased metastatic capactiy.

3D Organotypic results in this chapter show that collective, amoeboidal cell migration was predominant in both wild-type and SerpinB2$^{-/-}$ MEF collagen I matrices. This has also been reported by Wolf *et al.* (2003) where MMP inhibition did not impede MDA-MB-231 cell migration through collagen I matrices, with cells invading in an ameboidal migration modality (639). Whether this is a compensatory mechanism by MDA-MB-231 cells or perhaps a transition from proteolytic mesenchymal migratory phenotype towards a non-proteolytic amoeboidal movement mode is unclear, however it highlights the supramolecular plasticity of breast tumour cells to facilitate a migratory mechanism even after abrogation of pericellular proteolytic pathways.

Furthermore, the pilot 3D breast spheroid model was successful in showing that breast tumour spheroids can be utilised in this organotypic format. The invasion period was only 2 days, which is potentially why the addition of 500 nM SerpinB2 had no significant observable effect on the invasion of breast cancer cells. Nonetheless, this experimental model is feasible and should be repeated. Moreover, the addition of tumour-associated

macrophages (with modified expression levels of SerpinB2) would act as a biomimic for TME even more so and has been done by others. Dwyer *et al.* (2016) recently showed invasion in their co-culture spheroid model utilising PyVmT mouse mammary tumour-derived cells and mouse bone marrow-derived macrophages (640). Embedding of these "mammospheres" within Matrigel beds lead to invasion of both breast tumour cells and macrophages into the surrounding matrix (640). Utilising 3D live imaging on both breast and pancreatic spheroid organotypic invasions is now a viable experimental apparatus for our laboratory and one that should be definitely utilised.

In addition, not only do spheroid organotypic invasions recapitulate the human situation, the individual tumour cells of a spheroid will have a greater ability to infiltrate interstitial collagen networks without necessitating proteolytic remodeling and classical EMT pathways [(584) and refer to section 4.4 for more references]. It has been reported that dissemination of a primary tumour mass of ~1 cm size (corresponding to $\sim 1 \times 10^9$ cancer cells) can supply the circulatory system with one million tumour cells each day (641). However, subsequent extravasation and secondary site colonisation is limited because of incompatible distal tissue beds. Perhaps SerpinB2 expression within these metastatic populations can assist in cytoprotection in these new environments (164,305), but more often than not, SerpinB2 expression is downregulated in metastatic cells of secondary tumour sites.

As aforementioned, experimentation by Finak *et al.* (2008) reported that SerpinB2 expression within isolated human breast tumours was ~16-fold decreased within invasive carcinoma compared with matched normal breast stroma ($P < 0.0001$, n = 1440) (623). This reduction in SerpinB2 expression in invasive tumour stroma compared with normal breast stromal tissue over such a large cohort provides strong evidence that SerpinB2 deletion within stroma promotes breast cancer progression. Possibly, without SerpinB2, stromal remodelling around breast tumour tissue sites promotes tumour growth and invasion through a loose extracellular matrix phenotype, and may define disease progression and metastatic lesion development. Indeed, from the data presented in this chapter, and that within Chapter 4 (PDAC chapter), it is hypothesised that the apparent lack

of mechanical forces between the cells and the ECM allows for collective amoeboidal tumour invasion and demonstrates the cell plasticity to adapt to a defunct tensional landscape, allowing for dramatic increases in breast tumour size and invasion. Therefore, the transition to an invasive phenotype appears to be in part a mechanical one, aided by the surrounding tissue compliance of breast tumour systems. The deregulated ECM in breast tissue around these tumourigenic sites is a complex process requiring elucidation, which the SerpinB2 models appear to be useful for isolating specific elements of the mammary TME, allowing for the dissection of PAS componency in tumour versus stromal tissue. The changes in the stroma surrounding tumours is largely due to the actions of activated myofibroblasts/CAFs in the stroma (23,642-644). It is still unclear in the field whether or not CAFs are resident fibroblasts, activated by paracrine cytokines and growth factors, or whether they are of mesenchymal stem cell origination that are genetic precursors to fibroblasts and are reverted to fibroblast-like cells within the breast TME (645). Certainly, isolating individual cell types from tumour extracts is a difficult task. The unique and variable proportion of stromal and epithelial cells in patient extracted tumour tissue can sometimes not provide information on the actual levels or proportion of each protein produced by specific cellular compartments. Additionally, the relative contribution of specific cellular secretions (whether from tumour cell, stromal or immune cell) affecting tumour progression is assumed. It is not possible to know what particular gene expression change has occurred in a specific cell of origin and it must not be assumed that all cell types of a tumour extract are expressing this same genetic alteration. Additionally, only approximately 50% of BC tumour masses are composed of epithelial cells (646), thus there is a dire need for better classification of expression signatures. This pitfall needs to be addressed either through state-of-the-art cell-sorting technology, or through categorisation of the specific genetic signatures of cell types (647), or in patients and their treatment responsiveness to adjuvant or neo-adjuvant therapy, which is currently underway (648). SerpinB2 expression and quantification within stroma of clinical samples is warranted, and it would be ideal to see if there is a relationship between tumour stage and stromal SerpinB2 expression, as well as metastasic site SerpinB2 expression level vesus primary tumour SerpinB2 expression level.

The results of this chapter demonstrate that there is immense potential for the development and future utilisation of SerpinB2 re-introduction into specific BC TMEs. SerpinB2's relatively small size, immunoneutrality and proven *in vitro* and *in vivo* targeting ability, provide it with rapid internalisation through RME, beneficial for therapeutic regimen (19,130). With a better understanding of the signaling mechanisms most vital in the development and perpetuation of TNBC, particularly within the stroma, drug design and development can be enhanced with clearer rationale, affording increased ECM targeting, drug synergism and overall better outcomes for TNBC patients. Future treatments for TNBC cancer must reflect the critical pathways in an individual patients tumour tissue, to inhibit growth, progression, and perpetuation of the tumour stroma. The results of this chapter and many research groups, support a role for PAS in TNBC malignancy (649,650), thus in the pursuit of greater clinical efficacy and personalised treatment regimen, our laboratory has been attaining deeper understanding of the tumour stroma in a TNBC specific context, and optimising drugs to target PAS in these systems. In this regard, a uPA targeted combinatorial therapeutic could offer increased efficacy upon invasive BC tumour cells. As it has been shown that high levels of SerpinB2 do not produce any apparent associated health risks (626), this may allow for the simultaneous IV-administration of both free SerpinB2 and SerpinB2 drug formulations, which could improve the outcome for cancer patients at high yet tolerable concentrations. Moreover, SerpinB2 has been shown by our laboratory to have inhibitory effects on endothelial cell (EC) tubule formation at high concentrations, which is possibly linked to the reduction of plasmin generation and MMP knock on effects in activation of key growth factors such as bFGF, VEGF, PDGF and TGF-β. bFGF, VEGF, HGF and PDGF stimulate EC proliferation, migration and integrin expression and TGF-β enhances EC differentiation (651-656). Notably, HGF and bFGF can also stimulate ECs to produce uPA, further inducing ECM degradation and promoting the plasmin positive-feedback loop (651) Extracellular growth factors, as well as uPA, bind to cell surface receptors, enhancing and inducing the downstream activation of intracellular signalling cascades by prolonging tyrosine phosphorylation, which leads to the transcriptional activation of genes that express other growth factors (657). Moreover, activated ECs

recruited in the establishment of angiogenesis, facilitating tumour metastasis, have been shown to up-regulate uPA and uPAR (29).

Through a combined understanding of PAS functioning in diseased systems and concurrent drug design and development, our laboratory is enhancing understanding of TNBC biology and leading the way in uPA/uPAR targeting drug-loaded nanoparticle systems. Previously, our laboratory has shown that through the utilisation of a uPA targeting moiety, a highly cytotoxic anti-mitotic drug (*N*-AI) can be specifically delivered to, and kill, cancerous BC cells, while unaffecting normal, healthy tissue (129). Current *in vitro* and *in vivo* studies have proved promising, demonstrating specific and enhanced efficacy of SerpinB2 drug conjugates over their un-conjugated free drug counterpart (130). It is hypothesised that the selective targeting of different BC cell subtypes using a SerpinB2 prodrug formulation will provide a means to treat multi-drug resistant tumours in uPA-positive BC. There are multiple benefits available with this targeted approach: firstly, through an enhanced efficacy of the drug due to its targeted, receptor specific delivery; and secondly, by the decrease in systemic toxicity and side-effects due to the targeted drug only being activated at the site of interest (130). The mechanism of *N*-AI relies upon the destabilisation of microtubules, causing G2 and M phase arrest, inhibiting the normal function of mitosis (130,658). As such, the more proliferative a cell line, the more susceptible it is to *N*-AI during mitosis and cytokinesis, where tubulin polymerisation and microtubule formation is largely required, which produces a greater cytotoxic effect, hence ideal for most tumour systems (131).

Additionally, as PAS is also upregulated by activated endothelial cells, as found in angiogenic vessels; a SerpinB2 drug approach may additionally be very useful against angiogenesis. At present, there are many phase I and II clinical trials underway utilising monoclonal antibodies (WX-671/Mesupron and WX-UK1, respectively) which target uPA and interfere with the growth, spread and metastasis of solid malignant tumours (21). To date, there have been promising results in reducing metastatic spread and extending the lifespan of breast or pancreatic cancer patients (21). However, monoclonal antibodies are expensive to synthesise, meaning dosage

regimes are not affordable for many cancer patients. Additionally, several drugs targeting uPA have been reported to lack the specificity required to only interact with tumour-associated uPA, causing significant side effects (21). The production of the naturally occurring SerpinB2 ligand, conjugated to a potent cytotoxin that specifically targets uPA, would offer a more cost effective way to target uPA positive cancers and potentially reduce side effects. Conversely, the biggest problem with uPA targeting drugs is the interaction that can occur with healthy tissue, since uPA can be expressed and secreted by normal cells, supporting fibrinolysis, tissue remodeling, vessel growth or wound healing (81,659). To overcome this, experiments need to be conducted on different cancer types that are uPA expressive in order to determine when non-preferred uPA interaction is not a problem and what type of patients will benefit the most from uPA-specific targeted cancer therapy (219).

Albeit costly and time consuming, *in vivo* tests are warranted from the findings in this work and are essential because of the complex nature of vascular responses to test reagents, of which no *in vitro* model has the capacity to determine. This study provides deeper insight and impetus to further develop and test our laboratory's SerpinB2 cancer drugs upon *in vivo* in order to determine their potential therapeutic targeting in the inhibition of breast and other cancer types.

Finally, this chapter confirms SerpinB2's significant role in the progression of breast cancer invasion and metastasis, providing valuable information of TNBC biology. This work validates our laboratory's design and testing of SerpinB2 drug conjugates as potential chemotherapy options for both primary, metastatic and angiogenic cells, offering great potential therapeutic value in the future.

CHAPTER 6

CONCLUSIONS AND FUTURE DIRECTIONS

CHAPTER 6

CONCLUSIONS AND FUTURE DIRECTIONS

The findings in this thesis confirm SerpinB2 as a powerful modulator of the growth, progression and local invasion of both breast and pancreatic cancer. Through the utilisation of both *in vitro* and *in vivo* 2D and 3D imaging technology this study examined cancer progression at a sub-cellular and molecular level. We used both 3D organotypic matrices and *in vivo* models and advanced imaging approaches to decipher the cellular migration and tumour progression of both epithelial and stromal cell types, in which SerpinB2 expression was also modified. This approach allows for the real-time *in vivo* assessment of single-cell migration and invasion events, enabling the understanding of how tumour and stromal cells interact. Through elucidation of critical checkpoints (i.e. ECM remodeling, cell migration and local invasion) within these systems, a deeper knowledge of the effects of PAS regulation on breast and pancreatic cancer progression has been discovered. It is clear that without SerpinB2 in fibroblasts, the key cell component coordinating the majority of stromal remodeling within the TME of solid tumours, a diffuse stroma is generated, which can be infiltrated with both greater ease and collectively by both TNBC and PDAC cancer cells (Fig. 6.1). These findings provide strong evidence for a role for both SerpinB2 and uPA/uPAR in TNBC and PDAC stroma and certainly require further investigation. As such, this work opens up the potential for developing uPAS-targeted therapeutics for molecular subtypes of BC (personalised medicine) with enhanced activity and efficacy. Further understanding into the biochemical functioning of PAS in these (and other) contexts will help facilitate the design of novel therapies, offering structural and functional information for more efficient tumour-stroma targeting strategies.

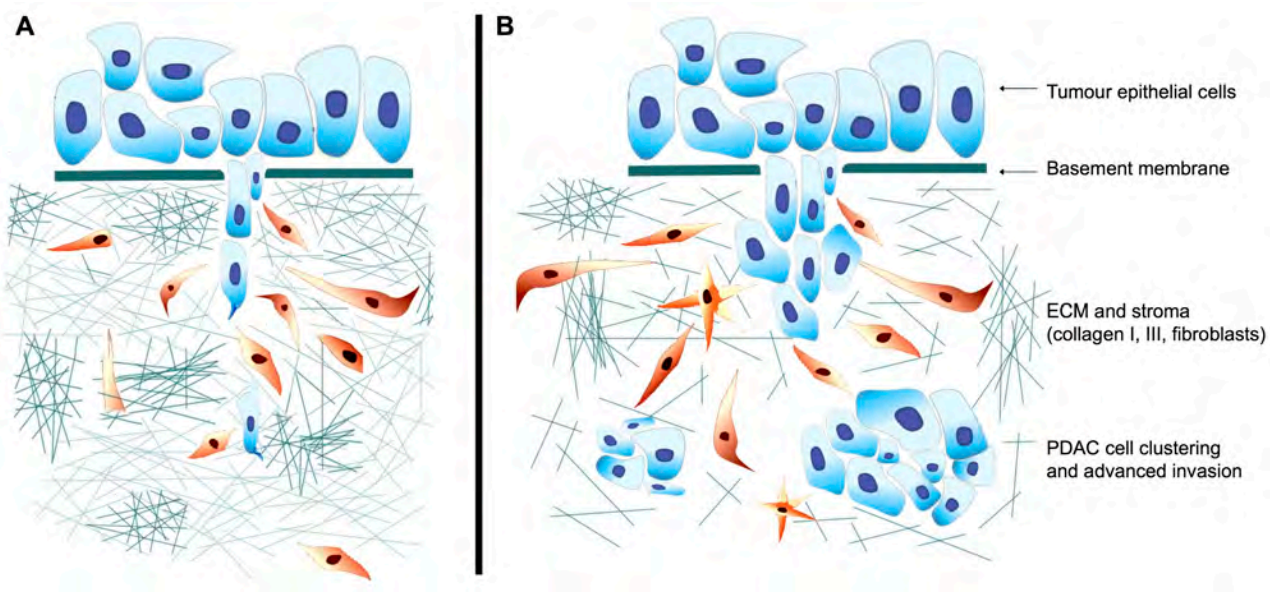

Fig 6.1. Schematic representation of the proposed effects of SerpinB2 within the TME. The TME with (**A**) and without (**B**) SerpinB2 expression. Tumour epithelial cells (blue) are able to degrade the basement membrane and invade into the underlying ECM with the help of CAFs (orange). The stromal composition of the SerpinB2 null/reduced ECM is decreased in stiffness and less occupied by collagen I networks allowing greater migration of tumour cells in (**B**).

Through the implementation of Gateway lentiviral systems for both overexpression and attenuation of SerpinB2 gene expression, the potential for development of SerpinB2 gene therapies was demonstrated and should be exploited as a targeted cancer therapy approach in the future. Lentiviral vectors provide a powerful method to inducibly manipulate SerpinB2 in both epithelial and fibroblast cell types. With the ability to over-express and knockdown genes of interest in a temporal, spatial, and cell-type specific fashion, this inducible genetic approach can not only help elucidate differential roles of SerpinB2 in the TME, but also could be used for gene editing. The use of CRISPR offers greater fidelity over lentiviral systems and could potentially revolutionise gene therapy, not just within the cancer arena. There are obviously beneficial applications for this within clinical studies, such as fibroblastic SerpinB2 modulation. The constructs produced herein could either be utilised directly or as a guide for future CRISPR work in the modification of SerpinB2 in other cell types and research platforms, including those used to study tumour-stroma interactions within pancreatic and breast cancer (refer to chapters 4 and 5, respectively).

Collectively, the findings in this thesis highlight the possibility that there are broader biological implications in stromal remodeling of SerpinB2. Potential associations between FAKs and TG2 are possible, and these explanations require elucidation. In the collagen contraction model, SerpinB2$^{-/-}$ MEFs potentially exhibit decreased integrin (α2ß1) binding (without TG2-fibronectin/fibrin/integrin bond stabilisation), reducing FAK (Vinculin, Paxillin and FAK) activation/phosphorylation, attenuating actin re-organisation and eventually ECM remodelling, causing changes in cellular adhesion, proliferation, migration and cell survival. Future experiments are required to investigate this further. Interestingly, actin-related protein 2/3 complex subunit 1B (ARPC1B) was present at twice the amount compared to that of wild-type matrices, as assessed by LC/MS. This increase was potentially to compensate for the decreased LOX pathway activity (refer to Fig. 3.10) as ARPC1B is a subunit of the Arp2/3 complex, involved in regulation of actin polymerisation and formation of branched actin networks. Welch *et al.* (1997) showed that Arp2/3 complex is localised to the lamellipodia of both stationary and motile fibroblasts and suggested that this complex promotes both actin assembly in lamellipodia and could facilitate lamellipodial protrusion (469). This 2-fold increase in SerpinB2$^{-/-}$ MEF ARPC1B level is potentially associated with the 0.7-fold up-regulation of actin within SerpinB2$^{-/-}$ MEF matrices (refer to Fig. 3.10) and may be a compensatory mechanism to stimulate proper fibroblast lamellipodial protrusion for adequate ECM remodelling. Thus, SerpinB2-FAK association studies are warranted.

Cell-cell and cell ECM signaling in the stroma and subcellular locations within both breast and pancreatic cancer (and probably other cancer types) may involve SerpinB2, with strong biological implications. The aspects of stromal biology that appear to aid both PDAC and TNBC tumour progression and invasion within our models involve collagen cross-linking and alignment, matrix stiffness and the influx and potential crosstalk of various tumour and stromal cells. Moreover, the observation that pancreatic and breast stromal density affects local invasion is clinically relevant and loose and stiff stromal ECM will become increasingly appreciated as influencing the initiation of metastases in both breast and pancreatic carcinomas. The challenge going forward is to determine a reliable diagnostic assay for both the presence of specific PAS biomarkers as early as possible,

and also in particular, for the assessment of collagen density and alignment within a patient's TME. This has the potential to assist surgeons and oncologists, for application during both biopsy and surgical resection, as SHG microscopy utilised for such imaging does not require any labeling and can be performed rapidly on fresh, unstained tissue. Already, collagen deposition and fibril alignment as a biomarker is paired with the determination of specific biomarkers (660). Further understanding of the contextual role of collagen deposition with the ECM of both breast and pancreatic cancer in facilitating tumour cell invasion is required and will present new opportunities to diagnose, predict and treat many different cancer types.

The biological implications of these thesis findings also have the power to deliver substantial improvements in patient prognostic outcome and predicting therapeutic response. There is potential that these stromal processes around tumour sites during specific ECM events could be manipulated *via* PAS regulation to increase clinical efficacy, particularly in identified patients with high uPA/uPAR. However, prior to such testing, the prognostic significance of cellular SerpinB2 expression within cellular and ECM events identified in this study must be elucidated clinically. The decreased survival of 1.6 years in patients with high uPA expressing PDAC tumours is testament to the significant effect of PAS in tumour aggression and metastatic potential, and this increases the likelihood that these data presented will be corroborated in clinical data. Considering the potent activity of SerpinB2 to inhibit the aggressive PDAC line in 3D organotypic matrices, subsequent experiments were undertaken in an effort to further ascertain the stromal versus epithelial cell effects of SerpinB2. Dramatic differences were seen in SerpinB2$^{-/-}$ matrices, offering clues to SerpinB2's role in stromal remodeling within the TME. In order to further understand the effects of SerpinB2 on collagen cross-linking and the stromal remodeling process, future SerpinB2$^{-/-}$ 3D models future experiments are required to essentially prove or disprove this. Future work should include state-of-the-art imaging systems such as FRAP and FLIM–FRET, to analyse SerpinB2-FAK co-localisation in fibroblast migration during both matrix contraction and PDAC/TNBC invasion experiments. In addition, these imaging techniques have the power to examine anti-uPA drugs

targeting the ECM, thereby offering early validation before more time-consuming, expensive and complex *in vivo* assessment. Additionally, there is a dire necessity for increased examination and imaging of the stroma around primary, peri-tumoural, micrometastatic and metastatic sites, as these zones still remain poorly understood. This would be ideal for testing in SerpinB2$^{-/-}$ tissues and SerpinB2$^{-/-}$ mice, as these are recapitulative of most highly invasive tumour systems and metastatic lesions, making it especially beneficial for the development of new combinatorial treatments targeting uPA/uPAR and/or the stroma of inoperable tumours.

Moreover, it would be extremely interesting to compare and contrast SerpinB2 expression (mRNA and protein) in the tumour vs. stroma of the APGI PDAC tumours. To elucidate whether stromal SerpinB2 expression was associated with increased survival in the APGI cohort would be ideal. From the results obtained in this project, it would be expected that high SerpinB2 expression specifically in the stroma of APGI PDAC tumours would signify good prognosis, with less invasive tumours versus a low stromal SerpinB2 expression. Therefore, future studies should examine SerpinB2 expression in both PDAC and TNBC tumours, where cohorts are available. The functional effects of SerpinB2 in a cell-specific context could be directly addressed in the APGI PDAC tumour cohorts. IHC for SerpinB2 in the stroma of this cohort could potentially be correlated to local invasion and perhaps overall survival. Concurrently, this should also be performed for the TNBC cohorts as available and stromal vs. cancer evaluation of SerpinB2 expression could be undertaken and correlated to clinicopathological indicators and survival. This could one day lead to SerpinB2 expression in stroma being utilised as a marker to personalise treatment for patients who have low or negligible levels of SerpinB2 in stroma. Recombinant SerpinB2 could be administered as an ECM block on tumour invasion, as an adjuvant to surgery and/or chemotherapy, as results within this project have illustrated. Furthermore, this thesis offers insight and impetus for the potential use of SerpinB2 as a drug delivery system to target uPA positive tumours and warrants further preclinical investigation (129-131). In this context, a SerpinB2 functionalised drug could be expected to exhibit an improved efficacy and *in vivo*, than corresponding free drug,

when administered to a patient with a uPA positive malignancy. In addition, the *ex vivo* results in this work demonstrated that the organotypic assay system can provide high *in vitro* fidelity to support further *in vivo* drug discovery. Despite great advances in 3D cell culture methodology, such as the organotypic model, it must also be considered that matrix specific effects upon the movement of molecules through tissue beds at both a micro- and macroscopic scale will impact upon the spatial distribution of oxygen, growth factors, metabolites and other signaling molecules (23). There are specific gradients of biological molecules within tissue beds modulated by the vasculature, angiogenesis and the ECM (23). As such, not all cells in the TME of a solid tumour are exposed to the same microenvironment and this diversity is a major factor contributing to the heterogeneity of tumour and stromal cell populations *in vivo* (661). This is tremendously difficult to reproduce *in vitro* and although it is not yet possible to recapitulate arterial blood flow within these 3D culture systems, the inclusion of endothelial cells together with fibroblasts, either within the collagen I matrix or beneath it, could allow for adequate angiogenic modeling, in conjunction with the investigation of tumour-stroma interactions. Additionally, the supplementation of immune cells to the culture system is another important area for development, as it is well known that T-cells and tumour-associated macrophages impinge upon cancer cell biology. Previous studies utilising co-cultures of macrophages and tumour cells on collagen gel beds have shown strong evidence of intercellular signaling loops that regulate 3D cell movement (565,662), and similar experiments are achievable and should be investigated within our organotypic culture approach. As demonstrated in Chapter 5 (refer to Section 5.3.7), a pilot 3D organotypic experiment was undertaken to investigate the effects of tumour spheroids within the matrices. This model was successful and recapitulates the human situation with greater biomimicry potentially allowing for increased therapeutic insight during drug design. Future studies in our laboratory will utilise this 3D organotypic spheroid model and further optimise it to be even more *in vivo* similar. Organotypic culture technology is fast becoming one of the most accessible and physiologically relevant models to study TME dynamics of both tumour and stromal cells in a controlled environment, and ECM equivalent matrices can be derived from a variety of sources, as exemplified by the

thesis work presented herein. At present, there is much interest in 3D organotypic culture models and commercial development of a more standardised, validated culture system would be extremely valuable in ensuring that the organotypic system becomes more inclusive and accessible to a wider range of academic and clinical scientists, thereby helping to maximise its potential. Through a more diverse yet defined ECM, specific for each tumour context, coupled with the appropriate cell culture media, it is foreseeable that a highly accurate, reproducible 3D organotypic culture model could emerge, potentially making it possible to offer real time translational experimentation from bench to bedside. Through coupling these types of benchside culture models with integrated analyses of a patient's genomic, epigenomic and transcriptomic characteristics, there is future therapeutic relevance and biological insights to be gained.

Most recently, a paper by Bailey *et al.* (2016), combining Australian researchers from the International Cancer Genome Consortium has identified four distinct types of PDAC, arising from 32 recurrently mutated genes from ten different cellular trigger points (663). These four subtypes identified were squamous, pancreatic progenitor, immunogenic and aberrantly differentiated endocrine exocrine PDAC, based on the differential expression of transcription factors and downstream targets in specific lineages during pancreas development and regeneration (663). This elegant paper not only highlights the extreme complexity of PDAC, but also reveals the fields increased appreciation of the role of the immune system in malignant progression. Immunotherapy is now a rapidly growing field in in cancer therapy, both academically and commercially. Many new therapies are specifically targeting mechanisms through which tumours evade the immune system. A large amount of clinical trials are underway utilising immunotherapies both individually and combinatorially with current gold-standard chemotherapies, with varied results of both increased and decreased efficacy. Indeed, patient selection is of, and will remain to be, consistently important for efficacy of cancer therapeutic regimen. Direct differences in the molecular evolution of a patient's unique cancer subtype is required to identify the best pathway for therapeutic success for every person.

In conclusion, the results of this thesis offer further insight and understanding into the biochemical properties and diverse cellular functions of SerpinB2. The relationships between SerpinB2 uPA inhibitory function and ECM remodeling provide further rationale for the use of SerpinB2 as both a marker of invasive potential and metastatic progression. These data impact on the potential future use of individual PAS components (i.e. uPA and uPAR) as biomarkers in pancreatic and breast cancer patients who are potentially at a higher risk of metastatic progression. Finally, these findings also further validate the importance for the continued development of SerpinB2 as a targeted cancer therapeutic. Through the combined understanding of PAS functioning and concurrent drug design and development, improved outcomes for cancer patients are surely on the horizon.

REFERENCES

1. Hanahan D, Weinberg RA. The hallmarks of cancer. Cell. 2000;100:57–70.

2. Weinstein IB, Joe A. Oncogene addiction. Cancer Research. American Association for Cancer Research; 2008;68:3077–80–discussion3080.

3. Brabletz T, Jung A, Spaderna S, Hlubek F, Kirchner T. Migrating cancer stem cells |[mdash]| an integrated concept of malignant tumour progression. Nature Publishing Group; 2005;5:744–9.

4. Im JH, Fu W, Wang H, Bhatia SK, Hammer DA, Kowalska MA, et al. Coagulation facilitates tumor cell spreading in the pulmonary vasculature during early metastatic colony formation. Cancer Research. American Association for Cancer Research; 2004;64:8613–9.

5. Neal CP, Berry DP. Basic principles of the molecular biology of cancer II: angiogenesis, invasion and metastasis. Surgery (Oxford). 2006.

6. Harris L, Fritsche H, Mennel R, Norton L, Ravdin P, Taube S, et al. American Society of Clinical Oncology 2007 update of recommendations for the use of tumor markers in breast cancer. J Clin Oncol. American Society of Clinical Oncology; 2007;25:5287–312.

7. Joyce JA, Pollard JW. Microenvironmental regulation of metastasis. 2009;9:239–52.

8. Allinen M, Beroukhim R, Cai L, Brennan C, Lahti-Domenici J, Huang H, et al. Molecular characterization of the tumor microenvironment in breast cancer. Cancer Cell. 2004;6:17–32.

9. Folkman J. Angiogenesis. Annu Rev Med. Annual Reviews; 2006;57:1–18.

10. Inda M-D-M, Bonavia R, Mukasa A, Narita Y, Sah DWY, Vandenberg S, et al. Tumor heterogeneity is an active process maintained by a mutant EGFR-induced cytokine circuit in glioblastoma. Genes Dev. Cold Spring Harbor Lab; 2010;24:1731–45.

11. Dolberg DS, Bissell MJ. Inability of Rous sarcoma virus to cause sarcomas in the avian embryo. Nature. Nature Publishing Group; 1984;309:552–6.

12. Bonnans C, Chou J, Werb Z. Remodelling the extracellular matrix in development and disease. Nat Rev Mol Cell Biol. 2014;15:786–801.

13. Wang Y, Steinbeisser H. Molecular basis of morphogenesis during vertebrate gastrulation. Cell Mol Life Sci. SP Birkhäuser Verlag Basel; 2009;66:2263–73.

14. Katoh M. Networking of WNT, FGF, Notch, BMP, and Hedgehog signaling pathways during carcinogenesis. Stem Cell Rev. Humana Press Inc; 2007;3:30–8.

15. Schmitt M, Wilhelm OG, Reuning U, Krüger A, Harbeck N, Lengyel E, et al. The urokinase plasminogen activator system as a novel target for tumour therapy. Fibrinolysis and Proteolysis. 2000;14:114–32.

16. Ranson M, Andronicos NM. Plasminogen binding and cancer: promises and pitfalls. Front Biosci. 2003;8:s294–304.

17. Duffy MJ, Duggan C. The urokinase plasminogen activator system: a rich source of tumour markers for the individualised management of patients with cancer. Clin Biochem. 2004;37:541–8.

18. Weigelt B, Peterse JL, van't Veer LJ. Breast cancer metastasis: markers and models. Nature Publishing Group; 2005;5:591–602.

19. Croucher DR, Saunders DN, Lobov S, Ranson M. Revisiting the biological roles of PAI2 (SERPINB2) in cancer. 2008;8:535–45.

20. Matthews H, Ranson M, Tyndall JDA, Kelso MJ. Synthesis and preliminary evaluation of amiloride analogs as inhibitors of the urokinase-type plasminogen activator (uPA). Bioorg Med Chem Lett. 2011;21:6760–6.

21. Schmitt M, Harbeck N, Brünner N, Jänicke F, Meisner C, Mühlenweg B, et al. Cancer therapy trials employing level-of-evidence-1 disease forecast cancer biomarkers uPA and its inhibitor PAI-1. Expert Rev Mol Diagn. Taylor & Francis; 2011;11:617–34.

22. Lu P, Takai K, Weaver VM, Werb Z. Extracellular matrix degradation and remodeling in development and disease. Cold Spring Harb Perspect Biol. Cold Spring Harbor Lab; 2011;3:a005058–8.

23. Cox TR, Erler JT. Remodeling and homeostasis of the extracellular matrix: implications for fibrotic diseases and cancer. Disease Models and Mechanisms. The Company of Biologists Ltd; 2011;4:165–78.

24. Croucher DR, Saunders DN, Stillfried GE, Ranson M. A structural basis for differential cell signalling by PAI-1 and PAI-2 in breast cancer cells. Biochem J. Portland Press Limited; 2007;408:203–10.

25. Cochran BJ, Croucher DR, Lobov S, Saunders DN, Ranson M. Dependence on endocytic receptor binding via a minimal binding motif underlies the differential prognostic profiles of SerpinE1 and SerpinB2 in cancer. J Biol Chem. American Society for Biochemistry and Molecular Biology; 2011;286:24467–75.

26. Bacharach E, Itin A, Keshet E. In vivo patterns of expression of urokinase and its inhibitor PAI-1 suggest a concerted role in regulating physiological angiogenesis. Proc Natl Acad Sci USA. National Academy of Sciences; 1992;89:10686–90.

27. Dichek DA, Anderson J, Kelly AB, Hanson SR, Harker LA. Enhanced in vivo antithrombotic effects of endothelial cells expressing recombinant plasminogen activators transduced with retroviral vectors. Circulation. 1996;93:301–9.

28. Dolan JM, Sim FJ, Meng H, Kolega J. Endothelial cells express a unique transcriptional profile under very high wall shear stress known to induce expansive arterial remodeling. American Journal of Physiology - Cell Physiology. American Physiological Society; 2012;302:C1109–18.

29. Alexander RA, Prager GW, Mihaly-Bison J, Uhrin P, Sunzenauer S, Binder BR, et al. VEGF-induced endothelial cell migration requires urokinase receptor (uPAR)-dependent integrin redistribution. Cardiovascular Research. The Oxford University Press; 2012;94:125–35.

30. Prager GW, Poettler M, Unseld M, Zielinski CC. Angiogenesis in cancer: Anti-VEGF escape mechanisms. Transl Lung Cancer Res. 2012;1:14–25.

31. Raffaghello L, Vacca A, Pistoia V, Ribatti D. Cancer associated fibroblasts in hematological malignancies. Oncotarget. Impact Journals; 2015;6:2589–603.

32. Fidler IJ. The pathogenesis of cancer metastasis: the "seed and soil" hypothesis revisited. Nat. Rev. Cancer. 2003. pages 453–8.

33. Chiang AC, Massagué J. Molecular basis of metastasis. N Engl J Med. Massachusetts Medical Society; 2008;359:2814–23.

34. Engbring JA, Kleinman HK. The basement membrane matrix in malignancy. Bosman FT, Stamenkovic I, editors. J Pathol. John Wiley & Sons, Ltd; 2003;200:465–70.

35. Lee M, Fridman R, Mobashery S. Extracellular proteases as targets for treatment of cancer metastases. Chem Soc Rev. The Royal Society of Chemistry; 2004;33:401–9.

36. Andreasen PA, Kjoller L, Christensen L. The urokinase-type plasminogen activator system in cancer metastasis: a review. International Journal of .... 1997.

37. Lugassy G. Thrombosis and cancer. Thrombosis and Anti-Thrombotic Therapy. 2001.

38. Guarino M. Epithelial–mesenchymal transition and tumour invasion. The International Journal of Biochemistry & Cell Biology. 2007;39:2153–60.

39. Tjalma WA, Weyler JJ, Bogers JJ, Pollefliet C, Baay M, Goovaerts GC, et al. The importance of biological factors (bcl-2, bax, p53, PCNA, MI, HPV and angiogenesis) in invasive cervical cancer. Eur J Obstet Gynecol Reprod Biol. 2001;97:223–30.

40. Hanahan D, Coussens LM. Accessories to the crime: functions of cells recruited to the tumor microenvironment. Cancer Cell. Elsevier; 2012;21:309–22.

41. Whatcott C, Han H, Posner RG, Hoff Von DD. Tumor-stromal interactions in pancreatic cancer. Crit Rev Oncog. 2013;18:135–51.

42. Sugimoto H, Mundel TM, Kieran MW, Kalluri R. Identification of fibroblast heterogeneity in the tumor microenvironment. Cancer Biol Ther. 2006;5:1640–6.

43. Kalluri R, Zeisberg M. Fibroblasts in cancer. 2006;6:392–401.

44. Greaves M, Maley CC. Clonal evolution in cancer. Nature. 2012;481:306–13.

45. Kandoth C, McLellan MD, Vandin F, Ye K, Niu B, Lu C, et al. Mutational landscape and significance across 12 major cancer types. Nature. Nature Research; 2013;502:333–9.

46. Zhang M, Atkinson RL, Rosen JM. Selective targeting of radiation-resistant tumor-initiating cells. Proc Natl Acad Sci USA. National Acad Sciences; 2010;107:3522–7.

47. Cabrera MC, Hollingsworth RE, Hurt EM. Cancer stem cell plasticity and tumor hierarchy. World J Stem Cells. 2015;7:27–36.

48. Ding L, Ley TJ, Larson DE, Miller CA, Koboldt DC, Welch JS, et al. Clonal evolution in relapsed acute myeloid leukaemia revealed by whole-genome sequencing. Nature. Nature Research; 2012;481:506–10.

49. Vignot S, Frampton GM, Soria J-C, Yelensky R, Commo F, Brambilla C, et al. Next-generation sequencing reveals high concordance of recurrent somatic alterations between primary tumor and metastases from patients with non-small-cell lung cancer. J Clin Oncol. American Society of Clinical Oncology; 2013;31:2167–72.

50. HAYFLICK L, MOORHEAD PS. The serial cultivation of human diploid cell strains. Exp Cell Res. 1961;25:585–621.

51. Bonnet D, Dick JE. Human acute myeloid leukemia is organized as a hierarchy that originates from a primitive hematopoietic cell. Nat Med. Nature Publishing Group; 1997;3:730–7.

52. Singh SK, Hawkins C, Clarke ID, Squire JA, Bayani J, Hide T, et al. Identification of human brain tumour initiating cells. Nature. 2004;432:396–401.

53. Zhang S, Balch C, Chan MW, Lai H-C, Matei D, Schilder JM, et al. Identification and characterization of ovarian cancer-initiating cells from primary human tumors. Cancer Research. American Association for Cancer Research; 2008;68:4311–20.

54. Eramo A, Lotti F, Sette G, Pilozzi E, Biffoni M, Di Virgilio A, et al. Identification and expansion of the tumorigenic lung cancer stem cell population. Cell Death Differ. Nature Publishing Group; 2008;15:504–14.

55. Al-Hajj M, Wicha MS, Benito-Hernandez A, Morrison SJ, Clarke MF. Prospective identification of tumorigenic breast cancer cells. Proc Natl Acad Sci USA. National Acad Sciences; 2003;100:3983–8.

56. O'Brien CA, Pollett A, Gallinger S, Dick JE. A human colon cancer cell capable of initiating tumour growth in immunodeficient mice. Nature. 2007;445:106–10.

57. Collins AT, Berry PA, Hyde C, Stower MJ, Maitland NJ. Prospective identification of tumorigenic prostate cancer stem cells. Cancer Research. American Association for Cancer Research; 2005;65:10946–51.

58. Li C, Heidt DG, Dalerba P, Burant CF, Zhang L, Adsay V, et al. Identification of pancreatic cancer stem cells. Cancer Research. American Association for Cancer Research; 2007;67:1030–7.

59. Crawford J. Stem cell therapies: Hype or reality? Journal of the Royal College of Physicians of Edinburgh. 2008;38:221–3.

60. Gupta PB, Chaffer CL, Weinberg RA. Cancer stem cells: mirage or reality? Nat Med. 2009;15:1010–2.

61. Mani SA, Guo W, Liao M-J, Eaton EN, Ayyanan A, Zhou AY, et al. The epithelial-mesenchymal transition generates cells with properties of stem cells. Cell. 2008;133:704–15.

62. Creighton CJ, Li X, Landis M, Dixon JM, Neumeister VM, Sjolund A, et al. Residual breast cancers after conventional therapy display mesenchymal as well as tumor-initiating features. Proc Natl Acad Sci USA. National Acad Sciences; 2009;106:13820–5.

63. Yao D, Dai C, Peng S. Mechanism of the mesenchymal-epithelial transition and its relationship with metastatic tumor formation. Mol Cancer Res. Molecular Cancer Research; 2011;9:1608–20.

64. Bao B, Ahmad A, Azmi AS, Ali S, Sarkar FH. Overview of cancer stem cells (CSCs) and mechanisms of their regulation: implications for cancer therapy. Curr Protoc Pharmacol. Hoboken, NJ, USA: John Wiley & Sons, Inc; 2013;Chapter 14:Unit14.25–14.25.14.

65. Reya T, Morrison SJ, Clarke MF, Weissman IL. Stem cells, cancer, and cancer stem cells. Nature. 2001;414:105–11.

66. Yeung TM, Gandhi SC, Bodmer WF. Hypoxia and lineage specification of cell line-derived colorectal cancer stem cells. Proc Natl Acad Sci USA. National Acad Sciences; 2011;108:4382–7.

67. Vermeulen L, De Sousa E Melo F, van der Heijden M, Cameron K, de Jong JH, Borovski T, et al. Wnt activity defines colon cancer stem cells and is regulated by the microenvironment. Nat Cell Biol. 2010;12:468–76.

68. Zellmer VR, Zhang S. Evolving concepts of tumor heterogeneity. Cell Biosci. BioMed Central; 2014;4:69.

69. Yap TA, Gerlinger M, Futreal PA, Pusztai L, Swanton C. Intratumor heterogeneity: seeing the wood for the trees. Sci Transl Med. American Association for the Advancement of Science; 2012;4:127ps10–0.

70. Andreasen PA, Egelund R, Petersen HH. The plasminogen activation system in tumor growth, invasion, and metastasis. Cell Mol Life Sci. Birkhäuser Verlag; 2000;57:25–40.

71. Ulisse S, Baldini E, Sorrenti S, D'Armiento M. The Urokinase Plasminogen Activator System: A Target for Anti-Cancer Therapy. Curr Cancer Drug Targets. 2009;9:32–71.

72. Strickland S, Reich E, Sherman MI. Plasminogen activator in early embryogenesis: enzyme production by trophoblast and parietal endoderm. Cell. 1976;9:231–40.

73. Rittirsch D, Flierl MA, Ward PA. Harmful molecular mechanisms in sepsis. Nat Rev Immunol. 2008;8:776–87.

74. Amara U, Flierl MA, Rittirsch D, Klos A, Chen H, Acker B, et al. Molecular intercommunication between the complement and coagulation systems. J Immunol. American

Association of Immunologists; 2010;185:5628–36.

75. Reich E. Activation of plasminogen: A general mechanism for producing localized extracellular proteolysis. Molecular Basis of Biological Degradative Processes. 1978;:155–69.

76. Choong P. Urokinase Plasminogen Activator System: A Multifunction Role in Tumor Progression and Metastasis. 2003.

77. Béné MC, Castoldi G, Knapp W, Rigolin GM, Escribano L, Lemez P, et al. CD87 (urokinase-type plasminogen activator receptor), function and pathology in hematological disorders: a review. Leukemia. Nature Publishing Group; 2004;18:394–400.

78. McMahon B, Kwaan HC. The plasminogen activator system and cancer. Pathophysiol Haemost Thromb. Karger Publishers; 2008;36:184–94.

79. Corte MD, Vérez P, Rodríguez JC, Roibás A, Domínguez ML, Lamelas ML, et al. Tissue-type plasminogen activator (tPA) in breast cancer: relationship with clinicopathological parameters and prognostic significance. Breast Cancer Res Treat. Kluwer Academic Publishers; 2005;90:33–40.

80. Wiman B, Collen D. On the mechanism of the reaction between human alpha 2-antiplasmin and plasmin. Journal of Biological Chemistry. 1979;254:9291–7.

81. Schaller J, Gerber SS. The plasmin-antiplasmin system: structural and functional aspects. Cell Mol Life Sci. SP Birkhäuser Verlag Basel; 2011;68:785–801.

82. Ulisse S, Baldini E, Sorrenti S, D'Armiento M. The urokinase plasminogen activator system: a target for anti-cancer therapy. Curr Cancer Drug Targets. 2009;9:32–71.

83. Nykjaer A, Conese M, Christensen EI, Olson D, Cremona O, Gliemann J, et al. Recycling of the urokinase receptor upon internalization of the uPA:serpin complexes. The EMBO Journal. EMBO Press; 1997;16:2610–20.

84. Danø K, Behrendt N, Høyer-Hansen G, Johnsen M, Lund LR, Ploug M, et al. Plasminogen activation and cancer. Thromb Haemost. Schattauer Publishers; 2005;93:676–81.

85. Look MP, van Putten WLJ, Duffy MJ, Harbeck N, Christensen IJ, Thomssen C, et al. Pooled analysis of prognostic impact of urokinase-type plasminogen activator and its inhibitor PAI-1 in 8377 breast cancer patients. J Natl Cancer Inst. Oxford University Press; 2002;94:116–28.

86. Ranson M, Andronicos NM, O'Mullane MJ, Baker MS. Increased plasminogen binding is associated with metastatic breast cancer cells: differential expression of plasminogen binding proteins. Br J Cancer. Nature Publishing Group; 1998;77:1586–97.

87. Kwaan HC, McMahon B. The role of plasminogen-plasmin system in cancer. Cancer Treat Res. Boston, MA: Springer US; 2009;148:43–66.

88. Kjøller L. The urokinase plasminogen activator receptor in the regulation of the actin cytoskeleton and cell motility. Biol Chem. 2002;383:5–19.

89. Smith HW, Marshall CJ. Regulation of cell signalling by uPAR. Nat Rev Mol Cell Biol. 2010;11:23–36.

90. List K, Jensen ON, Bugge TH, Lund LR, Ploug M, Danø K, et al. Plasminogen-independent initiation of the pro-urokinase activation cascade in vivo. Activation of pro-urokinase by glandular kallikrein (mGK-6) in plasminogen-deficient mice. Biochemistry. American Chemical Society; 2000;39:508–15.

91. Behrendt N. The urokinase receptor (uPAR) and the uPAR-associated protein (uPARAP/Endo180): membrane proteins engaged in matrix turnover during tissue remodeling. Biol Chem. 2004;385:103–36.

92. Blasi F, Vassalli JD, Danø K. Urokinase-type plasminogen activator: proenzyme, receptor, and inhibitors. The Journal of Cell Biology. The Rockefeller University Press; 1987;104:801–4.

93. Grøndahl-Hansen J, Lund LR, Ralfkiaer E, Ottevanger V, Danø K. Urokinase- and tissue-type plasminogen activators in keratinocytes during wound reepithelialization in vivo. J Invest Dermatol. 1988;90:790–5.

94. Fisher JL, Mackie PS, Howard ML, Zhou H, Choong PF. The expression of the urokinase plasminogen activator system in metastatic murine osteosarcoma: an in vivo mouse model. Clinical Cancer Research. 2001;7:1654–60.

95. Zeslawska E, Jacob U, Schweinitz A, Coombs G, Bode W, Madison E. Crystals of urokinase type plasminogen activator complexes reveal the binding mode of peptidomimetic inhibitors. J Mol Biol. 2003;328:109–18.

96. Duffy MJ, Duggan C, Mulcahy HE, McDermott EW, O'Higgins NJ. Urokinase plasminogen activator: a prognostic marker in breast cancer including patients with axillary node-negative disease. Clin Chem. American Association for Clinical Chemistry; 1998;44:1177–83.

97. Offersen BV, Pfeiffer P, Andreasen P, Overgaard J. Urokinase plasminogen activator and plasminogen activator inhibitor type-1 in nonsmall-cell lung cancer: relation to prognosis and angiogenesis. Lung Cancer. 2007;56:43–50.

98. Dear AE, Medcalf RL. The cellular and molecular biology of plasminogen activator inhibitor type-2. Fibrinolysis. 1995;9:321–30.

99. Zhang L, Zhao ZS, Ru GQ, Ma J. Correlative studies on uPA mRNA and uPAR mRNA expression with vascular endothelial growth factor, microvessel density, progression and survival time of …. World journal of gastroenterology. 2006;12:3970–6.

100. Takeuchi Y, Nakao A, Harada A, Nonami T, Fukatsu T, Takagi H. Expression of plasminogen activators and their inhibitors in human pancreatic carcinoma: immunohistochemical study. Am J Gastroenterol. 1993;88:1928–33.

101. Berger DH. Plasmin/Plasminogen System in Colorectal Cancer. World J Surg. 2002;26:767–71.

102. DeLano WL. The PyMOL Molecular Graphics System. (2002). 2002.

103. Blasi F, Carmeliet P. uPAR: a versatile signalling orchestrator. Nat Rev Mol Cell Biol. 2002;3:932–43.

104. D'Alessio S, Blasi F. The urokinase receptor as an entertainer of signal transduction. Front Biosci (Landmark Ed). 2009;14:4575–87.

105. Binder BR, Mihaly J. The plasminogen activator inhibitor "paradox" in cancer. Immunol Lett. 2008;118:116–24.

106. Hadler-Olsen E, Wetting HL, Ravuri C, Omair A, Rikardsen O, Svineng G, et al. Organ specific regulation of tumour invasiveness and gelatinolytic activity at the invasive front. European Journal of Cancer. 2011;47:305–15.

107. Cai Z, Li YF, Liu FY, FENG YL, HOU JH, ZHAO MQ. The expression and clinical significance of uPA and PAI-1 in epithelial ovarian cancer. Chin J Cancer. 2007.

108. Steiner E, Pollow K, Hasenclever D, Schormann W. Role of urokinase-type plasminogen activator (uPA) and plasminogen activator inhibitor type 1 (PAI-1) for prognosis in endometrial cancer. Gynecologic .... 2008.

109. Bhuvarahamurthy V, Schroeder J, Kristiansen G, Roigas J, Denkert C, Johannsen M, et al. Differential gene expression of urokinase-type plasminogen activator and its receptor in human renal cell carcinoma. Oncology Reports. 2005;14:777–82.

110. Gavrilov D, Kenzior O, Evans M, Calaluce R, Folk WR. Expression of urokinase plasminogen activator and receptor in conjunction with the ets family and AP-1 complex transcription factors in high grade prostate cancers. Eur J Cancer. 2001;37:1033–40.

111. Hundsdorfer B, Zeilhofer H-F, Bock KP, Dettmar P, Schmitt M, Horch H-H. [The prognostic importance of urinase type plasminogen activators (uPA) and plasminogen activator inhibitors (PAI-1) in the primary resection of oral squamous cell carcinoma]. Mund Kiefer Gesichtschir. Springer-Verlag; 2004;8:173–9.

112. Nomiya T, Nemoto K, Miyachi H, Fujimoto K, Takahashi C, Takeda K, et al. Significance of plasminogen-activation system in the formation of macroscopic types and invasion in esophageal carcinoma. Anticancer Res. 2002;22:2913–6.

113. Riisbro R, Christensen IJ, Nielsen HJ, Brünner N, Nilbert M, Fernebro E. Preoperative plasma soluble urokinase plasminogen activator receptor as a prognostic marker in rectal cancer patients. An EORTC-Receptor and Biomarker Group collaboration. Int J Biol Markers. 2005;20:93–102.

114. Zhou Q, Liang L-J, Peng B-G, Zhen Y-Y. [Expression and clinical significance of coagulate and fibrolysis factors in tissue and plasma from hepatocellular carcinoma patients]. Ai Zheng. 2006;25:1433–8.

115. Almasi CE, Høyer-Hansen G, Christensen IJ, Danø K, Pappot H. Prognostic impact of liberated domain I of the urokinase plasminogen activator receptor in squamous cell lung cancer tissue. Lung Cancer. Elsevier; 2005;48:349–55.

116. Almasi CE, Christensen IJ, Høyer-Hansen G, Danø K, Pappot H, Dienemann H, et al. Urokinase receptor forms in serum from non-small cell lung cancer patients: relation to prognosis. Lung Cancer. Elsevier; 2011;74:510–5.

117. K W, P SÂN, M B. Serum level of Urokinase Plasminogen Activator (uPA) Correlates with the Survival of Patients with Pancreatic Ductal Adenocarcinoma (PDAC). Pancreat Disord Ther. 2015;05:1–6.

118. Cantero D, Friess H, Deflorin J, Zimmermann A, Bründler MA, Riesle E, et al. Enhanced expression of urokinase plasminogen activator and its receptor in pancreatic carcinoma. Br J Cancer. Nature Publishing Group; 1997;75:388–95.

119. Graf M, Reif S, Hecht K, Pelka Fleischer R, Pfister K, Schmetzer H. High expression of urokinase plasminogen activator receptor (UPA - R) in acute myeloid leukemia (AML) is associated with worse prognosis. American Journal of Hematology. Wiley Subscription Services, Inc., A Wiley Company; 2005;79:26–35.

120. Silverman GA, Bird PI, Carrell RW, Church FC, Coughlin PB, Gettins PG, et al. The serpins are an expanding superfamily of structurally similar but functionally diverse proteins. Evolution, mechanism of inhibition, novel functions, and a revised nomenclature. Journal of Biological Chemistry. American Society for Biochemistry and Molecular Biology; 2001;276:33296.

121. Irving JA, Pike RN, Lesk AM, Whisstock JC. Phylogeny of the serpin superfamily: implications of patterns of amino acid conservation for structure and function. Genome Res. 2000;10:1845–64.

122. Levin EG, Santell L. Conversion of the active to latent plasminogen activator inhibitor from human endothelial cells. Blood. 1987;70:1090–8.

123. Astedt B, Lindoff C, Lecander I. Significance of the plasminogen activator inhibitor of placental type (PAI-2) in pregnancy. Semin Thromb Hemost. 1998;24:431–5.

124. Al-Ejeh F, Croucher D, Ranson M. Kinetic analysis of plasminogen activator inhibitor type-2: urokinase complex formation and subsequent internalisation by carcinoma cell lines. Exp Cell Res. 2004;297:259–71.

125. Lindahl TL, Sigurdardottir O, Wiman B. Stability of plasminogen activator inhibitor 1 (PAI-1). Thromb Haemost. 1989;62:748–51.

126. Risse BC, Brown H, Lavker RM, Pearson JM, Baker MS, Ginsburg D, et al. Differentiating cells of murine stratified squamous epithelia constitutively express plasminogen activator inhibitor type 2 (PAI-2). Histochem Cell Biol. 1998;110:559–69.

127. McMahon GA, Petitclerc E, Stefansson S, Smith E, Wong MK, Westrick RJ, et al. Plasminogen activator inhibitor-1 regulates tumor growth and angiogenesis. Journal of Biological Chemistry. American Society for Biochemistry and Molecular Biology; 2001;276:33964–8.

128. Stefansson S, McMahon GA, Petitclerc E, Lawrence DA. Plasminogen activator inhibitor-1 in tumor growth, angiogenesis and vascular remodeling. Curr Pharm Des. 2003;9:1545–64.

129. Vine KL, Lobov S, Indira Chandran V, Harris NLE, Ranson M. Improved pharmacokinetic and biodistribution properties of the selective urokinase inhibitor PAI-2 (SerpinB2) by site-specific PEGylation: implications for drug delivery. Pharm Res. Springer US; 2015;32:1045–54.

130. Vine KL, Indira Chandran V, Locke JM, Matesic L, Lee J, Skropeta D, et al. Targeting urokinase and the transferrin receptor with novel, anti-mitotic N-alkylisatin cytotoxin conjugates causes selective cancer cell death and reduces tumor growth. Curr Cancer Drug Targets. 2012;12:64–73.

131. Indira Chandran V, Matesic L, Locke JM, Skropeta D, Ranson M, Vine KL. Anti-cancer activity of an acid-labile N-alkylisatin conjugate targeting the transferrin receptor. Cancer Lett. 2012;316:151–6.

132. Gettins PGW. Serpin Structure, Mechanism, and Function. American Chemical Society; 2002. pages 4751–803.

133. Gooptu B, Lomas DA. Conformational pathology of the serpins: themes, variations, and therapeutic strategies. Annu Rev Biochem. Annual Reviews; 2009;78:147–76.

134. Kruithof EK, Tran-Thang C, Gudinchet A, Hauert J, Nicoloso G, Genton C, et al. Fibrinolysis in pregnancy: a study of plasminogen activator inhibitors. Blood. 1987;69:460–6.

135. Genton C, Kruithof EK, Schleuning WD. Phorbol ester induces the biosynthesis of glycosylated and nonglycosylated plasminogen activator inhibitor 2 in high excess over urokinase-type plasminogen activator in human U-937 lymphoma cells. The Journal of Cell Biology. The Rockefeller University Press; 1987;104:705–12.

136. Wohlwend A, Belin D, Vassalli JD. Plasminogen activator-specific inhibitors produced by human monocytes/macrophages. J Exp Med. The Rockefeller University Press; 1987;165:320–39.

137. Jensen PH, Lorand L, Ebbesen P, Gliemann J. Type-2 plasminogen-activator inhibitor is a substrate for trophoblast transglutaminase and factor XIIIa. Transglutaminase-catalyzed cross-linking to cellular and extracellular structures. Eur J Biochem. 1993;214:141–6.

138. Darnell GA, Schroder WA, Gardner J, Harrich D, Yu H, Medcalf RL, et al. SerpinB2 is an inducible host factor involved in enhancing HIV-1 transcription and replication. Journal of Biological Chemistry. American Society for Biochemistry and Molecular Biology; 2006;281:31348–58.

139. Tonnetti L, Netzel-Arnett S, Darnell GA, Hayes T, Buzza MS, Anglin IE, et al. SerpinB2 Protection of Retinoblastoma Protein from Calpain Enhances Tumor Cell Survival. Cancer Research. American Association for Cancer Research; 2008;68:5648–57.

140. Fan D, Takawale A, Lee J, Kassiri Z. Cardiac fibroblasts, fibrosis and extracellular matrix remodeling in heart disease. Fibrogenesis Tissue Repair. BioMed Central Ltd; 2012;5:15.

141. Boncela J, Przygodzka P, Papiewska-Pajak I, Wyroba E, Cierniewski CS. Association of plasminogen activator inhibitor type 2 (PAI-2) with proteasome within endothelial cells activated with inflammatory stimuli. J Biol Chem. American Society for Biochemistry and

Molecular Biology; 2011;286:43164–71.

142. Gan H, Newman GW, Remold HG. Plasminogen activator inhibitor type 2 prevents programmed cell death of human macrophages infected with Mycobacterium avium, serovar 4. J Immunol. American Association of Immunologists; 1995;155:1304–15.

143. Wilczynska M, Lobov S, Ohlsson PI, Ny T. A redox-sensitive loop regulates plasminogen activator inhibitor type 2 (PAI-2) polymerization. The EMBO Journal. EMBO Press; 2003;22:1753–61.

144. Heijne Von G, Liljeström P, Mikus P, Andersson H, Ny T. The efficiency of the uncleaved secretion signal in the plasminogen activator inhibitor type 2 protein can be enhanced by point mutations that increase its hydrophobicity. Journal of Biological Chemistry. American Society for Biochemistry and Molecular Biology; 1991;266:15240–3.

145. Medcalf RL, Stasinopoulos SJ. The undecided serpin. The ins and outs of plasminogen activator inhibitor type 2. FEBS J. 2005;272:4858–67.

146. Kruithof EK, Baker MS, Bunn CL. Biological and clinical aspects of plasminogen activator inhibitor type 2. Blood. 1995;86:4007–24.

147. Johnson TA, Buzza MS, Riley EAU, Antalis TM. Plasminogen Activator Inhibitor Type-2 (PAI-2)/SerpinB2: A Unique Multifunctional Serpin. The Serpin Family. Cham: Springer International Publishing; 2015. pages 107–26.

148. Udofa EA, Stringer BW, Gade P, Mahony D, Buzza MS, Kalvakolanu DV, et al. The Transcription Factor C/EBP-β Mediates Constitutive and LPS-Inducible Transcription of Murine SerpinB2. Spilianakis CB, editor. PLoS ONE. Public Library of Science; 2013;8:e57855.

149. Harrop SJ, Jankova L, Coles M, Jardine D, Whittaker JS, Gould AR, et al. The crystal structure of plasminogen activator inhibitor 2 at 2.0 Å resolution: implications for serpin function. Structure. 1999;7:43–54.

150. Eaton A, Nagy E, Pacault M, Fauconnier J, Bäck M. Cysteinyl leukotriene signaling through perinuclear CysLT1 receptors on vascular smooth muscle cells transduces nuclear calcium signaling and alterations of gene expression. J Mol Med. Springer-Verlag; 2012;90:1223–31.

151. Schroder WA, Le TTT, Major L, Street S, Gardner J, Lambley E, et al. A physiological function of inflammation-associated SerpinB2 is regulation of adaptive immunity. J Immunol. American Association of Immunologists; 2010;184:2663–70.

152. Antalis TM, La Linn M, Donnan K, Mateo L, Gardner J, Dickinson JL, et al. The serine proteinase inhibitor (serpin) plasminogen activation inhibitor type 2 protects against viral cytopathic effects by constitutive interferon alpha/beta priming. J Exp Med. The Rockefeller University Press; 1998;187:1799–811.

153. Krishnamurti C, Wahl LM, Alving BM. Stimulation of plasminogen activator inhibitor activity in human monocytes infected with dengue virus. Am J Trop Med Hyg. 1989;40:102–7.

154. Tyner JW, Uchida O, Kajiwara N, Kim EY, Patel AC, O'Sullivan MP, et al. CCL5-CCR5

interaction provides antiapoptotic signals for macrophage survival during viral infection. Nat Med. Nature Publishing Group; 2005;11:1180–7.

155. Montemurro P, Barbuti G, Dundon WG, Del Giudice G, Rappuoli R, Colucci M, et al. Helicobacter pylori neutrophil-activating protein stimulates tissue factor and plasminogen activator inhibitor-2 production by human blood mononuclear cells. J Infect Dis. Oxford University Press; 2001;183:1055–62.

156. Mirlashari MR, Høiby EA, Holst J, Lyberg T. Outer Membrane Vesicles from Neisseria meningitidis: Effects on Tissue Factor and Plasminogen Activator Inhibitor-2 Production in Human Monocytes. Thromb Res. 2001;102:375–80.

157. Losick VP, Isberg RR. NF-kappaB translocation prevents host cell death after low-dose challenge by Legionella pneumophila. J Exp Med. Rockefeller Univ Press; 2006;203:2177–89.

158. Schroder WA, Gardner J, Le TT, Duke M, BURKE ML, JONES MK, et al. SerpinB2 deficiency modulates Th1/Th2 responses after schistosome infection. Parasite Immunology. Blackwell Publishing Ltd; 2010;32:764–8.

159. Woodruff PG, Boushey HA, Dolganov GM, Barker CS, Yang YH, Donnelly S, et al. Genome-wide profiling identifies epithelial cell genes associated with asthma and with treatment response to corticosteroids. Proc Natl Acad Sci USA. National Acad Sciences; 2007;104:15858–63.

160. Palafox-Sanchez CA, Mercado MV-D, Orozco-Barocio G, la Torre IG-D, Torres-Carrillo N, Torres-Carrillo NM, et al. A Functional Ser413/Ser413 PAI-2 Polymorphism Is Associated With Susceptibility and Damage Index Score in Systemic Lupus Erythematosus. CLIN APPL THROMB HEMOST. SAGE Publications; 2008;15:233–8.

161. Major LD, Partridge TS, Gardner J, Kent SJ, de Rose R, Suhrbier A, et al. Induction of SerpinB2 and Th1/Th2 Modulation by SerpinB2 during Lentiviral Infections In Vivo. Ahuja SK, editor. PLoS ONE. Public Library of Science; 2013;8:e57343.

162. Cousin E, Medcalf RL, Bergonzelli GE, Kruithof EKO. Regulatory elements involved in constitutive and phorbol ester-inducible expression of the plasminogen activator inhibitor type 2 gene promoter. Nucleic Acids Res. Oxford University Press; 1991;19:3881–6.

163. Antalis TM, Costelloe E, Muddiman J, Ogbourne S, Donnan K. Regulation of the plasminogen activator inhibitor type-2 gene in monocytes: localization of an upstream transcriptional silencer. Blood. 1996;88:3686–97.

164. Stringer B, Udofa EA, Antalis TM. Regulation of the human plasminogen activator inhibitor type 2 gene: cooperation of an upstream silencer and transactivator. J Biol Chem. American Society for Biochemistry and Molecular Biology; 2012;287:10579–89.

165. Ameyar M, Wisniewska M, Weitzman JB. A role for AP-1 in apoptosis: the case for and against. Biochimie. 2003;85:747–52.

166. Shaulian E, Karin M. AP-1 in cell proliferation and survival. Oncogene. Nature Publishing Group; 2001;20:2390–400.

167. Schroder WA, Major LD, Le TT, Gardner J, Sweet MJ, Janciauskiene S, et al. Tumor cell-expressed SerpinB2 is present on microparticles and inhibits metastasis. Cancer Med. 2014;3:500–13.

168. van den Akker J, van Weert A, Afink G, Bakker ENTP, van der Pol E, Böing AN, et al. Transglutaminase 2 is secreted from smooth muscle cells by transamidation-dependent microparticle formation. Amino Acids. Springer Vienna; 2012;42:961–73.

169. Boncela J, Przygodzka P, Wyroba E, Papiewska-Pajak I, Cierniewski CS. Secretion of SerpinB2 from endothelial cells activated with inflammatory stimuli. Exp Cell Res. 2013;319:1213–9.

170. Bard-Chapeau EA, Jeyakani J, Kok CH, Muller J, Chua BQ, Gunaratne J, et al. Ecotopic viral integration site 1 (EVI1) regulates multiple cellular processes important for cancer and is a synergistic partner for FOS protein in invasive tumors. Proc Natl Acad Sci USA. National Acad Sciences; 2012;109:2168–73.

171. Glass C, Wuertzer C, Cui X, Bi Y, Davuluri R, Xiao Y-Y, et al. Global Identification of EVI1 Target Genes in Acute Myeloid Leukemia. Tse W, editor. PLoS ONE. Public Library of Science; 2013;8:e67134.

172. Yu H, Maurer F, Medcalf RL. Plasminogen activator inhibitor type 2: a regulator of monocyte proliferation and differentiation. Blood. American Society of Hematology; 2002;99:2810–8.

173. Copple BL, Bai S, Burgoon LD, Moon JO. Hypoxia-inducible factor-1α regulates the expression of genes in hypoxic hepatic stellate cells important for collagen deposition and angiogenesis. Liver Int. Blackwell Publishing Ltd; 2011;31:230–44.

174. Leung KC, Byatt JA, Stephens RW. Poly-D-lysine dependent inactivation of tissue plasminogen activator by a class PAI-2 inhibitor (minactivin). Thromb Res. Pergamon; 1987;46:767–77.

175. Schwartz BS. Differential inhibition of soluble and cell surface receptor-bound single-chain urokinase by plasminogen activator inhibitor type 2. A potential regulatory mechanism. Journal of Biological Chemistry. 1994;269:8319–23.

176. Cochran BJ, Gunawardhana LP, Vine KL, Lee JA, Lobov S, Ranson M. The CD-loop of PAI-2 (SERPINB2) is redundant in the targeting, inhibition and clearance of cell surface uPA activity. BMC Biotechnol. 2009;9:43.

177. Croucher DR. Defining the mechanism and functional consequences of PAI-2-mediated uPA/uPAR endocytosis. University of Wollongong Thesis Collection. 2006.

178. Nakamura M, Konno H, Tanaka T, Maruo Y, Nishino N, Aoki K, et al. Possible role of plasminogen activator inhibitor 2 in the prevention of the metastasis of gastric cancer tissues. Thromb Res. 1992;65:709–19.

179. Umeda T, Eguchi Y, Okino K, Kodama M, Hattori T. Cellular localization of urokinase-type plasminogen activator, its inhibitors, and their mRNAs in breast cancer tissues. Journal of Pathology. 1997;183:388–97.

180. Nozaki S, Endo Y, Kawashiri S, Nakagawa K, Yamamoto E, Yonemura Y, et al.

Immunohistochemical localization of a urokinase-type plasminogen activator system in squamous cell carcinoma of the oral cavity: association with mode of invasion and lymph node metastasis. Oral Oncol. 1998;34:58–62.

181. Jensen PH, Lorand L, Ebbesen P, Gliemann J. Type-2 plasminogen-activator inhibitor is a substrate for trophoblast transglutaminase and factor XIIIa. Transglutaminase-catalyzed cross-linking to cellular and extracellular structures. Eur J Biochem. 1993;214:141–6.

182. Delhase M, Kim S-Y, Lee H, Naiki-Ito A, Chen Y, Ahn E-R, et al. TANK-binding kinase 1 (TBK1) controls cell survival through PAI-2/serpinB2 and transglutaminase 2. Proc Natl Acad Sci USA. National Acad Sciences; 2012;109:E177–86.

183. Dickinson JL, Norris BJ, Jensen PH. The CD interhelical domain of the serpin plasminogen activator inhibitor-type 2 is required for protection from TNF- induced apoptosis. Cell death and .... 1998.

184. Shafren DR, Gardner J, Mann VH, Antalis TM, SUHRBIER A. Picornavirus receptor down-regulation by plasminogen activator inhibitor type 2. J Virol. American Society for Microbiology (ASM); 1999;73:7193–8.

185. Lavker RM, Risse B, Brown H, Jensen PJ, Ginsburg D, Pearson J, et al. Localization of Plasminogen Activator Inhibitor Type 2 (PAI-2) in Hair and Nail: Implications for Terminal Differentiation. Journal of Investigative Dermatology. 1998;110:917–22.

186. Chuang S-Y, Yang C-H, Chou C-C, Chiang Y-P, Chuang T-H, Hsu L-C. TLR-induced PAI-2 expression suppresses IL-1β processing via increasing autophagy and NLRP3 degradation. Proc Natl Acad Sci USA. National Acad Sciences; 2013;110:16079–84.

187. Sharon R, Abramovitz R, Miskin R. Plasminogen mRNA induction in the mouse brain after kainate excitation: codistribution with plasminogen activator inhibitor-2 (PAI-2) mRNA. Molecular Brain Research. 2002;104:170–5.

188. Oliverio S, Amendola A, Di Sano F, Farrace MG, Fesus L, Nemes Z, et al. Tissue transglutaminase-dependent posttranslational modification of the retinoblastoma gene product in promonocytic cells undergoing apoptosis. Mol Cell Biol. American Society for Microbiology (ASM); 1997;17:6040–8.

189. Greten FR, Arkan MC, Bollrath J, Hsu L-C, Goode J, Miething C, et al. NF-κB Is a Negative Regulator of IL-1β Secretion as Revealed by Genetic and Pharmacological Inhibition of IKKβ. Cell. 2007;130:918–31.

190. Hsu L-C, Ali SR, McGillivray S, Tseng P-H, Mariathasan S, Humke EW, et al. A NOD2-NALP1 complex mediates caspase-1-dependent IL-1beta secretion in response to Bacillus anthracis infection and muramyl dipeptide. Proc Natl Acad Sci USA. National Acad Sciences; 2008;105:7803–8.

191. Zhao A, Yang Z, Sun R, Grinchuk V, Netzel-Arnett S, Anglin IE, et al. SerpinB2 is critical to Th2 immunity against enteric nematode infection. J Immunol. American Association of Immunologists; 2013;190:5779–87.

192. Shea-Donohue T, Zhao A, Antalis TM. SerpinB2 mediated regulation of macrophage function during enteric infection. Gut Microbes. Taylor & Francis; 2014;5:254–8.

193. Vyhlidal CA, Riffel AK, Dai H, Rosenwasser LJ, Jones BL. Detecting gene expression in buccal mucosa in subjects with asthma versus subjects without asthma. Pediatr Allergy Immunol. 2013;24:138–43.

194. Poole A, Urbanek C, Eng C, Schageman J, Jacobson S, O'Connor BP, et al. Dissecting childhood asthma with nasal transcriptomics distinguishes subphenotypes of disease. J Allergy Clin Immunol. 2014;133:670–8.e12.

195. Ong W-Y, Ng MP-E, Loke S-Y, Jin S, Wu Y-J, Tanaka K, et al. Comprehensive Gene Expression Profiling Reveals Synergistic Functional Networks in Cerebral Vessels after Hypertension or Hypercholesterolemia. Arai K, editor. PLoS ONE. Public Library of Science; 2013;8:e68335.

196. Soler Palacios B, Estrada Capetillo L, Izquierdo E, Criado G, Nieto C, Municio C, et al. Macrophages from the synovium of active rheumatoid arthritis exhibit an activin A-dependent pro-inflammatory profile. J Pathol. John Wiley & Sons, Ltd; 2015;235:515–26.

197. Zhang S-J, Zou M, Lu L, Lau D, Ditzel DAW, Delucinge-Vivier C, et al. Nuclear Calcium Signaling Controls Expression of a Large Gene Pool: Identification of a Gene Program for Acquired Neuroprotection Induced by Synaptic Activity. Orr H, editor. PLoS Genet. Public Library of Science; 2009;5:e1000604.

198. Lee JA, Yerbury JJ, Farrawell N, Shearer RF, Constantinescu P, Hatters DM, et al. SerpinB2 (PAI-2) Modulates Proteostasis via Binding Misfolded Proteins and Promotion of Cytoprotective Inclusion Formation. Kampinga HH, editor. PLoS ONE. Public Library of Science; 2015;10:e0130136.

199. Katic J, Loers G, Kleene R, Karl N, Schmidt C, Buck F, et al. Interaction of the cell adhesion molecule CHL1 with vitronectin, integrins, and the plasminogen activator inhibitor-2 promotes CHL1-induced neurite outgrowth and neuronal migration. J Neurosci. Society for Neuroscience; 2014;34:14606–23.

200. Książek K, Mikuła Pietrasik J, Catar R, Dworacki G, Winckiewicz M, Frydrychowicz M, et al. Oxidative stress - dependent increase in ICAM - 1 expression promotes adhesion of colorectal and pancreatic cancers to the senescent peritoneal mesothelium. Int J Cancer. Wiley Subscription Services, Inc., A Wiley Company; 2010;127:293–303.

201. Tarcic G, Avraham R, Pines G, Amit I, Shay T, Lu Y, et al. EGR1 and the ERK-ERF axis drive mammary cell migration in response to EGF. FASEB J. Federation of American Societies for Experimental Biology; 2012;26:1582–92.

202. Lijnen HR, Frederix L, Scroyen I. Deficiency of plasminogen activator inhibitor-2 impairs nutritionally induced murine adipose tissue development. J Thromb Haemost. Blackwell Publishing Ltd; 2007;5:2259–65.

203. Dougherty KM, Pearson JM, Yang AY, Westrick RJ, Baker MS, Ginsburg D. The plasminogen activator inhibitor-2 gene is not required for normal murine development or survival. Proc Natl

Acad Sci USA. 1999;96:686–91.

204. Siefert SA, Chabasse C, Mukhopadhyay S, Hoofnagle MH, Strickland DK, Sarkar R, et al. Enhanced venous thrombus resolution in plasminogen activator inhibitor type-2 deficient mice. Journal of Thrombosis and Haemostasis. 2014;12:1706–16.

205. Kovacheva M, Zepp M, Berger SM, Berger MR. Sustained conditional knockdown reveals intracellular bone sialoprotein as essential for breast cancer skeletal metastasis. Oncotarget. Impact Journals; 2014;5:5510–22.

206. Chambers SK, Gertz RE, Ivins CM, Kacinski BM. The significance of urokinase-type plasminogen activator, its inhibitors, and its receptor in ascites of patients with epithelial ovarian cancer. Cancer. Wiley Subscription Services, Inc., A Wiley Company; 1995;75:1627–33.

207. Chambers SK, Ivins CM, Carcangiu ML. Expression of plasminogen activator inhibitor-2 in epithelial ovarian cancer: A favorable prognostic factor related to the actions of CSF-1. Int J Cancer. Wiley Subscription Services, Inc., A Wiley Company; 1997;74:571–5.

208. Ashton JM, Balys M, Neering SJ, Hassane DC, Cowley G, Root DE, et al. Gene sets identified with oncogene cooperativity analysis regulate in vivo growth and survival of leukemia stem cells. Cell Stem Cell. 2012;11:359–72.

209. Subimerb C, Wongkham C, Khuntikeo N, Leelayuwat C, McGrath MS, Wongkham S. Transcriptional profiles of peripheral blood leukocytes identify patients with cholangiocarcinoma and predict outcome. Asian Pac J Cancer Prev. 2014;15:4217–24.

210. Rushworth LK, Kidger AM, Delavaine L, Stewart G, van Schelven S, Davidson J, et al. Dual-specificity phosphatase 5 regulates nuclear ERK activity and suppresses skin cancer by inhibiting mutant Harvey-Ras (HRasQ61L)-driven SerpinB2 expression. Proc Natl Acad Sci USA. National Acad Sciences; 2014;111:18267–72.

211. Nordengren J, Fredstorp Lidebring M, Bendahl P-O, Brünner N, Fernö M, Högberg T, et al. High tumor tissue concentration of plasminogen activator inhibitor 2 (PAI-2) is an independent marker for shorter progression-free survival in patients with early stage endometrial cancer. Int J Cancer. 2002;97:379–85.

212. Zhou H-M, Bolon I, Nichols A, Wohlwend A, Vassalli J-D. Overexpression of Plasminogen Activator Inhibitor Type 2 in Basal Keratinocytes Enhances Papilloma Formation in Transgenic Mice. Cancer Research. American Association for Cancer Research; 2001;61:970–6.

213. Valiente M, Obenauf AC, Jin X, Chen Q, Zhang XH-F, Lee DJ, et al. Serpins promote cancer cell survival and vascular co-option in brain metastasis. Cell. 2014;156:1002–16.

214. Shimizu T, Sato K, Suzuki T, Tachibana K, Takeda K. Induction of plasminogen activator inhibitor-2 is associated with suppression of invasive activity in TPA-mediated differentiation of human prostate cancer cells. Biochem Biophys Res Commun. 2003;309:267–71.

215. Praus M, Wauterickx K, Collen D, Gerard RD. Reduction of tumor cell migration and metastasis by adenoviral gene transfer of plasminogen activator inhibitors. Gene Ther. Nature

Publishing Group; 1999;6:227–36.

216. Geiger M, Wahlmüller F, Furtmüller M. The serpin family: Proteins with multiple functions in health and disease. Geiger M, Wahlmüller F, Furtmüller M, editors. The Serpin Family: Proteins with Multiple Functions in Health and Disease. Cham: Springer International Publishing; 2015. pages 1–329.

217. Meng S, Tripathy D, Shete S, Ashfaq R, Saboorian H, Haley B, et al. uPAR and HER-2 gene status in individual breast cancer cells from blood and tissues. Proc Natl Acad Sci USA. National Acad Sciences; 2006;103:17361–5.

218. Harbeck N, Schmitt M, Paepke S, Allgayer H, Kates RE. Tumor-Associated Proteolytic Factors uPA and PAI-1: Critical Appraisal of Their Clinical Relevance in Breast Cancer and Their Integration into Decision-Support Algorithms. Critical Reviews in Clinical Laboratory Sciences. 2007;44:179–201.

219. Harbeck N, Thomssen C. A new look at node-negative breast cancer. The Oncologist. AlphaMed Press; 2010;15 Suppl 5:29–38.

220. Robert C, Bolon I, Gazzeri S, Veyrenc S, Brambilla C, Brambilla E. Expression of plasminogen activator inhibitors 1 and 2 in lung cancer and their role in tumor progression. Clinical Cancer Research. American Association for Cancer Research; 1999;5:2094–102.

221. Foekens JA, Peters HA, Look MP, Portengen H, Schmitt M, Kramer MD, et al. The urokinase system of plasminogen activation and prognosis in 2780 breast cancer patients. Cancer Research. American Association for Cancer Research; 2000;60:636–43.

222. Kuhn W, Pache L, Schmalfeldt B, Dettmar P, Schmitt M, Jänicke F, et al. Urokinase (uPA) and PAI-1 Predict Survival in Advanced Ovarian Cancer Patients (FIGO III) after Radical Surgery and Platinum-Based Chemotherapy. Gynecologic Oncology. Academic Press; 1994;55:401–9.

223. Tecimer C, Doering DL, Goldsmith LJ, Meyer JS, Abdulhay G, Wittliff JL. Clinical relevance of urokinase - type plasminogen activator, its receptor and inhibitor type 1 in ovarian cancer. International Journal of Gynecological Cancer. Blackwell Science Inc; 2000;10:372–81.

224. Van Veldhuizen PJ, Sadasivan R. Urokinase-type plasminogen activator expression in human prostate carcinomas. The American journal …. 1996.

225. Miyake H, Hara I, Yamanaka K, Arakawa S, Kamidono S. Elevation of urokinase-type plasminogen activator and its receptor densities as new predictors of disease progression and prognosis in men with prostate cancer. Int J Oncol. 1999;14:535–41.

226. Miyake H, Hara I, Yamanaka K, Gohji K, Arakawa S, Kamidono S. Elevation of serum levels of urokinase-type plasminogen activator and its receptor is associated with disease progression and prognosis in patients with prostate cancer. Prostate. 1999;39:123–9.

227. Li Y, Rizvi SMA, Ranson M, Allen BJ. 213Bi-PAI2 conjugate selectively induces apoptosis in PC3 metastatic prostate cancer cell line and shows anti-cancer activity in a xenograft animal model. Br J Cancer. Nature Publishing Group; 2002;86:1197–203.

228. Parolini S, Flagiello D, Cinquetti A, Gozzi R, Cristini S, Cappiello J, et al. Up-regulation of urokinase-type plasminogen activator in squamous cell carcinoma of human larynx. Br J Cancer. Nature Publishing Group; 1996;74:1168–74.

229. Leto G, Tumminello FM, Gebbia N, Bazan V, Tomasino RM, Dardanoni G, et al. Differential expression levels of urokinase-type plasminogen activator and cathepsin D in locally advanced laryngeal squamous cell carcinoma: clinical implications. Int J Biol Markers. 2001;16:245–9.

230. Hundsdorfer B, Zeilhofer H-F, Bock KP, Dettmar P, Schmitt M, Horch H-H. [Comparison of urokinase type plasminogen activators (uPA) and plasminogen activator inhibitors (PAI-1) in primary resection of oral squamous cell carcinoma]. Mund Kiefer Gesichtschir. Springer-Verlag; 2004;8:180–90.

231. Tang WH, Friess H, Kekis PB, Martignoni ME, Fukuda A, Roggo A, et al. Serine proteinase activation in esophageal cancer. Anticancer Res. 2001;21:2249–58.

232. Shiomi H, Eguchi Y, Tani T, Kodama M, Hattori T. Cellular distribution and clinical value of urokinase-type plasminogen activator, its receptor, and plasminogen activator inhibitor-2 in esophageal squamous cell carcinoma. Am J Pathol. 2000;156:567–75.

233. Harvey SR, Hurd TC, Markus G, Martinick MI, Penetrante RM, Tan D, et al. Evaluation of urinary plasminogen activator, its receptor, matrix metalloproteinase-9, and von Willebrand factor in pancreatic cancer. Clinical Cancer Research. 2003;9:4935–43.

234. Takeuchi Y, Nakao A, Harada A, Nonami T, Fukatsu T, Takagi H. Expression of plasminogen activators and their inhibitors in human pancreatic carcinoma: immunohistochemical study. Am J Gastroenterol. 1993;88:1928–33.

235. Sawai H, Okada Y, Funahashi H, Matsuo Y, Takahashi H, Takeyama H, et al. Interleukin-1alpha enhances the aggressive behavior of pancreatic cancer cells by regulating the alpha6beta1-integrin and urokinase plasminogen activator receptor expression. BMC Cell Biol. BioMed Central; 2006;7:8.

236. Tan X, Egami H, Nozawa F, Abe M, Baba H. Analysis of the invasion-metastasis mechanism in pancreatic cancer: involvement of plasmin(ogen) cascade proteins in the invasion of pancreatic cancer cells. Int J Oncol. 2006;28:369–74.

237. He Y, Liu X-D, Chen Z-Y, Zhu J, Xiong Y, Li K, et al. Interaction between cancer cells and stromal fibroblasts is required for activation of the uPAR-uPA-MMP-2 cascade in pancreatic cancer metastasis. Clinical Cancer Research. Clinical Cancer Research; 2007;13:3115–24.

238. Smith R, Xue A, Gill A, Scarlett C, Saxby A, Clarkson A, et al. High expression of plasminogen activator inhibitor-2 (PAI-2) is a predictor of improved survival in patients with pancreatic adenocarcinoma. World J Surg. Springer-Verlag; 2007;31:493–502–discussion503.

239. Zhi X, Lamperska K, Golusinski P, Schork NJ. Gene expression analysis of head and neck squamous cell carcinoma survival and recurrence. Oncotarget. 2015.

240. Y T, K M, K O, S M, M H, S N, et al. Protein expression profile related to cisplatin resistance in bladder cancer cell lines detected by two-dimensional gel electrophoresis. Biomed Res.

2014;36:253–61.

241. King KE, Reddi DM, Ponnamperuma RM, Gerdes M, Weinberg WC. Dysregulated ΔNp63α negatively regulates the maspin promoter in keratinocytes via blocking endogenous p73 binding. Mol Carcinog. 2014;53:698–710.

242. Li W, Ai N, Wang S, Bhattacharya N, Vrbanac V, Collins M, et al. GRK3 is essential for metastatic cells and promotes prostate tumor progression. Proc Natl Acad Sci USA. National Acad Sciences; 2014;111:1521–6.

243. Suwa D, Konno H, Tanaka T, Urano T. Intraperitoneal infusion of recombinant plasminogen activator inhibitor type 2 induced apoptosis in implanted human colon cancer and inhibited its growth and liver metastasis. Anticancer Res. 2008;28:693–8.

244. Mueller BM, Yu YB, Laug WE. Overexpression of plasminogen activator inhibitor 2 in human melanoma cells inhibits spontaneous metastasis in scid/scid mice. Proc Natl Acad Sci USA. National Academy of Sciences; 1995;92:205–9.

245. Zou Z, Zeng F, Xu W, Wang C, Ke Z, Wang QJ, et al. PKD2 and PKD3 promote prostate cancer cell invasion by modulating NF-κB- and HDAC1-mediated expression and activation of uPA. Journal of Cell Science. The Company of Biologists Ltd; 2012;125:4800–11.

246. De Wever O, Mareel M. Role of tissue stroma in cancer cell invasion. Bosman FT, Stamenkovic I, editors. J Pathol. 2003;200:429–47.

247. Mareel M, Madani I. Tumour-associated host cells participating at invasion and metastasis : targets for therapy? Acta Chir Belg. 2006;106:635–40.

248. Turner N, Grose R. Fibroblast growth factor signalling: From development to cancer. Nature Reviews Cancer. 2010;10:116–29.

249. Cox TR, Erler JT. Fibrosis, cancer and the premetastatic niche. http://dxdoiorg/102217/bmt1436. Future Medicine Ltd London, UK; 2014;3:453–5.

250. Bissell MJ, Hall HG, Parry G. How does the extracellular matrix direct gene expression? J Theor Biol. 1982;99:31–68.

251. Schultz GS, Davidson JM, Kirsner RS, Bornstein P, Herman IM. Dynamic reciprocity in the wound microenvironment. Wound Repair Regen. Blackwell Publishing Inc; 2011;19:134–48.

252. Bornstein P, McPherson J. Synthesis and secretion of structural macromolecules by endothelial cells in culture. … of the endothelial cell; 1982.

253. Roskelley CD, Bissell MJ. Dynamic reciprocity revisited: a continuous, bidirectional flow of information between cells and the extracellular matrix regulates mammary epithelial cell function. Biochem Cell Biol. 1995;73:391–7.

254. Di Lullo GA, Sweeney SM, Korkko J, Ala-Kokko L, San Antonio JD. Mapping the ligand-binding sites and disease-associated mutations on the most abundant protein in the human, type I collagen. Journal of Biological Chemistry. American Society for Biochemistry and Molecular

Biology; 2002;277:4223–31.

255. Chung HJ, Steplewski A, Chung KY, Uitto J, Fertala A. Collagen fibril formation. A new target to limit fibrosis. Journal of Biological Chemistry. American Society for Biochemistry and Molecular Biology; 2008;283:25879–86.

256. Kadler KE, Holmes DF, Trotter JA, Chapman JA. Collagen fibril formation. Biochem J. Portland Press Ltd; 1996;316 (Pt 1):1–11.

257. Bhattacharjee A, Bansal M. Collagen structure: the Madras triple helix and the current scenario. IUBMB Life. Informa Healthcare; 2005;57:161–72.

258. Bekhouche M, Colige A. The procollagen N-proteinases ADAMTS2, 3 and 14 in pathophysiology. Matrix Biol. 2015;44-46:46–53.

259. Steplewski A, Fertala A. Inhibition of collagen fibril formation. Fibrogenesis Tissue Repair. BioMed Central Ltd; 2012;5:S29.

260. López B, González A, Hermida N, Valencia F, de Teresa E, Díez J. Role of lysyl oxidase in myocardial fibrosis: from basic science to clinical aspects. Am J Physiol Heart Circ Physiol. American Physiological Society; 2010;299:H1–9.

261. Demou ZN, Awad M, McKee T, Perentes JY, Wang X, Munn LL, et al. Lack of telopeptides in fibrillar collagen I promotes the invasion of a metastatic breast tumor cell line. Cancer Research. American Association for Cancer Research; 2005;65:5674–82.

262. Netti PA, Berk DA, Swartz MA, Grodzinsky AJ, Jain RK. Role of extracellular matrix assembly in interstitial transport in solid tumors. Cancer Research. 2000;60:2497–503.

263. Pandol S, Edderkaoui M, Gukovsky I, Lugea A, Gukovskaya A. Desmoplasia of Pancreatic Ductal Adenocarcinoma. Clinical Gastroenterology and Hepatology. 2009;7:S44–7.

264. Cox TR, Bird D, Baker A-M, Barker HE, Ho MW-Y, Lang G, et al. LOX-mediated collagen crosslinking is responsible for fibrosis-enhanced metastasis. Cancer Research. American Association for Cancer Research; 2013;73:1721–32.

265. Brightman AO, Rajwa BP, Sturgis JE, McCallister ME, Robinson JP, Voytik-Harbin SL. Time-lapse confocal reflection microscopy of collagen fibrillogenesis and extracellular matrix assembly in vitro. Biopolymers. John Wiley & Sons, Inc; 2000;54:222–34.

266. Zeltz C, Orgel J, Gullberg D. Molecular composition and function of integrin-based collagen glues-introducing COLINBRIs. Biochim Biophys Acta. 2014;1840:2533–48.

267. Frantz C, Stewart KM, Weaver VM. The extracellular matrix at a glance. Journal of Cell Science. The Company of Biologists Ltd; 2010;123:4195–200.

268. Lucero HA, Kagan HM. Lysyl oxidase: an oxidative enzyme and effector of cell function. Cell Mol Life Sci. 2006;63:2304–16.

269. Sethi A, Mao W, Wordinger RJ, Clark AF. Transforming growth factor-beta induces

extracellular matrix protein cross-linking lysyl oxidase (LOX) genes in human trabecular meshwork cells. Invest Ophthalmol Vis Sci. The Association for Research in Vision and Ophthalmology; 2011;52:5240–50.

270. Welge-Lüßen U, May CA, Lütjen-Drecoll E. Induction of Tissue Transglutaminase in the Trabecular Meshwork by TGF-β1 and TGF-β2. Invest Ophthalmol Vis Sci. The Association for Research in Vision and Ophthalmology; 2000;41:2229–38.

271. Tovar-Vidales T, Roque R, Clark AF, Wordinger RJ. Tissue transglutaminase expression and activity in normal and glaucomatous human trabecular meshwork cells and tissues. Invest Ophthalmol Vis Sci. The Association for Research in Vision and Ophthalmology; 2008;49:622–8.

272. Tiger C-F. Cellular Interactions with Extracellular Matrix During Development and in Muscle Disease. Acta Universitatis Upsaliensis; 2002.

273. Kadler KE, Hill A, Canty-Laird EG. Collagen fibrillogenesis: fibronectin, integrins, and minor collagens as organizers and nucleators. Curr Opin Cell Biol. 2008;20:495–501.

274. Suarez E, Syed F, Rasgado TA, Walmsley A, Mandal P, Bayat A. Skin equivalent tensional force alters keloid fibroblast behavior and phenotype. Wound Repair Regen. 2014;22:557–68.

275. Aycock RS, Seyer JM. Collagens of Normal and Cirrhotic Human Liver. Connective Tissue Research. Taylor & Francis; 2009;23:19–31.

276. Imamura T, Iguchi H, Manabe T, Ohshio G, Yoshimura T, Wang Z-H, et al. Quantitative Analysis of Collagen and Collagen Subtypes I, III, and V in Human Pancreatic Cancer, Tumor-Associated Chronic Pancreatitis, and Alcoholic Chronic Pancreatitis. Pancreas. 1995;11:357.

277. Barsky SH, Rao CN, Grotendorst GR, Liotta LA. Increased content of Type V Collagen in desmoplasia of human breast carcinoma. Am J Pathol. American Society for Investigative Pathology; 1982;108:276–83.

278. Provenzano PP, Inman DR, Eliceiri KW, Knittel JG, Yan L, Rueden CT, et al. Collagen density promotes mammary tumor initiation and progression. BMC Med. BioMed Central; 2008;6:11.

279. Provenzano PP, Eliceiri KW, Campbell JM, Inman DR, White JG, Keely PJ. Collagen reorganization at the tumor-stromal interface facilitates local invasion. BMC Med. BioMed Central; 2006;4:38.

280. Merika EE, Syrigos KN, Saif MW. Desmoplasia in Pancreatic Cancer. Can We Fight It? Gastroenterology Research and Practice. Hindawi Publishing Corporation; 2012;2012:1–10.

281. Sethi A, Wordinger RJ, Clark AF. Focus on molecules: lysyl oxidase. Exp Eye Res. 2012;104:97–8.

282. Miller BW, Morton JP, Pinese M, Saturno G, Jamieson NB, McGhee E, et al. Targeting the LOX/hypoxia axis reverses many of the features that make pancreatic cancer deadly: inhibition of LOX abrogates metastasis and enhances drug efficacy. EMBO Molecular Medicine. EMBO

Press; 2015;7:1063–76.

283. El-Haibi CP, Bell GW, Zhang J, Collmann AY, Wood D, Scherber CM, et al. Critical role for lysyl oxidase in mesenchymal stem cell-driven breast cancer malignancy. Proc Natl Acad Sci USA. National Acad Sciences; 2012;109:17460–5.

284. Sivakumar P, Gupta S, Sarkar S, Sen S. Upregulation of lysyl oxidase and MMPs during cardiac remodeling in human dilated cardiomyopathy. Mol Cell Biochem. 2008;307:159–67.

285. Ueno T, Kaname S, Takaichi K, Nagase M, Tojo A, Onozato ML, et al. LOX-1, an oxidized low-density lipoprotein receptor, was upregulated in the kidneys of chronic renal failure rats. Hypertens Res. 2003;26:117–22.

286. Wong CC-L, Tse AP-W, Huang Y-P, Zhu Y-T, Chiu DK-C, Lai RK-H, et al. Lysyl oxidase-like 2 is critical to tumor microenvironment and metastatic niche formation in hepatocellular carcinoma. Hepatology. 2014;60:1645–58.

287. Ishida Y, Kanno Z, Soma K. Occlusal Hypofunction Induces Atrophic Changes in Rat Gingiva. 2009. pages 1015–22.

288. Hornstra IK, Birge S, Starcher B, Bailey AJ, Mecham RP, Shapiro SD. Lysyl oxidase is required for vascular and diaphragmatic development in mice. Journal of Biological Chemistry. American Society for Biochemistry and Molecular Biology; 2003;278:14387–93.

289. Royce PM, Camakaris J, Danks DM. Reduced lysyl oxidase activity in skin fibroblasts from patients with Menkes' syndrome. Biochem J. Portland Press Ltd; 1980;192:579–86.

290. Kaler SG, Gallo LK, Proud VK, Percy AK, Mark Y, Segal NA, et al. Occipital horn syndrome and a mild Menkes phenotype associated with splice site mutations at the MNK locus. Nature Publishing Group; 1994;8:195–202.

291. Friedl P, Wolf K. Tube travel: the role of proteases in individual and collective cancer cell invasion. Cancer Research. American Association for Cancer Research; 2008;68:7247–9.

292. Offenberg H, Brünner N, Mansilla F, Orntoft Torben F, Birkenkamp-Demtroder K. TIMP-1 expression in human colorectal cancer is associated with TGF-B1, LOXL2, INHBA1, TNF-AIP6 and TIMP-2 transcript profiles. Mol Oncol. 2008;2:233–40.

293. Baker AM, Bird D, Lang G, Cox TR, Erler JT. Lysyl oxidase enzymatic function increases stiffness to drive colorectal cancer progression through FAK. Oncogene. Nature Publishing Group; 2013;32:1863–8.

294. Barry-Hamilton V, Spangler R, Marshall D, McCauley S, Rodriguez HM, Oyasu M, et al. Allosteric inhibition of lysyl oxidase-like-2 impedes the development of a pathologic microenvironment. Nat Med. 2010;16:1009–17.

295. Melino G, Candi E, Steinert PM. Transglutaminases in cell death. Methods Enzymol; 1999.

296. Facchiano F, Facchiano A, Facchiano AM. The role of transglutaminase-2 and its substrates in human diseases. Front Biosci. 2006.

297. Klöck C, Diraimondo TR, Khosla C. Role of transglutaminase 2 in celiac disease pathogenesis. Semin Immunopathol. 2012;34:513–22.

298. Griffin M, Casadio R, Bergamini CM. Transglutaminases: nature's biological glues. Biochem J. Portland Press Limited; 2002;368:377–96.

299. Telci D, Wang Z, Li X, Verderio EAM, Humphries MJ, Baccarini M, et al. Fibronectin-tissue transglutaminase matrix rescues RGD-impaired cell adhesion through syndecan-4 and beta1 integrin co-signaling. Journal of Biological Chemistry. American Society for Biochemistry and Molecular Biology; 2008;283:20937–47.

300. Hansson T, Ulfgren AK, Lindroos E, DannÆus A, Dahlbom I, Klareskog L. Transforming Growth Factor - β (TGF - β) and Tissue Transglutaminase Expression in the Small Intestine in Children with Coeliac Disease. Scandinavian Journal of Immunology. Blackwell Science Ltd; 2002;56:530–7.

301. Sulic A-M, Kurppa K, Rauhavirta T, Kaukinen K, Lindfors K. Transglutaminase as a therapeutic target for celiac disease. Expert Opin Ther Targets. Informa Healthcare; 2015;19:335–48.

302. Telci D, Collighan RJ, Basaga H, Griffin M. Increased TG2 expression can result in induction of transforming growth factor beta1, causing increased synthesis and deposition of matrix proteins, which can be regulated by nitric oxide. J Biol Chem. American Society for Biochemistry and Molecular Biology; 2009;284:29547–58.

303. Gundemir S, Colak G, Tucholski J, Johnson GVW. Transglutaminase 2: A molecular Swiss army knife. Biochimica et Biophysica Acta (BBA) - Molecular Cell Research. 2012;1823:406–19.

304. Ritchie H, Lawrie LC, Crombie PW, Mosesson MW, Booth NA. Cross-linking of plasminogen activator inhibitor 2 and alpha 2-antiplasmin to fibrin(ogen). Journal of Biological Chemistry. American Society for Biochemistry and Molecular Biology; 2000;275:24915–20.

305. Lee JA, Cochran BJ, Lobov S, Ranson M. Forty years later and the role of plasminogen activator inhibitor type 2/SERPINB2 is still an enigma. Semin Thromb Hemost. © Thieme Medical Publishers; 2011;37:395–407.

306. Oji V, Oji ME, Adamini N, Walker T, Aufenvenne K, Raghunath M, et al. Plasminogen activator inhibitor-2 is expressed in different types of congenital ichthyosis: in vivo evidence for its cross-linking into the cornified cell envelope by transglutaminase-1. Br J Dermatol. Blackwell Publishing Ltd; 2006;154:860–7.

307. Bechtel MJ, Schaefer BM, Kramer MD. Plasminogen activator inhibitor type - 2 in the lesional epidermis of lupus erythematosus. British Journal of Dermatology. Blackwell Publishing Ltd; 1996;134:411–9.

308. Monk M, Holding C. Human embryonic genes re-expressed in cancer cells. Oncogene. Nature Publishing Group; 2001;20:8085–91.

309. Ma Y, Zhang P, Wang F, Yang J, Yang Z, Qin H. The relationship between early embryo development and tumourigenesis. J Cell Mol Med. 2010;14:2697–701.

310. Murray MJ, Lessey BA. Embryo implantation and tumor metastasis: common pathways of invasion and angiogenesis. Semin Reprod Endocrinol. 1999;17:275–90.

311. Preis M, Korc M. Kinase signaling pathways as targets for intervention in pancreatic cancer. Cancer Biol Ther. 2010;9:754–63.

312. Morris JP, Wang SC, Hebrok M. KRAS, Hedgehog, Wnt and the twisted developmental biology of pancreatic ductal adenocarcinoma. 2010;10:683–95.

313. Hruban RH, Goggins M, Parsons J, Kern SE. Progression model for pancreatic cancer. Clinical Cancer Research. American Association for Cancer Research; 2000;6:2969–72.

314. Hu ZY, Liu YX, Liu K, Byrne S, Ny T, Feng Q, et al. Expression of tissue type and urokinase type plasminogen activators as well as plasminogen activator inhibitor type-1 and type-2 in human and rhesus monkey placenta. J Anat. Wiley-Blackwell; 1999;194 (Pt 2):183–95.

315. Reith A, Booth NA, Moore NR, Cruickshank DJ, Bennett B. Plasminogen activator inhibitors (PAI-1 and PAI-2) in normal pregnancies, pre-eclampsia and hydatidiform mole. Br J Obstet Gynaecol. 1993;100:370–4.

316. Zini JM, Murray SC, Graham CH, Lala PK, Karikó K, Barnathan ES, et al. Characterization of urokinase receptor expression by human placental trophoblasts. Blood. 1992;79:2917–29.

317. MacPhee D. Focal adhesion kinase is a key mediator of human trophoblast development. Laboratory Investigation. 2001;81:1469–83.

318. Zemskov EA, Janiak A, Hang J, Waghray A. The role of tissue transglutaminase in cell-matrix interactions. Front Biosci. 2006.

319. Verma A, Mehta K. Tissue transglutaminase-mediated chemoresistance in cancer cells. Drug Resistance Updates. 2007;10:144–51.

320. Nurminskaya MV, Belkin AM. Cellular functions of tissue transglutaminase. … review of cell and molecular biology. 2012.

321. Robinson NJ, Glazier JD, Greenwood SL, Baker PN, Aplin JD. Tissue transglutaminase expression and activity in placenta. Placenta. 2006;27:148–57.

322. Knöfler M. Critical growth factors and signalling pathways controlling human trophoblast invasion. Int J Dev Biol. UPV/EHU Press; 2010;54:269–80.

323. Chau DYS, Collighan RJ, Verderio EAM, Addy VL, Griffin M. The cellular response to transglutaminase-cross-linked collagen. Biomaterials. 2005;26:6518–29.

324. Orban JM, Wilson LB, Kofroth JA, Kurdi El MS, Maul TM, Vorp DA. Crosslinking of collagen gels by transglutaminase. Journal of Biomedical Materials Research Part A. Wiley Subscription Services, Inc., A Wiley Company; 2004;68A:756–62.

325. Fortunati D, Chau DYS, Wang Z, Collighan RJ, Griffin M. Cross-linking of collagen I by tissue transglutaminase provides a promising biomaterial for promoting bone healing. Amino Acids.

Springer Vienna; 2014;46:1751–61.

326. Kumar S, Mehta K. Tissue transglutaminase, inflammation, and cancer: how intimate is the relationship? Amino Acids. Springer Vienna; 2013;44:81–8.

327. Verma A, Guha S, Diagaradjane P, Kunnumakkara AB, Sanguino AM, Lopez-Berestein G, et al. Therapeutic significance of elevated tissue transglutaminase expression in pancreatic cancer. Clinical Cancer Research. American Association for Cancer Research; 2008;14:2476–83.

328. Mehta K, Fok J, Miller FR, Koul D, Sahin AA. Prognostic significance of tissue transglutaminase in drug resistant and metastatic breast cancer. Clinical Cancer Research. American Association for Cancer Research; 2004;10:8068–76.

329. Herman JF, Mangala LS, Mehta K. Implications of increased tissue transglutaminase (TG2) expression in drug-resistant breast cancer (MCF-7) cells. Oncogene. Nature Publishing Group; 2006;25:3049–58.

330. Assi J, Srivastava G, Matta A, Chang MC, Walfish PG, Ralhan R. Transglutaminase 2 overexpression in tumor stroma identifies invasive ductal carcinomas of breast at high risk of recurrence. Mehta K, editor. PLoS ONE. Public Library of Science; 2013;8:e74437.

331. Verma A, Wang H, Manavathi B, Fok JY, Mann AP, Kumar R, et al. Increased expression of tissue transglutaminase in pancreatic ductal adenocarcinoma and its implications in drug resistance and metastasis. Cancer Research. American Association for Cancer Research; 2006;66:10525–33.

332. Balklava Z, Verderio E, Collighan R, Gross S, Adams J, Griffin M. Analysis of tissue transglutaminase function in the migration of Swiss 3T3 fibroblasts: the active-state conformation of the enzyme does not affect cell motility but is important for its secretion. Journal of Biological Chemistry. American Society for Biochemistry and Molecular Biology; 2002;277:16567–75.

333. Alberts B, Johnson A, Lewis J, Raff M, Roberts K, Walter P. Fibroblasts and Their Transformations: The Connective-Tissue Cell Family. Tissue Engineering Part A. Garland Science; 2002;19:1416–23.

334. Abercrombie M. Fibroblasts. J Clin Pathol Suppl (R Coll Pathol). BMJ Group; 1978;12:1–6.

335. Fries KM, Blieden T, Looney RJ, Sempowski GD, Silvera MR, Willis RA, et al. Evidence of fibroblast heterogeneity and the role of fibroblast subpopulations in fibrosis. Clin Immunol Immunopathol. 1994;72:283–92.

336. Rodemann HP, Müller GA. Characterization of human renal fibroblasts in health and disease: II. In vitro growth, differentiation, and collagen synthesis of fibroblasts from kidneys with interstitial fibrosis. Am J Kidney Dis. 1991;17:684–6.

337. Rollins BJ, Stier P, Ernst T, Wong GG. The human homolog of the JE gene encodes a monocyte secretory protein. Mol Cell Biol. American Society for Microbiology (ASM); 1989;9:4687–95.

338. Bhowmick NA, Neilson EG, Moses HL. Stromal fibroblasts in cancer initiation and progression. Nature. Nature Publishing Group; 2004;432:332–7.

339. Strieter RM, Wiggins R, Phan SH, Wharram BL, Showell HJ, Remick DG, et al. Monocyte chemotactic protein gene expression by cytokine-treated human fibroblasts and endothelial cells. Biochem Biophys Res Commun. 1989;162:694–700.

340. Ravikanth M, Soujanya P, Manjunath K, Saraswathi TR, Ramachandran CR. Heterogenecity of fibroblasts. Journal of Oral and Maxillofacial Pathology : JOMFP. Medknow Publications; 2011;15:247–50.

341. Lekic PC, Pender N, McCulloch CA. Is fibroblast heterogeneity relevant to the health, diseases, and treatments of periodontal tissues? Crit Rev Oral Biol Med. 1997;8:253–68.

342. Wu Y, Zhou BP. Inflammation: a driving force speeds cancer metastasis. Cell Cycle. NIH Public Access; 2009;8:3267–73.

343. Desmoulière A, Guyot C, Gabbiani G. The stroma reaction myofibroblast: a key player in the control of tumor cell behavior. Int J Dev Biol. 2004;48:509–17.

344. Gaggioli C, Hooper S, Hidalgo-Carcedo C, Grosse R, Marshall JF, Harrington K, et al. Fibroblast-led collective invasion of carcinoma cells with differing roles for RhoGTPases in leading and following cells. Nat Cell Biol. 2007;9:1392–400.

345. Sullivan DE, Ferris M, Nguyen H, Abboud E, Brody AR. TNF-alpha induces TGF-beta1 expression in lung fibroblasts at the transcriptional level via AP-1 activation. J Cell Mol Med. Blackwell Publishing Ltd; 2009;13:1866–76.

346. Lijnen HR, Van Hoef B, Lupu F, Moons L, Carmeliet P, Collen D. Function of the plasminogen/plasmin and matrix metalloproteinase systems after vascular injury in mice with targeted inactivation of fibrinolytic system genes. Arterioscler Thromb Vasc Biol. Lippincott Williams & Wilkins; 1998;18:1035–45.

347. Hildenbrand R, Jansen C, Wolf G, Böhme B, Berger S, Minckwitz von G, et al. Transforming growth factor-beta stimulates urokinase expression in tumor-associated macrophages of the breast. Lab Invest. 1998;78:59–71.

348. Farina AR, Coppa A, Tiberio A, Tacconelli A, Turco A, Colletta G, et al. Transforming growth factor-beta1 enhances the invasiveness of human MDA-MB-231 breast cancer cells by up-regulating urokinase activity. Int J Cancer. 1998;75:721–30.

349. Santibanez JF. Transforming growth factor-Beta and urokinase-type plasminogen activator: dangerous partners in tumorigenesis-implications in skin cancer. ISRN Dermatol. Hindawi Publishing Corporation; 2013;2013:597927–26.

350. Weaver VM, Petersen OW, Wang F, Larabell CA, Briand P, Damsky C, et al. Reversion of the malignant phenotype of human breast cells in three- dimensional culture and in vivo by integrin blocking antibodies. J Cell Biol. Rockefeller Univ Press; 1997;137:231–45.

351. Wiseman BS, Werb Z. Stromal effects on mammary gland development and breast cancer.

Science. American Association for the Advancement of Science; 2002;296:1046–9.

352. Rhim AD, Oberstein PE, Thomas DH, Mirek ET, Palermo CF, Sastra SA, et al. Stromal Elements Act to Restrain, Rather Than Support, Pancreatic Ductal Adenocarcinoma. Cancer Cell. Elsevier Inc; 2014;25:735–47.

353. Gore J, Korc M. Pancreatic cancer stroma: friend or foe? Cancer Cell. Elsevier; 2014;25:711–2.

354. Nyga A, Cheema U, Loizidou M. 3D tumour models: novel in vitro approaches to cancer studies. J Cell Commun Signal. Springer Netherlands; 2011;5:239–48.

355. Bissell MJ, Radisky D. Putting tumours in context. 2001;1:46–54.

356. Cukierman E, Pankov R, Yamada KM. Cell interactions with three-dimensional matrices. Curr Opin Cell Biol. 2002;14:633–9.

357. Erler JT, Weaver VM. Three-dimensional context regulation of metastasis. Clin Exp Metastasis. 2009;26:35–49.

358. Herrmann D, Conway JRW, Vennin C, Magenau A, Hughes WE, Morton JP, et al. Three-dimensional cancer models mimic cell-matrix interactions in the tumour microenvironment. Carcinogenesis. Oxford University Press; 2014;35:1671–9.

359. Timpson P, Mcghee EJ, Erami Z, Nobis M, Quinn JA, Edward M, et al. Organotypic Collagen I Assay: A Malleable Platform to Assess Cell Behaviour in a 3-Dimensional Context. JoVE. 2011;:e3089–9.

360. Mcghee EJ, Morton JP, Kriegsheim von A, Schwarz JP, Karim SA, Carragher NO, et al. FLIM-FRET imaging in vivo reveals 3D-environment spatially regulates RhoGTPase activity during cancer cell invasion. Small GTPases. Taylor & Francis; 2011;2:239–44.

361. Linder S, Aepfelbacher M. Podosomes: adhesion hot-spots of invasive cells. Trends in Cell Biology. 2003;13:376–85.

362. Geraldo S, Simon A, Elkhatib N, Louvard D, Fetler L, Vignjevic DM. Do cancer cells have distinct adhesions in 3D collagen matrices and in vivo? European Journal of Cell Biology. 2012;91:930–7.

363. Edmondson R, Broglie JJ, Adcock AF, Yang L. Three-dimensional cell culture systems and their applications in drug discovery and cell-based biosensors. Assay Drug Dev Technol. Mary Ann Liebert, Inc. 140 Huguenot Street, 3rd Floor New Rochelle, NY 10801 USA; 2014;12:207–18.

364. Trédan O, Galmarini CM, Patel K, Tannock IF. Drug resistance and the solid tumor microenvironment. J Natl Cancer Inst. Oxford University Press; 2007;99:1441–54.

365. Sodek KL, Ringuette MJ, Brown TJ. Compact spheroid formation by ovarian cancer cells is associated with contractile behavior and an invasive phenotype. Int J Cancer. Wiley Subscription Services, Inc., A Wiley Company; 2009;124:2060–70.

366. Yip D, Cho CH. A multicellular 3D heterospheroid model of liver tumor and stromal cells in collagen gel for anti-cancer drug testing. Biochem Biophys Res Commun. 2013;433:327–32.

367. Talukdar S, Kundu SC. A Non - Mulberry Silk Fibroin Protein Based 3D In Vitro Tumor Model for Evaluation of Anticancer Drug Activity. Advanced Functional Materials. WILEY - VCH Verlag; 2012;22:4778–88.

368. Longati P, Jia X, Eimer J, Wagman A, Witt M-R, Rehnmark S, et al. 3D pancreatic carcinoma spheroids induce a matrix-rich, chemoresistant phenotype offering a better model for drug testing. BMC Cancer. BioMed Central; 2013;13:95.

369. Doyle AD, Wang FW, Matsumoto K, Yamada KM. One-dimensional topography underlies three-dimensional fibrillar cell migration. The Journal of Cell Biology. Rockefeller Univ Press; 2009;184:481–90.

370. Suri S, Schmidt CE. Cell-Laden Hydrogel Constructs of Hyaluronic Acid, Collagen, and Laminin for Neural Tissue Engineering. http://dxdoiorg/101089/tentea20090381. Mary Ann Liebert, Inc. 140 Huguenot Street, 3rd Floor New Rochelle, NY 10801 USA; 2010;16:1703–16.

371. Schmeichel KL, Bissell MJ. Modeling tissue-specific signaling and organ function in three dimensions. Journal of Cell Science. The Company of Biologists Ltd; 2003;116:2377–88.

372. Conway JRW, Carragher NO, Timpson P. Developments in preclinical cancer imaging: innovating the discovery of therapeutics. Nature Publishing Group; 2014;14:314–28.

373. Ranson M, Tian Z, Andronicos NM, Rizvi S, Allen BJ. In vitro cytotoxicity of bismuth-213 (213Bi)-labeled-plasminogen activator inhibitor type 2 (alpha-PAI-2) on human breast cancer cells. Breast Cancer Res Treat. 2002;71:149–59.

374. Ramezani A, Hawley RG. Overview of the HIV - 1 Lentiviral Vector System. Hoboken, NJ, USA: John Wiley & Sons, Inc; 2002. pages 16.21.1–16.21.15.

375. Shearer RF, Saunders DN. Experimental design for stable genetic manipulation in mammalian cell lines: lentivirus and alternatives. Genes Cells. 2015;20:1–10.

376. Mautino MR. Lentiviral Vectors for Gene Therapy of HIV-1 Infection. Current gene therapy. Bentham Science Publishers; 2002;2:23–43.

377. Gilbert JR, Wong-Staal F. HIV-2 and SIV vector systems. Somat Cell Mol Genet. 2001;26:83–98.

378. Cockrell AS, Kafri T. Gene delivery by lentivirus vectors. Mol Biotechnol. 2007;36:184–204.

379. Goff SP. Intracellular trafficking of retroviral genomes during the early phase of infection: viral exploitation of cellular pathways. The Journal of Gene Medicine. John Wiley & Sons, Ltd; 2001;3:517–28.

380. Schlegel R, Tralka TS, Willingham MC, Pastan I. Inhibition of VSV binding and infectivity by phosphatidylserine: Is phosphatidylserine a VSV-binding site? Cell. 1983;32:639–46.

381. Akkina RK, Walton RM, Chen ML, Li QX, Planelles V, Chen IS. High-efficiency gene transfer into CD34+ cells with a human immunodeficiency virus type 1-based retroviral vector pseudotyped with vesicular stomatitis virus envelope glycoprotein G. J Virol. American Society for Microbiology (ASM); 1996;70:2581–5.

382. Naldini L, Blömer U, Gage FH, Trono D, Verma IM. Efficient transfer, integration, and sustained long-term expression of the transgene in adult rat brains injected with a lentiviral vector. Proc Natl Acad Sci USA. National Academy of Sciences; 1996;93:11382–8.

383. Reiser J, Harmison G, Kluepfel-Stahl S, Brady RO, Karlsson S, Schubert M. Transduction of nondividing cells using pseudotyped defective high-titer HIV type 1 particles. Proc Natl Acad Sci USA. National Academy of Sciences; 1996;93:15266–71.

384. Tolstoshev P. Retroviral-mediated gene therapy--safety considerations and preclinical studies. Bone Marrow Transplant. 1992;9 Suppl 1:148–50.

385. Sinn PL, Sauter SL, McCray PB. Gene Therapy Progress and Prospects: Development of improved lentiviral and retroviral vectors |[ndash]| design, biosafety, and production. Gene Ther. Nature Publishing Group; 2005;12:1089–98.

386. Jackson DA, Symons RH, Berg P. Biochemical method for inserting new genetic information into DNA of Simian Virus 40: circular SV40 DNA molecules containing lambda phage genes and the galactose operon of Escherichia coli. Proc Natl Acad Sci USA. National Acad Sciences; 1972;69:2904–9.

387. Proudfoot NJ. Ending the message: poly (A) signals then and now. Genes Dev. 2011.

388. Kafri T, Blömer U, Peterson DA, Gage FH, Verma IM. Sustained expression of genes delivered directly into liver and muscle by lentiviral vectors. Nature Publishing Group; 1997;17:314–7.

389. Wiznerowicz M, Trono D. Harnessing HIV for therapy, basic research and biotechnology. Trends Biotechnol. Elsevier; 2005;23:42–7.

390. Wiznerowicz M, Trono D. Conditional suppression of cellular genes: lentivirus vector-mediated drug-inducible RNA interference. J Virol. American Society for Microbiology (ASM); 2003;77:8957–61.

391. Sumimoto H, Kawakami Y. Lentiviral vector-mediated RNAi and its use for cancer research. http://dxdoiorg/102217/1479669436655. Future Medicine Ltd London, UK; 2007;3:655–64.

392. Pfeifer A, Ikawa M, Dayn Y, Verma IM. Transgenesis by lentiviral vectors: lack of gene silencing in mammalian embryonic stem cells and preimplantation embryos. Proc Natl Acad Sci USA. National Acad Sciences; 2002;99:2140–5.

393. Baekelandt V, Eggermont K, Michiels M, Nuttin B, Debyser Z. Optimized lentiviral vector production and purification procedure prevents immune response after transduction of mouse brain. Gene Ther. Nature Publishing Group; 2003;10:1933–40.

394. Kay MA, Glorioso JC, Naldini L. Viral vectors for gene therapy: the art of turning infectious

agents into vehicles of therapeutics. Nat Med. Nature Publishing Group; 2001;7:33–40.

395. Singer O, Verma IM. Applications of lentiviral vectors for shRNA delivery and transgenesis. Current gene therapy. NIH Public Access; 2008;8:483–8.

396. Bobbin ML, Burnett JC, Rossi JJ. RNA interference approaches for treatment of HIV-1 infection. Genome Med. BioMed Central Ltd; 2015;7:50.

397. Wu X, Wakefield JK, Liu H, Xiao H, Kralovics R, Prchal JT, et al. Development of a novel trans-lentiviral vector that affords predictable safety. Mol Ther. 2000;2:47–55.

398. Dull T, Zufferey R, Kelly M, Mandel RJ, Nguyen M, Trono D, et al. A third-generation lentivirus vector with a conditional packaging system. J Virol. American Society for Microbiology (ASM); 1998;72:8463–71.

399. Miyoshi H, Blömer U, Takahashi M, Gage FH, Verma IM. Development of a self-inactivating lentivirus vector. J Virol. American Society for Microbiology; 1998;72:8150–7.

400. Zufferey R, Dull T, Mandel RJ, Bukovsky A, Quiroz D, Naldini L, et al. Self-inactivating lentivirus vector for safe and efficient in vivo gene delivery. J Virol. American Society for Microbiology; 1998;72:9873–80.

401. Iwakuma T, Cui Y, Chang LJ. Self-inactivating lentiviral vectors with U3 and U5 modifications. Virology. 1999;261:120–32.

402. Zufferey R, Donello JE, Trono D, Hope TJ. Woodchuck hepatitis virus posttranscriptional regulatory element enhances expression of transgenes delivered by retroviral vectors. J Virol. American Society for Microbiology (ASM); 1999;73:2886–92.

403. Follenzi A, Ailles LE, Bakovic S, Geuna M, Naldini L. Gene transfer by lentiviral vectors is limited by nuclear translocation and rescued by HIV-1 pol sequences. 2000;25:217–22.

404. Barry SC, Harder B, Brzezinski M, Flint LY, Seppen J, Osborne WR. Lentivirus vectors encoding both central polypurine tract and posttranscriptional regulatory element provide enhanced transduction and transgene expression. Hum Gene Ther. Mary Ann Liebert, Inc; 2001;12:1103–8.

405. Mátrai J, Chuah MKL, VandenDriessche T. Recent advances in lentiviral vector development and applications. Mol Ther. Nature Publishing Group; 2010;18:477–90.

406. Landy A, Ross W. Viral integration and excision: structure of the lambda att sites. Science. NIH Public Access; 1977;197:1147–60.

407. Weisberg RA, Landy A. Site-specific Recombination in Phage Lambda. Cold Spring Harbor Monograph Archive. 1983;13:211–50.

408. Postle K, Nguyen TT, Bertrand KP. Nucleotide sequence of the repressor gene of the TN10 tetracycline resistance determinant. Nucleic Acids Res. Oxford University Press; 1984;12:4849–63.

409. Forster K, Helbl V, Lederer T, Urlinger S, Wittenburg N, Hillen W. Tetracycline-inducible expression systems with reduced basal activity in mammalian cells. Nucleic Acids Res. Oxford University Press; 1999;27:708–10.

410. Wimmel A, Lucibello FC, Sewing A, Adolph S, Müller R. Inducible acceleration of G1 progression through tetracycline-regulated expression of human cyclin E. Oncogene. 1994;9:995–7.

411. Gossen M, Bujard H. Efficacy of tetracycline-controlled gene expression is influenced by cell type: commentary. BioTechniques. Biotechniques; 1995;19:213–6–discussion216–7.

412. Shin K-J, Wall EA, Zavzavadjian JR, Santat LA, Liu J, Hwang J-I, et al. A single lentiviral vector platform for microRNA-based conditional RNA interference and coordinated transgene expression. Proc Natl Acad Sci USA. National Acad Sciences; 2006;103:13759–64.

413. Albrecht C, Hosiner S, Tichy B, Aldrian S, Hajdu S, Nürnberger S. Comparison of Lentiviral Packaging Mixes and Producer Cell Lines for RNAi Applications. Mol Biotechnol. Springer US; 2015;57:499–505.

414. Sena-Esteves M, Tebbets JC, Steffens S, Crombleholme T, Flake AW. Optimized large-scale production of high titer lentivirus vector pseudotypes. Journal of Virological Methods. 2004;122:131–9.

415. Kafri T, van Praag H, Ouyang L, Gage FH, Verma IM. A packaging cell line for lentivirus vectors. J Virol. American Society for Microbiology; 1999;73:576–84.

416. Farson D, Witt R, McGuinness R, Dull T, Kelly M, Song J, et al. A new-generation stable inducible packaging cell line for lentiviral vectors. Hum Gene Ther. Mary Ann Liebert, Inc; 2001;12:981–97.

417. Pacchia AL, Adelson ME, Kaul M, Ron Y, Dougherty JP. An inducible packaging cell system for safe, efficient lentiviral vector production in the absence of HIV-1 accessory proteins. Virology. 2001;282:77–86.

418. Qin JY, Zhang L, Clift KL, Hulur I, Xiang AP, Ren B-Z, et al. Systematic Comparison of Constitutive Promoters and the Doxycycline-Inducible Promoter. Hansen IA, editor. PLoS ONE. Public Library of Science; 2010;5:e10611.

419. Heldt SA, Ressler KJ. The Use of Lentiviral Vectors and Cre/loxP to Investigate the Function of Genes in Complex Behaviors. Front Mol Neurosci. Frontiers; 2009;2:22.

420. Thorsen F, Visted T, Lehtolainen P. Release of replication-deficient retroviruses from a packaging cell line: interaction with glioma tumor spheroids in vitro. … journal of cancer. 1997.

421. Haselhorst D, Kaye JF, Lever AM. Development of cell lines stably expressing human immunodeficiency virus type 1 proteins for studies in encapsidation and gene transfer. J Gen Virol. Microbiology Society; 1998;79 (Pt 2):231–7.

422. Ni Y, Sun S, Oparaocha I, Humeau L, Davis B, Cohen R, et al. Generation of a packaging cell

line for prolonged large-scale production of high-titer HIV-1-based lentiviral vector. The Journal of Gene Medicine. John Wiley & Sons, Ltd; 2005;7:818–34.

423. Logan AC, Nightingale SJ, Haas DL, Cho GJ, Pepper KA, Kohn DDB. Factors Influencing the Titer and Infectivity of Lentiviral Vectors. http://dxdoiorg/101089/hum200415976. Mary Ann Liebert, Inc. 2 Madison Avenue Larchmont, NY 10538 USA; 2004;15:976–88.

424. Nelson CM, Bissell MJ. Of extracellular matrix, scaffolds, and signaling: tissue architecture regulates development, homeostasis, and cancer. Annu Rev Cell Dev Biol. Annual Reviews; 2006;22:287–309.

425. Imamura Y, Mukohara T, Shimono Y, Funakoshi Y, Chayahara N, Toyoda M, et al. Comparison of 2D- and 3D-culture models as drug-testing platforms in breast cancer. Oncology Reports. Spandidos Publications; 2015;33:1837–43.

426. Pickl M, Ries CH. Comparison of 3D and 2D tumor models reveals enhanced HER2 activation in 3D associated with an increased response to trastuzumab. Oncogene. Nature Publishing Group; 2009;28:461–8.

427. Frigault MM, Lacoste J, Swift JL, Brown CM. Live-cell microscopy – tips and tools. Journal of Cell Science. The Company of Biologists Ltd; 2009;122:753–67.

428. Graf BW, Boppart SA. Imaging and analysis of three-dimensional cell culture models. Methods Mol Biol. Totowa, NJ: Humana Press; 2010;591:211–27.

429. Campagnola PJ, Clark HA, Mohler WA, Lewis A, Loew LM. Second-harmonic imaging microscopy of living cells. J Biomed Opt. International Society for Optics and Photonics; 2001;6:277–86.

430. Fine S, Hansen WP. Optical Second Harmonic Generation in Biological Systems. Appl Opt, AO. Optical Society of America; 1971;10:2350–3.

431. Thrasivoulou C, Virich G, Krenacs T, Korom I, Becker DL. Optical delineation of human malignant melanoma using second harmonic imaging of collagen. Biomed Opt Express. Optical Society of America; 2011;2:1282–95.

432. Millard AC, Jin L, Lewis A, Loew LM. Direct measurement of the voltage sensitivity of second-harmonic generation from a membrane dye in patch-clamped cells. Opt Lett. 2003;28:1221–3.

433. Moreaux L, Sandre O, Charpak S, Blanchard-Desce M, Mertz J. Coherent scattering in multi-harmonic light microscopy. Biophys J. Elsevier; 2001;80:1568–74.

434. Williams RM, Zipfel WR, Webb WW. Interpreting second-harmonic generation images of collagen I fibrils. Biophys J. Elsevier; 2005;88:1377–86.

435. Both M, Vogel M, Friedrich O, Wegner von F, Künsting T, Fink RHA, et al. Second harmonic imaging of intrinsic signals in muscle fibers in situ. J Biomed Opt. International Society for Optics and Photonics; 2004;9:882–92.

436. Brown RM, Millard AC, Campagnola PJ. Macromolecular structure of cellulose studied by second-harmonic generation imaging microscopy. Opt Lett. 2003;28:2207–9.

437. Kim BM, Eichler J, Reiser KM, Rubenchik AM, Da Silva LB. Collagen structure and nonlinear susceptibility: effects of heat, glycation, and enzymatic cleavage on second harmonic signal intensity. Lasers Surg Med. 2000;27:329–35.

438. Hoover EE, Squier JA. Advances in multiphoton microscopy technology. Nat Photonics. 2013;7:93–101.

439. Denk W, Svoboda K. Photon upmanship: why multiphoton imaging is more than a gimmick. Neuron. 1997;18:351–7.

440. Vernon-Parry KD. Scanning electron microscopy: an introduction. III-Vs Review. 2000;13:40–4.

441. Unakar NJ, Tsui JY, Harding CV. Scanning Electron Microscopy. Ophthalmic Res. Karger Publishers; 1981;13:20–35.

442. Gao J, Aksoy BA, Dogrusoz U, Dresdner G, Gross B, Sumer SO, et al. Integrative analysis of complex cancer genomics and clinical profiles using the cBioPortal. Sci Signal. 2013;6:pl1–pl1.

443. Cerami E, Gao J, Dogrusoz U, Gross BE, Sumer SO, Aksoy BA, et al. The cBio cancer genomics portal: an open platform for exploring multidimensional cancer genomics data. Cancer Discov. American Association for Cancer Research; 2012;2:401–4.

444. Andronicos NM, Ranson M. The topology of plasminogen binding and activation on the surface of human breast cancer cells. Br J Cancer. Nature Publishing Group; 2001;85:909–16.

445. Wilcox JR, Covington DS, Paez N. Doxycycline as a modulator of inflammation in chronic wounds. Wounds. 2012;24:339–49.

446. Goktolga U, Cavkaytar S, Altinbas SK, Tapisiz OL, Tapisiz A, Erdem O. Effect of the non-specific matrix metalloproteinase inhibitor Doxycycline on endometriotic implants in an experimental rat model. Experimental and Therapeutic Medicine. Spandidos Publications; 2015;9:1813–8.

447. Griffin MO, Jinno M, Miles LA, Villarreal FJ. Reduction of myocardial infarct size by doxycycline: A role for plasmin inhibition. Mol Cell Biochem. Kluwer Academic Publishers; 2005;270:1–11.

448. Pires PW, Rogers CT, McClain JL, Garver HS, Fink GD, Dorrance AM. Doxycycline, a matrix metalloprotease inhibitor, reduces vascular remodeling and damage after cerebral ischemia in stroke-prone spontaneously hypertensive rats. Am J Physiol Heart Circ Physiol. American Physiological Society; 2011;301:H87–H97.

449. Weißer J, Lai ZW, Bronsert P, Kuehs M, Drendel V, Timme S, et al. Quantitative proteomic analysis of formalin-fixed, paraffin-embedded clear cell renal cell carcinoma tissue using stable isotopic dimethylation of primary amines. BMC Genomics. BioMed Central; 2015;16:559.

450. Apte MV, Park S, Phillips PA, Santucci N, Goldstein D, Kumar RK, et al. Desmoplastic Reaction in Pancreatic Cancer: Role of Pancreatic Stellate Cells. Pancreas. 2004;29:179.

451. Sabeh F, Shimizu-Hirota R, Weiss SJ. Protease-dependent versus -independent cancer cell invasion programs: three-dimensional amoeboid movement revisited. The Journal of Cell Biology. Rockefeller Univ Press; 2009;185:11–9.

452. Telgenhoff D, Shroot B. Cellular senescence mechanisms in chronic wound healing. Cell Death Differ. Nature Publishing Group; 2005;:695–8.

453. Madhyastha HK, Radha KS, Nakajima Y, Omura S, Maruyama M. uPA dependent and independent mechanisms of wound healing by C-phycocyanin. J Cell Mol Med. Blackwell Publishing Ltd; 2008;12:2691–703.

454. Pöllänen J, Vaheri A, Tapiovaara H, Riley E, Bertram K, Woodrow G, et al. Prourokinase activation on the surface of human rhabdomyosarcoma cells: localization and inactivation of newly formed urokinase-type plasminogen activator by recombinant class 2 plasminogen activator inhibitor. Proc Natl Acad Sci USA. National Academy of Sciences; 1990;87:2230–4.

455. Suarez E, Syed F, Alonso-Rasgado T, Mandal P, Bayat A. Up-regulation of tension-related proteins in keloids: knockdown of Hsp27, α2β1-integrin, and PAI-2 shows convincing reduction of extracellular matrix production. Plast Reconstr Surg. 2013;131:158e–173e.

456. Arold ST, Hoellerer MK, Noble MEM. The structural basis of localization and signaling by the focal adhesion targeting domain. Structure. 2002;10:319–27.

457. Burridge K, Turner CE, Romer LH. Tyrosine phosphorylation of paxillin and pp125FAK accompanies cell adhesion to extracellular matrix: a role in cytoskeletal assembly. The Journal of Cell Biology. Rockefeller Univ Press; 1992;119:893–903.

458. Wong VW, Rustad KC, Akaishi S, Sorkin M, Glotzbach JP, Januszyk M, et al. Focal adhesion kinase links mechanical force to skin fibrosis via inflammatory signaling. Nat Med. 2012;18:148–52.

459. Thannickal VJ, Lee DY, White ES, Cui Z, Larios JM, Chacon R, et al. Myofibroblast differentiation by transforming growth factor-beta1 is dependent on cell adhesion and integrin signaling via focal adhesion kinase. Journal of Biological Chemistry. American Society for Biochemistry and Molecular Biology; 2003;278:12384–9.

460. Eckes B, Zweers MC, Zhang ZG, Hallinger R, Mauch C, Aumailley M, et al. Mechanical tension and integrin alpha 2 beta 1 regulate fibroblast functions. J Investig Dermatol Symp Proc. 2006;11:66–72.

461. Tomasek JJ, Gabbiani G, Hinz B, Chaponnier C, Brown RA. Myofibroblasts and mechano-regulation of connective tissue remodelling. Nat Rev Mol Cell Biol. 2002;3:349–63.

462. Popov C, Radic T, Haasters F, Prall WC, Aszodi A, Gullberg D, et al. Integrins α2β1 and α11β1 regulate the survival of mesenchymal stem cells on collagen I. Cell Death Dis. Nature Publishing Group; 2011;2:e186.

463. Paszek MJ, Zahir N, Johnson KR, Lakins JN, Rozenberg GI, Gefen A, et al. Tensional homeostasis and the malignant phenotype. Cancer Cell. Elsevier; 2005;8:241–54.

464. Desgrosellier JS, Cheresh DA. Integrins in cancer: biological implications and therapeutic opportunities. 2010;10:9–22.

465. Margadant C, Sonnenberg A. Integrin-TGF-beta crosstalk in fibrosis, cancer and wound healing. EMBO reports. EMBO Press; 2010;11:97–105.

466. Laczko R, Szauter KM, Jansen MK, Hollosi P, Muranyi M, Molnar J, et al. Active lysyl oxidase (LOX) correlates with focal adhesion kinase (FAK)/paxillin activation and migration in invasive astrocytes. Neuropathol Appl Neurobiol. Blackwell Publishing Ltd; 2007;33:631–43.

467. Seton-Rogers S. Stopping the spread. 2006.

468. Barker HE, Cox TR, Erler JT. The rationale for targeting the LOX family in cancer. Nature Publishing Group; 2012;12:540–52.

469. Welch MD, DePace AH, Verma S, Iwamatsu A, Mitchison TJ. The human Arp2/3 complex is composed of evolutionarily conserved subunits and is localized to cellular regions of dynamic actin filament assembly. The Journal of Cell Biology. The Rockefeller University Press; 1997;138:375–84.

470. Spessotto P, Cervi M, Mucignat MT, Mungiguerra G, Sartoretto I, Doliana R, et al. beta 1 Integrin-dependent cell adhesion to EMILIN-1 is mediated by the gC1q domain. Journal of Biological Chemistry. American Society for Biochemistry and Molecular Biology; 2003;278:6160–7.

471. Colombatti A, Spessotto P, Doliana R, Mongiat M, Bressan GM, Esposito G. The EMILIN/Multimerin family. Front Immunol. Frontiers; 2011;2:93.

472. Spessotto P, Bulla R, Danussi C, Radillo O, Cervi M, Monami G, et al. EMILIN1 represents a major stromal element determining human trophoblast invasion of the uterine wall. Journal of Cell Science. The Company of Biologists Ltd; 2006;119:4574–84.

473. Schönherr E, Witsch-Prehm P, Harrach B, Robenek H, Rauterberg J, Kresse H. Interaction of biglycan with type I collagen. Journal of Biological Chemistry. 1995;270:2776–83.

474. Furuta Y, Ilić D, Kanazawa S, Takeda N, Yamamoto T, Aizawa S. Mesodermal defect in late phase of gastrulation by a targeted mutation of focal adhesion kinase, FAK. Oncogene. 1995;11:1989–95.

475. Fässler R, Georges-Labouesse E, Hirsch E. Genetic analyses of integrin function in mice. Curr Opin Cell Biol. 1996;8:641–6.

476. Ridley AJ, Hall A. The small GTP-binding protein rho regulates the assembly of focal adhesions and actin stress fibers in response to growth factors. Cell. 1992;70:389–99.

477. Termine JD, Belcourt AB, Conn KM, Kleinman HK. Mineral and collagen-binding proteins of fetal calf bone. Journal of Biological Chemistry. American Society for Biochemistry and

Molecular Biology; 1981;256:10403–8.

478. Sage H, Johnson C, Bornstein P. Characterization of a novel serum albumin-binding glycoprotein secreted by endothelial cells in culture. Journal of Biological Chemistry. American Society for Biochemistry and Molecular Biology; 1984;259:3993–4007.

479. Engel J, Taylor W, Paulsson M, Sage H, Hogan B. Calcium binding domains and calcium-induced conformational transition of SPARC/BM-40/osteonectin, an extracellular glycoprotein expressed in mineralized and nonmineralized tissues. Biochemistry. 1987;26:6958–65.

480. Funk SE, Sage EH. The Ca2(+)-binding glycoprotein SPARC modulates cell cycle progression in bovine aortic endothelial cells. Proc Natl Acad Sci USA. National Acad Sciences; 1991;88:2648–52.

481. Visse R, Nagase H. Matrix metalloproteinases and tissue inhibitors of metalloproteinases: structure, function, and biochemistry. Circulation Research. Lippincott Williams & Wilkins; 2003;92:827–39.

482. Danial NN, Korsmeyer SJ. Cell death: critical control points. Cell. 2004;116:205–19.

483. Doolittle RF. Fibrinogen and Fibrin. Annu Rev Biochem. Annual Reviews 4139 El Camino Way, P.O. Box 10139, Palo Alto, CA 94303-0139, USA; 1984;53:195–229.

484. Sahni A, Sahni SK, Simpson Haidaris PJ, Francis CW. Fibrinogen binding potentiates FGF - 2 but not VEGF induced expression of u - PA, u - PAR, and PAI - 1 in endothelial cells. Journal of Thrombosis and Haemostasis. Blackwell Science Inc; 2004;2:1629–36.

485. Erler JT, Bennewith KL, Cox TR, Lang G, Bird D, Koong A, et al. Hypoxia-induced lysyl oxidase is a critical mediator of bone marrow cell recruitment to form the premetastatic niche. Cancer Cell. Elsevier; 2009;15:35–44.

486. Mosher DF, Schad PE, Kleinman HK. Inhibition of blood coagulation factor XIIIa-mediated cross-linking between fibronectin and collagen by polyamines. J Supramol Struct. Alan R. Liss, Inc; 1979;11:227–35.

487. Mosher DF, Schad PE. Cross-linking of fibronectin to collagen by blood coagulation Factor XIIIa. J Clin Invest. American Society for Clinical Investigation; 1979;64:781–7.

488. Madsen CD, Pedersen JT, Venning FA, Singh LB, Moeendarbary E, Charras G, et al. Hypoxia and loss of PHD2 inactivate stromal fibroblasts to decrease tumour stiffness and metastasis. EMBO reports. EMBO Press; 2015;16:1394–408.

489. Skiles JW, Gonnella NC, Jeng AY. The Design, Structure, and Clinical Update of Small Molecular Weight Matrix Metalloproteinase Inhibitors. CMC. Bentham Science Publishers; 2004;11:2911–77.

490. Fingleton B. MMPs as therapeutic targets--still a viable option? Semin Cell Dev Biol. 2008;19:61–8.

491. Devy L, Dransfield DT. New strategies for the next generation of matrix-metalloproteinase inhibitors: selectively targeting membrane-anchored MMPs with therapeutic antibodies. Biochemistry research .... 2010.

492. Morikawa K, Walker SM, Nakajima M, Pathak S, Jessup JM, Fidler IJ. Influence of organ environment on the growth, selection, and metastasis of human colon carcinoma cells in nude mice. Cancer Research. American Association for Cancer Research; 1988;48:6863–71.

493. Chakraborti S, Mandal M, Das S, Mandal A, Chakraborti T. Regulation of matrix metalloproteinases: An overview. Mol Cell Biochem. Kluwer Academic Publishers; 2003;253:269–85.

494. Butcher DT, Alliston T, Weaver VM. A tense situation: forcing tumour progression. Nature Publishing Group; 2009;9:108–22.

495. Biondi ML, Turri O, Leviti S, Seminati R, Cecchini F, Bernini M, et al. MMP1 and MMP3 polymorphisms in promoter regions and cancer. Clin Chem. 2000;46:2023–4.

496. Monea S, Lehti K, Keski Oja J, Mignatti P. Plasmin activates pro - matrix metalloproteinase - 2 with a membrane - type 1 matrix metalloproteinase - dependent mechanism. Journal of Cellular Physiology. Wiley Subscription Services, Inc., A Wiley Company; 2002;192:160–70.

497. Carmeliet P, Moons L, Herbert JM, Crawley J, Lupu F, Lijnen R, et al. Urokinase but not tissue plasminogen activator mediates arterial neointima formation in mice. Circulation Research. Lippincott Williams & Wilkins; 1997;81:829–39.

498. Carmeliet P, Moons L, Lijnen R, Baes M, Lemaître V, Tipping P, et al. Urokinase-generated plasmin activates matrix metalloproteinases during aneurysm formation. Nature Publishing Group; 1997;17:439–44.

499. Proteolytic networks in cancer. Elsevier Ltd; 2011;21:228–37.

500. Hanemaaijer R, Visser H, Koolwijk P, Sorsa T, Salo T, Golub LM, et al. Inhibition of MMP Synthesis by Doxycycline and Chemically Modified Tetracyclines (CMTs) in Human Endothelial Cells. ADR. SAGE Publications; 1998;12:114–8.

501. Ruoslahti E. Brain extracellular matrix. Glycobiology. 1996;6:489–92.

502. da Silva R, Uno M, Marie SKN, Oba-Shinjo SM. LOX expression and functional analysis in astrocytomas and impact of IDH1 mutation. Li J, editor. PLoS ONE. Public Library of Science; 2015;10:e0119781.

503. Rosenbloom J, Mendoza FA, Jimenez SA. Strategies for anti-fibrotic therapies. Biochim Biophys Acta. 2013;1832:1088–103.

504. Levental KR, Yu H, Kass L, Lakins JN, Egeblad M, Erler JT, et al. Matrix crosslinking forces tumor progression by enhancing integrin signaling. Cell. Elsevier; 2009;139:891–906.

505. Slebos R, Hoppin JA, Tolbert PE, Holly EA. K-ras and p53 in pancreatic cancer: association with medical history, histopathology, and environmental exposures in a population-based study.

… Biomarkers & Prevention. 2000.

506. Clinical and molecular characterization of HER2 amplified-pancreatic cancer. 2013;5:1–1.

507. Jemal A, Siegel R, Ward E, Hao Y, Xu J, Murray T, et al. Cancer Statistics, 2008. CA: A Cancer Journal for Clinicians. John Wiley & Sons, Ltd; 2008;58:71–96.

508. Sheikh R, Walsh N, Clynes M, O'Connor R, McDermott R. Challenges of drug resistance in the management of pancreatic cancer. Expert Rev Anticancer Ther. Informa HealthcareLondon; 2010;10:1647–61.

509. Chen F, Guo Y, Wang L. The Emerging Genetic Basis and Its Clinical Implication in Pancreatic Cancer. Gastrointest Tumors. Karger Publishers; 2015;2:131–43.

510. Bryant KL, Mancias JD, Kimmelman AC, Der CJ. KRAS: feeding pancreatic cancer proliferation. Trends Biochem Sci. Elsevier; 2014;39:91–100.

511. Biankin AV, Waddell N, Kassahn KS, Gingras M-C, Muthuswamy LB, Johns AL, et al. Pancreatic cancer genomes reveal aberrations in axon guidance pathway genes. Nature. Nature Publishing Group; 2012;491:399–405.

512. Habbe N, Langer P, Sina-Frey M, Bartsch DK. Familial pancreatic cancer syndromes. Endocrinol Metab Clin North Am. 2006;35:417–30–xi.

513. Wescott MP, Rustgi AK. Pancreatic cancer: translating lessons from mouse models and hereditary syndromes. Cancer Prev Res (Phila). American Association for Cancer Research; 2008;1:503–6.

514. Ruggeri B, Zhang SY, Caamano J, DiRado M, Flynn SD, Klein-Szanto AJ. Human pancreatic carcinomas and cell lines reveal frequent and multiple alterations in the p53 and Rb-1 tumor-suppressor genes. Oncogene. 1992;7:1503–11.

515. Scarpa A, Capelli P, Mukai K, Zamboni G, Oda T, Iacono C, et al. Pancreatic adenocarcinomas frequently show p53 gene mutations. Am J Pathol. American Society for Investigative Pathology; 1993;142:1534–43.

516. Alexandrov LB, Nik-Zainal S, Wedge DC, Aparicio SAJR, Behjati S, Biankin AV, et al. Signatures of mutational processes in human cancer. Nature. Nature Publishing Group; 2013;500:415–21.

517. Caldas C, Hahn SA, da Costa LT, Redston MS, Schutte M, Seymour AB, et al. Frequent somatic mutations and homozygous deletions of the p16 (MTS1) gene in pancreatic adenocarcinoma. Nature Publishing Group; 1994;8:27–32.

518. Hahn SA, Schutte M, Hoque AT, Moskaluk CA, da Costa LT, Rozenblum E, et al. DPC4, a candidate tumor suppressor gene at human chromosome 18q21.1. Science. 1996;271:350–3.

519. Waddell N, Pajic M, Patch A-M, Chang DK, Kassahn KS, Bailey P, et al. Whole genomes redefine the mutational landscape of pancreatic cancer. Nature. 2015;518:495–501.

520. Distler M, Aust D, Weitz J, Pilarsky C, Grützmann R. Precursor lesions for sporadic pancreatic cancer: PanIN, IPMN, and MCN. Biomed Res Int. Hindawi Publishing Corporation; 2014;2014:474905–11.

521. Kanda M, Matthaei H, Wu J, Hong S-M, Yu J, Borges M, et al. Presence of somatic mutations in most early-stage pancreatic intraepithelial neoplasia. Gastroenterology. Elsevier; 2012;142:730–9.

522. Hong S-M, Park JY, Hruban RH, Goggins M. Molecular signatures of pancreatic cancer. Archives of pathology & laboratory medicine. NIH Public Access; 2011;135:716–27.

523. Moriya T, Kimura W, Semba S, Sakurai F, Hirai I, Ma J, et al. Biological similarities and differences between pancreatic intraepithelial neoplasias and intraductal papillary mucinous neoplasms. Int J Gastrointest Cancer. Humana Press; 2005;35:111–9.

524. Maitra A, Fukushima N, Takaori K, Hruban RH. Precursors to Invasive Pancreatic Cancer. Advances in Anatomic Pathology. 2005;12:81.

525. Ismail MF, Aly MS, Khaled HM, Mohamed HM. Detection of HER-2/neu, c-myc amplification and p53 inactivation by FISH in Egyptian patients with breast cancer. Ger Med Sci. 2009;7:Doc03.

526. Yarden Y, Sliwkowski MX. Untangling the ErbB signalling network. Nat Rev Mol Cell Biol. Nature Publishing Group; 2001;2:127–37.

527. Moasser MM. The oncogene HER2: its signaling and transforming functions and its role in human cancer pathogenesis. Oncogene. Nature Publishing Group; 2007;26:6469–87.

528. Herreros-Villanueva M, Hijona E, Cosme A, Bujanda L. Mouse models of pancreatic cancer. World J Gastroenterol. Baishideng Publishing Group Inc; 2012;18:1286–94.

529. O'Hagan RC, Heyer J. KRAS Mouse Models Modeling Cancer Harboring KRAS Mutations. Genes & Cancer. SAGE Publications; 2011;2:335–43.

530. Hingorani SR, Petricoin EF, Maitra A, Rajapakse V, King C, Jacobetz MA, et al. Preinvasive and invasive ductal pancreatic cancer and its early detection in the mouse. Cancer Cell. Elsevier; 2003;4:437–50.

531. Aguirre AJ, Bardeesy N, Sinha M, Lopez L, Tuveson DA, Horner J, et al. Activated Kras and Ink4a/Arf deficiency cooperate to produce metastatic pancreatic ductal adenocarcinoma. Genes Dev. Cold Spring Harbor Lab; 2003;17:3112–26.

532. Hingorani SR, Wang L, Multani AS, Combs C, Deramaudt TB, Hruban RH, et al. Trp53R172H and KrasG12D cooperate to promote chromosomal instability and widely metastatic pancreatic ductal adenocarcinoma in mice. Cancer Cell. 2005;7:469–83.

533. Bardeesy N, Aguirre AJ, Chu GC, Cheng K-H, Lopez LV, Hezel AF, et al. Both p16(Ink4a) and the p19(Arf)-p53 pathway constrain progression of pancreatic adenocarcinoma in the mouse. Proc Natl Acad Sci USA. National Acad Sciences; 2006;103:5947–52.

534. Mollenhauer J, Roether I, Kern HF. Distribution of Extracellular Matrix Proteins in Pancreatic Ductal Adenocarcinoma and Its Influence on Tumor Cell Proliferation in Vitro. Pancreas. 1987;2:14.

535. Vasseur S, Tomasini R, Tournaire R, Iovanna JL. Hypoxia induced tumor metabolic switch contributes to pancreatic cancer aggressiveness. Cancers (Basel). Molecular Diversity Preservation International; 2010;2:2138–52.

536. Provenzano PP, Cuevas C, Chang AE, Goel VK, Hoff Von DD, Hingorani SR. Enzymatic targeting of the stroma ablates physical barriers to treatment of pancreatic ductal adenocarcinoma. Cancer Cell. Elsevier; 2012;21:418–29.

537. Whatcott CJ, Han H, Posner RG, Hostetter G, Hoff Von DD. Targeting the tumor microenvironment in cancer: why hyaluronidase deserves a second look. Cancer Discov. American Association for Cancer Research; 2011;1:291–6.

538. Esposito I, Menicagli M, Funel N, Bergmann F, Boggi U, Mosca F, et al. Inflammatory cells contribute to the generation of an angiogenic phenotype in pancreatic ductal adenocarcinoma. J Clin Pathol. BMJ Publishing Group Ltd and Association of Clinical Pathologists; 2004;57:630–6.

539. Mace TA, Ameen Z, Collins A, Wojcik S, Mair M, Young GS, et al. Pancreatic cancer-associated stellate cells promote differentiation of myeloid-derived suppressor cells in a STAT3-dependent manner. Cancer Research. American Association for Cancer Research; 2013;73:3007–18.

540. Omary MB, Lugea A, Lowe AW, Pandol SJ. The pancreatic stellate cell: a star on the rise in pancreatic diseases. Journal of Clinical Investigation. American Society for Clinical Investigation; 2007;117:50–9.

541. Masamune A, Shimosegawa T. Signal transduction in pancreatic stellate cells. J Gastroenterol. Springer Japan; 2009;44:249–60.

542. Apte MV, Haber PS, Applegate TL, Norton ID, McCaughan GW, Korsten MA, et al. Periacinar stellate shaped cells in rat pancreas: identification, isolation, and culture. Gut. BMJ Group; 1998;43:128–33.

543. Bachem MG, Schünemann M, Ramadani M, Siech M, Beger H, Buck A, et al. Pancreatic carcinoma cells induce fibrosis by stimulating proliferation and matrix synthesis of stellate cells. Gastroenterology. Elsevier; 2005;128:907–21.

544. Schneiderhan W, Diaz F, Fundel M, Zhou S, Siech M, Hasel C, et al. Pancreatic stellate cells are an important source of MMP-2 in human pancreatic cancer and accelerate tumor progression in a murine xenograft model and CAM assay. Journal of Cell Science. The Company of Biologists Ltd; 2007;120:512–9.

545. Xue A, Xue M, Jackson C, Smith RC. Suppression of urokinase plasminogen activator receptor inhibits proliferation and migration of pancreatic adenocarcinoma cells via regulation of ERK/p38 signaling. The International Journal of Biochemistry & Cell Biology. 2009;41:1731–8.

546. Asuthkar S, Stepanova V, Lebedeva T, Holterman AL, Estes N, Cines DB, et al. Multifunctional roles of urokinase plasminogen activator (uPA) in cancer stemness and chemoresistance of pancreatic cancer. Mol Biol Cell. American Society for Cell Biology; 2013;24:2620–32.

547. Morton JP, Timpson P, Karim SA, Ridgway RA, Athineos D, Doyle B, et al. Mutant p53 drives metastasis and overcomes growth arrest/senescence in pancreatic cancer. Proc Natl Acad Sci USA. National Acad Sciences; 2010;107:246–51.

548. Stutchbury TK, Vine KL, Locke JM, Chrisp JS, Bremner JB, Clingan PR, et al. Preclinical evaluation of novel, all-in-one formulations of 5-fluorouracil and folinic acid with reduced toxicity profiles. Anticancer Drugs. 2011;22:24–34.

549. Xue A, Scarlett CJ, Jackson CJ, Allen BJ, Smith RC. Prognostic significance of growth factors and the urokinase-type plasminogen activator system in pancreatic ductal adenocarcinoma. Pancreas. 2008;36:160–7.

550. Babur Ö, Gönen M, Aksoy BA, Schultz N, Ciriello G, Sander C, et al. Systematic identification of cancer driving signaling pathways based on mutual exclusivity of genomic alterations. Genome Biol. 2015;16:45.

551. Hartsock A, Nelson WJ. Adherens and tight junctions: structure, function and connections to the actin cytoskeleton. Biochim Biophys Acta. 2008;1778:660–9.

552. Ilina O, Friedl P. Mechanisms of collective cell migration at a glance. Journal of Cell Science. The Company of Biologists Ltd; 2009;122:3203–8.

553. Nobis M, Mcghee EJ, Morton JP, Schwarz JP, Karim SA, Quinn J, et al. Intravital FLIM-FRET imaging reveals dasatinib-induced spatial control of src in pancreatic cancer. Cancer Research. American Association for Cancer Research; 2013;73:4674–86.

554. Shekouh AR, Thompson CC, Prime W, Campbell F, Hamlett J, Herrington CS, et al. Application of laser capture microdissection combined with two-dimensional electrophoresis for the discovery of differentially regulated proteins in pancreatic ductal adenocarcinoma. Proteomics. WILEY - VCH Verlag; 2003;3:1988–2001.

555. Seymour AB, Hruban RH, Redston M, Caldas C, Powell SM, Kinzler KW, et al. Allelotype of pancreatic adenocarcinoma. Cancer Research. 1994;54:2761–4.

556. Boyd ZS, Raja R, Johnson S, Eberhard DA, Lackner MR. A tumor sorting protocol that enables enrichment of pancreatic adenocarcinoma cells and facilitation of genetic analyses. J Mol Diagn. 2009;11:290–7.

557. Grippo PJ, Munshi HG, Liss AS, Thayer SP. Therapeutic targeting of pancreatic stroma. Trivandrum (India): Transworld Research Network; 2012.

558. Friedl P, Wolf K. Tumour-cell invasion and migration: diversity and escape mechanisms. Nature Reviews Cancer. Nature Publishing Group; 2003;3:362–74.

559. Friedl P, Hegerfeldt Y, Tusch M. Collective cell migration in morphogenesis and cancer.

International Journal of …. 2004.

560. Ryu JK, Hong S-M, Karikari CA, Hruban RH, Goggins MG, Maitra A. Aberrant MicroRNA-155 expression is an early event in the multistep progression of pancreatic adenocarcinoma. Pancreatology. 2010;10:66–73.

561. Ferlay J, Soerjomataram I, Dikshit R, Eser S, Mathers C, Rebelo M, et al. Cancer incidence and mortality worldwide: sources, methods and major patterns in GLOBOCAN 2012. Int J Cancer. 2015;136:E359–86.

562. Schneider G, Siveke JT, Eckel F, Schmid RM. Pancreatic cancer: basic and clinical aspects. Gastroenterology. 2005;128:1606–25.

563. Albrengues J, Meneguzzi G, Gaggioli C. Analysis of collective invasion of carcinoma cells in a 3D organotypic model. Methods Mol Biol. Totowa, NJ: Humana Press; 2013;961:243–52.

564. Whitworth PW, Pak CC, Esgro J, Kleinerman ES, Fidler IJ. Macrophages and cancer. Cancer Metastasis Rev. 1990;8:319–51.

565. Chioni A-M, Grose R. Organotypic modelling as a means of investigating epithelial-stromal interactions during tumourigenesis. Fibrogenesis Tissue Repair. BioMed Central Ltd; 2008;1:8.

566. Li J, Wientjes MG, Au JL-S. Pancreatic cancer: pathobiology, treatment options, and drug delivery. AAPS J. Springer US; 2010;12:223–32.

567. Neesse A, Michl P, Frese KK, Feig C, Cook N, Jacobetz MA, et al. Stromal biology and therapy in pancreatic cancer. Gut. BMJ Publishing Group Ltd and British Society of Gastroenterology; 2011;60:861–8.

568. McCarroll JA, Naim S, Sharbeen G, Russia N, Lee J, Kavallaris M, et al. Role of pancreatic stellate cells in chemoresistance in pancreatic cancer. Front Physiol. Frontiers; 2014;5:141.

569. Stylianopoulos T, Martin JD, Chauhan VP, Jain SR, Diop-Frimpong B, Bardeesy N, et al. Causes, consequences, and remedies for growth-induced solid stress in murine and human tumors. Proc Natl Acad Sci USA. 2012;109:15101–8.

570. Özdemir BC, Pentcheva-Hoang T, Carstens JL, Zheng X, Wu C-C, Simpson TR, et al. Depletion of carcinoma-associated fibroblasts and fibrosis induces immunosuppression and accelerates pancreas cancer with reduced survival. Cancer Cell. Elsevier Inc; 2014;25:719–34.

571. Wyckoff JB, Pinner SE, Gschmeissner S, Condeelis JS, Sahai E. ROCK- and myosin-dependent matrix deformation enables protease-independent tumor-cell invasion in vivo. Curr Biol. Elsevier; 2006;16:1515–23.

572. Condeelis J, Segall JE. Intravital imaging of cell movement in tumours. 2003;3:921–30.

573. Kauppila S, Stenbäck F, Risteli J, Jukkola A, Risteli L. Aberrant type I and type III collagen gene expression in human breast cancer in vivo. J Pathol. John Wiley & Sons, Ltd; 1998;186:262–8.

574. Curino AC, Engelholm LH, Yamada SS, Holmbeck K, Lund LR, Molinolo AA, et al. Intracellular collagen degradation mediated by uPARAP/Endo180 is a major pathway of extracellular matrix turnover during malignancy. The Journal of Cell Biology. Rockefeller Univ Press; 2005;169:977–85.

575. Kedrin D, Gligorijevic B, Wyckoff J, Verkhusha VV, Condeelis J, Segall JE, et al. Intravital imaging of metastatic behavior through a mammary imaging window. Nat Methods. 2008;5:1019–21.

576. Li CY, Shan S, Huang Q, Braun RD, Lanzen J, Hu K, et al. Initial stages of tumor cell-induced angiogenesis: evaluation via skin window chambers in rodent models. J Natl Cancer Inst. 2000;92:143–7.

577. Hwang RF, Moore T, Arumugam T, Ramachandran V, Amos KD, Rivera A, et al. Cancer-associated stromal fibroblasts promote pancreatic tumor progression. Cancer Research. American Association for Cancer Research; 2008;68:918–26.

578. Polyak K, Weinberg RA. Transitions between epithelial and mesenchymal states: acquisition of malignant and stem cell traits. 2009;9:265–73.

579. Panková K, Rösel D, Novotný M, Brábek J. The molecular mechanisms of transition between mesenchymal and amoeboid invasiveness in tumor cells. Cell Mol Life Sci. SP Birkhäuser Verlag Basel; 2010;67:63–71.

580. Sahai E, Marshall CJ. Differing modes of tumour cell invasion have distinct requirements for Rho/ROCK signalling and extracellular proteolysis. Nat Cell Biol. 2003;5:711–9.

581. Even-Ram S, Yamada KM. Cell migration in 3D matrix. Curr Opin Cell Biol. 2005;17:524–32.

582. Bajénoff M, Egen JG, Koo LY, Laugier JP, Brau F, Glaichenhaus N, et al. Stromal cell networks regulate lymphocyte entry, migration, and territoriality in lymph nodes. Immunity. Elsevier; 2006;25:989–1001.

583. Pluen A, Boucher Y, Ramanujan S, McKee TD, Gohongi T, di Tomaso E, et al. Role of tumor-host interactions in interstitial diffusion of macromolecules: cranial vs. subcutaneous tumors. Proc Natl Acad Sci USA. National Acad Sciences; 2001;98:4628–33.

584. Beadle C, Assanah MC, Monzo P, Vallee R, Rosenfeld SS, Canoll P. The role of myosin II in glioma invasion of the brain. Mol Biol Cell. American Society for Cell Biology; 2008;19:3357–68.

585. Rosenthal EL, Johnson TM, Allen ED, Apel IJ, Punturieri A, Weiss SJ. Role of the plasminogen activator and matrix metalloproteinase systems in epidermal growth factor- and scatter factor-stimulated invasion of carcinoma cells. Cancer Research. 1998;58:5221–30.

586. Sabeh F, Ota I, Holmbeck K, Birkedal-Hansen H, Soloway P, Balbin M, et al. Tumor cell traffic through the extracellular matrix is controlled by the membrane-anchored collagenase MT1-MMP. The Journal of Cell Biology. Rockefeller Univ Press; 2004;167:769–81.

587. Macias H, Hinck L. Mammary gland development. Wiley Interdiscip Rev Dev Biol. John Wiley

& Sons, Inc; 2012;1:533–57.

588. Whyte J, Bergin O, Bianchi A, McNally S, Martin F. Key signalling nodes in mammary gland development and cancer. Mitogen-activated protein kinase signalling in experimental models of breast cancer progression and in mammary gland development. Breast Cancer Res. BioMed Central Ltd; 2009;11:209.

589. Ercan C, van Diest PJ, Vooijs M. Mammary development and breast cancer: the role of stem cells. Curr Mol Med. 2011;11:270–85.

590. Parmar H, Cunha GR. Epithelial-stromal interactions in the mouse and human mammary gland in vivo. Endocr Relat Cancer. 2004;11:437–58.

591. Fata JE, Werb Z, Bissell MJ. Regulation of mammary gland branching morphogenesis by the extracellular matrix and its remodeling enzymes. Breast Cancer Res. BioMed Central Ltd; 2003;6:1–11.

592. Lund LR, Bjørn SF, Sternlicht MD, Nielsen BS, Solberg H, Usher PA, et al. Lactational competence and involution of the mouse mammary gland require plasminogen. Development. The Company of Biologists Ltd; 2000;127:4481–92.

593. Selvarajan S, Lund LR, Takeuchi T, Craik CS, Werb Z. A plasma kallikrein-dependent plasminogen cascade required for adipocyte differentiation. Nat Cell Biol. 2001;3:267–75.

594. Simian M, Hirai Y, Navre M, Werb Z, Lochter A, Bissell MJ. The interplay of matrix metalloproteinases, morphogens and growth factors is necessary for branching of mammary epithelial cells. Development. The Company of Biologists Ltd; 2001;128:3117–31.

595. Wiseman BS, Sternlicht MD, Lund LR, Alexander CM, Mott J, Bissell MJ, et al. Site-specific inductive and inhibitory activities of MMP-2 and MMP-3 orchestrate mammary gland branching morphogenesis. The Journal of Cell Biology. Rockefeller Univ Press; 2003;162:1123–33.

596. Australian Cancer Incidence and Mortality (ACIM) books: Breast cancer. Canberra: AIHW. Australian Institute of Health and Welfare 2015. [Internet]. Available from: www.aihw.gov.au/acim-books

597. Curtis C, Shah SP, Chin S-F, Turashvili G, Rueda OM, Dunning MJ, et al. The genomic and transcriptomic architecture of 2,000 breast tumours reveals novel subgroups. Nature. Nature Publishing Group; 2012;486:346–52.

598. W B. **Preneoplasia of the Breast: A New Conceptual Approach to Proliferative Breast Disease**. 4 ed. Munich: Elsevier GmbH; 2006. pages 1–28.

599. Choudhury S, Almendro V, Merino VF, Wu Z, Maruyama R, Su Y, et al. Molecular profiling of human mammary gland links breast cancer risk to a p27(+) cell population with progenitor characteristics. Cell Stem Cell. Elsevier; 2013;13:117–30.

600. Tiede B, Kang Y. From milk to malignancy: the role of mammary stem cells in development, pregnancy and breast cancer. Cell Res. 2011;21:245–57.

601. Perou CM, Sørlie T, Eisen MB, van de Rijn M, Jeffrey SS, Rees CA, et al. Molecular portraits of human breast tumours. Nature. Nature Publishing Group; 2000;406:747–52.

602. Onitilo AA, Engel JM, Greenlee RT, Mukesh BN. Breast cancer subtypes based on ER/PR and Her2 expression: comparison of clinicopathologic features and survival. Clinical Medicine & Research. Marshfield Clinic; 2009;7:4–13.

603. Yang LH, Tseng HS, Lin C, Chen LS. Survival benefit of tamoxifen in estrogen receptor-negative and progesterone receptor-positive low grade breast cancer patients. Journal of breast …. 2012.

604. Camerini A, Donati S, Viacava P, Siclari O, Puccetti C, Tartarelli G, et al. Evaluation of HER2 and p53 expression in predicting response to docetaxel-based first-line chemotherapy in advanced breast cancer. J Exp Clin Cancer Res. BioMed Central; 2011;30:38.

605. Cleere DW. Triple-negative breast cancer: a clinical update. Community Oncology. Community Oncology; 2010. pages 203–11.

606. MCCARTHY N, MITCHELL G, BILOUS M, WILCKEN N, LINDEMAN GJ. Triple - negative breast cancer: making the most of a misnomer. Asia - Pacific Journal of Clinical Oncology. Blackwell Publishing Asia; 2012;8:145–55.

607. Bertucci F, Finetti P, Cervera N, Esterni B, Hermitte F, Viens P, et al. How basal are triple-negative breast cancers? Int J Cancer. Wiley Subscription Services, Inc., A Wiley Company; 2008;123:236–40.

608. Bidard F-C, Conforti R, Boulet T, Michiels S, Delaloge S, André F. Does triple-negative phenotype accurately identify basal-like tumour? An immunohistochemical analysis based on 143 "triple-negative" breast cancers. Ann Oncol. Oxford University Press; 2007;18:1285–6.

609. Sørlie T, Perou CM, Tibshirani R, Aas T, Geisler S, Johnsen H, et al. Gene expression patterns of breast carcinomas distinguish tumor subclasses with clinical implications. Proc Natl Acad Sci USA. National Acad Sciences; 2001;98:10869–74.

610. Carey LA, Perou CM, Livasy CA, Dressler LG, Cowan D, Conway K, et al. Race, breast cancer subtypes, and survival in the Carolina Breast Cancer Study. JAMA. American Medical Association; 2006;295:2492–502.

611. Boyle P. Triple-negative breast cancer: epidemiological considerations and recommendations. Ann Oncol. Oxford University Press; 2012;23 Suppl 6:vi7–12.

612. Brouckaert O, Wildiers H, Floris G, Neven P. Update on triple-negative breast cancer: prognosis and management strategies. Int J Womens Health. Dove Press; 2012;4:511–20.

613. Foulkes WD, Smith IE, Reis-Filho JS. Triple-negative breast cancer. N Engl J Med. 2010;363:1938–48.

614. Hudis CA, Gianni L. Triple-negative breast cancer: an unmet medical need. The Oncologist. AlphaMed Press; 2011;16 Suppl 1:1–11.

615. Cheang MCU, Voduc D, Bajdik C, Leung S, McKinney S, Chia SK, et al. Basal-like breast cancer defined by five biomarkers has superior prognostic value than triple-negative phenotype. Clinical Cancer Research. American Association for Cancer Research; 2008;14:1368–76.

616. Turner N, Lambros MB, Horlings HM, Pearson A, Sharpe R, Natrajan R, et al. Integrative molecular profiling of triple negative breast cancers identifies amplicon drivers and potential therapeutic targets. Oncogene. Nature Publishing Group; 2010;29:2013–23.

617. Minchinton AI, Tannock IF. Drug penetration in solid tumours. Nature Reviews Cancer. 2006;6:583–92.

618. Duffy MJ, O'Grady P, Devaney D, O'Siorain L, Fennelly JJ, Lijnen HJ. Urokinase-plasminogen activator, a marker for aggressive breast carcinomas. Preliminary report. Cancer. 1988;62:531–3.

619. Vine KL, Locke JM, Bremner JB, Pyne SG, Ranson M. Selective targeting of 2'-deoxy-5-fluorouridine to urokinase positive malignant cells in vitro. Bioorg Med Chem Lett. 2010;20:2908–11.

620. Satya-Prakash KL, Pathak S, Hsu TC, Olivé M, Cailleau R. Cytogenetic analysis on eight human breast tumor cell lines: high frequencies of 1q, 11q and HeLa-like marker chromosomes. Cancer Genet Cytogenet. 1981;3:61–73.

621. Huguet EL, McMahon JA, McMahon AP, Bicknell R, Harris AL. Differential expression of human Wnt genes 2, 3, 4, and 7B in human breast cell lines and normal and disease states of human breast tissue. Cancer Research. 1994;54:2615–21.

622. Stillfried GE, Saunders DN, Ranson M. Plasminogen binding and activation at the breast cancer cell surface: the integral role of urokinase activity. Breast Cancer Res. BioMed Central Ltd; 2007;9:R14.

623. Finak G, Bertos N, Pepin F, Sadekova S, Souleimanova M, Zhao H, et al. Stromal gene expression predicts clinical outcome in breast cancer. Nat Med. Nature Publishing Group; 2008;14:518–27.

624. Balsara RD, Castellino FJ, Ploplis VA. A novel function of plasminogen activator inhibitor-1 in modulation of the AKT pathway in wild-type and plasminogen activator inhibitor-1-deficient endothelial cells. Journal of Biological Chemistry. American Society for Biochemistry and Molecular Biology; 2006;281:22527–36.

625. Hunt BJ, Missfelder-Lobos H, Parra-Cordero M, Fletcher O, Parmar K, Lefkou E, et al. Pregnancy outcome and fibrinolytic, endothelial and coagulation markers in women undergoing uterine artery Doppler screening at 23 weeks. Journal of Thrombosis and Haemostasis. Blackwell Publishing Ltd; 2009;7:955–61.

626. Brenner B. Haemostatic changes in pregnancy. Thromb Res. Elsevier; 2004;114:409–14.

627. Leung KC, Byatt JA, Stephens RW. The resistance of fibrin-stimulated tissue plasminogen activator to inactivation by a class PAI-2 inhibitor (minactivin). Thromb Res. 1987;46:755–66.

628. Sumiyoshi K, Serizawa K, Urano T, Takada Y, Takada A, Baba S. Plasminogen activator system in human breast cancer. Int J Cancer. 1992;50:345–8.

629. Bouchet C, Spyratos F, Martin PM, Hacène K, Gentile A, Oglobine J. Prognostic value of urokinase-type plasminogen activator (uPA) and plasminogen activator inhibitors PAI-1 and PAI-2 in breast carcinomas. Br J Cancer. Nature Publishing Group; 1994;69:398–405.

630. Borstnar S, Vrhovec I, Svetic B, Cufer T. Prognostic value of the urokinase-type plasminogen activator, and its inhibitors and receptor in breast cancer patients. Clin Breast Cancer. Elsevier; 2002;3:138–46.

631. Spyratos F, Bouchet C, Tozlu S, Labroquere M, Vignaud S, Becette V, et al. Prognostic value of uPA, PAI-1 and PAI-2 mRNA expression in primary breast cancer. Anticancer Res. 2002;22:2997–3003.

632. Allen BJ, Tian Z, Rizvi SMA, Li Y, Ranson M. Preclinical studies of targeted alpha therapy for breast cancer using 213Bi-labelled-plasminogen activator inhibitor type 2. Br J Cancer. Nature Publishing Group; 2003;88:944–50.

633. Stutchbury TK, Al-Ejeh F, Stillfried GE, Croucher DR, Andrews J, Irving D, et al. Preclinical evaluation of 213Bi-labeled plasminogen activator inhibitor type 2 in an orthotopic murine xenogenic model of human breast carcinoma. Mol Cancer Ther. American Association for Cancer Research; 2007;6:203–12.

634. Xu S-G, Yan P-J, Shao Z-M. Differential proteomic analysis of a highly metastatic variant of human breast cancer cells using two-dimensional differential gel electrophoresis. J Cancer Res Clin Oncol. Springer-Verlag; 2010;136:1545–56.

635. Huschtscha LI, Napier CE, Noble JR, Bower K, Au AYM, Campbell HG, et al. Enhanced isolation of fibroblasts from human skin explants. BioTechniques. 2012;53:239–44.

636. Rajaram M, Li J, Egeblad M, Powers RS. System-wide analysis reveals a complex network of tumor-fibroblast interactions involved in tumorigenicity. Horwitz MS, editor. PLoS Genet. Public Library of Science; 2013;9:e1003789.

637. Olsen CJ, Moreira J, Lukanidin EM, Ambartsumian NS. Human mammary fibroblasts stimulate invasion of breast cancer cells in a three-dimensional culture and increase stroma development in mouse xenografts. BMC Cancer. BioMed Central; 2010;10:444.

638. Gray RS, Cheung KJ, Ewald AJ. Cellular mechanisms regulating epithelial morphogenesis and cancer invasion. Curr Opin Cell Biol. 2010;22:640–50.

639. Wolf K, Mazo I, Leung H, Engelke K, Andrian von UH, Deryugina EI, et al. Compensation mechanism in tumor cell migration: mesenchymal-amoeboid transition after blocking of pericellular proteolysis. The Journal of Cell Biology. Rockefeller Univ Press; 2003;160:267–77.

640. Dwyer AR, Ellies LG, Holme AL, Pixley FJ. A three-dimensional co-culture system to investigate macrophage-dependent tumor cell invasion. Journal of Biological Methods. 2016;3:e49.

641. Fidler IJ. Cancer biology is the foundation for therapy. Cancer Biol Ther. 2005.

642. Erez N, Truitt M, Olson P, Arron ST, Hanahan D. Cancer-Associated Fibroblasts Are Activated in Incipient Neoplasia to Orchestrate Tumor-Promoting Inflammation in an NF-kappaB-Dependent Manner. Cancer Cell. Elsevier; 2010;17:135–47.

643. Nazareth MR, Broderick L, Simpson-Abelson MR, Kelleher RJ, Yokota SJ, Bankert RB. Characterization of human lung tumor-associated fibroblasts and their ability to modulate the activation of tumor-associated T cells. J Immunol. 2007;178:5552–62.

644. Shimoda M, Mellody KT, Orimo A. Carcinoma-associated fibroblasts are a rate-limiting determinant for tumour progression. Semin Cell Dev Biol. 2010;21:19–25.

645. Augsten M. Cancer-associated fibroblasts as another polarized cell type of the tumor microenvironment. Frontiers in oncology. 2014.

646. Lewis CE, Pollard JW. Distinct role of macrophages in different tumor microenvironments. Cancer Research. American Association for Cancer Research; 2006;66:605–12.

647. Yoshihara K, Shahmoradgoli M, Martínez E, Vegesna R, Kim H, Torres-Garcia W, et al. Inferring tumour purity and stromal and immune cell admixture from expression data. Nat Commun. Nature Research; 2013;4:2612.

648. Kao K-J, Chang K-M, Hsu H-C, Huang AT. Correlation of microarray-based breast cancer molecular subtypes and clinical outcomes: implications for treatment optimization. BMC Cancer. BioMed Central; 2011;11:143.

649. LeBeau AM, Duriseti S, Murphy ST, Pepin F, Hann B, Gray JW, et al. Targeting uPAR with antagonistic recombinant human antibodies in aggressive breast cancer. Cancer Research. American Association for Cancer Research; 2013;73:2070–81.

650. LeBeau AM, Sevillano N, King ML, Duriseti S, Murphy ST, Craik CS, et al. Imaging the Urokinase Plasminongen Activator Receptor in Preclinical Breast Cancer Models of Acquired Drug Resistance. Theranostics. 2014;4:267–79.

651. Montesano R, Orci L. Transforming growth factor beta stimulates collagen-matrix contraction by fibroblasts: implications for wound healing. Proc Natl Acad Sci USA. National Academy of Sciences; 1988;85:4894–7.

652. Nangia-Makker P, Honjo Y, Sarvis R, Akahani S, Hogan V, Pienta KJ, et al. Galectin-3 induces endothelial cell morphogenesis and angiogenesis. American Journal of Pathology. 2000;156:899–909.

653. Bremnes RM, Camps C, Sirera R. Angiogenesis in non-small cell lung cancer: The prognostic impact of neoangiogenesis and the cytokines VEGF and bFGF in tumours and blood. Lung Cancer. 2006;51:143–58.

654. Avraamides CJ, Garmy-Susini B, Varner JA. Integrins in angiogenesis and lymphangiogenesis. 2008;8:604–17.

655. Rasheed S, McDonald PJ, Northover JM, Guenther T. Angiogenesis and hypoxic factors in colorectal cancer. Pathol Res Pract. 2008;204:501–10.

656. Sabrkhany S, Griffioen AW, Oude Egbrink MGA. The role of blood platelets in tumor angiogenesis. Biochim Biophys Acta. 2011;1815:189–96.

657. Jih Y-J, Lien W-H, Tsai W-C, Yang G-W, Li C, Wu L-W. Distinct regulation of genes by bFGF and VEGF-A in endothelial cells. Angiogenesis. Kluwer Academic Publishers; 2001;4:313–21.

658. Vine KL, Locke JM, Ranson M, Pyne SG, Bremner JB. An investigation into the cytotoxicity and mode of action of some novel N-alkyl-substituted isatins. J Med Chem. American Chemical Society; 2007;50:5109–17.

659. Rijken DC, Lijnen HR. New insights into the molecular mechanisms of the fibrinolytic system. Journal of Thrombosis and Haemostasis. Blackwell Publishing Ltd; 2009;7:4–13.

660. Conklin MW, Keely PJ. Why the stroma matters in breast cancer: insights into breast cancer patient outcomes through the examination of stromal biomarkers. Cell Adh Migr. Taylor & Francis; 2012;6:249–60.

661. Vaupel P, Kallinowski F, Okunieff P. Blood flow, oxygen and nutrient supply, and metabolic microenvironment of human tumors: a review. Cancer Research. 1989;49:6449–65.

662. Goswami S, Sahai E, Wyckoff JB, Cammer M, Cox D, Pixley FJ, et al. Macrophages promote the invasion of breast carcinoma cells via a colony-stimulating factor-1/epidermal growth factor paracrine loop. Cancer Research. American Association for Cancer Research; 2005;65:5278–83.

663. Bailey P, Chang DK, Nones K, Johns AL, Patch A-M, Gingras M-C, et al. Genomic analyses identify molecular subtypes of pancreatic cancer. Nature. Nature Publishing Group; 2016;531:47–52.

APPENDICES

APPENDIX A
SOLUTIONS AND MEDIA

Buffers and Solutions

Phosphate Buffered Saline (PBS), pH 7.4
12 mM Na_2HPO_4
2 mM Na_2HPO_4
2.7 mM KCl
137 mM NaCl

Phosphate Buffered Saline (PBS), pH 8.5
12 mM Na_2HPO_4
2 mM Na_2HPO_4
2.7 mM KCl
137 mM NaCl

Hanks binding buffer, pH 7.4
0.98% (w/v) Hanks balanced salts
20 mM HEPES
1 mM $CaCl_2$
1 mM $MgCl_2$
0.1% (w/v) BSA

Sodium phosphate buffer
20 mM NaH2PO4
pH 6.0

HEPES buffer, pH 7.5
150 mM NaCl
20 mM HEPES

DNA Purification

Cell Resuspension Solution
50 mM Tris-HCl, pH 7.5
10 mM EDTA
100 µg/mL RNase A

Cell Lysis Solution
0.2 M NaOH
1% (w/v) SDS

Bacterial culture media

Luria-Bertani Broth (LB)
1% (w/v) tryptone
0.5% (w/v) yeast extract
170 mM NaCl

LB Agar
1% (w/v) tryptone
0.5% (w/v) yeast extract
170 mM NaCl
1.5% (w/v) agar

Teriffic Broth (TB)
1.2% (w/v) tryptone
2.4% (w/v) yeast extract
0.4% (v/v) glycerol

Protein Purification

Binding Buffer, pH 7.0
50 mM NaH_2PO_4
300 mM NaCl

Wash Buffer, pH 7.0
50 mM NaH_2PO_4
300 mM NaCl
5 mM imidazole

Elution Buffer, pH 7.0
50 mM NaH_2PO_4
300 mM NaCl
150 mM imidazole

SDS-PAGE

4 X SDS Sample Buffer
20% (v/v) 1 M Tris-HCl, pH 6.8
8% (w/v) SDS
40% (w/v) glycerol
4% (v/v) 14.7 M β-mercaptoethanol
10% (v/v) 0.5 M EDTA
0.08% (w/v) bromophenol blue

10% Resolving Acrylamide Gel
25% (v/v) 37.5:1 bis/acrylamide
25% (v/v) 1.5 M Tris base, pH 8.8

0.1% (w/v) SDS
0.04% (v/v) TEMED
0.1% (w/v) ammonium persulfate

5% Stacking Acrylamide Gel
12.5% (v/v) 37.5:1 bis/acrylamide
12.5% (v/v) 0.5M Tris base, pH 6.8
0.1% (w/v) SDS
0.1% (v/v) TEMED
0.1% (w/v) ammonium persulfate

SDS Running Buffer, pH 8.3
120 mM Tris base
120 mM glycine
2 mM SDS

Coomassie Staining Solution
0.2% (w/v) Coomassie blue R-250
40% (v/v) methanol
10% (v/v) glacial acetic acid

Coomassie Destaining Solution
40% (v/v) methanol
10% (v/v) glacial acetic acid

Ion-exchange chromatography

Start Buffer
20 mM Tris-HCl
pH 8.0

Elution Buffer
20 mM Tris-HCl
0.5 M NaCl
pH 8.0

Washing Buffer
20 mM Tris-HCl
1 M NaCl
pH 8.0

Tissue Culture Media

MDA-MB-231 Tissue Culture Media
94% (v/v) RPMI Media
5% (v/v) foetal bovine serum
1% (v/v) glutamine

MDA-MB-231HM Tissue Culture Media
89% (v/v) RPMI 1640 Media
9 % (v/v) foetal bovine serum
1% (v/v) 1M HEPES Buffer
125 IU Insulin

PDAC R172H Tissue Culture Media
90% (v/v) DMEM Media
10% (v/v) foetal bovine serum

MEF Tissue Culture Media
90% (v/v) DMEM Media
10% (v/v) foetal bovine serum

Cell Freeze-Down Media
80% (v/v) RPMI 1640 or DMEM Media
10% (v/v) foetal bovine serum
10% (v/v) dimethyl sulfoxide

APPENDIX B
IMMUNOFLUORESCENCE ANTIBODY CONTROL

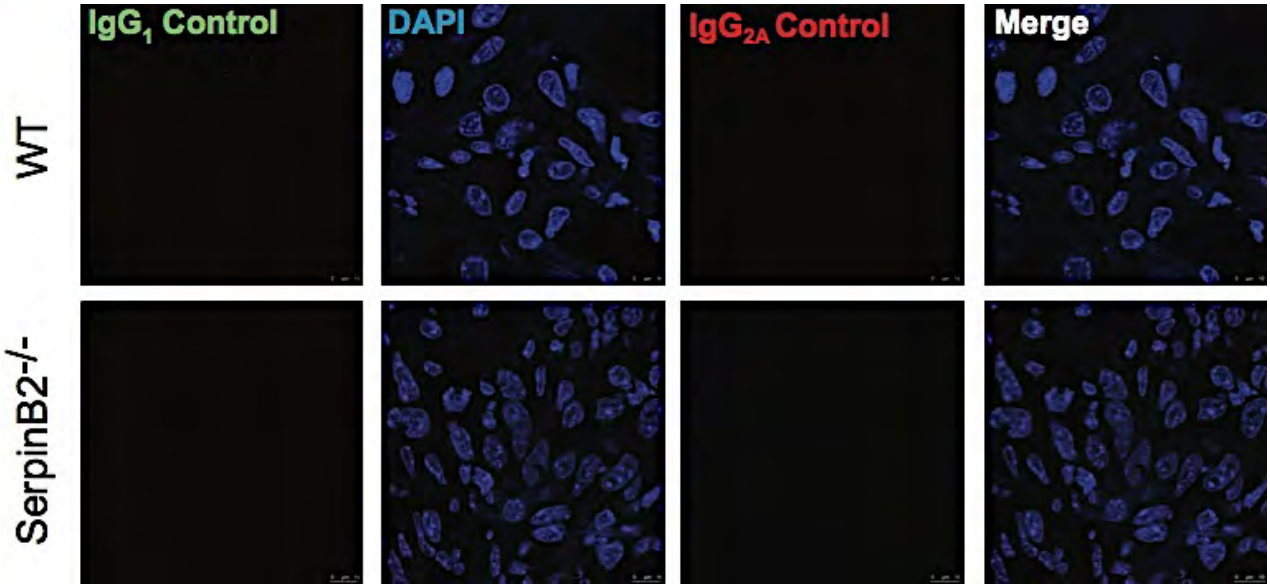

Fig. A1. Immunofluorescence isotope controls. Immunofluorescence imaging of cryosections from wild-type or SerpinB2$^{-/-}$ MEF:PDAC tumour allografts probed with Antibody isotype controls (IgG_1, IgG_{2A}). Merged images include DAPI nuclear staining.

APPENDIX C
LIST OF ANTIBODIES

Table A1. Antibodies used for immunohistochemistry, immunofluorescence and western blotting.

Antigen	Antibody description	Antibody supplier & catalog #	Antibody dilutions used	Secondary antibodies[2]
Actin	Mouse monoclonal, recognises multiple species (IgG_1)	Abcam; ab3280	IF: N/A IHC: N/A WB: 1:2500	Anti-mouse IgG-HRP[3]
Murine α-smooth muscle actin	Mouse monoclonal, cross-reacts with human (IgG_{2A})	Abcam; ab7817	IF: 1:500 IHC: N/A WB: N/A	Anti-mouse IgG Alexa Fluor 647
Human E-cadherin	Mouse monoclonal, cross-reacts with mouse (IgG_1)	BD Biosciences; 610181	IF: N/A IHC: 1:200 WB: N/A	IHC: Goat–anti mouse IgG-HRP[4]
Murine N-cadherin	Rabbit polyclonal, cross-reacts with human (IgG)	Santa Cruz; SC-7939	IF: N/A IHC: 1:200 WB: N/A	Goat–anti rabbit IgG-HRP
Chicken IgG	Mouse monoclonal (IgG_1)	Merck Millipore; MABC002	Negative control antibody - diluted to the same concentration as the test antibodies	
Human cleaved caspase-3	Rabbit polyclonal, cross-reacts with mouse (IgG)	Cell Signaling; #9661	IF: N/A IHC: 1:300 WB: N/A	Goat–anti rabbit IgG-HRP
Human Ki67	Rabbit monoclonal (IgG)	Thermo Scientific; RM9106-S1	IF: N/A IHC: 1:500 WB: N/A	Goat–anti rabbit IgG-HRP
Murine Multi-Cytokeratin	Mouse monoclonal (IgG_1)	Novocastra; NCL-C11	IF: N/A IHC: 1:500 WB: N/A	Goat–anti mouse IgG-HRP
Naïve rabbit sera Rabbit	Rabbit polyclonal (IgG)	Various	Negative control antibody - diluted to the same concentration as the test antibodies	
Murine SerpinB1	Rabbit Polyclonal (IgG)	Abcam; ab28207	IF: 1:500	Goat anti-rabbit Alexa-Fluor 488

[2] For flow cytometry, IgG-FITC secondary antibodies were from Sigma-Aldrich. For IF, IgG-Alexa Fluor secondary antibodies were from Life Technologies. For IHC and western blotting, IgG-HRP secondary antibodies were from DAKO and Sigma-Aldrich, respectively. Secondary antibodies were used within concentration ranges recommended by the manufacturers.

[3] Bound secondary antibodies detected using PicoWest ECL reagent (Pierce) and autoradiography

[4] Bound secondary antibodies detected using Liquid DAB+ Substrate Chromogen System K3468 (DAKO)

Murine/human SerpinB2	Rabbit polyclonal (IgG)	Abcam; ab137588	IF: 1:500 IHC: N/A WB: 1:2000	Goat anti-rabbit Alexa-Fluor 488 Anti-rabbit IgG –HRP
Murine SerpinB2	Rabbit polyclonal (IgG) (raised against the CD loop)	(198)	IF: 1:500 IHC: N/A WB: 1:2000	Goat anti-rabbit Alexa Fluor 488 Anti-rabbit IgG –HRP
Trinitrophenyl–KLH	Rat monoclonal (IgG_{2A})	BD Pharmingen;553996	Negative control antibody - diluted to the same concentration as the test antibodies	
Human uPA	Mouse monoclonal (IgG_1)	Sekisui Diagnostics GmbH: ADG3689	IF: 1:250 IHC: N/A WB: N/A	Goat anti-mouse IgG-FITC
Murine uPA	Rabbit polyclonal (IgG)	Abcam; ab20789	IF: 1:500 IHC: N/A WB: N/A	Goat anti-rabbit Alexa Fluor 488
Human uPAR	Mouse monoclonal (IgG_1)	R&D Systems; MAB807	IF: 1:500 IHC: N/A WB: N/A	Goat anti-mouse IgG-FITC
Murine uPAR	Rat monoclonal (IgG_{2A})	R&D Systems; MAB531	IF: 1:500 IHC: N/A WB: N/A	Goat anti-rat IgG-FITC or IgG-Alexa Fluor 555
Murine IgG	Negative Control Mouse monoclonal (IgG_1)	DAKO; X0943	Negative control antibody - diluted to the same concentration as the test antibodies	
Rabbit IgG	Rabbit polyclonal	DAKO; X0903	Negative control antibody - diluted to the same concentration as the test antibodies	

APPENDIX D
SUPPLEMENTARY MOVIE LEGENDS

Movie 1. Animated z-stack of SHG imaging from wild-type MEF contracted matrices at Day 4 of contraction.

Movie 2. Animated z-stack of SHG imaging from wild-type MEF contracted matrices at Day 12 of contraction.

Movie 3. Animated z-stack of SHG imaging from SerpinB2$^{-/-}$ MEF contracted matrices at Day 4 of contraction.

Movie 4. Animated z-stack of SHG imaging from SerpinB2$^{-/-}$ MEF contracted matrices at Day 12 of contraction.

Movie 5. Animation of rendered z-stacks of SHG imaging from SerpinB2$^{-/-}$ (L) and wild-type (R) MEF contracted matrices at Day 12 of contraction.

Movie 6 and 7. Animation of migration of wild-type (movie 6) or SerpinB2$^{-/-}$ (movie 7) MEFs through Collagen I matrices over 10 h at the midpoint of matrix contraction (day 6). Collagen (magenta) was detected using SHG and wild-type or SerpinB2$^{-/-}$ MEFs were detected through stable GFP expression.

APPENDIX E
LENTIVIRAL CONSTRUCT SEQUENCES

A

CTTGGTCGTACTAGGCCTAGGCGTCTGATCACTAGTGACTCTAGTCCTAGTCGACTAGGGATAACAGGGTAATTGTTTGAAT
GAGGCTTCAGTACTTTACAGAATCGTTGCCTGCACATCTTGGAAACACTTGCTGGGATTACTTCTTCAGGTTAACCCAACAGA
AGGCTCGAGAAGGTATATTGCTGTTGACAGTGAGCGAGGTAGTTATCCTGATGCGATTTAGTGAAGCCACAGATGTAAATCG
CATCAGGATAACTACCCTGCCTACTGCCTCGGAATTCAAGGGGCTACTTTAGGAGCAATTATCTTGTTTACTAAAACTGAATA
CCTTGCTATCTCTTTGATACATTTTTACAAAGCTGAATTAAAATGGTATAAATTAAATCACTTTTTTCAATTGGAAGACTAATG
CGTTTTCGAGATATCTAGACCCAGCTTTCTTGTACAAAGTTGGCATTATAAGAAAGCTGTGTCTAGCTATCTCGTGAACGCAT
TAGTCCTCTAATTGAAAAAAGTGATTTATTTTTTGCCTTTTAATTGCATTTCTGATGTTTTCAGAGGGAATCTGGGATGTGGC
TTTGTACAAAAGAAAATTATATCATGATGAGCCAGAAATCTGGGGTGGTTACCGGGGTAGTAATACGATGGGTGTTATGAGG
TCATATTCTACAGGATACGTCGATGCCTCGATTAGATTCCAACATGCATGCTCATTTATATGGGTATAAATGTTTCTCGCGAT
GATGTCGCGGAATCAGGTGCGACTATCTATCGCTTGTATGGGAAGCCCGATGCGCCATATTTGTTTCTGAAACATGGTGTAG
GTATCGTTGCCCAATGATGTTACAGATGAGATGGTCAGACTAAACTGGCTGACGGAAATTTATGCCTCTTCCGAACCATCAA
GCATTTTTATCCGCTAGCTCCATGATGATGCATGGTTTACATCGACCCAGCTGCCGAATCCCCCCGAGAACAAACCAGCAAT
TTCGACGTTATTTAGAAAGAAATATCTCTGCAATTCAGGGGATGAAAAATTATTTGGATTGGATGGCAGCATGAGAGCAGGT
GTTCGCTTGACGACTCGGATTTGCAGAATTCCGAAATGTTCTCGCTCTGGGTATCCAG

B

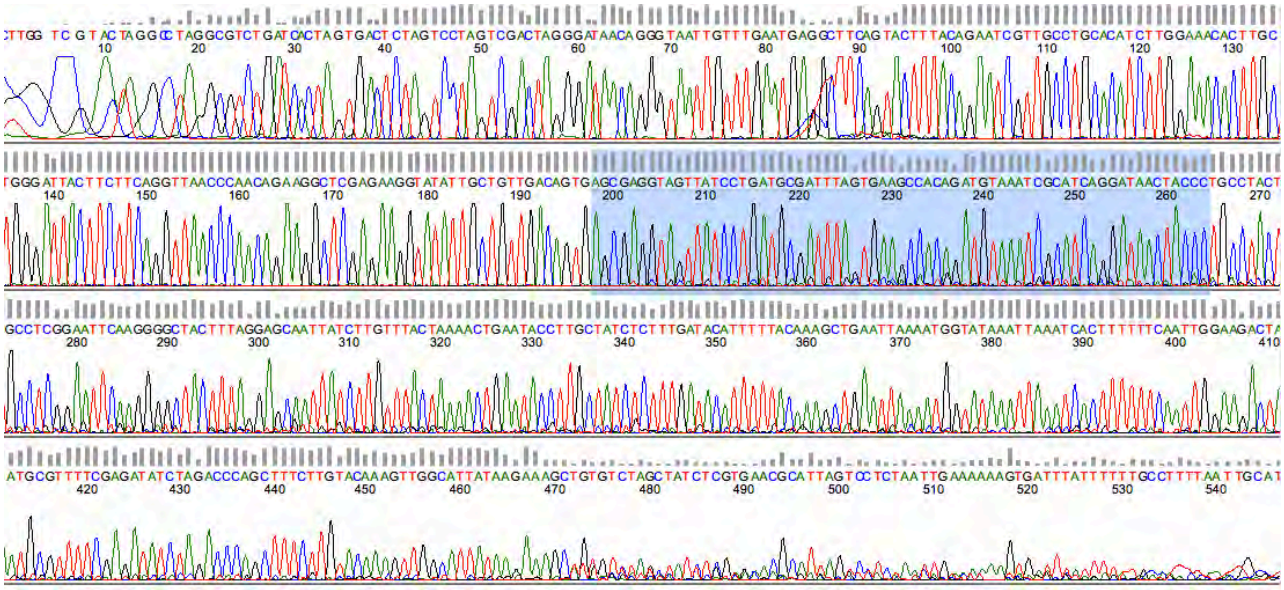

Fig A2. Entry clone analysis of pEN_TmiRc3-SerpinB2 shRNA1 vector sequence. A. Wt SerpinB2 sequence with SerpinB2 shRNA1, highlighted in green. **B.** Sequence analysis of entry clone pEN_TmiRc3-SerpinB2 shRNA1 using Finch TV analysis program. SerpinB2 shRNA1 sequence is highlighted.

A

CTTCGGCCGTACTAGGCCTAGGCGTCTGATCACTAGTGACTCTAGTCCTAGTCGACTAGGGATAACAGGGTAATTGTTT
GAATGAGGCTTCAGTACTTTACAGAATCGTTGCCTGCACATCTTGGAAACACTTGCTGGGATTACTTCTTCAGGTTAACC
CAACAGAAGGCTCGAGAAGGTATATTGCTGTTGACAGTGAGCGCGCAGGCACAAGCTGCAGATAATAGTGAAGCCACAG
ATGTATTATCTGCAGCTTGTGCCTGCATGCCTACTGCCTCGGAATTCAAGGGGCTACTTTAGGAGCAATTATCTTGTTTA
CTAAAACTGAATACCTTGCTATCTCTTTGATACATTTTTACAAAGCTGAATTAAAATGGTATAAATTAAATCACTTTTTTCA
ATTGGAAGACTAATGCGTTTTCGAGATATCTAGACCCAGCTTTCTTGTACAAAGTTGGCATTATAAGAAAGCAGTGCTTA
TCTATTTGGTGCACGCATTAGGCCTCTATTTGTCAAAAGTGAGTCATTTTTTGCCATCCAGCTGCAGCTCTGGGCCGTGT
CTCAAAATCTCTGATGTGACATTGCACAAAAGAAAATTATATCATGATGAGCCAGTAGTCTGGCTGGTTACAGAAGCAGT
AAGACGAGGGGTGTTATGAGCCATATTCGACGGGAAACGTCGAGGGCGCGATTACATTCCAACATGGATGCTGATTTAT
ATGTGTATAAATGGGCTCGCGATAATGTCGGGCAATCAGGTGCGACAATCTATCGCTTGTATGGGAAGCCCGATGCGCC
AGAGTTGTTTCTGAAACATGGGAAAGGTAGCGTTGCCAATGATGTTACAGATGAGATGGTCAGACGTAAACTGGCTGAC
GGAATTTATGCCTCTTCCGACCATCAAGCATTTTTATCCCGTACTCCTGATGATGCCATGGTTTACTCACCACCTGCGAA
TCCCCCGGAAAAACAGGCATTTCCAGGTATTAGAAGAAATATCCTGATTTCCAGTTGAAAAATATTGCTTGATGCCGCTG
GCAGTGATCCCCTGCCGCCGGTTTGCCAATTCCGAATTCCTGTTATTGTAATTGATCCCCTTTCTTTTCTAAAACCAGGC
CGAGCA

B

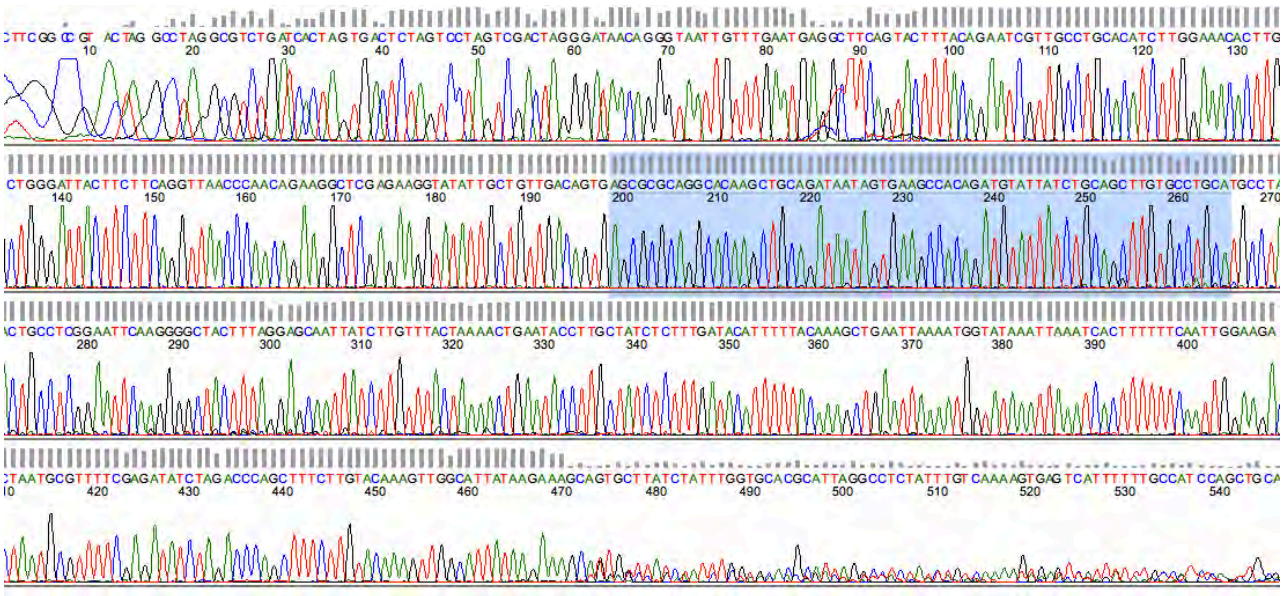

Fig. A3. Entry clone analysis of pEN_TmiRc3-SerpinB2 shRNA2 vector sequence. A. Wt SerpinB2 sequence with SerpinB2 shRNA2, highlighted in green. **B.** Sequence analysis of entry clone pEN_TmiRc3-SerpinB2 shRNA2 using Finch TV analysis program. SerpinB2 shRNA2 sequence is highlighted.

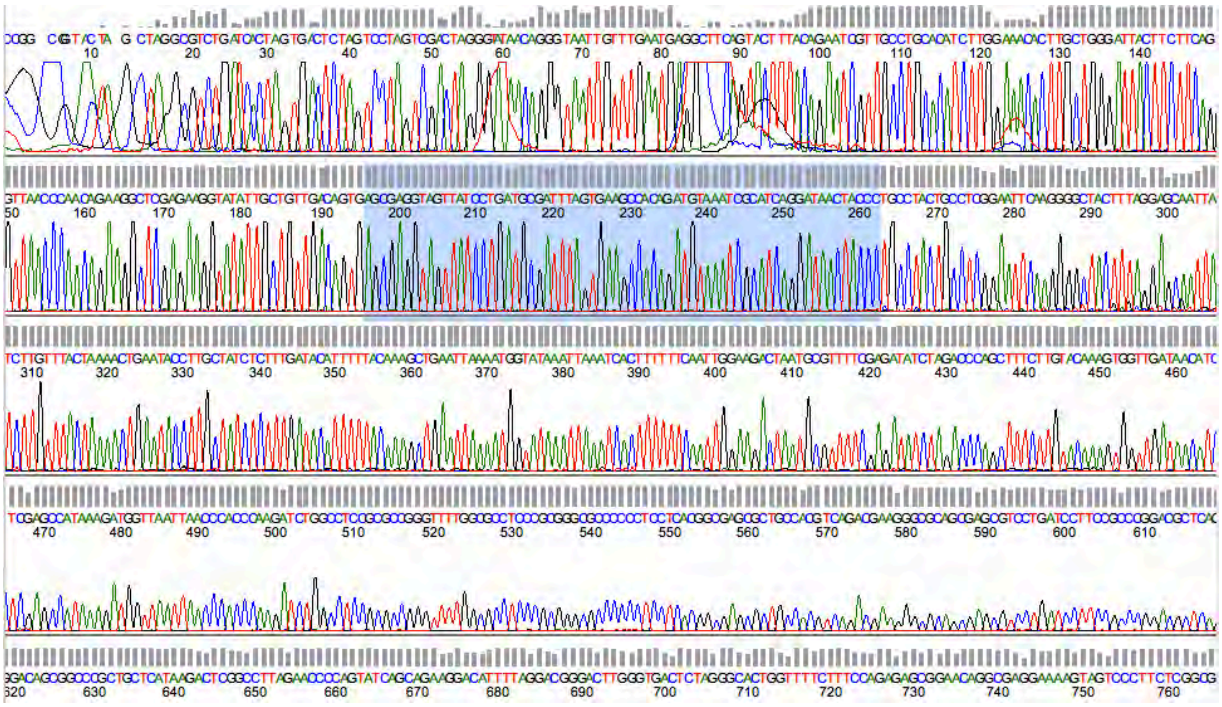

Fig A4. Destination clone analysis of pSLIK-SerpinB2 shRNA1 vector sequence. A. Wt SerpinB2 sequence with SerpinB2 shRNA 1C1, highlighted in green. **B.** Sequence analysis of destination clone pSLIK-SerpinB2 shRNA1 using Finch TV analysis program. SerpinB2 shRNA2 sequence is highlighted.

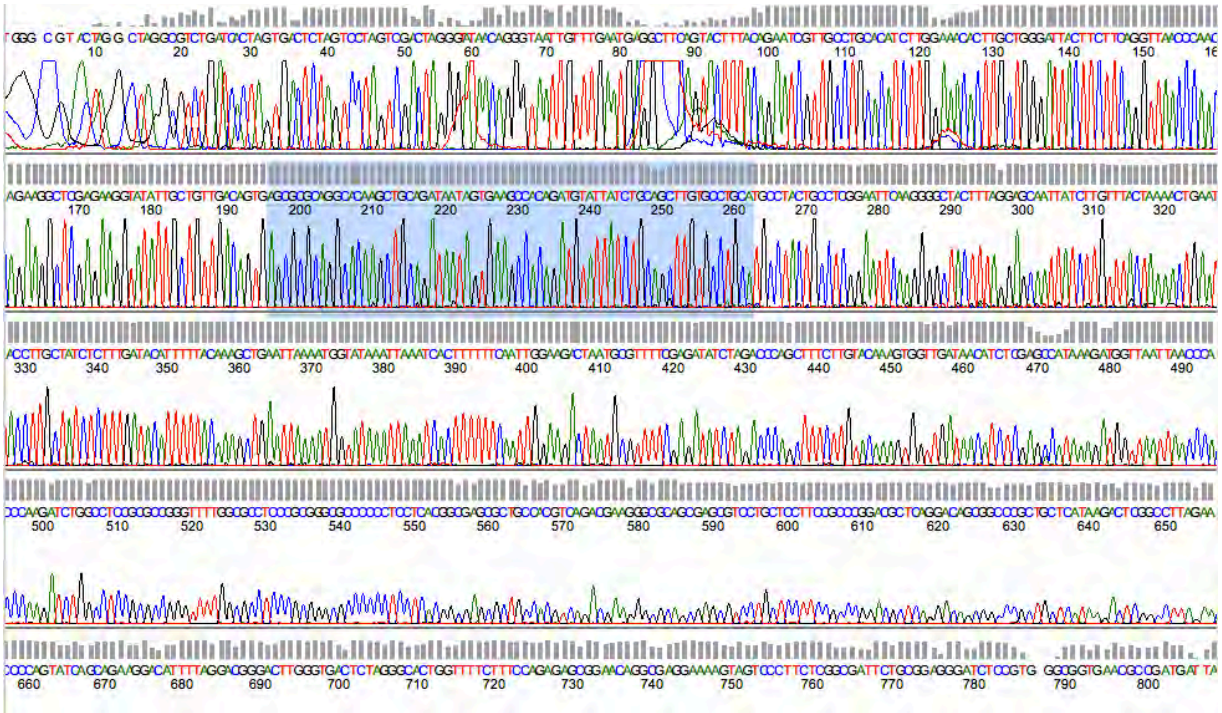

Fig. A5. Destination clone analysis of pSLIK-SerpinB2 shRNA2 vector sequence. A. Wt SerpinB2 sequence with SerpinB2 shRNA 1C1, highlighted in green. **B.** Sequence analysis of pSLIK-SerpinB2 shRNA2 using Finch TV analysis program. SerpinB2 shRNA2 sequence is highlighted.

A

File: pDONR221SerpinB2

Sample Name: pDONR221SerpinB2_CD1_Forward
Mobility: KB_3130_POP7_BDTv3.mob
Spacing: 12.9521
Comment: n/a

Signal Strengths: A = 73, C = 57, G = 125, T = 86
Lane/Cap#: 9
Matrix: n/a
Direction: Native

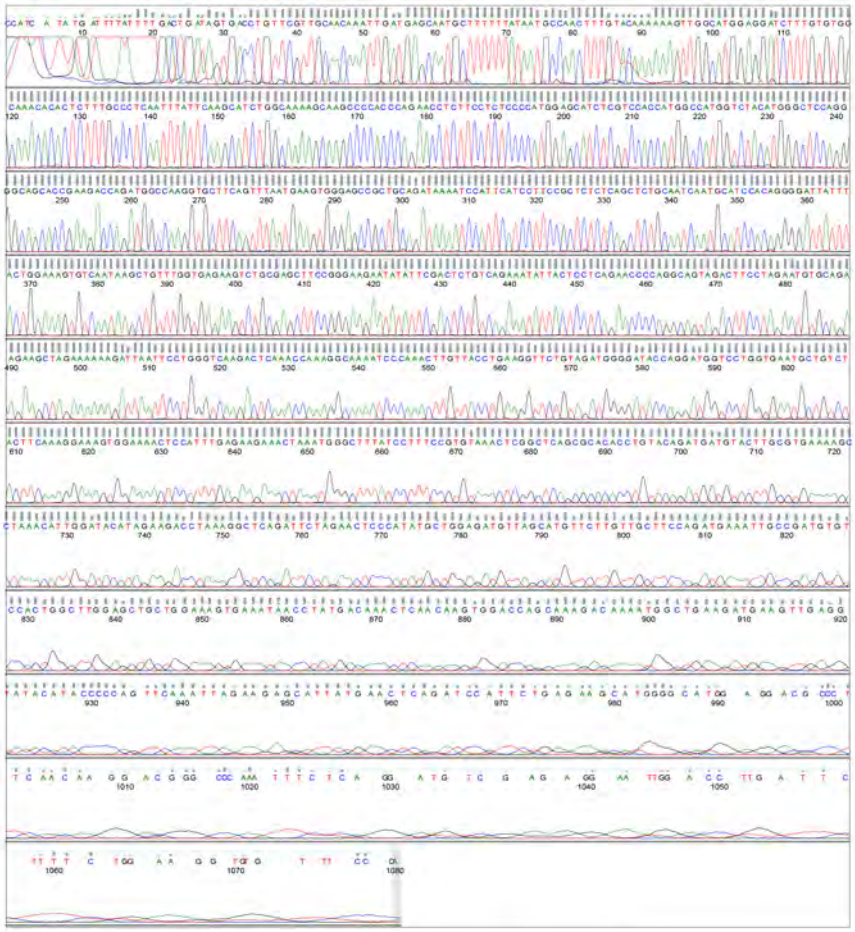

B

Chain A, Human Plasminogen Activator Inhibitor-2 [loop (66-98) Deletion Mutant]
Sequence ID: **gi|112489999|pdb|2ARQ|A** Length: 382 Number of Matches: 1

Score	Expect	Method	Identities	Positives	Gaps
545 bits(1403)	0.0()	Compositional matrix adjust.	382/382(100%)	382/382(100%)	0/382(0%)

Features:

```
Query   129   MEDLCVANTLFALNLFKHLAKASPTQNLFLSPWSISSTMAMVYMGSRGSTEDQMAKVLQF  308
SB2 ΔCD 1     MEDLCVANTLFALNLFKHLAKASPTQNLFLSPWSISSTMAMVYMGSRGSTEDQMAKVLQF  60
Query   309   NEVGAAADKIHSSFRSLSSAINASTGNYLLESVNKLFGEKSASFREEYIRLCQKYYSSEP  488
SB2 ΔCD 61    NEVGAAADKIHSSFRSLSSAINASTGNYLLESVNKLFGEKSASFREEYIRLCQKYYSSEP  120
Query   489   QAVDFLECAEEARKKINSWVKTQTKGKIPNLLPEGSVDGDTRMVLVNAVYFKGKWKTPFE  668
SB2 ΔCD 121   QAVDFLECAEEARKKINSWVKTQTKGKIPNLLPEGSVDGDTRMVLVNAVYFKGKWKTPFE  180
Query   669   KKLNGLYPFRVNSAQRTPVQMMYLREKLNIGYIEDLKAQILELPYAGDVSMFLLLPDEIA  848
SB2 ΔCD 181   KKLNGLYPFRVNSAQRTPVQMMYLREKLNIGYIEDLKAQILELPYAGDVSMFLLLPDEIA  240
Query   849   DVSTGLELLESEITYDKLNKWTSKDKMAEDEVEVYIPQFQLKEHYELRSILRSMGMEDAF  1028
SB2 ΔCD 241   DVSTGLELLESEITYDKLNKWTSKDKMAEDEVEVYIPQFQLKEHYELRSILRSMGMEDAF  300
Query   1029  NKGRANFSGMSERNDLFLSEVFHQAMVDVNEEGTEAAAGTGGVMTGRTGHGGPQFVADHP  1208
SB2 ΔCD 301   NKGRANFSGMSERNDLFLSEVFHQAMVDVNEEGTEAAAGTGGVMTGRTGHGGPQFVADHP  360
Query   1209  FLFLIMHKITNCILFFGRFSSP  1230
SB2 ΔCD 361   FLFLIMHKITNCILFFGRFSSP  382
```

Fig. A6. Entry clone sequence analysis of pDONR221 SerpinB2 ΔCD1 vector sequence. A. Nucelotide sequence analysis of entry vector, pDONR221 SerpinB2 ΔCD1. **B.** Translated protein analysis of sequence of pDONR221 SerpinB2 ΔCD1 construct versus SerpinB2 ΔCD (Homo sapiens) protein sequence. Plasmid sample was extracted from transformed DH5α *E. coli* and sequenced as described in section 2.2.2. Sequence analysis performed using Finch TV and 4 Peaks analysis programs, compared to SerpinB2 template using blastx. The red line undermarks the R380A mutation – arginine residue at position 380 with an alanine residue.

A

File: pDONR221SerpinB2_CD2

Sample Name: pDONR221SerpinB2_CD2_Forward
Mobility: KB_3130_POP7_BDTv3.mob
Spacing: 12.9356
Comment: n/a

Signal Strengths: A = 46, C = 39, G = 89, T = 56
Lane/Cap#: 11
Matrix: n/a
Direction: Native

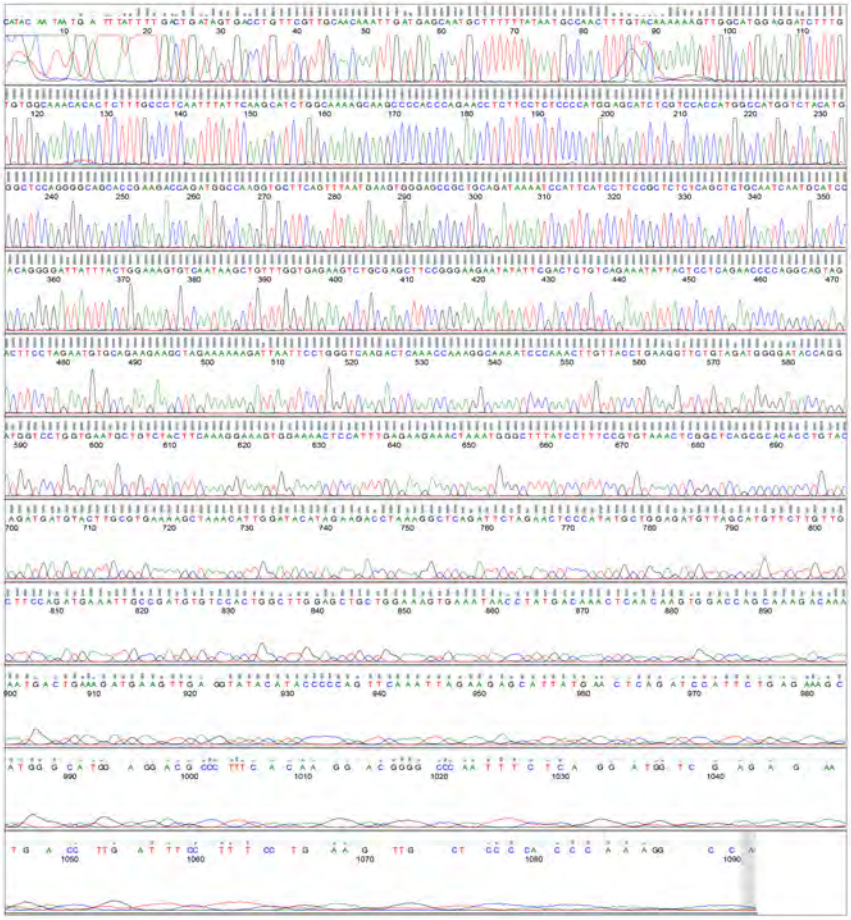

B

Chain A, Human Plasminogen Activator Inhibitor-2.[loop (66-98) Deletion Mutant]
Sequence ID: **gi|112489999|pdb|2ARQ|A** Length: 382 Number of Matches: 1

Score	Expect	Method	Identities	Positives	Gaps	Frame
545 bits(1403)	0.0()	Compositional matrix adjust.	382/382(100%)	382/382(100%)	0/382(0%)	+3

Features:

```
Query   129   MEDLCVANTLFALNLFKHLAKASPTQNLFLSPWSISSTMAMVYMGSRGSTEDQMAKVLQF  308
SB2 ΔCD 1     MEDLCVANTLFALNLFKHLAKASPTQNLFLSPWSISSTMAMVYMGSRGSTEDQMAKVLQF  60
Query   309   NEVGAAADKIHSSFRSLSSAINASTGNYLLESVNKLFGEKSASFREEYIRLCQKYYSSEP  488
SB2 ΔCD 61    NEVGAAADKIHSSFRSLSSAINASTGNYLLESVNKLFGEKSASFREEYIRLCQKYYSSEP  120
Query   489   QAVDFLECAEEARKKINSWVKTQTKGKIPNLLPEGSVDGDTRMVLVNAVYFKGKWKTPFE  668
SB2 ΔCD 121   QAVDFLECAEEARKKINSWVKTQTKGKIPNLLPEGSVDGDTRMVLVNAVYFKGKWKTPFE  180
Query   669   KKLNGLYPFRVNSAQRTPVQMMYLREKLNIGYIEDLKAQILELPYAGDVSMFLLLPDEIA  848
SB2 ΔCD 181   KKLNGLYPFRVNSAQRTPVQMMYLREKLNIGYIEDLKAQILELPYAGDVSMFLLLPDEIA  240
Query   849   DVSTGLELLESEITYDKLNKWTSKDKMAEDEVEVYIPQFQLKEHYELRSILRSMGMEDAF  1028
SB2 ΔCD 241   DVSTGLELLESEITYDKLNKWTSKDKMAEDEVEVYIPQFQLKEHYELRSILRSMGMEDAF  300
Query   1029  NKGRANFSGMSERNDLFLSEVFHQAMVDVNeegteaaagtggvmtgrtghggPQFVADHP  1208
SB2 ΔCD 301   NKGRANFSGMSERNDLFLSEVFHQAMVDVNEEGTEAAAGTGGVMTGRTGHGGPQFVADHP  360
Query   1209  FLFLIMHKITNCILFFGRFSSP  1230
SB2 ΔCD 361   FLFLIMHKITNCILFFGRFSSP  382
```

Fig. A7. Entry clone sequence analysis of pDONR221 SerpinB2 ΔCD2 vector sequence. A. Nucelotide sequence analysis of entry vector, pDONR221 ^{R380A}SerpinB2 ΔCD1. **B.** Translated protein analysis of sequence of pDONR221 SerpinB2 ΔCD2 construct versus SerpinB2 ΔCD (Homo sapiens) protein sequence. Plasmid sample was extracted from transformed DH5α *E. coli* and sequenced as described in section 2.2.2. Sequence analysis performed using Finch TV and 4 Peaks analysis programs, compared to SerpinB2 template using blastx.

A

File: pDONR221_SerpinB2R380Awt1

Sample Name: SerpinB2R380Awt1_Forward
Mobility: KB_3130_POP7_BDTv3.mob
Spacing: 12.7999
Comment: n/a

Signal Strengths: A = 32, C = 30, G = 61, T = 41
Lane/Cap#: 13
Matrix: n/a
Direction: Native

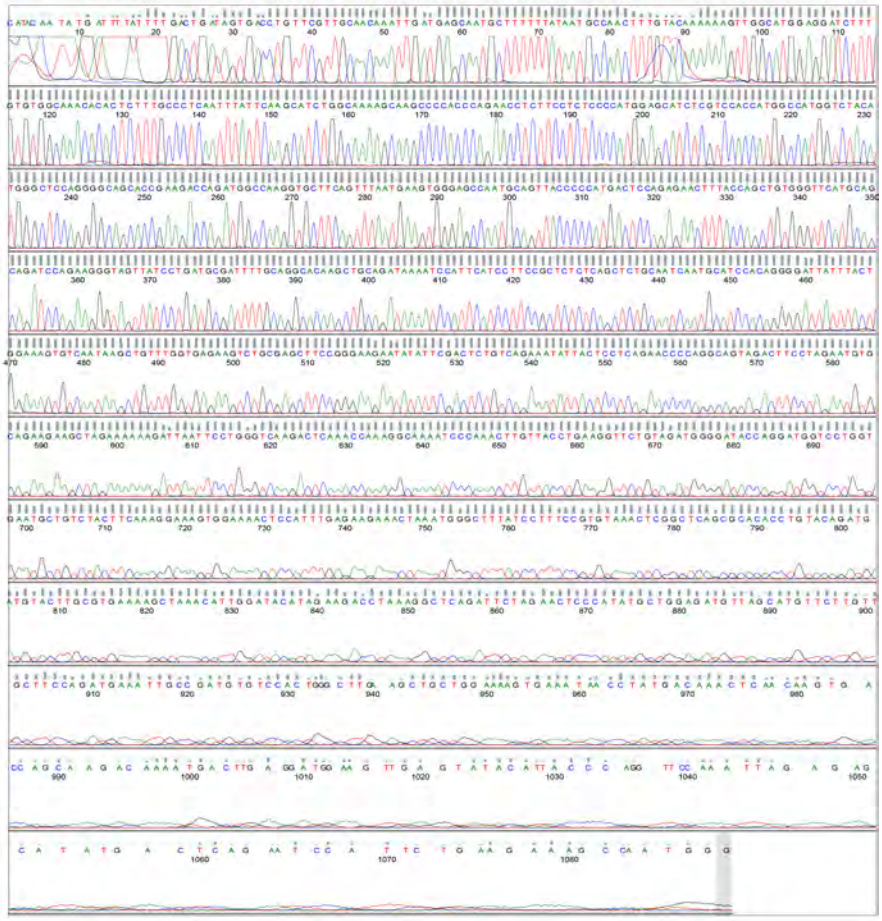

B

plasminogen activator inhibitor 2 [Homo sapiens]
Sequence ID: **gi|4505595|NP_002566.1** Length: 415 Number of Matches: 2

Range 1: 167 to 415

Score	Expect	Method	Identities	Positives	Gaps	Frame
466 bits(1200)	3e-161()	Compositional matrix adjust.	247/249(99%)	247/249(99%)	0/249(0%)	-1

Features:

```
Query  874  KKINSWVKTQTKGKIPNLLPEGSVDGDTRMVLVNAVYFKGKWKTPFEKKLNGLYPFRVNS  695
wt SB2 167  KKINSWVKTQTKGKIPNLLPEGSVDGDTRMVLVNAVYFKGKWKTPFEKKLNGLYPFRVNS  226
Query  694  AQRTPVQMMYLREKLNIGYIEDLKAQILELPYAGDVSMFLLLPDEIADVSTGLELLESEI  515
wt SB2 227  AQRTPVQMMYLREKLNIGYIEDLKAQILELPYAGDVSMFLLLPDEIADVSTGLELLESEI  286
Query  514  TYDKLNKWTSKDKMAEDEVEVYIPQFKLEEHYELRSILRSMGMEDAFNKGRANFSGMSER  335
wt SB2 287  TYDKLNKWTSKDKMAEDEVEVYIPQFKLEEHYELRSILRSMGMEDAFNKGRANFSGMSER  346
Query  334  NDLFLSEVFHQAMVDVNEEGTEAAAGTGGVMTGATGHGGPQFVADHPFLFLIMHKITKCI  155
wt SB2 347  NDLFLSEVFHQAMVDVNEEGTEAAAGTGGVMTGRTGHGGPQFVADHPFLFLIMHKITNCI  406
Query  154  LFFGRFSSP  128
wt SB2 407  LFFGRFSSP  415
```

Fig. A8. Entry clone sequence analysis of pDONR221 ^{R380A}SerpinB2 full-length 1 vector sequence. A. Nucelotide sequence analysis of entry vector, pDONR221 ^{R380A}SerpinB2 full-length 1. **B.** Translated protein analysis of both Forward and Reverse sequence of pDONR221 ^{R380A}SerpinB2 full-length 1 construct versus SerpinB2 (Homo sapiens) protein sequence. Plasmid sample was extracted from transformed DH5α *E. coli* and sequenced as described in section 2.2.2. Sequence analysis performed using Finch TV and 4 Peaks analysis programs, compared to SerpinB2 template using blastx. The red line undermarks the R380A mutation – arginine residue at position 380 with an alanine residue.

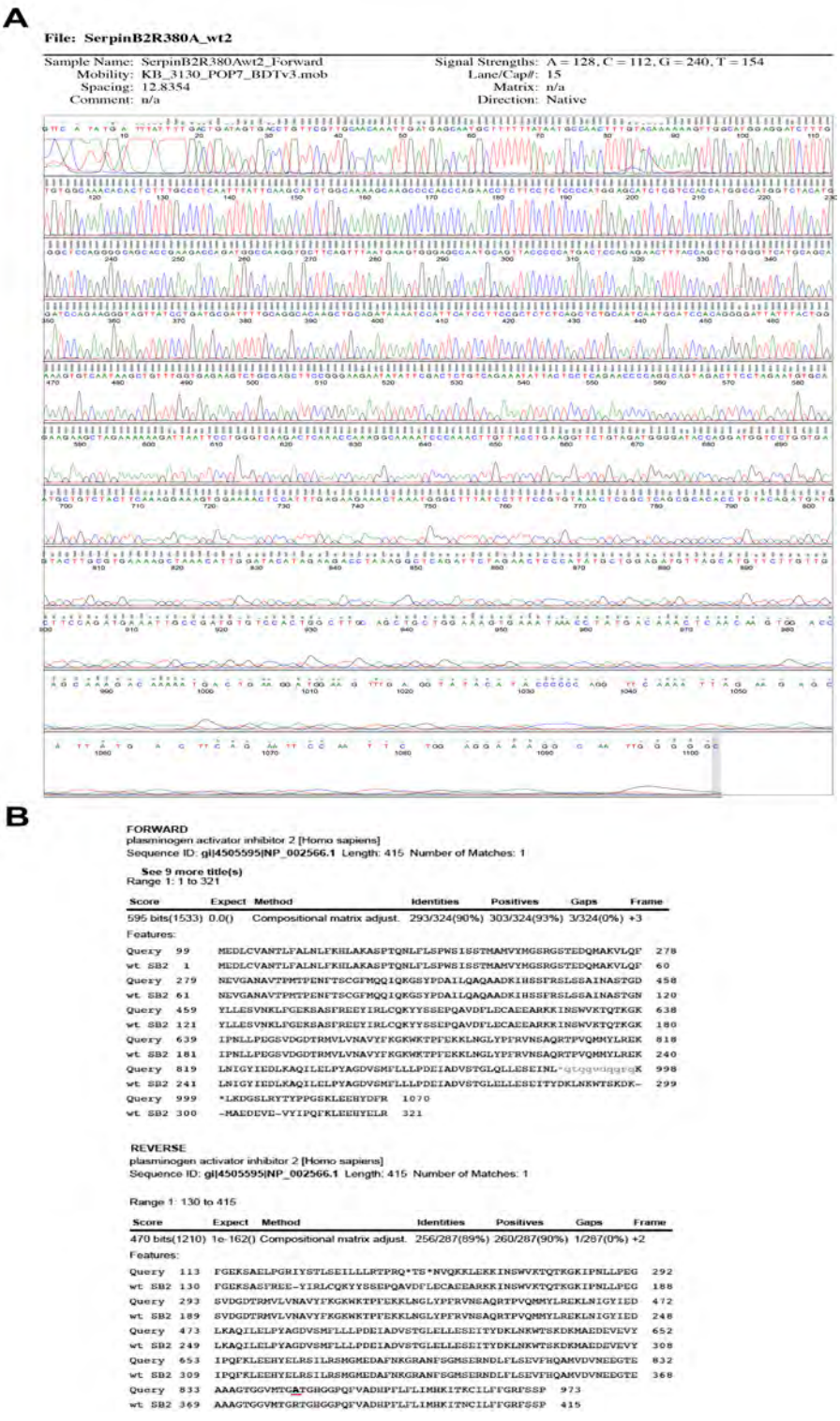

Fig. A9. Entry clone sequence analysis of pDONR221 ^{R380A}SerpinB2 full-length 2 vector sequence. A. Nucelotide sequence analysis of entry vector, pDONR221 ^{R380A}SerpinB2 full-length 2. **B.** Translated protein analysis of both Forward and Reverse sequence of pDONR221 ^{R380A}SerpinB2 full-length 2 construct versus SerpinB2 (Homo sapiens) protein sequence. Plasmid sample was extracted from transformed DH5α *E. coli* and sequenced as described in section 2.2.2. Sequence analysis performed using Finch TV and 4 Peaks analysis programs, compared to SerpinB2 template using blastx. The red line undermarks the R380A mutation – arginine residue at position 380 with an alanine residue.

A

File: pDONR221SerpinB2R380A

Sample Name: pDONR221SerpinB2R380A_CD1_Forward
Mobility: KB_3130_POP7_BDTv3.mob
Spacing: 12.777
Comment: n/a

Signal Strengths: A = 114, C = 108, G = 197, T = 146
Lane/Cap#: 2
Matrix: n/a
Direction: Native

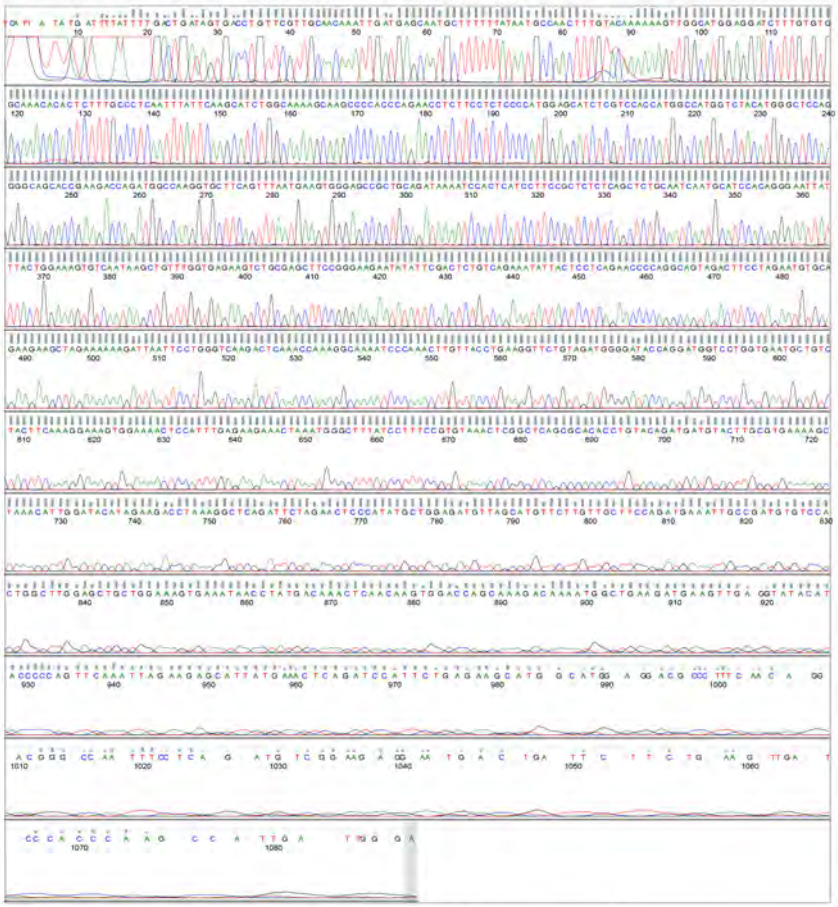

B

Chain A, Human Plasminogen Activator Inhibitor-2.[loop (66-98) Deletion Mutant]
Sequence ID: **gi|112489999|pdb|2ARQ|A** Length: 382 Number of Matches: 1

Score	Expect	Method	Identities	Positives	Gaps	Frame
545 bits(1403)	0.0()	Compositional matrix adjust.	381/382(99%)	381/382(99%)	1/382(0%)	+3

Features:

```
Query   129   MEDLCVANTLFALNLFKHLAKASPTQNLFLSPWSISSTMAMVYMGSRGSTEDQMAKVLQF  308
SB2 ΔCD 1     MEDLCVANTLFALNLFKHLAKASPTQNLFLSPWSISSTMAMVYMGSRGSTEDQMAKVLQF  60
Query   309   NEVGAAADKIHSSFRSLSSAINASTGNYLLESVNKLFGEKSASFREEYIRLCQKYYSSEP  488
SB2 ΔCD 61    NEVGAAADKIHSSFRSLSSAINASTGNYLLESVNKLFGEKSASFREEYIRLCQKYYSSEP  120
Query   489   QAVDFLECAEEARKKINSWVKTQTKGKIPNLLPEGSVDGDTRMVLVNAVYFKGKWKTPFE  668
SB2 ΔCD 121   QAVDFLECAEEARKKINSWVKTQTKGKIPNLLPEGSVDGDTRMVLVNAVYFKGKWKTPFE  180
Query   669   KKLNGLYPFRVNSAQRTPVQMMYLREKLNIGYIEDLKAQILELPYAGDVSMFLLLPDEIA  848
SB2 ΔCD 181   KKLNGLYPFRVNSAQRTPVQMMYLREKLNIGYIEDLKAQILELPYAGDVSMFLLLPDEIA  240
Query   849   DVSTGLELLESEITYDKLNKWTSKDKMAEDEVEVYIPQFQL*KEHY*ELRSILRSMGMED  1028
SB2 ΔCD 241   DVSTGLELLESEITYDKLNKWTSKDKMAEDEVEVYIPQFQL-KEHY-ELRSILRSMGMED  300
Query   1029  AFNKGRANFSGMSERNDLFLSEVFHQAMVDVNEEGTEAAAGTGGVMTGATGHGGPQFVAD  1208
SB2 ΔCD 301   AFNKGRANFSGMSERNDLFLSEVFHQAMVDVNEEGTEAAAGTGGVMTGRTGHGGPQFVAD  360
Query   1209  HPFLFLIMHKITNCILFFGRFSSP  1230
SB2 ΔCD 361   HPFLFLIMHKITNCILFFGRFSSP  382
```

Fig. A10. Entry clone sequence analysis of pDONR221 ^{R380A}SerpinB2 ΔCD1 vector sequence. A. Nucelotide sequence analysis of entry vector, pDONR221 ^{R380A}SerpinB2 ΔCD1. **B.** Translated protein analysis of sequence of pDONR221 ^{R380A}SerpinB2 ΔCD1 construct versus SerpinB2 ΔCD (Homo sapiens) protein sequence. Plasmid sample was extracted from transformed DH5α *E. coli* and sequenced as described in section 2.2.2. Sequence analysis performed using Finch TV and 4 Peaks analysis programs, compared to SerpinB2 template using blastx. The red line undermarks the R380A mutation – arginine residue at position 380 with an alanine residue.

A

File: pDONR221_SerpinB2R380A_CD2

Sample Name: SerpinB2R380A_CD2_Forward
Mobility: KB_3130_POP7_BDTv3.mob
Spacing: 13.4548
Comment: n/a

Signal Strengths: A = 114, C = 103, G = 217, T = 149
Lane/Cap#: 4
Matrix: n/a
Direction: Native

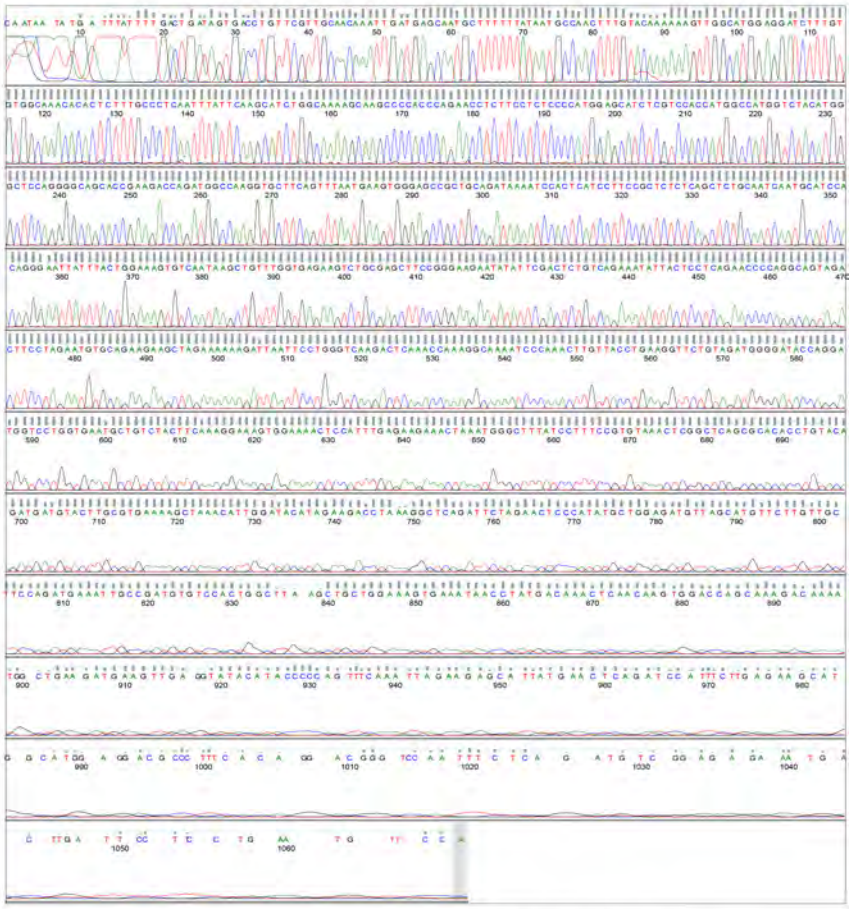

B

Chain A, Human Plasminogen Activator Inhibitor-2 [CD loop (66-98) Deletion Mutant]
Sequence ID: **gi|112489999|pdb|2ARQ|A** Length: 382 Number of Matches: 1

Score	Expect	Method	Identities	Positives	Gaps	Frame
522 bits(1345)	0.0()	Compositional matrix adjust.	339/382(88%)	345/382(90%)	2/382(0%)	+1

Features:

```
Query  16   MEDLCVANTLFALNLFKHLAKASPTQNLFLSPWSISSTMAMVYMGSRGSTEDQMAKVLQF  75
SB2ΔCD 1    MEDLCVANTLFALNLFKHLAKASPTQNLFLSPWSISSTMAMVYMGSRGSTEDQMASVLQF  60
Query  76   NEVGAAADKIHSSFRSLSSAINASTGNYLLESVNKLFGEKSASFREEYIRLCQKYYSSEP  135
SB2ΔCD 61   NEVGAAADKIHSSFRSLSSAINASTGNYLLESVNKLFGEKSASFREEYIRLCQKYYSSEP  120
Query  136  QAVDFLECAEEARKKINSWVKTQTKGKIPNLLPEGSVDGDTRMVLVNAVYFKGKWKTPFE  195
SB2ΔCD 121  QAVDFLECAEEARKKINSWVKTQTKGKIPNLLPEGSVDGDTRMVLVNAVYFKGKWKTPFE  180
Query  556  KKLNGLYPFRVNSAQRTPVQMMYLREKLNIGYIEDLKAQILELPYAGDVSMFLLLPDEIA  255
SB2ΔCD 181  KKLNGLFPFRVNSAQRTPVQMMYLREKLNIGYIEDLKAQILELPYAGDVSMFLLLPDEIA  240
Query  256  DVSTGLELLESEITYDKLNKWTSKDKMAEDEVEVYIPQFKLEEHYELRSILRSMGMEDAF  315
SB2ΔCD 241  DVSTGLELLESEITYDKLNKWTSKDKMAEDEVEVYIPQFKLEEHYELRSILRSMGMEDAF  300
Query  316  NKGRANFSGMSERNDLFLSEVFHQAMVDVNEEGTEAAAGTGGVMTGATGHGGPQFVADHP  375
SB2ΔCD 301  NKGRANFSGMSERNDLFLSEVFHQAMVDVNEEGTEAAAGTGGVMTGRTGHGGPQFVADHP  360
Query  376  FLFLIMHKITKCILFFGRFSSP 397
SB2ΔCD 361  FLFLIMHKITNCILFFGRFSSP 382
```

Fig. A11. Entry clone sequence analysis of pDONR221 ^{R380A}SerpinB2 ΔCD2 vector sequence. A. Nucelotide sequence analysis of entry vector, pDONR221 ^{R380A}SerpinB2 ΔCD2. **B.** Translated protein analysis of sequence of pDONR221 ^{R380A}SerpinB2 ΔCD2 construct versus SerpinB2 ΔCD (Homo sapiens) protein sequence. Plasmid sample was extracted from transformed DH5α *E. coli* and sequenced as described in section 2.2.2. Sequence analysis performed using Finch TV and 4 Peaks analysis programs, compared to SerpinB2 template using blastx. The red line undermarks the R380A mutation – arginine residue at position 380 with an alanine residue.